ADDRESSING ROLES FOR GLYCANS IN IMMUNOLOGY USING CHEMICAL BIOLOGY

EDITED BY: Matthew S. Macauley, Christoph Rademacher and Karina Valeria Mariño

PUBLISHED IN: Frontiers in Chemistry

frontiers Research Topics

ISSN 1664-8714
ISBN 978-2-88963-866-6
DOI 10.3389/978-2-88963-866-6

About Frontiers

Frontiers is more than just an open-access publisher of scholarly articles: it is a pioneering approach to the world of academia, radically improving the way scholarly research is managed. The grand vision of Frontiers is a world where all people have an equal opportunity to seek, share and generate knowledge. Frontiers provides immediate and permanent online open access to all its publications, but this alone is not enough to realize our grand goals.

Frontiers Journal Series

The Frontiers Journal Series is a multi-tier and interdisciplinary set of open-access, online journals, promising a paradigm shift from the current review, selection and dissemination processes in academic publishing. All Frontiers journals are driven by researchers for researchers; therefore, they constitute a service to the scholarly community. At the same time, the Frontiers Journal Series operates on a revolutionary invention, the tiered publishing system, initially addressing specific communities of scholars, and gradually climbing up to broader public understanding, thus serving the interests of the lay society, too.

Dedication to Quality

Each Frontiers article is a landmark of the highest quality, thanks to genuinely collaborative interactions between authors and review editors, who include some of the world's best academicians. Research must be certified by peers before entering a stream of knowledge that may eventually reach the public - and shape society; therefore, Frontiers only applies the most rigorous and unbiased reviews.
Frontiers revolutionizes research publishing by freely delivering the most outstanding research, evaluated with no bias from both the academic and social point of view. By applying the most advanced information technologies, Frontiers is catapulting scholarly publishing into a new generation.

What are Frontiers Research Topics?

Frontiers Research Topics are very popular trademarks of the Frontiers Journals Series: they are collections of at least ten articles, all centered on a particular subject. With their unique mix of varied contributions from Original Research to Review Articles, Frontiers Research Topics unify the most influential researchers, the latest key findings and historical advances in a hot research area! Find out more on how to host your own Frontiers Research Topic or contribute to one as an author by contacting the Frontiers Editorial Office: researchtopics@frontiersin.org

ADDRESSING ROLES FOR GLYCANS IN IMMUNOLOGY USING CHEMICAL BIOLOGY

Topic Editors:
Matthew S. Macauley, University of Alberta, Canada
Christoph Rademacher, Max Planck Institute of Colloids and Interfaces, Germany
Karina Valeria Mariño, Institute of Biology and Experimental Medicine (IBYME), Argentina

Citation: Macauley, M. S., Rademacher, C., Mariño, K. V., eds. (2020). Addressing Roles for Glycans in Immunology using Chemical Biology. Lausanne: Frontiers Media SA. doi: 10.3389/978-2-88963-866-6

Table of Contents

frontiers in Chemistry

EDITORIAL
published: 11 June 2020
doi: 10.3389/fchem.2020.00471

Editorial: Addressing Roles for Glycans in Immunology Using Chemical Biology

Matthew S. Macauley[1]*, *Christoph Rademacher*[2]* and *Karina V. Mariño*[3]*

[1] Departments of Chemistry, Medical Microbiology and Immunology, University of Alberta, Edmonton, AB, Canada, [2] Department of Biomolecular Systems, Max Planck Institute of Colloids and Interfaces, Potsdam, Germany, [3] Laboratorio de Glicómica Funcional y Molecular, Instituto de Biología y Medicina Experimental (IBYME-CONICET), Buenos Aires, Argentina

Keywords: glycans, carbohydrates, glycoimmunology, glycan binding protein (GBP), chemical biology

Editorial on the Research Topic

Addressing Roles for Glycans in Immunology Using Chemical Biology

INTRODUCTION TO CHEMICAL GLYCOIMMUNOLOGY

Advances in genetic techniques have enabled the identification of disease-susceptibility genes and the development of experimental models for mechanistic studies. However, this progress has only partially translated into new therapies, highlighting the relevance of both epigenetic control of gene expression and post-translational modifications as control points in the transition from genotype to phenotype. The cell surface provides a tightly-regulated temporal and spatial signature containing crucial biological information, and much of its dynamic response to environmental factors remains to be explored.

Glycoconjugates, macromolecules containing carbohydrates (glycans) linked to proteins or lipids, are a central component of the cell surface. These structurally diverse biomolecules expose their carbohydrate portion outside the cell, and in doing so, are essential in storing and transmitting information and regulating cell-cell interactions. One of the many fields where glycans have arisen as key communicators is immunology, as they mediate diverse immunological functions (Zhou et al., 2018). The complex mechanisms involved in the biosynthesis and assembly of glycans is a non-template driven manner, which results in a high, natural heterogeneity that is key to adapting cellular responses. However, structural characterization of these glycans and the functional interpretation of the array of carbohydrates on a cell surface, generally referred to as the glycome, remains an analytical challenge for chemists.

Since the glycome is unique to each cell type and significantly different between organisms, "self" and "non-self" signals are imbedded in the glycome (Varki, 2011). Moreover, glycans on immune cells are involved in different processes such as cell differentiation, trafficking, and response to pathogens (Varki, 2017). In this sense, glycan information is translated by glycan binding proteins (GBPs), also called lectins. The abilities of these GBPs to modulate immune cell function is intimately connected to their ability to differentiate glycan structures in a precise and effective manner. Evolution of lectins has granted these proteins a selective recognition, which is influenced not only by structure, but also by multivalency of their cognate glycan ligand, reflecting the naturally crowded and heterogeneous state of the cell surface (Kaltner et al., 2019). Consequently, chemistry has been crucial in untangling the roles of GBP-glycan interactions. Chemical tools and approaches provide a powerful complementary approach that has greatly aided our understanding of GBPs by designing inhibitors and synthetic ligands able to control immune cell function via glycan recognition. Below, we discuss the 13 manuscripts within this series in the context of three themes: GBPs, immunomodulation, and technological advances.

OPEN ACCESS

Edited and reviewed by:
John D. Wade,
University of Melbourne, Australia

***Correspondence:**
Matthew S. Macauley
macauley@ualberta.ca
Christoph Rademacher
christoph.rademacher@mpikg.mpg.de
Karina V. Mariño
kmarino@ibyme.conicet.gov.ar

Specialty section:
This article was submitted to Chemical Biology, a section of the journal Frontiers in Chemistry

Received: *29 April 2020*
Accepted: *06 May 2020*
Published: *11 June 2020*

Citation:
Macauley MS, Rademacher C and Mariño KV (2020) Editorial: Addressing Roles for Glycans in Immunology Using Chemical Biology. Front. Chem. 8:471. doi: 10.3389/fchem.2020.00471

TARGETING AND EXPLOITING GBPs

In mammals, immune cells are modulated by three major GBP families: C-type lectins (Brown et al., 2018), Galectins (Cerliani et al., 2017), and Siglecs (Duan and Paulson, 2020; Laubli and Varki, 2020). Galectins are a family of evolutionary-conserved, soluble lectins involved in multiple immunoregulatory pathways. Unraveling the molecular determinants of ligand recognition has and will continue to provide a path toward lectin engineering for improved function and efficient inhibition. This topic is reviewed by Modenutti et al., providing a synopsis of the available tools for studying galectins and their structural characterization, with emphasis on the role of water molecules in galectin-glycan binding. An alternative for modulating immune responses is using recombinant lectins to target cell surface glycans. Working with an engineered galectin1-galectin3 tetramer, Farhadi et al. investigated induction of apoptosis in cultured T cells. Through amplifying and integrating galectin-1 and−3 activities, these synthetic constructs provide new tools for understanding how these lectins, and their glycan ligands, influence innate and adaptive immunity. Beyond the human immune response, Vasta et al. provide a review on simpler organisms lacking adaptive immunity that also leverage galectins. Focusing on oysters and a parasite called *Perkinsus marinus*, that can deplete oyster stocks, the authors review recent evidence implicating galectin-like proteins produced by the oysters as a defense mechanism against the parasite. An intriguing mechanism is proposed whereby these oyster-derived GBPs bind both "self" and "non-self" glycans on host and pathogen to bring the parasite to the phagocytic hemocytes of the host.

Even though lectin families are defined by their affinity toward certain monosaccharides or oligosaccharide structures, most GBPs have low monovalent affinities, which is greatly enhanced through cell surface multivalency. Inspired by this principle of avidity, Li et al. and Goyard et al. designed synthetic multivalent glycoclusters to target GBPs on mammalian immune cells or pathogens, respectively. In the first manuscript, the focus is on DC-SIGN, a C-type lectin on dendritic cells (Li et al.). A comprehensive 20-member library of mannosides was synthesized based on 5 substructures of a high mannose N-glycan, each displayed at four valencies, and the most multivalent (hexameric) constructs showed the best binding to DC-SIGN. A TLR agonist and peptide T cell epitope were conjugated to the hexameric constructs and, surprisingly, their ability to induce monocyte maturation and T cell activation did not directly correlate with ligand potency. Accordingly, the avidity for DC-SIGN may have other consequences, such as intracellular routing and antigen presentation. In the second manuscript, a synthetic strategy is presented to prepare heteroglycoclusters designed to interact with LecA (galactose-binding lectin) and LecB (fucose binding lectin) (Goyard et al.). These lectins are virulence factors from *Pseudomonas aeruginosa*. Working with cyclopeptide-based heteroglycoclusters, fucose, mannose, and galactose can be co-presented to mimic the natural cell surface diversity and simultaneously target multiple lectins.

IMMUNOMODULATION USING GLYCOCONJUGATES OR MANIPULATING GLYCANS

Two major classes of glycoproteins are N-glycans and mucin-type O-glycans (Moremen et al., 2012). Heavily O-glycosylated mucins are an important component of the molecular shield of gastrointestinal, respiratory, and reproductive epithelial tissues. Pinzón Martín et al. reviewed the role of mucins in immunomodulation from a chemical perspective, pointing out the current challenges in their synthesis, expression, and structural characterization as fundamental and necessary steps toward understanding their clinical application. Glycoproteins can also be used for antibody development of anti-carbohydrate antibodies, which often requires the glycan to be chemically conjugated to a carrier protein. Pillot et al. address an important question, asking whether the protein conjugation site matters. Working with the Pneumococcal surface adhesin A protein, five mutants were engineered each with a single cysteine at different distances from known T-helper epitopes. A synthetic tetrasaccharide carbohydrate antigen, from the capsular polysaccharide of *S. pneumoniae*, was conjugated to the mutants via maleimide chemistry. The conjugation site furthest from the T-helper epitopes generated the highest anti-carbohydrate antibody titers, indicating that the site of conjugation does matter, which has important implications for the design of conjugate vaccines.

Glycolipids are another major class of glycoconjugates. Work by Lai et al. and Howlader et al. demonstrate applications of synthetically-prepared glycolipids and inhibitors of glycolipid-acting enzymes, respectively. Invariant NKT (iNKT) cells recognize glycolipids presented by CD1d (Rossjohn et al., 2012), and Lai et al. explore how iNKT cells respond to α-Lactosyl Ceramide (α-LacCer) relative to the commonly used α-Galactosyl Ceramide (α-GalCer). α-LacCer was synthesized and found to stimulate much weaker iNKT cell responses compared to α-GalCer. Consequently, α-LacCer suppressed iNKT responses to α-GalCer, which the authors use as a means of modulate iNKT responses and disease in the context of several iNKT-dependent injury mouse models. In the second manuscript, the ability of catabolic enzymes (sialidases) to remodel glycolipids were examined in the context of leukocyte adhesion. Using a neuraminidase-3 (Neu3) inhibitor, Howlader et al. report that interactions between the integrin LFA1 and ICAM, a key step in leukocyte adhesion and migration to inflammatory sites, is altered. Modulating Neu3 activity not only affected cell glycolipid composition, but also altered LFA1 sialylation, expression on the cell surface, and lateral mobility.

TECHNOLOGICAL ADVANCES FOR STUDYING IMMUNE CELL-RELATED GLYCOCONJUGATES

Chemistry has been instrumental in generating libraries of natural oligosaccharides. Such libraries have enabled the study of GBP specificity and glycoprofiling of diverse, complex

biological samples, such as human plasma to investigate aberrant glycosylation as a source of disease biomarkers. Specifically, Glycan libraries continue to be strongly leveraged for use in glycan microarrays. A review of glycan microarrays is presented by Gao et al., which begins by exploring chemical linking strategies used for immobilizing glycans to solid supports. An overview is presented on applications of glycan microarrays for studying the glycan binding specificity of Siglecs and Galectins, entry receptors for pathogens, and naturally occurring anti-glycan antibodies in humans (Gao et al.). Next generation approaches, such as those using DNA-encoding and cell-based approaches, are also discussed.

The natural heterogeneity of glycans has, for many years, delayed their detailed structural characterization and impaired a thorough understanding of their biological relevance. Three articles deal with the analytical challenge of glycan characterization from different perspectives (Lippold et al.; Rebello et al.; de Haas et al.). de Haas et al. review the advances in understanding the role of N-glycans on cell surface immune receptors. Here, available methodologies are discussed in relation to their potential to study this post-translational modification on processes such as pathogen recognition, antigen presentation, and immune signaling. Considering that monoclonal antibodies as therapeutics have revolutionized clinical approaches to treat many diseases, and the fact that their glycosylation can regulate their therapeutic efficacy through modulating their interactions with antibody receptors, glycoprofiling of antibodies has reached the spotlight in recent years (Mimura et al., 2018). Lippold et al. present the development of an affinity chromatography-mass spectrometry approach to understand the relevance of heterogeneous glycosylation of monoclonal antibodies. Their methodology focuses in the heterogeneous glycosylation of mAbs and its interaction with FCgIIIA, which is critically important in antibody-dependent cellular cytotoxicity. This functional separation was applied to Cetuximab as a case study, since this antibody contains a glycosylation site in both the Fc and Fab regions. Finally, and beyond biotherapeutics, the human plasma N-glycome has arisen as a source of biomarkers for different pathologies. Rebello et al. present a mass spectrometry assay for the relative quantitation of antennary fucosylation in total plasma N-glycome. The utility of this application was highlighted by its ability to detect and quantify antennary fucosylation in the plasma of colorectal cancer patients.

FUTURE PERSPECTIVES

This collection of articles highlights the relevance of chemical approaches for studying glyco-related immune pathways, exemplified with probes to target GBPs, structure–function relationships, and new analytical techniques. A close collaboration and interplay between chemists and immunologists have and will continue to lead to new breakthrough in the roles of glycosylation in immunity. Indeed, outcomes of this interdisciplinary strategy is facilitating and will certainly accelerate vaccine design, identification of new biomarkers and moreover, precise modulation of biotherapeutic activities.

AUTHOR CONTRIBUTIONS

All authors listed have made a substantial, direct and intellectual contribution to the work, and approved it for publication.

REFERENCES

Brown, G. D., Willment, J. A., and Whitehead, L. (2018). C-type lectins in immunity and homeostasis. *Nat. Rev. Immunol.* 18, 374–389. doi: 10.1038/s41577-018-0004-8

Cerliani, J. P., Blidner, A. G., Toscano, M. A., Croci, D. O., and Rabinovich, G. A. (2017). Translating the 'sugar code' into immune and vascular signaling programs. *Trends Biochem. Sci.* 42, 255–273. doi: 10.1016/j.tibs.2016.11.003

Duan, S., and Paulson, J. C. (2020). Siglecs as immune cell checkpoints in disease. *Annu Rev Immunol.* 38, 365–395. doi: 10.1146/annurev-immunol-102419-035900

Kaltner, H., Abad-Rodríguez, J., Corfield, A. P., Kopitz, J., and Gabius, J.-H. (2019). The sugar code: letters and vocabulary, writers, editors and readers and biosignificance of functional glycan–lectin pairing. *Biochem. J.* 476, 2623–2655. doi: 10.1042/BCJ20170853

Laubli, H., and Varki, A. (2020). Sialic acid-binding immunoglobulin-like lectins (Siglecs) detect self-associated molecular patterns to regulate immune responses. *Cell Mol. Life Sci.* 77, 593–605. doi: 10.1007/s00018-019-03288-x

Mimura, Y., Katoh, T., Saldova, R., O'Flaherty, R., Izumi, T., Mimura-Kimura, Y., et al. (2018). Glycosylation engineering of therapeutic IgG antibodies: challenges for the safety, functionality and efficacy. *Protein Cell.* 9, 47–62. doi: 10.1007/s13238-017-0433-3

Moremen, K. W., Tiemeyer, M., and Nairn, A. V. (2012). Vertebrate protein glycosylation: diversity, synthesis and function. *Nat. Rev. Mol. Cell Biol.* 13, 448–462. doi: 10.1038/nrm3383

Rossjohn, J., Pellicci, D. G., Patel, O., Gapin, L., and Godfrey, D. I. (2012). Recognition of CD1d-restricted antigens by natural killer T cells. *Nat. Rev. Immunol.* 12, 845–857. doi: 10.1038/nri3328

Varki, A. (2011). Since there are PAMPs and DAMPs, there must be SAMPs? Glycan "self-associated molecular patterns" dampen innate immunity, but pathogens can mimic them. *Glycobiology* 21, 1121–1124. doi: 10.1093/glycob/cwr087

Varki, A. (2017). Biological roles of glycans. *Glycobiology* 27, 3–49. doi: 10.1093/glycob/cww086

Zhou, J. Y., Oswald, D. M., Oliva, K. D., Kreisman, L. S. C., and Cobb, B. A. (2018). The glycoscience of immunity. *Trends Immunol.* 39, 523–535. doi: 10.1016/j.it.2018.04.004

Conflict of Interest: The authors declare that the research was conducted in the absence of any commercial or financial relationships that could be construed as a potential conflict of interest.

frontiers in Chemistry

ORIGINAL RESEARCH
published: 02 October 2019
doi: 10.3389/fchem.2019.00666

Heteroglycoclusters With Dual Nanomolar Affinities for the Lectins LecA and LecB From *Pseudomonas aeruginosa*

David Goyard[1], *Baptiste Thomas*[1], *Emilie Gillon*[2], *Anne Imberty*[2]* *and Olivier Renaudet*[1]*

[1] Univ. Grenoble Alpes, CNRS, DCM UMR 5250, Grenoble, France, [2] Univ. Grenoble Alpes, CNRS, CERMAV, Grenoble, France

Multivalent structures displaying different instead of similar sugar units, namely heteroglycoclusters (hGCs), are stimulating the efforts of glycochemists for developing compounds with new biological properties. Here we report a four-step strategy to synthesize hexadecavalent hGCs displaying eight copies of αFuc and βGal. These compounds were tested for the binding to lectins LecA and LecB from *Pseudomonas aeruginosa*. While parent fucosylated (**19**) and galactosylated (**20**) homoclusters present nanomolar affinity with LecB and LecA, respectively, we observed that hGCs combining these sugars (**11** and **13**) maintain their binding potency with both lectins despite the presence of an unspecific sugar. The added multivalency is therefore not a barrier for efficient recognition by bacterial receptors and it opens the route for adding different sugars that can be selected for their immunomodulatory properties.

Keywords: heteroglycocluster, multivalency, orthogonal ligation, lectin, *Pseudomonas aeruginosa*

OPEN ACCESS

Edited by:
Karina Valeria Mariño, Institute of Biology and Experimental Medicine (IBYME), Argentina

Reviewed by:
Maria Laura Uhrig, Universidad de Buenos Aires, Argentina
Juan M. Benito, Institute of Chemical Research (IIQ), Spain

***Correspondence:**
Anne Imberty
anne.imberty@cermav.cnrs.fr
Olivier Renaudet
olivier.renaudet@univ-grenoble-alpes.fr

Specialty section:
This article was submitted to Chemical Biology, a section of the journal Frontiers in Chemistry

Received: *29 July 2019*
Accepted: *18 September 2019*
Published: *02 October 2019*

Citation:
Goyard D, Thomas B, Gillon E, Imberty A and Renaudet O (2019) Heteroglycoclusters With Dual Nanomolar Affinities for the Lectins LecA and LecB From Pseudomonas aeruginosa. Front. Chem. 7:666. doi: 10.3389/fchem.2019.00666

INTRODUCTION

Glycoclusters and glycodendrimers remain a growing source of interest in glycosciences (Renaudet and Roy, 2013). For a long time, synthetic chemists focused their efforts on structures displaying multiple copies of a single sugar unit to both clarify and modulate biological and pathological processes involving multivalent interactions with proteins (Bernardi et al., 2013; Cecioni et al., 2015; Arsiwala et al., 2019). However, these compounds only partially reflect the heterogeneous expression of glycans at the cell surface (i.e., glycocalyx) and completely underestimate that other sugar units may participate or promote additional biological events (Jiménez Blanco et al., 2013; Müller et al., 2016). For this reason, the development of structures displaying different rather than unique sugars, namely heteroglycoclusters (hGCs), as mimics of the glycocalyx is renewing the enthusiasm in this field.

So far, several heterovalent structures have been reported for studying the interaction process with a large class of carbohydrate-specific proteins (i.e., glycosidases, glycosyltransferases, lectins, antibodies) (Deguise et al., 2007; Ortega-Muñoz et al., 2009; Gómez-García et al., 2010; Lindhorst et al., 2010; Karskela et al., 2012; Abellán Flos et al., 2016; Vincent et al., 2016; Ortiz Mellet et al., 2017; Gade et al., 2018; Ogura et al., 2018) or for triggering multifaceted immune response against tumor cells (Ragupathi et al., 2002; Zhu et al., 2009; Pett et al., 2017). These studies highlight the complexity of heterocluster effects and reinforce the need of new structures to go one step further toward the understanding of naturally occurring recognition events and the

development of more active compounds. Among recent reports, J. M. Garcia Fernandez and coworkers have demonstrated the impact of heterovalent display in both glycosidase inhibition and lectin binding using a competitive enzyme-lectin binding assay (Abellán Flos et al., 2016; García-Moreno et al., 2017). In addition, the Wong group have shown by glycan array that ligand density and neighboring sugars significantly affect the binding with antibodies (Liang et al., 2011). In another study, Reymond and co-workers focused their interest on the lectins LecA and LecB from *Pseudomonas aeruginosa* (Michaud et al., 2016). These two lectins play central roles in both the adhesion of the bacteria to host cells and the biofilm formation, causing severe damages in particular for immunocompromised patients (Mitchell et al., 2002; Imberty et al., 2004). Instead of using homovalent structures specific for either LecA or LecB, the authors postulated that the utilization of compounds combining both α-fucose (αFuc) and β-galactose (βGal) could bind simultaneously LecA and LecB, thus improving inhibitory effect to fight this antibiotic resistant bacterium. To this aim, glycodendrimers decorated with βGal and αFuc have been synthesized and promising activity in comparison with their previous homoclusters has been observed. This pioneering study prompted us to design new heterovalent glycodendrimers and to study their ability to bind these two lectins with high affinity and without loss of efficiency.

In the course of developing multivalent glycoconjugates (Galan et al., 2013; Daskhan et al., 2015), we recently focused on the synthesis of a variety of cyclopeptide-based hGCs using orthogonal chemoselective conjugation methods such as the oxime ligation (OL), the Cu(I)-catalyzed azide-alkyne cycloaddition (CuAAC), and the thiol-ene, thiol-chloroactetyl and diethyl squarate couplings (TEC, TCC, DSC). We thus synthesized diverse 4-, 8-, and 16-valent structures displaying from 2 to 4 different sugars in well-defined shuffled proportion and disposition (Thomas et al., 2012; Daskhan et al., 2016; Pifferi et al., 2017). In addition, sequential one-pot multi-click and iterative divergent strategies gave access to glycoconjugates with unprecedented structural complexity in excellent yields and purity (Thomas et al., 2015a). In the present study, we capitalized on these methodologies to synthesize glycodendrimers bearing βGal and αFuc with different chemical linkage and evaluated their binding to LecA and LecB. Because αMan is ligand of LecB, though with a lower affinity than αFuc, we also synthesized different combinations of hGCs containing this residue to evaluate its potential influence in the binding to these two lectins.

RESULTS AND DISCUSSION

In a previous report, we described a series of homovalent glycodendrimers with nanomolar affinity for LecB (Berthet et al., 2013). These compounds have been prepared by a convergent oxime conjugation of cyclopeptides and/or polylysine dendrons then aminooxylated sugar units have been grafted at the periphery. However, the same strategy is not compatible to introduce two different sugars in a regioselective and controlled manner (Bossu et al., 2011). Instead, we used here OL and CuAAC to secure the molecular assembly and the final purification of complex structures (Thomas et al., 2015b). To do so, the construction of the dendrimer core was first carried out from a central cyclopeptide **A** (**Figure 1**) containing two aminooxy groups and two serine as oxo-aldehyde precursors as previously described (Pifferi et al., 2017). This scaffold **A** was successively functionalized with two cyclopeptides: the first one **B** (right arm) contains one aldehyde and four azido groups, whereas the second one **C** (left arm) displays one aminooxy and four serines. Treatment with sodium periodate of the resulting hexadecavalent dendrimer afforded **1** which was functionalized with aminooxylated αFuc (**2**), βGal (**3**), and αMan (**4**) in aqueous solution containing 0.1% TFA at 37°C for 30 min. These three octavalent conjugates displaying eight copies of αFuc (**5**), βGal (**6**), and αMan (**7**) were subsequently conjugated without further purification with propargylated αFuc (**8**), βGal (**9**), and/or αMan (**10**) in PBS (pH 7.4, 10 mM) with $CuSO_4$, tris(3-hydroxypropyltriazolylmethylamine) (THPTA) and sodium ascorbate (**Figure 2**). After RP-HPLC purification, the resulting hGCs **11**–**14** were obtained in 76–84% yield.

The resulting hGCs were tested in solution with lectins by Isothermal Titration Calorimetry (**Table 1**) and their binding properties were compared with homoclusters **15**–**20** (Berthet et al., 2013; Thomas et al., 2015b) displaying either 4 and 16 βGal or αFuc units attached with an oxime or a triazole linker (**Figure 3**). Methyl α-L-fucoside (αFuc-OMe) and methyl β-D-galactoside (βGal-OMe) were used as monovalent references for LecB and LecA to calculate the relative potency (α) and relative potency per sugar (β) of each multivalent compound. Experiments were performed in direct injection mode (i.e., ligand in syringe and protein in cell) to minimize aggregation problems.

For LecB, we observed modest and similar *K*d (0.3 μM) for tetravalent compounds **15** and **16**, with negligible improvement factor α compared to αFuc-OMe indicating the absence of cluster effect (**Table 1**, **Figure 4A**, and **Supplementary Information**). Instead strong aggregation is observed as shown on the thermogram in **Figure 4A**. The analysis of the thermodynamic contributions indicates a strong gain in enthalpy but that is completely counterbalanced by the entropy cost. This again indicates that the tetravalent compound is bridging between different lectin tetramers instead of clustering neighboring binding sites.

By contrast, for LecA, a very strong improvement of binding was observed for both tetravalent compounds **17** and **18** (*K*d = 22 nM) compared to βGal-OMe (**Table 1**). This suggests a favorable presentation of sugar for the binding to LecA (Cecioni et al., 2012) with geometry allowing for a real clustering effect, also reflected in the huge enthalpy gain. Compound **18** that contains a triazole linkage instead of oxime (**17**) is the most efficient with a factor α of 7,000 and factor β of 1,700 when reported to the number of sugar (**Table 1**, **Figure 4B**, and **Supplementary Information**). This result is in good agreement with the well-known preference of LecA for β-galactoside containing an aromatic moiety near the anomeric position (Cecioni et al., 2012).

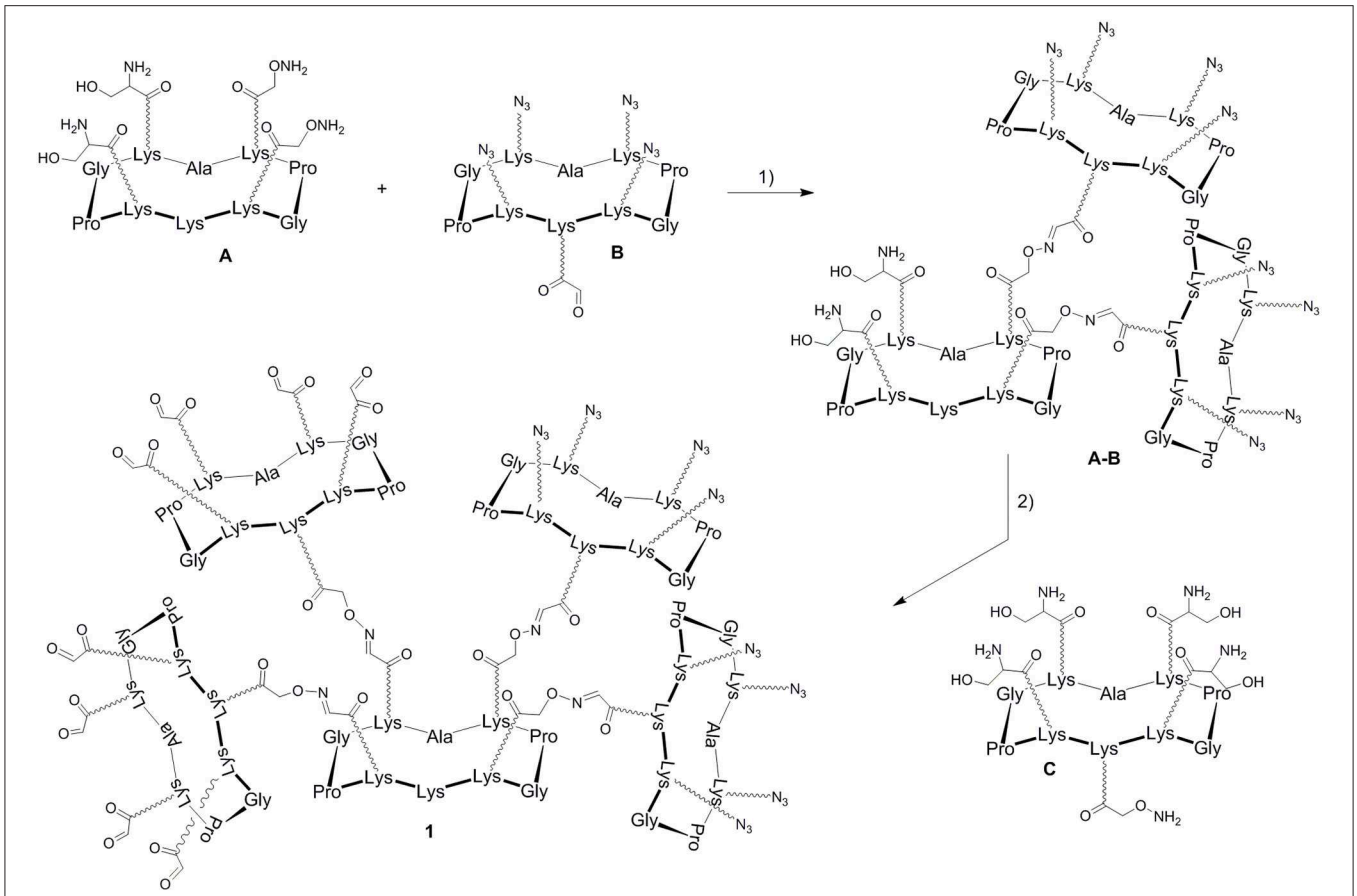

FIGURE 1 | Strategy for the construction of the hexadecavalent scaffold 1. Reagents and conditions (Pifferi et al., 2017): (1) 0.1% TFA in H_2O/CH_3CN (1:1), 37°C, 30 min; (2) i: $NaIO_4$, H_2O, r.t., 40 min; ii: 0.1% TFA in H_2O/CH_3CN (1:1), 37°C, 30 min; (3) $NaIO_4$, H_2O, r.t., 40 min.

Interestingly, multimerisation of the tetravalent structures **15** and **18** as the hexadecavalent dendrimers **19** and **20** allowed 10-fold binding improvement for fucosylated compounds with LecB (Kd = 44 nM for **19**). Only minor difference in Kd was observed between **18** and **20** and LecA (Kd = 22 and 14 nM, respectively), despite a more favorable binding enthalpy for **20** (−ΔH = 378 kJ/mol) and a higher improvement factor α (10,000) compared to βGal-OMe. While both **18** and **20** are excellent ligands for LecA, compound **20** shows a 2.5-lower β factor than **18** which suggests that increasing valency over four sugars units has low effect for enhancing affinity with LecA. Similar observations have been already reported in other studies (Cecioni et al., 2012; Michaud et al., 2016).

We next evaluated the binding potency of hGCs for LecA and LecB by ITC (**Table 1**, **Figure 5**, and **Supplementary Information**). Two compounds **11** and **13** display eight copies of αFuc and βGal with either oxime or triazole linkers and two other hGCs combine αMan with αFuc (**12**) or βGal (**14**). As observed with tetravalent clusters **15**–**16** with LecB, a higher affinity (Kd = 85–92 nM) was measured when the fucose unit is linked by an oxime linkage. These compounds **11** and **12** showed a more favorable binding enthalpy (−ΔH = 212 kJ/mol), suggesting a more favorable geometry and presentation of fucose. Moreover, no significant difference of affinity was observed between **11** and **12** with binding improvement in the same range of magnitude than homovalent compounds (i.e., β factor lower than 1), indicating the absence of influence of the partner sugar (Man or Gal).

As for LecA, as mentioned with homovalent structures **17**–**20**, hGCs displaying βGal **11**, **13**, and **14** lead to similar Kd (21–35 nM), showing strong binding entropy contribution (−ΔS = 173–199 kJ/mol) counterbalanced by favorable binding enthalpy (−ΔH = 216–243 kJ/mol).

When the binding is compared to parent galactosyl-homoclusters, the β factor was ∼500 for both βGal-αFuc hGCs **11** and **13** and 900 for **14** which displays βGal-αMan combination. The stoichiometry data for these three compounds indicated that approximately six βGal can bind to a monomer of LecA, which indicates a good accessibility despite the presence of non-specific sugars close to βGal. This results supports the fact that high affinity could be due to an aggregative binding mode. In the case of LecB, the stoichiometry measured for **11**–**13** (n = 0.1) lead to a similar hypothesis. Altogether, our data suggest that hGCs combining both βGal and αFuc derivatives not only bind to both

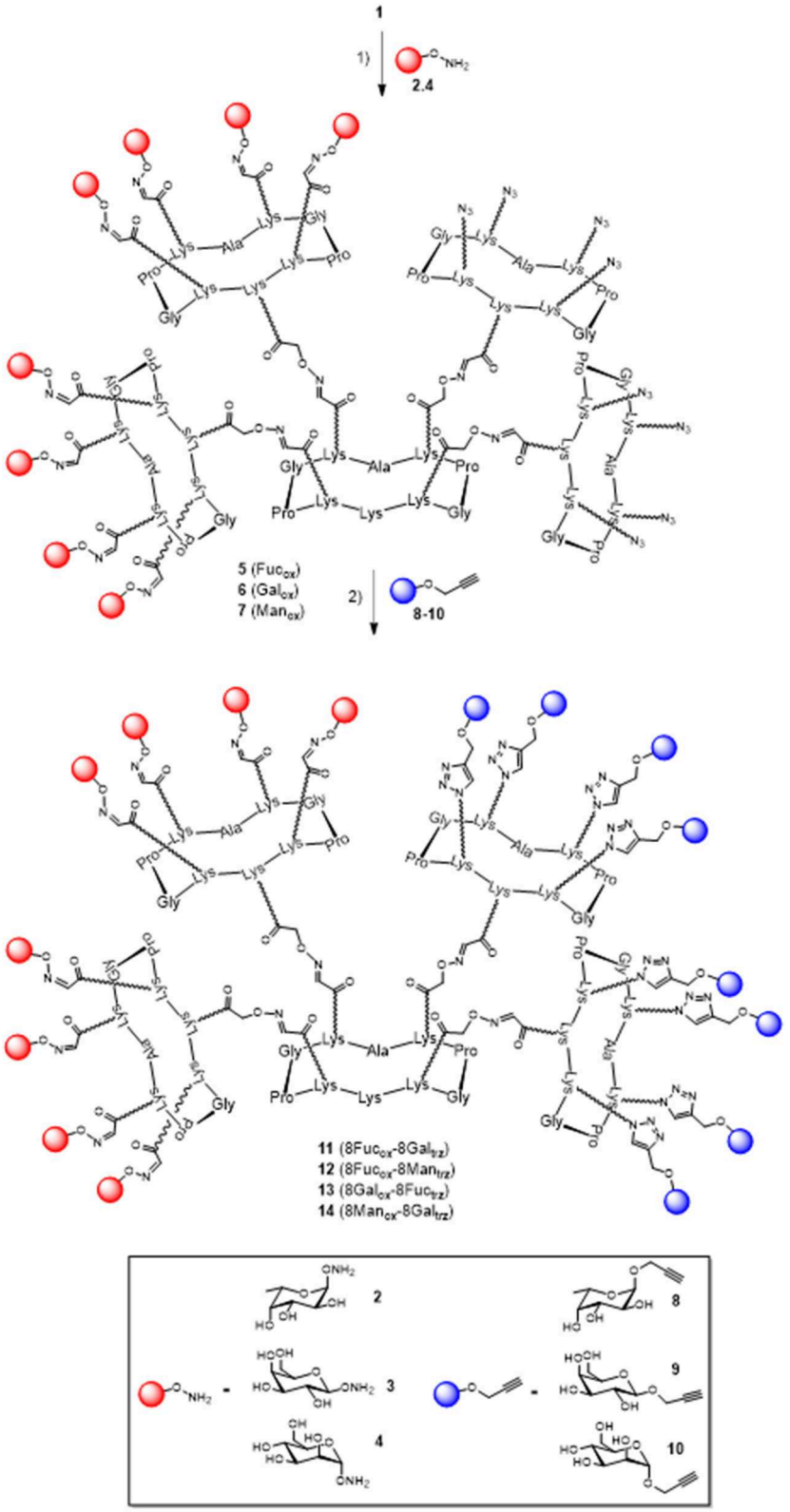

FIGURE 2 | Synthesis of hGCs **11**–**14** by a mixed OL and CuAAC strategy. Reagents and conditions: (1) **2**, **3**, or **4**, 0.1% TFA in H_2O/CH_3CN, 37°C, 30 min; (2) **8**, **9**, or **10**, $CuSO_4$, Na ascorbate, THPTA, PBS (pH 7.4, 10 mM), r.t., 90 min, 81% for **11**, 84% for **12**, 77% for **13**, and 76% for **14**.

TABLE 1 | Isothermal titration microcalorimetry data for binding to LecA and LecB[a].

Lectin	Compound	Kd [nM]	n	$-\Delta H$ [kJ.mol^{-1}]	$-\Delta G$ [kJ.mol^{-1}]	$-T\Delta S$ [kJ.mol^{-1}]	α	β
LecB	αFuc-OMe[b]	430	0.77	41	36.4	–5	1	1
	15 ($4Fuc_{ox}$)	334 ± 35	0.17	103.5 ± 2	37.1	66.5	1.3	0.3
	16 ($4Fuc_{trz}$)	367 ± 26	0.19	119.5 ± 1	36.8	82.8	1.2	0.3
	19 ($16Fuc_{ox}$)	44 ± 5	0.06	321.0 ± 14	42.0	279.0	9.8	0.6
	11 ($8Fuc_{ox}$-$8Gal_{trz}$)	92 ± 14	0.10	212.1 ± 6	40.2	171.9	4.7	0.8
	12 ($8Fuc_{ox}$-$8Man_{trz}$)	85 ± 16	0.08	211.0 ± 3	40.4	170.6	5.1	0.6
	13 ($8Gal_{ox}$-$8Fuc_{trz}$)	118 ± 15	0.10	182.9 ± 8	39.5	143.3	3.6	0.5
LecA	βGal-OMe[c]	150,000	0.8	39	22	15	1	1
	17 ($4Gal_{ox}$)	91 ± 4	0.32	139.5 ± 5	40.2	99.6	1,648	412
	18 ($4Gal_{trz}$)	22 ± 2	0.26	139.0 ± 1	43.8	95.5	6,818	1,705
	20 ($16Gal_{trz}$)	14 ± 0.7	0.09	378.6 ± 15	44.8	333.8	10,714	670
	11 ($8Fuc_{ox}$-$8Gal_{trz}$)	34 ± 7	0.16	232.6 ± 2	42.6	189.9	4,412	551
	13 ($8Gal_{ox}$-$8Fuc_{trz}$)	35 ± 0.1	0.16	216 ± 3	42.5	173.6	4,286	536
	14 ($8Man_{ox}$-$8Gal_{trz}$)	21 ± 4	0.16	243.2 ± 19	43.8	199	7,142	893

[a] *Thermodynamic data are referred to moles of glycoclusters and stoichiometry expressed as the number of glycocluster molecules per lectin monomer. Standard deviations are indicated on experimentally derived values (at least two experiments). α factor is the relative potency compared to the monovalent compound. β factor is the relative potency per sugar unit.*
[b] *see Berthet et al. (2013).*
[c] *see Cecioni et al. (2011).*

lectins with nanomolar affinity, but also that the presence of the other sugar does not affect the binding potency.

CONCLUSION

We have developed a synthetic strategy to prepare a series of heteroglycoclusters displaying eight copies of αFuc and βGal. Binding assays with both LecA and LecB lectins from *Pseudomonas aeruginosa* have revealed that the combination of αFuc and βGal with unspecific sugars maintain the binding potency of the parent homoclusters with both lectins. The review by Jiménez Blanco et al. (2013) opened the questions of the effect of functional promiscuity of glycoligands on different heteroglycocompounds, since such complex architecture are efficient mimics of cell surfaces. The authors raised concerns that the complexity may create "messiness or noise in the processes they participate in." We could demonstrate here that the crowding with an alternate sugar does not lower the efficiency of the glycocluster to bind to the bacteria lectins. In the future, this could be of importance for designing active compounds that will have the capacity of both binding to the bacterial surface and activating the immune system by different clusters of sugars.

EXPERIMENTAL SECTION

Materials

All chemical reagents were purchased from Aldrich (Saint Quentin Fallavier, France) or Acros (Noisy-Le-Grand, France). All protected amino acids and Fmoc-Gly-Sasrin® resin was obtained from Advanced ChemTech Europe (Brussels, Belgium). For peptides and glycopeptides, analytical RP-HPLC was performed on Waters system equipped with a Waters 2695 separations module and a Waters 2487 Dual Absorbance UV/Visible Detector. Analysis was carried out at 1.0 mL/min (EC 125/3 nucleosil 300-5 C_{18}) with UV monitoring at 214 nm and 250 nm using a linear A–B gradient (buffer A: 0.09% CF_3CO_2H in water; buffer B: 0.09% CF_3CO_2H in 90% acetonitrile). Purifications were carried out at 22.0 mL/min (VP 250/21 nucleosil 100-7 C_{18}) with UV monitoring at 214 nm and 250 nm using a linear A–B gradient. HRMS and ESI-MS and HRMS spectra of peptides and glycopeptides were measured on an Esquire 3000 spectrometer from Bruker. Lectins LecA and LecB were produced in recombinant form in *Escherichia coli* BL21(DE3) as described previously (Mitchell et al., 2005; Blanchard et al., 2008).

Synthetic Procedures

Synthesis of Compound 11

Cyclopeptide **1** (4.5 mg, 0.72 μmol) and aminooxy Fuc **2** (1.6 mg, 8.7 μmol) were dissolved in 0.1% TFA in H_2O (10 mM). After stirring for 30 min at room temperature, the propargyl Gal **9** (5.1 mg, 23.2 μmol) dissolved in DMF (1 mL) and a solution of $CuSO_4$ (1,4 mg, 5.8 μmol) in PBS buffer (500 μL, 100 mM) were added. Then was added a solution of THPTA (10.1 mg, 23.2 μmol) and sodium ascorbate (5.1 mg, 40.1 μmol) in PBS buffer (500 μL, 100 mM). All solutions were previously degassed under argon. The reaction was stirred at room temperature under argon and after 1 h analytical HPLC indicated complete reaction coupling. Then Chelex resin was added to remove excess of copper and the reaction mixture was directly purified by RP-HPLC affording pure compound as a white powder. Yield: 81% (5.4 mg, 0.59 μmol); RP-HPLC: Rt = 4.28 min (C_{18}, 214 nm 5–100% B in 15 min); MS (ESI^+) *m/z* calcd. for $C_{387}H_{619}N_{103}O_{158}$ $[M+5H]^{5+}$: 1847.3, found 1847.4.

Synthesis of Compound 12

Compound **12** was obtained from compound **1**, aminooxy Fuc **2,** and propargyl Man **10** following the procedure

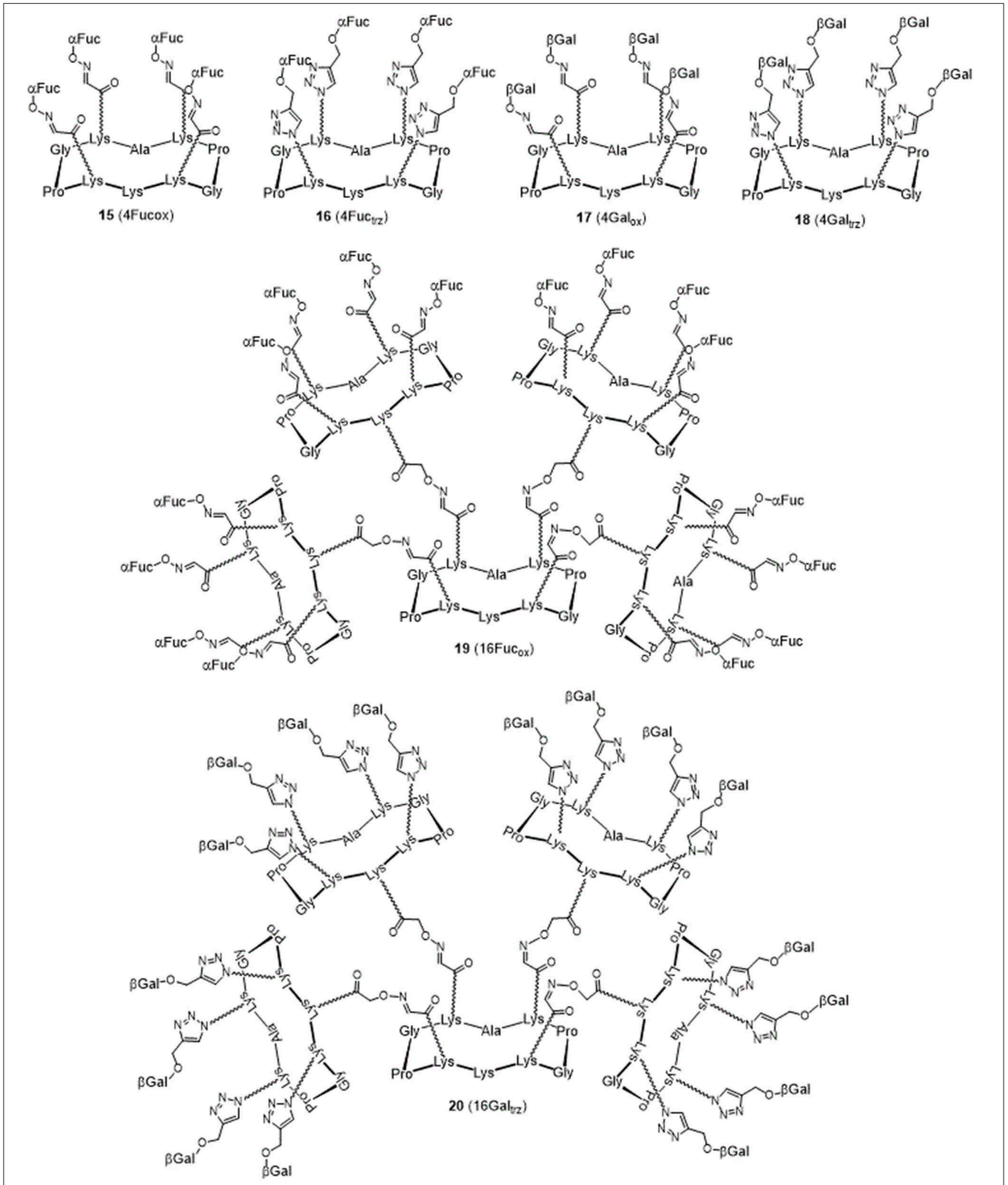

FIGURE 3 | Structure of the tetravalent (**15–18**) and hexadecavalent (**19–20**) homoclusters.

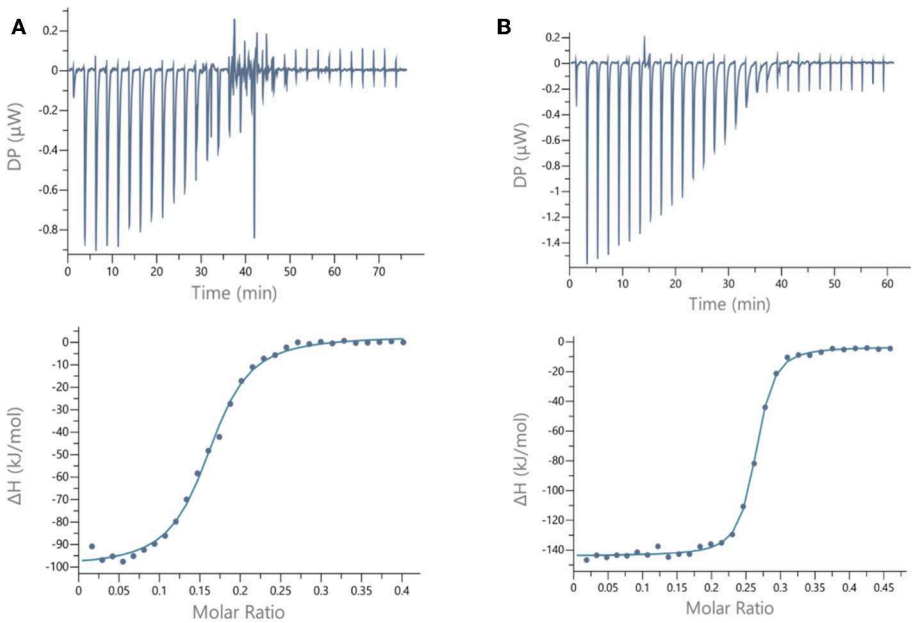

FIGURE 4 | ITC data. Thermograms obtained by injections of **(A)** glycocluster **16** at 140 µM in a solution of LecB (70 µM) and **(B)** glycocluster **18** at 80 µM in a solution of LecA (35 µM) with corresponding integrated titration curves. Molar ratio is indicated as number of glycocluster molecules per lectin monomer.

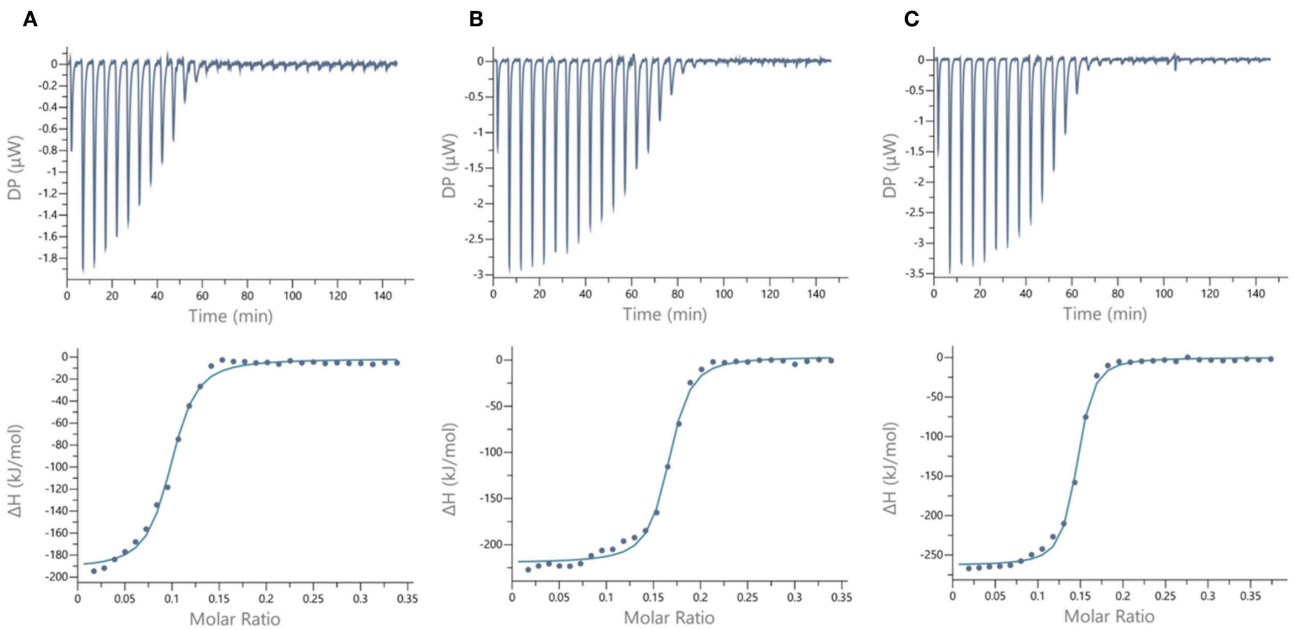

FIGURE 5 | ITC data. Thermograms obtained by injections of **(A)** glycodendrimer **11** at 50 µM in a solution of LecB (32 µM), **(B)** glycodendrimer **11** (50 µM) in a solution of LecA (32 µM), and **(C)** glycodendrimer **14** (40 µM) in a solution of LecA (29 µM) with corresponding integrated titration curves. Molar ratio is indicated as number of glycocluster molecules per lectin monomer.

described for **11**. Yield: 84% (5.6 mg, 0.61 µmol); RP-HPLC: Rt = 4.33 min (C_{18}, 214 nm 5–100% B in 15 min); MS (ESI^+) *m/z* calcd. for $C_{387}H_{618}N_{103}O_{158}$ $[M+4H]^{4+}$: 2309.1, found 2308.7

Synthesis of Compound 13

Compound **13** was obtained from compound **1**, aminooxy Gal **3** and propargyl Fuc **8** following the procedure described for **11**. Yield: 77% (3.5 mg, 0.38 µmol); RP-HPLC: Rt = 4.34 min

(C_{18}, 214 nm 5–100% B in 15 min); MS (ESI^+) *m/z* calcd. for $C_{387}H_{619}N_{103}O_{158}$ $[M+5H]^{5+}$: 1847.3, found 1847.3.

Synthesis of Compound 14

Compound **14** was obtained from compound **1**, aminooxy Man **4** and propargyl Gal **9** following the procedure described for **11**. Yield: 76% (3.1 mg, 0.33 μmol); RP-HPLC: Rt = 10.62 min (C_{18}, 214 nm 5–100% B in 20 min); MS (ESI^+) *m/z* calcd. for $C_{387}H_{619}N_{103}O_{166}$ $[M+5H]^{5+}$: 1873.7, found: 1874.1.

Synthesis of Compound 15

Aldehyde-containing cyclopeptide (Singh et al., 2005) (10.0 mg, 8.04 μmol) and aminooxy Fuc **2** (8.6 mg, 48.23 μmol) were dissolved in 0.1% TFA in H_2O (10 mM). After stirring for 30 min at room temperature, the crude mixture was purified by RP-HPLC. Fractions containing the product were combined and lyophilized to afford the title compound as a white fluffy powder (12.8 mg, 6.75 μmol, 84%). RP-HPLC: Rt = 4.77 min (C_{18}, 214 nm 5–60% B in 15 min); HRMS (ESI^+) *m/z* calcd. for $C_{79}H_{130}N_{19}O_{34}$ $[M+H]^+$: 1888.9027, found: 1888.9058.

Synthesis of Compound 16

The title compound was prepared according to already published protocol. Analytical data were in agreement with the literature (Ribeiro et al., 2018).

Synthesis of Compound 17

The title compound was prepared following the procedure described for **15** using aminooxy Gal **3** (7.5 mg, 38.6 μmol) and was obtained as a white fluffy powder after lyophilisation (13.7 mg, 7.02 μmol, 80%). RP-HPLC: Rt = 3.38 min (C_{18}, 214 nm 5–60% B in 15 min); HRMS (ESI^+) *m/z* calcd. for $C_{79}H_{130}N_{19}O_{38}$ $[M+H]^+$: 1952.8824, found: 1952.8890.

Synthesis of Compound 18

The title compound was prepared following the procedure described for **16** from propargyl Gal **9** (13 mg, 58.7 μmol) and was obtained as a white fluffy powder after lyophilisation (13.7 mg, 7.02 μmol, 80%). RP-HPLC: Rt = 4.17 min (C_{18}, 214 nm 5–60% B in 15 min); HRMS (ESI^+) *m/z* calcd. for $C_{83}H_{134}N_{22}O_{34}$ $[M+H]^+$: 1996.9464, found: 1996.9428.

Synthesis of Compound 19

The title compound was prepared according to already published protocol. Analytical date were in agreement with the literature (Berthet et al., 2013).

Synthesis of Compound 20

The title compound was prepared according to the same protocol as compound **18** and was obtained as a white fluffy powder after lyophilisation (4.8 mg, 0.51 μmol, 69%). RP-HPLC: Rt = 3.98 min (C_{18}, 214 nm 5–60% B in 15 min); MS (ESI^+) *m/z* calcd. for $C_{395}H_{628}N_{111}O_{158}$ $[M+7H]^{7+}$: 1350.2, found: 1351.8

Isothermal Titration Microcalorimetry

ITC experiments of compounds **15–18** were perfomed with a PEAQ-ITC titration calorimeter (Microcal). Other compounds were assayed with a VP-ITC isothermal titration calorimeter (Microcal). The experiments were carried out at 25°C. All glycocompounds and lectins LecB and LecA were dissolved in the same buffer composed of 20 mM Tris with 100 mM NaCl and 0.1 mM $CaCl_2$ at pH 7.5. For PEAQ-ITC, the lectins were placed in the microcalorimeter cell (200 μL) at concentrations varying from 35 to 70 μM. A total of 29 injections of 1.3 μL of glycoclusters at concentrations varying from 80 to 140 μM were performed. For VP-ITC, the microcalorimeter cell (1.447 mL) contained the lectins with concentrations between 30 and 100 μM. A total of 30 injections of 10 μL were performed intervals of 5 min while stirring at 310 rpm with glycoclusters concentrations varying from 0.40 to 0.150 μM. The experimental data were fitted to a theoretical titration curve using the Microcal PEAQ-ITC analysis software, with ΔH (enthalpy change), Ka (association constant), and N (number of binding sites per monomer) as adjustable parameters. Dissociation constant (Kd), free energy change (ΔG), and entropy contributions (TΔS) were derived from the previous ones. Two or three independent titrations were performed for each ligand tested.

DATA AVAILABILITY STATEMENT

All datasets generated for this study are included in the manuscript/**Supplementary Files**.

AUTHOR CONTRIBUTIONS

OR designed the study. DG and BT synthetized the compounds. DG and EG performed the ITC analysis. DG, AI, and OR wrote the manuscript.

FUNDING

This work was supported by CNRS, Université Grenoble Alpes, ICMG FR 2607, the French ANR project Glyco@Alps (ANR-15-IDEX-02), Labex ARCANE, and CBH-EUR-GS (ANR-17-EURE-0003).

ACKNOWLEDGMENTS

OR acknowledge the European Research Council Consolidator Grant LEGO (647938) for DG.

SUPPLEMENTARY MATERIAL

The Supplementary Material for this article can be found online at: https://www.frontiersin.org/articles/10.3389/fchem.2019.00666/full#supplementary-material

REFERENCES

Abellán Flos, M., García Moreno, M. I., Ortiz Mellet, C., García Fernández, J. M., Nierengarten, J. F., and Vincent, S. P. (2016). Potent glycosidase inhibition with heterovalent fullerenes: unveiling the binding modes triggering multivalent inhibition. *Chemistry* 22, 11450–11460. doi: 10.1002/chem.201601673

Arsiwala, A., Castro, A., Frey, S., Stathos, M., and Kane, R. S. (2019). Designing multivalent ligands to control biological interactions: from vaccines and cellular effectors to targeted drug delivery. *Chem. Asian J.* 14, 244–255. doi: 10.1002/asia.201801677

Bernardi, A., Jiménez-Barbero, J., Casnati, A., De Castro, C., Darbre, T., Fieschi, F., et al. (2013). Multivalent glycoconjugates as anti-pathogenic agents. *Chem. Soc. Rev.* 42, 4709–4727. doi: 10.1039/C2CS35408J

Berthet, N., Thomas, B., Bossu, I., Dufour, E., Gillon, E., Garcia, J., et al. (2013). High affinity glycodendrimers for the lectin LecB from *Pseudomonas aeruginosa*. *Bioconjug. Chem.* 24, 1598–1611. doi: 10.1021/bc400239m

Blanchard, B., Nurisso, A., Hollville, E., Tétaud, C., Wiels, J., Pokorná, M., et al. (2008). Structural basis of the preferential binding for globo-series glycosphingolipids displayed by *Pseudomonas aeruginosa* lectin I. *J. Mol. Biol.* 383, 837–853. doi: 10.1016/j.jmb.2008.08.028

Bossu, I., Šulc, M., Krenek, K., Dufour, E., Garcia, J., Berthet, N., et al. (2011). Dendri-RAFTs: a second generation of cyclopeptide-based glycoclusters. *Org. Biomol. Chem.* 9, 1948–1959. doi: 10.1039/c0ob00772b

Cecioni, S., Faure, S., Darbost, U., Bonnamour, I., Parrot-Lopez, H., Roy, O., et al. (2011). Selectivity among two lectins: probing the effect of topology, multivalency and flexibility of "clicked" multivalent glycoclusters. *Chemistry* 17, 2146–2159. doi: 10.1002/chem.201002635

Cecioni, S., Imberty, A., and Vidal, S. (2015). Glycomimetics versus multivalent glycoconjugates for the design of high affinity lectin ligands. *Chem. Rev.* 115, 525–561. doi: 10.1021/cr500303t

Cecioni, S., Praly, J. P., Matthews, S. E., Wimmerov,á, M., Imberty, A., and Vidal, S. (2012). Rational design and synthesis of optimized glycoclusters for multivalent lectin-carbohydrate interactions: influence of the linker arm. *Chemistry* 18, 6250–6263. doi: 10.1002/chem.201200010

Daskhan, G. C., Berthet, N., Thomas, B., Fiore, M., and Renaudet, O. (2015). Multivalent glycocyclopeptides: toward nano-sized glycostructures. *Carbohydr. Res.* 405, 13–22. doi: 10.1016/j.carres.2014.07.017

Daskhan, G. C., Pifferi, C., and Renaudet, O. (2016). Synthesis of a new series of sialylated homo- and heterovalent glycoclusters by using orthogonal ligations. *ChemistryOpen* 5, 477–484. doi: 10.1002/open.201600062

Deguise, I., Lagnoux, D., and Roy, R. (2007). Synthesis of glycodendrimers containing both fucoside and galactoside residues and their binding properties to Pa-IL and PA-IIL lectins from *Pseudomonas aeruginosa*. *N. J. Chem.* 31, 1321–1331. doi: 10.1039/b701237c

Gade, M., Alex, C., Leviatan Ben-Arye, S., Monteiro, J. T., Yehuda, S., Lepenies, B., et al. (2018). Microarray analysis of oligosaccharide-mediated multivalent carbohydrate–protein interactions and their heterogeneity. *Chembiochem* 19, 1170–1177. doi: 10.1002/cbic.201800037

Galan, M. C., Dumy, P., and Renaudet, O. (2013). Multivalent glyco(cyclo)peptides. *Chem. Soc. Rev.* 42, 4599–4612. doi: 10.1039/C2CS35413F

García-Moreno, M. I., Ortega-Caballero, F., Rísquez-Cuadro, R., Ortiz Mellet, C., and García Fernández, J. M. (2017). The impact of heteromultivalency in lectin recognition and glycosidase inhibition: an integrated mechanistic study. *Chemistry* 23, 6295–6304. doi: 10.1002/chem.201700470

Gómez-García, M., Benito, J. M., Gutiérrez-Gallego, R., Maestre, A., Mellet, C. O., Fernández, J. M., et al. (2010). Comparative studies on lectin–carbohydrate interactions in low and high density homo- and heteroglycoclusters. *Org. Biomol. Chem.* 8, 1849–1860. doi: 10.1039/b920048g

Imberty, A., Wimmerová, M., Mitchell, E. P., and Gilboa-Garber, N. (2004). Structures of the lectins from *Pseudomonas aeruginosa*: insight into the molecular basis for host glycan recognition. *Microbes Infect.* 6, 221–228. doi: 10.1016/j.micinf.2003.10.016

Jiménez Blanco, J. L., Ortiz Mellet, C., and García Fernández, J. M. (2013). Multivalency in heterogeneous glycoenvironments: hetero-glycoclusters, -glycopolymers and -glycoassemblies. *Chem. Soc. Rev.* 42, 4518–4531. doi: 10.1039/C2CS35219B

Karskela, M., von Usedom, M., Virta, M., Lönnberg, P. (2012). Synthesis of biotinylated multipodal glycoclusters on a solid support. *Eur. J. Org. Chem.* 2012, 6594–6605. doi: 10.1002/ejoc.201200926

Liang, C. H., Wang, S. K., Lin, C. W., Wang, C. C., Wong, C. H., and Wu, C. Y. (2011). Effects of neighboring glycans on antibody-carbohydrate interaction. *Angew. Chem. Int. Ed Engl.* 50, 1608–1612. doi: 10.1002/anie.201003482

Lindhorst, T. K., Bruegge, K., Fuchs, A., and Sperling, O. (2010). A bivalent glycopeptide to target two putative carbohydrate binding sites on FimH. *Beilstein J. Org. Chem.* 6, 801–809. doi: 10.3762/bjoc.6.90

Michaud, G., Visini, R., Bergmann, M., Salerno, G., Bosco, R., Gillon, E., et al. (2016). Overcoming antibiotic resistance in *Pseudomonas aeruginosa* biofilms using glycopeptide dendrimers. *Chem. Sci.* 7, 166–182. doi: 10.1039/C5SC03635F

Mitchell, E., Houles, C., Sudakevitz, D., Wimmerova, M., Gautier, C., Pérez, S., et al. (2002). Structural basis for oligosaccharide-mediated adhesion of *Pseudomonas aeruginosa* in the lungs of cystic fibrosis patients. *Nat. Struct. Biol.* 9, 918–921. doi: 10.1038/nsb865

Mitchell, E. P., Sabin, C., Snajdrová, L., Pokorná, M., Perret, S., Gautier, C., et al. (2005). High affinity fucose binding of *Pseudomonas aeruginosa* lectin PA-IIL: 1.0 A resolution crystal structure of the complex combined with thermodynamics and computational chemistry approaches. *Proteins* 58, 735–746. doi: 10.1002/prot.20330

Müller, C., Despras, G., and Lindhorst, T. K. (2016). Organizing multivalency in carbohydrate recognition. *Chem. Soc. Rev.* 45, 3275–3302. doi: 10.1039/C6CS00165C

Ogura, A., Urano, S., Tahara, T., Nozaki, S., Sibgatullina, R., Vong, K., et al. (2018). A viable strategy for screening the effects of glycan heterogeneity on target organ adhesion and biodistribution in live mice. *Chem. Commun.* 54, 8693–8696. doi: 10.1039/C8CC01544A

Ortega-Muñoz, M., Perez-Balderas, F., Sanfrutos, J. M., Hernandez-Mateo, F., Isac-García, J., Santoyo-González, F., et al. (2009). Click multivalent heterogeneous neoglycoconjugates – modular synthesis and evaluation of their binding affinities. *Eur. J. Org. Chem.* 2009, 2454–2473. doi: 10.1002/ejoc.200801169

Ortiz Mellet, C., J.-,Nierengarten, F., and García Fernández, J. M. (2017). Multivalency as an action principle in multimodal lectin recognition and glycosidase inhibition: a paradigm shift driven by carbon-based glyconanomaterials. *J. Mater. Chem. B* 5, 6428–6436. doi: 10.1039/C7TB00860K

Pett, C., Cai, H., Liu, J., Palitzsch, B., Schorlemer, M., Hartmann, S., et al. (2017). Microarray analysis of antibodies induced with synthetic antitumor vaccines: specificity against diverse mucin core structures. *Chemistry* 23, 3875–3884. doi: 10.1002/chem.201603921

Pifferi, C., Thomas, B., Goyard, D., Berthet, N., and Renaudet, O. (2017). Heterovalent glycodendrimers as epitope carriers for antitumor synthetic vaccines. *Chemistry* 23, 16283–16296. doi: 10.1002/chem.201702708

Ragupathi, G., Coltart, D. M., Williams, L. J., Koide, F., Kagan, E., Allen, J., et al. (2002). On the power of chemical synthesis: immunological evaluation of models for multiantigenic carbohydrate-based cancer vaccines. *Proc. Natl. Acad. Sci. U.S.A.* 99, 13699–13704. doi: 10.1073/pnas.202427599

Renaudet, O., and Roy, R. (2013). Multivalent scaffolds in glycoscience: an overview. *Chem. Soc. Rev.* 42, 4515–4517. doi: 10.1039/c3cs90029k

Ribeiro, J. P., Villringer, S., Goyard, D., Coche-Guerente, L., Höferlin, M., Renaudet, O., et al. (2018). Tailor-made Janus lectin with dual avidity assembles glycoconjugate multilayers and crosslinks protocells. *Chem. Sci.* 9, 7634–7641. doi: 10.1039/C8SC02730G

Singh, Y., Renaudet, O., Defrancq, E., and Dumy, P. (2005). Preparation of a multitopic glycopeptide-oligonucleotide conjugate. *Org. Lett.* 7, 1359–1362. doi: 10.1021/ol050134n

Thomas, B., Fiore, M., Bossu, I., Dumy, P., and Renaudet, O. (2012). Synthesis of heteroglycoclusters by using orthogonal chemoselective ligations. *Beilstein J. Org. Chem.* 8, 421–427. doi: 10.3762/bjoc.8.47

Thomas, B., Fiore, M., Daskhan, G. C., Spinelli, N., and Renaudet, O. (2015a). A multi-ligation strategy for the synthesis of heterofunctionalized glycosylated scaffolds. *Chem. Commun.* 51, 5436–5439. doi: 10.1039/C4CC05451B

Thomas, B., Pifferi, C., Daskhan, G. C., Fiore, M., Berthet, N., and Renaudet, O. (2015b). Divergent and convergent synthesis of

GalNAc-conjugated dendrimers using dual orthogonal ligations. *Org. Biomol. Chem.* 13, 11529–11538. doi: 10.1039/C5OB01870F

Vincent, S. P., Buffet, K., Nierengarten, I., Imberty, A., and Nierengarten, J. F. (2016). Biologically active heteroglycoclusters constructed on a pillar[5]arene-containing [2]rotaxane scaffold. *Chemistry* 22, 88–92. doi: 10.1002/chem.201504110

Zhu, J., Wan, Q., Lee, D., Yang, G., Spassova, M. K., Ouerfelli, O., et al. (2009). From synthesis to biologics: preclinical data on a chemistry derived anticancer vaccine. *J. Am. Chem. Soc.* 131, 9298–9303. doi: 10.1021/ja901415s

Conflict of Interest: The authors declare that the research was conducted in the absence of any commercial or financial relationships that could be construed as a potential conflict of interest.

frontiers in Chemistry

ORIGINAL RESEARCH
published: 04 October 2019
doi: 10.3389/fchem.2019.00650

Systematic Dual Targeting of Dendritic Cell C-Type Lectin Receptor DC-SIGN and TLR7 Using a Trifunctional Mannosylated Antigen

Rui-Jun Eveline Li[1†], Tim P. Hogervorst[2†], Silvia Achilli[3‡], Sven C. Bruijns[1], Tim Arnoldus[1], Corinne Vivès[3], Chung C. Wong[2], Michel Thépaut[3], Nico J. Meeuwenoord[2], Hans van den Elst[2], Herman S. Overkleeft[2], Gijs A. van der Marel[2], Dmitri V. Filippov[2], Sandra J. van Vliet[1], Franck Fieschi[3], Jeroen D. C. Codée[2*] and Yvette van Kooyk[1*]*

[1] Department of Molecular Cell Biology and Immunology, Cancer Center Amsterdam, Amsterdam Infection and Immunity Institute, Amsterdam Universitair Medische Centra, Vrije Universiteit Amsterdam, Amsterdam, Netherlands, [2] Department of Bio-organic Synthesis, Faculty of Science, Leiden Institute of Chemistry, Leiden University, Leiden, Netherlands, [3] Univ. Grenoble Alpes, CNRS, CEA, Institut de Biologie Structurale, Grenoble, France

Dendritic cells (DCs) are important initiators of adaptive immunity, and they possess a multitude of Pattern Recognition Receptors (PRR) to generate an adequate T cell mediated immunity against invading pathogens. PRR ligands are frequently conjugated to tumor-associated antigens in a vaccination strategy to enhance the immune response toward such antigens. One of these PPRs, DC-SIGN, a member of the C-type lectin receptor (CLR) family, has been extensively targeted with Lewis structures and mannose glycans, often presented in multivalent fashion. We synthesized a library of well-defined mannosides (mono-, di-, and tri-mannosides), based on known "high mannose" structures, that we presented in a systematically increasing number of copies (n = 1, 2, 3, or 6), allowing us to simultaneously study the effect of mannoside configuration and multivalency on DC-SIGN binding via Surface Plasmon Resonance (SPR) and flow cytometry. Hexavalent presentation of the clusters showed the highest binding affinity, with the hexa-α1,2-di-mannoside being the most potent ligand. The four highest binding hexavalent mannoside structures were conjugated to a model melanoma gp100-peptide antigen and further equipped with a Toll-like receptor 7 (TLR7)-agonist as adjuvant for DC maturation, creating a trifunctional vaccine conjugate. Interestingly, DC-SIGN affinity of the mannoside clusters did not directly correlate with antigen presentation enhancing properties and the α1,2-di-mannoside cluster with the highest binding affinity in our library even hampered T cell activation. Overall, this systematic study has demonstrated that multivalent glycan presentation can improve DC-SIGN binding but enhanced binding cannot be directly translated into enhanced antigen presentation and the sole assessment of binding affinity is thus insufficient to determine further functional biological activity. Furthermore, we show that well-defined antigen conjugates combining two different PRR ligands can be generated in a modular fashion to increase the effectiveness of vaccine constructs.

Keywords: DC-SIGN, TLR7, glyco-antigen, vaccine model, peptide conjugate, tumor-associated antigens, mannoside

OPEN ACCESS

Edited by:
Matthew S. Macauley, University of Alberta, Canada

Reviewed by:
Mare Cudic, Florida Atlantic University, United States
Gregory A. Hudalla, University of Florida, United States

***Correspondence:**
Franck Fieschi
Franck.Fieschi@ibs.fr
Jeroen D. C. Codée
JCodee@chem.leidenuniv.nl
Yvette van Kooyk
Y.vanKooyk@vumc.nl

[†] These authors have contributed equally to this work

[‡] Present address:
Silvia Achilli, Univ. Grenoble Alpes, CNRS, Departement de Pharmacochimie Moléculaire, Grenoble, France; Institut de Biologie Structurale, Grenoble, France

Specialty section:
This article was submitted to Chemical Biology, a section of the journal Frontiers in Chemistry

Received: *19 June 2019*
Accepted: *11 September 2019*
Published: *04 October 2019*

Citation:
Li R-JE, Hogervorst TP, Achilli S, Bruijns SC, Arnoldus T, Vivès C, Wong CC, Thépaut M, Meeuwenoord NJ, van den Elst H, Overkleeft HS, van der Marel GA, Filippov DV, van Vliet SJ, Fieschi F, Codée JDC and van Kooyk Y (2019) Systematic Dual Targeting of Dendritic Cell C-Type Lectin Receptor DC-SIGN and TLR7 Using a Trifunctional Mannosylated Antigen. Front. Chem. 7:650. doi: 10.3389/fchem.2019.00650

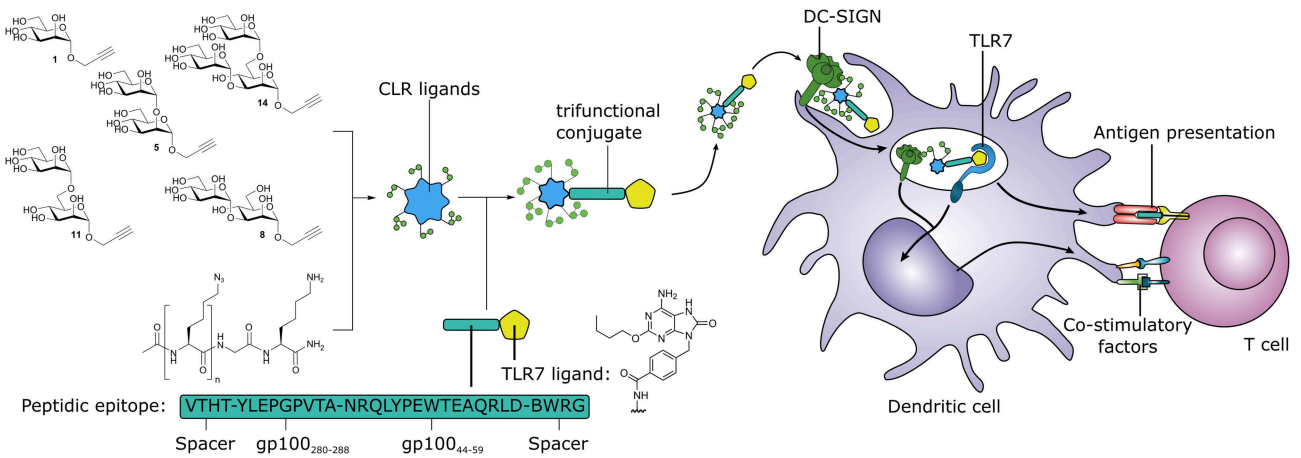

GRAPHICAL ABSTRACT | Synthetic multivalent presentation of CLR ligands on tumor antigens together with TLR7 agonist, provides DC targeting and induction of tumor specific T cells.

INTRODUCTION

DC-SIGN (CD209) is an extensively studied receptor, due to its expression on various dendritic cell (DC) populations and its role in infection of certain viruses, like HIV (Bernardi et al., 2013; van Kooyk et al., 2013). This C-type Lectin Receptor (CLR) recognizes carbohydrate-based Pathogen-Associated Molecular Patterns (PAMPs) containing Lewis structures and high mannose glycans commonly found on bacteria, fungi and viruses (Geijtenbeek and Van Kooyk, 2003). DC-SIGN occurs on the cell surface as a tetramer, and therefore multivalent presentation of its carbohydrate ligand is favored for high affinity binding (van Kooyk et al., 2013).

Two strategies have been developed to target DC-SIGN using mannose-based ligands to deliver cargo to DCs. The first strategy uses mannosyl monosaccharides or analogs thereof, as these are readily available. Because the binding affinity of the mono-mannosides for DC-SIGN is relatively low with respect to larger and more complex oligo-mannosides (van Liempt et al., 2006), they are generally incorporated into dendrimers, liposomes or nanoparticles to achieve a multivalent presentation, enhancing the binding to DC-SIGN (Fehres et al., 2015; Ordanini et al., 2015; Silva et al., 2015; Berzi et al., 2016; Le Moignic et al., 2018). The other strategy uses larger and more complex oligomannosides with intrinsic multivalence. Various oligosaccharides have been explored for DC-SIGN binding (Ni et al., 2006; McIntosh et al., 2015), a prime example being the "high mannose" structure Man_9 (**Figure 1A**). Both strategies have previously been used to deliver cancer antigens to DCs to enhance uptake and antigen presentation for the development of more effective cancer immunotherapies (Buskas et al., 2005; Moyle et al., 2007; Srinivas et al., 2007; McIntosh et al., 2015; Glaffig et al., 2018).

Another approach for the development of well-defined anti-cancer vaccines entails the covalent attachment of other adjuvants to the antigens of choice, targeting other Pattern Recognition Receptors (PRR), such as members of the Toll-Like Receptor (TLR) family (Deres et al., 1989; Cho et al., 2000; Blander and Medzhitov, 2006; Fujita and Taguchi, 2012; Willems et al., 2014), the NOD-like receptor (NLR) family (Willems et al., 2016), or combinations thereof (Buskas et al., 2005; Moyle et al., 2007; Sedaghat et al., 2016; Zom et al., 2019). PAMP recognition by TLRs induces DC maturation, stimulating antigen processing, and presentation for the induction of pathogen-specific T cells (Ackerman and Cresswell, 2003). The covalent attachment of a TLR agonist to an antigen can accelerate uptake and enhances antigen presentation while DC maturation *via* the TLR-ligands is maintained (Khan et al., 2007; Ignacio et al., 2018). Furthermore, it has been shown by simultaneous targeting of CLRs and TLRs, that CLR stimulation influences the TLR signaling cascades. For example, simultaneous triggering of DC-SIGN with TLR4 strengthens and prolongs TLR- signaling to enhance pro-inflammatory cytokine production in DCs (Fritz et al., 2005; Gringhuis et al., 2007). Since DC maturation is a necessity for upregulation of antigen processing and presentation, we hypothesized that a peptide-antigen conjugate, equipped with both a mannose-based DC-SIGN targeting glycan and a TLR-ligand, could lead to synergy in antigen presentation and improve specific T cell activation. We here describe the generation of such conjugate vaccine modalities, composed of a well-defined DC-SIGN targeting oligomannose cluster, a synthetic long peptide gp100 antigen, and a TLR7-agonist. TLR7 was selected as candidate due to its residency within the endosomes. We hypothesized that upon binding and internalization via DC-SIGN, the vaccine conjugate would be processed in endosomes where it can encounter TLR7. Using this strategy, we additionally avoid competition between binding of DC-SIGN and other cell surface TLRs.

Synthesizing high mannose structures is time and labor intensive and obtaining these structures in large quantities is challenging (Evers et al., 1998; Umekawa et al., 2008; Amin

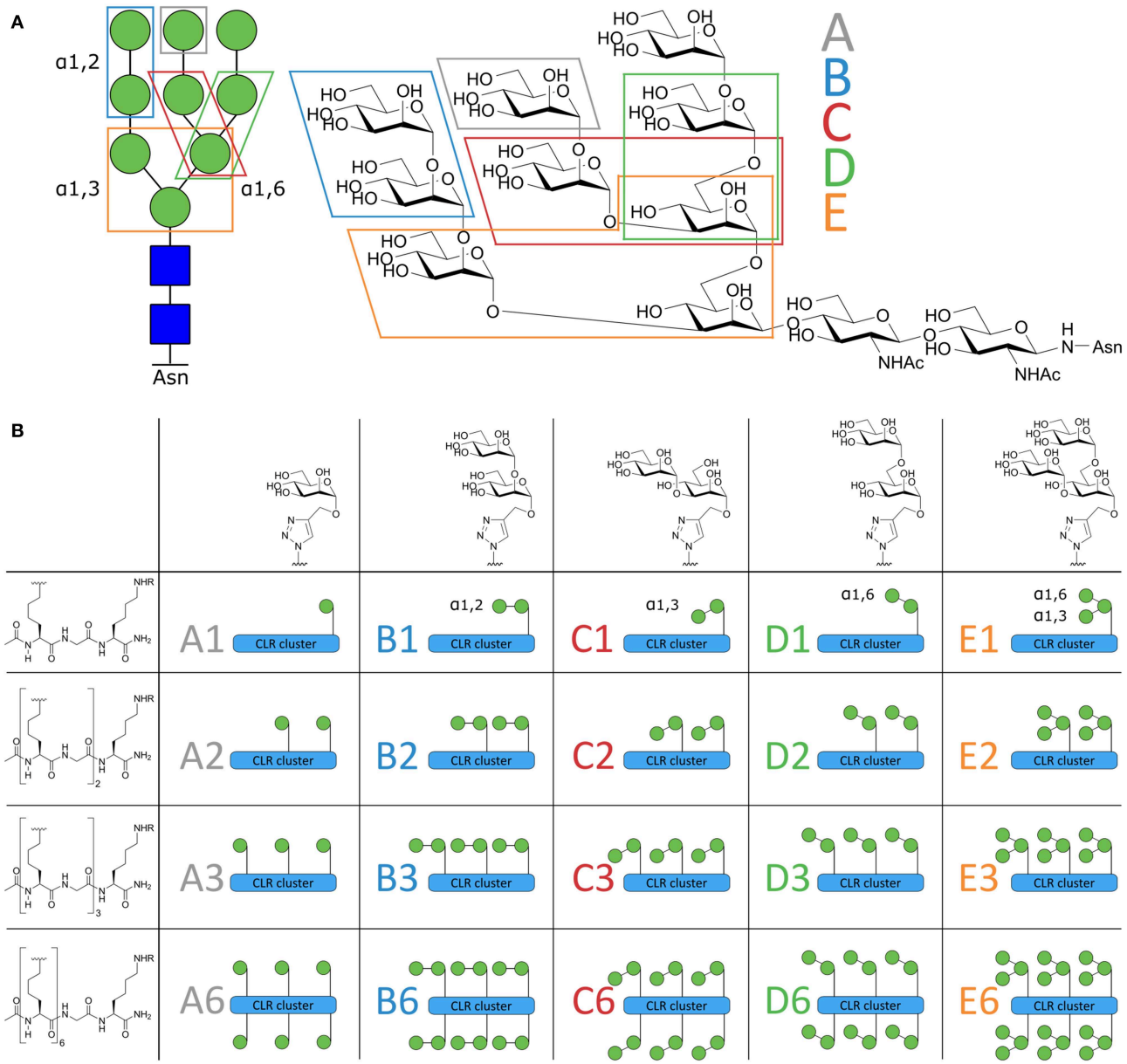

FIGURE 1 | Schematic overview of the Mannose-cluster library. **(A)** Symbolic and chemical representation of the high affinity DC-SIGN ligand high mannose N-glycan Man_9. The 5 mannoside configurations within Man9 are indicated in the figure. **(B)** From left to right, the 5 different oligomannosides. Top-down, the peptide backbone with increased valency. The total library of 20 mannoside clusters are illustrated as symbols and coded **A1–E6**.

et al., 2011; Temme et al., 2013). We have therefore dissected the "high mannose" Man_9-structure in smaller oligomannosides to explore which oligomannoside configurations could be used as a tool to effectively target the DC-SIGN receptor. To this end, we synthesized an array of oligomannose containing clusters (**Figure 1B**) that varied in number (ranging from 1 to 6 copies) and type of mannoside, each representing a part of the Man_9 oligosaccharide (mono-; α1,2-di-; α1,3-di-; α1,6-di-; and an α1,3-α1,6-tri-mannoside, coded **A–E**, **Figure 1A**). This library has allowed us to compare side-by-side, the different mannoside configurations in different, well-defined clustered representations. The high affinity binders were used for conjugation to a model peptide antigen, containing the helper T cell epitope $gp100_{280-288}$ and effector T cell epitope $gp100_{44-59}$, to generate conjugates that could be targeted to DCs. To enhance the presentation of the antigens embedded in the conjugates by the DCs, we equipped the conjugates with a previously reported 8-oxo-adenosine analog (Jin et al., 2006; Gential et al., 2019), a ligand for the endosomal TLR7 which resulted in

trifunctional conjugates (CLR-antigen-TLR). Using monocyte-derived dendritic cells (moDCs) we showed that the generated trifunctional conjugates represent attractive vaccine modalities that effectively targeted and activated DCs allowing effective antigen presentation.

RESULTS AND DISCUSSION

Synthesis of the Oligomannoside Clusters

The design of the oligomannoside cluster array is based on the Man_9–N-glycan structure as depicted in **Figure 1A** and encompasses structures displaying 1, 2, 3, or 6 copies of mono-, di-, or trimannosides. The assembly of the array is shown in **Figure 2** and it employs an oligo-azidolysine (6-azidonorleucine) backbone to which propargyl mannosides can be coupled. The required oligomannosides were all generated using propargyl α-D-mannopyranoside **1** as a starting compound (Daly et al., 2012). In order to keep the anomeric alkyne moiety intact, reductive transformations were avoided and acid/base labile protective groups were applied throughout the syntheses. Selective protection of the equatorial hydroxyls in **1** with a 1,2-butane diacetal, was followed by silylation of the primary hydroxyl to yield acceptor **3** in 54% yield over two steps. Glycosylation of **3** with imidate donor **2** (Thomas et al., 2007) provided the protected 1,2-linked disaccharide **4** in 82% yield. Acidic removal of the ketal and silyl ethers was followed by a basic deacetylation leading to α1,2-di-mannoside **6** in 58% yield over two steps. For the assembly of the 1,3-linked dimannoside, the higher nucleophilicity of the C-3-OH in **6** with respect to the neighboring, axial C-2-OH (van der Vorm et al., 2018) was exploited in a regio- and stereoselective glycosylation reaction. The condensation of acceptor **6** and donor **2** (Carpenter and Nepogodiev, 2005; Sauer et al., 2019) provided disaccharide **7** in 80% yield. Subsequent removal of the protective groups by sequential acid and base treatment resulted in α1,3-di-mannoside **8** in 90% yield over two steps. The 1,6-linked disaccharide was obtained by tritylation of the primary hydroxyl in propargyl mannopyranoside **1**, acetylation of secondary hydroxyls and trityl removal to give acceptor **9** in 63% yield over three steps. Glycosylation of **9** with donor **2** yielded disaccharide **10** in 79% yield, and after deacetylation α1,6-di-mannoside **11** was obtained in 66% yield. The set of propargyl mannnosides was completed with the previously described synthesis of tri-mannoside **14** from 2,4-di-*O*-benzoyl mannose acceptor **12**. This diol was mannosylated with two copies of donor **2** to yield the fully protected trisaccharide **13** in 82% yield, which was deacylated to effectively generate trimer **14** (Wong et al., 2015).

With the required propargyl mannosides in hand, the assembly of the array was undertaken. Using solid phase peptide synthesis (SPPS), four different backbones with 1, 2, 3, or 6 azides were synthesized for the attachment of the mannose clusters (**15–18**). To match the length of the hexavalent scaffold **18** with the trivalent backbone, glycine residues were incorporated in the latter scaffold to separate the azidolysines in **17**. Similarly, the azidolysines in the divalent scaffold **16** were also separated by a glycine residue. All backbones contained a lysine at the C-terminus for further functionalization. Via Cu(I) catalyzed Azide-Alkyne Cycloaddition (CuAAC) reactions the propargyl mannosides (**5**, **8**, **11, 14**) and peptides backbones (**15–18**) were clicked together. This resulted in a library of 20 well-defined structures (**A1–A6**; **B1–B6**; **C1–C6**; **D1–D6**; **E1–E6**, **Figures 1B**, **2**), subdivided in five series in which the **A** series bears α-mannose **1**, the **B** series carries α1,2-di-mannoside **5**, the **C** series presents α1,3-di-mannoside **8**, the **D** series displays α1,6-di-mannoside **11**, and the **E** series is equipped with α1,3-α1,6-tri-mannoside **14**. All mannoside-clusters were equipped with a biotin handle for cellular assays by reacting the primary amine of the C-terminal lysine with Biotin-OSu to provide compounds **a1–e6**. For conjugation with the model epitope clusters the clusters **B6, C6, D6**, and **E6** were functionalized with an alkyne handle resulting in conjugation-ready compounds **19–22**.

Binding Profile of the Mannoside Library

The affinity of the clusters for the extracellular domain (ECD) of the DC-SIGN receptor (DC-SIGN ECD) was estimated *via* surface plasmon resonance (SPR) assays (Tabarani et al., 2009). The apparent K_d was calculated in direct interaction mode using a surface functionalized in an oriented manner with DC-SIGN ECD. In this assay, tetrameric DC-SIGN ECD is attached to the surface of the sensor chip via the N-terminus of its neck oligomerization domain, thus presenting its four carbohydrate recognition domains toward the solvent, realistically mimicking the presentation of the receptor on cell surface (Porkolab et al., 2019). For some of the low affinity ligands, in the mM range, it was not possible to determine their affinity with this assay, and therefore a competition experiment was performed providing IC_{50} values (Timpano et al., 2008) (**Figure 3A**). A-specific interactions with the peptide backbone were excluded, since control clusters **G1** and **G2** (propargyl β-D-galactose clicked to backbones **15** and **16**) showed no interaction (**Supplementary Figures 1A, 5**). When comparing equivalent clusters, the α1,2-di-mannoside (**B** series) bound with the highest affinity (**Figure 3A**). Hexavalent presentation ($n = 6$) of the oligomannosides showed micromolar affinity toward DC-SIGN. **B6** had the highest affinity in the library with an apparent K_d of 0.95 μM, followed by the α1,3-dimannoside cluster **C6** (1.17 μM), and the trimannoside clusters **E3** (2.44 μM) and **E6** (2.78 μM). Interestingly, the affinity of the trisaccharide series (**E** series) did not improve going form the tri- to the hexavalent representation (**E3** vs. **E6**, **Figure 3A**). A potential explanation for this effect could be that the spacing of clusters is more important for the larger tri-mannosides. For the monovalent mannosides **A1** and **C1** we could not determine a reliable IC_{50} in this setup, indicating that their binding affinity for DC-SIGN is too weak (see **Supplementary Figures 2, 3** for all SPR sensorgrams).

Next, we assessed the binding of our clusters to cellular DC-SIGN using moDCs (**Figure 3B**, **Supplementary Figure 1B**). To this end, binding of the clusters **a1–a6**, **b1–b6**, **c1–c6**, **d1–d6,** and **e1–e6**, decorated with a biotin handle, was determined by flow cytometry. Clusters were bound to moDCs for 30 min at 4°C. By staining using fluorophore-conjugated streptavidin and washing at 4°C, the bound clusters could be quantified by flow cytometry. Complementary to the SPR assays, the flow cytometric experiments revealed an enhancement in binding

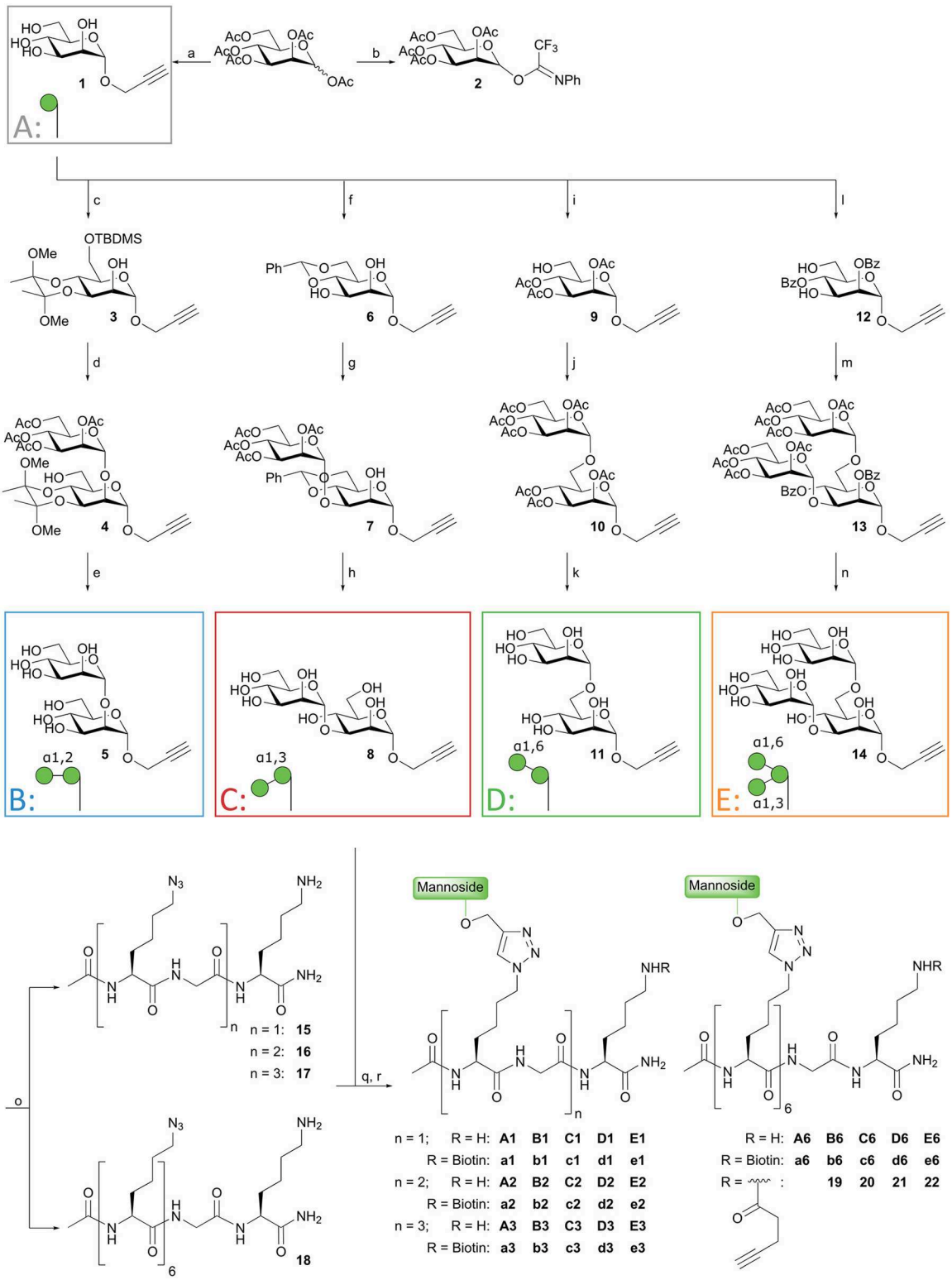

FIGURE 2 | Synthesis of mannoside clusters. *Reagents and conditions:* (a) Daly et al. (2012); (b) Thomas et al. (2007); (c) *i.* 2,3-butanedione, $HC(OMe)_3$, MeOH, CSA, reflux, 55%; *ii.* TBDMSCl, imidazole, DMF, 99%; (d) Donor **2**, TMSOTf, DCM, −20°C, 82%; (e) *i.* TFA, H_2O, 71%; *ii.* NaOMe, MeOH, 82%; (f) $PhCH(OMe)_2$, CSA, ACN, 50°C, 300 mbar, 51%; (g) Donor **2**, TMSOTf, DCM, −20°C, 80%; (h) *i.* AcOH, H_2O, 95%; *ii.* NaOMe, MeOH, 95%; (i) *i.* Ph_3CCl, imidazole, DCM, followed by Ac_2O, pyridine, 90%; *ii.* $BF_3{\cdot}Et_2O$, MeOH, toluene, 70%; (j) *i.* Donor **2**, TMSOTf, DCM, −20°C, 79%; (h) NaOMe, MeOH, 66%; (l) *i.* $PhC(OMe)_3$, CSA, ACN; *ii.* H_2O, 52%; (m) Donor **2**, TMSOTf, DCM, −25°C, 82%; (n) NaOMe, MeOH, 75% (see reference Wong et al., 2015); (o) Fmoc-SPPS; (q) CuI, THPTA, DIPEA, DMSO, H_2O; (r) BiotinOSu or Pent-4-ynoic acid succinimidyl ester, DIPEA, DMSO.

A

Cluster	IC_{50} (μM)	Kd_{app} (μM)
A1	N.D.	
A2	2605±95	
A3	736.7±3.4	
A6		7.82±.44
B1	2343±109	
B2	189.25±3.45	
B3		19.5±0.5
B6		0.946±0.04
C1	N.D.	
C2	567.45±1.15	
C3	171.95±1.45	
C6		1.17±0.25
D1	6961.5±3038.5	
D2	410.9±0.3	
D3		48.74±2.57
D6		6.56±1.2
E1	1518.5±250.5	
E2	305.55±4.75	
E3		2.435±0.035
E6		2.78±0.015

C

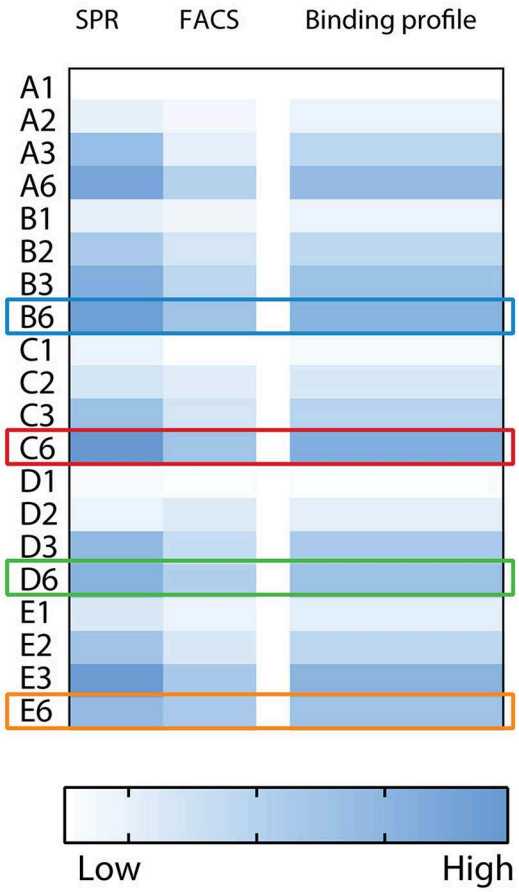

B

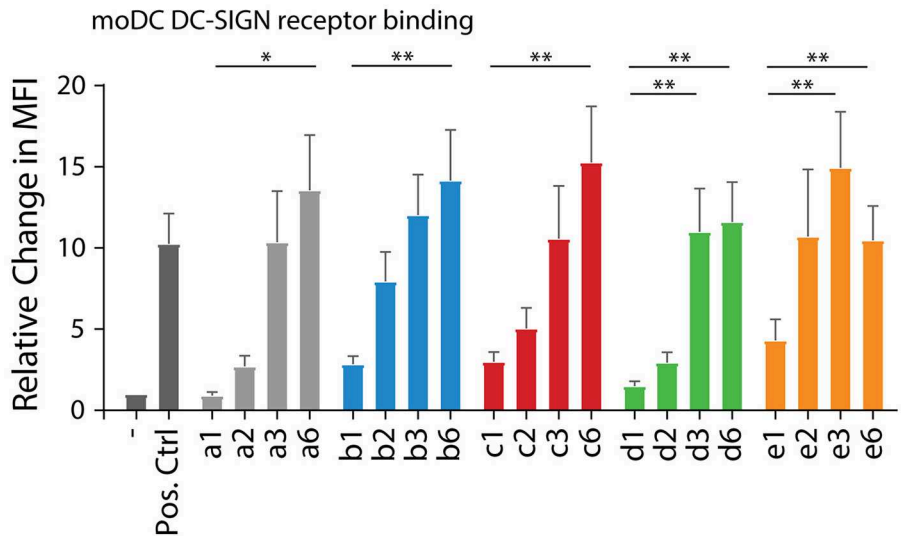

FIGURE 3 | DC-SIGN has the highest affinity for α1,2-di-mannoside in a hexavalent configuration on multiple interaction levels. **(A)** Surface plasmon resonance (SPR) analysis demonstrates increase of affinity for DC-SIGN with increasing multivalence ($n = 1 > 2 > 3 > 6$). Clusters presenting the α1,2-di-mannoside **5** (**B** series) have the highest affinity in comparison to the other mannosides in this array. **(B)** Binding of the biotinylated mannoside library to DC-SIGN on moDC was measured by flow cytometry. Normalized to the unbound control, the clusters displayed increased binding with increasing multivalence. **(C)** Overall binding profile of the library, normalized to **A1**, indicating that the highest affinity binders are the **B6**, **C6**, **D6**, **E3,** and **E6** clusters. $^{*}p < 0.05$ and $^{**}p < 0.01$.

with increasing amount of mannosides for the **a**, **b**, and **c** series (**Figure 3B**). We observed significantly higher binding for the hexavalent mono-mannoside compared to the monovalent mannoside (**a1** vs. **a6**). These results are in agreement with earlier work suggesting DC-SIGN has a preference for high mannose like mannosides (Feinberg et al., 2007). The α1,2-mannosides (**b** series) showed enhanced binding in comparison to the mono-mannoside and the α1,6- or α1,3-dimannosides, in line with the SPR results and earlier results (Feinberg et al., 2007). In the cellular assay we also did not observe an increase in binding with an increasing number of tri-mannosides from the trivalent to the hexavalent cluster (**e3** vs. **e6**), in line with the SPR results. This result again illustrates the need to carefully consider the spacing between oligomannoses in multivalent mannoside clusters. The cellular assay also showed no increase in binding of the α1,6-dimannoside clusters when increasing the valency from **d3** to **d6**, again highlighting the potential influence of the scaffold design. In control experiments ligand binding to DC-SIGN was inhibited using a blocking anti-DC-SIGN antibody (**Supplementary Figure 1C**). Small residual binding remained, revealing a cluster-dependent increase in binding for the **a–c** series and a similar trend in binding of the **d**- and **e**-series. This suggests that other carbohydrate binding receptors, such as the mannose receptor, may play a role in binding the mannoside clusters (Raiber et al., 2010; He et al., 2015).

The binding profile of all mannose clusters is graphically summarized in **Figure 3C**. The strongest binding was observed for the hexavalent scaffolds, engaging DC-SIGN with μM affinity. The α1,2-di saccharide (**B** series) bound strongest and the monosaccharide (**A** series) bound with the lowest affinity. Therefore, we selected the **B6, C6, D6,** and **E6** clusters for conjugation to the melanoma gp100 antigen-TLR7 construct. Although cluster **E6** bound without affinity improvement for DC-SIGN comparing to **E3**, the former cluster was selected to allow for a direct comparison between the different clusters at the glycoconjugate level.

Antigen and Adjuvant Conjugation

We next proceeded by synthesizing the mannose cluster-peptide-TLR7-agonist-conjugates via Fmoc-SPPS chemistry. Starting from Tentagel® S RAM amide resin we coupled Fmoc-Lys(Mmt)-OH as the first amino acid to allow the conjugation of the TLR7 ligand after assembly of the peptide (see **Figure 4**). The gp100 peptide contains the $gp100_{280-288}$ sequence for antigen presentation to $CD4^+$ T cells connected to the N-terminus of the $gp100_{44-59}$ sequence for $CD8^+$ T cells. The epitope was elongated with four extra amino acids on each side to act as spacers. To prevent potential oxidation Cys_{60} was replaced by its isosteric analog α-amino-butyric acid (Wlodawer et al., 1989), which did not influence the antigen presentation of the peptide (**Supplementary Figures 1G, 6**). The peptide was elongated with Fmoc-Lys(N_3)-OH followed by acetylation of the N-terminus resulting in **24**. C-terminal functionalization was achieved by selective removal of the Lys(Mmt) group, and subsequent coupling of an ethylene glycol spacer followed by introduction of the TLR7 agonist (Chan et al., 2009). Using our previously described protocol (Gential et al., 2019), we could introduce Boc protected TLR7-ligand **23** on-resin, resulting in functionalized solid support **25**. Release of the peptide-TLR7 ligand conjugate from the resin and concomitant global deprotection of the side chains under acidic conditions resulted in azido-peptide **26**, which was purified by HPLC. Control peptides lacking the N-terminal azide and/or the TLR7 ligand were synthesized to investigate the effect of the CLR clusters (**gp100** and **gp100-TLR7L**, see **Supplementary Figure 6**).

Attempts to synthesize gp100 peptides elongated with six azidolysines through SPPS proved to be troublesome and therefore we used a modular approach in which the pre-assembled CLR clusters (**19–22**) (**Figure 2**) were ligated to TLR7-peptide conjugate **26** via a CuAAC click reaction (**Figure 4**) (Conibear et al., 2016). This resulted in four conjugates containing a TLR7 agonist and a hexavalent α1,2-dimannnoside cluster (**B6-gp100-TLR7L**); an α1,3-dimannoside cluster (**C6-gp100-TLR7L**); an α1,6-dimannoside cluster (**D6-gp100-TLR7L**); or an α1,3-α1,6-trimannoside cluster (**E6-gp100-TLR7L**) that could be tested for their antigen presenting capacities.

Targeting Efficacy of the Mannoside-Peptide Conjugates

Immature dendritic cells are present in the peripheral tissue, acting as the first-line of defense against pathogens. In immature state, dendritic cells are optimized for phagocytosis of extracellular material and antigens. Upon maturation, triggered by e.g., pathogenic stimuli that activates TLRs, phagocytic processes are downregulated, while co-stimulatory molecules for T cell activation are upregulated and antigen presentation is enhanced (Ackerman and Cresswell, 2003). After the trifunctional peptides are internalized, the maturation process prepares the dendritic cell for optimal antigen presentation to T cells. To assess the efficacy of the selected compounds, we analyzed different biological processes that the trifunctional peptides are routed through. First, the uptake of biotinylated clusters by immature DCs was measured, followed by the ability of the trifunctional conjugates to induce DC maturation, and lastly the capability of the gp100 epitopes to be presented (**Figure 5A**).

Among the various conjugates produced, two could be evaluated by SPR for their binding properties to ensure that conjugating the mannose-cluster to gp100 alone or gp100-TLR7L modules do not mask their accessibility for DC-SIGN recognition. **B6-gp100** and **E6-gp100-TLR7L** are still binders with μM affinities of DC-SIGN surfaces, however the conjugation to either gp100 or gp100-TLR7L module decreased this affinity by a factor of about 10, suggesting that gp100 conjugation reduced binding somewhat (Comparing **Figure 3A** and **Supplementary Figure 1A**, the K_{d-app} goes from 0.9 to 10.6 μM for **B6** to **B6-gp100**, and for **E6** to **E6-gp100-TLR7L** the K_{d-app} goes from 2.7 to 31 μM, each time increasing by about a factor 10, **Supplementary Figure 3**).

For the internalization, the moDCs were incubated with clusters **b6, c6, d6,** and **e6** for 1 h at 4°C, where after unbound ligands were washed away with ice-cold medium. Warm medium

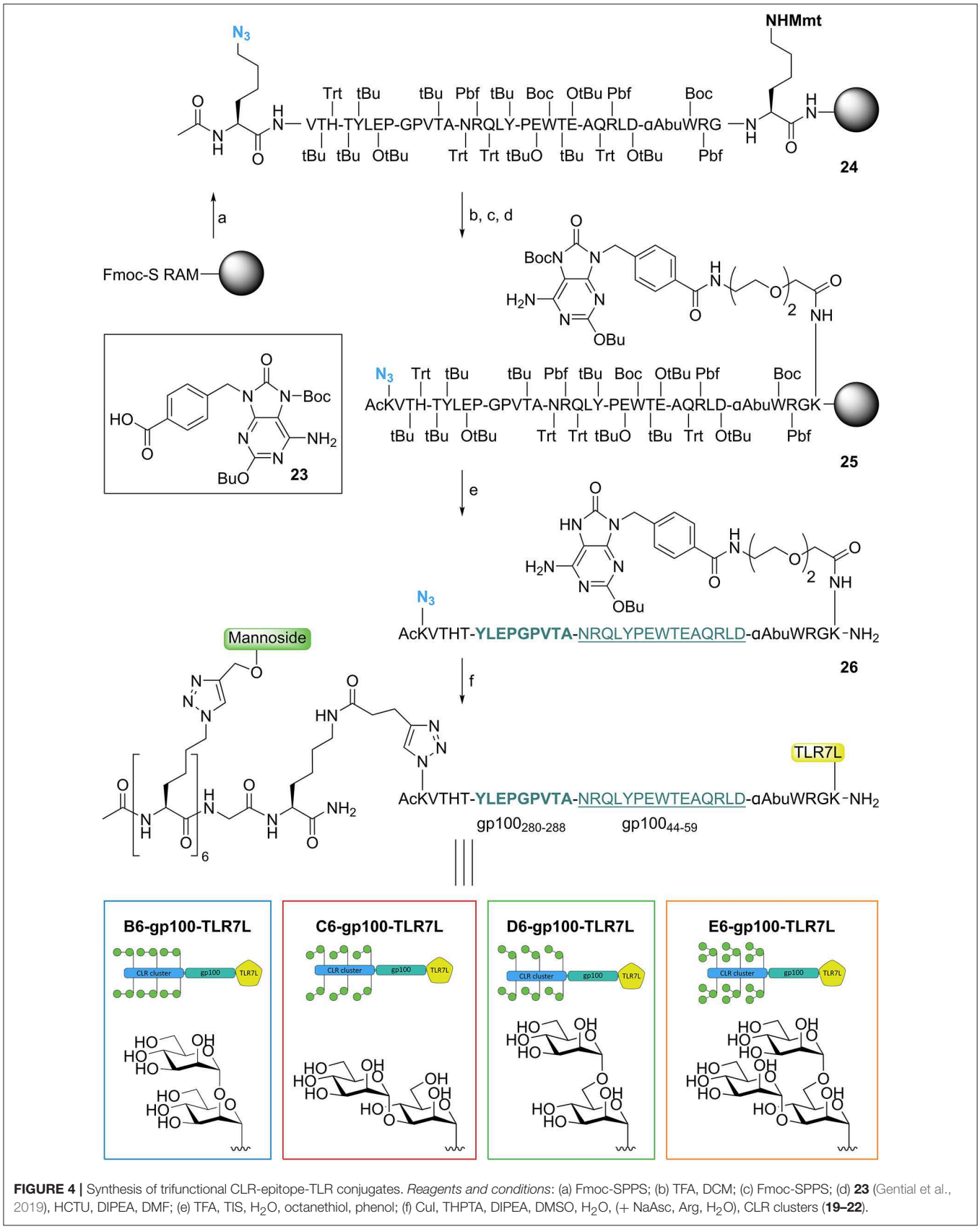

FIGURE 4 | Synthesis of trifunctional CLR-epitope-TLR conjugates. *Reagents and conditions*: (a) Fmoc-SPPS; (b) TFA, DCM; (c) Fmoc-SPPS; (d) **23** (Gential et al., 2019), HCTU, DIPEA, DMF; (e) TFA, TIS, H_2O, octanethiol, phenol; (f) CuI, THPTA, DIPEA, DMSO, H_2O, (+ NaAsc, Arg, H_2O), CLR clusters (**19–22**).

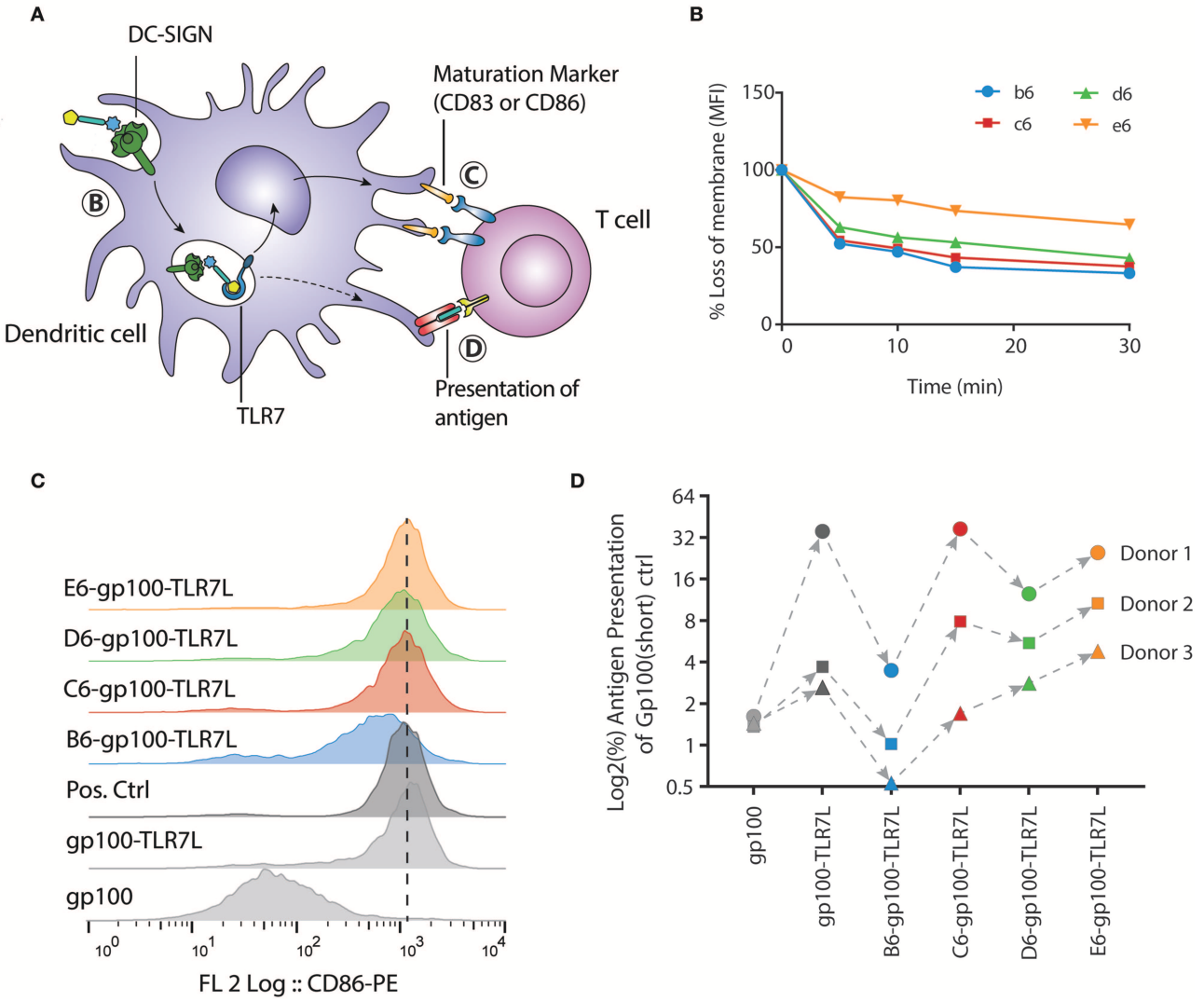

FIGURE 5 | E-gp100-TLR7L increases antigen presentation of monocyte-derived dendritic cells despite slower internalization. **(A)** Schematic representation of the moDC readouts used. **(B)** The internalization of the hexavalent mannoside clusters by moDCs was measured by flow cytometry. One donor is depicted here as representation of four individual clusters **b6**, **c6**, **d6** are rapidly internalized, while **e6** remains longer at the surface. **(C)** Expression of the DC maturation marker CD86 upon overnight stimulation with the trifunctional conjugates is measured by flow cytometry. All compounds harboring the mannoside cluster and a TLR7 ligand induce expression of CD86. LPS stimulation (10 ng/mL) is used as positive control. **(D)** Antigen presentation by the moDCs was determined by IFNγ release of the activated T cells. The **B6-gp100-TLR7L** conjugate shows minimal T cell activation while the **C6**-, **D6**-, and **E6-gp100-TLR7L** conjugates increased T cell activation compared to **gp100-TLR7L**. Overall, conjugate **E6-gp100-TLR7L** showed the strongest antigen presentation enhancement by moDCs.

was added to the moDCs, and samples were taken at the indicated time points and put on ice. Upon staining the moDCs with fluorophore-conjugated streptavidin, we could measure the signal loss of the membrane *via* flow cytometry. To exclude ligand-receptor dissociation before internalization, the moDCs were fixed under gentle conditions, hereby inhibiting receptor-mediated endocytosis. On fixed moDCs the clusters remained at the surface, as no signal loss could be detected (**Supplementary Figure 1D**). Notably, the uptake of clusters **b6, c6, d6,** and **e6** by immature moDCs did not correlate with their affinity for DC-SIGN (**Figures 3B**, **5B**). The di-mannoside clusters (**b6**, **c6,** and **d6**) were internalized relatively fast, with a 50% uptake within 5 min (**Figure 5B**). The tri-mannoside cluster **e6** however remained longer at the membrane surface and only a 25% uptake was seen after 30 min. Similar results were seen using a pH-sensitive fluorophore. In acidic environments, such as the endosomes and lysosomes, the fluorescence of this dye increases. Pre-complexed clusters mirrored the accelerated uptake of the di-mannoside clusters over the **e6** cluster (**Supplementary Figure 1E**). Although the DC-SIGN mediated uptake mechanism is known (Cambi et al., 2009), the initiation trigger for endocytosis upon DC-SIGN-ligand binding remains unclear. Recognition of the di-mannoside clusters could induce signaling leading to accelerated uptake, whereas the

tri-mannoside cluster could trigger a different signaling pathway. Nonetheless, the clusters harboring the smaller mannosides are preferred. Although the binding affinity of the clusters ranged from 0.9 to 6.6 μM, the di-mannosides induce more rapid DC-SIGN internalization over the tri-mannosides, and can thus increase intracellular peptide concentrations more efficiently for further antigen processing and presentation.

Next, the four trifunctional-conjugates were evaluated for their ability to mature moDCs and compared to non-mannosylated conjugates **gp100** and **gp100-TLR7L**. Maturation of the moDCs was measured by the expression of CD86 and CD83, two costimulatory molecules necessary for T cell activation. As expected, **gp100**, lacking the TLR7 agonist, did not induce maturation of the moDCs. All the conjugates with the mannoside clusters and the TLR7 ligand induced the expression of the moDCs maturation marker CD86 (**Figure 5C**), as well as CD83 (**Supplementary Figure 1F**) compared to the TLR7 agonist lacking gp100 control, indicating the DCs potential to activate T cells. These results show that the conjugation of TLR7 ligand to the peptide antigen or the peptide-mannose cluster conjugates does not hamper the TLR activating ability of the ligand.

Lastly, antigen presentation was determined in a human T cell antigen presentation model (**Figure 5D**). In this assay, the potency of DCs to present the internalized gp100 antigen on the cell surface to gp100-specific T cells is analyzed. The IFNγ secretion of activated T cells upon recognition of the cell surface presented gp100 is measured. Day 5 moDCs were stimulated for 30 min, as the internalization was relatively fast, with the glycopeptides at the assay-optimized concentration of 20 μM (**Supplementary Figure 1H**). The constructs were washed away before overnight co-culture with gp100-specific T cells. Although we observed significant natural donor variability, all conjugates showed similar mannoside-dependent trends in response. Surprisingly, although the α1,2-di-mannoside cluster **B6** showed the strongest binding affinity and **b6** was internalized rapidly, **B6-gp100-TLR7L** did not enhance antigen presentation. The obstruction of antigen presentation was primarily seen with the **B6-gp100-TLR7L** contradicting the assumption that the best binding constructs will simultaneously maximize T cell activation. The other di-mannoside conjugates (**C6-gp100-TLR7L** & **D6-gp100-TLR7L**) performed better in the antigen presentation assay than **B6-gp100-TLR7L**. **E6-gp100-TLR7L** demonstrated the strongest antigen presentation in the three donors tested. With some exceptions in donor 1, the antigen presentation was readily enhanced compared to **gp100-TLR7L** and all other constructs within each donor, even though the binding affinity of **E6** was a 3-fold lower than **B6**. The enhancement in antigen presentation of tri-mannoside conjugate **E6-gp100-TLR7L** may be a result of the stagnant uptake of tri-mannoside clusters (**Figure 5B**), altered DC-SIGN signaling and/or different intracellular routing or processing of the conjugates, compared to the di-mannosides. This indicates that oligosaccharides with high binding affinity for DC-SIGN are not *per se* the most suitable for use in covalent saccharide-antigen conjugates, designed for optimal antigen presentation and that the size of the clusters may affect the rate by which peptidases trim the conjugates enabling loading on MHC molecules for presentation.

It has previously been reported that a negative correlation between high internalization efficiency and antigen presentation may be due to altered intracellular processing (Chatterjee et al., 2012) and that DC-SIGN endocytosed ligands can traffic to differential endosomal compartments upon internalization. The trifunctional conjugates here are assumed to dissociate from the DC-SIGN receptor in the early endosomes, to allow triggering of TLR7 and enable their processing (Engering et al., 2002; Wilson et al., 2019). Our data may be explained by differential routing of the conjugates or differences in processing efficiency (Chatterjee et al., 2012). Alternatively, binding of the clusters to different mannose binding lectins, may also impact uptake and routing. In this regard, the mannose receptor could be a contributing inhibitory factor as high affinity binding of the smaller mannoside clusters to this receptor is known to prohibit ligand-receptor dissociation, halting further antigen processing in the early endosomes (Hiltbold et al., 2000). Future experiments will have to shed light on how and where conjugates of this type are processed, to enable the further optimization of rationally designed self-adjuvating peptide vaccines.

CONCLUSION

With the field of dendritic cell-based immunotherapy in acceleration, the range of glycoconjugates aimed at modulating the dendritic cell phenotype has rapidly expanded (Hotaling et al., 2014). Our paper documents a systematic array of DC-SIGN-targeting clusters, with well-defined mannoside structures (mono-, di-, and tri-mannosides) and controlled (mono-, di-, tri-, hexavalent) presentation. From this array, we have identified multiple hexavalent ligands that bind DC-SIGN with micromolar affinity, with the α1,2-dimannoside cluster **B6** being the best binder. The hexavalent clusters were conjugated to a model antigen and a TLR7 agonist, and tested for their ability to mature DCs and to enhance antigen presentation. Conjugation of the peptide to the sugar clusters does not hamper their binding to DC-SIGN nor does the conjugation impede TLR7 activation. Improved antigen presentation was observed for three of the four conjugates that were equipped with a TLR7 ligand and a mannoside cluster. Surprisingly, the conjugate harboring the highest affinity DC-SIGN binder, **B6**, showed lower antigen presentation that its **C6**-, **D6,** and **E6**-counterparts. This indicates that the affinity for DC-SIGN of particular mannoside clusters does not directly translate into enhanced antigen presentation of conjugates equipped with the clusters. Differences in processing pathways and speed of the multifunctional conjugates have to be taken into account and future research will be directed at mapping the events between uptake and presentation to enable the design of the next generation vaccine conjugates with tailor made activity. Taking natural variations between donors into account, the **E6-gp100-TLR7L** conjugate showed the best T cell activating properties and will serve as a lead for further conjugate development. The modular chemistry developed here, allows the future design of conjugates bearing multiple PRR ligands in a

single molecule. The multivalent presentation of a TLR ligand may enhance the activation of its cognate TLR, and different PRR-ligands may be combined to achieve synergistic activation of DCs, for example by exploiting simultaneous TLR and NLR activation (Ignacio et al., 2018).

MATERIALS AND METHODS

General Synthesis

The brief general synthetic procedures are described below, comprehensive experimental descriptions and analytical spectra for each construct can be found in the **Supplementary Materials** section.

The solid-phase peptide synthesis of the azidolysine backbones was performed on a TRIBUTE® Peptide Synthesizer (Gyros Protein Technologies AB, Arizona, USA) applying Fmoc based protocol starting with Tentagel S-RAM resin (∼0.22 mmol/g) on a 100 μmol scale using established synthetic protocols (Chan and White, 2000).

For the conjugation of propargyl glycosides and azidopeptides, all solvents were degassed by sonicating while bubbling argon through the solutions. A solution of azidopeptides in DMSO (0.5 M, 1 eq) was mixed with a solution of propargyl glycoside in water (0.5 M, 1.2 eq per azide) followed by addition of an aliquot of a stock solution of CuI (0.1 eq), THPTA (0.3 eq), and DIPEA (0.2 eq) in water ($[Cu^+] = 0.5$ M). The reaction was stirred at 40°C and the process was followed via LC-MS. When reactions did not progress and turned blue, a sodium ascorbate solution (0.2–1 eq, 1 M, aq) was added. Generally, reactions were stirred overnight at 40°C. When not complete after 16 h an extra aliquot of the copper stock was added. After completion a small amount of Quadrasil® AP (washed with water) was added, stirred for 1 h, filtered and applied on gel filtration (Toyopearl HW40S, 150 mM NH_4HCO_3, 1.6 × 60 cm, 1 mL/min) followed by lyophilization.

To introduce the biotin handle, glycoclusters (**A1–E6**) were dissolved in DMSO (0.02 M). To this, a stock solution of Biotin-OSu (0.15 M, 3–4 eq) and DIPEA (0.015 M, 0.3–0.4 eq) in DMSO were added and shaken overnight after which compounds were purified via RP-HPLC (linear gradient 10–16 % B in A, 12 min, 5 mL/min, Develosil RPAQUEOUS 10.0 × 250 mm) followed by lyophilization.

For the synthesis of alkyne labeled clusters **19–22,** a solution of glycoclusters (**B6, C6, D6,** or **E6**) in water (0.2 M, 1 eq) was mixed with a stock solution of **S9** (0.15 M, 3 eq) and DIPEA (0.05 M, 1 eq) in DMSO and shaken 1 h. Reaction progress was followed via LC-MS and when completed, the 4-pentynoic amides were purified via gel filtration (Toyopearl HW-40S, 1.6 × 60 cm, 150 mM NH_4HCO_3, 1 mL/min) or RP-HPLC followed by lyophilization.

The solid-phase peptide synthesis of the gp100 peptides was performed on a TRIBUTE® Peptide Synthesizer (Gyros Protein Technologies AB, Arizona, USA) applying Fmoc based protocol starting with Tentagel S-RAM resin (∼0.22 mmol/g) on a 100–250 μmol scale using established synthetic protocols (Chan and White, 2000). The consecutive steps for synthesis on 250 μmol scale* performed in each cycle were:

(1) DMF wash (1x) followed by nitrogen purge; *(2)* Deprotection of the Fmoc-group with 20% piperidine in DMF (8 mL) (3 × 3 min at 50°C); *(3)* DMF wash (3x) followed by nitrogen purge; *(4.1)* Coupling of the appropriate amino acid** in 4-fold excess (unless stated otherwise)***; *(4.2)* Step 4.1 was repeated; *(5)* DMF wash (3x) followed by nitrogen purge; *(6)* capping with a solution of Ac_2O/DMF/DIPEA (8 mL, 10/88/2, v/v/v) for 2 min; *(7)* DMF wash (2x).

After the complete sequence the resin was washed with DMF (3x), DCM (3x), Et_2O (3x), followed by nitrogen purge before treatment with the cleavage cocktail.

*All amounts are scaled-down in equimolar proportions for smaller scale.

The amino acids applied in this synthesis were: Fmoc-Lys(Mmt)-OH, Fmoc-Gly-OH, Fmoc-Arg(Pbf)-OH, Fmoc-Trp(Boc)-OH, Fmoc-L-α-aminobutyric acid, Fmoc-Asp(O*t*Bu)-OH**, Fmoc-Leu-OH****, Fmoc-Gln(Trt)-OH, Fmoc-Ala-OH, Fmoc-Glu(O*t*Bu)-OH, Fmoc-Thr(*t*Bu)-OH, Fmoc-Pro-OH, Fmoc-Tyr(*t*Bu)-OH, Fmoc-Asn(Trt)-OH, Fmoc-Val-OH, Fmoc-His(Trt)-OH, Fmoc-AEEA-OH *(Fmoc-8-amino-3,6-dioxaoctanoic acid)* (Carbosynth), Fmoc-Cys(Trt)-OH, Fmoc-Lys(N_3)-OH (IRIS biotech), and **23**.

***Generally, the Fmoc amino acid is dissolved in a HCTU solution in DMF (5.00 mL, 0.20 M, 1.0 mmol, 4 eq) The resulting solution was transferred to the reaction vessel followed by a DIPEA solution in DMF (4.00 mL, 0.50 M, 2.0 mmol, 8 eq) to initiate the coupling. The reaction vessel was shaken for 30 min at 50°C (unless stated otherwise).

****Aspartic acid and the adjacent Leucine and Arginine were introduced at with 1 h reaction time at room temperature. Fmoc removal was achieved with piperide/DMF in 3 × 5 min at room temperature (Behrendt and Offer, 2016).

For the final conjugation of the gp100 peptide **26** with glycoclusters **19–22**, all solvents were degassed by sonicating while bubbling argon through the solutions. A solution of azidopeptide **26** in DMSO was mixed with a solution of alkyne functionalized glycoclusters in water (**19, 20, 21,** or **22**) followed by addition of an aliquot of a stock solution of CuI (0.1 eq), THPTA (0.3 eq), and DIPEA (0.2 eq) in water ($[Cu^+] = 0.5$ M). The reaction was stirred at 45°C and the process was followed via LC-MS. When reactions did not progress and turned blue, a stock solution of sodium ascorbate (0.25 M) and arginine (Conibear et al., 2016) (0.5 M) (0.2–1 eq ascorbate) in water was added. After completion a small amount of Quadrasil® AP (washed with water) was added, stirred for 1 h, filtered and applied on gel filtration (Toyopearl HW40S, 150 mM NH_4HCO_3, 1.6 × 60 cm, 1 mL/min) or purified via RP-HPLC followed by lyophilization.

(All compound characterization can be found in the **Supplementary Materials** section page 30 and further).

Cell Isolation and Culture

Monocytes were isolated from buffy coats of healthy donors (Sanquin Amsterdam, reference: S03.0023-XT) using sequential Ficoll (STEMCELL Technologies) and Percoll (Sigma) gradient centrifugation, and cultured for 5 days in RPMI 1640 (Invitrogen) with 10% FCS (Biowittaker), 1.000 U/mL penicillin (Lonza), 1 U/mL streptomycin (Lonza), 262.5 U/mL IL-4 (Biosource), and

112.5 U/mL GM-CSF (Biosource). The differentiation of the moDCs was monitored via flow cytometric analysis of DC-SIGN AZN-D1-Alexa488, in house (Geijtenbeek et al., 2002), CD83 and CD86 (both PE-conjugated, Becton Dickinson) expression.

Surface Plasmon Resonance Analysis

The ECD of DC-SIGN (residues 66–404) was overexpressed and purified as previously described (Tabarani et al., 2009). The DC-SIGN S-ECD construct used for direct interaction experiment (see below) has been overexpressed and purified as described elsewhere (Porkolab et al., 2019). The SPR competition experiments were performed on a BIAcore T200 using a CM3 series S sensor chip. Flow cells were activated as previously described (Halary et al., 2002). Flow cell 1 was functionalized with BSA, blocked with ethanolamine and subsequently used as a control surface. Flow cells 2 and 3 were treated with BSA-Man α1-3[Manα1-6]Man (Dextra) (60 μg/mL) in 10 mM NaOAc pH 4 and blocked with ethanolamine. The final densities on flow cells 2 and 3 were about 2,100 RU. The affinities of the various compounds for DC-SIGN ECD were evaluated via an established inhibition assay (Andreini et al., 2011) in which DCSIGN ECD was injected at 20 μM alone or in the presence of increasing concentration of inhibitors. Injections were performed at 5 μL/min using 25 mM Tris-HCl pH 8, 150 mM NaCl, 4 mM $CaCl_2$, 0.05% P20 surfactant as running buffer. The surface was regenerated by the injection of 50 mM EDTA. The data was analyzed in BIAcore BIAevaluation software using four parameter equation.

The direct interaction experiments were executed on a T200 Biacore with a CM3 series S sensor chip. Contrary to the competition assay described above, in this test, DC-SIGN ECD used harbors a StreptagII in its N-terminus (DC-SIGN S-ECD) to allow its capture and functionalization onto the surface in an oriented manner. Flow cells were functionalized as previously described (Porkolab et al., 2019). Briefly, after EDC/NHS activation, flow cells were functionalized with streptactin protein in a first step. Flow cell 1 was used as control, while other flow cells were, in a second round of activation, functionalized with 100 μg/mL of a DC-SIGN S-ECD up to a final density ranging between 2,500 and 3,000 RU, via tag specific capture and linkage by amine coupling chemistry simultaneously. The compounds were injected in running buffer of 25 mM Tris pH 8, 150 mM NaCl, 4 mM $CaCl_2$, 0.05% Tween 20 onto the surface at increasing concentrations with a flow rate of 30 μL/min. The ligand titration led to the determination of an apparent K_d value. The data was analyzed in BIAcore BIAevaluation software for direct interaction 1:1 calculation assuming that the K_d will reflect the affinity of the ligands (glycoclusters) for the DC-SIGN oriented surface used as a whole.

Binding of the Mannose Library to moDCs

Approximately 10^5 day 5 moDCs were washed and resuspended in 100 μL culture medium (pre-cooled to 4°C). 20 μg/mL AZN-D1 (anti-DC-SIGN, in house Geijtenbeek et al., 2002) or purified mouse anti-human CD206 antibody (Clone 19.2, BD Bioscience) was added to the moDCs and pre-incubated for 45 min on ice. Subsequently, 10 μM of the biotinylated mannoside clusters or 1 μg/mL of $Lewis^Y$-conjugated polyacrylamide (positive control) was added, and incubated for 30 min at 4°C. Cells were then washed with pre-cooled PBS (4°C), and stained with Alexa647-labeled streptavidin (Invitrogen™) in PBS supplemented with 0.5% BSA and 0.02% NaN_3 (PBA) for 30 min at 4°C. Upon washing in ice-cold PBA and fixation in PBS with 0.5% PFA, the fluorescence was measured by flow cytometry (CyAn™ ADP with Summit™ Software), and further analyzed using FlowJo v10.

Antigen Presentation

Immature day 5 moDCs were seeded in 96-well plates (Greiner) at $50{\cdot}10^3$ cells/well and incubated with 20 μM of the different gp100-conjugates in the presence or absence of the TLR4 ligand LPS (10 ng/mL) or the TLR7 ligand Imiquimod (2.5 μg/mL). The gp100 short peptide, containing the $gp100_{280-288}$ sequence, was taken along as control, as well as the gp100 long peptide without the four C-terminal linker amino acids (gp100(ctrl)). After 30 min, moDCs were washed, and co-cultured overnight with $CD8^+$ HLA-A2.1 restricted T cell clone transduced with the TCR specific for the $gp100_{280-288}$ peptide (10^5 cells per well, E:T ratio 1:2) (Schaft et al., 2003). IFNγ in the supernatant was measured by sandwich ELISA according to the manufacturer's protocol (Biosource), and measured by spectrophotometric analysis on the iMarkTM Microplate Absorbance Reader (Bio-RAD) at 450 nm.

Internalization Assay

Immature day 5 moDCs were harvested and washed with cold HBSS (Thermo Fischer), after which half of the moDCs were gently fixed for 20 min at RT with 1% PFA in PBS. Afterwards, 20 μM of the different biotinylated mannose-clusters in cold HBSS were added. The moDCs were incubated for 1 h on ice, and washed in cold HBSS. Subsequently, warm HBSS was added to the cells, and cells were incubated at 37°C in a shaking heating block. At the indicated time points, a sample of the cells was taken and put on ice. After the last time point, the cells were stained with Streptavidin-Alexa647 (Thermo Fisher), measured using flow cytometry (CyAn™ ADP with Summit™ Software), and further analyzed using FlowJo v10. The same procedure was used for internalization with pHrodo™ Red Avidin (Thermo Fischer). The different biotinylated mannose-clusters were however incubated with pHrodo-Avidin (ratio 2:1) for 15 min at 37°C, prior to moDC exposure. The fluorescence upon internalization was measured using flow cytometry (BD LSRFortessa™ X-20 with FACSDiva Software), and further analyzed using FlowJo v10.

Statistics

Unless otherwise stated, data are presented as the mean ± SD of at least three independent experiments or healthy donors. Statistical analyses were performed in GraphPad Prism v7.04. Statistical significance was set at $P < 0.05$ and was evaluated by the Mann–Whitney U-test.

DATA AVAILABILITY STATEMENT

All datasets generated for this study are included in the manuscript/**Supplementary Files**.

AUTHOR CONTRIBUTIONS

R-JL and TH wrote the first drafts of this manuscript. TH synthesized the described constructs under supervision of HO, DF, GM, and JC. CW synthesized some of the propargyl mannosides. NM and HE assisted in purification and high resolution mass measurements. R-JL determined the cellular affinity, uptake, maturation, and antigen presentation aided by SB and TA under supervision of SV and YK. SPR experiments were performed by SA and CV under supervision of FF. MT was involved in the preparation of DC-SIGN samples.

FUNDING

This work was funded by the NWO gravitation program 2013 granted to the Institute for Chemical Immunology (ICI-024.002.009) and by the European Union's Horizon 2020 research and innovation program under the Marie Sklowdowska-Curie grant Agreement No. 642870 (Immunoshape). The Multistep Protein Purification Platform (MP3) was exploited for human DC-SIGN ECD, and S-ECD production and the SPR platform for the competition and direct interaction tests of the Grenoble Instruct center (ISBG; UMS 3518 CNRS-CEA-UJF-EMBL) with support from FRISBI (ANR-10-INSB-05-02) and GRAL (ANR-10-LABX-49-01) within the Grenoble Partnership for Structural Biology.

SUPPLEMENTARY MATERIAL

The Supplementary Material for this article can be found online at: https://www.frontiersin.org/articles/10.3389/fchem.2019.00650/full#supplementary-material

REFERENCES

Ackerman, A. L., and Cresswell, P. (2003). Regulation of MHC class I transport in human dendritic cells and the dendritic-like cell line KG-1. *J. Immunol.* 170, 4178–4188. doi: 10.4049/jimmunol.170.8.4178

Amin, M. N., Huang, W., Mizanur, R. M., and Wang, L.-X. (2011). Convergent synthesis of homogeneous Glc 1 Man 9 GlcNAc 2 - protein and derivatives as ligands of molecular chaperones in protein quality control. *J. Am. Chem. Soc.* 133, 14404–14417. doi: 10.1021/ja204831z

Andreini, M., Doknic, D., Sutkeviciute, I., Reina, J. J., Duan, J., Chabrol, E., et al. (2011). Second generation of fucose-based DC-SIGN ligands: affinity improvement and specificity versus Langerin. *Org. Biomol. Chem.* 9, 5778–5786. doi: 10.1039/c1ob05573a

Behrendt, R., and Offer, J. (2016). Advances in Fmoc solid-phase peptide synthesis. *J. Pept.* 22, 4–27. doi: 10.1002/psc.2836

Bernardi, A., Jiménez-Barbero, J., Casnati, A., De Castro, C., Darbre, T., Fieschi, F., et al. (2013). Multivalent glycoconjugates as anti-pathogenic agents. *Chem. Soc. Rev.* 42, 4709–4727. doi: 10.1039/C2CS35408J

Berzi, A., Ordanini, S., Joosten, B., Trabattoni, D., Cambi, A., Bernardi, A., et al. (2016). Pseudo-mannosylated DC-SIGN ligands as immunomodulants. *Sci. Rep.* 6:35373. doi: 10.1038/srep35373

Blander, J. M., and Medzhitov, R. (2006). Toll-dependent selection of microbial antigens for presentation by dendritic cells. *Nature* 440, 808–812. doi: 10.1038/nature04596

Buskas, T., Ingale, S., and Boons, G.-J. (2005). Towards a fully synthetic carbohydrate-based anticancer vaccine: synthesis and immunological evaluation of a lipidated glycopeptide containing the tumor-associated Tn antigen. *Angew. Chemie Int. Ed.* 44, 5985–5988. doi: 10.1002/anie.200501818

Cambi, A., Beeren, I., Joosten, B., Fransen, J. A., and Figdor, C. G. (2009). The C-type lectin DC-SIGN internalizes soluble antigens and HIV-1 virions via a clathrin-dependent mechanism. *Eur. J. Immunol.* 39, 1923–1928. doi: 10.1002/eji.200939351

Carpenter, C., and Nepogodiev, S. A. (2005). Synthesis of a αMan(1→3)αMan(1→2)αMan glycocluster presented on aβ-cyclodextrin scaffold. *Eur. J. Org. Chem.* 2005, 3286–3296. doi: 10.1002/ejoc.200500146

Chan, M., Hayashi, T., Kuy, C. S., Gray, C. S., Wu, C. C. N., Corr, M., et al. (2009). Synthesis and immunological characterization of toll-like receptor 7 Agonistic conjugates. *Bioconjug. Chem.* 20, 1194–1200. doi: 10.1021/bc900054q

Chan, W. C., and White, P. D. (2000). *Fmoc Solid Phase Peptide Synthesis: a Practical Approach*. Nottingham: Oxford University Press.

Chatterjee, B., Smed-Sörensen, A., Cohn, L., Chalouni, C., Vandlen, R., Lee, B.-C., et al. (2012). Internalization and endosomal degradation of receptor-bound antigens regulate the efficiency of cross presentation by human dendritic cells. *Blood* 120, 2011–2020. doi: 10.1182/blood-2012-01-402370

Cho, H. J., Takabayashi, K., Cheng, P.-M., Nguyen, M.-D., Corr, M., Tuck, S., et al. (2000). Immunostimulatory DNA-based vaccines induce cytotoxic lymphocyte activity by a T-helper cell-independent mechanism. *Nat. Biotechnol.* 18, 509–514. doi: 10.1038/75365

Conibear, A. C., Farbiarz, K., Mayer, R. L., Matveenko, M., Kählig, H., and Becker, C. F. W. (2016). Arginine side-chain modification that occurs during copper-catalysed azide–alkyne click reactions resembles an advanced glycation end product. *Org. Biomol. Chem.* 14, 6205–6211. doi: 10.1039/C6OB00932H

Daly, R., Vaz, G., Davies, A. M., Senge, M. O., and Scanlan, E. M. (2012). Synthesis and biological evaluation of a library of glycoporphyrin compounds. *Chem. Eur. J.* 18, 14671–14679. doi: 10.1002/chem.201202064

Deres, K., Schild, H., Wiesmüller, K.-H., Jung, G., and Rammensee, H.-G. (1989). *In vivo* priming of virus-specific cytotoxic T lymphocytes with synthetic lipopeptide vaccine. *Nature* 342, 561–564. doi: 10.1038/342561a0

Engering, A., Geijtenbeek, T. B. H., van Vliet, S. J., Wijers, M., Liempt, E., van, Demaurex, N., et al. (2002). The dendritic cell-specific adhesion receptor DC-SIGN internalizes antigen for presentation to T cells. *J. Immunol.* 168, 2118–2126. doi: 10.4049/jimmunol.168.5.2118

Evers, D. L., Hung, R. L., Thomas, V. H., and Rice, K. G. (1998). Preparative purification of a high-mannose type N-glycan from soy bean agglutinin by hydrazinolysis and tyrosinamide derivatization. *Anal. Biochem.* 265, 313–316. doi: 10.1006/abio.1998.2895

Fehres, C. M., Kalay, H., Bruijns, S. C. M., Musaafir, S. A. M., Ambrosini, M., Bloois, L., et al. (2015). Cross-presentation through langerin and DC-SIGN targeting requires different formulations of glycan-modified antigens. *J. Control. Release* 203, 67–76. doi: 10.1016/j.jconrel.2015.01.040

Feinberg, H., Castelli, R., Drickamer, K., Seeberger, P. H., and Weis, W. I. (2007). Multiple modes of binding enhance the affinity of DC-SIGN for high mannose N-linked glycans found on viral glycoproteins. *J. Biol. Chem.* 282, 4202–4209. doi: 10.1074/jbc.M609689200

Fritz, J. H., Girardin, S. E., Fitting, C., Werts, C., Mengin-Lecreulx, D., Caroff, M., et al. (2005). Synergistic stimulation of human monocytes and dendritic cells by Toll-like receptor 4 and NOD1- and NOD2-activating agonists. *Eur. J. Immunol.* 35, 2459–2470. doi: 10.1002/eji.200526286

Fujita, Y., and Taguchi, H. (2012). Overview and outlook of Toll-like receptor ligand–antigen conjugate vaccines. *Ther. Deliv.* 3, 749–760. doi: 10.4155/tde.12.52

Geijtenbeek, T. B. H., van Duijnhoven, G. C. F., van Vliet, S. J., Krieger, E., Vriend, G., Figdor, C. G., et al. (2002). Identification of different binding sites in the dendritic cell-specific receptor DC-SIGN for intercellular adhesion

molecule 3 and HIV-1. *J. Biol. Chem.* 277, 11314–11320. doi: 10.1074/jbc.M111532200

Geijtenbeek, T. B. H., and Van Kooyk, Y. (2003). Pathogens target DC-SIGN to influence their fate DC-SIGN functions as a pathogen receptor with broad specificity. *APMIS* 111, 698–714. doi: 10.1034/j.1600-0463.2003.11107803.x

Gential, G. P. P., Hogervorst, T. P., Tondini, E., van de Graaff, M. J., Overkleeft, H. S., Codée, J. D. C., et al. (2019). Peptides conjugated to 2-alkoxy-8-oxo-adenine as potential synthetic vaccines triggering TLR7. *Bioorg. Med. Chem. Lett.* 29, 1340–1344. doi: 10.1016/j.bmcl.2019.03.048

Glaffig, M., Stergiou, N., Hartmann, S., Schmitt, E., and Kunz, H. (2018). A Synthetic MUC1 anticancer vaccine containing mannose ligands for targeting macrophages and dendritic cells. *ChemMedChem* 13, 25–29. doi: 10.1002/cmdc.201700646

Gringhuis, S. I., den Dunnen, J., Litjens, M., van Het Hof, B., van Kooyk, Y., and Geijtenbeek, T. B. H. (2007). C-Type lectin DC-SIGN modulates toll-like receptor signaling via Raf-1 kinase-dependent acetylation of transcription factor NF-κB. *Immunity* 26, 605–616. doi: 10.1016/j.immuni.2007.03.012

Halary, F., Amara, A., Lortat-Jacob, H., Messerle, M., Delaunay, T., Houlès, C., et al. (2002). Human cytomegalovirus binding to DC-SIGN is required for dendritic cell infection and target cell trans-infection. *Immunity* 17, 653–664. doi: 10.1016/S1074-7613(02)00447-8

He, L.-Z., Weidlick, J., Sisson, C., Marsh, H. C., and Keler, T. (2015). Toll-like receptor agonists shape the immune responses to a mannose receptor-targeted cancer vaccine. *Cell. Mol. Immunol.* 12, 719–728. doi: 10.1038/cmi.2014.100

Hiltbold, E. M., Vlad, A. M., Ciborowski, P., Watkins, S. C., and Finn, O. J. (2000). The mechanism of unresponsiveness to circulating tumor antigen MUC1 is a block in intracellular sorting and processing by dendritic cells. *J. Immunol.* 165, 3730–3741. doi: 10.4049/jimmunol.165.7.3730

Hotaling, N. A., Ratner, D. M., Cummings, R. D., and Babensee, J. E. (2014). Presentation modality of glycoconjugates modulates dendritic cell phenotype. *Biomater. Sci.* 2, 1426–1439. doi: 10.1039/C4BM00138A

Ignacio, B. J., Albin, T. J., Esser-Kahn, A. P., and Verdoes, M. (2018). Toll-like receptor agonist conjugation: a chemical perspective. *Bioconjug. Chem.* 29, 587–603. doi: 10.1021/acs.bioconjchem.7b00808

Jin, G., Wu, C. C. N., Tawatao, R. I., Chan, M., Carson, D. A., and Cottam, H. B. (2006). Synthesis and immunostimulatory activity of 8-substituted amino 9-benzyladenines as potent Toll-like receptor 7 agonists. *Bioorg. Med. Chem. Lett.* 16, 4559–4563. doi: 10.1016/j.bmcl.2006.06.017

Khan, S., Bijker, M. S., Weterings, J. J., Tanke, H. J., Adema, G. J., van Hall, T., et al. (2007). Distinct uptake mechanisms but similar intracellular processing of two different toll-like receptor ligand-peptide conjugates in dendritic cells. *J. Biol. Chem.* 282, 21145–21159. doi: 10.1074/jbc.M701705200

Le Moignic, A., Malard, V., Benvegnu, T., Lemiègre, L., Berchel, M., Jaffrès, P.-A., et al. (2018). Preclinical evaluation of mRNA trimannosylated lipopolyplexes as therapeutic cancer vaccines targeting dendritic cells. *J. Control. Release* 278, 110–121. doi: 10.1016/j.jconrel.2018.03.035

McIntosh, J. D., Brimble, M. A., Brooks, A. E. S., Dunbar, P. R., Kowalczyk, R., Tomabechi, Y., et al. (2015). Convergent chemo-enzymatic synthesis of mannosylated glycopeptides; targeting of putative vaccine candidates to antigen presenting cells. *Chem. Sci.* 6, 4636–4642. doi: 10.1039/C5SC00952A

Moyle, P. M., Olive, C., Ho, M.-F., Pandey, M., Dyer, J., Suhrbier, A., et al. (2007). Toward the development of prophylactic and therapeutic human papillomavirus type-16 lipopeptide vaccines. *J. Med. Chem.* 50, 4721–4727. doi: 10.1021/jm070287b

Ni, J., Song, H., Wang, Y., Stamatos, N. M., and Wang, L. X. (2006). Toward a carbohydrate-based HIV-1 vaccine: synthesis and immunological studies of oligomannose-containing glycoconjugates. *Bioconjug. Chem.* 17, 493–500. doi: 10.1021/bc0502816

Ordanini, S., Varga, N., Porkolab, V., Thépaut, M., Belvisi, L., Bertaglia, A., et al. (2015). Designing nanomolar antagonists of DC-SIGN-mediated HIV infection: ligand presentation using molecular rods. *Chem. Commun.* 51, 3816–3819. doi: 10.1039/C4CC09709B

Porkolab, V., Pifferi, C., Sutkeviciute, I., Ordanini, S., Taouai, M., Thepaut, M., et al. (2019). Development of c-type lectin oriented surfaces for high avidity glycoconjugates: towards mimicking multivalent interactions on the cell surface. *bioRxiv [Preprint]*. doi: 10.1101/780452

Raiber, E.-A., Tulone, C., Zhang, Y., Martinez-Pomares, L., Steed, E., Sponaas, A. M., et al. (2010). Targeted delivery of antigen processing inhibitors to antigen presenting cells via mannose receptors. *ACS Chem. Biol.* 5, 461–476. doi: 10.1021/cb100008p

Sauer, M. M., Jakob, R. P., Luber, T., Canonica, F., Navarra, G., Ernst, B., et al. (2019). Binding of the bacterial adhesin FimH to its natural, multivalent high-mannose type glycan targets. *J. Am. Chem. Soc.* 141, 936–944. doi: 10.1021/jacs.8b10736

Schaft, N., Willemsen, R. A., de Vries, J., Lankiewicz, B., Essers, B. W., Gratama, J.-W., et al. (2003). Peptide fine specificity of anti-glycoprotein 100 CTL is preserved following transfer of engineered TCR genes into primary human T lymphocytes. *J. Immunol.* 170, 2186–2194. doi: 10.4049/jimmunol.170.4.2186

Sedaghat, B., Stephenson, R. J., Giddam, A. K., Eskandari, S., Apte, S. H., Pattinson, D. J., et al. (2016). Synthesis of mannosylated lipopeptides with receptor targeting properties. *Bioconjug. Chem.* 27, 533–548. doi: 10.1021/acs.bioconjchem.5b00547

Silva, J. M., Zupancic, E., Vandermeulen, G., Oliveira, V. G., Salgado, A., Videira, M., et al. (2015). *In vivo* delivery of peptides and Toll-like receptor ligands by mannose-functionalized polymeric nanoparticles induces prophylactic and therapeutic anti-tumor immune responses in a melanoma model. *J. Control. Release* 198, 91–103. doi: 10.1016/j.jconrel.2014.11.033

Srinivas, O., Larrieu, P., Duverger, E., Boccaccio, C., Bousser, M. T., Monsigny, M., et al. (2007). Synthesis of glycocluster - Tumor antigenic peptide conjugates for dendritic cell targeting. *Bioconjug. Chem.* 18, 1547–1554. doi: 10.1021/bc070026g

Tabarani, G., Thépaut, M., Stroebel, D., Ebel, C., Vivès, C., Vachette, P., et al. (2009). DC-SIGN neck domain is a pH-sensor controlling oligomerization. *J. Biol. Chem.* 284, 21229–21240. doi: 10.1074/jbc.M109.021204

Temme, J. S., Drzyzga, M. G., MacPherson, I. S., and Krauss, I. J. (2013). Directed evolution of 2G12-targeted nonamannose glycoclusters by SELMA. *Chem. Eur. J.* 19, 17291–17295. doi: 10.1002/chem.201303848

Thomas, M., Gesson, J.-P., and Papot, S. (2007). First O-Glycosylation of hydroxamic acids. *J. Org. Chem.* 72, 4262–4264. doi: 10.1021/jo0701839

Timpano, G., Tabarani, G., Anderluh, M., Invernizzi, D., Vasile, F., Potenza, D., et al. (2008). Synthesis of novel DC-SIGN ligands with an α-fucosylamide anchor. *ChemBioChem* 9, 1921–1930. doi: 10.1002/cbic.200800139

Umekawa, M., Huang, W., Li, B., Fujita, K., Ashida, H., Wang, L. X., et al. (2008). Mutants of Mucor hiemalis endo-β-N-acetylglucosaminidase show enhanced transglycosylation and glycosynthase-like activities. *J. Biol. Chem.* 283, 4469–4479. doi: 10.1074/jbc.M707137200

van der Vorm, S., van Hengst, J. M. A., Bakker, M., Overkleeft, H. S., van der Marel, G. A., and Codée, J. D. C. (2018). Mapping the relationship between glycosyl acceptor reactivity and glycosylation stereoselectivity. *Angew. Chemie Int. Ed.* 57, 8240–8244. doi: 10.1002/anie.201802899

van Kooyk, Y., Unger, W. W., Fehres, C. M., Kalay, H., and García-Vallejo, J. J. (2013). Glycan-based DC-SIGN targeting vaccines to enhance antigen cross-presentation. *Mol. Immunol.* 55, 143–145. doi: 10.1016/j.molimm.2012.10.031

van Liempt, E., Bank, C. M., Mehta, P., Garciá-Vallejo, J. J., Kawar, Z. S., Geyer, R., et al. (2006). Specificity of DC-SIGN for mannose- and fucose-containing glycans. *FEBS Lett.* 580, 6123–6131. doi: 10.1016/j.febslet.2006.10.009

Willems, M. M., Zom, G. G., Khan, S., Meeuwenoord, N., Melief, C. J. M., Stelt, M., et al. (2014). N-tetradecylcarbamyl lipopeptides as novel agonists for toll-like receptor 2. *J. Med. Chem.* 57, 6873–6878. doi: 10.1021/jm500722p

Willems, M. M., Zom, G. G., Meeuwenoord, N., Khan, S., Ossendorp, F., Overkleeft, H. S., et al. (2016). Lipophilic muramyl dipeptide-antigen conjugates as immunostimulating agents. *ChemMedChem* 11, 190–198. doi: 10.1002/cmdc.201500196

Wilson, D. S., Hirosue, S., Raczy, M. M., Bonilla-Ramirez, L., Jeanbart, L., Wang, R., et al. (2019). Antigens reversibly conjugated to a polymeric glyco-adjuvant induce protective humoral and cellular immunity. *Nat. Mater.* 18, 175–185. doi: 10.1038/s41563-018-0256-5

Wlodawer, A., Miller, M., Jaskólski, M., Sathyanarayana, B., Baldwin, E., Weber, I. T., et al. (1989). Conserved folding in retroviral proteases: crystal structure of a synthetic HIV-1 protease. *Science* 245, 616–621. doi: 10.1126/science.2548279

Wong, C. S., Hoogendoorn, S., van der Marel, G. A., Overkleeft, H. S., and Codée, J. D. C. (2015). Targeted delivery of fluorescent high-mannose-type oligosaccharide cathepsin inhibitor conjugates. *Chempluschem* 80, 928–937. doi: 10.1002/cplu.201500004

Zom, G. G., Willems, M. M. J. H., Meeuwenoord, N., Reintjens, N. R. M., Tondini, E., Khan, S., et al. (2019). Dual synthetic peptide conjugate vaccine simultaneously triggers TLR2 and NOD2 and activates human dendritic cells. *Bioconjug. Chem.* 30, 1150–1161. doi: 10.1021/acs.bioconjchem.9b00087

Conflict of Interest: The authors declare that the research was conducted in the absence of any commercial or financial relationships that could be construed as a potential conflict of interest.

frontiers in Chemistry

REVIEW
published: 22 October 2019
doi: 10.3389/fchem.2019.00710

Mucins and Pathogenic Mucin-Like Molecules Are Immunomodulators During Infection and Targets for Diagnostics and Vaccines

Sandra Pinzón Martín[1,2], *Peter H. Seeberger*[1,2] *and Daniel Varón Silva*[1,2]*

[1] Department of Biomolecular Systems, Max Planck Institute of Colloids and Interfaces, Potsdam, Germany, [2] Department of Biology, Chemistry and Pharmacy, Freie Universität Berlin, Berlin, Germany

Mucins and mucin-like molecules are highly O-glycosylated proteins present on the cell surface of mammals and other organisms. These glycoproteins are highly diverse in the apoprotein and glycan cores and play a central role in many biological processes and diseases. Mucins are the most abundant macromolecules in mucus and are responsible for its biochemical and biophysical properties. Mucin-like molecules cover various protozoan parasites, fungi and viruses. In humans, modifications in mucin glycosylation are associated with tumors in epithelial tissue. These modifications allow the distinction between normal and abnormal cell conditions and represent important targets for vaccine development against some cancers. Mucins and mucin-like molecules derived from pathogens are potential diagnostic markers and targets for therapeutic agents. In this review, we summarize the distribution, structure, role as immunomodulators, and the correlation of human mucins with diseases and perform a comparative analysis of mucins with mucin-like molecules present in human pathogens. Furthermore, we review the methods to produce pathogenic and human mucins using chemical synthesis and expression systems. Finally, we present applications of mucin-like molecules in diagnosis and prevention of relevant human diseases.

Keywords: mucins, mucin-like molecules, O-glycoproteins, cancer, parasites, virus, infection

OPEN ACCESS

Edited by:
Karina Valeria Mariño, Molecular and Functional Glycomics Lab, Institute of Biology and Experimental Medicine (IBYME), Argentina

Reviewed by:
Carlos A. Buscaglia, National Council for Scientific and Technical Research (CONICET), Argentina
Rosa Muchnik De Lederkremer, University of Buenos Aires, Argentina

***Correspondence:**
Daniel Varón Silva
daniel.varon@mpikg.mpg.de

Specialty section:
This article was submitted to Chemical Biology, a section of the journal Frontiers in Chemistry

Received: *12 August 2019*
Accepted: *09 October 2019*
Published: *22 October 2019*

Citation:
Pinzón Martín S, Seeberger PH and Varón Silva D (2019) Mucins and Pathogenic Mucin-Like Molecules Are Immunomodulators During Infection and Targets for Diagnostics and Vaccines. Front. Chem. 7:710. doi: 10.3389/fchem.2019.00710

INTRODUCTION

Physical protection from external pathogens and molecules is essential for cell survival. Most mammal cells exposed to the external environment use complex molecular shields and coats that are present either as a hard shell (skin) or as a soft secretion (mucus) (Hansson, 2019). Mucus is present on the ocular surface and in organs of respiratory, gastrointestinal, and reproductive tracts. It covers human organs and glands and contains proteins having highly O-glycosylated repeats, called mucins (Corfield, 2015; Bansil and Turner, 2018).

Some human pathogens use similar protection mechanisms involving highly O-glycosylated proteins (Buscaglia et al., 2006). These molecules are present in parasites, viruses and fungi and include mucin-like regions (Herpes virus), mucin-like domains (Ebola virus and *Toxoplasma Gondii*), mucin-like glycoproteins (*Cryptosporidium parvum*), mucin-associated surface proteins MASPs (*Trypanosoma cruzi*), and mucin-type proteins (*Candida albicans*), among others. In this review, we use the term mucin-like molecules (MLMs) to denote all these molecules.

Mucins and MLMs share, as a structural feature, the presence of a dense array of O-linked oligosaccharides attached to serine or threonine residues of the protein. These glycans form a cover acting as a shield for protection and interaction with receptors (Buscaglia et al., 2006). A human mucin barrier protects the mucosal membranes and takes part in cellular regeneration, differentiation, signaling, adhesion, immune response, and tumor progression (Kufe, 2009; Senapati et al., 2010). Mucins and MLMs of protozoa, viruses and fungi protect these pathogens from the vector and vertebrate-host defense mechanisms and can have a critical role in targeting, attachment and invasion of specific host cells and tissues (Buscaglia et al., 2006; Lee and Saphire, 2009).

Comprehensive reviews about the structure, properties, role in cancer, and other aspects of mucins (Corfield, 2017; van Putten and Strijbis, 2017; Bansil and Turner, 2018; Dhanisha et al., 2018; Wagner et al., 2018; Kasprzak and Adamek, 2019) prompt us to cover these aspects only briefly by providing an overview of mucins and their comparison with MLMs. We will focus in the distribution, role in diseases and chemical structure of human mucins and pathogenic MLMs and review the role of these molecules as immunomodulators and their potential use in the diagnosis and prevention of diseases. Finally, we summarize the strategies required to obtain these complex molecules.

Human Mucins

Mucus is a complex dilute aqueous viscoelastic secretion containing water, electrolytes, lipids, and proteins (Bansil and Turner, 2018). It is abundantly present in the epithelium of the gastrointestinal, respiratory and reproductive tracts and the secretory epithelial surfaces of liver, pancreas, gallbladder, kidney, and eyes, as well as in salivary and lacrimal glands. Mucus has diverse functions attributed to its primary structural component, mucins, which are present at concentrations between 1 and 5% (Rachagani et al., 2009; Corfield, 2015; Bansil and Turner, 2018). Mucins are expressed by epithelial cells (including endothelial cells), specialized epithelial cells known as goblet cells, leukocytes, and glands of the gastrointestinal tract (Tarp and Clausen, 2008; Rachagani et al., 2009; Dhanisha et al., 2018; Kasprzak and Adamek, 2019). They are present in the ocular surface and ear epithelium (Dhanisha et al., 2018) and cover the epithelial cell surfaces of the respiratory, digestive, and urogenital tracts forming gel-like structures (Johansson et al., 2008, 2014). Mucins form a protective barrier on the cell membrane and participate in regulation of solute transport, and as receptors for commensal and pathogenic microbes and for leukocyte targeting (Pelaseyed et al., 2014; Birchenough et al., 2015). Mucins are also associated with cellular regeneration, differentiation, integration, signaling, adhesion, and apoptosis (Bergstrom and Xia, 2013; Pelaseyed et al., 2014; Corfield, 2017; Kasprzak and Adamek, 2019).

Human mucins are encoded by 22 genes, designated MUC1 to MUC22, have a variable expression among tissues and display in the gastrointestinal tract the highest level and diversity (Behera et al., 2015). Mucins have a complex molecular organization and are classified into secreted and membrane bounded (transmembrane-) mucins considering their structure and localization (Kufe, 2009; Rachagani et al., 2009; Lang et al., 2016; Dhanisha et al., 2018). Secreted mucins form an extracellularly protective layer over the organs working as a barrier against external pathogens (Dhanisha et al., 2018). They can be gel-forming mucins (MUC 2, 5AC, 5B, 6, 19) or non-gel forming mucins (MUC 7, 8). MUC1, 3A, 3B, 4, 12, 13, 15, 16, 17, 18, 20, and 21 have a transmembrane domain attaching the glycoprotein to the membrane. Besides protection, they have a role in signaling, monitoring and repairing damaged epithelia (Martínez-Sáez et al., 2017; van Putten and Strijbis, 2017; Bansil and Turner, 2018; Dhanisha et al., 2018). Three mucins remain unclassified, the oviductal glycoprotein 1 (MUC9), endomucin MUC14 and MUC22 (Wagner et al., 2018).

Mucins contain variable glycosylated tandem repeat domains rich in proline (Pro), threonine (Thr) and/or serine (Ser) (PTS domains), and cysteine-rich regions localized at the amino and carboxy terminus and interspersed between the PTS domains (Bansil and Turner, 2018). The apomucin, or protein core, and the oligosaccharides are different among mucins (Corfield, 2015). An altered expression, up or down regulation, qualitative disturbances in glycosylation, changes in protein sequence, and in the structure of the glycans are generally associated with diseases, i.e., cancer (Brockhausen, 2003; Sheng et al., 2012; Nath and Mukherjee, 2014; Kasprzak and Adamek, 2019).

The expression of mucins was initially associated with epithelial tissues and later on with the immune system. This was particularly valid to MUC1 expressed by T and B cells (Agrawal et al., 1998; Chang et al., 2000; Treon et al., 2000; Correa et al., 2003; Fremd et al., 2016), MUC15 is expressed in adult human spleen, thymus, peripheral blood leukocyte, bone marrow, and lymph node (Pallesen et al., 2008), and MUC21 is expressed in thymus (Itoh et al., 2007). However, some mucins are found in other organs with certain specificity. Examples of these mucins are MUC14, a membrane bound mucin highly expressed in vascular tissues (dela Paz and D'Amore, 2009; Zuercher et al., 2012); MUC9, a non-gel-forming mucin, that is secreted by oviductal epithelial cells of the female reproductive tract (Slayden et al., 2018); and MUC3A and MUC3B have only been detected in the gastrointestinal tract and ear (Pratt et al., 2000; Sheng et al., 2012; Dhanisha et al., 2018; Kasprzak and Adamek, 2019). Other mucins genes such as MUC10 and MUC11 have not been identified in humans (Dhanisha et al., 2018). Detailed information about the distribution of human mucins has previously been reviewed (Behera et al., 2015; Dhanisha et al., 2018).

Membrane and secreted mucins have a high molecular weight (>200 kDa) and are composed of a long peptide chain with multiple O-linked glycans that correspond to more than 50% (w/w) of the glycoprotein. In mammals, the glycans are attached to the side chain of the serine or threonine via a N-acetylgalactosamine (GalNAc) that can be further elongated into different structures. The protein core is organized into two broadly distinct regions: a central region rich in Pro, Ser, and Thr residues containing multiple O-glycosylation and the carboxy- and amino-terminal non-repeat regions with low amounts of Ser/Thr and relatively few O-glycosylations. These non-repeat regions are generally rich in cysteine and contain N-glycans involved in the folding, oligomerization, and surface location

of the proteins (Linden et al., 2008; Jonckheere et al., 2013; Martínez-Sáez et al., 2017; Bansil and Turner, 2018).

The structure of the O-glycans present in human mucins comprises three main parts: the GalNAc linked to the protein; a backbone or extension part corresponding to an elongation of the GalNAc with either α-(1-3)- or β-(1-3)-linked galactose or by β-(1-6)-, β-(1-3)-, or α-(1-6)-linked N-acetylglucosamine; and a high variable peripheral part containing fucose and N-acetyl neuraminic acid terminal units. Glycan structures are summarized in **Figure 1** and by Corfield (2015).

Human mucin genes exhibit a specific domain called the variable number tandem repeat region (VNTR), encoding the tandem repeats region (TR) rich in PTS-domains and glycosylations. The presence of the PTS-domain is conserved in all mucins; however, the amino acid sequences and glycans within a mucin are identical but can vary among mucins. Secreted-gel-forming mucins have a TR with cysteine-rich regions flanked at its amino- and carboxy-terminus and interspersed between PTS domains (Bansil and Turner, 2018; Wagner et al., 2018). In addition, these mucins can also have von Willebrand-D-like-domains (VWF) flanking the amino and carboxy terminus of TR and cysteine knot (CK) at the carboxy terminus (**Figure 2**) (Ridley and Thornton, 2018). Differently, secreted non-gel-forming mucins only contain PTS and histamine-like domains. Membrane-bound-mucins have a common structure containing TRs, a transmembrane and a cytoplasmic tail domain (Xu et al., 2016; van Putten and Strijbis, 2017). Most of these mucins also contain Epidermal Growth Factor-like (EGF) and Sea Urchin Sperm Protein, Enterokinase, and Agrin (SEA) domains (Johansson et al., 2013; Jonckheere et al., 2013).

Pathogenic Mucins

MLMs have been identified in the parasites *Trypanosoma cruzi* (Di Noia et al., 2002), *Leishmania* (Ilg et al., 1999), *Toxoplasma gondii* (Tomita et al., 2018), *Cryptosporidium parvum* (Bhalchandra et al., 2013), and *Fasciola hepatica* (Noya et al., 2016). They are also present on the surface of the Ebola Virus (Lee et al., 2008), Herpes Simplex Virus (Altgärde et al., 2015) and in fungi, i.e., in *Candida albicans* (Altgärde et al., 2015). MLMs and mucins have similar functions acting as barrier to protect the membrane of the expressing cells (Buscaglia et al., 2006; Bergstrom and Xia, 2013), mediating interaction for cell penetration (Ricketson et al., 2015) or acting as signaling receptors in cells (van Putten and Strijbis, 2017).

Similar to human mucins, MLMs have domains rich in Pro, Thr and Ser containing multiple O-glycosylations. The structure of the glycan in MLMs from many pathogens is unknown, but some differences have been reported. Characterization of protozoan MLMs and *in vitro* studies showed important variations in the glycan core and the attachment of the glycans to Ser or Thr residues in *T. cruzi* MLMs via an N-acetylglucosamine (Previato et al., 1995).

In some Leishmania MLMs, oligosaccharides are linked to proteins by a phosphodiester bond between the carbohydrate and

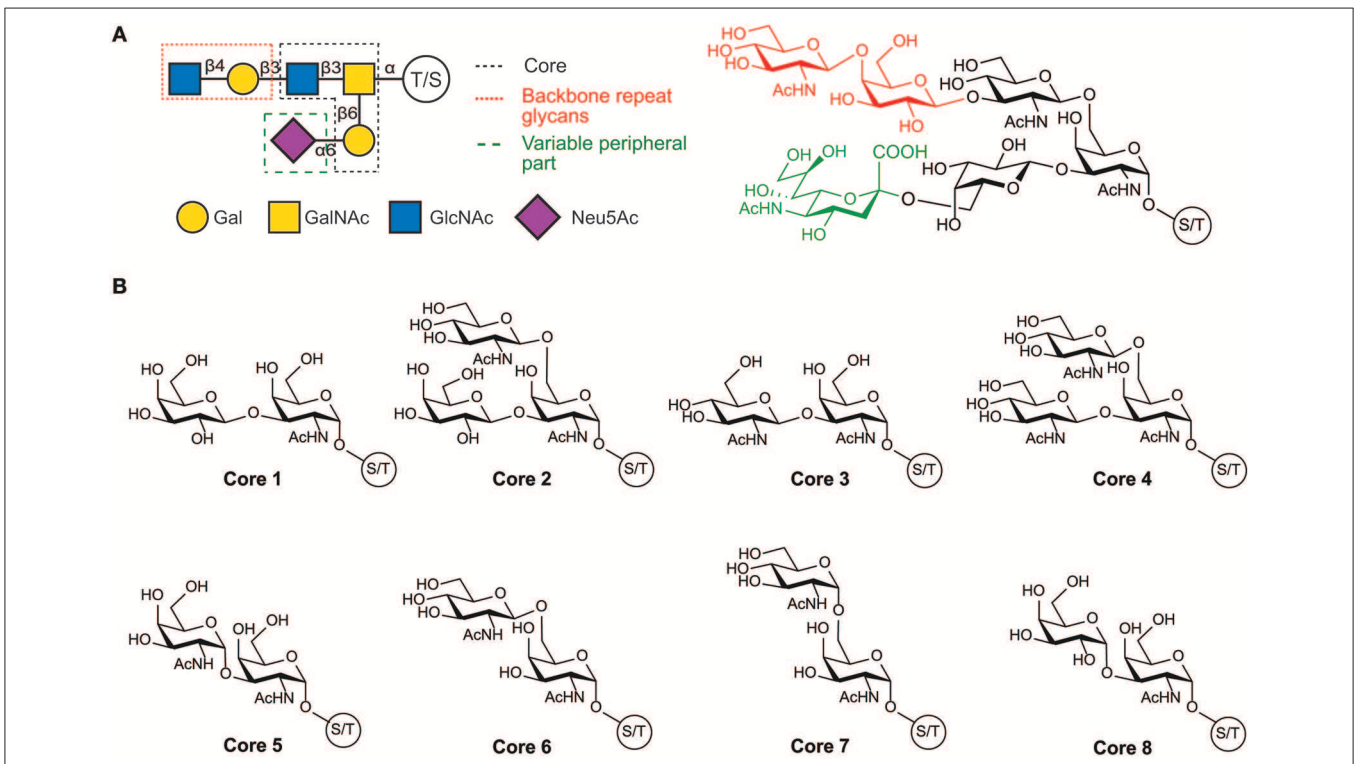

FIGURE 1 | Structure of human mucin glycans. **(A)** Schematic and chemical representation of the organization of mucins glycans, **(B)** Structure of the glycan cores present in mucins.

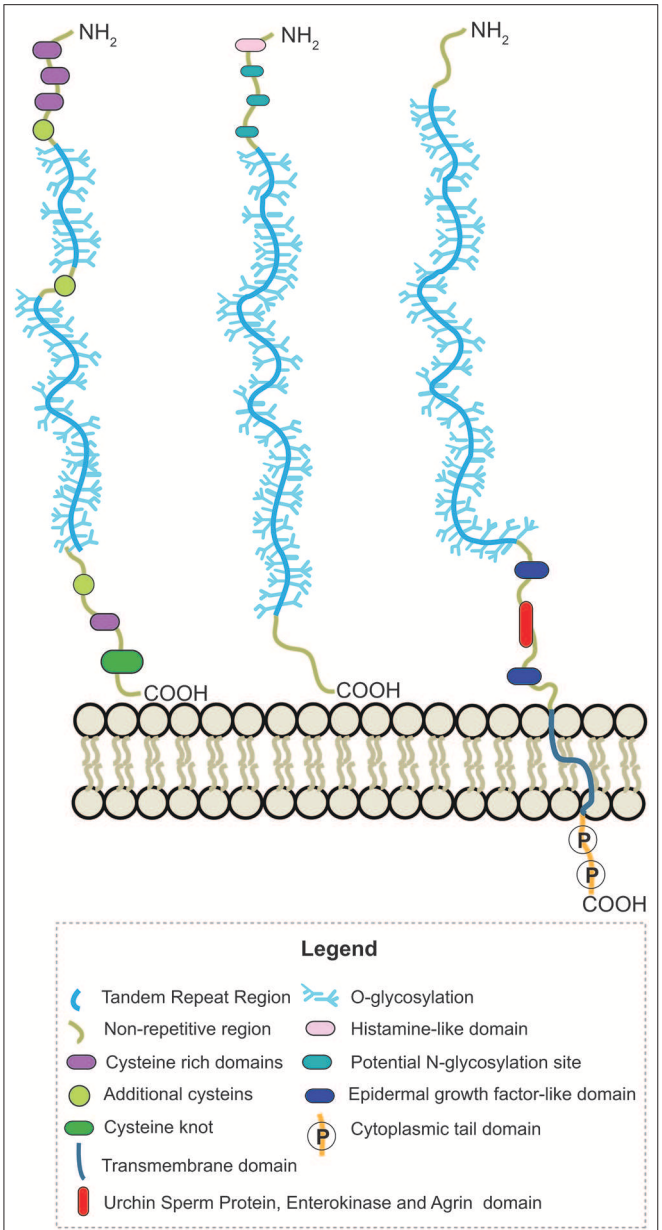

FIGURE 2 | Schematic representation of the structure from secreted-gel-forming, secreted-non-gel forming and transmembrane human mucins.

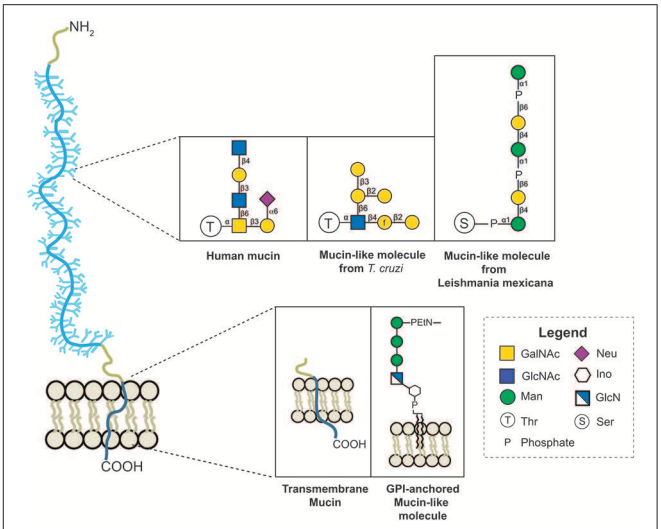

FIGURE 3 | Variation of the protein-glycan and membrane linkage and glycan structures in human mucins and protozoan MLMs.

Ser or Thr (see **Figure 3**) (Ilg et al., 1996; Ilg, 2000; Jain et al., 2001).

Besides Protozoa, trematode parasites also express MLMs that protect them from the host immune system and mediate their interaction with the host cells (Buscaglia et al., 2006; Wanyiri and Ward, 2006; Bhalchandra et al., 2013; Cancela et al., 2015). Characterization of cDNAs of proteins in *Fasciola hepatica* showed as particularities of these glycoproteins the presence of repeat Ser/Thr rich motifs with different lengths, minor amino acid variation and the absence of hydrophobic amino acids. The parasite *Cryptosporidium parvum* also express a MLM, *Cp*Clec, a type 1 transmembrane glycoprotein containing a canonical C-type lectin domain (CTDL), a signature long loop region hydrophobic core, a WIGL motif and highly O-glycosylated Ser-/Thr-rich domains (Bhalchandra et al., 2013). This composition suggests a role in attachment and invasion of host cells (Bouzid et al., 2013).

The protozoa *T. gondii* contains ML-domains in different surface related sequence proteins (SRS) that attach the parasite to the mammalian host cells and induce immune subversion during the acute infection. CST1, a key structural component of *T. gondii* cyst, is a glycoprotein conferring the sturdiness critical for persistence of bradyzoite forms (Tomita et al., 2013). CST1 contains 13 SRS domains and a stretch region with multiple Thr-rich tandem repeats that are similar to mucin-like domains observed in *C. parvum.* Recently, a similar 169 amino acid long stretch domain containing Thr-rich tandem repeats was determined in the SRS13 cyst wall protein between two SRS domains. These domains in SRS13 and CST1 cyst wall protein provide a physical barrier against proteolytic enzymes and may help to maintain the identity and hydration of the parasite (Tomita et al., 2018).

Leishmania parasites contain highly glycosylated MLMs with unique structural features, so-called proteophosphoglycans PPGs. These proteins contain phosphoglycosylation, Manα1-PO_4-Ser, as a unique linkage between protein and glycan (Ilg et al., 1994, 1996; Moss et al., 1999). PPGs are secreted in the surface of the parasite and along with the lipophosphoglycan (LPG) form a dense matrix of filaments, so called filamentous PPG (fPPG), that surround the parasites and promote Leishmaniasis (Rogers et al., 2004; Rogers, 2012). A characterization of fPPG stablished that mostly phosphoglycans are present in the filaments (~96%). However, a small amount of amino acids (~4%) is also observed, and from them more than

half of the amino acids are Ser and a large proportion of Ala or Pro. Most of the Ser residues are phosphoglycosylated (Ilg et al., 1999; Ilg, 2000).

The surface of the protozoan parasite *T. cruzi* is covered with MLMs and GPI-anchored glycoconjugates, termed mucins and mucin-associated surface proteins (MASP) (El-Sayed et al., 2005). *T. cruzi* mucins contribute to parasite protection and to establish a persistent infection (Buscaglia et al., 2006). These mucins have been extensively studied and encoded in two gene families: TcMUC encoding mucins in the mammalian stage and TcSMUG encoding mucins in the insect stages (Di Noia et al., 1998; Pech-Canul et al., 2017). These mucins share a common structure with three domains: a N-terminal SP, a central region showing high content (60–80%) of Thr, Ser, Pro, Gly, and Ala residues and a C-terminal signal for glycosylphosphatidylinositol (GPI) anchoring. The central region, present in the mature form of the proteins, bears multiple O-glycosylation sites and in some cases, a few (1-3) *N*-glycans (Cánepa et al., 2012b).

Early reports describing particular features of MLMs glycans derived from *T. cruzi* determined the linkage of glycans to threonine or serine *via* N-acetylglucosamine (Previato et al., 1994), and the abundance of GPI-anchored mucins in trypomastigotes (tGPI) containing glycans with terminal, non-reducing α-galactose (α-Gal) residues (Almeida et al., 1991). This α-Gal is part of the highly immunogenic epitope Galα(1,3)Galβ(1,4)GlcNAcα present on a mucin-like GPI-anchored glycoprotein present in sera of patients with chronic Chagas' disease that is recognized by anti-α-Gal antibodies (Almeida et al., 1993). This glycoprotein has a high carbohydrate content (60%), substantial amounts of Thr, Ser, Glu, Gly, Ala, Pro, *myo*-inositol, ethanolamine, and 1-O-hexadecylglycerol (Almeida et al., 1994).

Besides morphological variations in the life cycle of *T. cruzi*, there are important changes in the structure of glycolipids, GPIs attaching MLMs and carbohydrates characterizing the different stages of the parasite (de Lederkremer and Agusti, 2009). These changes include, among others, a higher content of GIPLs in epimastigotes than in trypomastigotes (Golgher et al., 1993; Pereira-Chioccola et al., 2000) and a change in the lipid part of GPILs from epismatigotes during the exponential and stationary growth phases from 1-*O*-hexadecyl-2-*O*-hexadecanoylglycerol to ceramide (de Lederkremer et al., 1993). Variations on the GPIs attaching MLMs include the lack of galactofuranose (Gal*f*) in the GPI-glycan of epimastigotes and trypomastigotes and a lipid change in trypomastigotes, which contain an alkylacylglycerol having mainly oleic and linoleic acid (Acosta Serrano et al., 1995; Previato et al., 1995; Almeida et al., 2000).

The first O-glycan characterized from *T. cruzi* MLMs showed oligosaccharide chains containing between three and six monosaccharide units that are conserved between *epimastigotes* and metacyclic *trypomastigotes* (Acosta Serrano et al., 1995). However, binding of anti-glycan antibodies showed the presence of the αGal(1,3)Gal epitope only in mucins from mammals, indicating a difference in mucins' glycosylation between mammals and insects (Almeida et al., 1994). In addition, there is polymorphism among the strains, the main difference being the presence of galactofuranose in glycans of the strains belonging to lineage I which includes G, Colombiana, and tulahuen (**Figure 4**) (Previato et al., 1994, 1995; Agrellos et al., 2003; Jones et al., 2004; Todeschini et al., 2009). Of particular interest is the *O*-glycans from mucins of *T. cruzi* from the Colombiana strain, due to the resistance of this strain to drugs used in Chagas' disease treatment. This strain, similar to the G-strain, presents a β-galactofuranose residue attached to N-acetylglucosamine (Todeschini et al., 2009). Additional glycosylated antigens described in *T. cruzi* may include a small surface antigen expressed in *trypomastigotes* (TSSA), which provides the first immunological marker to allow discrimination between lineages (Di Noia et al., 2002). Sequence analysis of TSSA showed high content of Ser and Thr residues in the protein backbone and multiple signals for putative O-glycosylation, suggesting that the gene encodes for a *T.cruzi* MLM (Di Noia et al., 2002). Further studies showed that TSSA play a role in host immune evasion, in maintaining the infection (Buscaglia et al., 2006) and in T. *cruzi* infectivity (Cánepa et al., 2012a). Contrary to initial studies suggesting that TSSA is glycosylated (Di Noia et al., 2002), a recent report described TSSA as a hypo-glycosylated molecule (Camara et al., 2017). Therefore, further research is still required to fully elucidate the TSSA structure and the presence of glycans.

An important group of MLMs are the viral mucin-like regions (MLRs). They are pathogenic factors in the Ebola virus (EBOV), Herpes Simplex Virus (HSV), Margburg virus (MARV), Crimean-Congo hemorrhagic fever virus (CCHFV), and human respiratory syncytial virus (hRSV) (Wertheim and Worobey, 2009). These regions should stretch the proteins to enhance their availability for binding, protecting the protein against proteolytic degradation, and acting as modulators of the host immune response (Wertheim and Worobey, 2009). EBOV has an envelope of glycoproteins that are crucial factors in determining virulence, including the MLR, called GP1. This highly glycosylated motif has N- and O-glycans (Kiley, 1988; Groseth et al., 2012) and has a similar structure to the HSV MLR (Altgärde et al., 2015). GP1 is essential for the infectivity of Zaire Ebola virus (ZEBOV) (Yang et al., 2000), and for the attachment of EBOV to host cells *via* interaction with surface lectins of hepatocytes, dendritic cells, macrophages, and endothelial cells (Fujihira et al., 2018). In HSV infections, a similar region from the gC glycoprotein balances the interaction and facilitate the attachment of viral particles to cells allowing an efficient release of viral progeny from the surface of infected cells (Altgärde et al., 2015).

MLMS are also present in fungi, with the Msb2 glycoprotein of *Candida albicans* as a main example. This high molecular weight and heavily glycosylated transmembrane protein is a sensor protein that takes part in the biosynthesis of the cell wall and in the invasion of solid surfaces (Whiteway and Oberholzer, 2004; Román et al., 2009; Szafranski-Schneider et al., 2012; Puri et al., 2015). Msb2 also protects *C. albicans* against antimicrobial peptides and can release its extracellular domain through a proteolytic cleavage generating a mucous layer to protect the cell. This protein is considered a functional analog of mammalian MUC1/MUC2 (Szafranski-Schneider et al., 2012).

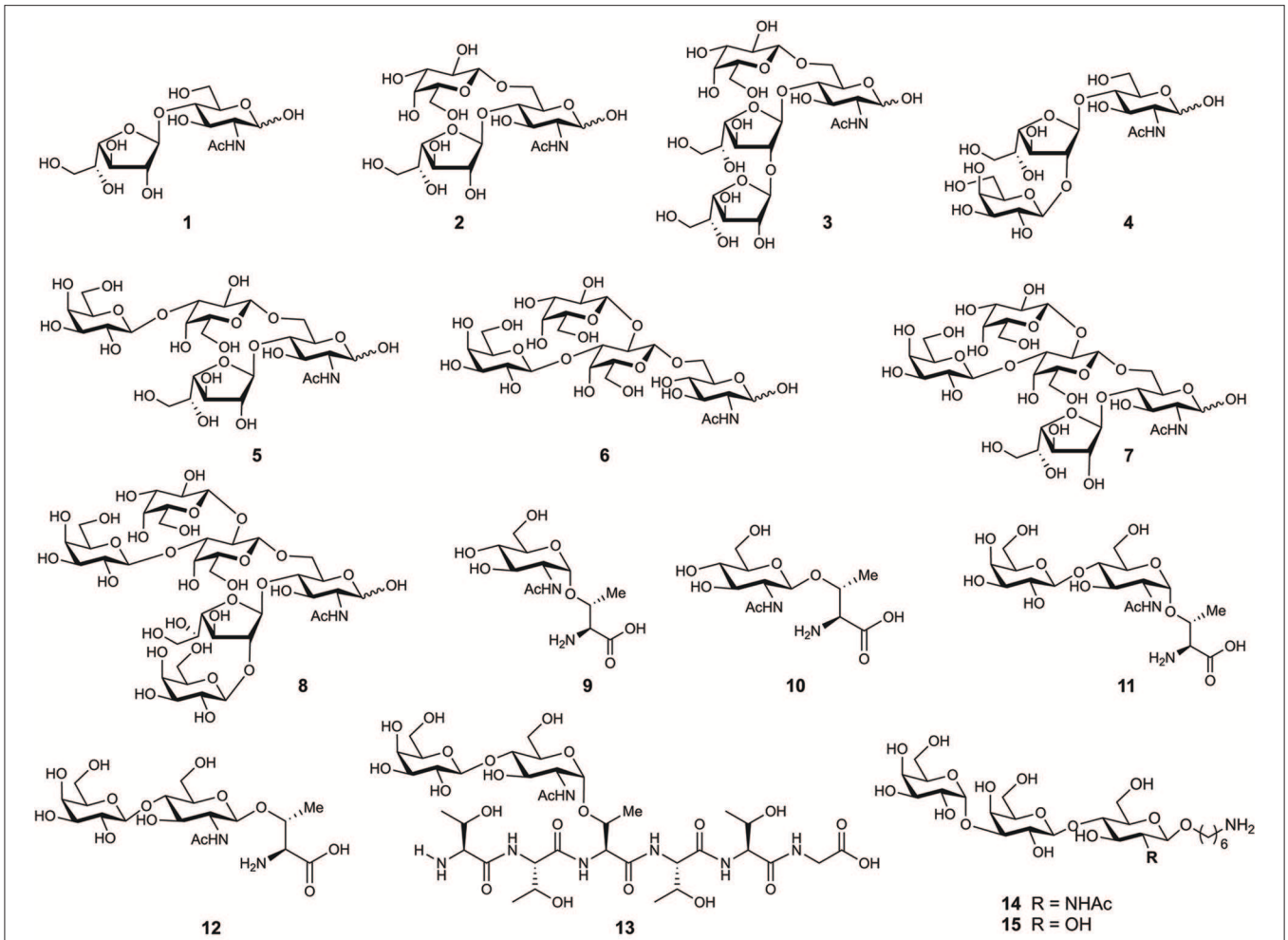

FIGURE 4 | Chemical structure of synthesized glycans from MLMs of *Trypanosoma cruzi* Colombiana strain (**1**–**8**) and Y strain (**9**–**13**).

MUCINS, MLMS, AND DISEASES

Modifications in mucins are strongly associated with diseases, susceptibility to pathogens, and the diagnosis and prognosis of cancer (Kasprzak and Adamek, 2019). An altered expression, up or down regulation of mucins, disturbances in glycosylation, and changes in the protein structure of mucins occur in many types of cancer (Rachagani et al., 2009; Hasnain et al., 2013; Nath and Mukherjee, 2014), inflammatory bowel disease, ocular surface diseases, and ulcerative colitis, among others (Dhanisha et al., 2018). Similarly, modification of MLMs protect pathogens from host proteases and recognition by the immune system, contributing to several infections (Ricketson et al., 2015; Noya et al., 2016; van Putten and Strijbis, 2017).

Cancer is a major global public health problem (Siegel et al., 2019) and its burden rose to 18.1 million new cases and 9.6 million cancer deaths in 2018 (Bray et al., 2018). In recent years, correlation studies showed an association between mucin overexpression and glycosylation with cancer formation, prognosis, and metastasis (Behera et al., 2015). MUC 1, 2, 3, 5AC, 5B, 8, 16, and 21 are related, to a different degree, in breast (Masaki et al., 1999), ovarian (Yin and Lloyd, 2001; Wang and El-Bahrawy, 2015), endometrial tumors (Hebbar et al., 2005), prostate (Xiong et al., 2006), pancreatic (Levi et al., 2004), gastric and cervical (Kaur et al., 2013), colorectal (Chang et al., 1994), renal cell carcinoma (Leroy et al., 2002), pseudoxyoma periotonei (Ciriza et al., 2000), and recently studied lung cancer (Yoshimoto et al., 2019). There are multiple recent reviews about the role on mucins and cancer for further reading (Chugh et al., 2015; Dhanisha et al., 2018; Kasprzak and Adamek, 2019).

In addition to cancer, mucins are also involved in other human diseases that commonly affect populations like asthma and otitis. Mucins 2, 5AC, 5B, and 6 are associated with diseases in epithelial tissue such as cystic fibrosis (Li et al., 1997; Puchelle et al., 2002; Thornton et al., 2008), MUC 3, 4, and 5AC in cap polyposis (Buisine et al., 1998), MUC19 in Sjörgen syndrome (Yu et al., 2008), and MUC 5B in diffuse panbronchiolitis (Kamio et al., 2005). Specific conditions in the eye and ear are also associated with mucins. Ethmoid chronic sinusitis is associated with MUC 4, 5AC, 5B, 7, and 8 (Jung et al., 2000), asthma with MUC 5AC

and 7 (Watson et al., 2009) and chronic otitis media with MUC 4, 5AC, and 5B (Moon et al., 2000; Lin et al., 2001). Particular changes in mucins in diseases have been reported (Behera et al., 2015; van Putten and Strijbis, 2017; Kasprzak and Adamek, 2019).

In contrast to human mucins, little is known about the role of MLMs in infections. MLMs protect the pathogens (Puri et al., 2015) and ensure the targeting and invasion of specific cells or tissues (Buscaglia et al., 2006). Human secreted gel-forming mucins coat and protect mucosal surfaces from chemical, enzymatic, and mechanical damages (Portal et al., 2017) and from penetration and pathogen invasion. MLMs from pathogens may have similar functions; however, more studies are necessary to determine the mechanisms involving these molecules in pathogen protection from the host defense and in the degradation of protective mucus gels of the host.

Changes in sialylation levels in glycolipids and glycoproteins are a hallmark of human diseases (Amon et al., 2014). Nonetheless, this modification of glycans is also used by pathogens to improve their survival and pathogenicity. *T. cruzi* uses sialylation of proteins to avoid lysis by serum factors and to enhance the interaction with the host cells (Tomlinson et al., 1994). The parasites do not synthesize sialic acid (Jain et al., 2001), however, the mucins of the parasite membrane are acceptors for sialic acid that is transferred from the host proteins using trans-sialidases (Giorgi and de Lederkremer, 2011). Sialylation may also reduce the susceptibility of the parasite to anti-α-Gal antibodies present in the mammalian bloodstream (Pereira-Chioccola et al., 2000), allowing colonization and infection. Recently, *T. cruzi* mucins were also associated with parasite attachment to the internal cuticle of the triatomine rectal ampoule, a critical step leading to *T. cruzi* differentiation into infective forms to mammalian host cells (Cámara et al., 2019).

Proteophosphoglycans (PPG) from Leishmania parasites have different roles during infection. They contribute to binding of *Leishmania major* promastigotes and the survival of the parasites within the macrophages (Piani et al., 1999). Secreted PPG of *Leishmania mexicana* amastigotes activates the complement system binding to serum mannan-binding proteins, reducing hemolytic activity of normal serum and preventing the opsonization of amastigotes (Peters et al., 1997). *Cryptosporidium parvum* employs the CpMuc4 and CpMuc5 ML-proteins for attachment and invasion of intestinal epithelial cells (Connor et al., 2009). Similarly, highly polymorphic ML-proteins from *Schistosma mansoni* are key factors for the compatibility and interaction of schistosomes with the snail host (Roger et al., 2008).

Recent studies of the mucin-like regions in EBOV and HSV revealed their role in infection. A mouse study of EBOV's mucin-like glycoprotein (Emuc) in virus pathogenesis showed Emuc as a pathogenic factor of EBOV; it causes acute inflammation and tissue injury. In mouse muscle, Emuc induced cell death, and this tissue lesion could be directly mediated by the cytotoxicity of Emuc (Ning et al., 2018). Similarly, the MLR at the N-terminus of HSV-1 surface glycoprotein modulates the HSV-glycosaminoglycan interactions and regulate the affinity, type, and number of glycoproteins involved in the interaction and in the attachment and release of the virus (Delguste et al., 2019).

Many parasitic and viral infections that use MLMs during the infection are life-long, debilitating, and life-threatening diseases (Steverding, 2014; Malvy et al., 2019) with a substantial epidemic potential and need for further research (Malvy et al., 2019). Mucins and MLMs are becoming important markers for diagnostics and targets for drug and vaccine design. MUC1-based structures are used as targets for cancer immunotherapy (Martínez-Sáez et al., 2017) and antibodies against ML-proteins are employed to discriminate *T. cruzi* lineages and to diagnose Chagas disease (Bhattacharyya et al., 2014). However, mucins and MLMs research is still limited by access to pure materials and a poor understanding of the function of these molecules in diseases.

PRODUCTION OF MUCINS AND MUCIN-LIKE MOLECULES AND THEIR USE AS IMMUNOMODULATORS

The physicochemical and biological properties of mucins render them interesting biomarkers for tumor diagnosis (Pett et al., 2017) and models for the production of new biomaterials (Petrou and Crouzier, 2018).

Recombinant protein expression enables the evaluation of mucin structures and their biological role. Human MUC2 structures have been studied using the expression of the C- and N-terminal parts as a recombinant tagged protein in Chinese hamster ovary cells (CHO-K1 cells) (Godl et al., 2002; Lidell et al., 2003). Similarly, the expression of the C-terminal cysteine-rich part of the human MUC5AC mucin in CHO-K1 and a structural analysis, showed that MUC2 and MUC5AC share the sequence (Gly-Asp-Pro-His) for the site of cleavage situated in the GDPH sequence found in the von Wildebrad D4 domain (Lidell and Hansson, 2006). These facts guarantees further progress to study the role of these mucins in human mucus.

To evaluate the role of MUC6 in gastrointestinal cancer; MUC6 was expressed in COS-7, PANC-1, LS 180, and MCF7 cell lines and used in cell invasion and adhesion studies. MUC6 may inhibit tumor cell invasion and slow the development of infiltrating carcinoma (Leir and Harris, 2011). Similarly, the role of MUC5B in pancreatic cancer and respiratory epithelia was assessed by cloning and expression using a mammalian episomal expression vector pCEP-His in 293-EBNA and human lung carcinoma cells (A549) (Ridley et al., 2014). A truncated MUC5AC was employed to assess the interaction of *Helicobacter pylori* with the gastric epithelia using AGS cells. The production of recombinant mucins with diverse structures in different cells is a novel platform to analyze mucin biosynthesis, secretion and functions (Dunne et al., 2017). More recently, larger-scale biomanufacturing of human mucins utilized a codon-scrambling strategy to generate synonymous genes of two mucins of commercial interest in Freestyle 293-F cells. Methods for cDNA design and mucin production in mammalian host production systems were established (Shurer et al., 2019).

The heterogeneity and difficult characterization of isolated glycoproteins together with the need for homogeneous material for drug and vaccine design prompted the chemical synthesis of

mucin and MLM related structures. Synthetic antigens induce a strong immune response for diagnostic and vaccine purposes. Mucin glycans from Type-1 core (Pett and Westerlind, 2014) and Type-2 core (Pett et al., 2013) and the combination of synthetic glycans with peptide synthesis by Fmoc-SPPS to obtain core mucin glycopeptides have been reported (Pett et al., 2013; Pett and Westerlind, 2014).

Synthetic tumor-associated mucin glycopeptides have been intensely studied as potential cancer vaccines over the past decade. Cancer cells can be distinguished from normal cells by overexpression of molecular markers on the membrane. Thus, some Tumor-associated carbohydrate antigens (TACAs) are promising targets for the design of anticancer vaccines (Wilson and Danishefsky, 2013; Feng et al., 2016). The MUC1 glycopeptide, which is aberrantly glycosylated and overexpressed in a variety of epithelial cancer has received much attention. MUC1 and Tumor-associated MUC1 are important antigens for tumor vaccines design (Wilson and Danishefsky, 2013) and the induction of MUC1-specific humoral and cellular responses (Martínez-Sáez et al., 2017). High antibody titers were observed for mono- and di-glycosylated glycopeptide vaccine candidates, with sialyl-T_N and T_N antigens from MUC1 tandem repeats connected to OVA T-cell peptide epitope (Westerlind et al., 2008, 2009). A TA-MUC1 Sialyl-T_N glycopeptide (Kaiser et al., 2009) and a fluorinated-substituent analog bearing the Thomsen-Friedenreich antigen also showed a strong and highly specific immune response in mice (Hoffmann-Röder et al., 2010). Recently, a synthetic cancer vaccine candidate consisting of a MUC1 glycopeptide and B-cell epitope was used to break the self-tolerance of the immune system. The glycopeptides were combined with tetanus toxoid as the immune-stimulating carrier to obtain high IgG antibodies titers. A monoclonal antibody generated from the immunization, exclusively bound to tumor-associated MUC1, allowing for the discrimination of human pancreatic cancer (Palitzsch et al., 2016).

Determining the structure of mucin derivatives is important to design specific antigens. Some recent studies in this field include the analysis of the structure of Ser and Thr-linked glycopeptides at an atomic level using X-ray, showing that there is no equivalence of O-glycosylation in Ser and Thr during molecular recognition processes (Martínez-Sáez et al., 2015). A revision of the specificity of cancer-related monoclonal antibodies and a combination of microarray screening and saturation transfer difference STD-NMR also supported the notion that there is specificity for the amino acid (Ser or Thr) in the recognition process (Coelho et al., 2015). Other studies showed that besides the role of the amino acid, the glycosylation in MUC1 peptide strongly affects antibody binding (Movahedin et al., 2017).

Structural studies include the evaluation of a synthetic antitumor vaccine candidate with an unnatural MUC1 α-methylserine in transgenic mice, to show the important role in presentation and dynamics of the sugar moiety displayed by the MUC1 derivative in immune recognition (Martínez-Sáez et al., 2016). In other studies, a library of more than 100 synthetic MUC1 glycopeptides was used to assess the recognition of antibodies induced by three different vaccines, and provided important insights concerning the specificity of anti-glycan antibodies for the design of antitumor vaccines (Pett et al., 2017). Synthetic antitumor vaccine candidates based on mucin glycopeptides and the rational design of cancer vaccines have been reviewed (Gaidzik et al., 2013; Martínez-Sáez et al., 2017).

One of the most studied MLMs are the glycoproteins from *T. cruzi*. The characterization of the glycans and protein core of these molecules, has served as a model to synthesize mucin-like O-glycans, peptides, glycosyl-amino acids, and glycopeptides. Initial synthesis includes the preparation of the O-linked saccharides **1**–**5** (**Figure 4**) present in *T. cruzi* Colombiana and Tulahuen strains (de Lederkremer and Agusti, 2009). The first synthetic target was disaccharide **1** (Gallo-Rodriguez et al., 1996), which is the basis of synthesizing other molecules including trisaccharides **2** (Gallo-Rodriguez et al., 1998), **3** and **4** (Mendoza et al., 2010), tetrasaccharide **5** (Gallo-Rodriguez et al., 2003), pentasaccharide **6** (Mendoza et al., 2006), and hexasaccharide **7** (Agusti et al., 2015). Further reports include the synthesis of glycan **8** from the *T. cru*zi Y strain (**Figure 4**) (van Well et al., 2008). Glycosyl amino acids **9** and **10** and disaccharides glycosides **11** and **12** derived from the *T. cruzi* Y strain were synthesized to study the mucins as substrates for *trans*-sialidase activities; i.e., a chemoenzymatic reaction on the glycosyl amino acid **9** was used to obtain the glycopeptide **13**. These studies delivered information about the relaxed acceptor substrate specificity of the *T. cruzi trans*-sialidase, which is important to understand the role of this enzyme during *T. cruzi* infections (Campo et al., 2007).

Further derivatives from *T. cruzi* ML-proteins can be used to discriminate Chagas disease infection for proper diagnostics and treatment. Seven lineage-specific peptides based on the *T. cruzi* trypomastigote small surface antigen (TSSA) with a N-terminal biotinylation, PEG spacer, Gly, and the terminal Cys were synthesized. Analysis of these epitopes showed the potential of synthetic peptides to provide *T. cruzi* antigens and to confirm the disparate geographical distribution in some samples. However, peptides alone were not sufficient to discriminate the strains. But new glycan and glycopeptide epitopes may provide new clinical biomarkers for the prognosis of Chagas disease (Bhattacharyya et al., 2014).

The use of recombinant TSSA and peptides derived from this antigen as a serological marker has been evaluated. Studies done in the last 10 years show detection of specific antibodies in human sera for the diagnosis of Chagas disease (De Marchi et al., 2011), mapping of the antigenic structure, validation of its use as a novel tool for Chagas' disease diagnosis (Balouz et al., 2015), and evaluation of TSSA as an early serological marker of drug efficacy in *T cruzi*-infected children (Balouz et al., 2017). These studies have shown that TSSA is useful as a marker for diagnosis and assessment of treatment efficiency, exhibiting improved sensitivity and specificity.

The interest in antigens from *T. cruzi* MLMs as markers for diagnostics and the development of vaccines has increased over the last years. Recent studies used the trisaccharide derivative **14** containing the immunodominant tGPI-mucin α-Gal epitope from *T. cruzi* to obtain a glycoconjugate with human serum

albumin (HSA) as a carrier protein. Mice with an α1,3-galactosyltransferase-knockout, a mouse model for acute Chagas Disease, were immunized with this glycoconjugate and were fully protected from a lethal *T. cruzi* infection (Portillo et al., 2019). Similarly, a conjugate containing the synthetic trisaccharide **15** and BSA was recently introduced as a potential marker for the detection of Chagas disease using serum samples of *T. cruzi*-infected patients (Lopez et al., 2019). Despite these promising results, an effective vaccine against *T. cruzi* infections and a gold standard method for Chagas disease diagnosis are still needed.

CONCLUSION AND PERSPECTIVES

Mucin and mucin-like molecules are important markers and targets for diagnostics and the prognosis of worldwide impact, lifelong, life-threatening, or even potential epidemic diseases such as cancer, Chagas disease, and Ebola Virus infections. There is a link between human mucins, pathogenic mucin-like molecules and their expression in multiple diseases. Changes in mucin and MLM glycosylation is an important factor that modulates molecular recognition by the immune system, differentiation of healthy tumor tissues, and can facilitate infections by pathogens. However, further research is necessary to establish the mechanisms of glycan modifications and other effects of these modifications in the structure and interactions of the glycoproteins.

Diverse challenges remain in using mucin- and MLMs in diagnosis, mucin-based vaccine designs, and the production of mucin-based materials. New strategies for the production of mucins and MLMs through chemical synthesis or expression systems are needed as methods to determine the properties of these molecules. It is also necessary to find methods for easy determination, characterization, and quantification of mucin glycosylation in normal and abnormal tissues. We require further analysis of mucin like molecules from pathogens to understand the interaction of these molecules with human receptors, and to determine how MLMs support the evasion of pathogens from the immune system. In addition, future research should also include the synthesis of new epitopes to provide new clinical biomarkers for diagnostics and the development of new antigens for the design of cancer vaccines.

AUTHOR CONTRIBUTIONS

SP and DV wrote the review. DV and PS revised the manuscript.

FUNDING

This work was supported by the Max Planck Society and the RIKEN-Max Planck Joint Center for Systems Chemical Biology.

ACKNOWLEDGMENTS

We thank the Max-Planck-Society and the RIKEN-Max-Planck Joint Research Center for Systems Chemical Biology for financial support.

REFERENCES

Acosta Serrano, A., Schenkman, S., Yoshida, N., Mehlert, A., Richardson, J. M., and Ferguson, M. A. (1995). The lipid structure of the glycosylphosphatidylinositol-anchored mucin-like sialic acid acceptors of *Trypanosoma cruzi* changes during parasite differentiation from epimastigotes to infective metacyclic trypomastigote forms. *J. Biol. Chem.* 270, 27244–27253. doi: 10.1074/jbc.270.45.27244

Agrawal, B., Krantz, M. J., Parker, J., and Longenecker, B. M. (1998). Expression of MUC1 mucin on activated human T cells: implications for a role of MUC1 in normal immune regulation. *Cancer Res.* 58, 4079–4081.

Agrellos, O. A., Jones, C., Todeschini, A. R., Previato, J. O., and Mendonca-Previato, L. (2003). A novel sialylated and galactofuranose-containing O-linked glycan, Neu5Ac-alpha-(2-3)-Galp-beta-(1-6)-(Galf-beta-(1-4)GlcNAc, is expressed on the sialoglycoprotein of *Trypanosoma cruzi* Dm28c. *Mol. Biochem. Parasitol.* 126, 93–96. doi: 10.1016/S0166-6851(02)00245-1

Agusti, R., Giorgi, M. E., Mendoza, V. M., Kashiwagi, G. A., de Lederkremer, R. M., and Gallo-Rodriguez, C. (2015). Synthesis of the O-linked hexasaccharide containing beta-D-Galp-(1-2)-D-Galf in *Trypanosoma cruzi* mucins. Differences on sialylation by trans-sialidase of the two constituent hexasaccharides. *Bioorg. Med. Chem.* 23, 1213–1222. doi: 10.1016/j.bmc.2015.01.056

Almeida, I. C., Camargo, M. M., Procopio, D. O., Silva, L. S., Mehlert, A., Travassos, L. R., et al. (2000). Highly purified glycosylphosphatidylinositols from *Trypanosoma cruzi* are potent proinflammatory agents. *EMBO J.* 19, 1476–1485. doi: 10.1093/emboj/19.7.1476

Almeida, I. C., Ferguson, M. A., Schenkman, S., and Travassos, L. R. (1994). Lytic anti-alpha-galactosyl antibodies from patients with chronic Chagas' disease recognize novel O-linked oligosaccharides on mucin-like glycosyl-phosphatidylinositol-anchored glycoproteins of *Trypanosoma cruzi*. *Biochem. J.* 304(Pt 3), 793–802. doi: 10.1042/bj3040793

Almeida, I. C., Krautz, G. M., Krettli, A. U., and Travassos, L. R. (1993). Glycoconjugates of *Trypanosoma cruzi*: a 74 kD antigen of trypomastigotes specifically reacts with lytic anti-alpha-galactosyl antibodies from patients with chronic Chagas disease. *J. Clin. Lab. Anal.* 7, 307–316. doi: 10.1002/jcla.1860070603

Almeida, I. C., Milani, S. R., Gorin, P. A., and Travassos, L. R. (1991). Complement-mediated lysis of *Trypanosoma cruzi* trypomastigotes by human anti-alpha-galactosyl antibodies. *J. Immunol.* 146, 2394–2400.

Altgärde, N., Eriksson, C., Peerboom, N., Phan-Xuan, T., Moeller, S., Schnabelrauch, M., et al. (2015). Mucin-like region of Herpes Simplex virus type 1 attachment protein glycoprotein C (gC) modulates the virus-glycosaminoglycan interaction. *J. Biol. Chem.* 290, 21473–21485. doi: 10.1074/jbc.M115.637363

Amon, R., Reuven, E. M., Leviatan Ben-Arye, S., and Padler-Karavani, V. (2014). Glycans in immune recognition and response. *Carbohydr. Res.* 389, 115–122. doi: 10.1016/j.carres.2014.02.004

Balouz, V., Cámara, Mde. L. Cánepa, G. E., Carmona, S. J., Volcovich, R., Gonzalez, N., et al. (2015). Mapping antigenic motifs in the trypomastigote small surface antigen from *Trypanosoma cruzi*. *Clin. Vaccine Immunol.* 22, 304–312. doi: 10.1128/CVI.00684-14

Balouz, V., Melli, L. J., Volcovich, R., Moscatelli, G., Moroni, S., González, N., et al. (2017). The trypomastigote small surface antigen from *Trypanosoma cruzi* improves treatment evaluation and diagnosis in pediatric chagas disease. *J. Clin. Microbiol.* 55, 3444–3453. doi: 10.1128/JCM.01317-17

Bansil, R., and Turner, B. S. (2018). The biology of mucus: composition, synthesis and organization. *Adv. Drug. Deliv. Rev.* 124, 3–15. doi: 10.1016/j.addr.2017.09.023

Behera, S. K., Praharaj, A. B., Dehury, B., and Negi, S. (2015). Exploring the role and diversity of mucins in health and disease with special insight into non-communicable diseases. *Glyconconj. J.* 32, 575–613. doi: 10.1007/s10719-015-9606-6

Bergstrom, K. S. B., and Xia, L. (2013). Mucin-type O-glycans and their roles in intestinal homeostasis. *Glycobiology* 23, 1026–1037. doi: 10.1093/glycob/cwt045

Bhalchandra, S., Ludington, J., Coppens, I., and Ward, H. D. (2013). Identification and characterization of *Cryptosporidium parvum* Clec, a novel C-Type lectin domain-containing mucin-Like glycoprotein. *Infect. Immun.* 81, 3356–3365. doi: 10.1128/IAI.00436-13

Bhattacharyya, T., Falconar, A. K., Luquetti, A. O., Costales, J. A., Grijalva, M. J., Lewis, M. D., et al. (2014). Development of peptide-based lineage-specific serology for chronic chagas disease: geographical and clinical distribution of epitope recognition. *PLOS Negl. Trop. Dis.* 8:e2892. doi: 10.1371/journal.pntd.0002892

Birchenough, G. M. H., Johansson, M. E., Gustafsson, J. K., Bergström, J. H., and Hansson, G. C. (2015). New developments in goblet cell mucus secretion and function. *Mucosal Immunol.* 8:712. doi: 10.1038/mi.2015.32

Bouzid, M., Hunter, P. R., Chalmers, R. M., and Tyler, K. M. (2013). Cryptosporidium pathogenicity and virulence. *Clin. Microbiol. Rev.* 26, 115–134. doi: 10.1128/CMR.00076-12

Bray, F., Ferlay, J., Soerjomataram, I., Siegel, R. L., Torre, L. A., and Jemal, A. (2018). Global cancer statistics 2018: GLOBOCAN estimates of incidence and mortality worldwide for 36 cancers in 185 countries. *CA Cancer J. Clin.* 68, 394–424. doi: 10.3322/caac.21492

Brockhausen, I. (2003). *Glycodynamics of Mucin Biosynthesis in Gastrointestinal Tumor Cells*. Boston, MA: Springer.

Buisine, M. P., Colombel, J. F., Lecomte-Houcke, M., Gower, P., Aubert, J. P., Porchet, N., et al. (1998). Abnormal mucus in cap polyposis. *Gut* 42, 135–138. doi: 10.1136/gut.42.1.135

Buscaglia, C. A., Campo, V. A., Frasch, A. C., and Di Noia, J. M. (2006). *Trypanosoma cruzi* surface mucins: host-dependent coat diversity. *Nat. Rev. Microbiol.* 4, 229–236. doi: 10.1038/nrmicro1351

Cámara, M. L. M., Balouz, V., Centeno Cameán, C., Cori, C. R., Kashiwagi, G. A., Gil, S. A., et al. (2019). *Trypanosoma cruzi* surface mucins are involved in the attachment to the Triatoma infestans rectal ampoule. *PLOS Negl. Trop. Dis.* 13:e0007418. doi: 10.1371/journal.pntd.0007418

Camara, M. L. M., Cánepa, G. E., Lantos, A. B., Balouz, V., Yu, H., Chen, X., et al. (2017). The Trypomastigote Small Surface Antigen (TSSA) regulates *Trypanosoma cruzi* infectivity and differentiation. *PLOS Negl. Trop. Dis.* 11:e0005856. doi: 10.1371/journal.pntd.0005856

Campo, V. L., Carvalho, I., Allman, S., Davis, B. G., and Field, R. A. (2007). Chemical and chemoenzymatic synthesis of glycosyl-amino acids and glycopeptides related to *Trypanosoma cruzi* mucins. *Org. Biomol. Chem.* 5, 2645–2657. doi: 10.1039/b707772f

Cancela, M., Santos, G. B., Carmona, C., Ferreira, H. B., Tort, J. F., and Zaha, A. (2015). *Fasciola hepatica* mucin-encoding gene: expression, variability and its potential relevance in host–parasite relationship. *Parasitology* 142, 1673–1681. doi: 10.1017/S0031182015001134

Cánepa, G. E., Degese, M. S., Budu, A., Garcia, C. R. S., and Buscaglia, C. A. (2012a). Involvement of TSSA (trypomastigote small surface antigen) in *Trypanosoma cruzi* invasion of mammalian cells. *Biochem. J.* 444, 211–118. doi: 10.1042/BJ20120074

Cánepa, G. E., Mesias, A. C., Yu, H., Chen, X., and Buscaglia, C. A. (2012b). Structural features affecting trafficking, processing, and secretion of *Trypanosoma cruzi* mucins. *J. Biol. Chem.* 287, 26365–26376. doi: 10.1074/jbc.M112.354696

Chang, J.-F., Zhao, H.-L., Phillips, J., and Greenburg, G. (2000). The epithelial mucin, MUC1, is expressed on resting T lymphocytes and can function as a negative regulator of T cell activation. *Cell. Immunol.* 201, 83–88. doi: 10.1006/cimm.2000.1643

Chang, S.-K., Dohrman, A. F., Basbaum, C. B., Ho, S. B., Tsuda, T., Toribara, N. W., et al. (1994). Localization of mucin (MUC2 and MUC3) messenger RNA and peptide expression in human normal intestine and colon cancer. *Gastroenterology* 107, 28–36. doi: 10.1016/0016-5085(94)90057-4

Chugh, S., Gnanapragassam, V. S., Jain, M., Rachagani, S., Ponnusamy, M. P., and Batra, S. K. (2015). Pathobiological implications of mucin glycans in cancer: sweet poison and novel targets. *Biochim. Biophys. Acta* 1856, 211–225. doi: 10.1016/j.bbcan.2015.08.003

Ciriza, C., Valerdiz, S., Toribio, C., Dajil, S., Romero, M. J., Urquiza, O., et al. (2000). Mucinous adenocarcinoma of the appendix associated with ovarian tumors and pseudomyxoma peritonei. The difficulty in differential diagnosis. *An. Med. Interna.* 17, 540–542.

Coelho, H., Matsushita, T., Artigas, G., Hinou, H., Cañada, F. J., Lo-Man, R., et al. (2015). The quest for anticancer vaccines: deciphering the fine-epitope specificity of cancer-related monoclonal antibodies by combining microarray screening and saturation transfer difference NMR. *J. Am. Chem. Soc.* 137, 12438–12441. doi: 10.1021/jacs.5b06787

Connor, R. M., Burns, P. B., Ha-Ngoc, T., Scarpato, K., Khan, W., Kang, G., et al. (2009). Polymorphic mucin antigens CpMuc4 and CpMuc5 are integral to *Cryptosporidium parvum* infection *in vitro*. *Eukaryot. Cell* 8:461. doi: 10.1128/EC.00305-08

Corfield, A. (2017). Eukaryotic protein glycosylation: a primer for histochemists and cell biologists. *Histochem. Cell Biol.* 147, 119–147. doi: 10.1007/s00418-016-1526-4

Corfield, A. P. (2015). Mucins: a biologically relevant glycan barrier in mucosal protection. *Biochem. Biophys. Acta* 1850, 236–252. doi: 10.1016/j.bbagen.2014.05.003

Correa, I., Plunkett, T., Vlad, A., Mungul, A., Candelora-Kettel, J., Burchell, J. M., et al. (2003). Form and pattern of MUC1 expression on T cells activated *in vivo* or *in vitro* suggests a function in T-cell migration. *Immunology* 108, 32–41. doi: 10.1046/j.1365-2567.2003.01562.x

de Lederkremer, R. M., and Agusti, R. (2009). Glycobiology of *Trypanosoma cruzi*. *Adv. Carbohydr. Chem. Biochem.* 62, 311–366. doi: 10.1016/S0065-2318(09)00007-9

de Lederkremer, R. M., Lima, C. E., Ramirez, M. I., Goncalvez, M. F., and Colli, W. (1993). Hexadecylpalmitoylglycerol or ceramide is linked to similar glycophosphoinositol anchor-like structures in *Trypanosoma cruzi*. *Eur. J. Biochem.* 218, 929–936. doi: 10.1111/j.1432-1033.1993.tb18449.x

De Marchi, C. R., Di Noia, J. M., Frasch, A. C. C., Amato Neto, V., Almeida, I. C., and Buscaglia, C. A. (2011). Evaluation of a recombinant *Trypanosoma cruzi* mucin-like antigen for serodiagnosis of Chagas' disease. *Clin. Vaccine Immunol.* 18, 1850–1855. doi: 10.1128/CVI.05289-11

dela Paz, N. G., and D'Amore, P. A. (2009). Arterial versus venous endothelial cells. *Cell. Tissue Res.* 335, 5–16. doi: 10.1007/s00441-008-0706-5

Delguste, M., Peerboom, N., Le Brun, G., Trybala, E., Olofsson, S., Bergström, T., et al. (2019). Regulatory mechanisms of the mucin-like region on herpes simplex virus during cellular attachment. *ACS Chem. Biol.* 14, 534–542. doi: 10.1021/acschembio.9b00064

Dhanisha, S. S., Guruvayoorappan, C., Drishya, S., and Abeesh, P. (2018). Mucins: structural diversity, biosynthesis, its role in pathogenesis and as possible therapeutic targets. *Crit. Rev. Oncol. Hematol.* 122, 98–122. doi: 10.1016/j.critrevonc.2017.12.006

Di Noia, J. M., Buscaglia, C. A., De Marchi, C. R., Almeida, I. C., and Frasch, A. C. (2002). A *Trypanosoma cruzi* small surface molecule provides the first immunological evidence that Chagas' disease is due to a single parasite lineage. *J. Exp. Med.* 195, 401–413. doi: 10.1084/jem.20011433

Di Noia, J. M., D'Orso, I., Åslund, L., Sánchez, D. O., and Frasch, A.C.C. (1998). The *Trypanosoma cruzi* mucin family is transcribed from hundreds of genes having hypervariable regions. *J. Biol. Chem.* 273, 10843–10850. doi: 10.1074/jbc.273.18.10843

Dunne, C., McDermot, A., Anjan, K., Ryan, A., Reid, C., and Clyne, M. (2017). Use of recombinant mucin glycoprotein to assess the interaction of the gastric pathogen helicobacter pylori with the secreted human mucin MUC5AC. *Bionengineering* 4:E34. doi: 10.3390/bioengineering4020034

El-Sayed, N. M., Myler, P. J., Bartholomeu, D. C., Nilsson, D., Aggarwal, G., Tran, A.-N., et al. (2005). The genome sequence of *Trypanosoma cruzi*, etiologic agent of Chagas disease. *Science* 309, 409–415. doi: 10.1126/science.1112631

Feng, D., Shaikh, A. S., and Wang, F. (2016). Recent advance in Tumor-associated Carbohydrate Antigens (TACAs)-based antitumor vaccines. *ACS Chem. Biol.* 11, 850–863. doi: 10.1021/acschembio.6b00084

Fremd, C., Stefanovic, S., Beckhove, P., Pritsch, M., Lim, H., Wallwiener, M., et al. (2016). Mucin 1-specific B cell immune responses and their impact on overall survival in breast cancer patients. *Oncoimmunology* 5:e1057387. doi: 10.1080/2162402X.2015.1057387

Fujihira, H., Usami, K., Matsuno, K., Takeuchi, H., Denda-Nagai, K., and Furukawa, J.-,i., et al. (2018). A critical domain of ebolavirus envelope glycoprotein determines glycoform and infectivity. *Sci. Rep.* 8:5495. doi: 10.1038/s41598-018-23357-8

Gaidzik, N., Westerlind, U., and Kunz, H. (2013). The development of synthetic antitumour vaccines from mucin glycopeptide antigens. *Chem. Soc. Rev.* 42, 4421–4442. doi: 10.1039/c3cs35470a

Gallo-Rodriguez, C., Gil Libarona, M., M., Mendoza, V., and Lederkremer, R. (2003). Synthesis of β-D-Galp-(1-3)-β-D-Galp-(1-6)-(β-D-Galf-(1-4))-D-GlcNAc, a tetrasaccharide component of mucins of *Trypanosoma cruzi*. *Tetrahedron* 34, 163–170. doi: 10.1002/chin.200304193

Gallo-Rodriguez, C., Varela, O., and Lederkremer, R. (1998). One-pot synthesis of beta-D-Galf(1-4)[beta-D-Galp(1-4)]-D-GlcNAc, a 'core' trisaccharide linked O-glycosidically in glycoproteins of *Trypanosoma cruzi*. *Carbohydr. Res.* 305, 163–170. doi: 10.1016/S0008-6215(97)00256-5

Gallo-Rodriguez, C., Varela, O., and Lederkremer, R. M. (1996). First Synthesis of beta-D-Galf(1-4)GlcNAc, a structural unit attached O-glycosidically in glycoproteins of *Trypanosoma cruzi*. *J. Org. Chem.* 61, 1886–1889. doi: 10.1021/jo951934m

Giorgi, M. E., and de Lederkremer, R. M. (2011). Trans-sialidase and mucins of *Trypanosoma cruzi*: an important interplay for the parasite. *Carbohydr. Res.* 346, 1389–1393. doi: 10.1016/j.carres.2011.04.006

Godl, K., Johansson, M. E. V., Lidell, M. E., Mörgelin, M., Karlsson, H., Olson, F. J., et al. (2002). The N terminus of the MUC2 mucin forms trimers that are held together within a trypsin-resistant core fragment. *J. Biol. Chem.* 277, 47248–47256. doi: 10.1074/jbc.M208483200

Golgher, D. B., Colli, W., Souto-Padron, T., and Zingales, B. (1993). Galactofuranose-containing glycoconjugates of epimastigote and trypomastigote forms of *Trypanosoma cruzi*. *Mol. Biochem. Parasitol.* 60, 249–264. doi: 10.1016/0166-6851(93)90136-L

Groseth, A., Marzi, A., Hoenen, T., Herwig, A., Gardner, D., Becker, S., et al. (2012). The Ebola virus glycoprotein contributes to but is not sufficient for virulence *in vivo*. *PLOS Pathog.* 8:e1002847. doi: 10.1371/journal.ppat.1002847

Hansson, G. C. (2019). Mucus and mucins in diseases of the intestinal and respiratory tracts. *J. Intern. Med.* 285, 479–490. doi: 10.1111/joim.12910

Hasnain, S. Z., Gallagher, A. L., Grencis, R. K., and Thornton, D. J. (2013). A new role for mucins in immunity: insights from gastrointestinal nematode infection. *Int. J. Biochem. Cell Biol.* 45, 364–374. doi: 10.1016/j.biocel.2012.10.011

Hebbar, V., Damera, G., and Sachdev, G. P. (2005). Differential expression of MUC genes in endometrial and cervical tissues and tumors. *BMC Cancer* 5:124. doi: 10.1186/1471-2407-5-124

Hoffmann-Röder, A., Kaiser, A., Wagner, S., Gaidzik, N., Kowalczyk, D., Westerlind, U., et al. (2010). Synthetic antitumor vaccines from tetanus toxoid conjugates of MUC1 glycopeptides with the Thomsen–Friedenreich antigen and a fluorine-substituted analogue. *Angew. Chem. Int. Ed.* 49, 8498–8503. doi: 10.1002/anie.201003810

Ilg, T. (2000). Proteophosphoglycans of Leishmania. *Parasitol. Today* 16, 489–497. doi: 10.1016/S0169-4758(00)01791-9

Ilg, T., Handman, E., Ng, K., Stierhof, Y.-D., and Bacic, A. (1999). Mucin-like proteophosphoglycans from the protozoan parasite *Leishmania*. *Trends Glycosci. Glycotechnol.* 11, 53–71. doi: 10.4052/tigg.11.53

Ilg, T., Overath, P., Ferguson, M., Rutherford, T., Campbell, D., and, McConville, J., et al. (1994). O- and N-glycosylation of the leishmania mexicana-secreted acid phosphatase: characterization of a new class of phosphoserine-linked glycans. *J. Biol. Chem.* 269, 24073–24081.

Ilg, T., Stierhof, Y. D., Craik, D., Simpson, R., Handman, E., and Bacic, A. (1996). Purification and structural characterization of a filamentous, mucin-like proteophosphoglycan secreted by *Leishmania* parasites. *J. Biol. Chem.* 271, 21583–21596. doi: 10.1074/jbc.271.35.21583

Itoh, Y., Kamata-Sakurai, M., Denda-Nagai, K., Nagai, S., Tsuiji, M., Ishii-Schrade, K., et al. (2007). Identification and expression of human epiglycanin/MUC21: a novel transmembrane mucin. *Glycobiology* 18, 74–83. doi: 10.1093/glycob/cwm118

Jain, M., Karan, D., Batra, S., and Varshney, G. (2001). Mucins in protozoan parasites. *Front. Biosci.* 6, D1276–D1283. doi: 10.2741/Jain

Johansson, M. E. V., Gustafsson, J. K., Holmén-Larsson, J., Jabbar, K. S., Xia, L., Xu, H., et al. (2014). Bacteria penetrate the normally impenetrable inner colon mucus layer in both murine colitis models and patients with ulcerative colitis. *Gut* 63, 281–291. doi: 10.1136/gutjnl-2012-303207

Johansson, M. E. V., Phillipson, M., Petersson, J., Velcich, A., Holm, L., and Hansson, G. C. (2008). The inner of the two Muc2 mucin-dependent mucus layers in colon is devoid of bacteria. *Proc. Natl. Acad. Sci. U.S.A* 105, 15064–15069. doi: 10.1073/pnas.0803124105

Johansson, M. E. V., Sjövall, H., and Hansson, G. C. (2013). The gastrointestinal mucus system in health and disease. *Nat. Rev. Gastroenterol. Hepatol.* 10:352. doi: 10.1038/nrgastro.2013.35

Jonckheere, N., Skrypek, N., Frenois, F., and Van Seuningen, I. (2013). Membrane-bound mucin modular domains: from structure to function. *Biochimie* 95, 1077–1086. doi: 10.1016/j.biochi.2012.11.005

Jones, C., Todeschini, A. R., Agrellos, O. A., Previato, J. O., and Mendonca-Previato, L. (2004). Heterogeneity in the biosynthesis of mucin O-glycans from *Trypanosoma cruzi* tulahuen strain with the expression of novel galactofuranosyl-containing oligosaccharides. *Biochemistry* 43, 11889–11897. doi: 10.1021/bi048942u

Jung, H. H., Lee, J. H., Kim, Y. T., Lee, S. D., and Park, J. H. (2000). Expression of mucin genes in chronic ethmoiditis. *Am. J. Rhinol.* 14, 163–170. doi: 10.2500/105065800782102690

Kaiser, A., Gaidzik, N., Westerlind, U., Kowalczyk, D., Hobel, A., Schmitt, E., et al. (2009). A synthetic vaccine consisting of a tumor-associated sialyl-TN-MUC1 tandem-repeat glycopeptide and tetanus toxoid: induction of a strong and highly selective immune response. *Angew. Chem. Int. Ed.* 48, 7551–7555. doi: 10.1002/anie.200902564

Kamio, K., Matsushita, I., Hijikata, M., Kobashi, Y., Tanaka, G., Nakata, K., et al. (2005). Promoter analysis and aberrant expression of the MUC5B gene in diffuse panbronchiolitis. *Am. J. Respir. Crit. Care Med.* 171, 949–957. doi: 10.1164/rccm.200409-1168OC

Kasprzak, A., and Adamek, A. (2019). Mucins: the old, the new and the promising factors in hepatobiliary carcinogenesis. *Int. J. Mol. Sci.* 20:E1288. doi: 10.3390/ijms20061288

Kaur, S., Kumar, S., Momi, N., Sasson, A. R., and Batra, S. K. (2013). Mucins in pancreatic cancer and its microenvironment. *Nat. Rev. Gastroenterol. Hepatol.* 10, 607–620. doi: 10.1038/nrgastro.2013.120

Kiley, M. P. (1988). "Filoviridae: Marburg and Ebola Viruses," in *Laboratory Diagnosis of Infectious Diseases Principles and Practice: Viral, Rickettsial, and Chlamydial Diseases*, eds E. H. Lennette, P. Halonen, F. A. Murphy, A. Balows, and W. J. Hausler (New York, NY: Springer New York), 595–601.

Kufe, D. W. (2009). Mucins in cancer: function, prognosis and therapy. *Nat. Rev. Cancer* 9, 874–885. doi: 10.1038/nrc2761

Lang, T., Klasson, S., Larsson, E., Johansson, M. E. V., Hansson, G. C., and Samuelsson, T. (2016). Searching the evolutionary origin of epithelial mucus protein components—mucins and FCGBP. *Mol. Biol. Evol.* 33, 1921–1936. doi: 10.1093/molbev/msw066

Lee, J. E., Fusco, M. L., Hessell, A. J., Oswald, W. B., Burton, D. R., and Saphire, E. O. (2008). Structure of the Ebola virus glycoprotein bound to an antibody from a human survivor. *Nature* 454, 177–182. doi: 10.1038/nature07082

Lee, J. E., and Saphire, E. O. (2009). Ebolavirus glycoprotein structure and mechanism of entry. *Fut. Virol.* 4, 621–635. doi: 10.2217/fvl.09.56

Leir, S.-H., and Harris, A. (2011). MUC6 mucin expression inhibits tumor cell invasion. *Exp. Cell Res.* 317, 2408–2419. doi: 10.1016/j.yexcr.2011.07.021

Leroy, X., Copin, M. C., Devisme, L., Buisine, M. P., Aubert, J. P., Gosselin, B., et al. (2002). Expression of human mucin genes in normal kidney and renal cell carcinoma. *Histopathology* 40, 450–457. doi: 10.1046/j.1365-2559.2002.01408.x

Levi, E., Klimstra, D. S., Andea, A., Basturk, O., and Adsay, N. V. (2004). MUC1 and MUC2 in pancreatic neoplasia. *J. Clin. Pathol.* 57, 456–462. doi: 10.1136/jcp.2003.013292

Li, J. D., Dohrman, A. F., Gallup, M., Miyata, S., Gum, J. R., Kim, Y. S., et al. (1997). Transcriptional activation of mucin by Pseudomonas aeruginosa lipopolysaccharide in the pathogenesis of cystic fibrosis lung disease. *Proc. Natl. Acad. Sci. U.S.A.* 94, 967–972. doi: 10.1073/pnas.94.3.967

Lidell, M. E., and Hansson, G, C. (2006). Cleavage in the GDPH sequence of the C-terminal cysteine-rich part of the human MUC5AC mucin. *Biochem. J.* 399, 121–129. doi: 10.1042/BJ20060443

Lidell, M. E., Johansson, M. E. V., and Hansson, G. C. (2003). An autocatalytic cleavage in the C terminus of the human MUC2 mucin occurs at the low pH of the late secretory pathway. *J. Biol. Chem.* 278, 13944–13951. doi: 10.1074/jbc.M210069200

Lin, J., Tsuprun, V., Kawano, H., Paparella, M. M., Zhang, Z., Anway, R., et al. (2001). Characterization of mucins in human middle ear and

Eustachian tube. *Am. J. Physiol. Lung Cell Mol. Physiol.* 280, L1157–L1167. doi: 10.1152/ajplung.2001.280.6.L1157

Linden, S. K., Sutton, P., Karlsson, N. G., Korolik, V., and McGuckin, M. A. (2008). Mucins in the mucosal barrier to infection. *Mucosal Immunol.* 1, 183–197. doi: 10.1038/mi.2008.5

Lopez, R., Giorgi, M. E., Melgarejo, L. T., Ducrey, I., Balouz, V., Gonzalez-Salas, D., et al. (2019). Synthesis and characterization of alpha-D-Galp-(1-3)-beta-D-Galp epitope-containing neoglycoconjugates for chagas disease serodiagnosis. *Carbohydr. Res.* 478, 58–67. doi: 10.1016/j.carres,.2019.04.007

Malvy, D., McElroy, A. K., de Clerck, H., Günther, S., and van Griensven, J. (2019). Ebola virus disease. *Lancet* 393, 936–948. doi: 10.1016/S0140-6736(18)33132-5

Martínez-Sáez, N., Castro-López, J., Valero-González, J., Madariaga, D., Compañón, I., Somovilla, V. J., et al. (2015). Deciphering the non-equivalence of serine and threonine O-glycosylation points: implications for molecular recognition of the Tn antigen by an anti-MUC1 antibody. *Angew. Chem. Int. Ed.* 54, 9830–9834. doi: 10.1002/anie.201502813

Martínez-Sáez, N., Peregrina, J. M., and Corzana, F. (2017). Principles of mucin structure: implications for the rational design of cancer vaccines derived from MUC1-glycopeptides. *Chem. Soc. Rev.* 46, 7154–7175. doi: 10.1039/C6CS00858E

Martínez-Sáez, N., Supekar, N. T., Wolfert, M. A., Bermejo, I. A., Hurtado-Guerrero, R., Asensio, J. L., et al. (2016). Mucin architecture behind the immune response: design, evaluation and conformational analysis of an antitumor vaccine derived from an unnatural MUC1 fragment. *Chem. Sci.* 7, 2294–2301. doi: 10.1039/C5SC04039F

Masaki, Y., Oka, M., Ogura, Y., Ueno, T., Nishihara, K., Tangoku, A., et al. (1999). Sialylated MUC1 mucin expression in normal pancreas, benign pancreatic lesions, and pancreatic ductal adenocarcinoma. *Hepatogastroenterology* 46, 2240–2245.

Mendoza, V. M., Agusti, R., Gallo-Rodriguez, C., and de Lederkremer, R. M. (2006). Synthesis of the O-linked pentasaccharide in glycoproteins of *Trypanosoma cruzi* and selective sialylation by recombinant trans-sialidase. *Carbohydr. Res.* 341, 1488–1497. doi: 10.1016/j.carres.2006.03.033

Mendoza, V. M., Kashiwagi, G. A., de Lederkremer, R. M., and Gallo-Rodriguez, C. (2010). Synthesis of trisaccharides containing internal galactofuranose O-linked in *Trypanosoma cruzi* mucins. *Carbohydr. Res.* 345, 385–396. doi: 10.1016/j.carres.2009.12.005

Moon, S. K., Lim, D. J., Lee, H. K., Kim, H. N., and Yoo, J. H. (2000). Mucin gene expression in cultured human middle ear epithelial cells. *Acta Otolaryngol.* 120, 933–939. doi: 10.1080/00016480050218654

Moss, J. M., Reid, G. E., Mullin, K. A., Zawadzki, J. L., Simpson, R. J., and McConville, M. J. (1999). Characterization of a Novel GDP-mannose:Serine-protein Mannose-1-phosphotransferase from *Leishmania mexicana*. *J. Biol. Chem.* 274, 6678–6688. doi: 10.1074/jbc.274.10.6678

Movahedin, M., Brooks, T. M., Supekar, N. T., Gokanapudi, N., Boons, G.-J., and Brooks, C. L. (2017). Glycosylation of MUC1 influences the binding of a therapeutic antibody by altering the conformational equilibrium of the antigen. *Glycobiology* 27, 677–687. doi: 10.1093/glycob/cww131

Nath, S., and Mukherjee, P. (2014). MUC1: a multifaceted oncoprotein with a key role in cancer progression. *Trends Mol. Med.* 20, 332–342. doi: 10.1016/j.molmed.2014.02.007

Ning, Y.-J., Kang, Z., Xing, J., Min, Y.-Q., Liu, D., Feng, K., et al. (2018). Ebola virus mucin-like glycoprotein (Emuc) induces remarkable acute inflammation and tissue injury: evidence for Emuc pathogenicity *in vivo*. *Protein Cell* 9, 389–393. doi: 10.1007/s13238-017-0471-x

Noya, V., Brossard, N., Berasaín, P., Rodríguez, E., Chiale, C., Mazal, D., et al. (2016). A mucin-like peptide from *Fasciola hepatica* induces parasite-specific Th1-type cell immunity. *Parasitol. Res.* 115, 1053–1063. doi: 10.1007/s00436-015-4834-z

Palitzsch, B., Gaidzik, N., Stergiou, N., Stahn, S., Hartmann, S., Gerlitzki, B., et al. (2016). A synthetic glycopeptide vaccine for the induction of a monoclonal antibody that differentiates between normal and tumor mammary cells and enables the diagnosis of human pancreatic cancer. *Angew. Chem. Int. Ed.* 55, 2894–2898. doi: 10.1002/anie.201509935

Pallesen, L. T., Pedersen, L. R. L., Petersen, T. E., Knudsen, C. R., and Rasmussen, J. T. (2008). Characterization of human mucin (MUC15) and identification of ovine and caprine orthologs. *J. Dairy Sci.* 91, 4477–4483. doi: 10.3168/jds.2008-1204

Pech-Canul, A. C., Monteon, V., and Solis-Oviedo, R. L. (2017). A brief view of the surface membrane proteins from *Trypanosoma cruzi*. *J. Parasitol. Res.* 2017:3751403. doi: 10.1155/2017/3751403

Pelaseyed, T., Bergström, J. H., Gustafsson, J. K., Ermund, A., Birchenough, G. M. H., Schütte, A., et al. (2014). The mucus and mucins of the goblet cells and enterocytes provide the first defense line of the gastrointestinal tract and interact with the immune system. *Immunol. Rev.* 260, 8–20. doi: 10.1111/imr.12182

Pereira-Chioccola, V. L., Acosta-Serrano, A., Correia de Almeida, I., Ferguson, M. A., Souto-Padron, T., Rodrigues, M. M., et al. (2000). Mucin-like molecules form a negatively charged coat that protects *Trypanosoma cruzi* trypomastigotes from killing by human anti-alpha-galactosyl antibodies. *J. Cell Sci.* 113, 1299–1307.

Peters, C., Kawakami, M., Kaul, M., Ilg, T., Overath, P., and Aebischer, T. (1997). Secreted proteophosphoglycan of Leishmania mexicana amastigotes activates complement by triggering the mannan binding lectin pathway. *Eur. J. Immunol.* 27, 2666–2672. doi: 10.1002/eji.1830271028

Petrou, G., and Crouzier, T. (2018). Mucins as multifunctional building blocks of biomaterials. *Biomater. Sci.* 6, 2282–2297. doi: 10.1039/C8BM00471D

Pett, C., Cai, H., Liu, J., Palitzsch, B., Schorlemer, M., Hartmann, S., et al. (2017). Microarray analysis of antibodies induced with synthetic antitumor vaccines: specificity against diverse mucin core structures. *Chem. Eur. J.* 23, 3875–3884. doi: 10.1002/chem.201603921

Pett, C., Schorlemer, M., and Westerlind, U. (2013). A unified strategy for the synthesis of mucin cores 1–4 saccharides and the assembled multivalent glycopeptides. *Chem. Eur. J.* 19, 17001–17010. doi: 10.1002/chem.201302921

Pett, C., and Westerlind, U. (2014). A convergent strategy for the synthesis of type-1 elongated mucin cores 1–3 and the corresponding glycopeptides. *Chem. Eur. J.* 20, 7287–7299. doi: 10.1002/chem.201400162

Piani, A., Ilg, T., Elefanty, A. G., Curtis, J., and Handman, E. (1999). *Leishmania* major proteophosphoglycan is expressed by amastigotes and has an immunomodulatory effect on macrophage function. *Microbes Infect.* 1, 589–599. doi: 10.1016/S1286-4579(99)80058-6

Portal, C., Gouyer, V., Magnien, M., Plet, S., Gottrand, F., and Desseyn, J.-L. (2017). *In vivo* imaging of the Muc5b gel-forming mucin. *Sci. Rep.* 7:44591. doi: 10.1038/srep44591

Portillo, S., Zepeda, B. G., Iniguez, E., Olivas, J. J., Karimi, N. H., Moreira, O. C., et al. (2019). A prophylactic alpha-Gal-based glycovaccine effectively protects against murine acute Chagas disease. *NPJ Vaccines* 4:13. doi: 10.1038/s41541-019-0107-7

Pratt, W. S., Crawley, S., Hicks, J., Ho, J., Nash, M., Kim, Y. S., et al. (2000). Multiple transcripts of MUC3: evidence for two genes, MUC3A and MUC3B. *Biochem. Biophys. Res. Commun.* 275, 916–923. doi: 10.1006/bbrc.2000.3406

Previato, J. O., Jones, C., Goncalves, L. P., Wait, R., Travassos, L. R., and Mendonca-Previato, L. (1994). O-glycosidically linked N-acetylglucosamine-bound oligosaccharides from glycoproteins of *Trypanosoma cruzi*. *Biochem. J.* 301(Pt 1), 151–159. doi: 10.1042/bj3010151

Previato, J. O., Jones, C., Xavier, M. T., Wait, R., Travassos, L. R., Parodi, A. J., et al. (1995). Structural characterization of the major glycosylphosphatidylinositol membrane-anchored glycoprotein from epimastigote forms of *Trypanosoma cruzi* Y-strain. *J. Biol. Chem.* 270, 7241–7250. doi: 10.1074/jbc.270.13.7241

Puchelle, E., Bajolet, O., and Abely, M. (2002). Airway mucus in cystic fibrosis. *Paediatr. Respir. Rev.* 3, 115–119. doi: 10.1016/S1526-0550(02)00005-7

Puri, S., Friedman, J., Saraswat, D., Kumar, R., Li, R., Ruszaj, D., et al. (2015). Candida albicans shed Msb2 and host mucins affect the candidacidal activity of salivary Hst 5. *Pathogens* 4, 752–763. doi: 10.3390/pathogens4040752

Rachagani, S., Torres, M. P., Moniaux, N., and Batra, S. K. (2009). Current status of mucins in the diagnosis and therapy of cancer. *Biofactors* 35, 509–527. doi: 10.1002/biof.64

Ricketson, R., Roberts, L., and Mutombo, P. (2015). *The Glycoprotein Mucin-Like Domain (MLD) in the Zaire ebolavirus (EBOV) May be Responsible for the Manifestations of Post-Ebola Virus Disease Syndrome (PEVDS)*. Web Med Cen.

Ridley, C., Kouvatsos, N., Raynal, B. D., Howard, M., Collins, R. F., Desseyn, J.-L., et al. (2014). Assembly of the respiratory mucin MUC5B: a new model for a gel-forming mucin. *J. Biol. Chem.* 289, 16409–16420. doi: 10.1074/jbc.M114.566679

Ridley, C., and Thornton, D. J. (2018). Mucins: the frontline defence of the lung. *Biochem. Soc. Trans.* 46, 1099–1106. doi: 10.1042/BST20170402

Roger, E., Gourbal, B., Grunau, C., Pierce, R. J., Galinier, R., and Mitta, G. (2008). Expression analysis of highly polymorphic mucin proteins (Sm PoMuc) from the parasite *Schistosoma mansoni*. *Mol. Biochem. Parasitol.* 157, 217–227. doi: 10.1016/j.molbiopara.2007.11.015

Rogers, M. (2012). The role of *Leishmania* proteophosphoglycans in sand fly transmission and infection of the mammalian host. *Front. Microbiol.* 3:223. doi: 10.3389/fmicb.2012.00223

Rogers, M. E., Ilg, T., Nikolaev, A. V., Ferguson, M. A. J., and Bates, P. A. (2004). Transmission of cutaneous leishmaniasis by sand flies is enhanced by regurgitation of fPPG. *Nature* 430, 463–467. doi: 10.1038/nature02675

Román, E., Cottier, F., Ernst, J. F., and Pla, J. (2009). Msb2 Signaling mucin controls activation of Cek1 mitogen-activated protein kinase in *Candida albicans*. *Eukaryot. Cell* 8, 1235–1249. doi: 10.1128/EC.00081-09

Senapati, S., Das, S., and Batra, S. K. (2010). Mucin-interacting proteins: from function to therapeutics. *Trends Biochem. Sci.* 35, 236–245. doi: 10.1016/j.tibs.2009.10.003

Sheng, Y. H., Hasnain, S. Z., Florin, T. H. J., and McGuckin, M. A. (2012). Mucins in inflammatory bowel diseases and colorectal cancer. *J. Gastroenterol. Hepatol.* 27, 28–38. doi: 10.1111/j.1440-1746.2011.06909.x

Shurer, C. R., Wang, Y., Feeney, E., Head, S. E., Zhang, V. X., Su, J., et al. (2019). Stable recombinant production of codon-scrambled lubricin and mucin in human cells. *Biotechnol. Bioeng.* 116, 1292–1303. doi: 10.1002/bit.26940

Siegel, R. L., Miller, K. D., and Jemal, A. (2019). Cancer statistics, 2019. *CA Cancer J. Clin.* 69, 7–34. doi: 10.3322/caac.21551

Slayden, O. D., Friason, F. K. E., Bond, K. R., and Mishler, E. C. (2018). Hormonal regulation of oviductal glycoprotein 1 (OVGP1; MUC9) in the rhesus macaque cervix. *J. Med. Primatol.* 47, 362–370. doi: 10.1111/jmp.12357

Steverding, D. (2014). The history of Chagas disease. *Parasit. Vect.* 7:317. doi: 10.1186/1756-3305-7-317

Szafranski-Schneider, E., Swidergall, M., Cottier, F., Tielker, D., Román, E., Pla, J., et al. (2012). Msb2 shedding protects *Candida albicans* against antimicrobial peptides. *PLOS Pathog.* 8:e1002501. doi: 10.1371/journal.ppat.1002501

Tarp, M. A., and Clausen, H. (2008). Mucin-type O-glycosylation and its potential use in drug and vaccine development. *Biochim. Biophys. Acta* 1780, 546–563. doi: 10.1016/j.bbagen.2007.09.010

Thornton, D. J., Rousseau, K., and McGuckin, M. A. (2008). Structure and function of the polymeric mucins in airways mucus. *Annu. Rev. Physiol.* 70, 459–486. doi: 10.1146/annurev.physiol.70.113006.100702

Todeschini, A. R., de Almeida, E. G., Agrellos, O. A., Jones, C., Previato, J. O., and Mendonca-Previato, L. (2009). Alpha-N-acetylglucosamine-linked O-glycans of sialoglycoproteins (Tc-mucins) from *Trypanosoma cruzi* colombiana strain. *Mem. Inst. Oswaldo Cruz* 104(Suppl. 1), 270–274. doi: 10.1590/S0074-02762009000900035

Tomita, T., Bzik, D. J., Ma, Y. F., Fox, B. A., Markillie, L. M., Taylor, R. C., et al. (2013). The *Toxoplasma gondii* cyst wall protein CST1 is critical for cyst wall integrity and promotes bradyzoite persistence. *PLOS Pathog.* 9:e1003823. doi: 10.1371/journal.ppat.1003823

Tomita, T., Ma, Y., and Weiss, L. (2018). Characterization of a SRS13: a new cyst wall mucin-like domain containing protein. *Parasitol. Res.* 117, 2457–2466. doi: 10.1007/s00436-018-5934-3

Tomlinson, S., Pontes de Carvalho, L. C., Vandekerckhove, F., and Nussenzweig, V. (1994). Role of sialic acid in the resistance of *Trypanosoma cruzi* trypomastigotes to complement. *J. Immunol.* 153, 3141–3147.

Treon, S. P., Maimonis, P., Bua, D., Young, G., Raje, N., Mollick, J., et al. (2000). Elevated soluble MUC1 levels and decreased anti-MUC1 antibody levels in patients with multiple myeloma. *Blood* 96, 3147–3153. doi: 10.1182/blood.V96.9.3147.h8003147_3147_3153

van Putten, J. P. M., and Strijbis, K. (2017). Transmembrane mucins: signaling receptors at the intersection of inflammation and cancer. *J. Innate Immun.* 9, 281–299. doi: 10.1159/000453594

van Well, R. M., Collet, B., and Field, R. (2008). Synthesis of mucin glycans from the protozoon parasite *Trypanosoma cruzi*. *Synlett 2008* 14, 2175–2177. doi: 10.1055/s-2008-1078249

Wagner, C. E., Wheeler, K. M., and Ribbeck, K. (2018). Mucins and their role in shaping the functions of mucus barriers. *Annu. Rev. Cell Dev. Biol.* 34, 189–215. doi: 10.1146/annurev-cellbio-100617-062818

Wang, J., and El-Bahrawy, M. (2015). Expression profile of mucins (MUC1, MUC2, MUC5AC, and MUC6) in ovarian mucinous tumours: changes in expression from benign to malignant tumours. *Histopathology* 66, 529–535. doi: 10.1111/his.12578

Wanyiri, J., and Ward, H. (2006). Molecular basis of *Cryptosporidium*–host cell interactions: recent advances and future prospects. *Fut. Microbiol.* 1, 201–208. doi: 10.2217/17460913.1.2.201

Watson, A. M., Ngor, W.-M., Gordish-Dressman, H., Freishtat, R. J., and Rose, M. C. (2009). MUC7 polymorphisms are associated with a decreased risk of a diagnosis of asthma in an African American population. *J. Investig. Med.* 57, 882–886. doi: 10.2310/JIM.0b013e3181c0466d

Wertheim, J. O., and Worobey, M. (2009). Relaxed selection and the evolution of RNA virus mucin-like pathogenicity factors. *J. Virol.* 83, 4690–4694. doi: 10.1128/JVI.02358-08

Westerlind, U., Hobel, A., Gaidzik, N., Schmitt, E., and Kunz, H. (2008). Synthetic vaccines consisting of tumor-associated MUC1 glycopeptide antigens and a T-cell epitope for the induction of a highly specific humoral immune response. *Angew. Chem. Int. Ed.* 47, 7551–7556. doi: 10.1002/anie.200802102

Westerlind, U., Schröder, H., Hobel, A., Gaidzik, N., Kaiser, A., Niemeyer, C. M., et al. (2009). Tumor-associated MUC1 tandem-repeat glycopeptide microarrays to evaluate serum– and monoclonal–antibody specificity. *Angew. Chem. Int. Ed.* 48, 8263–8267. doi: 10.1002/anie.200902963

Whiteway, M., and Oberholzer, U. (2004). Candida morphogenesis and host–pathogen interactions. *Curr. Opin. Microbiol.* 7, 350–357. doi: 10.1016/j.mib.2004.06.005

Wilson, R. M., and Danishefsky, S. J. (2013). A vision for vaccines built from fully synthetic tumor-associated antigens: from the laboratory to the clinic. *J. Am. Chem. Soc.* 135, 14462–14472. doi: 10.1021/ja405932r

Xiong, C. Y., Natarajan, A., Shi, X. B., Denardo, G. L., and Denardo, S. J. (2006). Development of tumor targeting anti-MUC-1 multimer: effects of di-scFv unpaired cysteine location on PEGylation and tumor binding. *Protein Eng. Des. Sel.* 19, 359–367. doi: 10.1093/protein/gzl020

Xu, D., Pavlidis, P., Thamadilok, S., Redwood, E., Fox, S., Blekhman, R., et al. (2016). Recent evolution of the salivary mucin MUC7. *Sci. Rep.* 6:31791. doi: 10.1038/srep31791

Yang, Z. Y., Duckers, H. J., Sullivan, N. J., Sanchez, A., Nabel, E. G., and Nabel, G. J. (2000). Identification of the Ebola virus glycoprotein as the main viral determinant of vascular cell cytotoxicity and injury. *Nat. Med.* 6, 886–889. doi: 10.1038/78654

Yin, B. W. T., and Lloyd, K. O. (2001). Molecular cloning of the CA125 ovarian cancer antigen: identification as a new mucin, MUC16. *J. Biol. Chem.* 276, 27371–27375. doi: 10.1074/jbc.M103554200

Yoshimoto, T., Matsubara, D., Soda, M., Ueno, T., Amano, Y., Kihara, A., et al. (2019). MUC21 is a key molecule involved in the incohesive growth pattern in lung adenocarcinoma. *Cancer Sci.* 110, 3006–3011. doi: 10.1111/cas.14129

Yu, D. F., Chen, Y., Han, J. M., Zhang, H., Chen, X. P., Zou, W. J., et al. (2008). MUC19 expression in human ocular surface and lacrimal gland and its alteration in Sjögren syndrome patients. *Exp. Eye Res.* 86, 403–411. doi: 10.1016/j.exer.2007.11.013

Zuercher, J., Fritzsche, M., Feil, S., Mohn, L., and Berger, W. (2012). Norrin stimulates cell proliferation in the superficial retinal vascular plexus and is pivotal for the recruitment of mural cells. *Hum. Mol. Genet.* 21, 2619–2630. doi: 10.1093/hmg/dds087

Conflict of Interest: The authors declare that the research was conducted in the absence of any commercial or financial relationships that could be construed as a potential conflict of interest.

frontiers in Chemistry

CORRECTION
published: 05 December 2019
doi: 10.3389/fchem.2019.00846

Corrigendum: Mucins and Pathogenic Mucin-Like Molecules Are Immunomodulators During Infection and Targets for Diagnostics and Vaccines

Sandra Pinzón Martín[1,2], *Peter H. Seeberger*[1,2] *and Daniel Varón Silva*[1,2]*

[1] Department of Biomolecular Systems, Max Planck Institute of Colloids and Interfaces, Potsdam, Germany, [2] Department of Biology, Chemistry and Pharmacy, Freie Universität Berlin, Berlin, Germany

Keywords: mucins, mucin-like molecules, O-glycoproteins, cancer, parasites, virus, infection

OPEN ACCESS

Edited by:
Karina Valeria Mariño, Institute of Biology and Experimental Medicine (IBYME), Argentina

Reviewed by:
Rosa Muchnik De Lederkremer, University of Buenos Aires, Argentina

***Correspondence:**
Daniel Varón Silva
daniel.varon@mpikg.mpg.de

Specialty section:
This article was submitted to Chemical Biology, a section of the journal Frontiers in Chemistry

Received: *29 October 2019*
Accepted: *21 November 2019*
Published: *05 December 2019*

Citation:
Pinzón Martín S, Seeberger PH and Varón Silva D (2019) Corrigendum: Mucins and Pathogenic Mucin-Like Molecules Are Immunomodulators During Infection and Targets for Diagnostics and Vaccines. Front. Chem. 7:846. doi: 10.3389/fchem.2019.00846

A Corrigendum on

Mucins and Pathogenic Mucin-Like Molecules Are Immunomodulators During Infection and Targets for Diagnostics and Vaccines
by Pinzón Martín, S., Seeberger, P. H., and Varón Silva, D. (2019). Front. Chem. 7:710. doi: 10.3389/fchem.2019.00710

In the original article, there was a mistake in **Figure 4** as published. The strain for three structures was incorrectly assigned in the figure legend. Structures 3 and 6 were corrected and structures 6–8 required renumbering to fit the text. The correct **Figure 4** and legend appear below.

The authors apologize for this error and state that this does not change the scientific conclusions of the article in any way. The original article has been updated.

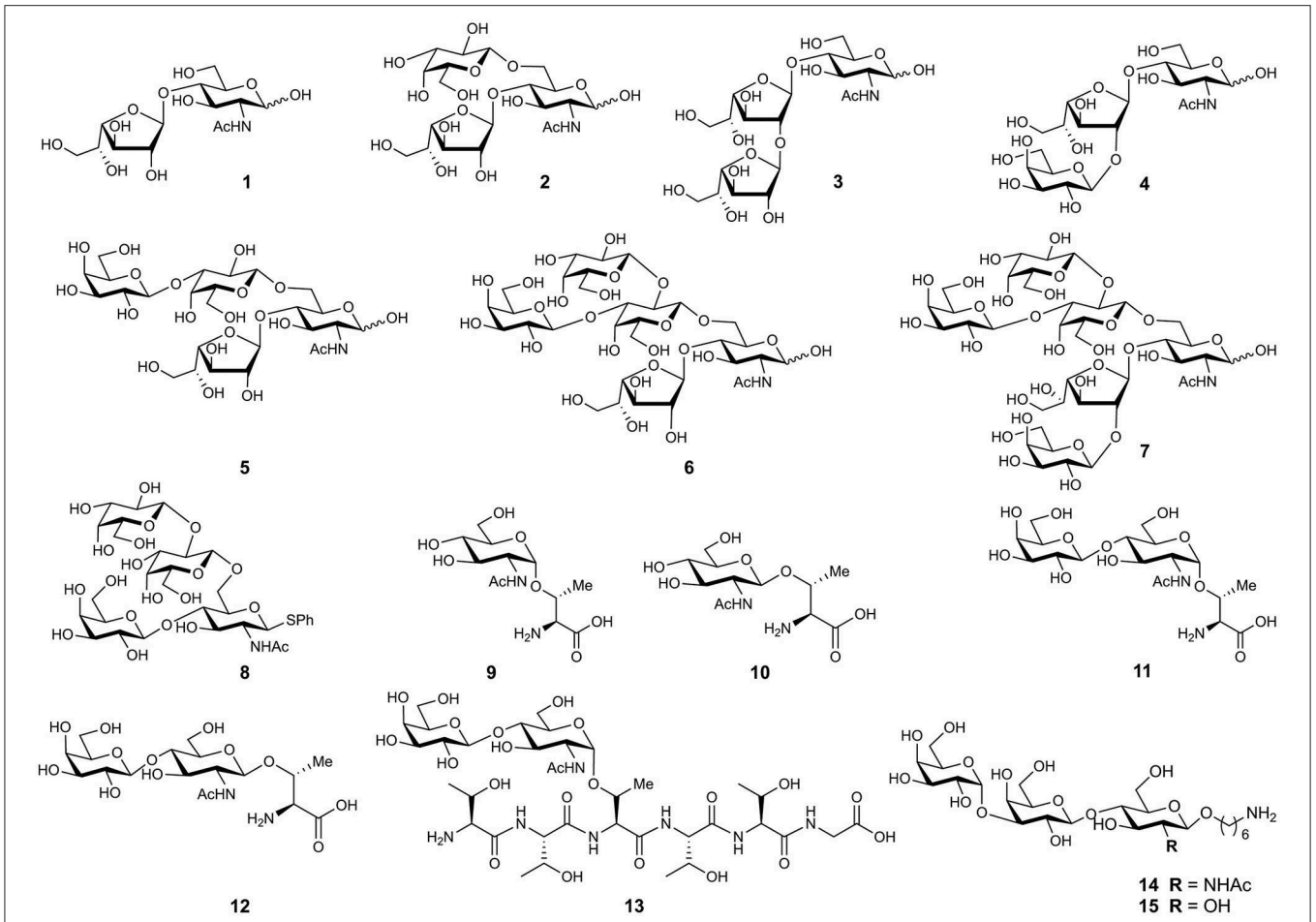

FIGURE 4 | Chemical structure of synthesized glycans from MLMs of *Trypanosoma cruzi* Colombiana strain (**1**, **2**, **6**, **7**), Tulahuen strain (**3**–**5**), and Y strain (**8**–**13**).

frontiers in Chemistry

ORIGINAL RESEARCH
published: 24 October 2019
doi: 10.3389/fchem.2019.00698

Proteoform-Resolved FcγRIIIa Binding Assay for Fab Glycosylated Monoclonal Antibodies Achieved by Affinity Chromatography Mass Spectrometry of Fc Moieties

*Steffen Lippold, Simone Nicolardi, Manfred Wuhrer and David Falck**

Center for Proteomics and Metabolomics, Leiden University Medical Center, Leiden, Netherlands

FcγR receptors (FcγR) mediate key functions in immunological responses. For instance, FcγRIIIa is involved in antibody-dependent cell-mediated cytotoxicity (ADCC). FcγRIIIa interacts with the fragment crystallizable (Fc) of immunoglobulin G (IgG). This interaction is known to be highly dependent on IgG Fc glycosylation. Thus, the impact of glycosylation features on this interaction has been investigated in several studies by numerous analytical and biochemical techniques. FcγRIIIa affinity chromatography (AC) hyphenated to mass spectrometry (MS) is a powerful tool to address co-occurring Fc glycosylation heterogeneity of monoclonal antibodies (mAbs). However, MS analysis of mAbs at the intact level may provide limited proteoform resolution, for example, when additional heterogeneity is present, such as antigen-binding fragment (Fab) glycosylation. Therefore, we investigated middle-up approaches to remove the Fab and performed AC-MS on the IgG Fc to evaluate its utility for FcγRIIIa affinity assessment compared to intact IgG analysis. We found the protease Kgp to be particularly suitable for a middle-up FcγRIIIa AC-MS workflow as demonstrated for the Fab glycosylated cetuximab. The complexity of the mass spectra of Kgp digested cetuximab was significantly reduced compared to the intact level while affinity was fully retained. This enabled a reliable assignment and relative quantitation of Fc glycoforms in FcγRIIIa AC-MS. In conclusion, our workflow allows a functional separation of differentially glycosylated IgG Fc. Consequently, applicability of FcγRIIIa AC-MS is extended to Fab glycosylated IgG, i.e., cetuximab, by significantly reducing ambiguities in glycoform assignment vs. intact analysis.

Keywords: affinity chromatography, mass spectrometry, middle-up protein analysis, cetuximab, Fc glycosylation, Fab glycosylation, FcγRIIIa, Kgp

OPEN ACCESS

Edited by:
Christoph Rademacher, Max Planck Institute of Colloids and Interfaces, Germany

Reviewed by:
Harald Kolmar, Darmstadt University of Technology, Germany
Francisco Solano, University of Murcia, Spain

***Correspondence:**
David Falck
d.falck@lumc.nl

Specialty section:
This article was submitted to Chemical Biology, a section of the journal Frontiers in Chemistry

Received: *31 July 2019*
Accepted: *08 October 2019*
Published: *24 October 2019*

Citation:
Lippold S, Nicolardi S, Wuhrer M and Falck D (2019) Proteoform-Resolved FcγRIIIa Binding Assay for Fab Glycosylated Monoclonal Antibodies Achieved by Affinity Chromatography Mass Spectrometry of Fc Moieties. Front. Chem. 7:698. doi: 10.3389/fchem.2019.00698

INTRODUCTION

The fragment crystallizable (Fc) of antibodies mediates immunological responses, for example through binding to Fc receptors (Nimmerjahn and Ravetch, 2008; Pincetic et al., 2014). Fc glycosylation has a key role in modulating Fc receptor-mediated effector functions, such as antibody-dependent cell-mediated cytotoxicity (ADCC) (Reusch and Tejada, 2015; Cymer et al., 2018; Saunders, 2019). The affinity toward FcγRIIIa is known to be crucial for ADCC

(Nimmerjahn and Ravetch, 2008). Fucosylation of Fc glycans drastically decreases FcγRIIIa affinity which is attributable to an unique glycan-glycan interaction (Ferrara et al., 2011). Other glycosylation features such as galactosylation were also shown to affect the Fc-FcγRIIIa interaction (Thomann et al., 2015; Dekkers et al., 2017). The binding of the Fc to FcγRIIIa is asymmetric in a 1:1 stoichiometry (Sondermann et al., 2000). Nonetheless, FcγRIIIa affinity is influenced by the pairing of Fc glycans (Shatz et al., 2013). While differential affinity of glycoforms is dominated by the stronger binding glycan, the second glycan modulates affinity to a smaller extent, but along the same structural features (Shatz et al., 2013; Lippold et al., 2019). Nowadays, therapeutic monoclonal antibodies (mAbs) are most often derived from human immunoglobulin G 1 (IgG1, schematic overview in **Figure 1**). They are used in the treatment of various diseases, such as cancers or autoimmune diseases (Chan and Carter, 2010; Weiner et al., 2010). In the biopharmaceutical industry, mAbs are very successful and currently dominate new approvals (Walsh, 2018). Recently, glycoengineering for enhanced FcγRIIIa affinity and ADCC has been therapeutically exploited (Jefferis, 2009; Beck and Reichert, 2012).

Numerous analytical technologies exist for assessing the effector functions of therapeutic antibodies (Jiang et al., 2011; Cymer et al., 2018). They vary largely in information content, generally with a negative correlation between complexity and resolution. Complex cellular assays are more easily translated to the *in vivo* situation. Contrary, physicochemical assays provide higher molecular resolution and better robustness. Though immune responses depend on the formation of immune complexes, receptor binding studies on monomeric IgG are highly relevant and widely used (Nimmerjahn and Ravetch, 2008; Cymer et al., 2018). Ultimately, combining information from different assays is essential to fully understand antibody effector functions. Glycosylation heterogeneity is a major challenge for the assessment of individual contributions of specific glycoforms to the effector functions, especially considering pairing possibilities. Several studies applied laborious glycoengineering in order to assess receptor binding and effector functions of specific glycoforms (Dashivets et al., 2015; Thomann et al., 2015; Dekkers et al., 2017; Wada et al., 2019). Affinity chromatography (AC) represents a cell-free physicochemical assay which provides a functional separation and correlates well with surface plasmon resonance (SPR) assays and ADCC assays (Dashivets et al., 2015; Thomann et al., 2015; Wada et al., 2019). We reported recently on coupling of FcγRIIIa AC to mass spectrometry (AC-MS) (Lippold et al., 2019). This approach allows the differential assessment of Fc glycoforms in heterogeneously glycosylated mAbs with high resolution of proteoforms and affinity on an intact protein level. Whereas it should be very powerful for most mAbs, proteoform resolution may be insufficient for more complex formats (Ayoub et al., 2013). This applies to mAbs with a higher degree of heterogeneity due to sequence variants or post translational modifications (PTMs), especially additional glycosylation sites in the antigen-binding fragment (Fab). In addition, the analysis of new antibody-derived therapeutic formats, such as bispecific antibodies or fusion proteins, may be challenging (Klein et al., 2016).

Cetuximab is an approved mAb with additional Fab glycosylation and ADCC is described as one mechanisms of action (Kurai et al., 2007; Kol et al., 2017). Each heavy chain (HC) contains an *N*-glycosylation site at the Fab (N_{88}) and at the Fc (N_{299}) resulting in a high number of possible glycoforms. The proteoform heterogeneity of cetuximab is further increased by C-terminal lysine variants of the HC (Ayoub et al., 2013). Hence, glycoform assignment of the heavily glycosylated cetuximab by intact mass analysis is hindered by a high degree of ambiguities (Ayoub et al., 2013; Bern et al., 2018). Middle-up approaches are highly advantageous alternatives for obtaining information about individual subunit (e.g., Fc, Fc/2, Fab) modifications, especially for complex formats (Beck et al., 2013; Sjögren et al., 2016; Lermyte et al., 2019). Bacterial enzymes are important tools for middle-up approaches, since they cleave IgG specifically within the hinge region. Robust and simple workflows for the middle-up analysis of (therapeutic) mAbs are established (Zhang et al., 2016; Moelleken et al., 2017; Sjögren et al., 2017; Bern et al., 2018; van der Burgt et al., 2019). IdeS, SpeB, and Kgp are frequently used commercial IgG hinge-specific proteases (cleavage sites and products are indicated in **Figure 1** and **Supplementary Figure 1**, respectively). As opposed to papain, for example, additional cleavages outside of the hinge region are not reported under standard conditions. Their characteristics were recently summarized (Sjögren et al., 2017). IdeS based middle-up MS analysis of cetuximab is commonly applied to unravel the (glycosylation) microheterogeneity (Ayoub et al., 2013; Janin-Bussat et al., 2013; Bern et al., 2018).

This study combines our recently reported FcγRIIIa AC-MS with middle-up analysis. Therefore, we investigated how cleavages within the hinge region affect the FcγRIIIa binding properties of the obtained Fc. Three different commercial IgG hinge-specific proteases were tested, namely IdeS, SpeB, and Kgp (Sjögren et al., 2017). We demonstrate comparability of middle-up and intact affinity assessment by FcγRIIIa AC-MS upon Kgp digestion. Furthermore, we applied this workflow to cetuximab and simultaneously assessed the FcγRIIIa affinity, characterized the Fc glycoform pairings and analyzed the Fab glycosylation.

MATERIALS AND METHODS

Chemicals, Proteases, and Antibodies

All chemicals in this study had at least analytical grade quality. Deionized water was obtained from a Purelab ultra (ELGA Labwater, Ede, The Netherlands). Preparation of mobile phase was performed with ammonium acetate solution (7.5 M, Sigma-Aldrich, Steinheim Germany) and glacial acetic acid (Honeywell, Seelze, Germany). IdeS (FabRICATOR®), SpeB (FabULOUS®), and Kgp (GingisKHAN®) proteases were purchased from Genovis (Lund, Sweden). A reference standard therapeutic mAb produced in CHO cells (referred to as mAb1) and the FcγRIIIa affinity column was obtained from Roche Diagnostics (Penzberg, Germany). An EMA-approved cetuximab (Erbitux®) was used in this study. Cetuximab is a chimeric IgG1, produced by SP2/0

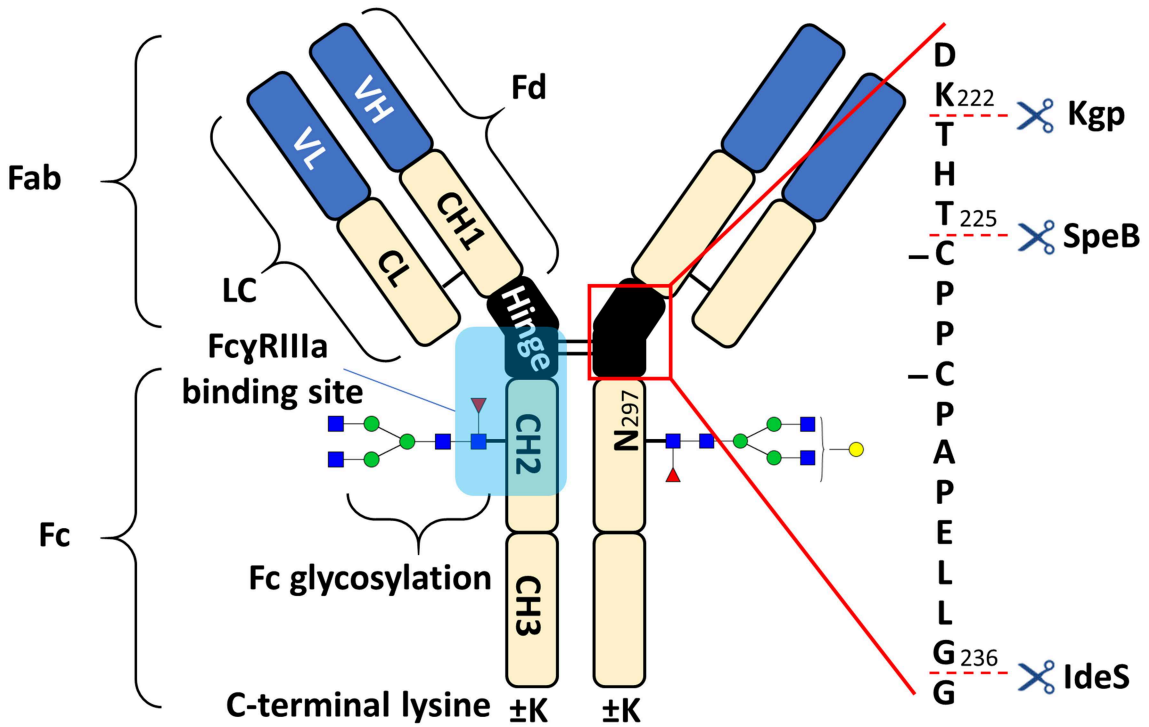

FIGURE 1 | Schematic overview of human IgG1 with a zoom into the hinge region, indicating cleavage sites of IdeS, SpeB, and Kgp. The heavy chain (HC) contains three constant domains (CH1–CH3) and a variable domain (VH), whereas the light chain (LC) has only one constant domain (CL) and a variable domain (VL). The Fd consists of VH and CH1. LC and Fd together form the antigen binding fragment (Fab). About 15% of plasma IgG contain one or more additional *N*-glycosylation sites in the variable domains (Anumula, 2012). CH2 and CH3 of the two heavy chains build the fragment crystallizable (Fc). Within the Fc is a conserved glycosylation site at N_{297} in the CH2 (Jefferis, 2009). Between the CH1 and CH2 of the heavy chains is a mostly flexible hinge region and the four chains are covalently connected via disulfide bridges. Amino acids are presented with single letter code and numbered according to the Kabat system (Kabat et al., 1991).

murine myeloma cells, which binds to the epidermal growth factor receptor (EGFR).

Antibody Digestion (IdeS, SpeB, Kgp)

All IgG hinge-specific proteases were reconstituted in deionized water following the manufacturer's instructions (IdeS: 67 units/μL, SpeB 40 units/μL, Kgp: 10 units/μL). Buffers and reducing conditions were selected from the recommended options. mAbs were digested at a concentration of 5 mg/mL (1 unit of protease per 1 μg of mAb) and incubated for 1 h at 37°C. In case of Kgp, the samples were buffer exchanged prior to digestion (10 kDa molecular weight cut-off filter, Merck, Darmstadt, Germany) to digestion buffer. 100 mM Tris buffer (pH 8) was used with mild reducing conditions (2 mM cysteine) for Kgp and reducing conditions (1 mM DTT) for SpeB, respectively. IdeS digestion was performed under non-reducing conditions with 100 mM ammonium bicarbonate (pH 7). After digestion, samples were buffer exchanged to a final concentration of 5 mg/mL in 50 mM ammonium acetate pH 5 (10 kDa molecular weight cut-off filter).

FcγRIIIa Affinity Chromatography—Mass Spectrometry

The FcγRIIIa AC-MS system was previously described in detail (Lippold et al., 2019). In short, a biocompatible Thermo Ultimate3000 instrument coupled to a 15 T solariX XR FT-ICR mass spectrometer (Bruker Daltonics, Bremen, Germany) was used. The column was operated at 25°C and a flow rate of 500 μL/min was applied. Prior to MS detection, the flow rate was reduced to 30 μL/min via flow-splitting. Mobile phase A was 50 mM ammonium acetate pH 5 and mobile phase B 50 mM ammonium acetate pH 3. Upon injection (50–100 μg sample), the column was washed for 10.5 min (5 column volumes) with 100% mobile phase A and then a linear gradient to 42 min to 100% mobile phase B (15 column volumes) was applied. For electrospray ionization (ESI), the capillary voltage was set to 4,000 V, the nebulizer gas to 0.8 bar, the dry gas flow to 3 L/min dry gas and the source temperature to 200°C.

Data Analysis

Average masses were calculated using the web-based Protein Tool (https://www.protpi.ch) based on the protein sequences and expected modifications. For mAb1 and cetuximab, C-terminal lysine clipping and 16 disulfide bridges were set as modifications. N-terminal pyroglutamic acid was additionally added as modification for cetuximab. Visualization and processing of mass spectra was performed in DataAnalysis 5.0 (Bruker Daltonics). Extracted ion chromatograms (EICs) were generated based on the theoretical *m/z* (±0.2 Th) for all observed charge states. For deconvolution, the Maximum Entropy tool was

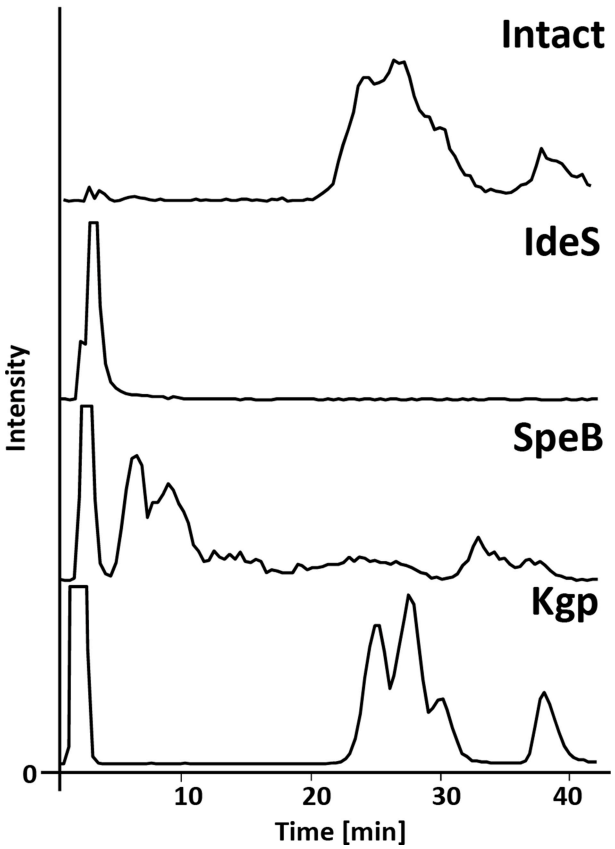

FIGURE 2 | FcγRIIIa AC-MS base peak chromatograms of intact and IdeS-, SpeB-, and Kgp-digested mAb1. For intact and Kgp-digested mAb1, two distinct groups of peaks were detected, namely fucosylated forms with lower affinity (RT 20–35 min) and afucosylated glycoforms with higher affinity (RT higher than 35 min); see **Figure 3**.

used (deconvolution range indicated in table headings, data point spacing = 1, instrument resolving power = 3,000). All described Fc glycans can be found in **Supplementary Table 1** which provides information about composition and structure.

RESULTS AND DISCUSSION

IgG Protease Evaluation

The FcγRIIIa AC-MS retention profiles of hinge cleaved mAb1, obtained by either IdeS, SpeB, or Kgp, and of intact mAb1 were compared (**Figure 2**). Although digestion sites of the three proteases are in close proximity in the hinge region (**Figure 1**), vastly different retention profiles were observed for the differently cleaved Fc. Kgp generated Fc was found to exhibit a remarkably comparable retention profile to the intact mAb1. IdeS digested mAb1 did not show retention on the FcγRIIIa column and the expected cleavage products, including the Fc, were detected in the injection peak (**Supplementary Figure 2**). Under native conditions, Fc fragments consisting of paired polypeptide chains were observed rather than single Fc/2 chains which is attributable to non-covalent interactions of the Fc polypeptides (Bern et al., 2018). The lack of retention can be explained by the removal of amino acids that form an essential part of the FcγRIIIa binding motif (Sondermann et al., 2000). In particular, L_{234} and L_{235} are crucial amino acids. The mutation of these amino acids to alanines (LALA mutant) is known to eliminate FcγRIIIa binding and thus ADCC (Schlothauer et al., 2016; Saunders, 2019). In contrast to IdeS, the protease SpeB does not remove these key amino acids from the Fc. The Fab was observed in the injection peak while the Fc was retained on the FcγRIIIa column (**Supplementary Figure 3**). However, in contrast to Kgp, the Fc retention profile upon SpeB cleavage was vastly different from that of the intact mAb. SpeB derived Fc spread over the entire chromatogram and most of the Fc eluted already before the pH gradient started. Two differences from Kgp derived Fc might provide an explanation. Firstly, the removed amino acids (THT) might lead to an impaired conformational stability of the Fc obtained by SpeB. Furthermore, substitution of H, at this position, was shown to influence FcγRIIIa binding and ADCC (Yan et al., 2012). Finally, partial reduction, which is likely to occur under the applied reducing conditions of 1 mM DTT (Sjögren et al., 2017), is discussed to influence binding to Fc receptors and ADCC (Liu and May, 2012). Under milder reducing conditions SpeB does not show sufficient activity (data not shown). Besides the impaired retention profile, an increased heterogeneity is a disadvantage for MS analysis, when comparing SpeB to Kgp. Heterogeneity is caused by additional cleavages between H_{224} and T_{225} or T_{223} and H_{224} (**Supplementary Figure 3**). These products showed a similar impaired binding behavior. In contrast to SpeB, Kgp protease retains T_{223}, H_{224}, and T_{225} and works under mild reducing conditions (2 mM cysteine) which prevents reduction of the hinge interchain disulfide bonds (Moelleken et al., 2017). Both, the additional amino acids and intact disulfide bonds, might be responsible for improved binding of Kgp derived Fc over SpeB derived Fc. Interestingly, the Fab was removed in a previous study using papain to exclude that the Fab influences the FcγRIIIa binding (Dashivets et al., 2015). In line with our observations for Kgp in FcγRIIIa AC-MS, binding of papain generated Fc was comparable to intact IgG (glycovariants). Total binding strength as well as glycoform differences were preserved in the SPR analysis (Dashivets et al., 2015). Papain digestion is performed under conditions (5–10 mM cysteine) which are only slightly more reductive than for Kgp (2 mM cysteine) (Dashivets et al., 2015; Moelleken et al., 2017). The preferred cleavage site of papain is between the Kgp and SpeB cleavage site (H_{224} and T_{225}) (Kim et al., 2016; van den Bremer et al., 2017) and corresponds to the observed additional cleavage site of SpeB. Hence, the harsher incubation conditions are more likely to cause the differences between Kgp, or papain, and SpeB than the presence or absence of H_{224}. However, by-products (due to cleavage outside the hinge region), insufficient yields and glycoform dependency make papain less favorable as an IgG middle-up protease (Raju and Scallon, 2007; Moelleken et al., 2017). Moreover, papain might degrade the receptor material of the affinity column, since it is not an IgG-specific protease. Consequently, due to the preservation

of the affinity separation and the specificity, Kgp was chosen for the middle-up FcγRIIIa AC-MS workflow. Interestingly, an IdeS middle-up approach is described for neonatal Fc receptor (FcRn) AC (Schlothauer et al., 2013). In this study, an impact of the Fab on the FcRn interaction was shown for several mAbs. The influence of different Fabs might also be relevant for other Fc receptor interactions. Thus, middle-up AC-MS also has high potential for investigating Fab-Fc structure-function relationships in a proteoform-resolved manner.

Comparability of Intact and Middle-Up FcγRIIIa Affinity Chromatography

FcγRIIIa AC, separates two distinct groups of peaks, representing fucosylated glycoforms (2x fucosylated glycoforms) with lower affinity and (partially) afucosylated glycoforms (2x and 1x afucosylated glycoforms) with higher affinity (**Figures 2**, **3**) (Lippold et al., 2019). It has to be noticed that the column performance was slightly different for late eluting glycoforms compared to previous experiments on intact mAb1 (Lippold et al., 2019). Fc glycoforms are discussed in a nomenclature as listed in **Supplementary Table 1**. Middle-up FcγRIIIa AC-MS exhibited sharper peaks than its intact counterpart (**Figure 3**). In general, decreasing the size of proteins in chromatography, in this case from 150 to 50 kDa, increases the diffusion coefficient (Tyn and Gusek, 1990). This improves the mass transfer kinetics of the protein (Gritti and Guiochon, 2012; Astefanei et al., 2017). Sharper peaks and a similar retention resulted in better separation efficiency for the middle-up FcγRIIIa AC-MS. Mainly, several partially separated species in the EICs of **Figure 3** indicate separation of glycoforms with terminal galactose present on the 1,3-arm or the 1,6-arm of G1F. Differential FcγRIIIa affinity of G1F(1,3) and G1F(1,6) glycoforms has recently been reported [G2F = G1F(1,6) > G1F(1,3) = G0F] (Aoyama et al., 2019). Based on this, G0F/G1F(1,3) has a similar affinity as G0F/G0F. G0F/G1F(1,6) exhibits an increased FcγRIIIa affinity comparable to G0F/G2F. Similarly, the G1F/G1F (G0F/G2F) peak shows partial separation. The first peak was assigned to G0F/G2F and G1F(1,3)/G1F(1,6) while the second peak likely represents G1F(1,6)/G1F(1,6). In addition, a third species [G1F(1,3)/G1F(1,3)] might populate the front of the peak. However, in this case peak asymmetry might provide an alternative explanation. For G1F/G2F, an early eluting peak [G1F(1,3)/G2F] was observed for the middle-up as well as the intact analysis. The affinity of G1F(1,6)/G2F was similar to G2F/G2F. A comparable glycoform ranking for mAb1 glycoforms is achieved in middle-up and intact FcγRIIIa AC-MS analysis. The masses corresponded to the expected Fc fragments (**Supplementary Table 2**) and comparability of glycoform affinity ranking to the intact mAb1 was demonstrated by comparing retention time differences (**Figure 3** and **Supplementary Figure 4**).

FcγRIIIa Affinity Analysis of Cetuximab Proteoforms

FcγRIIIa AC-MS of intact cetuximab is illustrated in **Figure 4** by EICs using *m/z* values of the three most abundant fucosylated and afucosylated Fc glycoforms, assuming H7N4F1/H7N4F1 as Fab glycosylation. Fab glycans are presented and discussed at a compositional level to avoid confusion with Fc glycans. Mainly fucosylated complex and high mannose glycoforms with little terminal galactose-α-1,3 galactose (α-gal) are described for the Fc glycosylation of SP2/0 produced cetuximab. For the Fab glycosylation, highly heterogeneous complex glycans with a high amount of α-gal and *N*-glycolylneuraminic acid (S) are reported (Jefferis, 2009; Biacchi et al., 2015). Intact cetuximab analysis proposed G0F/G1F and M5/G1F as the main fucosylated and (partially) afucosylated glycoforms, respectively (**Figure 5**). Based on literature, G0F/G0F and M5/G0F should be the most abundant Fc fucosylated and (partially) afucosylated glycoforms, respectively (Ayoub et al., 2013; Bern et al., 2018). This was later confirmed by middle-up analysis. FcγRIIIa AC-MS of intact cetuximab reduced the MS spectral complexity by separating fucosylated from (partially) afucosylated Fc glycoforms (**Figure 5**) compared to previously reported intact analysis (Ayoub et al., 2013; Bern et al., 2018). However, one MS peak may still be assigned to various combinations of Fc and Fab glycoforms with the same mass or similar masses. The degree of overlapping glycoforms and the resulting assignment ambiguities were exemplified by permutating three high abundant Fab glycoforms (H6N4F1, H6N4F1S1, H7N4F1) with the three most abundant Fc glycoforms (G0F, G1F, M5) already resulting in 36 different combinations (**Figure 5** and **Supplementary Table 3**). This is excluding heavy chain positional isomers within one site, such as G0F-H6N4F1/G1F-H7N4F1 and G0F-H7N4F1/G1F-H6N4F1. The theoretical number of possible glycoforms is significantly higher when considering all possible Fc and Fab glycans. Thus, at the intact level, assessing FcγRIIIa affinity of cetuximab glycoforms by AC-MS based on EICs is prevented by the high number of isomeric and non-resolved proteoforms. For example, Fc glycoforms G0F/G0F and G0F/G1F will be extracted as the same mass, when combined with Fab glycans of composition H7N4F1/H7N4F1 and H7N4F1/H6N4F1, respectively. The MS analysis of mAbs is generally affected by an increased signal heterogeneity derived from additional non-resolved proteoforms and adducts (Campuzano et al., 2019). In particular for native MS of complex proteins, the applied deconvolution (algorithm, settings) can have an influence on the data evaluation with respect to resolving heterogeneous mass spectra (Campuzano et al., 2019). Cetuximab glycoforms, containing H7N4F1/H6N4F1S1 and H6N4F1/H6N4F1S1 Fab glycoform pairings (**Figure 5** and **Supplementary Table 3**), were not resolved. A mass difference of 17 Da with H7N4F1/H7N4F1 and H6N4F1/H7N4F1 means the *m/z* difference for the most abundant charge state (28+) is 0.6 Th. This difference cannot be resolved under the applied conditions. Additionally, isomeric and non-resolved proteoforms lead to the distortion of the relative abundances as mentioned at the start of this paragraph. This becomes quite apparent when comparing the intact to the middle-up analysis in **Figures 4**, **5**.

In contrast, middle-up FcγRIIIa AC-MS of cetuximab simplified MS spectra enough to confidently assign Fc glycoforms and lysine variants (**Figures 4**, **5**). Nonetheless, the Fc glycoform pairing assignments also showed some degree of ambiguity

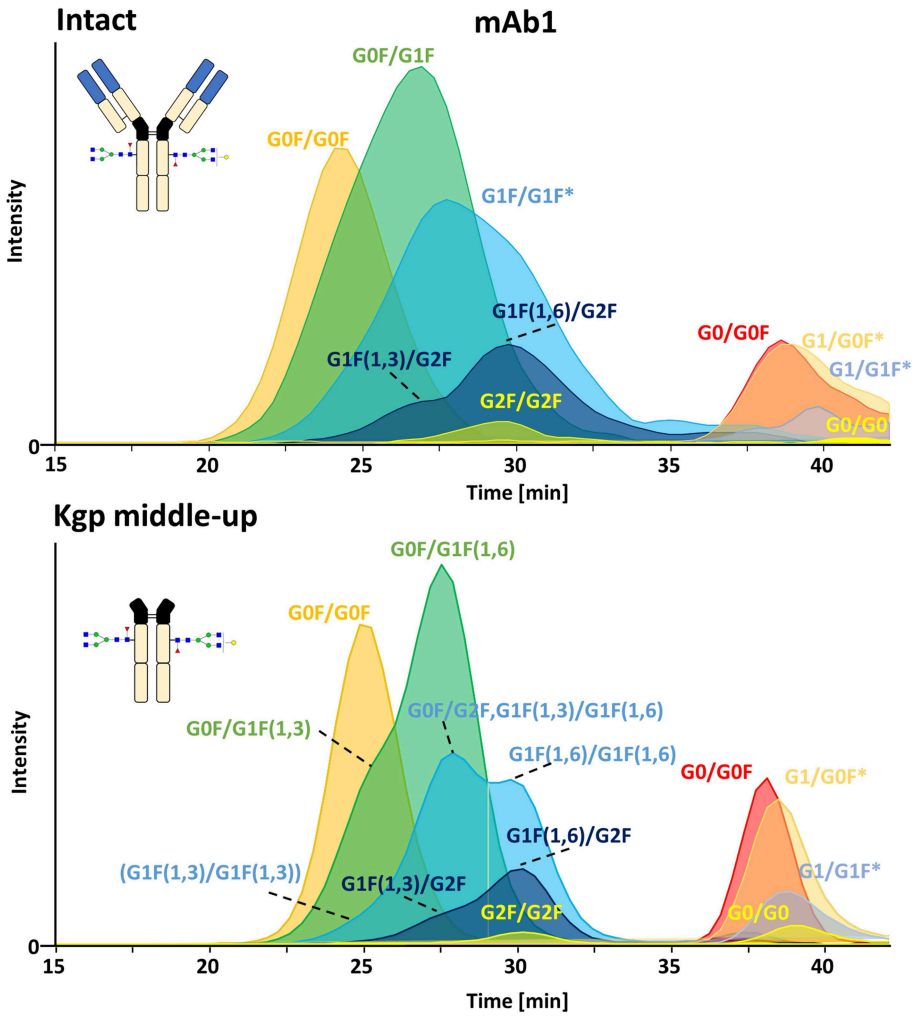

FIGURE 3 | Extracted ion chromatograms of major glycoforms assigned for FcγRIIIa AC-MS of mAb1 on intact and Kgp middle-up level. *indicates additional isomers listed in **Supplementary Table 2**.

(**Supplementary Table 4**, e.g., M5/G1F vs. M6/G0F). However, these ambiguities were minor compared to the intact mass analysis of cetuximab. Relative abundancies were in line with literature on Fc/2 glycoforms (Ayoub et al., 2013; Bern et al., 2018). The Fc glycan pairing of cetuximab was so far only briefly mentioned in a recent study, using IdeS digestion and direct infusion with native MS conditions (Bern et al., 2018). We observed G0F/G0F as the main fucosylated glycoform. Additional galactosylation variants were observed as for mAb1. M5/G0F was determined as main (partially) afucosylated glycoform. Further high mannose glycoforms (M5/M5, M5/G1F, M5/G2F) were detected. Low amounts of G0/G0F, G0/G1F were also found. Relative FcγRIIIa affinity was comparable to mAb1 (**Figure 3**) and/or consistent with literature (Lippold et al., 2019). For example, a strong decrease and a mild increase in FcγRIIIa binding was observed for fucosylation and galactosylation, respectively (Dashivets et al., 2015; Thomann et al., 2015). High mannose glycoforms exhibited a higher affinity than the fucosylated glycoforms but their affinity is decreased compared to the afucosylated complex-type glycoforms (Yu et al., 2012). Interestingly, different pairings of high mannose glycoforms with fucosylated complex-type glycans (M5/G1F. M5/G2F) could be studied and were found with slightly higher FcγRIIIa affinity compared to M5/M5. M5/G1F and M5/G2F showed a slightly increased affinity over M5/G0F. This confirms and extends our previous findings, which were limited to the comparison of low abundant M5/M5 and M5/G0F (Lippold et al., 2019). Though it is difficult to compare affinity of the intact and the Fc, the latter seems to show a higher affinity (**Figure 4**). This is comparable to the negative influence of the Fab on FcRn binding reported for cetuximab (Schlothauer et al., 2013).

Furthermore, C-terminal lysine variants (+K, **Figure 1**) could be studied in the middle-up analysis with respect to FcγRIIIa affinity. Investigations of incomplete lysine clipping with respect to different Fc glycoforms and FcγRIIIa affinity have not been described yet (Brorson and Jia, 2014). The C-terminal lysine

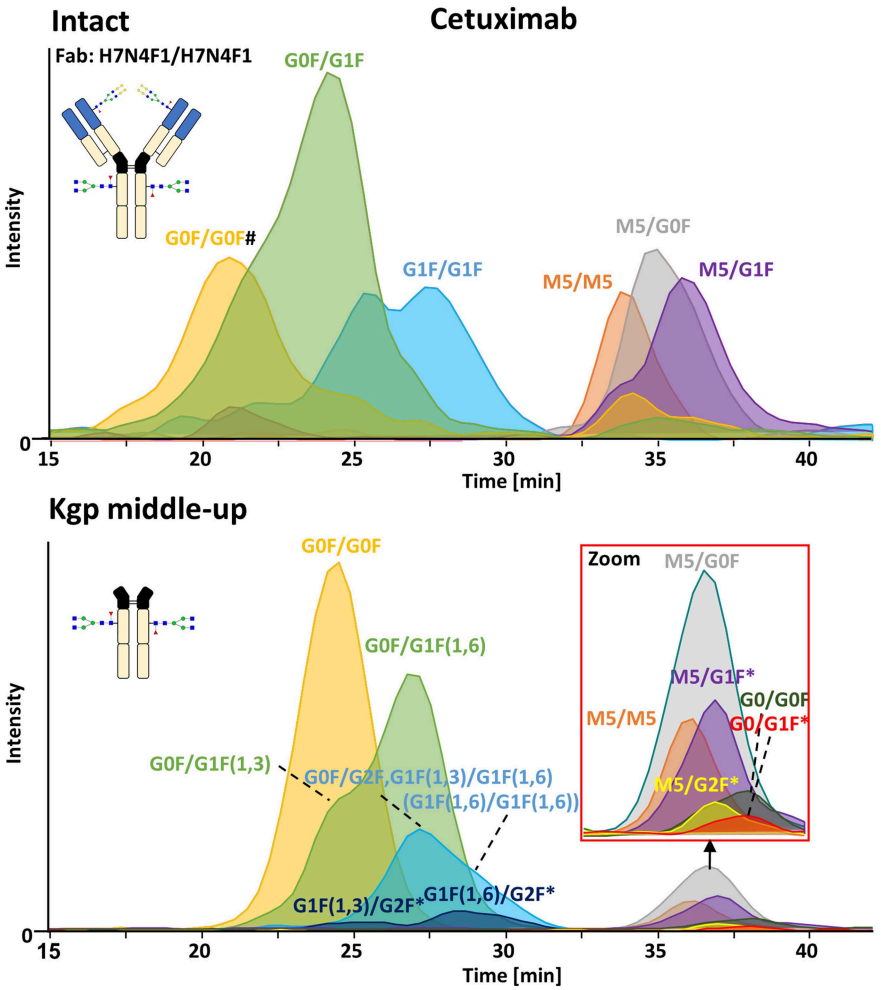

FIGURE 4 | FcγRIIIa AC-MS of cetuximab on intact and Kgp middle-up level. Intact analysis was restricted to the main Fab glycoform (H7N4F1/H7N4F1) and the most abundant Fc glycoforms (G0F, G1F, M5). G0F/G0F# is marked exemplarily for isomeric EICs: G0F/G1F exhibits the same EIC if the Fab glycoform is H7N4F1/H6N4F1. For middle-up FcγRIIIa AC-MS analysis, EICs of all detected Fc glycoforms are presented. Data for C-terminal lysine variants (+K) are omitted for clarity. *indicates additional isomers listed in **Supplementary Table 4**.

appeared not to influence the Fc glycoform retention strongly (**Supplementary Table 4**) which is not surprising as the receptor binds far away from the C-terminus (**Figure 1**). In contrast, C-terminal lysine may interfere with complement activation. However physiological relevance may anyhow be small as the lysine is enzymatically removed upon administration (van den Bremer et al., 2015).

Moreover, middle-up FcγRIIIa AC-MS allowed a simultaneous determination of Fab glycosylation by evaluating the injection peak (**Figure 5** and **Supplementary Table 5**). Fab glycosylation might be relevant for antigen binding and pharmacokinetic behavior (Huang et al., 2006; Jefferis, 2007). In total, 11 Fab glycoforms were assigned. Our results are qualitatively and quantitatively in line with reported Fab glycosylation of SP2/0 produced cetuximab (Ayoub et al., 2013; Bern et al., 2018). H7N4F1 was determined to be the most abundant glycoform followed by H6N4F1S1, in line with a previous report (Ayoub et al., 2013) and in contrast to a recent study (H7N4F2) (Bern et al., 2018). The two differently reported Fab glycoforms vary only by 1 Da. However, based on in-depth structural studies on cetuximab glycosylation reporting a high amount of S and only minor abundancies of antenna fucosylation, Fab glycoforms are more likely to contain H6N4F1S1 than additional H7N4F2 (Wiegandt and Meyer, 2014).

By applying middle-up FcγRIIIa AC-MS to cetuximab, 10 Fc glycoforms could be assigned, of which 5 Fc glycoforms were also found with the C-terminal lysine (amounting to 21 possible isomers, **Supplementary Table 4**). The combination of the 21 assigned Fc glycoform pairings (**Supplementary Table 4**) with the 11 assigned Fab glycoforms (**Supplementary Table 5**), belonging to 66 Fab glycoform pairings in theory, would result in 1,386 proteoforms for the intact cetuximab. This underlines the limitations of intact FcγRIIIa AC-MS for Fab glycosylated

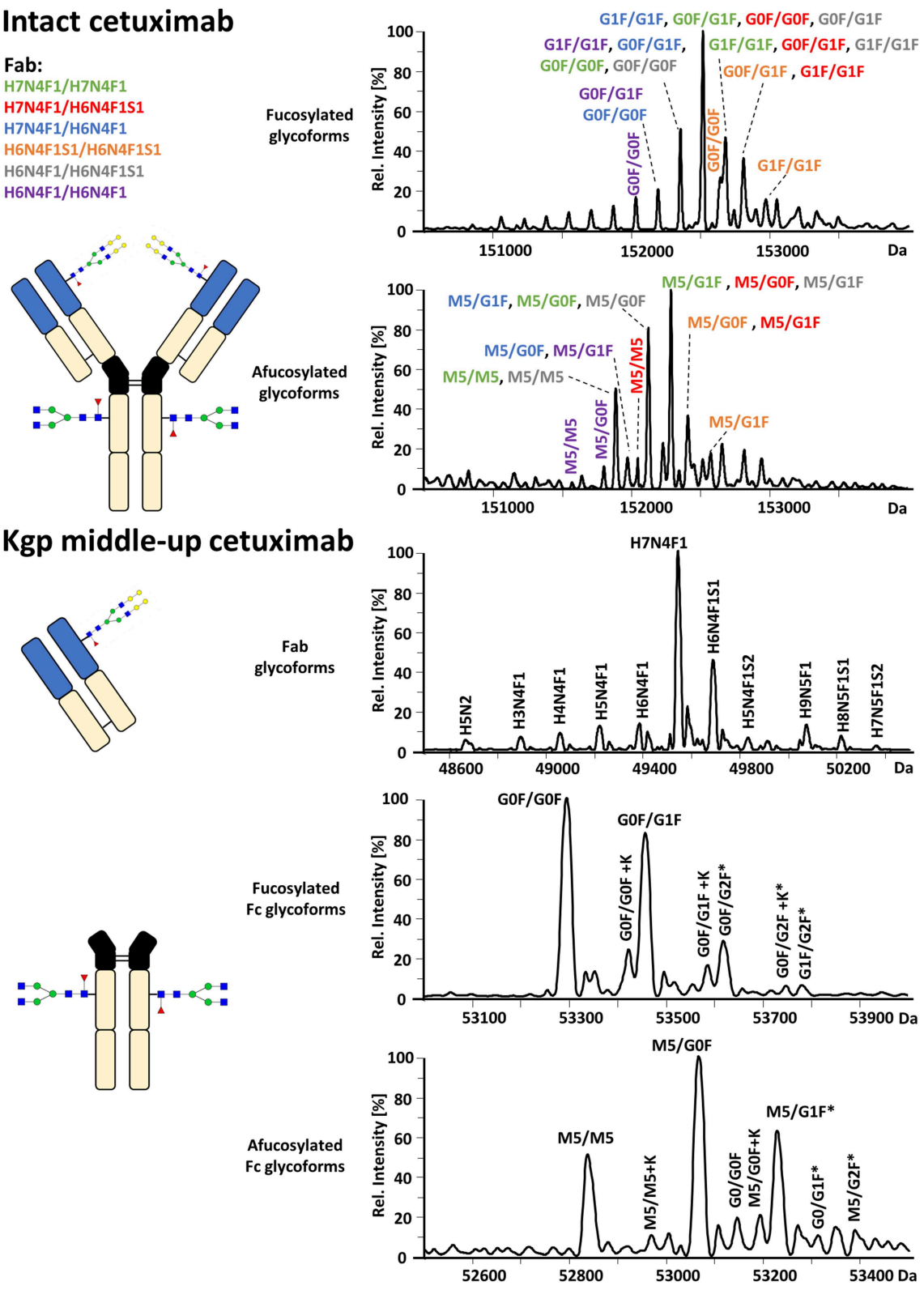

FIGURE 5 | Assignment of cetuximab glycoforms on intact and Kgp middle-up level by FcγRIIIa AC-MS. Fc glycoform assignment of intact cetuximab was restricted to 6 different Fab glycoform pairings indicated by a color code. The broad peaks often contain multiple isomeric and non-resolved glycoforms (**Supplementary Table 3**). Thirty four out of thirty six possibilities are assigned to peaks. For Kgp middle-up FcγRIIIa AC-MS, the composition of Fab glycoforms were assigned as well as the Fc fragments (*indicates additional isomers). All observed deconvoluted masses for intact and middle-up analysis are listed in **Supplementary Tables 3–5**.

IgGs and highlights the degree of simplification obtained by the middle-up workflow.

CONCLUSION

IgG Fc, generated by three established IgG middle-up proteases (IdeS, SpeB, Kgp), demonstrated differences in retention behavior in FcγRIIIa AC-MS. Kgp derived Fc showed a remarkably similar retention profile and glycoform ranking as the intact mAb. Advantages of the Kgp middle-up FcγRIIIa AC-MS workflow were demonstrated in the application to the Fab glycosylated therapeutic mAb, cetuximab. The middle-up workflow provided significantly reduced MS complexity compared to the intact level. Consequently, it revealed important information about cetuximab Fc glycoforms by enabling their confident assignment and quantitation while retaining the Fc pairing and FcγRIIIa AC retention. Simultaneously, Fab glycosylation could be determined.

In the future, middle-up AC-MS might also be a tool to investigate the interplay of the Fab and the Fc in structure-function studies of IgG-Fc receptor interactions. Since the presented workflow with Kgp is limited to human IgG1, further development of hinge-specific antibody proteases with broader subclass coverage would be highly desired. AC-MS workflows may thus be further expanded toward clinical applications and polyclonal therapeutic samples (e.g., intravenous IgGs). Moreover, the complexity of antibody-derived therapeutics is growing. Hence, the interest in middle-up approaches might further evolve in order to characterize new generations of therapeutic proteins.

DATA AVAILABILITY STATEMENT

The raw data supporting the conclusions of this manuscript will be made available by the authors, without undue reservation, to any qualified researcher.

AUTHOR CONTRIBUTIONS

SL performed and evaluated the experiments, supported by SN and supervised by DF. SL, MW, and DF designed the experiments. SL, SN, and DF drafted the manuscript. All authors contributed to finalizing the manuscript.

FUNDING

This research was supported by the European Union (Analytics for Biologics project, Grant No. 765502), as well as by the NWO (Vernieuwingsimpuls Veni Project No. 722.016.008).

SUPPLEMENTARY MATERIAL

The Supplementary Material for this article can be found online at: https://www.frontiersin.org/articles/10.3389/fchem.2019.00698/full#supplementary-material

REFERENCES

Anumula, K. R. (2012). Quantitative glycan profiling of normal human plasma derived immunoglobulin and its fragments Fab and Fc. *J. Immunol. Methods* 382, 167–176. doi: 10.1016/j.jim.2012.05.022

Aoyama, M., Hashii, N., Tsukimura, W., Osumi, K., Harazono, A., Tada, M., et al. (2019). Effects of terminal galactose residues in mannose α1-6 arm of Fc-glycan on the effector functions of therapeutic monoclonal antibodies. *MAbs* 11, 826–836. doi: 10.1080/19420862.2019.1608143

Astefanei, A., Dapic, I., and Camenzuli, M. (2017). Different stationary phase selectivities and morphologies for intact protein separations. *Chromatographia* 80, 665–687. doi: 10.1007/s10337-016-3168-z

Ayoub, D., Jabs, W., Resemann, A., Evers, W., Evans, C., Main, L., et al. (2013). Correct primary structure assessment and extensive glyco-profiling of cetuximab by a combination of intact, middle-up, middle-down and bottom-up ESI and MALDI mass spectrometry techniques. *MAbs* 5, 699–710. doi: 10.4161/mabs.25423

Beck, A., and Reichert, J. M. (2012). Marketing approval of mogamulizumab: a triumph for glyco-engineering. *MAbs* 4, 419–425. doi: 10.4161/mabs.20996

Beck, A., Wagner-Rousset, E., Ayoub, D., Van Dorsselaer, A., and Sanglier-Cianferani, S. (2013). Characterization of therapeutic antibodies and related products. *Anal. Chem.* 85, 715–736. doi: 10.1021/ac3032355

Bern, M., Caval, T., Kil, Y. J., Tang, W., Becker, C., Carlson, E., et al. (2018). Parsimonious charge deconvolution for native mass spectrometry. *J. Proteome Res.* 17, 1216–1226. doi: 10.1021/acs.jproteome.7b00839

Biacchi, M., Gahoual, R., Said, N., Beck, A., Leize-Wagner, E., and Francois, Y. N. (2015). Glycoform separation and characterization of cetuximab variants by middle-up off-line capillary zone electrophoresis-UV/electrospray ionization-MS. *Anal. Chem.* 87, 6240–6250. doi: 10.1021/acs.analchem.5b00928

Brorson, K., and Jia, A. Y. (2014). Therapeutic monoclonal antibodies and consistent ends: terminal heterogeneity, detection, and impact on quality. *Curr. Opin. Biotechnol.* 30, 140–146. doi: 10.1016/j.copbio.2014.06.012

Campuzano, I. D. G., Robinson, J. H., Hui, J. O., Shi, S. D. H., Netirojjanakul, C., Nshanian, M., et al. (2019). Native and denaturing MS protein deconvolution for biopharma: monoclonal antibodies and antibody–drug conjugates to polydisperse membrane proteins and beyond. *Anal. Chem.* 91, 9472–9480. doi: 10.1021/acs.analchem.9b00062

Chan, A. C., and Carter, P. J. (2010). Therapeutic antibodies for autoimmunity and inflammation. *Nat. Rev. Immunol.* 10, 301–316. doi: 10.1038/nri2761

Cymer, F., Beck, H., Rohde, A., and Reusch, D. (2018). Therapeutic monoclonal antibody N-glycosylation–Structure, function and therapeutic potential. *Biologicals* 52, 1–11. doi: 10.1016/j.biologicals.2017.11.001

Dashivets, T., Thomann, M., Rueger, P., Knaupp, A., Buchner, J., and Schlothauer, T. (2015). Multi-angle effector function analysis of human monoclonal IgG glycovariants. *PLoS ONE* 10:e0143520. doi: 10.1371/journal.pone.0143520

Dekkers, G., Treffers, L., Plomp, R., Bentlage, A. E. H., de Boer, M., Koeleman, C. A. M., et al. (2017). Decoding the human immunoglobulin G-Glycan repertoire reveals a spectrum of Fc-receptor- and complement-mediated-effector activities. *Front. Immunol.* 8:877. doi: 10.3389/fimmu.2017.00877

Ferrara, C., Grau, S., Jäger, C., Sondermann, P., Brünker, P., Waldhauer, I., et al. (2011). Unique carbohydrate–carbohydrate interactions are required for high affinity binding between FcγRIII and antibodies lacking core fucose. *Proc. Natl. Acad. Sci. U.S.A.* 108, 12669–12674. doi: 10.1073/pnas.1108455108

Gritti, F., and Guiochon, G. (2012). Mass transfer kinetics, band broadening and column efficiency. *J. Chromatogr. A* 1221, 2–40. doi: 10.1016/j.chroma.2011.04.058

Huang, L., Biolsi, S., Bales, K. R., and Kuchibhotla, U. (2006). Impact of variable domain glycosylation on antibody clearance: an LC/MS characterization. *Anal. Biochem.* 349, 197–207. doi: 10.1016/j.ab.2005.11.012

Janin-Bussat, M. C., Tonini, L., Huillet, C., Colas, O., Klinguer-Hamour, C., Corvaia, N., et al. (2013). Cetuximab Fab and Fc N-glycan fast characterization using IdeS digestion and liquid chromatography coupled to electrospray ionization mass spectrometry. *Methods Mol. Biol.* 988, 93–113. doi: 10.1007/978-1-62703-327-5_7

Jefferis, R. (2007). Antibody therapeutics: isotype and glycoform selection. *Expert Opin. Biol. Ther.* 7, 1401–1413. doi: 10.1517/14712598.7.9.1401

Jefferis, R. (2009). Glycosylation as a strategy to improve antibody-based therapeutics. *Nat. Rev. Drug Discov.* 8, 226–234. doi: 10.1038/nrd2804

Jiang, X.-R., Song, A., Bergelson, S., Arroll, T., Parekh, B., May, K., et al. (2011). Advances in the assessment and control of the effector functions of therapeutic antibodies. *Nat. Rev. Drug Discov.* 10, 101–111. doi: 10.1038/nrd3365

Kabat, E. A., Te Wu, T., Perry, H. M., Foeller, C., and Gottesman, K. S. (1991). *Sequences of Proteins of Immunological Interest.* Washington, DC: NIH Publication.

Kim, H. S., Kim, I., Zheng, L., Vernes, J.-M., Meng, Y. G., and Spiess, C. (2016). Evading pre-existing anti-hinge antibody binding by hinge engineering. *MAbs* 8, 1536–1547. doi: 10.1080/19420862.2016.1219006

Klein, C., Schaefer, W., and Regula, J. T. (2016). The use of CrossMAb technology for the generation of bi- and multispecific antibodies. *MAbs* 8, 1010–1020. doi: 10.1080/19420862.2016.1197457

Kol, A., Terwisscha van Scheltinga, A., Pool, M., Gerdes, C., de Vries, E., and de Jong, S. (2017). ADCC responses and blocking of EGFR-mediated signaling and cell growth by combining the anti-EGFR antibodies imgatuzumab and cetuximab in NSCLC cells. *Oncotarget* 8, 45432–45446. doi: 10.18632/oncotarget.17139

Kurai, J., Chikumi, H., Hashimoto, K., Yamaguchi, K., Yamasaki, A., Sako, T., et al. (2007). Antibody-dependent cellular cytotoxicity mediated by cetuximab against lung cancer cell lines. *Clin. Cancer Res.* 13, 1552–1561. doi: 10.1158/1078-0432.CCR-06-1726

Lermyte, F., Tsybin, Y. O., O'Connor, P. B., and Loo, J. A. (2019). Top or middle? Up or down? Toward a standard lexicon for protein top-down and allied mass spectrometry approaches. *J. Am. Soc. Mass Spectrom.* 30, 1149–1157. doi: 10.1007/s13361-019-02201-x

Lippold, S., Nicolardi, S., Domínguez-Vega, E., Heidenreich, A.-K., Vidarsson, G., Reusch, D., et al. (2019). Glycoform-resolved FcγRIIIa affinity chromatography–mass spectrometry. *MAbs* 11, 1191–1196. doi: 10.1080/19420862.2019.1636602

Liu, H., and May, K. (2012). Disulfide bond structures of IgG molecules: structural variations, chemical modifications and possible impacts to stability and biological function. *MAbs* 4, 17–23. doi: 10.4161/mabs.4.1.18347

Moelleken, J., Endesfelder, M., Gassner, C., Lingke, S., Tomaschek, S., Tyshchuk, O., et al. (2017). GingisKHAN^{TM} protease cleavage allows a high-throughput antibody to Fab conversion enabling direct functional assessment during lead identification of human monoclonal and bispecific IgG1 antibodies. *MAbs* 9, 1076–1087. doi: 10.1080/19420862.2017.1364325

Nimmerjahn, F., and Ravetch, J. V. (2008). Fcγ receptors as regulators of immune responses. *Nat. Rev. Immunol.* 8, 34–47. doi: 10.1038/nri2206

Pincetic, A., Bournazos, S., DiLillo, D. J., Maamary, J., Wang, T. T., Dahan, R., et al. (2014). Type I and type II Fc receptors regulate innate and adaptive immunity. *Nat. Immunol.* 15, 707–716. doi: 10.1038/ni.2939

Raju, T. S., and Scallon, B. (2007). Fc glycans terminated with N-acetylglucosamine residues increase antibody resistance to papain. *Biotechnol. Prog.* 23, 964–971. doi: 10.1002/bp070118k

Reusch, D., and Tejada, M. L. (2015). Fc glycans of therapeutic antibodies as critical quality attributes. *Glycobiology* 25, 1325–1334. doi: 10.1093/glycob/cwv065

Saunders, K. O. (2019). Conceptual approaches to modulating antibody effector functions and circulation half-life. *Front. Immunol.* 10:1296. doi: 10.3389/fimmu.2019.01296

Schlothauer, T., Herter, S., Koller, C. F., Grau-Richards, S., Steinhart, V., Spick, C., et al. (2016). Novel human IgG1 and IgG4 Fc-engineered antibodies with completely abolished immune effector functions. *Protein Eng. Des. Sel.* 29, 457–466. doi: 10.1093/protein/gzw040

Schlothauer, T., Rueger, P., Stracke, J. O., Hertenberger, H., Fingas, F., Kling, L., et al. (2013). Analytical FcRn affinity chromatography for functional characterization of monoclonal antibodies. *MAbs* 5, 576–586. doi: 10.4161/mabs.24981

Shatz, W., Chung, S., Li, B., Marshall, B., Tejada, M., Phung, W., et al. (2013). Knobs-into-holes antibody production in mammalian cell lines reveals that asymmetric afucosylation is sufficient for full antibody-dependent cellular cytotoxicity. *MAbs* 5, 872–881. doi: 10.4161/mabs.26307

Sjögren, J., Andersson, L., Mejàre, M., and Olsson, F. (2017). "Generating and purifying Fab fragments from human and mouse IgG using the bacterial enzymes IdeS, SpeB and Kgp," in *Bacterial Pathogenesis: Methods and Protocols,* eds P. Nordenfelt and M. Collin (New York, NY: Springer New York), 319–329. doi: 10.1007/978-1-4939-6673-8_21

Sjögren, J., Olsson, F., and Beck, A. (2016). Rapid and improved characterization of therapeutic antibodies and antibody related products using IdeS digestion and subunit analysis. *Analyst* 141, 3114–3125. doi: 10.1039/C6AN00071A

Sondermann, P., Huber, R., Oosthuizen, V., and Jacob, U. (2000). The 3.2-Å crystal structure of the human IgG1 Fc fragment–FcγRIII complex. *Nature* 406, 267–273. doi: 10.1038/35018508

Thomann, M., Schlothauer, T., Dashivets, T., Malik, S., Avenal, C., Bulau, P., et al. (2015). *In vitro* glycoengineering of IgG1 and its effect on Fc receptor binding and ADCC activity. *PLoS ONE* 10:e0134949. doi: 10.1371/journal.pone.0134949

Tyn, M. T., and Gusek, T. W. (1990). Prediction of diffusion coefficients of proteins. *Biotechnol. Bioeng.* 35, 327–338. doi: 10.1002/bit.260350402

van den Bremer, E. T., Beurskens, F. J., Voorhorst, M., Engelberts, P. J., de Jong, R. N., van der Boom, B. G., et al. (2015). Human IgG is produced in a pro-form that requires clipping of C-terminal lysines for maximal complement activation. *MAbs* 7, 672–680. doi: 10.1080/19420862.2015.1046665

van den Bremer, E. T. J., Labrijn, A. F., van den Boogaard, R., Priem, P., Scheffler, K., Melis, J. P. M., et al. (2017). Cysteine-SILAC mass spectrometry enabling the identification and quantitation of scrambled interchain disulfide bonds: preservation of native heavy-light chain pairing in bispecific IgGs generated by controlled Fab-arm exchange. *Anal. Chem.* 89, 10873–10882. doi: 10.1021/acs.analchem.7b02543

van der Burgt, Y. E. M., Kilgour, D. P. A., Tsybin, Y. O., Srzentić, K., Fornelli, L., Beck, A., et al. (2019). Structural analysis of monoclonal antibodies by ultrahigh resolution MALDI in-source decay FT-ICR mass spectrometry. *Anal. Chem.* 91, 2079–2085. doi: 10.1021/acs.analchem.8b04515

Wada, R., Matsui, M., and Kawasaki, N. (2019). Influence of N-glycosylation on effector functions and thermal stability of glycoengineered IgG1 monoclonal antibody with homogeneous glycoforms. *MAbs* 11, 350–372. doi: 10.1080/19420862.2018.1551044

Walsh, G. (2018). Biopharmaceutical benchmarks 2018. *Nat. Biotechnol.* 36, 1136–1145. doi: 10.1038/nbt.4305

Weiner, L. M., Surana, R., and Wang, S. (2010). Monoclonal antibodies: versatile platforms for cancer immunotherapy. *Nat. Rev. Immunol.* 10, 317–327. doi: 10.1038/nri2744

Wiegandt, A., and Meyer, B. (2014). Unambiguous characterization of N-glycans of monoclonal antibody cetuximab by integration of LC-MS/MS and 1H NMR spectroscopy. *Anal. Chem.* 86, 4807–4814. doi: 10.1021/ac404043g

Yan, B., Boyd, D., Kaschak, T., Tsukuda, J., Shen, A., Lin, Y., et al. (2012). Engineering upper hinge improves stability and effector function of a human IgG1. *J. Biol. Chem.* 287, 5891–5897. doi: 10.1074/jbc.M111.311811

Yu, M., Brown, D., Reed, C., Chung, S., Lutman, J., Stefanich, E., et al. (2012). Production, characterization, and pharmacokinetic properties of antibodies with N-linked mannose-5 glycans. *MAbs* 4, 475–487. doi: 10.4161/mabs.20737

Zhang, Z., Perrault, R., Zhao, Y., and Ding, J. (2016). SpeB proteolysis with imaged capillary isoelectric focusing for the characterization of domain-specific charge heterogeneities of reference and biosimilar Rituximab. *J. Chromatogr. B* 1020, 148–157. doi: 10.1016/j.jchromb.2016.03.031

Conflict of Interest: The authors declare that the research was conducted in the absence of any commercial or financial relationships that could be construed as a potential conflict of interest.

frontiers in Chemistry

ORIGINAL RESEARCH
published: 01 November 2019
doi: 10.3389/fchem.2019.00726

Site-Specific Conjugation for Fully Controlled Glycoconjugate Vaccine Preparation

*Aline Pillot[1,2], Alain Defontaine[1], Amina Fateh[1], Annie Lambert[1], Maruthi Prasanna[1,3], Mathieu Fanuel[4], Muriel Pipelier[2], Noemi Csaba[3], Typhaine Violo[1], Emilie Camberlein[1] and Cyrille Grandjean[1]**

[1] Université de Nantes, CNRS, Unité Fonctionnalité et Ingénierie des Protéines (UFIP), UMR 6286, Nantes, France, [2] Université de Nantes, CNRS, Chimie Et Interdisciplinarité: Synthèse, Analyse, Modélisation (CEISAM), UMR 6230, Nantes, France, [3] Department of Pharmacology, Pharmacy and Pharmaceutical Technology, Center for Research in Molecular Medicine and Chronic Diseases (CIMUS), School of Pharamacy, Health Research Institute of Santiago de Compostela (IDIS), University of Santiago de Compostela, Santiago de Compostela, Spain, [4] Unité Biopolymères Interactions Assemblages Plate-Forme BIBS, INRA, Nantes, France

Glycoconjugate vaccines are formed by covalently link a carbohydrate antigen to a carrier protein whose role is to achieve a long lasting immune response directed against the carbohydrate antigen. The nature of the sugar antigen, its length, its ratio per carrier protein and the conjugation chemistry impact on both structure and the immune response of a glycoconjugate vaccine. In addition it has long been assumed that the sites at which the carbohydrate antigen is attached can also have an impact. These important issue can now be addressed owing to the development of novel chemoselective ligation reactions as well as techniques such as site-selective mutagenesis, glycoengineering, or extension of the genetic code. The preparation and characterization of homogeneous bivalent pneumococcal vaccines is reported. The preparation and characterization of homogeneous bivalent pneumococcal vaccines is reported. A synthetic tetrasaccharide representative of the serotype 14 capsular polysaccharide of *Streptococcus pneumoniae* has been linked using the thiol/maleimide coupling chemistry to four different Pneumococcal surface adhesin A (PsaA) mutants, each harboring a single cysteine mutation at a defined position. Humoral response of these 1 to 1 carbohydrate antigen/PsaA conjugates have been assessed in mice. Our results showed that the carbohydrate antigen-PsaA connectivity impacts the anti-carrier response and raise questions about the design of glycoconjugate vaccine whereby the protein plays the dual role of immunogen and carrier.

Keywords: glycoconjugate vaccine, cysteine mutagenesis, chemoselective ligation, protein conjugation, pneumococcal vaccine, thio/maleimide ligation

OPEN ACCESS

Edited by:
Christoph Rademacher, Max Planck Institute of Colloids and Interfaces, Germany

Reviewed by:
Rino Rappuoli, GlaxoSmithKline, Italy
Neil Ravenscroft, University of Cape Town, South Africa

***Correspondence:**
Cyrille Grandjean
cyrille.grandjean@univ-nantes.fr

Specialty section:
This article was submitted to Chemical Biology, a section of the journal Frontiers in Chemistry

Received: *28 July 2019*
Accepted: *10 October 2019*
Published: *01 November 2019*

Citation:
Pillot A, Defontaine A, Fateh A, Lambert A, Prasanna M, Fanuel M, Pipelier M, Csaba N, Violo T, Camberlein E and Grandjean C (2019) Site-Specific Conjugation for Fully Controlled Glycoconjugate Vaccine Preparation. Front. Chem. 7:726. doi: 10.3389/fchem.2019.00726

INTRODUCTION

Surface exposed polysaccharides of bacterial pathogens are perceived as non-self by the host immune system. Therefore, they are often the target of a protective humoral immune response. Immunization using polysaccharides from capsulated bacteria has been introduced by Gotschlich in the late 1960s (Gotschlich et al., 1972). Capsular polysaccharides are typical T cell-independent

type 2 antigens (Mond et al., 1995). This group of antigens is able to deliver prolonged and persistent signaling to the B cell through B cell receptor cross-linking. However, these vaccines fail to be active in children, the population which is the major target of the infectious diseases caused by pathogenic bacteria. A major breakthrough in the field has been later achieved by the development of the glycoconjugate vaccines (Rappuoli, 2018). A purified capsular polysaccharide or a fragment thereof or a synthetic oligosaccharide mimicking the antigenic determinants expressed by capsular polysaccharide is conjugated to a protein scaffold referred to as carrier protein. In this case, the protein moiety of the conjugate is processed by carbohydrate antigen-specific B cells after engagement of their B cell receptor. This leads to the presentation of peptides—T helper epitopes—in association with major histocompatibility complex of type II (MHCII) molecules to carrier peptide-specific $CD4^+$ T lymphocytes. These T helper cells, in turn, stimulate the production of both plasma cells and memory B cells (Pollard et al., 2009). This vaccine strategy proved highly efficient even in infants. Consequently several vaccines active against meningococcus, streptococcus, or *Haemophilus influenza* type b have been launched (Berti and Adamo, 2018). Alternatively it has recently been shown that a carbohydrate epitope presented in the form of a glycopeptide by the MHCII molecules could strongly stimulate $CD4^+$ T cells (Avci et al., 2011; Berti and Adamo, 2013). While both mechanisms probably coexist, this discovery might considerably impact the design of future glycoconjugate vaccines. Indeed, it has long been established that both length and density of the carbohydrate antigens on the carrier protein influence the immunogenicity of the conjugates in an interconnected manner. At a fixed sugar/protein ratio, the anti-carbohydrate antigen titers vary according to a bell curve as a function of density (Pozsgay et al., 1999). On the other hand, the observed optimum depends on the length of the antigen, this value being usually lowered when one increases the chain length (Anderson et al., 1989). However, if second mechanism has to be considered, the selection of the glycosylation sites is equally important. Along this line, Peng et al. have taken advantage of the propensity of flagellin to self-assemble in a supercoiled structure to selectively modify the sole lysines exposed to the solvent and thus preserving the protein properties to activate immune response (Peng et al., 2018). Stefanetti et al. recently prepared a series of glycoconjugates made of CRM_{197} and *Salmonella O*-antigen as the carrier protein and the carbohydrate antigen, respectively (Stefanetti et al., 2015). An average of one up to four *O*-antigen chains per protein was introduced at controlled positions. The *O*-antigen chains were randomly linked to surface accessible glutamic/aspartic acid or lysine residues or at more defined sites upon exploiting the kinetically favored reactivity of lysines having the lowest pK_a (Crotti et al., 2014; Matos et al., 2018), the rarity of surface exposed tyrosine selectively activated (Hu et al., 2013; Nilo et al., 2014), the transglutaminase catalyzed modification of a lysine (Nilo et al., 2015b) or upon designing stapled conjugate from a reduced disulfide bond. This study was useful to demonstrate that the conjugation site plays a role in determining the immunogenicity. However, the tested formulations still contained heterogeneous mixtures of conjugates since the derivatization processes remain largely empirical. Moreover, further discrepancies arose from structural differences among the linkers used in the study although the same strain promoted azide-alkyne cycloaddition reaction was applied for the preparation of every conjugate. Such biases do not allow an unequivocal interpretation of observed results. Yet recent progress made in unnatural amino acid incorporation (Quast et al., 2015), protein glycan coupling technology (PGCT) (Ma et al., 2018) or site-selective mutagenesis (Grayson et al., 2011) offer unique opportunities to access fully defined glycoconjugate vaccines and further elucidate the relationship between carbohydrate antigen/carrier protein connectivity and immunogenicity. We report herein the preparation and the characterization of homogeneous bivalent pneumococcal conjugates. A synthetic tetrasaccharide derived from *Streptococcus pneumoniae* serotype 14 capsular polysaccharide equipped of a maleimido-functionalized spacer arm at its reducing end has been site-specifically attached to four different cysteine mono-mutants of the Pneumococcal surface adhesin A (PsaA).

RESULTS AND DISCUSSION

Conjugate Design, Synthesis, and Characterization

Pneumococcal infections are still a leading cause of mortality worldwide. Available prophylactic pneumococcal glycoconjugate vaccines induce capsule-specific memory B-cells and IgG capable to prevent colonization and disease (Jochems et al., 2017). Vaccine effectiveness is considerably improved by increasing the valency e.g., from 7 up to 13 serotypes (van der Linden et al., 2016). However, inclusion of serotype-independent immunogens able to control pneumococcal carriage to these vaccines has been identified as an appealing strategy (Jochems et al., 2017). PsaA is a nasopharyngeal colonization factor which is expressed by more than 99% of pneumococcal strains in a highly conserved form (Rajam et al., 2008a). These features have thus designed PsaA as a possible protein immunogen candidate (Wang et al., 2010; Gor et al., 2011; Olafsdottir et al., 2012; Lu et al., 2015). Concomitant administration of PsaA with PCV7 was accompanied with reduced colonization in a murine model (Whaley et al., 2010) and its protective effect in association with a panel of pneumococcal protein immunogens later assessed in phase I clinical trials (Schmid et al., 2011; Entwisle et al., 2017). Moreover, the successful use of PsaA both as an immunogen and a carrier protein PsaA by several laboratories including ours in mice models further encouraged us to select it as a model protein (Lin et al., 2010; Chen et al., 2016; Prasanna et al., 2019). Mature PsaA (mPsaA) i.e., PsaA deprived from its signal peptide, was therefore conjugated to the tetrasaccharide $\beta-\text{D}-Galp-(1\rightarrow4)-\beta-\text{D}-Glcp-(1\rightarrow6)-[\beta-\text{D}-Galp-(1\rightarrow4)]\beta$-D-GlcpNAc **1** (referred to as Pn14TS) (**Figure 1A**). This easily synthesized tetrasaccharide is the minimal structure from the capsule of serotype 14, one of the prevalent pneumococcal serotype which has developed high antibiotic resistance (Yahiaoui et al., 2018), able to induce functional antibodies (Abs) (Safari et al., 2008).

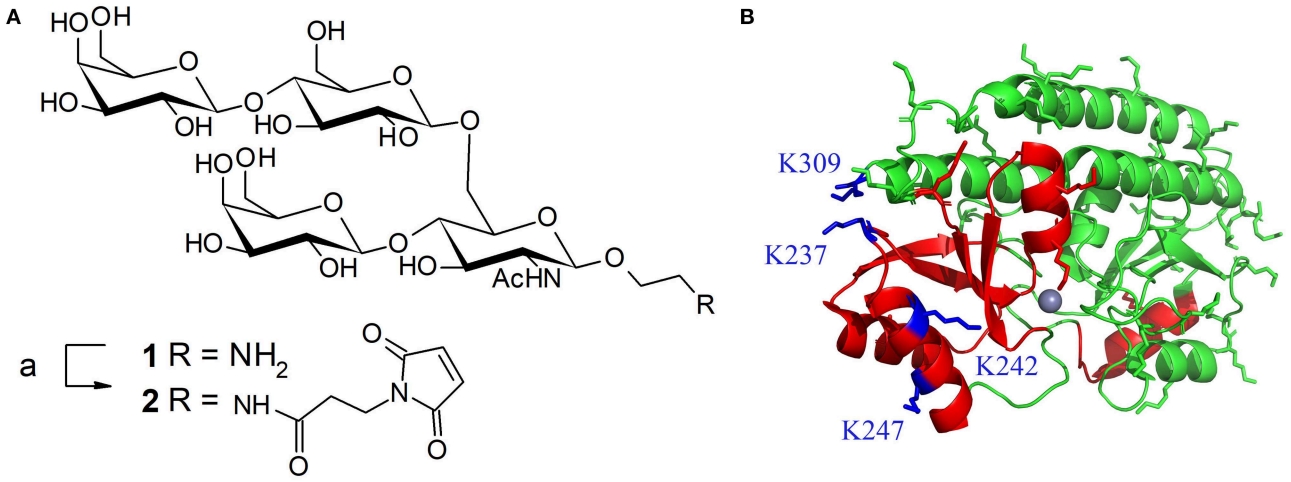

FIGURE 1 | (A) Structure of tetrasaccharide antigen **1** from *S. pneumoniae* serotype 14 capsule and its activation with a maleimide linker; reagents and conditions: (a) 3-maleimidopropionic acid *N*-hydrosysuccimide ester (1.45 equiv), DIEA (2 equiv), DMF, RT, overnight, 58%. **(B)** Ribbon diagram of PsaA (green). Regions containing known Th and B-epitopes are colored in red. Lysine side-chain are represented in green except the four lysines targeted for mutagenesis (in blue). Representation based on the 1PSZ PDB file, with a resolution of 2.0 Å (Lawrence et al., 1998).

We observed that while high anti-mPsaA Ab titers were induced in mice immunized with mPsaA alone, this response was much lower when mice where immunized with a conjugate whereby Pn14TS was randomly coupled to surface-exposed lysine side-chains of mPsaA at a 5.4:1 average value for carbohydrate:protein ratio (Prasanna et al., 2019). This observation might result from mPsaA B epitope masking due to Pn14TS conjugation on the protein, immune-dominance of antigenic determinants expressed by Pn14TS over the mPsaA B epitopes or different processing of free vs. conjugated mPsaA. Developing an access to homogeneous Pn14TS-mPsaA conjugates will therefore provide tools to address these issues and document structure-immunogenicity relationships useful for future pneumococcal vaccine design.

mPsaA is a 32.4 kDa-protein which corresponds to amino acids 21-309 of PsaA sequence. mPsaA essentially adopts alpha-helical secondary structures and contains 37 lysines, most of them accessible for conjugation (**Figure 1B**) (Couñago et al., 2014). Interestingly, mPsaA does not contain any cysteine residue which makes site-selective cysteine mutagenesis an attractive approach to envision homogenous mPsaA conjugate synthesis (Grayson et al., 2011). Previous studies based on secondary structure predictions, endopeptidase site analyses and *in silico* MCHII peptide-binding affinity screening helped identifying a panel of 24 putative PsaA T-helper epitopes. Three out of them proved to be able to provoke Th cell proliferation: $PsaA^{67-82}$, $PsaA^{199-221}$, and $PsaA^{231-268}$. The last one was deduced from three potent overlapping 15-mer peptides among which sequence 243–257 was the most potent (Singh et al., 2014). Identification of PsaA B epitopes has also been carried out using a phage display peptide library and monoclonal Abs. Two sequences in the region 132–146 and 253–267 showed promises for their immunogenicity in mice noticeably for reducing carriage and colonization (Srivastava et al., 2000; Johnson et al., 2002). Further studies have demonstrated that the sequence $PsaA^{251-278}$ was involved in PsaA-mediated adherence of *S. pneumoniae* to epithelial cells (Romero-Steiner et al., 2006; Rajam et al., 2008b). In view of these data, we elected to mutate C-terminal lysine 309 located in an apparently non-relevant region for immunity into a cysteine. The preparation of three additional cysteine mutants at K237, K242, and K247 i.e., within or close to the potent T-helper epitope was also envisaged (**Figure 1B**).

We have recently reported the production in *Escherichia coli* BL21(DE3) of the mPsaA *N*-terminated by a poly-6-histidine tag sequence to facilitate its purification by immobilized-Ni affinity chromatography plus a Tabacco Etch Protease (TEV) specific cleavage site to remove the tag after purification (Prasanna et al., 2019). mPsaA production level has been increased by 5–6 fold upon adopting time/temperature/induction conditions reported by Laurentis et al. and replacing the LB by the TB growth medium (**Supplementary Figure 1** and **Supplementary Table 1**) (Larentis et al., 2011). The four mutants have been produced accordingly after having introduced every desired mutation in the original sequence using the QuickChange method. Culture have been carried out at a 250 ml scale and yielded about 19 mg of each mutant after purification and histidine tag removal (**Figure 2**).

Having the four mutants in hand we next examined their respective conjugation with the carbohydrate antigen. To this aim, known tetrasaccharide **1** (Prasanna et al., 2019) was derivatized with a maleimide linker to provide **2** in 58% yield following RP-HPLC purification (**Figure 1A**). The four mutants were treated separately with DTT to reduce any inter-protein disulfide bond which might have formed during their preparation and further reacted with no more than 5 equivalent of **2** in degassed PBS, pH 7.0 at room temperature overnight. Each

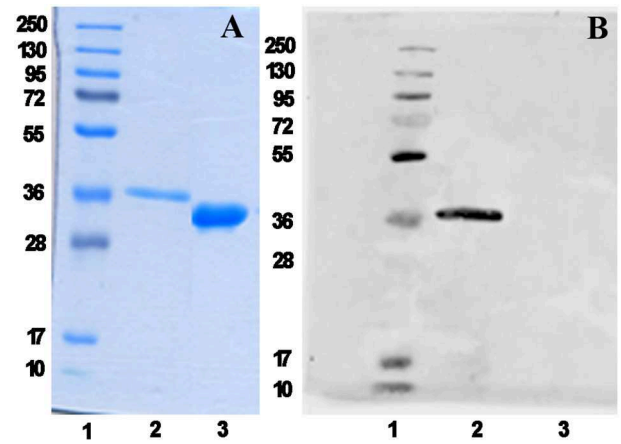

FIGURE 2 | mPsaA K309C characterization as a representative example. Analysis of histidine tag removal from mutant mPsaA K309C by SDS-PAGE **(A)** and by Western blot **(B)**. Lane 1: unstained protein marker; Lane 2: tagged mPsaA K309C; Lane 3: purified mPsaA K309C after removal of poly-histidine tag.

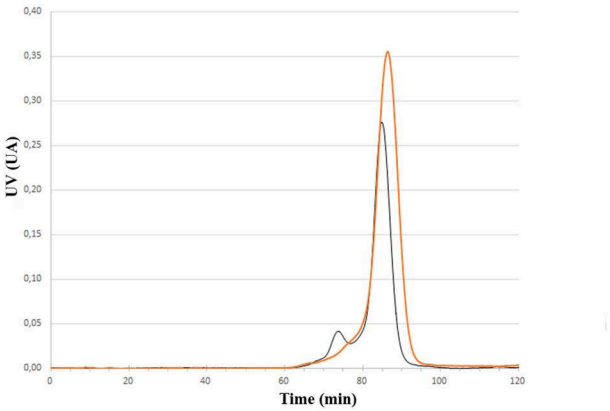

FIGURE 3 | Comparison of size exclusion chromatography profile of Pn14TS-mPsaA K247C (red trace) and Pn14TS-mPsaA K309C (Black trace) conjugates. Column HiLoad 15/600 Superdex^{TM} 75 pg (GE Healthcare) column and PBS 0.1 M, pH 7.3 as eluent.

conjugate was then subjected to gel filtration purification to remove excess tetrasaccharide (**Figure 3**) and freeze-dried for storage. Gel filtration chromatography profiles of conjugates associated to mPsaA K237C, K242C, and K247C were very similar and essentially composed of a single peak. A second unidentified peak which is eluted earlier is apparent in the Pn14TS-mPsaA K309C profile (**Figure 3**). We first thought that it corresponds to a dimer of the mPsaA K309C whose formation had been favored due to a greater exposure of the cysteine at the C-terminus. However, mass spectrometry experiments ruled out this hypothesis. Effectiveness of the conjugation was checked by gel electrophoresis which uniformly showed that spots are shifted toward higher molecular weight, compatible with the attachment of a single tetrasaccharide (**Figure 4A**). These results were confirmed by MALDI mass spectrometry experiments which indicate that parent mutant mPsaA proteins were incremented by 896–906 mass unit (calculated +901 Da) within the error range mass measurements (**Figure 4B**). In the end homogenous 1:1 carbohydrate antigen/carrier protein K237C, K242C, K247C, K309C conjugates have been obtained in 55, 36, 44, and 30% yield, respectively, with a purity superior to 90%.

Humoral Response Evaluation

Groups of five C57/BL6 mice were immunized thrice at 2 weeks interval with each of the four conjugates and PBS as a negative control formulated in chitosan and Ribi as adjuvant. The antibody response against both mPsaA and capsular polysaccharide of *S. pneumoniae* serotype 14 (CP14), was then determined by ELISA assays 1 week after the second and third immunization (i.e., on Days 21 and 35). The IgG response raised against CP14 by the conjugates was very low and not significant compared to the negative control group (data not shown). This response was equally low when we used Pn14TS as the coating antigen indicating that the observed results were not due to a lack of recognition of CP14 by anti-Pn14TS Abs. Anti-CP14 IgM response was also determined after the second and the third immunizations. Low titers of anti-CP14 IgM Abs could be measured in the sera of mice for any of the tested formulations after the second immunization **(Supplementary Figure 2A).** Highest titers of anti-CP14 Abs seem to be induced by Pn14TS-mPsaA K247C conjugate in comparison with other conjugates and PBS. Pn14TS-mPsaA K309C gave rise to the weakest response comparable to that induced by PBS. However, these tendencies were not statistically significant. Anti-IgM responses further diminished after the boost although the expected IgM to IgG switch was not observed **(Supplementary Figure 2B).** In fact, we and other experienced in the past that Pn14Ts was able to efficiently mimic native CP14 (Safari et al., 2008; Kurbatova et al., 2017; Prasanna et al., 2019). However, as mentioned in the introduction, it is assumed that the level of the anti-carbohydrate antigen response depends on intricate related parameters such as carbohydrate antigen length, carbohydrate antigen:carrier (S/P) ratio and administered sugar dose (Pozsgay et al., 1999). For examples, significant humoral response has been previously observed against Pn14TS: this hapten being used at a S/P ratio of 4, at a 2.5 μg dose using adipic acid coupling chemistry and CRM_{197} as the carrier (Mawas et al., 2002); at a S/P ratio of 4.8 or 6, at a 2.5 μg dose, using squarate coupling chemistry and CRM_{197} as carrier protein (Mawas et al., 2002; Safari et al., 2008); at a S/P ratio of 11, at 1.25–10 μg dose, using squarate chemistry and BSA as carrier; at a S/P ratio of 5.4, at 3 μg dose using thio/maleimide coupling chemistry and PsaA as carrier protein. Testing of Pn14TS at a S/P of 1 is unprecedented. Absence of anti-CP14 IgG response might be circumvented upon increasing the length of the antigen. Effective response was nicely observed when a dodecasaccharide (corresponding to 3 × Pn14TS units), conjugated to CRM_{197} was used in a 1:1 carbohydrate antigen/carrier protein ratio (Safari et al., 2008). Increasing the administered dose could also

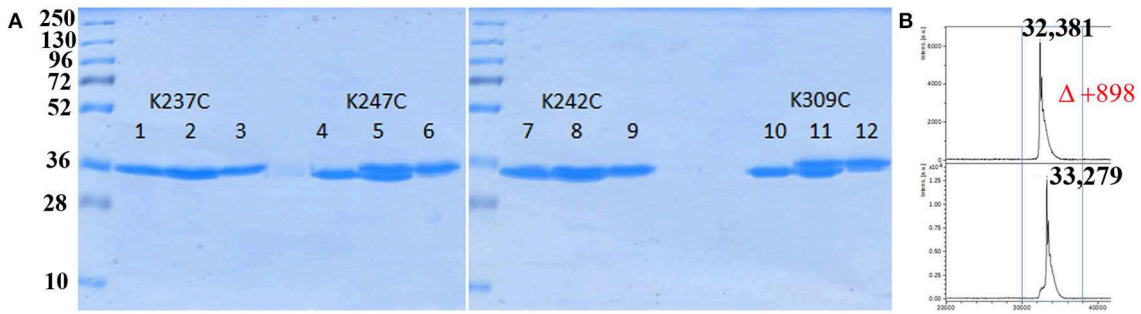

FIGURE 4 | Analysis of bioconjugation efficiency by SDS PAGE and mass spectrometry. **(A)** Comparison of each mPsaA mutant before, mix of before and after, and after conjugation. Lanes 1–3: mPsaA K237C; Lanes 4–6: mPsaA K247C; Lanes 7–9: mPsaA K242C; Lanes 10–12: mPsaA K309C. Two micrograms protein sample/lane, 12% SDS-PAGE, 100 V, 2 h; **(B)** MALDI MS spectrum of mPsaA K309C (top spectrum) and Pn14TS-mPsaA K309C (bottom spectrum).

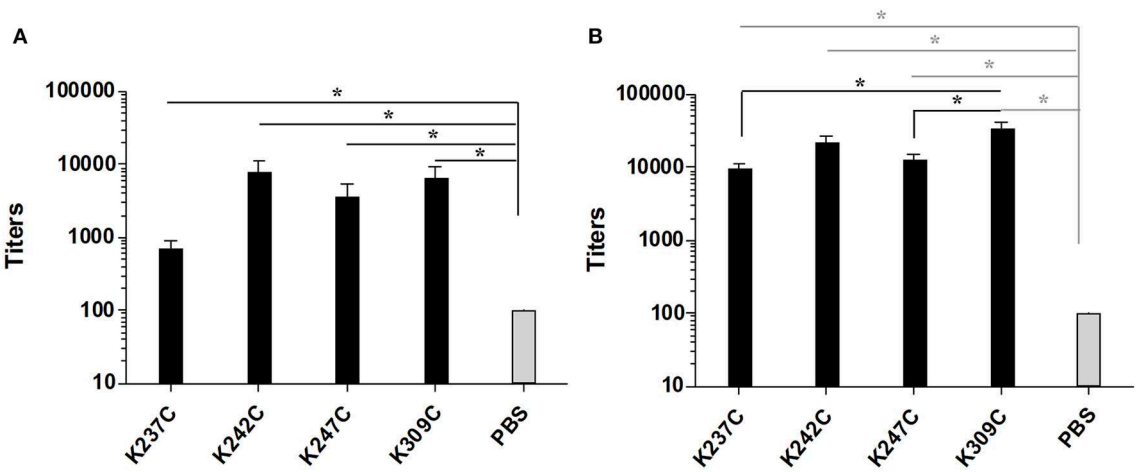

FIGURE 5 | Titers of anti-mPsaA (coated on microtiter plates) IgG Abs of mice immunized with Pn14TS-mPsaA K237C, K242C, K247C, K309C, PBS 1 week after the 2nd (J21) **(A)** and the 3rd (J35) immunization **(B)**. The serum samples data presented as geometric mean titer ± standard deviation of five mice per group. Statistical analysis was performed using one-way ANOVA with Tukey analysis for multiple comparisons. Statistical difference between the groups is $^*P < 0.05$.

been envisaged. A very low amount of carbohydrate antigens (0.5 μg/dose/mouse) was indeed used for immunizations. This value was chosen to keep the amount of injected mPsaA equal to 25 μg/dose/mouse and remaining coherent with our previous experiments (Prasanna et al., 2019). The adopted strategy was nevertheless applicable to the investigation of the anti-mPsaA response. IgM Ab response was absent in all tested sera in agreement with our previous findings (data not shown) (Prasanna et al., 2019). Contrasting with these results a significant response was observed in the secondary sera of mice immunized with the conjugates in comparison with the control group ($P < 0.05$) **(Figure 5A)**. Level of anti-mPsaA IgG titers was further raised up to 1/8,000–1/64,000 for all sera after the third immunization. The highest titers were observed in sera of mice immunized with Pn14TS-mPsaA K242C and K309C. Noticeably, anti-mPsaA IgG Abs induced by the later conjugate was significantly higher than those induced by Pn14TS-mPsaA K237C or Pn14TS-mPsaA K247C ($P < 0.05$) but not Pn14TS-mPsaA K242C **(Figure 5B)**. We have recently shown that mPsaA was highly immunogenic in mice while introduction of only five tetrasaccharide haptens by classic lysine random conjugation severely impaired its immunogenicity (Prasanna et al., 2019). Maintaining the protective properties of the mPsaA epitopes is of paramount importance if a dual role of both vaccine immunogen and carrier for carbohydrate antigens is envisaged. Dual anti-Group B *Streptococcus* glycoconjugate vaccines have been prepared using transglutaminase or tyrosine-directed conjugation technology. This coupling strategy was shown to preserve the antigenicity of the *Streptococcus* proteins used as the carriers (Nilo et al., 2014). Immunogenicity of the conjugates with defined connectivity was essentially comparable to that observed for conjugates obtained upon conjugation of surface-exposed lysine side-chains (Nilo et al., 2015a,b). In a different study, PGCT was applied to the controlled transfer of *E. coli* O157:H7 *O*-polysaccharide to the asparagine residue amino acid sequence $(DQNAT)_4$ introduced at the C-terminus of the maltose-binding protein used as carrier protein model (Ma et al., 2018). The glycosylation had slight interference on

the global anti-MBP response. However, for the first time it has been shown that the carbohydrate antigen decreased the response against the peptides containing or adjacent to the polysaccharide but not against peptide at distal site. Our results are in agreement with these data. Immunogenicity of mPsaA is globally conserved but finely tuned by the grafting of a single carbohydrate antigen. The highest anti-mPsaA response is observed when Pn14TS is introduced at position 309 of mPsaA i.e., in a peptide segment distant from the identified T-helper epitope and not when it is introduced at position 237, 242, or 247. This result makes sense if mPsaA B-cell epitopes and Pn14TS antigen compete for the assistance of the same T-helper epitopes. CRM_{197} remains the best carrier protein develop so far for use in humans. Structural alteration of the epitopes expressed by CRM_{197} during conjugation and detoxification processes have been proposed to explain its superiority as a carrier protein over diphtheria toxoid or tetanus toxoid (Pecetta et al., 2015). Beyond, if one cannot improve the response against one antigen at the detriment of the response against another equally important one then the strategy consisting in using a protein with dual role of antigen and carrier is questionable. Consistent with this assumption, the weakest anti-Pn14TS response was measured in sera of mice immunized with the Pn14TS-mPsaA K309C conjugate. However, further studies are required to confirm this tendency since the anti-CP14 titers were weak and limited to IgM Abs. In a study based on the use of group B streptococcal type III polysaccharide, it has been calculated that approximately eight repeat units of a polysaccharide branched to a T-helper peptide could be presented in complex with a MCHII molecule to a T-cell receptor (TCR) (Avci et al., 2011).We herein elected to work with a short tetrasaccharide antigen. It is conceivable that a TCR can recognize both our small carbohydrate antigen and part of the T-helper peptide sequence even though this is not yet demonstrated. Access to longer synthetic oligosaccharides is more demanding from the synthetic aspect and not necessarily associated with improved antigenicity (Safari et al., 2008). Also the use of purified CP will be accompanied by a loss of conjugate homogeneity while complexing its immune investigation. However, administration of a higher dose of sugar might improve the response against the Pn14TS and allow assessment of the variation of both anti-sugar and anti-protein responses. Alternatively, such study could be envisaged upon coupling not one but several carbohydrate antigen at controlled positions. Further work is also needed to assess the protective properties of the Abs and to investigate in detail the B-cell response, in particular which part of the protein is targeted by the humoral response.

CONCLUSION

The development of technologies based on site-directed or site-specific conjugation for example relying on cysteine mutagenesis as exemplified in this study can lead to fully characterized glycoconjugate vaccines while ensuring higher batch-to-batch reproducibility. Moreover, it offers unique opportunity to study structure-immunogenicity relationship while unraveling molecular aspects of the immune response and giving rise to an optimized generation of glycoconjugate vaccines.

EXPERIMENTAL SECTION

Mutagenesis

Mutations K237C, K242C, K247C, and K309C have been performed by PCR amplification Phusion polymerase (Thermo Scienyific), followed by DpnI digestion using the following primers: K237C forward 5′-GCACCCCGGAGCAAATCT GCACCCTGGTGGAAAAGC, reverse 5′-GCTTTTCCACCA GGGTGCAGATTTGCTCCGGGGTGC; K242C forward 5′-CAAATCAAAACCCTGGTGGAATGCCTGCGTCAGACCAA AGTTCCG, reverse 5′-CGGAACTTTGGTCTGACGCAGG CATTCCACCAGGGTTTTGATTTG; K247C forward 5′- GAA AAGCTGCGTCAGACCTGCGTTCCGAGCCTGTTCGTG, reverse 5′-CACGAACAGGCTCGGAACGCAGGTCTGACG CAGCTTTTC; K309C forward 5′-GGAGGGTCTGGCGTGC TAAGGATCCGGC, reverse 5′-GCCGGATCCTTAGCACGCCA GACC CTCC. The plasmids obtained are then transformed into competent XL1 blue bacteria. For each mutation, extraction of the plasmid (Quiaprep®Miniprep from Quiagen) on three different clones is carried out according to manufacturer protocol, and insertion of the mutations checked by sequencing.

Mutant mPsaA Expression

The validated plasmids have been used to transform *E. coli* BL21 (DE3) strains for expression of the different mutants. The expression of mPsaA mutant proteins was performed according to the following protocol. Briefly, 250 mL of fresh TB medium with 100 μg/ml ampicillin were inoculated with 0.5 mL of overnight pre-culture and left to grow at 37°C, 180 rpm until they reach the exponential phase (approximately OD of 0.6/0.7 is reached) and at this point the HtTEV-mPsaA expression in the cultures were induced with IPTG (0.1 mM final concentration). The cultures were left to grow for another 16 h at 25°C and 180 rpm. The cells were harvested at 10,000 rpm. The pellet were re-suspended in 25 ml cold lysis buffer (50 mM NaH_2PO_4, 150 mM NaCl, pH 8.0 + 5 mM Imidazole + 1 mM PMSF) + 1 μg/mL DNAse, and 1 mg/mL of lysozyme incubated at 4°C under stirring during 30 min and were subjected to sonication (7 min, 50% amplitude, pulse of 5 s ON/OFF) while they were kept in ice, and the cell debris were removed by centrifugation (30 min, 13,000 rpm). The obtained supernatant was filtered (0.45 μm) and incubated with 0.5 ml of preconditioned Ni NTA beads for 1 h on rotating disk at 4°C, 12 rpm. Unbound fraction was collected, and the beads were washed with a lysis buffer containing 2–10 mM imidazole. The elution was performed with a lysis buffer containing 300 mM imidazole. The eluted fractions were subjected to SDS-PAGE to identify the fractions containing target protein. Later, the eluted fractions, containing the target protein (100 mg/L of culture), were pooled and dialyzed against water at 4°C.

Removal of Poly-6-Histidine Tag and Western Blot Analysis

The enzymatic cleavage of the histidine tag from mutants was performed using a 5:1 HtTEV-mPsaA/AcTEV^{TM} protease ratio in the reaction buffer (50 mM Tris-HCl (pH 7.6), 1 mM EDTA, 1 mM DTT), for 16 h at 20°C, without stirring. The crude reaction mixtures were then dialyzed against water and incubated with the Ni NTA beads for the separation of the cleaved mPsaA mutants from the histidine tag, parent mPsaA mutants if not entirely digested and the tagged TEV protease. The eluate was collected and was subjected to SDS-PAGE and western blot analyses to confirm the removal of the histidine tag and assess their purity.

For the western blot, the vertical SDS-PAGE was carried out using 12% acrylamide gels with the loadings of the reaction mixture and tagged mPsaA mutants as controls using the Bio-rad system. The proteins were transferred to a nitrocellulose membrane at 150 mA for 90 min. For the antibody probing, the nitrocellulose membrane was initially blocked with TBS containing 5% skim milk and 0.1% tween 20 for 1 h at RT. A primary antibody to mouse anti-poly histidine (Sigma H1029, diluted 1:1,000), was applied to the membrane and incubated for 16 h at RT with agitation. The membranes were washed thrice with PBS containing 0.1% tween 20 and incubated with secondary antibody (Goat anti-Mouse IgG (H+L) Secondary Antibody, Alexa Fluor 680) for 1 h at RT on a shaker. Membranes were subjected to a final wash with PBS, and the detection was performed using an Odyssey CLx scanner (LI-COR) at 700 nm.

2-(*N*-3-maleimidopropanoyl)ethyl(β − *d* − *galactopyranosyl*) − (1 → 4) − (β − *d* − *galactopyranosyl*) − (1 → 6) − [(β − *d* − *galactopyranosyl*) − (1 → 4)] − 2 − *deoxy* − 2 − *acetamido* − β-d-glucopyranoside 2

To a solution of 2-amino-ethyl (β − D − *galactopyranosyl*) − (1 → 4) − (β − D − *galactopyranosyl*) − (1 → 6) − [(β − D − *galactopyranosyl*) − (1 → 4)] − 2 − *deoxy* − 2 − *acetamido* − β-D-glucopyranoside **1** (17.5 mg, 0.023 mmol, 1 equiv) in DMF were successively added 3-maleimido-propionic acid succinimidyl ester (9 mg, 1.45 equiv) and DIEA (8.30 μL, 2 equiv) at RT. The reaction mixture was stirred at RT overnight, diluted in water and freeze-dried. The crude residue was purified by RP-HPLC to provide **2** (12.2 mg, 58% yield); R_f 0.39 (nBuOH/EtOH/H_2O 5:5:3); ^{1}H NMR (400 MHz, D_2O): δ 6.85 (s, 2H), 4.52 (d, J = 8.2 Hz, 1H), 4.51 (d, J = 7.8 Hz, 2H), 4.43 (d, J = 7.8 Hz, 1H), 4.26 (dd, J = 1.9, 11.7 Hz, 1H), 3.99–3.88 (m, 4H), 3.84–3.62 (m, 20H), 3.60–3.55 (m, 1H), 3.54–3.48 (m, 2H), 3.36 (ddd, J = 2.5, 7.8, 9.8 Hz, 1H), 3.28 (t, J = 4.1 Hz, 2H), 2.48 (t, J = 7.0 Hz 2H), 2.00 (s, 3H); ^{13}C NMR (100 MHz, D_2O): δ 174.7, 173.5, 172.6, 134.5, 103.0, 102.8, 102.5, 101.2, 78.5, 77.9, 75.4, 75.3, 74.7, 74.3, 73.5, 72.7, 72.6, 72.6, 72.4, 71.0, 71.0, 68.9, 68.6, 68.2, 67.4, 61.1, 61.0, 60.2, 55.1, 39.3, 34.7, 34.5, 22.3; HR-ESI-MS: *m/z* Calcd for $C_{35}H_{55}N_3O_{24}[M+Na]^+$ 924.3073, found 924.3088.

Glycoconjugate Syntheses

mPsaA mutants proteins are rehydrated with ultrapure water to reconstitute 50 mM phosphate buffer. The pH are tested and adjusted to pH 8 with NaOH 0.1 M if necessary. mPsaA solutions are then treated with DTT (1.6 mg/mg of protein). Solutions are mixed first by flush and next let in rotary shaker at room temperature for 15 min. DTT is eliminated with desalting column (Zeba Spin, 7 MWCO) prior equilibrated with *degassed* pH 7 PBS buffer using swing centrifuge. Protein contents are quantified using Nanodrop spectrophotometer at 280 nm prior their conjugation. To a solution of mPsaA mutants (4.8–7.2 mg) in degassed 40 mM PBS, pH 7.0 (1.8–2.4 mg/mL), was added **2** (5 equiv) dissolved in water (1 mg/mL), and the resulting mixture stirred overnight and then purified by gel filtration using a HiLoad 15/600 Superdex^{TM} 75 pg (GE Healthcare) column and 0.1 M PBS, pH 7.3 as eluent at 0.8 ml/min. Collected fractions were concentrated by centrifugal concentrators (cut-off 3 MWCO) (Vivaspin; 1 h 7,000 g 4°C) and then freeze-dried to give the corresponding conjugates which were analyzed for identity and purity by gel electrophoresis and mass spectrometry.

Immunizations

The conjugates (40 μl of a 5 mg/ml solution in PBS), were first formulated with a mixture of chitosan/poloxamer/TPP (1:1:1) (6 mL) under stirring (600 rpm) for 30 min. The particles were concentrated by centrifugation at 12000 RCF for 12 min at 15°C, using 10 μL of glycerol bed. After the centrifugation, the pellet in the bottom is carefully collected and re-suspended in PBS (50 μL). The Groups of 5 male C57/BL6JRj (5 week old) mice were injected sub-cutaneously (s.c.) with PBS, Pn14TS-mPsaA K237C, Pn14TS-mPsaA K242C, Pn14TS-mPsaA K247C, or Pn14TS-mPsaA K309C (25 μg protein/dose-−0.5 μg tetrasaccharide/dose) diluted with 50 μL of RIBI in PBS. The mice were immunized at day 0, 14, and 28. The sera were collected on days 21 and 35. Sera were stored at −80°C.

Measurement of Humoral Response

The Ab responses induced upon immunizations were assessed 1 week after the second and the third injections by ELISA. mPsaA and capsular polysaccharide serotype 14 (CP14) (Alliance Bio Expertise), were used as coated antigens to define the anti-mPsaA or anti-CP14 Ab titers. mPsaA (0.1 μg/well) in 10 mM PBS, pH 7.3 (100 μL/well), was coated on 96 wells microtiter plates Nunc Maxisorp (ThermoFisher Scientific) plates overnight at 4°C. CP14 (1 μg/well) was coated for 48 h at 4°C in 10 mM PBS, pH 7.3 (100 μL/well). Plates were then washed with PBS 0.05% Tween 20 (3 × 200 μL), saturated using PBS containing 10% skimmed milk at 37°C for 2 h, then washed using PBS Tween 20 (PBST, 50 mM Tris, 150 mM NaCl, 0,1% Tween 20) (3 × 200 μL). Series of dilution of sera in PBS containing 10% skimmed milk (100 μL/well), were incubated at 37°C for 2 h. Plates were then washed with PBST (3 × 200 μL) and then incubated with goat anti-mouse IgG(H+L)-horse radish peroxidase-labeled conjugate (CliniSciences) used as secondary Ab at a dilution of 1/6,000, for 1 h at 37°C and further washed with PBST (5 × 200 μL). The enzyme substrate, o-phenylenediamine dihydrochloride (100 μL at 0.4 mg mL^{-1}) in 0.1 M sodium citrate

(pH 5.2), containing 0.02% hydrogen peroxide, was added to each well and the plate incubated for 20 min at RT in the dark. The reaction was terminated by adding 3 M HCl (1,000 μL per well), and the A492 was read in an Infinite M1000 spectrophotometer (TECAN). The Ab titer was defined as the dilution of immune serum that gave an OD (405 nm) at least twice that observed with pre-immune serum.

DATA AVAILABILITY STATEMENT

All datasets generated for this study are included in the article/**Supplementary Material**.

ETHICS STATEMENT

The animal study was reviewed and approved by ethical permit number from Comité d'Ethique en Expérimentation Animale (CEEA): 7897.

AUTHOR CONTRIBUTIONS

CG designed the research and wrote the manuscript with AP, AD, and AL. MPr developed the route for the production of PsaA under EC, NC, and CG supervision. AP and AD produced the PsaA mutants under MPi, TV, and EC guidance. AL and CG carried out the conjugation step and the purification of the conjugates. AP and AF performed the ELISA assays. MF assisted in mass measurements.

FUNDING

AP, MPr, and TV acknowledge their respective doctoral fellowship from the Région Pays de la Loire/Université de Nantes, under the GlycoOuest Program, from the European Commission, Education, Audiovisual and Culture Executive Agency (EACEA), under the Erasmus Mundus program, NanoFar and from the Région Pays de la Loire, under the Pari Scientifique BioSynProt program.

ACKNOWLEDGMENTS

The authors gratefully acknowledge Dorian Caudal and Aude Lafoux from platform Therassey (Nantes) for animal experiments.

SUPPLEMENTARY MATERIAL

The Supplementary Material for this article can be found online at: https://www.frontiersin.org/articles/10.3389/fchem.2019.00726/full#supplementary-material

REFERENCES

Anderson, P. W., Pichichero, M. E., Stein, E. C., Porcelli, S., Betts, R. F., Connuck, D. M., et al. (1989). Effect of oligosaccharide chain length, exposed terminal group, and hapten loading on the antibody response of human adults and infants to vaccines consisting of haemophilus influenzae type b capsular antigen unterminally coupled to the diphtheria protein CRM197. *J. Immunol.* 142, 2464–2468.

Avci, F. Y., Xiangming, L., Moriya, T., and Kasper, D. L. (2011). A mechanism for glycoconjugate vaccine activation of the adaptive immune system and its implications for vaccine design. *Nat. Med.* 17, 1602–1609. doi: 10.1038/nm.2535

Berti, F., and Adamo, R. (2013). Recent mechanistic insights on glycoconjugate vaccines and future perspectives. *ACS Chem. Biol.* 8, 1653–1663. doi: 10.1021/cb400423g

Berti, F., and Adamo, R. (2018). Antimicrobial glycoconjugate vaccines: an overview of classic and modern approaches for protein modification. *Chem. Soc. Rev.* 47, 9015–9025. doi: 10.1039/C8CS00495A

Chen, Z., Guo, R., Xu, J., and Qiu, C. (2016). Immunogenicity and protective immunity against otitis media caused by pneumococcus in mice of Hib conjugate vaccine with PsaA protein carrier. *Front. Med.* 10, 490–498. doi: 10.1007/s11684-016-0470-y

Couñago, R. M., Ween, M. P., Begg, S. L., Bajaj, M., Zuegg, J., O'Mara, M. L., et al. (2014). Imperfect coordination chemistry facilitates metal ion release in the Psa permease. *Nat. Chem. Biol.* 10, 35–41. doi: 10.1038/nchembio.1382

Crotti, S., Zhai, H., Zhou, J., Allan, M., Proietti, D., Pansegrau, W., et al. (2014). Defined conjugation of glycans to the lysines of CRM197 guided by their reactivity mapping. *Chembiochem* 15, 836–843. doi: 10.1002/cbic.201300785

Entwisle, C., Hill, S., Pang, Y., Joachim, M., McIlgorm, A., Colaco, C., et al. (2017). Safety and immunogenicity of a novel multiple antigen pneumococcalvaccine in adults: a Phase 1 randomised clinical trial. *Vaccine* 35, 7181–7186. doi: 10.1016/j.vaccine.2017.10.076

Gor, D. O., Ding, X., Li, Q., Sultana, D., Mambula, S. S., Bram, R. J., et al. (2011). Enhanced immunogenicity of pneumococcal surface adhesin A (PsaA) in mice via fusion to recombinant human B lymphocyte stimulator (BLyS). *Biol. Direct* 6:9. doi: 10.1186/1745-6150-6-9

Gotschlich, E. C., Rey, M., Triau, R., and Sparks, K. J. (1972). Quantitative determination of the human immune response to immunization with meningococcal vaccines. *J. Clin. Invest.* 51, 89–96. doi: 10.1172/JCI106801

Grayson, E. J., Bernardes, G. J. L., Chalker, J. M., Boutureira, O., Koeppe, J. R., and Davis, B. J. (2011). A coordinated synthesis and conjugation strategy for the preparation of homogeneous glycoconjugate vaccine candidates. *Angew. Chem. Int. Ed.* 50, 4127–4132. doi: 10.1002/anie.201006327

Hu, Q.-Y., Allan, M., Adamo, R., Quinn, D., Zhai, H., Wu, G., et al. (2013). Synthesis of a well-defined glycoconjugate vaccine by a tyrosine-selective conjugation strategy. *Chem. Sci.* 4, 3827–3832. doi: 10.1039/c3sc51694f

Jochems, S. P., Weiser, J. N., Malley, R., and Ferreira, D. M. (2017). The immunological mechanisms that control pneumococcal carriage. *PLoS Pathog.* 13:e1006665. doi: 10.1371/journal.ppat.1006665

Johnson, S. E., Dykes, J. K., Jue, D. L., Sampson, J. S., Carlone, G. M., and Ades, E. W. (2002). Inhibition of pneumococcal carriage in mice by subcutaneous immunization with peptides from the common surface protein pneumococcal surface adhesin A. *J. Infect.Dis.* 185, 489–496. doi: 10.1086/338928

Kurbatova, E. A., Akhmatova, N. K., Akhmatova, E. A., Egorova, N. B., Yastrebova, N. E., Sukhova, E. V., et al. (2017). Neoglycoconjugate of tetrasaccharide representing one repeating unit of the *Streptococcus pneumoniae* type 14 capsular polysaccharide induces the production of opsonizing IgG1 antibodies and possesses the highest protective activity as compared to hexa- and octasaccharide conjugates. *Front. Immunol.* 8:659. doi: 10.3389/fimmu.2017.00659

Larentis, A. L., Corrêa Argondizzo, A. P., dos Santos Esteves, G., Jessouron, E., Galler, R., and Medeiros, M. A. (2011). Cloning and optimization of induction conditions for mature PsaA (Pneumococcal Surface Adhesin A) expression in *Escherichia coli* and recombinant protein stability during long-term storage. *Protein Exp. Purif.* 78, 38–47. doi: 10.1016/j.pep.2011.02.013

Lawrence, M. C., Pilling, P. A., Epa, V. C., Berry, A. M., Ogunniyi, A. D., and Paton, J. C. (1998). The crystal structure of pneumococcal surface antigen PsaA reveals

a metal-binding site and a novel structure for a putative ABC-type binding protein. *Structure* 6, 1553–1561. doi: 10.1016/S0969-2126(98)00153-1

Lin, H., Lin, Z., Meng, C., Huang, J., and Guo, Y. (2010). Preparation and immunogenicity of capsular polysaccharide-surface adhesin A (PsaA) conjugate of *Streptococcus pneumoniae*. *Immunobiology* 215, 545–550. doi: 10.1016/j.imbio.2009.08.008

Lu, J., Sun, T., Wang, D., Dong, Y., Xu, M., Hou, H., et al. (2015). Protective immune responses elicited by fusion protein containing PsaA and PspA fragments. *Immunol. Invest.* 44, 482–496. doi: 10.3109/08820139.2015.1037956

Ma, Z., Zhang, H., Wang, P. G., Liu, X.-W., and Chen, M. (2018). Peptide adjacent to glycosylation sites impacts immunogenicity of glycoconjugate vaccine. *Oncotarget* 9, 75–82. doi: 10.18632/oncotarget.19944

Matos, M. J., Oliveira, B. L., Martínez-Sáez, N., Guerreiro, A., Cal, P. M. S. D., Bertoldo, J., et al. (2018). Chemo- and regioselective lysine modification on native proteins. *J. Am. Chem. Soc.* 140, 4004–4017. doi: 10.1021/jacs.7b12874

Mawas, F., Niggemann, J., Jones, C., Corbel, M. J., Kamerling, J. P., and Vliegenthart, J. F. (2002). Immunogenicity in a mouse model of a conjugate vaccine made with a synthetic single repeating unit of type 14 pneumococcal polysaccharide coupled to CRM197. *Infect. Immun.* 70, 5107–5114. doi: 10.1128/IAI.70.9.5107-5114.2002

Mond, J. J., Lees, A., and Snapper, C. M. (1995). T cell-independent antigens type 2. *Ann. Rev. Immunol.* 13, 655–692. doi: 10.1146/annurev.iy.13.040195.003255

Nilo, A., Allan, M., Brogioni, B., Proietti, D., Cattaneo, V., Crotti, S., et al. (2014). Tyrosine-directed conjugation of large glycans to proteins via copper-free click chemistry. *Bioconj. Chem.* 25, 2105–2111. doi: 10.1021/bc500438h

Nilo, A., Morelli, L., Passalacqua, I., Brogioni, B., Allan, M., Carboni, F., et al. (2015a). Anti-group B streptococcus glycan-conjugate vaccines using pilus protein GBS80 as carrier and antigen: comparing lysine and tyrosine-directed conjugation. *ACS Chem. Biol.* 10, 1737–1746. doi: 10.1021/acschembio.5b00247

Nilo, A., Passalacqua, I., Fabbrini, M., Allan, M., Usera, A., Carboni, F., et al. (2015b). Exploring the effect of conjugation site and chemistry on the immunogenicity of an anti-group B streptococcus glycoconjugate vaccine based on GBS67 pilus protein and type V polysaccharide. *Bioconj. Chem.* 26, 1839–1849. doi: 10.1021/acs.bioconjchem.5b00480

Olafsdottir, T. A., Lingnau, K., Nagy, E., and Jonsdottir, I. (2012). Novel protein-based pneumococcal vaccines administered with the Th1-promoting adjuvant IC31 induce protective immunity against pneumococcal disease in neonatal mice. *Infect. Immun.* 80, 461–468. doi: 10.1128/IAI.05801-11

Pecetta, S., Lo Surdo, P., Tontini, M., Proietti, D., Zambonelli, C., Bottomley, M. J., et al. (2015). Carrier priming with CRM 197 or diphtheria toxoid has a different impact on the immunogenicity of the respective glycoconjugates: biophysical and immunochemical interpretation. *Vaccine* 33, 314–320. doi: 10.1016/j.vaccine.2014.11.026

Peng, C.-J., Chen, H.-L., Chiu, C.-H., and Fang, J.-M. (2018). Site-selective functionalization of flagellin by steric self-protection: a strategy to facilitate flagellin as a self-adjuvanting carrier in conjugate vaccine. *Chembiochem* 19, 805–814. doi: 10.1002/cbic.201700634

Pollard, A. J., Perrett, K. P., and Beverley, P. C. (2009). Maintaining protection against invasive bacteria with protein-polysaccharide conjugate vaccines. *Nat. Rev. Immunol.* 9, 213–220. doi: 10.1038/nri2494

Pozsgay, V., Chu, C., Pannell, L., Wolfe, J., Robbins, J. B., and Schneerson, R. (1999). Protein conjugates of synthetic saccharides elicit higher levels of serum IgG lipopolysaccharide antibodies in mice than do those of the O-specific polysaccharide from *Shigella Dysenteriae* type 1. *Proc. Natl Acad. Sci. U.S.A.* 96, 5194–5197. doi: 10.1073/pnas.96.9.5194

Prasanna, M., Soulard, D., Camberlein, E., Ruffier, N., Lambert, A., Trottein, F., et al. (2019). Semisynthetic glycoconjugate based on dual role protein/PsaA as a pneumococcal vaccine. *Eur. J. Pharm. Sci.* 129, 31–41. doi: 10.1016/j.ejps.2018.12.013

Quast, R. B., Mrusek, D., Hoffmeister, C., Sonnabend, A., and Kubick, S. (2015). Cotranslational incorporation of non-standard amino acids using cell-free protein synthesis. *FEBS Lett.* 589, 1703–1712. doi: 10.1016/j.febslet.2015.04.041

Rajam, G., Anderton, J. M., Carlone, G. M., Sampson, J. S., and Ades, E. W. (2008a). Pneumococcal surface adhesin A (PsaA): a review. *Crit. Rev. Microbiol.* 34, 131–142. doi: 10.1080/10408410802275352

Rajam, G., Phillips, D. J., White, E., Anderton, J., Hooper, C. W., Sampson, J. S., et al. (2008b). A functional epitope of the pneumococcal surface adhesin A activates nasopharyngeal cells and increases bacterial internalization. *Microb. Pathog.* 44, 186–196. doi: 10.1016/j.micpath.2007.09.003

Rappuoli, R. (2018). Glycoconjugate vaccines: principles and mechanisms. *Sci. Transl. Med.* 10:eaat4615. doi: 10.1126/scitranslmed.aat4615

Romero-Steiner, S., Caba, J., Rajam, G., Langley, T., Floyd, A., Johnson, S. E., et al. (2006). Adherence of recombinant pneumococcal surface adhesin A (RPsaA)-coated particles to human nasopharyngeal epithelial cells for the evaluation of anti-PsaA functional antibodies. *Vaccine* 24, 3224–3231. doi: 10.1016/j.vaccine.2006.01.042

Safari, D., Dekker, H. A. T., Joosten, J. A. F., Michalik, D., Carvalho de Souza, A., Adamo, R., et al. (2008). Identification of the smallest structure capable of evoking opsonophagocytic antibodies against *Streptococcus pneumoniae* type 14. *Infect. Immun.* 76, 4615–4623. doi: 10.1128/IAI.00472-08

Schmid, P., Selak, S., Keller, M., Luhan, B., Magyarics, Z., Seidel, S., et al. (2011). Th17/Th1 biased immunity to the pneumococcal proteins PcsB, StkP and PsaA in adults of different age. *Vaccine* 29, 3982–3989. doi: 10.1016/j.vaccine.2011.03.081

Singh, R., Gupta, P., Sharma, P. K., Ades, E. W., Hollingshead, S. K., Singh, S., et al. (2014). Prediction and characterization of helper T-cell epitopes from pneumococcal surface adhesin A. *Immunology* 141, 514–530. doi: 10.1111/imm.12194

Srivastava, N., Zeiler, J. L., Smithson, S. L., Carlone, G. M., Ades, E. W., Sampson, J. S., et al. (2000). Selection of an immunogenic and protective epitope of the PsaA protein of *Streptococcus pneumoniae* using a phage display library. *Hybridoma* 19, 23–31. doi: 10.1089/027245700315761

Stefanetti, G., Hu, Q.-Y., Usera, A., Robinson, Z., Allan, M., Singh, A., et al. (2015). Sugar-protein connectivity impacts on the immunogenicity of site-selective salmonella O-Antigen glycoconjugate vaccines. *Angew. Chem. Int. Ed.* 54, 13198–13203. doi: 10.1002/anie.201506112

van der Linden, M., Falkenhorst, G., Perniciaro, S., Fitzner, C., and Imöhl, M. (2016). Effectiveness of pneumococcal conjugate vaccines (PCV7 and PCV13) against invasive pneumococcal disease among children under two years of age in Germany. *PLoS ONE* 11:e0161257. doi: 10.1371/journal.pone.0161257

Wang, S., Li, Y., Shi, H., Scarpellini, G., Torres-Escobar, A., Roland, K. L., et al. (2010). Immune responses to recombinant pneumococcal PsaA antigen delivered by a live attenuated Salmonella vaccine. *Infect. Immun.* 78, 3258–3271. doi: 10.1128/IAI.00176-10

Whaley, M. J., Sampson, J. S., Johnson, S. E., Rajam, G., Stinson-Parks, A., Holder, P., et al. (2010). Concomitant administration of recombinant PsaA and PCV7 reduces *Streptococcus pneumoniae* serotype 19A colonization in a murine model. *Vaccine* 28, 3071–3075. doi: 10.1016/j.vaccine.2010.02.086

Yahiaoui, R. Y., Bootsma, H. J., den Heijer, C. D. J., Pluister, G. N., Paget, W. J., Spreeuwenberg, P., et al. (2018). Distribution of serotypes and patterns of antimicrobial resistance among commensal *Streptococcus pneumoniae* in nine European countries. *BMC Infect. Dis.* 18:440. doi: 10.1186/s12879-018-3341-0

Conflict of Interest: The authors declare that the research was conducted in the absence of any commercial or financial relationships that could be construed as a potential conflict of interest.

frontiers in Chemistry

ORIGINAL RESEARCH
published: 22 November 2019
doi: 10.3389/fchem.2019.00791

Neuraminidase-3 Is a Negative Regulator of LFA-1 Adhesion

*Md. Amran Howlader, Caishun Li, Chunxia Zou, Radhika Chakraberty, Njuacha Ebesoh and Christopher W. Cairo**

Department of Chemistry, University of Alberta, Edmonton, AB, Canada

Within the plasma membrane environment, glycoconjugate-receptor interactions play an important role in the regulation of cell-cell interactions. We have investigated the mechanism and activity of the human neuraminidase (NEU) isoenzyme, NEU3, on T cell adhesion receptors. The enzyme is known to prefer glycolipid substrates, and we confirmed that exogenous enzyme altered the glycolipid composition of cells. NEU3 was able to modify the sialic acid content of purified LFA-1 *in vitro*. Enzymatic activity of NEU3 resulted in re-organization of LFA-1 into large clusters on the membrane. This change was facilitated by an increase in the lateral mobility of LFA-1 upon NEU3 treatment. Changes to the lateral mobility of LFA-1 were specific for NEU3 activity, and we observed no significant change in diffusion when cells were treated with a bacterial NEU (NanI). Furthermore, we found that NEU3 treatment of cells increased surface expression levels of LFA-1. We observed that NEU3-treated cells had suppressed LFA-1 adhesion to an ICAM-1 coated surface using an *in vitro* static adhesion assay. These results establish that NEU3 can modulate glycoconjugate composition and contribute to the regulation of integrin activity. We propose that NEU3 should be investigated to determine its role on LFA-1 within the inflammatory cascade.

Keywords: integrin, adhesion, glycolipid, glycosyl hydrolase, inflammation

OPEN ACCESS

Edited by:
Karina Valeria Mariño, Institute of Biology and Experimental Medicine (IBYME), Argentina

Reviewed by:
Kazunori Yamaguchi, Miyagi Cancer Center, Japan
Eugenio Monti, University of Brescia, Italy

****Correspondence:***
Christopher W. Cairo
ccairo@ualberta.ca

Specialty section:
This article was submitted to Chemical Biology, a section of the journal Frontiers in Chemistry

Received: *21 August 2019*
Accepted: *04 November 2019*
Published: *22 November 2019*

Citation:
Howlader MA, Li C, Zou C, Chakraberty R, Ebesoh N and Cairo CW (2019) Neuraminidase-3 Is a Negative Regulator of LFA-1 Adhesion. Front. Chem. 7:791. doi: 10.3389/fchem.2019.00791

INTRODUCTION

The process of leukocyte rolling, extravasation, and homing to sites of inflammation is critical to cellular immunity, and is known as the leukocyte adhesion cascade (Ley et al., 2007). Along each step of this process different cell adhesion molecules and their ligands mediate recognition between leukocytes and endothelial cells. The initial attachment of the leukocyte to the endothelial wall, usually referred to as rolling, is mediated by selectins and their carbohydrate ligands (e.g., sialyl Lewis-X; CD15s) (Varki, 1994). Later steps of the process must arrest the cell (firm adhesion) to allow for transmigration. These later steps of the process are largely mediated by integrin receptors and their ligands. Integrins are a major class of adhesion receptors and an important therapeutic target (Hynes, 2002; Cox et al., 2010; Desgrosellier and Cheresh, 2010). The first integrin in the inflammatory cascade is LFA-1 (known as the αLβ2 integrin; or CD11a, CD18), a transmembrane glycoprotein which binds to ICAM-1 (inter-cellular adhesion molecule-1; CD54) and conveys an outside-in intracellular signal to the leukocyte (Hogg et al., 2004). These and subsequent integrin-mediated processes, including interactions of the very-late antigens (VLA-4, the α4β1 integrin or VLA-5, the α5β1 integrin), allow cells to migrate to the site of inflammation (Hogg et al., 2003; Simmons, 2005; Cox et al., 2010). Thus, processes which modulate leukocyte integrin function are of potential interest for the development of anti-adhesive and anti-inflammatory therapeutics (Hogg et al., 2003; Simmons, 2005; Cox et al., 2010).

Cell surface glycoconjugates are critical components of the plasma membrane. Sialic acid-containing glycolipids, known as gangliosides, play important structural and functional roles. Sialic acid (also known as neuraminic acid, or Neu5Ac) has long been recognized to participate in the regulation of immune cell function. The sialic acid content of lymphocyte receptors is known to be altered as part of cell development (Bi and Baum, 2009), infection (Galvan et al., 1998), and activation (Hernandez et al., 2007). The enzymes that remove sialic acid, known as neuraminidases (NEU; also called sialidases), increase trans-endothelial migration (Sakarya et al., 2004), reduce expression of CD15s (Gadhoum and Sackstein, 2008), and expose integrin activation epitopes (Feng et al., 2011). Early reports dubbed increases in B cell antigen sensitivity a "neuraminidase effect," (Cowing and Chapdelaine, 1983) and recent evidence has ascribed this phenomenon to sialic acid acting as a negative regulator of immune cell interactions (Bagriacik and Miller, 1999). The prominent role of sialic acid in adhesion suggests that changes which affect sialoglycoconjugates (SGC) may be critical to regulation of cell-cell interactions.

Catabolic remodeling of glycoconjugates is likely to be more rapid than biosynthetic processes (Parker and Kohler, 2010). Membrane-associated glycosyl hydrolase (GH) enzymes could play a role in signaling pathways through processing of glycolipids or glycoproteins. This hypothesis is consistent with the increased turnover of terminal glycan residues (e.g., neuraminic acid and fucose) relative to core glycan residues (Tauber et al., 1983), and the rapid loss of sialylated antigens on neutrophils (Gadhoum and Sackstein, 2008). The family of human neuraminidases (hNEU) have been shown to participate in a variety of signaling pathways and pathologies including inflammation, adhesion, tumorigenesis, and cancer metastasis (Miyagi, 2010; Miyagi and Yamaguchi, 2012). However, the role of specific hNEU isoenzymes has not been well-defined within inflammation.

The NEU3 isoenzyme is known as a plasma-membrane-associated GH which has a strong preference for glycolipid targets (Monti et al., 2000; Kopitz et al., 2001; Papini et al., 2004; Seyrantepe et al., 2004; Zanchetti et al., 2007). Interestingly, NEU3 has been shown to modulate β1 integrin activity (Tringali et al., 2012). Additionally, the enzymatic activity of NEU3 is modulated by signaling events such as protein kinase C stimulation in immune cells (Wang et al., 2004). The specificity of NEU3 for glycolipids, and its localization to membrane microdomains (Wang Y. et al., 2002), suggests a central role for the enzyme in cellular signaling (Kopitz et al., 2001). The glycolipid GM3 is a key component of lipid rafts, as well as a substrate for NEU3 (Sandbhor et al., 2011). Our group has been interested in the function of NEU3 in regulating membrane organization. We wanted to investigate the effects of NEU3 on integrin-mediated leukocyte adhesion through its regulation of SGC. Glycolipid interactions with integrins have been examined by a number of groups (Pande, 2000). Lactosyl ceramide (LacCer) has been shown to activate β1 integrins (Sharma et al., 2005; Chatterjee and Pandey, 2008). The activation of LFA-1 in neutrophils has been found to require LacCer-enriched domains (Chatterjee and Pandey, 2008). Imaging studies have found that LFA-1 on monocytes is associated with raft markers (Cambi et al., 2006); and activation of cells allows LFA-1 nanodomains to assemble into larger clusters with GPI-associated proteins (van Zanten et al., 2009). Taken together, these reports suggest an important role for glycolipids in the regulation of integrin organization and function on lymphocytes.

In this study, we investigated the role of the human NEU3 isoenzyme in regulating LFA-1 adhesion in a T cell model (Jurkat) and peripheral blood mononuclear cells (PBMC). We found that exogenous enzyme altered the glycolipid composition of cells, as well as the organization of LFA-1 in the membrane. By measuring the lateral mobility of LFA-1, we provide mechanistic insight into the altered distribution of LFA-1. We observed that NEU3 activity significantly increased LFA-1 lateral mobility and endocytosis, and blocked LFA-1–ICAM-1 adhesion. We also found that NEU3 treatment did not block all adhesion pathways, as homotypic aggregation of cells was increased. Together, our results suggest that NEU3 may have a role in the regulation of lymphocyte integrins critical to the inflammatory cascade.

RESULTS

NEU3 Treatment Reduced Sialylated-Glycolipids in Cells

To gain insight into gross changes in the composition of membrane glycosphinolipids (GSL), we first employed high-performance thin layer chromatography (HPTLC). Jurkat T cells were treated with conditions expected to alter integrin function, and GSL were extracted and analyzed by HPTLC (Muthing, 1996). We observed only minor variations in sialo- and asialo-forms of gangliosides which were difficult to quantitate (data not shown). To provide more quantitative insights we implemented an LC-MS-FLD analysis of gangliosides based on previous reports (Neville et al., 2004; Albrecht et al., 2016). We detected glycolipids extracted from Jurkat cells including LacCer, GM1, GM2, GM3, and GD1a (**Figure 1A** and **Figure S7**). We focused on changes to the ratio of LacCer to GM3 since GM3 is a well-known substrate for NEU3. This analysis showed no significant changes on treatment with phorbol 12-myristate 13-acetate (PMA; a protein kinase C activator), and minor, but not significant, changes with cytochalasin D (cytoD; a cytoskeletal disruptor) (van Kooyk and Figdor, 2000). Human cell types typically express multiple isoforms of NEU (Miyagi and Yamaguchi, 2012). In order to probe the role of a single NEU isoenzyme in cells, we treated cells with recombinant NEU3 enzyme and a bacterial NEU from *Clostridium perfringens* (NanI) (Peter et al., 1995; Albohy et al., 2010). We found that treatment with NanI had no detectable effect on glycolipid composition; however, NEU3 showed a significant increase in asialo forms of GM3 (**Figure 1B**). This result suggested that NanI did not substantially alter ganglioside composition, while NEU3 showed more specific activity for glycolipid substrates (Ha et al., 2004; Sandbhor et al., 2011). We concluded that treatment of cells with NEU3 resulted in an altered composition of membrane glycolipids, which included reduction in GM3 and an increase in LacCer.

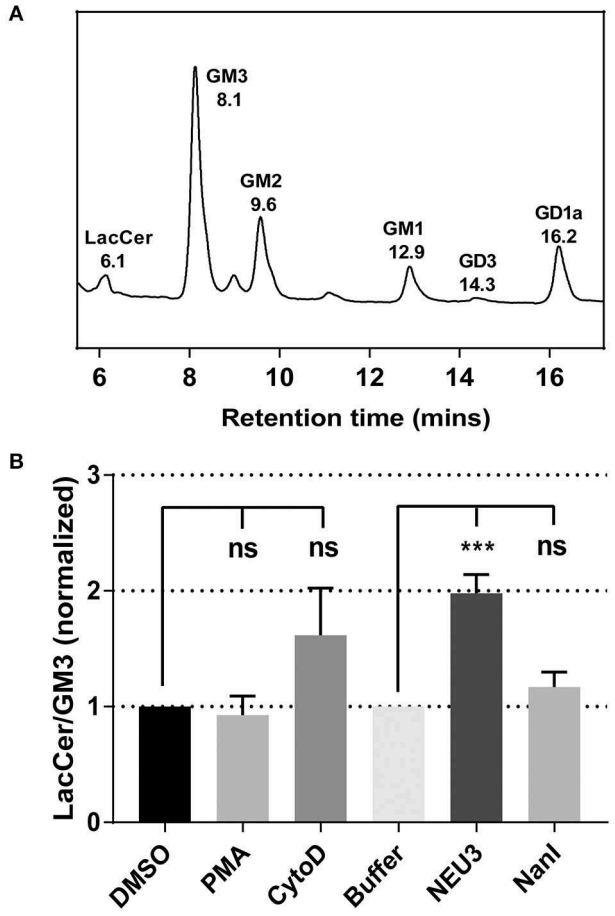

FIGURE 1 | Analysis of the change of cell membrane GSLs. GSLs were extracted from treated or control cells and analyzed by LC-MS. **(A)** Glycolipids extracted from Jurkat cells were digested with endoglycoceramidase, labeled and resolved by LC-MS-FLD. The major glycolipids observed were LacCer, GM3, GM2, GM1, and GD1a. **(B)** LC-MS-FLD analysis was performed on four replicate samples ($N = 4$) for Jurkat cells treated as indicated. The ratio of LacCer to GM3 was calculated using the peak areas for each condition and normalized to the respective control. Data were compared to the indicated control using a student *t*-test to determine *p*-values; $^{***}p \leq 0.005$; ns, not significant.

NEU3 Treatment Altered the Glycosylation of LFA-1

We used lectin blotting to detect changes in the glycosylation state of LFA-1 after NEU treatment (**Figure 2** and **Figures S4–S6**). We selected the *Sambucus nigra* agglutinin (SNA), peanut agglutinin (PNA), and *Maackia amurensis* agglutinin (MAA) for this analysis. The PNA lectin binds terminal galactose residues, while SNA and MAA bind to terminal sialic acid residues (Freeze, 2001). We observed that treatment of purified LFA-1 with NEU3 and NanI resulted in a significant decrease in SNA and MAA staining for LFA-1, consistent with loss of sialic acid. Treatment with either NEU enzyme gave a corresponding increase in PNA staining, suggesting a corresponding increase in terminal galactose residues after loss of sialic acid. These results were consistent for both the α- and β-chains of LFA-1. Together, these data are consistent with desialylation of the LFA-1 complex, leading to an increased amount of exposed galactose sites in the presence of NEU3 or NanI activity.

Fluorescence Imaging of LFA-1

We next sought to determine if NEU3 treatment of cells would result in changes to the localization of LFA-1. Cells were imaged by total internal reflection fluorescence (TIRF) microscopy, limiting visualization to portions of the cell in close apposition to the glass surface. Cells were stained with a Cy5-conjugated anti-LFA-1 antibody (clone TS2/4) and a FITC-conjugated Cholera Toxin subunit B (CTB-FITC) to visualize gangliosides (Blank et al., 2007). Untreated cells showed relatively diffuse LFA-1 microclusters, while CTB gave diffuse staining and large patches with partial LFA-1–CTB colocalization (**Figure 3A**). Treatment of cells with NEU3 resulted in more punctate CTB staining and more diffuse LFA-1 microclusters. In contrast, NanI treatment resulted in larger co-localized regions of LFA-1 and CTB staining. A portion of the localized aggregates appeared at cell-cell contacts. Treatment of cells with PMA resulted in larger and more distinct microclusters of LFA-1 and minimal CTB colocalization (**Figure 3B**). Treatment of cells with cytoD disrupted CTB-positive aggregates and reduced co-localization with LFA-1 microclusters. LFA-1 is known to form nanoclusters on resting and activated cells, and the membrane domains in which LFA-1 is found tend to be heterogeneous (Marwali et al., 2003; Cambi et al., 2006). We also note that CTB staining may include reactivity to glycoprotein antigens, and therefore imaging results with this stain should be interpreted with caution. Previous reports have suggested that GM1 is the major CTB reactive glycoconjugate in Jurkat cells (Wands et al., 2015).

To quantitate changes in LFA-1 cluster size, we analyzed TIRF images of individual cells ($N = 15$) from each condition by determining the amount of LFA-1 found in clusters. Images were processed in ImageJ to identify clusters and to determine the total area per cell found within them (**Figure 4** and **Table S2**) (Schneider et al., 2012). The distribution of total cluster area per cell is shown in **Figure 4A**. Clear increases in cluster size were observed for cytoD, NEU3, and NanI treatments. Treatment with NanI showed the largest increase in cluster area (consistent with **Figure 3**). Our observation that NEU3 has similar effects to cytoD in both lateral mobility and clustering indicated that enzyme activity influenced cytoskeletal regulation of the receptor (Cairo et al., 2006; Cairo and Golan, 2008).

Lateral Mobility of LFA-1 Was Altered by NEU3 Treatment

We next examined the lateral mobility of LFA-1 on Jurkat T cells using single-particle tracking (SPT) methods (Saxton and Jacobson, 1997; Jaqaman et al., 2008; Alenghat and Golan, 2013). Cells were labeled with Cy5-conjugated anti-LFA-1 (clone TS2/4) at low enough concentrations to achieve sparse labeling of the receptors as observed by TIRF. Videos were recorded and analyzed to determine trajectories of LFA-1 on live cells (10 s, 10 FPS). This strategy allowed us to obtain many trajectories rapidly;

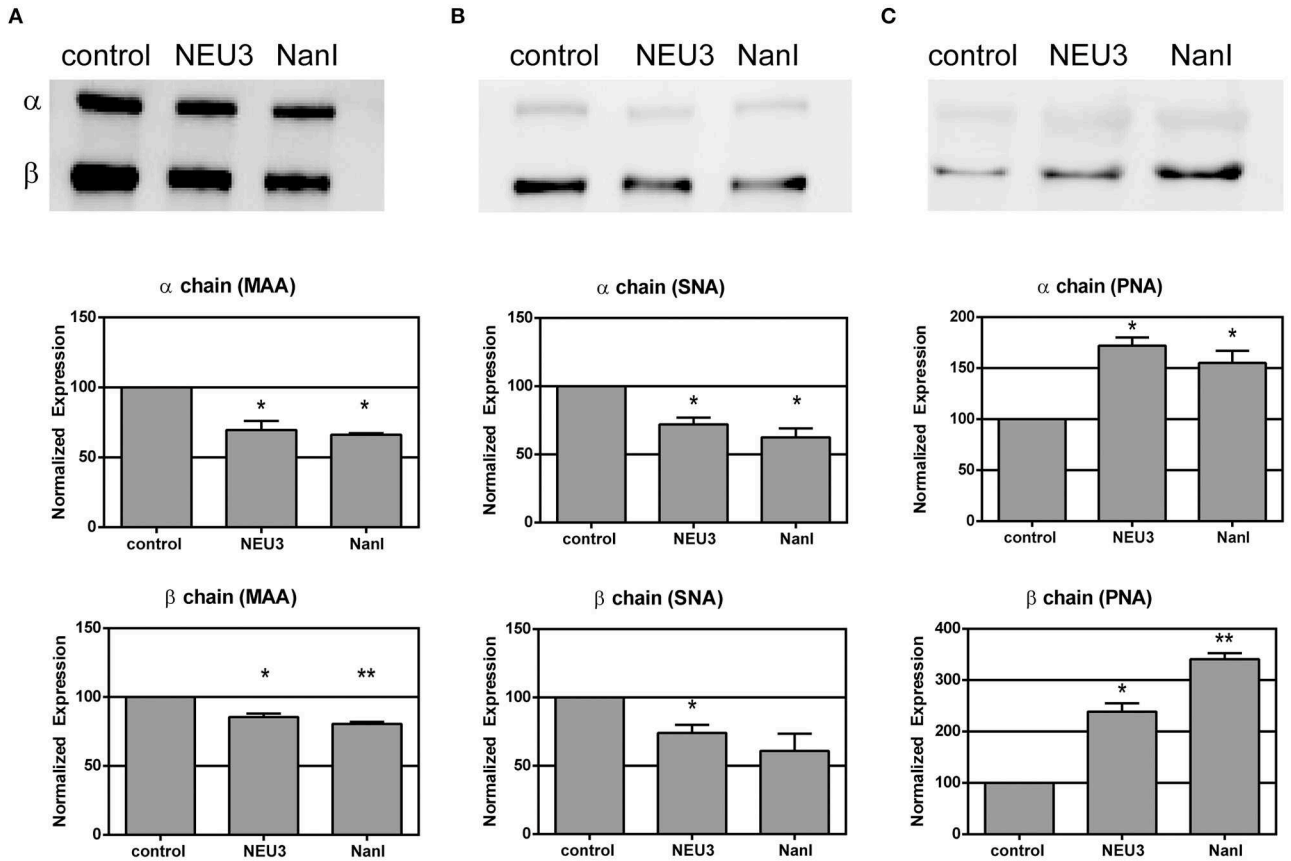

FIGURE 2 | Lectin blotting of LFA-1 shows sensitivity of LFA-1 to NEU treatment. Purified LFA-1 was treated with NEU3 and NanI for 3 h at 37°C. The protein was then blotted and probed with biotinylated lectins. Lectins **(A)** MAA, **(B)** SNA, and **(C)** PNA were used. MAA and SNA recognize terminal sialic acid residues, while PNA recognizes terminal galactose residues. Chemiluminescent blots were developed and analyzed for changes in band intensities, and a representative image from two experiments are shown at the top of each panel (see **Supporting Information**). Data are shown as the mean ± SEM and were compared to the appropriate control using *t*-test to determine *p*-values; $^{*}p \leq 0.05$; $^{**}p \leq 0.01$.

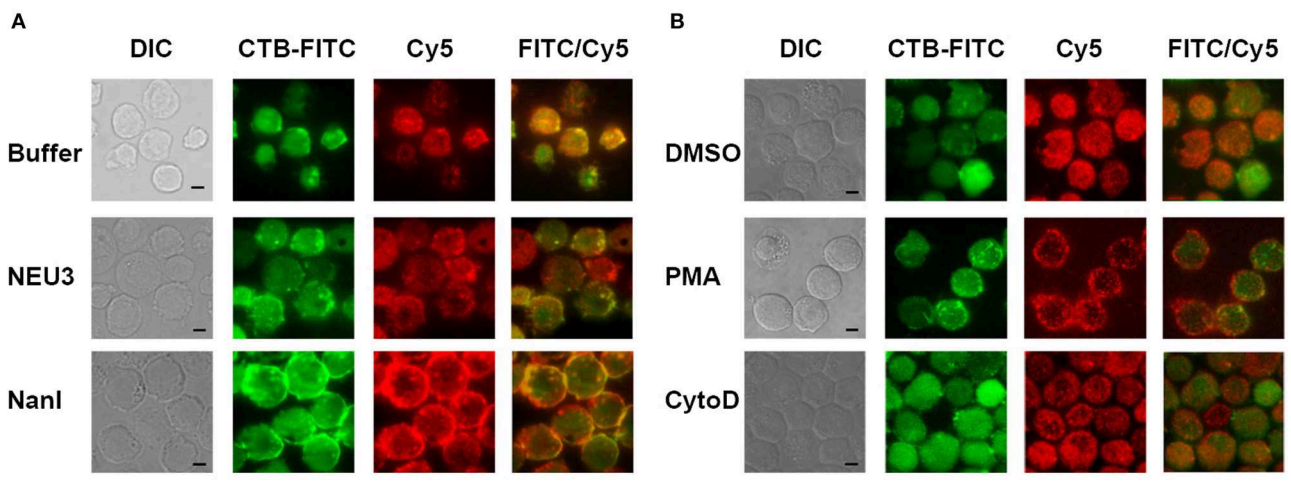

FIGURE 3 | TIRF imaging of LFA-1 on treated cells. Jurkat cells were fixed after treatment with **(A)** buffer (control), NEU3, or *NanI*; and **(B)** DMSO, PMA, or cytoD. The fixed cells were then labeled with Cholera toxin subunit B (CTB-FITC) to label gangliosides and a TS2/4-Cy5 conjugate to label LFA-1. Cells were imaged by DIC and TIRF. Merged FITC and Cy5 images are shown in the last column with yellow indicating co-localization. Scale Bar = 5 μm.

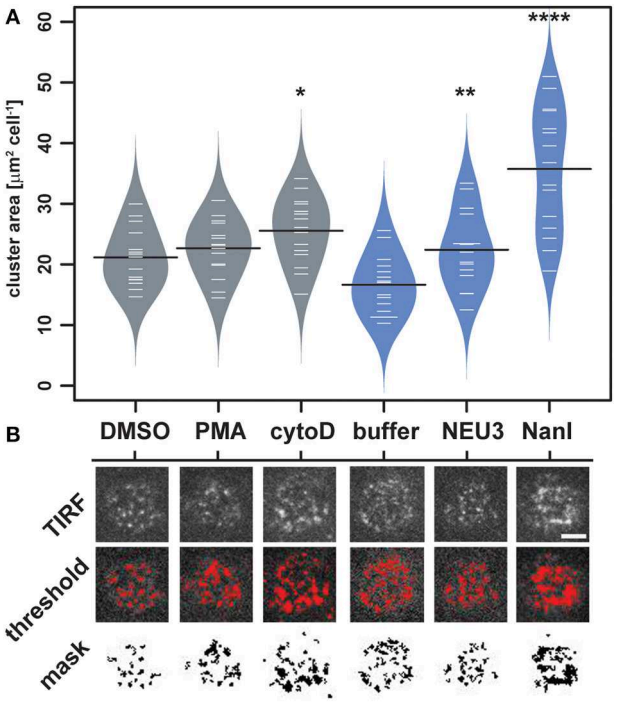

FIGURE 4 | Changes in LFA-1 clustering after neuraminidase treatment. The amount of clustered LFA-1 on individual cells was determined using TIRF imaging. Cells were labeled with a TS2/4-Cy5 antibody conjugate, and 15 individual cells were compared for each condition. **(A)** Clusters that were larger than 4 pixel^2 were measured using ImageJ, and the average area was tabulated for each cell. Data are plotted using a beanplot, with solid lines representing the mean of each population (Kampstra, 2008). **(B)** Representative TIRF images for individual cells are shown from each condition. A mask was generated from the TIRF image using a threshold for quantitation. Data were compared to the appropriate control using a *t*-test to determine *p*-values; $^*p \leq 0.05$; $^{**}p \leq 0.01$; $^{****}p \leq 0.0001$. Scale bar = 5 μm.

TABLE 1 | Diffusion of LFA-1 determined using SPT.

Condition	*N*	D_{micro} †			
		Mean (linear)	Median (linear)	Mean (log transformed)	Median‡ (log normal)
DMSO (control)	321	5.2 ± 0.3	3.28	2 ± 1	2.2 ± 0.4
PMA	334	5.9 ± 0.4	4.31	2 ± 1	2.4 ± 0.5
cytoD	422	7.7 ± 0.7**	4.32	3 ± 1**	3.0 ± 0.5
Buffer (control)	294	6.1 ± 0.6	3.28	2 ± 1	1.8 ± 0.4
NEU3	210	11 ± 1****	6.11	4 ± 1****	4.3 ± 0.9
NanI	216	5.5 ± 0.4	3.32	2 ± 1	2.3 ± 0.5

Data was analyzed using u-Track (Jaqaman et al., 2008) and custom scripts implemented in Matlab (Cairo et al., 2006). Values listed are either the arithmetic mean, arithmetic median, or the median determined for a log normal distribution (see ***Supporting Information****). Error is given as the standard error of the mean.* † *Diffusion coefficients are in units of × 10^{-10} [cm^2s^{-1}] or × 10^{-2} [μm^2s^{-1}]; Data were compared to the appropriate control using a t-test to determine p-values; **p ≤ 0.01; ****p ≤ 0.0001.* ‡ *Median calculated based on a lognormal fit as described in* ***Supporting Information****.*

however, due to photobleaching, trajectories recorded in this experiment tend to be shorter than those obtained from tracking of polystyrene beads or quantum dots. Trajectories were analyzed with u-Track and processed with custom scripts in MATlab (Cairo et al., 2006; Jaqaman et al., 2008). Data were pooled from multiple cells for each condition and are summarized in **Table 1**. All diffusion measurements were calculated as microdiffusion coefficients (D_{micro}) due to the short duration of the trajectories (Qian et al., 1991). Our observations were in general agreement with SPT studies of fusion-protein labeled LFA-1 (Ishibashi et al., 2015). In previous SPT observations of LFA-1 at high time resolution the diffusion coefficients were found to have a non-normal distribution (Cairo et al., 2006). We found this to also be the case in our SPT data set, as the measured diffusion coefficients spanned up to four decades. Therefore, we proceeded to analyze these data as normal and lognormal distributions (**Table S1** and **Figure S1**). Comparisons of the linear and logarithmic means found that LFA-1 on cytoD- and NEU3-treated cells exhibited significantly increased diffusion. Beanplots showing the distribution of diffusion coefficients are shown in **Figure 5**, and illustrate the shifts in LFA-1 diffusion in logarithmic scale (Kampstra, 2008). Further analysis of these data as cumulative distribution functions (CDF) illustrate the clear increase in LFA-1 diffusion upon NEU3 treatment. Our measurements were in general agreement with previous studies of LFA-1 lateral mobility using other methods (Gaborski et al., 2013). These data allowed us to conclude that NEU3 had a significant positive effect on the lateral mobility of LFA-1. Interestingly, the bacterial neuraminidase, NanI, had no significant effect on LFA-1 mobility in this experiment. These data support a specific role for NEU3 enzyme activity in the regulation of integrin mobility.

LFA-1–ICAM-1 Adhesion Was Blocked by NEU3

To determine if NEU3 had a functional effect on LFA-1–mediated adhesion we employed a flow cytometry-based assay, similar to previous reports (See Experimental Procedures section) (Crucian et al., 2006). Fluorescent polystyrene beads were coated with recombinant ICAM-1, and cell–bead conjugates were detected by flow cytometry. Binding to beads was normalized to ICAM-1 coated beads as a positive control and bovine serum albumin (BSA) coated beads as a negative control. We found that PMA treatment of Jurkat cells increased adhesion as expected (**Figure 6A**). To test the role of native neuraminidase enzymes, we treated the cells with a general neuraminidase inhibitor, 2,3-dehydro-2-deoxy-*N*-acetylneuraminic acid (DANA). DANA is known to inhibit multiple human NEU isoenzymes (Cairo, 2014; Richards et al., 2018), and we observed a significant increase in LFA-1 adhesion after DANA treatment in the absence and presence of PMA. This result was consistent with a role for native NEU activity that negatively regulates LFA-1–ICAM-1 adhesion. Treatment of cells with purified NEU3 or NanI resulted in a dramatic block of LFA-1–ICAM-1 adhesion (**Figure 6B**). Experiments with a NEU3(Y370F) mutant confirmed that the effect of NEU3 was due to its enzymatic activity (**Figure S2**)

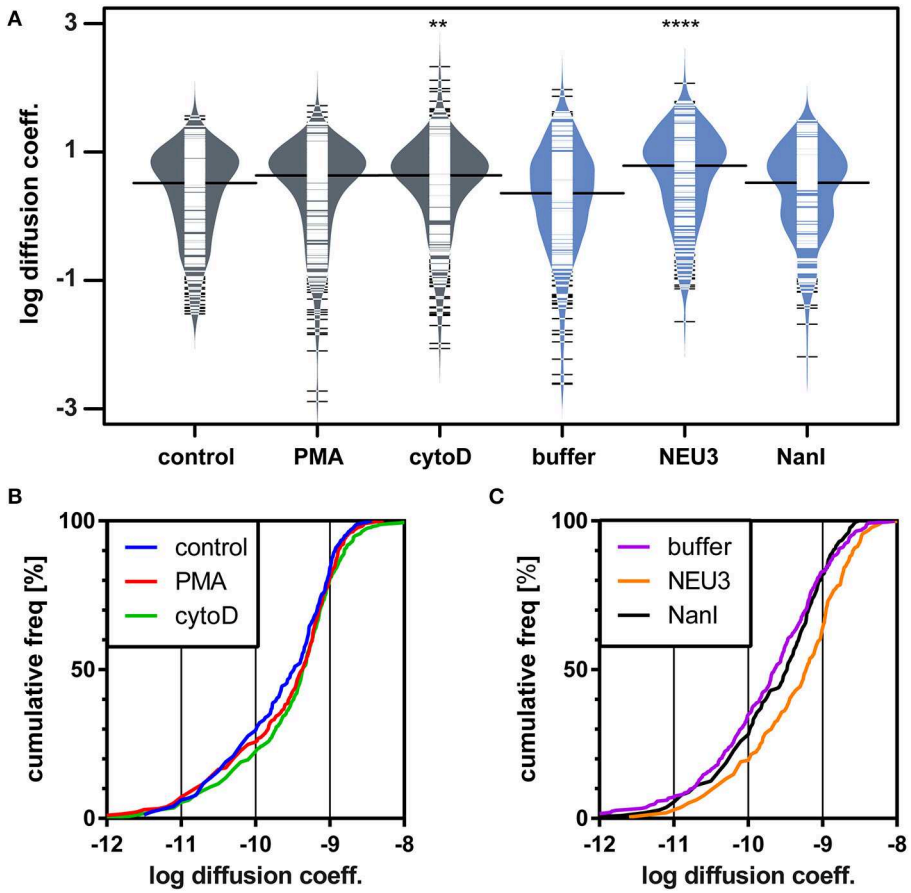

FIGURE 5 | LFA-1 diffusion is altered by NEU treatment. The lateral mobility of LFA-1 on Jurkat was determined using SPT. **(A)** A beanplot of each population is shown with the logarithmic median of diffusion coefficients indicated by a solid line for each population (same data as in **Table 1**) (Kampstra, 2008). Each population is shown with a density estimate and horizontal lines indicate individual diffusion coefficient measurements. **(B)** A cumulative frequency distribution is shown for the control, PMA, and cytoD conditions. **(C)** A cumulative frequency distribution is shown for the buffer, NEU3, and NanI conditions. Diffusion coefficients are given as log(D), where D is in units of $\times 10^{-10}$ [cm^2s^{-1}] or $\times 10^{-2}$ [μm^2s^{-1}]. Data were compared to the appropriate control using a *t*-test to determine *p*-values; $^{**}p \leq 0.01$; $^{****}p \leq 0.0001$.

(Albohy et al., 2010). Furthermore, to resolve the likely substrate of each enzyme we performed additional controls. Control experiments with ICAM-1 beads pre-treated with either NEU3 or NanI found that NEU3 treatment had no effect on ICAM-1–LFA-1 adhesion; while treatment of the same beads with NanI resulted in a large decrease in adhesion. Thus, we concluded that the two enzymes inhibited adhesion through modification of different substrates: Treatment with NanI blocked adhesion as a result of desialylation of the ICAM-1 ligand, while NEU3 blocked adhesion through enzymatic modification of a cell-surface target.

We further confirmed our observations beyond model cells by testing the effect NEU3 on ICAM-1 adhesion in PBMC (**Figure 6C**). Treatment of PBMC with NEU3 or NanI enzymes resulted in a significant decrease in ICAM-1 adhesion. Notably, NEU3 treatment of Jurkat and PBMC cells partially suppressed PMA-activated adhesion suggesting a regulatory role for the enzyme late in the activation pathway.

NEU3 Enhanced Homotypic Aggregation

Once we had concluded that NEU3 could act as a negative regulator of β2-integrin mediated adhesion, we investigated the effect of NEU3 on an alternative cell adhesion process—homotypic aggregation. The homotypic aggregation of T cells is generally considered to be mediated by multiple receptors (Kansas and Tedder, 1991; Andrew et al., 1994; Cho et al., 2001) including LFA-1 (Rothlein and Springer, 1986) and VLA-4 (Bednarczyk and McIntyre, 1990; Campanero et al., 1990). We determined the number of cells involved in aggregates using microscopy (**Figure 6D** and **Figure S3**). Cells were treated with NEU3 or NanI, both of which resulted in significantly increased aggregation. Previous results have found that NEU3 increased fibronectin–β1 integrin cell migration in epithelial cells, and the effect was not due to desialylation of fibronectin (Jia et al., 2016). Homotypic aggregation of neutrophils has been reported to be increased by treatment with NanI (Cross and

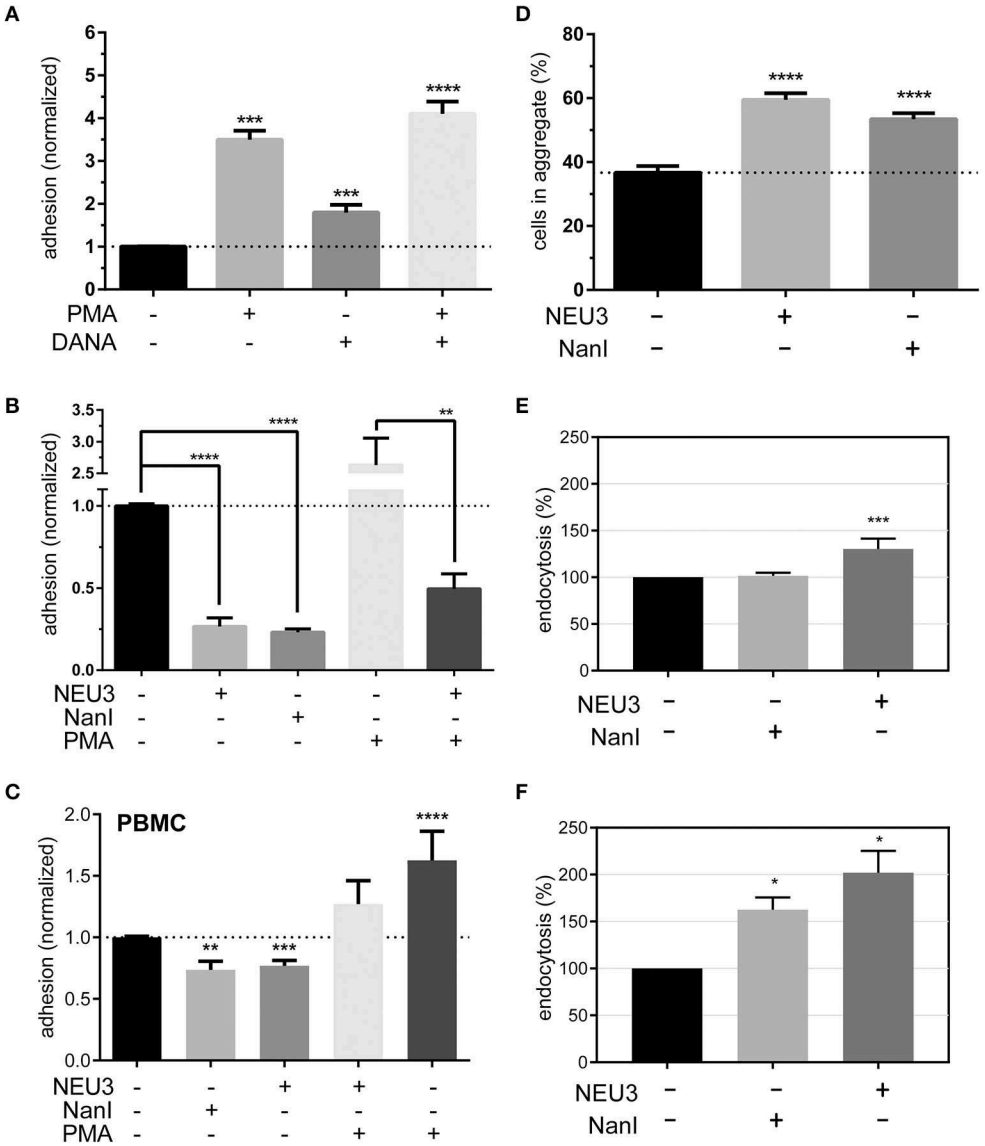

FIGURE 6 | Adhesion of T cells is altered by Neu treatment. **(A)** Adhesion of Jurkat cells to ICAM-1 was determined using flow cytometry and fluorescent beads (1 μm) under the indicated conditions. Control samples were treated with DMSO (0.05 %), PMA, or DANA for 30 min. **(B)** Adhesion of Jurkat cells to ICAM-1 was determined using flow cytometry and fluorescent beads; samples were treated with buffer or enzyme for 3 h, followed by incubation with buffer, PMA, or DANA (100 μM) for 30 min. All cytometry data were normalized to the appropriate control after background subtraction (BSA coated beads). **(C)** Isolated PBMC were treated as indicated and adhesion to ICAM-1 coated beads was determined by flow cytometry. Data shown are from at least three healthy donors for each condition. Values shown in **(A–C)** are the average of $N = 6$–12 replicates, error is the standard error of the mean. **(D)** Homotypic aggregation of Jurkat cells was determined using microscopy. Cells were incubated under the indicated conditions for 3 h. Aggregation was determined by imaging to determine the total number of cells and the number of cells found within aggregates. Aggregation is expressed as the percentage of cells in all samples found within an aggregate ($N = 24$, from two separate experiments), and error is shown as the standard error of the mean. **(E)** Changes in the endocytosis of β2-integrin ($N = 4$) and **(F)** β1-integrin ($N = 2$) in Jurkat cells after treatment with NanI or NEU3 (30 min at 37°C). Error bars are shown as standard error of the mean, all data were compared to the indicated control using a *t*-test; $^{*}p \leq 0.05$; $^{**}p \leq 0.01$; $^{***}p \leq 0.005$; $^{****}p \leq 0.0001$.

Wright, 1991). We concluded that while NEU3 disrupted LFA-1–ICAM-1 interactions (*vide infra*), desialylation of cell surface targets by NEU3 or NanI could also stimulate other adhesion mechanisms. These two results indicate that sialic acid can be either activating or inhibitory in adhesion, likely due to the specific target SGC involved.

NEU3 Altered Endocytosis of β1 and β2 Integrins

Previous studies have supported a role for glycolipids in the regulation of integrin endocytosis (Sharma et al., 2005). Our examination of the effect of NEU3 on integrin adhesion suggested differential regulation of these two adhesion receptors.

Perturbation of the balance of exo- and endocytosis of integrins is well-known as a mechanism to regulate adhesion (Caswell and Norman, 2006; Pellinen and Ivaska, 2006). We used biotin labeling of cell-surface proteins to interrogate changes in endocytosis of β2 and β1 integrins in Jurkat after exposure to NEU enzymes. We observed a significant increase in endocytosis of the β2 integrin after NEU3 treatment, but NanI appeared to have no significant effect (**Figure 6E**). In contrast, the β1 integrin showed a large increase in endocytosis after both NEU3 and NanI treatment (**Figure 6F**). We note that these analyses are based on densitometry of multiple western blots and are best interpreted qualitatively.

Neuraminidases Altered Expression of LFA-1 Epitopes

Our observation that NEU3 activity blocked LFA-1 adhesion could be the result of multiple mechanisms. To gain some insight into the process, we measured changes in known surface epitopes of LFA-1. The MEM148 epitope is found in the membrane proximal domain of CD18, and is an activation-dependent epitope of LFA-1 (Drbal et al., 2001). The TS1/22 antibody binds to the LFA-1 α-chain, and is both adhesion blocking and conformationally independent (Kuwano et al., 2010). To detect changes in epitope expression after treatment with NEU, we used flow cytometry (**Figure 7**). The TS1/22 epitope showed a large increase in expression on both cell types after NEU3 treatment, while NanI had no detectable effect on this epitope. Treatment of cells with NEU3 showed a significant increase in the MEM148 activation epitope on Jurkat, but not on PBMC. NanI treatment resulted in a decrease in the MEM148 epitope on both cell types. These data are consistent with increased LFA-1 total expression levels upon NEU3 treatment, with minor changes to the MEM148 activation epitope. Increased LFA-1 expression may be a result of delivery of LFA-1 to the surface from intracellular stores (Miller et al., 1987). We note that previous reports have observed increased expression of the MEM148 epitope and increased surface-localized LFA-1 on neutrophils after NanI treatment (Feng et al., 2011).

DISCUSSION

Our data demonstrated that the human NEU3 enzyme can act as a negative regulator of LFA-1–ICAM-1 mediated adhesion in lymphocytes. We confirmed that treatment of cells with exogenous NEU3 produced a reduction of sialylated glycolipids (e.g., GM3) on cells and reduced sialylation of the LFA-1 glycoprotein *in vitro*. NEU3 has been previously shown to prefer glycolipid substrates over glycoproteins, due to its requirement for substrates with a hydrophobic aglycone (Ha et al., 2004; Sandbhor et al., 2011). Treatment of cells with NEU3 or NanI (which lacks activity for gangliosides) (Peter et al., 1995), produced increased LFA-1 clustering as observed by fluorescence microscopy. Quantitative analysis of single-cell images confirmed that LFA-1 clustering was increased in NEU-treated cells. Analysis of the lateral mobility of LFA-1 found that NEU3 treatment resulted in an increase in integrin diffusion. Importantly, substantial effects on lateral mobility were only observed after NEU3 treatment, consistent with a role for gangliosides in regulating integrin diffusion (Sharma et al., 2005). NEU activity had a significant influence on LFA-1–ICAM-1 adhesion, and we concluded that NEU3 blocked LFA-1 adhesion through desialylation of a cell-surface target (e.g., glycolipids or glycoproteins). Control experiments confirmed that the NEU3 anti-adhesive effect was not a result of changes to ICAM-1 glycosylation, as was the case for NanI. Furthermore, we confirmed that NEU3 activity was distinct from NanI in that NEU3 induced an increase in surface expression of LFA-1. We observed that NEU3 activity increased endocytosis of both β1 and β2 integrins while NanI only affected the β1 integrin, suggesting a role for glycolipids in regulating the balance of exo- and endocytosis of adhesion receptors. We note that our experiments have focused on exogenous NEU3, which is a limitation of our study. However, the observation that treatment with an inhibitor of native NEU activity (DANA) blocks LFA-1-mediated adhesion is consistent with a role for native NEU. Together, our results implicate NEU3 as a potential regulator of β2-integrin mediated adhesion.

LFA-1 activity is governed by the interplay of avidity and affinity regulation; and these factors correspond to receptor clustering and conformational change, respectively (van Kooyk and Figdor, 2000; Carman and Springer, 2003; Kim et al., 2004). A quantitative analysis of single-cell images obtained by TIRF microscopy confirmed that a larger proportion of LFA-1 was found in clusters on NEU–treated cells. In accord with this observation, we found that the lateral mobility of LFA-1 on NEU–treated cells was increased, providing a mechanism for the change in integrin organization (Cairo and Golan, 2008). LFA-1 has been observed to cluster in microdomains (Scheiermann et al., 2010) with tightly regulated lateral mobility (Bakker et al., 2012). The size of LFA-1 clusters has been estimated over a wide range between 50 and 200 nm (Cambi et al., 2006; van Zanten et al., 2009; Rajani et al., 2011). Our observations using TIRF microscopy are limited by diffraction, and therefore changes observed for cluster size (**Figure 4**) were likely due to co-localization of multiple microclusters. The lateral mobility of LFA-1 has been found to be dependent on conformational state and stimulation of the cell (Cairo et al., 2006; Alenghat and Golan, 2013). Furthermore, LFA-1 mobility is linked to the ability of the cell to form a stable adhesion (Ishibashi et al., 2015).

The two NEU enzymes studied here had distinct effects on LFA-1. We observed that NEU3 activity induced an LFA-1 activation epitope on Jurkat, but had no effect on PBMC (Drbal et al., 2001). Treatment of cells with NanI showed a uniform decrease in the MEM148 activation epitope. Glycosylation of integrins is known to influence both conformation and function (Bellis, 2004; Gu and Taniguchi, 2004; Liu et al., 2008), and our lectin blots confirm that these enzymes modify glycosylation of LFA-1. While NanI activity also resulted in a blockade of LFA-1–ICAM-1 interactions, this effect can be ascribed to modification of the ICAM-1 ligand, rather than targets on the lymphocyte. These observations may be specific to cell type, as NEU activity directed at LFA-1 is reported to enhance adhesion of neutrophils (Feng et al., 2011). In addition to conformational changes of

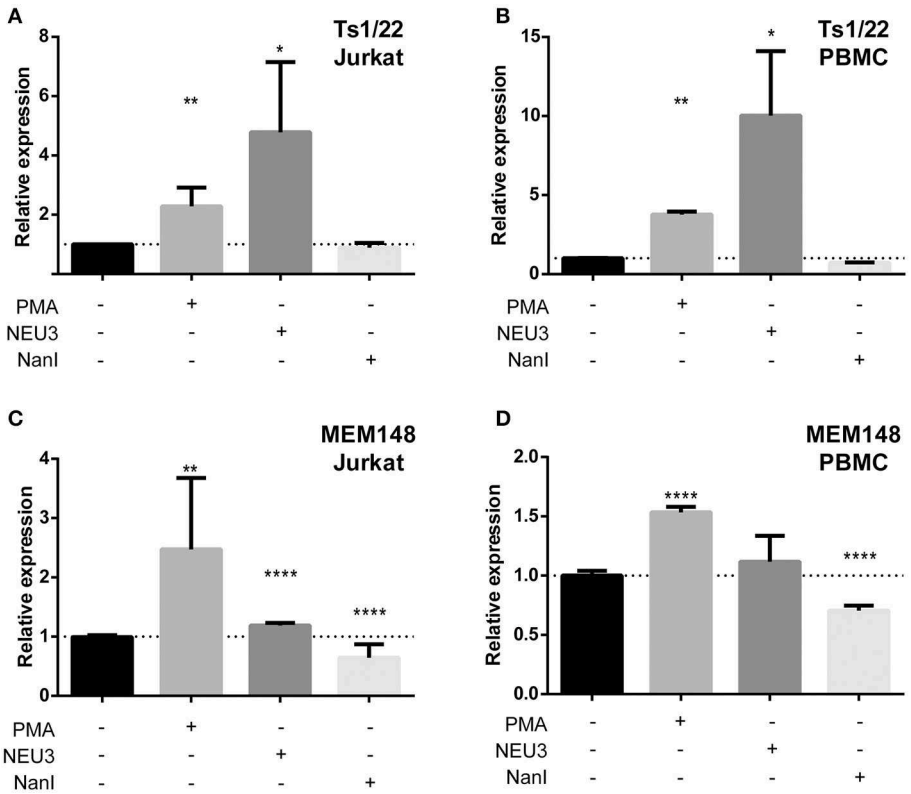

FIGURE 7 | Alteration of LFA-1 epitopes by neuraminidase treatment. Jurkat T cells **(A,C)** or PBMC **(B,D)** were treated with the indicated conditions. Treated cells were labeled with primary antibodies (TS1/22 or MEM148), followed by an AF647-conjugated secondary antibody. Cells were fixed with 1% PFA, analyzed by flow cytometry, and normalized to control (buffer) treatment. Data shown are the mean of three replicates for each sample and error is shown as the standard error of mean. Data were compared to the appropriate control using a *t*-test to determine *p*-values; $^{*}p \leq 0.05$; $^{**}p \leq 0.01$; $^{****}p \leq 0.0001$.

integrins, desialylation may alter inter-molecular interactions which depend on the revealed galactoside epitopes generated by NEU activity (Zhuo et al., 2008; Yang et al., 2017).

Signaling mechanisms known to negatively regulate LFA-1 include the protein tyrosine phosphatase receptor type γ (Mirenda et al., 2015), and the Lyn kinase (Nakata et al., 2006; Malik et al., 2008). Notably, Lyn activity suppresses LFA-1–ICAM-1 adhesion, but enhances cell migration. Lyn activity is known to be regulated by glycolipid composition of the outer leaflet (Sonnino et al., 2010). Furthermore, Lyn is known to be found at the leading edge of migrating cells (He et al., 2011), as is NEU3 and consistent with our imaging in **Figure 3** (Yamaguchi et al., 2006). We note that Lyn-mediated activation of alternative adhesion mechanisms is consistent with our homotypic aggregation results (**Figure 6**). Future investigations will need to address a link between Lyn and NEU3 as it pertains to LFA-1 down-regulation. While our data suggest NEU3 is a negative regulator of LFA-1 adhesion, we also observed an increase in homotypic aggregation in NEU3-treated cells. Homotypic aggregation of lymphocytes is mediated by receptors including the αLβ2 (Rothlein and Springer, 1986), α4β1, and α5β1 integrins (Caixia et al., 1991). The activity of NEU3 on simple gangliosides (e.g., GM3) would generate neutral glycosphingolipids, which are known to be activators of homotypic aggregation in hematopoietic cells (Yamaji et al., 1997). Furthermore, changes in membrane cholesterol or GM1 are known to disrupt LFA-1 adhesion, and our results may suggest that changes to other glycolipid components of microdomains have a similar effect (Marwali et al., 2003). Increased NEU3 activity may alter the concentration of additional degradation products of GSL. Ceramide is known to increase surface expression of β2 integrin, and to block β2-integrin–dependent adhesion while preserving homotypic aggregation (Feldhaus et al., 2002).

How do NEU enzymes affect LFA-1 function? First, the mechanisms of action of each NEU enzyme used in this study have important differences. The substrate profile of each enzyme is different, with NanI acting on glycoproteins while NEU3 uses glycolipids as its favored substrates (Peter et al., 1995; Wang Y. et al., 2001). Thus, NanI treatment is likely to alter glycoprotein substrates, while NEU3 modifies both glycolipids and LFA-1. Changes to glycoprotein epitopes of LFA-1 may block adhesive interactions (Ardman et al., 1992) or induce engagement of new protein-glycan interactions (Wang X.Q. et al., 2002; Rossi et al., 2006; Rabinovich et al., 2007). Galectins are secreted lectins that bind to β-galactoside epitopes, which are often revealed by NEU

activity (Rabinovich and Toscano, 2009). Galectin-1 can inhibit leukocyte adhesion (He and Baum, 2006; Norling et al., 2008), while Galectin-3 can promote neutrophil adhesion (Kuwabara and Liu, 1996). Previous work has found that native NEU activity in neutrophils positively regulates LFA-1 adhesion, which may implicate other isoenzymes, such as NEU1, for this activity (Feng et al., 2011). NEU3 activity altered lipid composition and could therefore influence membrane microdomain recruitment, function, or trafficking of integrins (Gopalakrishna et al., 2004; Ledeen and Wu, 2007; Nakayama et al., 2008). It is possible that direct integrin-glycolipid interactions are responsible for the reorganization of LFA-1 observed here, as β1-integrins are known to bind directly to gangliosides (Wang X. et al., 2001). Indeed, changes in membrane glycolipid composition have been shown to affect the recruitment of integrins and Src kinases to membrane microdomains (Kazui et al., 2000). Ectoenzymes are emerging as important regulators of leukocyte migration (Salmi and Jalkanen, 2005). NEU3 has been established as a plasma membrane-associated enzyme (Zanchetti et al., 2007), and our work here confirms that its activity can negatively regulate leukocyte adhesion.

The data presented here provide evidence that the human NEU3 enzyme can act as a negative regulator of LFA-1–ICAM-1 adhesion. However, it is important to emphasize that the enzyme also activates other cell-adhesion mechanisms (**Figure 6D**). The enzyme alters glycolipid composition, which likely leads to a shift in clustering and increased endocytosis of LFA-1. This mechanism of LFA-1 regulation was able to substantially block PMA-activated adhesion of leukocytes, and may present a novel target for pharmacological intervention in inflammation (Cairo, 2014). Although blocking of NEU3 would result in positive regulation of LFA-1, inhibition may also block the downstream adhesion mechanisms which are activated by NEU3. Future work should address the specific adhesion mechanisms which NEU3 may positively regulate, and the role of NEU3 within the inflammatory cascade (Ley et al., 2007).

EXPERIMENTAL PROCEDURES

Cell Culture

Jurkat cells (clone E6.1) were grown in RPMI 1640 medium with 10% fetal bovine serum (FBS) at 37°C under 5% CO_2 to ∼1.5 × 10^6 cells mL^{-1}. Phorbol 12-myristate 13-acetate (PMA) (Sigma-Aldrich. Oakville, Ontario, Canada) and cytochalasin D (cytoD) (ENZO Life Sciences. Farmingdale, NY, USA) were dissolved in dimethyl sulfoxide (DMSO) as stock solutions (Sigma-Aldrich. Oakville, Ontario, Canada). Human neuraminidase 3 (NEU3) and NanI (Sigma-Aldrich. Oakville, Ontario, Canada) were stored in the same NEU3 buffer (0.2 M NaCl, 10% glycerol, 10 mM maltose, 20 mM MOPS pH 7.2). NEU3 was produced as a recombinant MBP fusion as previously reported (Albohy et al., 2010).

Peripheral blood mononuclear cells (PBMC) were isolated from whole blood samples of healthy donors following a protocol approved by the Health Research Ethics Board of the University of Alberta (Pro00016491). Briefly, cells were centrifuged over a ficoll gradient, transferred to a culture flask, and incubated overnight at 37°C with 5% CO_2 in RPMI medium (10% FBS and 1% penicillin-streptomycin).

Cell treatments were performed using the conditions indicated below. A suspension of 1 × 10^6 cells was taken from the culture flask and washed three times with buffer. In all washing steps, the cells were spun at 1,200 rpm for 2 min in a desktop centrifuge. For PMA and cytoD conditions, cells were re-suspended in 1 mL of buffer (PBS) with DMSO (0.05% final concentration) or the same buffer with DMSO containing PMA (200 ng mL^{-1}) or cytoD (2.5 μg mL^{-1}). The samples were then incubated at 37°C under 5% CO_2 for 30 min. For enzyme treatments, cells were re-suspended in PBS alone, NEU3 enzyme (0.01875 U), or NanI enzyme (0.01875 U). One unit of enzyme activity was defined as, 1 U = 1 μmol 4MU-NANA substrate cleavage min^{-1}, this calibration was done at pH 4.5. Enzyme samples were then incubated at 37°C under 5% CO_2 for 3 h. After incubation all treated cells were then washed 3 times with PBS before further labeling, analysis, or extraction steps.

High-Performance Thin Layer Chromatography (HPTLC)

For high-performance thin layer chromatography (HPTLC) experiments, phosphate buffered saline (PBS) was used as washing buffer. All treatments were done with 1 × 10^7 cells in a 10 mL volume. After treatment, the cells were centrifuged to a pellet and re-suspended in 60 μL water, and sonicated for 30 s. Cells were extracted with a mixture of chloroform and methanol (1:1, 400 μL × 3) and agitated for 10 min. The sample was centrifuged (10,000 rpm for 10 min), and the supernatant was transferred to a glass bottle, dried under a flow of N_2, and stored at −20°C. Before analysis, the cell extract was dissolved in a chloroform and methanol solution (1:1, 200 μL) and applied to a HPTLC plate (Sigma-Aldrich) using a glass micropipette. Chromatography was performed with acetic acid, *n*-butanol, and 0.25% $CaCl_2$ (1:2:1) as the eluent followed by staining with orcinol (0.5 g orcinol, 200 mL 8% H_2SO_4 in ethanol).

Extraction and Purification of Gangliosides

Ganglioside extraction and purification was performed following previous reports (Neville et al., 2004). Briefly, a lysate of 1 × 10^6 Jurkat T cells was diluted with ice cold water (4 mL g^{-1} based on weight of sample). After homogenization, methanol was added to make the final ratio of methanol:water 8:3. Chloroform was added after vigorous mixing of this suspension to make the chloroform:methanol:water mixture to the ratio 4:8:3 (v/v/v). This mixture was vortexed and centrifuged at 1,500 RPM for 15 min. The supernatant was carefully recovered, volume measured, then diluted with 0.173 volumes of water. After mixing, the suspension was centrifuged again. The upper phase was recovered and transferred to a fresh tube, purified on a SepPak C18 cartridge (Waters Corporation, Milford, MA, USA), evaporated to dryness under a stream of nitrogen, and re-dissolved in methanol.

LC-MS Analysis of Gangliosides

Expression and purification of EGCase was performed following previous reports with a pET30 vector (Albrecht et al., 2016).

Samples of extracted GSLs were dissolved in a 50 mM sodium acetate buffer (pH 5.2) containing 1 mg mL^{-1} sodium cholate and incubated for 18 h at 30°C with 0.086U EGCase. One unit of EGCase I was defined as the amount of enzyme that hydrolyzes 1 μmol of GM3 per minute at 30°C. Released glycans were labeled with a mixture containing 30 mg anthranilic acid, 20 mg boric acid, 40 mg sodium acetate, and 45 mg sodium cyanoborohydride at 80°C for 45 min.

Labeled glycans were analyzed using an Agilent 1200 SL HPLC system and a normal-phase column (Accucore-150-Amide-HILIC, 2.6 μm, 2.1 × 150 mm, Thermo Fisher). Dried samples were re-solubilized in water:DMF:acetonitrile in the ratio 1:1:2 and 15 μL was injected. The fluorescence detector was set to monitor at 320 nm excitation and 420 nm emission, and all chromatography was performed at 40°C. Mass spectra were acquired in negative mode using an Agilent 6220 Accurate-Mass TOF HPLC/MS system with a dual spray electrospray ionization source along with a secondary reference sprayer for a reference mass solution. Data analysis was performed using the Agilent MassHunter Qualitative Analysis software package version B.07.01.

Single-Particle Tracking of Integrin Receptors

In single particle tracking and TIRF imaging experiments the washing buffer was HBSSB (1% BSA, Hank's Balanced Salt Solution). TS2/4 mAb was purified from HB244 cell line (American Type Culture Collection, ATCC). A Cy5-antibody conjugate was generated using an NHS ester of Cy5 (GE Healthcare, Buckinghamshire, UK) using the manufacturer's protocol. The dye:antibody ratio was measured at 3.7 dye per antibody after purification. A final concentration of 30 ng mL^{-1} of labeled protein was added into a sample of 1 × 10^6 treated cells. Cells were washed 3 times with HBSSB buffer after labeling at 37°C for 15 min. Labeled cells were re-suspended in 1 mL HBSSB and transferred to a 24-well cell culture plate containing a coverglass which was previously treated with 10 μg mL^{-1} of poly-L-lysine. The plate was spun at 400 g for 7 min, and the well was washed 3 times with HBSSB to remove unattached cells. The coverglass was transferred onto a microscopy slide and sealed with Cytoseal 60 (Thermo Fisher Scientific, Waltham, MA). All tracking data were acquired within 30 min of sealing. Tracking videos were taken on a NIKON Ti TIRF microscopy with 638 nm laser excitation and a 690 ± 40 nm filter with a 60 × TIRF objective (NA 1.49) with an additional 1.5 × magnifier (providing a final resolution of 252 nm $pixel^{-1}$). Videos were acquired at 10 FPS for 10 s and analyzed with u-track (Jaqaman et al., 2008) in Matlab (2012b). Trajectories with fewer than 20 steps were discarded. The intensity of the trajectories was used to exclude the top and bottom 5 % of trajectories from the analysis. The data were processed using custom scripts in MATlab (Cairo et al., 2006).

Total Internal Reflection Fluorescence Microscope (TIRF) Imaging and Cluster Analysis

Cells were treated identically to those used for SPT, followed by fixation with 1% paraformaldehyde (PFA) in PBS at 4°C for 60 min. The fixed cells were washed with PBS twice, and 2 × 10^5 fixed cells from each treatment were re-suspended in 200 μL PBS. The cells were labeled with Cholera toxin B FITC (CTB-FITC, 5 μg mL^{-1}; Sigma-Aldrich, Oakville, Ontario, Canada) and TS2/4-Cy5 (500 ng mL^{-1}) at room temperature for 10 min. Labeled cells were washed twice with PBS, re-suspended in 1 mL PBS, and transferred to a 24-well cell culture plate containing a coverglass (poly-L-Lysine treated). The plate was spun at 400 g for 7 min, and the well was washed 3 times with PBS. The coverglass was transferred to a microscope slide and sealed with Cytoseal 60, followed by imaging using TIRF. More than three independent labeling samples were imaged for each treatment.

TIRF imaging for cluster analysis was performed using an identical protocol as described above, with a lower concentration of the TS2/4-Cy5 conjugate (80 ng mL^{-1}). Fifteen cells were chosen for analysis based on DIC (the cells were apparently healthy and round) and staining (TIRF image showed TS2/4 labeling on the whole cell). Images of individual cells were processed in ImageJ by applying a threshold to identify labeled pixels and processed using the analyze particle function to measure clusters larger than 4 $pixel^2$ (0.07 mm^2).

ICAM-1 Adhesion Assay

To prepare ICAM-1–bead complexes purified ICAM-1 protein (5 μg, R&D systems, Minneapolis, MN, USA) was incubated with 25 μL of a 2% solution of 1 μm microbeads (yellow-green sulfate microspheres; Life Technologies, Burlington, ON, Canada) in a final volume of 100 μL (in 50 mM PBS, pH 8.3) for 8 h at 4°C. After incubation, a solution of PBS (50 mM) containing 2% BSA (100 μL) was added and the suspension of beads and was incubated overnight at 4°C. The beads were stored at 4°C and used within 24 h.

Jurkat T cells or PBMC were treated as above with PBS as the washing buffer. Treatment with DANA was at 100 μM. Treated cell samples contained 3 × 10^6 cells in 1 mL PBS, and were labeled with 10 μL of ICAM-1 or control beads followed by incubation at 37°C for 15 min. The labeled cells were washed with PBS three times and resuspended in 1 mL of PBS followed by analysis on an Accuri C6 flow cytometer.

Homotypic Aggregation of Jurkat Cells

Jurkat cells were washed with PBS three times and re-suspended in PBS at a concentration of 2 × 10^5 cells mL^{-1}. Cells were transferred to solutions with the following conditions: buffer alone, NEU3 (0.01875 U), or NanI (0.01875 U). All samples had a final concentration of 10% NEU3 storage buffer and 0.6% binding buffer (100 mM CAPS, 0.15M NaCl, 1 mM calcium chloride, pH 11.0). All samples were stained with 1 μg mL^{-1} Calcein AM (Life Technologies, Burlington, ON, Canada). Samples were transferred to a 96-well- plate (200 μL per well). The plate was incubated at 37°C for 3 h. Fluorescent images were taken with

a NIKON Ti microscope using a 20x objective and a FITC filter set. Four images were taken for each well to provide 24 images for each condition. The images were analyzed with CellProfiler (Version 2.1.1) (Carpenter et al., 2006; Bray et al., 2015). The total number of the cells in each image, and the number of single cells (cells not in any clusters) were counted in CellProfiler. The amount of aggregation was calculated as (total number of cells – numbers of single cells)/total number of cells. Results were confirmed using at least two independent repeats.

Integrin Endocytosis

Samples of sulfo-NHS-SS-Biotin and streptavidin-resin were obtained from Thermofisher, USA. Glutathione (GSH) was purchased from Sigma-Aldrich. Antibodies for β1 integrin (clone EP1041Y), β2 integrin (clone EP1286Y), HRP-conjugated goat anti-rabbit secondary antibody (ab6721) were obtained from Abcam, USA.

Biotin-based endocytosis assays were performed as previously described with slight modifications (Cihil and Swiatecka-Urban, 2013). Jurkat T cells were grown in 10% FBS-containing medium T-75 flasks (Corning, USA). Cells were collected by centrifugation at 300 g for 2 min and 2×10^6 cells were placed in separate Eppendorf tubes. Samples were placed on ice and washed once with cold PBS, and then labeled with 0.8 mg mL^{-1} of sulfo-NHS-SS-biotin for 60 min at 4°C. Cells were then centrifuged again and unbound biotin was washed away with cold medium. Cells were then resuspended in prewarmed medium with or without treatment and biotin-labeled surface proteins were allowed to internalize at 37°C for 30 min. Enzyme treatments were performed in PBS buffer (pH 7.0) with 0.02 U of NEU3 or NanI. Cold medium was immediately added, and samples were put over ice. Any remaining biotin at the cell surface was removed with GSH buffer (75 mM sodium chloride, 1 mM magnesium chloride, 0.1 mM calcium chloride, 50 mM GSH, and 80 mM sodium hydroxide) for 30 min at 4°C, followed by multiple washes with cold PBS. The cells were pelleted and treated with lysis buffer [150 mM sodium chloride, 1.0% Triton X-100, 0.5% sodium deoxycholate, 0.1% SDS, 50 mM Tris, pH 8.0 and phosphatase and protease inhibitor cocktails (Roche, USA)] at 4°C for 30 min. The lysate was clarified by ultra-centrifugation at 18,000 × g for 10 min. Supernatants were collected, and a BCA assay was used to calibrate protein concentrations. Equal amounts of protein were incubated with streptavidin-resin with agitation at 4°C overnight. The resin was washed once with lysis buffer and boiled with 2x Laemmeli sample buffer containing 100 mM DTT. Endocytosed biotinylated β1 and β2 integrins were measured by separate western blots for the respective β-chains.

LFA-1 Antibody Binding

MEM148 antibody was purchased from AbD Serotec (Raleigh, NC, USA); TS1/22 antibody was purchased from Fisher Scientific Ottawa, ON, Canada. A sample of cells (Jurkat or PBMC, 1×10^6) were treated with NEU3 (0.01875 U) or NanI (0.01875 U) for 3 h, or PMA (200 ng mL^{-1}) for 30 min. Incubations were done at 37°C at 5% CO_2, followed by washing with PBS, centrifugation, and re-suspension in PBS buffer (900 μL). Cells were then divided into aliquots and labeled with TS1/22 or MEM148 antibodies for 30 min. Cells were then washed three times with PBS and re-suspended with PBS with AF-647–conjugated secondary antibody at 1:1000 dilution for 10 min. Cells were again washed three times and fixed with 1 % PFA for 10 min before analyzing using an Accuri C6 flow cytometer.

Lectin Blotting of LFA-1

Purified LFA-1 (R&D systems, USA; 50 μg) was biotinylated with sulfo-NHS-SS-biotin and immobilized on Neutravidin resin (600 μL) overnight at pH 7. The suspension was then washed three times with PBS buffer (pH 7.0). The immobilized LFA-1 was then treated with NEU3 (0.01875 U) or NanI (0.01875 U) and the mixture was incubated for 3 h at 37°C. The resin was washed three times to remove contaminating proteins, followed by incubation at 95°C for 10 min in the presence of DTT (100 mM) to release LFA-1 from the resin. Buffer exchange was done to remove excess DTT, and a BCA assay was carried out to determine the protein concentration of each sample. Equal amounts of the protein were then loaded on an SDS-PAGE gel, transferred to a nitrocellulose membrane, and detected using biotinylated peanut agglutinin (PNA), *M. amurensis* agglutinin (MAA), or *S. nigra* (SNA) lectins (Bio-World, Ohio, USA) at 1:500 dilution. Lectins were imaged with streptavidin-HRP (1:200 dilution) and band intensity was analyzed using ImageJ.

DATA AVAILABILITY STATEMENT

All datasets generated for this study are included in the article/**Supplementary Material**.

ETHICS STATEMENT

The studies involving human participants were reviewed and approved by University of Alberta, Health Research Ethics Board. The patients/participants provided their written informed consent to participate in this study.

AUTHOR CONTRIBUTIONS

MH designed and performed endocytosis, epitope expression, lectin blotting experiments, and wrote the manuscript. CL performed and analyzed fluorescence microscopy, SPT, antibody binding, FN aggregation experiments, and edited the manuscript. RC designed and performed glycolipid analysis and wrote the manuscript. CZ designed and performed ICAM binding experiments and produced NEU3 protein. NE designed antibody binding experiments. CC designed and coordinated the study, analyzed data, and wrote the manuscript.

FUNDING

This work was supported by the Natural Sciences and Engineering Research Council of Canada (NSERC), the Alberta Glycomics Center, and the Canadian Glycomics Network (GlycoNet). Instrumentation for this study was supported in part by the Canadian Foundation for Innovation (CFI).

ACKNOWLEDGMENTS

MH acknowledges support from an NSERC CGS-D scholarship. We thank the University of Alberta Department of Chemistry for access to LC-MS facilities.

SUPPLEMENTARY MATERIAL

The Supplementary Material for this article can be found online at: https://www.frontiersin.org/articles/10.3389/fchem.2019.00791/full#supplementary-material

REFERENCES

Albohy, A., Li, M. D., Zheng, R. B., Zou, C., and Cairo, C. W. (2010). Insight into substrate recognition and catalysis by the mammalian neuraminidase 3 (NEU3) through molecular modeling and site directed mutagenesis. *Glycobiology* 20, 1127–1138. doi: 10.1093/glycob/cwq077

Albrecht, S., Vainauskas, S., Stockmann, H., McManus, C., Taron, C. H., and Rudd, P. M. (2016). Comprehensive profiling of glycosphingolipid glycans using a novel broad specificity endoglycoceramidase in a high-throughput workflow. *Anal. Chem.* 88, 4795–4802. doi: 10.1021/acs.analchem.6b00259

Alenghat, F. J., and Golan, D. E. (2013). Membrane protein dynamics and functional implications in mammalian cells. *Curr. Top. Membr.* 72, 89–120. doi: 10.1016/B978-0-12-417027-8.00003-9

Andrew, D. P., Berlin, C., Honda, S., Yoshino, T., Hamann, A., Holzmann, B., et al. (1994). Distinct but overlapping epitopes are involved in alpha 4 beta 7-mediated adhesion to vascular cell adhesion molecule-1, mucosal addressin-1, fibronectin, and lymphocyte aggregation. *J. Immunol.* 153, 3847–3861.

Ardman, B., Sikorski, M. A., and Staunton, D. E. (1992). CD43 interferes with T-lymphocyte adhesion. *Proc. Natl. Acad. Sci. U.S.A.* 89, 5001–5005. doi: 10.1073/pnas.89.11.5001

Bagriacik, E. U., and Miller, K. S. (1999). Cell surface sialic acid and the regulation of immune cell interactions: the neuraminidase effect reconsidered. *Glycobiology* 9, 267–275. doi: 10.1093/glycob/9.3.267

Bakker, G. J., Eich, C., Torreno-Pina, J. A., Diez-Ahedo, R., Perez-Samper, G., van Zanten, T. S., et al. (2012). Lateral mobility of individual integrin nanoclusters orchestrates the onset for leukocyte adhesion. *Proc. Natl. Acad. Sci. U.S.A.* 109, 4869–4874. doi: 10.1073/pnas.1116425109

Bednarczyk, J. L., and McIntyre, B. W. (1990). A monoclonal antibody to VLA-4 alpha-chain (CDw49d) induces homotypic lymphocyte aggregation. *J. Immunol.* 144, 777–784.

Bellis, S. L. (2004). Variant glycosylation: an underappreciated regulatory mechanism for beta 1 integrins. *Biochim. Biophys. Acta Biomembr.* 1663, 52–60. doi: 10.1016/j.bbamem.2004.03.012

Bi, S., and Baum, L. G. (2009). Sialic acids in T cell development and function. *Biochim. Biophys. Acta* 1790, 1599–1610. doi: 10.1016/j.bbagen.2009.07.027

Blank, N., Schiller, M., Krienke, S., Wabnitz, G., Ho, A. D., and Lorenz, H.-M. (2007). Cholera toxin binds to lipid rafts but has a limited specificity for ganglioside GM1. *Immunol. Cell Biol.* 85, 378–382. doi: 10.1038/sj.icb.7100045

Bray, M. A., Vokes, M. S., and Carpenter, A. E. (2015). Using cellprofiler for automatic identification and measurement of biological objects in images. *Curr. Protoc. Mol. Biol.* 109, 14.17.1–14.17.13. doi: 10.1002/0471142727.mb1417s109

Cairo, C. W. (2014). Inhibitors of the human neuraminidase enzymes. *MedChemComm* 5, 1067–1074. doi: 10.1039/C4MD00089G

Cairo, C. W., and Golan, D. E. (2008). T cell adhesion mechanisms revealed by receptor lateral mobility. *Biopolymers* 89, 409–419. doi: 10.1002/bip.20898

Cairo, C. W., Mirchev, R., and Golan, D. E. (2006). Cytoskeletal regulation couples LFA-1 conformational changes to receptor lateral mobility and clustering. *Immunity* 25, 297–308. doi: 10.1016/j.immuni.2006.06.012

Caixia, S., Stewart, S., Wayner, E., Carter, W., and Wilkins, J. (1991). Antibodies to different members of the β1 (CD29) integrins induce homotypic and heterotypic cellular aggregation. *Cell. Immunol.* 138, 216–228. doi: 10.1016/0008-8749(91)90146-3

Cambi, A., Joosten, B., Koopman, M., de Lange, F., Beeren, I., Torensma, R., et al. (2006). Organization of the integrin LFA-1 in nanoclusters regulates its activity. *Mol. Biol. Cell* 17, 4270–4281. doi: 10.1091/mbc.e05-12-1098

Campanero, M., Pulido, R., Ursa, M., Rodriguez-Moya, M., De Landazuri, M., and Sanchez-Madrid, F. (1990). An alternative leukocyte homotypic adhesion mechanism, LFA-1/ICAM-1-independent, triggered through the human VLA-4 integrin. *J. Cell Biol.* 110, 2157–2165. doi: 10.1083/jcb.110.6.2157

Carman, C. V., and Springer, T. A. (2003). Integrin avidity regulation: are changes in affinity and conformation underemphasized? *Curr. Opin. Cell Biol.* 15, 547–556. doi: 10.1016/j.ceb.2003.08.003

Carpenter, A. E., Jones, T. R., Lamprecht, M. R., Clarke, C., Kang, I. H., Friman, O., et al. (2006). CellProfiler: image analysis software for identifying and quantifying cell phenotypes. *Genome Biol.* 7:R100. doi: 10.1186/gb-2006-7-10-r100

Caswell, P. T., and Norman, J. C. (2006). Integrin trafficking and the control of cell migration. *Traffic* 7, 14–21. doi: 10.1111/j.1600-0854.2005.00362.x

Chatterjee, S., and Pandey, A. (2008). The Yin and Yang of lactosylceramide metabolism: implications in cell function. *Biochim. Biophys. Acta Gen. Subjects* 1780, 370–382. doi: 10.1016/j.bbagen.2007.08.010

Cho, J. Y., Fox, D. A., Horejsi, V., Sagawa, K., Skubitz, K. M., Katz, D. R., et al. (2001). The functional interactions between CD98, β1-integrins, and CD147 in the induction of U937 homotypic aggregation. *Blood* 98, 374–382. doi: 10.1182/blood.V98.2.374

Cihil, K. M., and Swiatecka-Urban, A. (2013). The cell-based L-glutathione protection assays to study endocytosis and recycling of plasma membrane proteins. *J. Visual. Exp.* 82:e50867. doi: 10.3791/50867

Cowing, C., and Chapdelaine, J. M. (1983). T-cells discriminate between Ia antigens expressed on allogeneic accessory cells and B-cells - A potential function for carbohydrate side-chains on Ia molecules. *Proc. Natl. Acad. Sci. U.S.A.* 80, 6000–6004. doi: 10.1073/pnas.80.19.6000

Cox, D., Brennan, M., and Moran, N. (2010). Integrins as therapeutic targets: lessons and opportunities. *Nat. Rev. Drug Discov.* 9, 804–820. doi: 10.1038/nrd3266

Cross, A. S., and Wright, D. G. (1991). Mobilization of sialidase from intracellular stores to the surface of human neutrophils and its role in stimulated adhesion responses of these cells. *J. Clin. Investig.* 88, 2067–2076. doi: 10.1172/JCI115536

Crucian, B., Nelman-Gonzalez, M., and Sams, C. (2006). Rapid flow cytometry method for quantitation of LFA-1-adhesive T cells. *Clin. Vaccine Immunol.* 13, 403–408. doi: 10.1128/CVI.13.3.403-408.2006

Desgrosellier, J. S., and Cheresh, D. A. (2010). Integrins in cancer: biological implications and therapeutic opportunities. *Nat. Rev. Cancer* 10, 9–22. doi: 10.1038/nrc2748

Drbal, K., Angelisova, P., Cerny, J., Hilgert, I., and Horejsi, V. (2001). A novel anti-CD18 mAb recognizes an activation-related epitope and induces a high-affinity conformation in leukocyte integrins. *Immunobiology* 203, 687–698. doi: 10.1016/S0171-2985(01)80017-6

Feldhaus, M. J., Weyrich, A. S., Zimmerman, G. A., and McIntyre, T. M. (2002). Ceramide Generation *in situ* alters leukocyte cytoskeletal organization and β2-integrin function and causes complete degranulation. *J. Biol. Chem.* 277, 4285–4293. doi: 10.1074/jbc.M106653200

Feng, C., Zhang, L., Almulki, L., Faez, S., Whitford, M., Hafezi-Moghadam, A., et al. (2011). Endogenous PMN sialidase activity exposes activation epitope on CD11b/CD18 which enhances its binding interaction with ICAM-1. *J. Leukocyte Biol.* 90, 313–321. doi: 10.1189/jlb.1210708

Freeze, H. H. (2001). Lectin analysis of proteins blotted onto filters. *Curr. Protoc. Mol. Biol.* Chapter 17, Unit17.7. doi: 10.1002/0471142727.mb1707s23

Gaborski, T. R., Sealander, M. N., Waugh, R. E., and McGrath, J. L. (2013). Dynamics of adhesion molecule domains on neutrophil membranes: surfing the dynamic cell topography. *Eur. Biophys. J.* 42, 851–855. doi: 10.1007/s00249-013-0931-z

Gadhoum, S. Z., and Sackstein, R. (2008). CD15 expression in human myeloid cell differentiation is regulated by sialidase activity. *Nat. Chem. Biol.* 4, 751–757. doi: 10.1038/nchembio.116

Galvan, M., Murali-Krishna, K., Ming, L. L., Baum, L., and Ahmed, R. (1998). Alterations in cell surface carbohydrates on T cells from virally infected mice

can distinguish effector/memory CD8(+) T cells from naive cells. *J. Immunol.* 161, 641–648.

Gopalakrishna, P., Rangaraj, N., and Pande, G. (2004). Cholesterol alters the interaction of glycosphingolipid GM3 with alpha 5 beta 1 integrin and increases integrin-mediated cell adhesion to fibronectin. *Exp. Cell Res.* 300, 43–53. doi: 10.1016/j.yexcr.2004.06.012

Gu, J. G., and Taniguchi, N. (2004). Regulation of integrin functions by N-glycans. *Glycoconjugate J.* 21, 9–15. doi: 10.1023/B:GLYC.0000043741.47559.30

Ha, K. T., Lee, Y. C., Cho, S. H., Kim, J. K., and Kim, C. H. (2004). Molecular characterization of membrane type and ganglioside-specific sialidase (Neu3) expressed in *E-coli*. *Mol. Cells* 17, 267–273.

He, J., and Baum, L. G. (2006). Endothelial cell expression of galectin-1 induced by prostate cancer cells inhibits T-cell transendothelial migration. *Lab. Investig.* 86, 578–590. doi: 10.1038/labinvest.3700420

He, Y., Kapoor, A., Cook, S., Liu, S., Xiang, Y., Rao, C. V., et al. (2011). The non-receptor tyrosine kinase Lyn controls neutrophil adhesion by recruiting the CrkL–C3G complex and activating Rap1 at the leading edge. *J. Cell Sci.* 124, 2153–2164. doi: 10.1242/jcs.078535

Hernandez, J. D., Klein, J., Van Dyken, S. J., Marth, J. D., and Baum, L. G. (2007). T-cell activation results in microheterogeneous changes in glycosylation of CD45. *Int. Immunol.* 19, 847–856. doi: 10.1093/intimm/dxm053

Hogg, N., Laschinger, M., Giles, K., and McDowall, A. (2003). T-cell integrins: more than just sticking points. *J. Cell Sci.* 116, 4695–4705. doi: 10.1242/jcs.00876

Hogg, N., Smith, A., McDowall, A., Giles, K., Stanley, P., Laschinger, M., et al. (2004). How T cells use LFA-1 to attach and migrate. *Immunol. Lett.* 92, 51–54. doi: 10.1016/j.imlet.2003.10.014

Hynes, R. O. (2002). Integrins: bidirectional, allosteric signaling machines. *Cell* 110, 673–687. doi: 10.1016/S0092-8674(02)00971-6

Ishibashi, M., Miyanaga, Y., Matsuoka, S., Kozuka, J., Togashi, Y., Kinashi, T., et al. (2015). Integrin LFA-1 regulates cell adhesion via transient clutch formation. *Biochem. Biophys. Res. Commun.* 464, 459–466. doi: 10.1016/j.bbrc.2015.06.155

Jaqaman, K., Loerke, D., Mettlen, M., Kuwata, H., Grinstein, S., Schmid, S. L., et al. (2008). Robust single-particle tracking in live-cell time-lapse sequences. *Nat. Methods* 5, 695–702. doi: 10.1038/nmeth.1237

Jia, F., Howlader, M. A., and Cairo, C. W. (2016). Integrin-mediated cell migration is blocked by inhibitors of human neuraminidase. *Biochim. Biophys. Acta Mol. Cell Biol. Lipids* 1861(9, Part A), 1170–1179. doi: 10.1016/j.bbalip.2016.06.013

Kampstra, P. (2008). Beanplot: a boxplot alternative for visual comparison of distributions. *J. Stat. Softw.* 28, 1–9. doi: 10.18637/jss.v028.c01

Kansas, G., and Tedder, T. (1991). Transmembrane signals generated through MHC class II, CD19, CD20, CD39, and CD40 antigens induce LFA-1-dependent and independent adhesion in human B cells through a tyrosine kinase-dependent pathway. *J. Immunol.* 147, 4094–4102.

Kazui, A., Ono, M., Handa, K., and Hakomori, S. I. (2000). Glycosylation affects translocation of integrin, Src, and caveolin into or out of GEM. *Biochem. Biophys. Res. Commun.* 273, 159–163. doi: 10.1006/bbrc.2000.2903

Kim, M., Carman, C. V., Yang, W., Salas, A., and Springer, T. A. (2004). The primacy of affinity over clustering in regulation of adhesiveness of the integrin alpha(L)beta 2. *J. Cell Biol.* 167, 1241–1253. doi: 10.1083/jcb.200404160

Kopitz, J., Oehler, C., and Cantz, M. (2001). Desialylation of extracellular GD1a-neoganglioprotein suggests cell surface orientation of the plasma membrane-bound ganglioside sialidase activity in human neuroblastoma cells. *FEBS Lett.* 491, 233–236. doi: 10.1016/S0014-5793(01)02207-4

Kuwabara, I., and Liu, F.-T. (1996). Galectin-3 promotes adhesion of human neutrophils to laminin. *J. Immunol.* 156, 3939–3944.

Kuwano, Y., Spelten, O., Zhang, H., Ley, K., and Zarbock, A. (2010). Rolling on E- or P-selectin induces the extended but not high-affinity conformation of LFA-1 in neutrophils. *Blood* 116, 617–624. doi: 10.1182/blood-2010-01-266122

Ledeen, R., and Wu, G. (2007). GM1 in the nuclear envelope regulates nuclear calcium through association with a nuclear sodium-calcium exchanger. *J. Neurochem.* 103(Suppl. 1), 126–134. doi: 10.1111/j.1471-4159.2007.04722.x

Ley, K., Laudanna, C., Cybulsky, M. I., and Nourshargh, S. (2007). Getting to the site of inflammation: the leukocyte adhesion cascade updated. *Nat. Rev. Immunol.* 7, 678–689. doi: 10.1038/nri2156

Liu, Y. M., Pan, D., Bellis, S. L., and Song, Y. H. (2008). Effect of altered glycosylation on the structure of the I-like domain of beta 1 integrin: a molecular dynamics study. *Proteins Struct. Funct. Bioinformatics* 73, 989–1000. doi: 10.1002/prot.22126

Malik, M., Chen, Y.-Y., Kienzle, M. F., Tomkowicz, B. E., Collman, R. G., and Ptasznik, A. (2008). Monocyte migration and LFA-1-mediated attachment to brain microvascular endothelia is regulated by SDF-1α through Lyn kinase. *J. Immunol.* 181, 4632–4637. doi: 10.4049/jimmunol.181.7.4632

Marwali, M. R., Rey-Ladino, J., Dreolini, L., Shaw, D., and Takei, F. (2003). Membrane cholesterol regulates LFA-1 function and lipid raft heterogeneity. *Blood* 102, 215–222. doi: 10.1182/blood-2002-10-3195

Miller, L. J., Bainton, D. F., Borregaard, N., and Springer, T. A. (1987). Stimulated mobilization of monocyte Mac-1 and p150,95 adhesion proteins from an intracellular vesicular compartment to the cell surface. *J. Clin. Investig.* 80, 535–544. doi: 10.1172/JCI113102

Mirenda, M., Toffali, L., Montresor, A., Scardoni, G., Sorio, C., and Laudanna, C. (2015). Protein tyrosine phosphatase receptor type γ is a JAK phosphatase and negatively regulates leukocyte integrin activation. *J. Immunol.* 194, 2168–2179. doi: 10.4049/jimmunol.1401841

Miyagi, T. (2010). Mammalian sialidases and their functions. *Trends Glycosci. Glycotechnol.* 22, 162–172. doi: 10.4052/tigg.22.162

Miyagi, T., and Yamaguchi, K. (2012). Mammalian sialidases: physiological and pathological roles in cellular functions. *Glycobiology* 22, 880–896. doi: 10.1093/glycob/cws057

Monti, E., Bassi, M. T., Papini, N., Riboni, M., Manzoni, M., Venerando, B., et al. (2000). Identification and expression of NEU3, a novel human sialidase associated to the plasma membrane. *Biochem. J.* 349, 343–351. doi: 10.1042/bj3490343

Muthing, J. (1996). High-resolution thin-layer chromatography of gangliosides. *J. Chromatogr. A* 720, 3–25. doi: 10.1016/0021-9673(95)00499-8

Nakata, Y., Tomkowicz, B., Gewirtz, A. M., and Ptasznik, A. (2006). Integrin inhibition through Lyn-dependent cross talk from CXCR4 chemokine receptors in normal human CD34+ marrow cells. *Blood* 107, 4234–4239. doi: 10.1182/blood-2005-08-3343

Nakayama, H., Yoshizaki, F., Prinetti, A., Sonnino, S., Mauri, L., Takamori, K., et al. (2008). Lyn-coupled LacCer-enriched lipid rafts are required for CD11b/CD18-mediated neutrophil phagocytosis of nonopsonized microorganisms. *J. Leukocyte Biol.* 83, 728–741. doi: 10.1189/jlb.0707478

Neville, D. C., Coquard, V., Priestman, D. A., te Vruchte, D. J., Sillence, D. J., Dwek, R. A., et al. (2004). Analysis of fluorescently labeled glycosphingolipid-derived oligosaccharides following ceramide glycanase digestion and anthranilic acid labeling. *Anal. Biochem.* 331, 275–282. doi: 10.1016/j.ab.2004.03.051

Norling, L. V., Sampaio, A. L., Cooper, D., and Perretti, M. (2008). Inhibitory control of endothelial galectin-1 on *in vitro* and *in vivo* lymphocyte trafficking. *FASEB J.* 22, 682–690. doi: 10.1096/fj.07-9268com

Pande, G. (2000). The role of membrane lipids in regulation of integrin functions. *Curr. Opin. Cell Biol.* 12, 569–574. doi: 10.1016/S0955-0674(00)00133-2

Papini, N., Anastasia, L., Tringali, C., Croci, G., Bresciani, R., Yamaguchi, K., et al. (2004). The plasma membrane-associated sialidase MmNEU3 modifies the ganglioside pattern of adjacent cells supporting its involvement in cell-to-cell interactions. *J. Biol. Chem.* 279, 16989–16995. doi: 10.1074/jbc.M400881200

Parker, R. B., and Kohler, J. J. (2010). Regulation of intracellular signaling by extracellular glycan remodeling. *ACS Chem. Biol.* 5, 35–46. doi: 10.1021/cb9002514

Pellinen, T., and Ivaska, J. (2006). Integrin traffic. *J. Cell Sci.* 119, 3723–3731. doi: 10.1242/jcs.03216

Peter, R., Reinhard, G., and Roland, S. (1995). Diversity in the properties of two sialidase isoenzymes produced by *Clostridium perfringens* spp. *Biol. Chem. Hoppe Seyler* 376, 569–576. doi: 10.1515/bchm3.1995.376.9.569

Qian, H., Sheetz, M. P., and Elson, E. L. (1991). Single particle tracking. Analysis of diffusion and flow in two-dimensional systems. *Biophys. J.* 60, 910–921. doi: 10.1016/S0006-3495(91)82125-7

Rabinovich, G. A., and Toscano, M. A. (2009). Turning 'sweet' on immunity: galectin-glycan interactions in immune tolerance and inflammation. *Nat. Rev. Immunol.* 9, 338–352. doi: 10.1038/nri2536

Rabinovich, G. A., Toscano, M. A., Jackson, S. S., and Vasta, G. R. (2007). Functions of cell surface galectin-glycoprotein lattices. *Curr. Opin. Struct. Biol.* 17, 513–520. doi: 10.1016/j.sbi.2007.09.002

Rajani, V., Carrero, G., Golan, D. E., de Vries, G., and Cairo, C. W. (2011). Analysis of molecular diffusion by first-passage time variance identifies the size of confinement zones. *Biophys. J.* 100, 1463–1472. doi: 10.1016/j.bpj.2011.01.064

Richards, M. R., Guo, T., Hunter, C. D., and Cairo, C. W. (2018). Molecular dynamics simulations of viral neuraminidase inhibitors with the human neuraminidase enzymes: insights into isoenzyme selectivity. *Bioorgan. Med. Chem.* 26, 5349–5358. doi: 10.1016/j.bmc.2018.05.035

Rossi, B., Espeli, M., Schiff, C., and Gauthier, L. (2006). Clustering of pre-B cell integrins induces galectin-1-dependent pre-B cell receptor relocalization and activation. *J. Immunol.* 177, 796–803. doi: 10.4049/jimmunol.177.2.796

Rothlein, R., and Springer, T. A. (1986). The requirement for lymphocyte function-associated antigen 1 in homotypic leukocyte adhesion stimulated by phorbol ester. *J. Exp. Med.* 163, 1132–1149. doi: 10.1084/jem.163.5.1132

Sakarya, S., Rifat, S., Zhou, J., Bannerman, D. D., Stamatos, N. M., Cross, A. S., et al. (2004). Mobilization of neutrophil sialidase activity desialylates the pulmonary vascular endothelial surface and increases resting neutrophil adhesion to and migration across the endothelium. *Glycobiology* 14, 481–494. doi: 10.1093/glycob/cwh065

Salmi, M., and Jalkanen, S. (2005). Cell-surface enzymes in control of leukocyte trafficking. *Nat. Rev. Immunol.* 5, 760–771. doi: 10.1038/nri1705

Sandbhor, M. S., Soya, N., Albohy, A., Zheng, R. B., Cartmell, J., Bundle, D. R., et al. (2011). Substrate recognition of the membrane-associated sialidase NEU3 requires a hydrophobic aglycone. *Biochemistry* 50, 6753–6762. doi: 10.1021/bi200449j

Saxton, M. J., and Jacobson, K. (1997). Single-particle tracking: applications to membrane dynamics. *Annu. Rev. Biophys. Biomol. Struct.* 26, 373–399. doi: 10.1146/annurev.biophys.26.1.373

Scheiermann, C., Kunisaki, Y., Jang, J.-E., and Frenette, P. S. (2010). Neutrophil microdomains: linking heterocellular interactions with vascular injury. *Curr. Opin. Hematol.* 17:25. doi: 10.1097/MOH.0b013e328333d2a3

Schneider, C. A., Rasband, W. S., and Eliceiri, K. W. (2012). NIH image to ImageJ: 25 years of image analysis. *Nat. Methods* 9, 671–675. doi: 10.1038/nmeth.2089

Seyrantepe, V., Landry, K., Trudel, S., Hassan, J. A., Morales, C. R., and Pshezhetsky, A. V. (2004). Neu4, a novel human lysosomal lumen sialidase, confers normal phenotype to sialidosis and galactosialidosis cells. *J. Biol. Chem.* 279, 37021–37029. doi: 10.1074/jbc.M404531200

Sharma, D. K., Brown, J. C., Cheng, Z., Holicky, E. L., Marks, D. L., and Pagano, R. E. (2005). The glycosphingolipid, lactosylceramide, regulates β1-integrin clustering and endocytosis. *Cancer Res.* 65, 8233–8241. doi: 10.1158/0008-5472.CAN-05-0803

Simmons, D. L. (2005). Anti-adhesion therapies. *Curr. Opin. Pharmacol.* 5, 398–404. doi: 10.1016/j.coph.2005.02.009

Sonnino, S., Aureli, M., Loberto, N., Chigorno, V., and Prinetti, A. (2010). Fine tuning of cell functions through remodeling of glycosphingolipids by plasma membrane-associated glycohydrolases. *FEBS Lett.* 584, 1914–1922. doi: 10.1016/j.febslet.2009.11.020

Tauber, R., Park, C. S., and Reutter, W. (1983). Intramolecular heterogeneity of degradation in plasma membrane glycoproteins - evidence for a general characteristic. *Proc. Natl. Acad. Sci. U.S.A.* 80, 4026–4029. doi: 10.1073/pnas.80.13.4026

Tringali, C., Lupo, B., Silvestri, I., Papini, N., Anastasia, L., Tettamanti, G., et al. (2012). The plasma membrane sialidase NEU3 regulates the malignancy of renal carcinoma cells by controlling β1 integrin internalization and recycling. *J. Biol. Chem.* 287, 42835–428345. doi: 10.1074/jbc.M112.407718

van Kooyk, Y., and Figdor, C. G. (2000). Avidity regulation of integrins: the driving force in leukocyte adhesion. *Curr. Opin. Cell Biol.* 12, 542–547. doi: 10.1016/S0955-0674(00)00129-0

van Zanten, T. S., Cambi, A., Koopman, M., Joosten, B., Figdor, C. G., and Garcia-Parajo, M. F. (2009). Hotspots of GPI-anchored proteins and integrin nanoclusters function as nucleation sites for cell adhesion. *Proc. Natl. Acad. Sci. U.S.A.* 106, 18557–18562. doi: 10.1073/pnas.0905217106

Varki, A. (1994). Selectin ligands. *Proc. Natl. Acad. Sci. U.S.A.* 91, 7390–7397. doi: 10.1073/pnas.91.16.7390

Wands, A. M., Fujita, A., McCombs, J. E., Cervin, J., Dedic, B., Rodriguez, A. C., et al. (2015). Fucosylation and protein glycosylation create functional receptors for cholera toxin. *eLife* 4:e09545. doi: 10.7554/eLife.09545

Wang, P., Zhang, J., Bian, H., Wu, P., Kuvelkar, R., Kung, T. T., et al. (2004). Induction of lysosomal and plasma membrane-bound sialidases in human T-cells via T-cell receptor. *Biochem. J.* 380, 425–433. doi: 10.1042/bj20031896

Wang, X., Sun, P., Al-Qamari, A., Tai, T., Kawashima, I., and Paller, A. S. (2001). Carbohydrate-carbohydrate binding of ganglioside to integrin alpha(5) modulates alpha(5)beta(1) function. *J. Biol. Chem.* 276, 8436–8444. doi: 10.1074/jbc.M006097200

Wang, X. Q., Sun, P., and Paller, A. S. (2002). Ganglioside modulation regulates epithelial cell adhesion and spreading via ganglioside-specific effects on signaling. *J. Biol. Chem.* 277, 40410–40419. doi: 10.1074/jbc.M207117200

Wang, Y., Yamaguchi, K., Shimada, Y., Zhao, X. J., and Miyagi, T. (2001). Site-directed mutagenesis of human membrane-associated ganglioside sialidase - Identification of amino-acid residues contributing to substrate specificity. *Eur. J. Biochem.* 268, 2201–2208. doi: 10.1046/j.1432-1327.2001.02069.x

Wang, Y., Yamaguchi, K., Wada, T., Hata, K., Zhao, X. J., Fujimoto, T., et al. (2002). A close association of the ganglioside-specific sialidase Neu3 with caveolin in membrane microdomains. *J. Biol. Chem.* 277, 26252–26259. doi: 10.1074/jbc.M110515200

Yamaguchi, K., Hata, K., Wada, T., Moriya, S., and Miyagi, T. (2006). Epidermal growth factor-induced mobilization of a ganglioside-specific sialidase (NEU3) to membrane ruffles. *Biochem. Biophys. Res. Commun.* 346, 484–490. doi: 10.1016/j.bbrc.2006.05.136

Yamaji, T., Miyake, Y., Kozutsumi, Y., and Kawasaki, T. (1997). Neutral glycosphingolipids induce cell-cell aggregation of a variety of hematopoietic cell lines. *European J. Biochem.* 247, 21–29. doi: 10.1111/j.1432-1033.1997.t01-1-00021.x

Yang, E. H., Rode, J., Howlader, M. A., Eckermann, M., Santos, J. T., Hernandez Armada, D., et al. (2017). Galectin-3 alters the lateral mobility and clustering of β1-integrin receptors. *PLoS ONE* 12:e0184378. doi: 10.1371/journal.pone.0184378

Zanchetti, G., Colombi, P., Manzoni, M., Anastasia, L., Caimi, L., Borsani, G., et al. (2007). Sialidase NEU3 is a peripheral membrane protein localized on the cell surface and in endosomal structures. *Biochem. J.* 408, 211–219. doi: 10.1042/BJ20070503

Zhuo, Y., Chammas, R., and Bellis, S. L. (2008). Sialylation of β1 integrins blocks cell adhesion to galectin-3 and protects cells against galectin-3-induced apoptosis. *J. Biol. Chem.* 283, 22177–22185. doi: 10.1074/jbc.M800015200

Conflict of Interest: The authors declare that the research was conducted in the absence of any commercial or financial relationships that could be construed as a potential conflict of interest.

frontiers in Chemistry

ORIGINAL RESEARCH
published: 28 November 2019
doi: 10.3389/fchem.2019.00811

α-Lactosylceramide Protects Against iNKT-Mediated Murine Airway Hyperreactivity and Liver Injury Through Competitive Inhibition of Cd1d Binding

Alan Chuan-Ying Lai[1], Po-Yu Chi[1], Christina Li-Ping Thio[1], Yun-Chiann Han[1], Hsien-Neng Kao[1], Hsiao-Wu Hsieh[2], Jacquelyn Gervay-Hague[2] and Ya-Jen Chang[1]**

[1] Institute of Biomedical Sciences, Academia Sinica, Taipei, Taiwan, [2] Department of Chemistry, University of California, Davis, Davis, CA, United States

Invariant natural killer T (iNKT) cells, which are activated by T cell receptor (TCR)-dependent recognition of lipid-based antigens presented by the CD1d molecule, have been shown to participate in the pathogenesis of many diseases, including asthma and liver injury. Previous studies have shown the inhibition of iNKT cell activation using lipid antagonists can attenuate iNKT cell-induced disease pathogenesis. Hence, the development of iNKT cell-targeted glycolipids can facilitate the discovery of new therapeutics. In this study, we synthesized and evaluated α-lactosylceramide (α-LacCer), an α-galactosylceramide (α-GalCer) analog with lactose substitution for the galactose head and a shortened acyl chain in the ceramide tail, toward iNKT cell activation. We demonstrated that α-LacCer was a weak inducer for both mouse and human iNKT cell activation and cytokine production, and the iNKT induction by α-LacCer was CD1d-dependent. However, when co-administered with α-GalCer, α-LacCer inhibited α-GalCer-induced IL-4 and IFN-γ production from iNKT cells. Consequently, α-LacCer also ameliorated both α-GalCer and GSL-1-induced airway hyperreactivity and α-GalCer-induced neutrophilia when co-administered *in vivo*. Furthermore, we were able to inhibit the increases of ConA-induced AST, ALT and IFN-γ serum levels through α-LacCer pre-treatment, suggesting α-LacCer could protect against ConA-induced liver injury. Mechanistically, we discerned that α-LacCer suppressed α-GalCer-stimulated cytokine production through competing for CD1d binding. Since iNKT cells play a critical role in the development of AHR and liver injury, the inhibition of iNKT cell activation by α-LacCer present a possible new approach in treating iNKT cell-mediated diseases.

Keywords: NKT cell, glycolipid, CD1d, asthma, liver injury, ConA

OPEN ACCESS

Edited by:
Christoph Rademacher, Max Planck Institute of Colloids and Interfaces, Germany

Reviewed by:
Seung Bum Park, Seoul National University, South Korea
Chang-Chun Ling, University of Calgary, Canada

***Correspondence:**
Jacquelyn Gervay-Hague
jgervayhague@ucdavis.edu
Ya-Jen Chang
yajchang@ibms.sinica.edu.tw

Specialty section:
This article was submitted to Chemical Biology, a section of the journal Frontiers in Chemistry

Received: *12 June 2019*
Accepted: *11 November 2019*
Published: *28 November 2019*

Citation:
Lai AC-Y, Chi P-Y, Thio CL-P, Han Y-C, Kao H-N, Hsieh H-W, Gervay-Hague J and Chang Y-J (2019) α-Lactosylceramide Protects Against iNKT-Mediated Murine Airway Hyperreactivity and Liver Injury Through Competitive Inhibition of Cd1d Binding. Front. Chem. 7:811. doi: 10.3389/fchem.2019.00811

INTRODUCTION

Invariant natural killer T (iNKT) cells are a rare subset of T cells that possess properties of both conventional T and natural killer (NK) cells (Wu and Van Kaer, 2011; Cameron et al., 2015). Unlike conventional T cells, iNKT cells express a highly restricted T cell receptor (TCR)-α chain (Vα14/Jα18 in mice and Vα24/Jα18 in humans) and a moderately diverse TCR-β chain (Vβ2, Vβ7,

and Vβ8 in mice and Vβ11 in humans; Carreno et al., 2016). iNKT cells are activated through invariant TCR by the recognition of lipid-based antigens presented by the MHC class I-like CD1d molecule found on antigen presenting cells (Laurent et al., 2014; Cameron et al., 2015). Activated iNKT cells produce large quantities of cytokines including the Th2 cytokine IL-4 and the Th1 cytokine IFN-γ, which can enhance the function of other immune cells such as NK, B and T cells (Carnaud et al., 1999; Kitamura et al., 2000; Brigl et al., 2003). Therefore, iNKT cells play a key role in bridging the innate and adaptive immunity.

Due to their restricted TCR rearrangements, all iNKT cells share the ability to recognize glycolipids with their sugar head attached in an α-anomeric configuration to the polar head group of a lipid (Kjer-Nielsen et al., 2006). α-galactosylceramide (α-GalCer), also known as KRN7000, is the prototypical glycolipid of this type and has the capability to activate all iNKT cells with a mixed Th1 and Th2 response when presented by CD1d molecule (Kawano et al., 1997; Zhang et al., 2008). α-Glucuronosylceramide (GSL-1), a glycolipid extracted from *Sphingomonas* bacteria, represents another CD1d ligand with α-linked glucuronic acid and a mixture of at least three different sphingosine bases (Perola et al., 2002; Kinjo et al., 2005). Similar to α-GalCer, GSL-1 is also a potent stimulator of iNKT cells, primarily by engaging the TCR expressed by these cells (Perola et al., 2002; Kinjo et al., 2005; Long et al., 2007). Consequently, both α-GalCer and GSL-1 are commonly used to study the function of iNKT cells or iNKT cell-related diseases.

iNKT cells have been implicated in a number of immune-related diseases due to their multi-functional responses. Activated iNKT cells can enhance tumor immunity (Kawano et al., 1999; Aspeslagh et al., 2013) as well as suppress autoimmune disease (Singh et al., 2001). However, they are also associated with the disruption of mucosal homeostasis in the intestines and airways (Nau et al., 2014) and contribute to allergic airway inflammation in various allergen models, including ovalbumin (OVA) and house dust mite (HDM) extract, through Th2-biased cytokine responses (Akbari et al., 2003; Lisbonne et al., 2003; Wingender et al., 2011). Furthermore, both α-GalCer and GSL-1 have been shown to induce airway hyperreactivity (AHR) through iNKT cell activation as glycolipid-induced AHR was abolished in iNKT cell-deficient $CD1d^{-/-}$ (human CD1d analog) and $Jα18^{-/-}$ mice (Meyer et al., 2006). Additionally, iNKT cells also contribute to concavalin A (ConA)-induced hepatitis by inducing liver injury (Kaneko et al., 2000; Takeda et al., 2000). Given their pathogenic roles, the development of lipid antagonist that limit the activation of pathogenic iNKT cells may be of therapeutic relevance.

In this paper, we examined the effects of α-lactosylceramide (α-LacCer), an α-GalCer analog with a lactose head instead of galactose head and a shortened acyl chain in the ceramide tail, on iNKT cells. We found that α-LacCer weakly induced mouse and human iNKT cell activation in a CD1d-dependent manner. However, when co-treated with α-GalCer, α-LacCer suppressed the iNKT cell-activating properties of α-GalCer in terms of IL-4 and IFN-γ production. The therapeutic application of α-LacCer was evaluated *in vivo*, in which this glycolipid effectively attenuated α-GalCer- and GSL-1-induced AHR and Con-A-mediated liver injury. Lastly, our results in the plate-bound CD1d binding assay suggested the inhibitory function of α-LacCer was mediated by competitive CD1d binding.

MATERIALS AND METHODS

Mice

Eight- to ten-week-old C57BL/6 and BALB/c female mice were purchased from National Laboratory Animal Center (Taipei, Taiwan). $CD1d^{-/-}$ (human CD1d analog) mice (Stock No: 002962) were purchased from The Jackson Laboratory (Maine, USA). All animals were housed under specific pathogen-free conditions. This study (13-03-525) was carried out in accordance with the recommendations and guidelines of Academia Sinica Institutional Animal Care and Use Committee (IACUC), and all protocols were approved by the IACUC.

Reagents

α-GalCer (KRN7000) was purchased from Funakoshi (Tokyo, Japan). RPMI 1640, DMEM, newborn calf serum (NBCS), and red blood cell (RBC) lysis buffer were purchased from Gibco™ (Waltham, MA, USA). Fetal bovine serum (FBS) was purchased from Biological Industries (Beit-Haemek, Israel). Recombinant mouse IL-2 and GM-CSF were purchased from BioLegend (San Diego, CA, USA). Recombinant mouse IL-15, human IL-4, and GM-CSF were purchased from PeproTech (Rocky Hill, NJ, USA). Recombinant human IL-2 was purchased from eBioscience (San Diego, CA, USA).

In vitro Stimulation of Mouse $Vα14^+$T Hybridomas, Splenocytes, and iNKT Cells

$Vα14^+$T hybridomas (NK1.2), A20 and A20-CD1d cells, which were maintained in cRPMI medium, were kindly provided by Dr. Mitchell Kronenberg (La Jolla Institute, CA). For mouse $Vα14^+$T hybridoma stimulation, NK1.2 cells (10^5) were co-cultured with A20 or A20-CD1d cells (5×10^4) and stimulated with glycolipid. Splenic iNKT cells were expanded with α-GalCer, and CD1d tetramer$^+$ TCRβ$^+$ cells were sorted by FACSAria (BD Bioscience, San Jose, CA, USA) with a purity of >95%, and sorted iNKT cells were cultured with IL-2 and IL-15 and rested for 24 h before use. For mouse iNKT cell stimulation, sorted mouse iNKT cells (10^5) were co-cultured with irradiated GM-CSF-treated bone marrow-derived dendritic cells (3×10^4) and before stimulation with glycolipids. Mouse splenocytes (10^6) were isolated from fresh mouse spleen via mechanical dissociation before stimulation with glycolipids. Neutralization of CD1d was performed with 0.5 μg/well of anti-CD1d antibody (1B1, eBioscience).

In vitro Culture of Human PBMCs and iNKT Cells

Human peripheral blood mononuclear cells (PBMCs) from healthy volunteers were collected from whole blood through gradient-centrifugation with Histopaque-1077 (Sigma-Aldrich). Human iNKT cells were isolated from PBMCs as described previously (Kim et al., 2011). This study (AS-IRB-BM-15054 v.1) was carried out in accordance with the recommendations and

guidelines of Academia Sinica Institutional Review Board on Biomedical Science Research (IRB-BM) with written informed consent from all subjects. All subjects gave written informed consent in accordance with the Declaration of Helsinki. The protocol was approved by the IRB-BM. 0.5 μg/well of anti-CD1b antibody (SN13, BioLegend) and anti-CD1d antibody (51.1, BioLegend) were used for blocking CD1b and CD1d, respectively.

Measurement of Airway Hyperreactivity in Mice

BALB/c mice were intranasally (i.n.) administered with 1 μg of α-GalCer or 10 μg of GSL-1 in the presence or absence of 1 μg α-LacCer for 24 h. Mice were anesthetized with 100 mg/kg in body weight of pentobarbital (Sigma-Aldrich), tracheotomized and mechanically ventilated via the FinePointe RC system (Buxco Research Systems, Wilmington, NC, USA). AHR was assessed by measuring the lung resistance and dynamic compliance in response to increasing doses of aerosolized methacholine (1.25–40 mg/mL, Sigma-Aldrich).

Collection and Analysis of BALF From Mice

Upon exposure of trachea, the airway was lavaged twice with 1 ml of PBS supplemented with 2% FCS. BALF was pooled, and cells were pelleted by centrifugation and fixed onto slides. The slides were stained with Diff-Quik solution (Polysciences Inc.), and differential cell count was performed.

Murine Lung Cell Isolation

The whole lungs were flushed by PBS injection (supplemented with 2% FCS) through the right ventricle and minced prior to incubation in 3 ml DMEM medium with 0.1% (v/v) DNase I (Worthington Biochemicals) and 1.6 mg/mL collagenase IV (Worthington Biochemicals) for 40 min at 37°C. Tissues were filtered through a 100 μm mesh to obtain single cell suspensions. Red blood cells were removed by incubating in ACK lysing buffer (GIBCO) for 5 min at 25°C. Single cell suspensions were suspended in the appropriate buffer for further processing.

Flow Cytometry

Single cell suspensions were stained with fixable viability dye eFluor® 780 (eBioscience) for 30 min at 4°C, and Fc receptors were blocked with anti-CD16/32 (BioLegend) blocking antibody prior to surface staining with antibodies. Antibodies for surface staining used are listed, mouse: CD45 (30-F11, BioLegend), TCR β (H57-597, BioLegend), CD69 (H1.2F3, eBioscience), CD1d tetramer (NIH); human: CD45 (HI30, eBioscience), TCRα/β (IP26, BioLegend), CD69 (FN50, BioLegend), Vα24 (6B11, BD Bioscience). For intracellular staining, single cell suspensions were stimulated with 50 ng/mL phorbol 12-myristate 13-acetate (PMA) (Sigma-Aldrich), 1 μg/mL ionomycin (Sigma-Aldrich) and 1 μg/mL Golgi stop A (BD Biosciences) for 4 h. After surface staining, cells were fixed and permeabilized with Cytofix/Cytoperm solution (BD biosciences) and further stained intracellularly with human IFNγ (B27, BioLegend) and human IL-4 (MP4-25D2, BioLegend). For Ki67 staining, cells were fixed and permeabilized with Cytofix/Cytoperm solution (eBioscience), and further stained with Ki67 (SolA15, eBioscience). Data were acquired using LSR II (BD Biosciences) and analyzed using the FlowJo software (BD Biosciences).

Murine ConA-Induced Liver Injury Model

BALB/c or $CD1^{-/-}$ mice were injected intravenously (i.v.) with 25 mg/kg ConA (Sigma-Aldrich) for 24 h. In α-LacCer protection experiments, BALB/c mice were pre-treated with 5 μg/ml α-LacCer (i.p.) for 24 h prior to ConA treatment. Serum was collected at 0, 6, and 24 h for aspartate aminotransferase (AST) and alanine aminotransferase (ALT) detection, and livers were harvested at 24 h post-injection for H&E staining.

Plate-Bound CD1d Binding Assay

96-well strepavidin plates (Thermo scientific) were incubated with 0.5 μg of mouse CD1 or human CD1d monomer protein per well in PBS for 24 h in dark at room temperature. Plate was washed with PBS twice, and indicated glycolipids were loaded and incubated overnight under 37°C. After 24 h, the plate was washed twice, and 10^5 iNKT cells were added and cultured for 48 h. The supernatant was harvested, and the levels of IFN-γ and IL-4 were detected by ELISA.

ELISA

Cytokines (mouse IL-2, IL-4, and IFNγ; human IFNγ and IL-4) in culture supernatant, lung lysate, serum, or BALF of mice were analyzed with ELISA kits from Biolegend, with the exception of mouse IL-13 (eBioscience). For the determination of cytokine concentrations *in vivo*, lungs were flushed and minced thoroughly prior to sonication with Bioruptor® Plus sonicator (Diagenode) in RIPA buffer. Lung protein lysate was obtained via centrifugation. To determine cytokine concentrations in the serum, blood samples collected from mice were incubated at room temperature to allow coagulation and the collection of sera.

Statistics

Data were analyzed with the GraphPad Prism software (GraphPad Prism software, San Diego, CA, USA). Statistical analysis was determined using the Student's two-tailed *t*-test and the two-way analysis of variance (ANOVA).

RESULTS

α-LacCer Activates NK1.2 Hybridoma and Mouse iNKT Cells in a CD1d-Dependent Manner

The synthetic protocol of α-LacCer, a new α-GalCer analog with lactose substitution at the galactose head (Hsieh et al., 2014), is shown in **Supplementary Figure 1**, where a trimethylsilyl protected ceramide was reacted with an activated lactosyl iodide to give the alpha-lactoside in 61% purified yield. Deprotection of the acetate protecting groups quantitatively afforded the desired material for this study. The structures of α-GalCer and α-LacCer are shown in **Figure 1A**, respectively.

We first assessed their immune-stimulating activities in both $Vα14^+$T hybridoma cells (NK1.2) and primary mouse iNKT

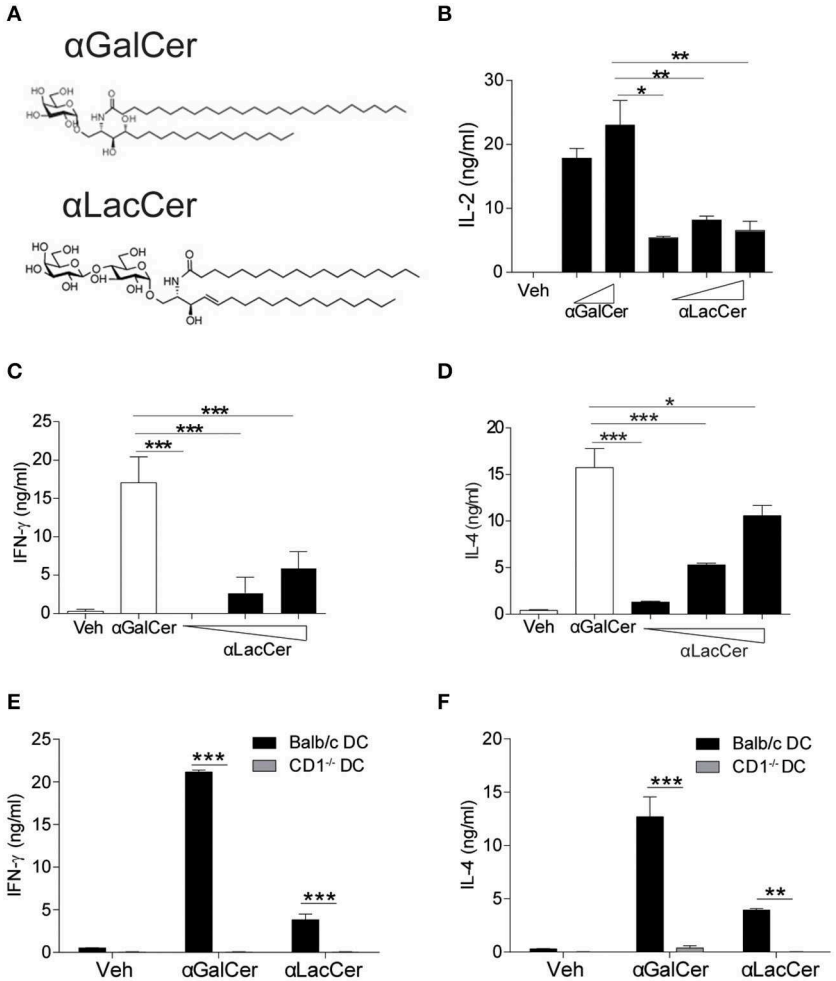

FIGURE 1 | α-LacCer activates NK1.2 hybridoma and mouse iNKT cells in a CD1d-dependent manner. **(A)** The structures of α-galactosyl ceramide (α-GalCer) and its analogs, α-lactosyl ceramide (α-LacCer). **(B)** Vα14^{+} T hybridoma cells (NK1.2) were co-cultured with A20-CD1d cells in the presence of α-GalCer (100, 1,000 ng/ml) or α-LacCer (10, 100, 1,000 ng/ml) for 48 h. The level of IL-2 in the supernatant was measured ($n = 3$–4). **(C,D)** Sorted mouse iNKT cells in co-culture with irradiated BMDCs were stimulated with α-GalCer (100 ng/ml) or α-LacCer (10, 100, 1,000 ng/ml) for 48 h, and the levels of IFN-γ **(C)** and IL-4 **(D)** in the supernatant were measured ($n = 3$). **(E,F)** Sorted mouse iNKT cells in co-culture with irradiated CD1d$^{-/-}$ or WT BMDCs were stimulated with α-GalCer (100 ng/ml) or α-LacCer (100 ng/ml) for 48 h. The levels of IFN-γ **(E)** and IL-4 **(F)** in the supernatant were measured ($n = 3$). Data are representative of three independent experiments and presented as means ± s.e.m. [$^{*}P < 0.05$, $^{**}P < 0.01$, and $^{***}P < 0.001$; Student's *t*-test **(B–F)**].

cells. In comparison to α-GalCer, α-LacCer induced a lower level of IL-2 production by NK1.2 cells (**Figure 1B**). Similarly, the levels of IFN-γ (**Figure 1C**) and IL-4 (**Figure 1D**) produced by α-LacCer-treated iNKT cells co-cultured with DCs were lower than cells treated with α-GalCer. Moreover, mouse iNKT cells failed to produce IFN-γ (**Figure 1E**) and IL-4 (**Figure 1F**) in response to both glycolipids when co-cultured with CD1d$^{-/-}$ DCs, suggesting both α-GalCer and α-LacCer induce mouse iNKT cell activation in a CD1d-dependent manner.

α-LacCer Suppresses α-GalCer-Induced Cytokine Production *in vitro* and *in vivo*

Since α-LacCer has been shown as a CD1d ligand weakly inducing iNKT cell activation, we theorized α-LacCer might be a good candidate to suppress iNKT cell activation by competing for CD1d-binding. To prove this hypothesis, we co-treated splenocytes with α-GalCer and α-LacCer. We observed that α-LacCer co-treatment reduced α-GalCer-induced IFN-γ (**Figure 2A**) and IL-4 (**Figure 2B**) production by mouse splenocytes. Additionally, α-LacCer inhibited α-GalCer-induced IL-2 production by NK1.2 hybridomas (**Figure 2C**), as well as IFN-γ (**Figure 2D**) and IL-4 (**Figure 2E**) production by mouse iNKT cells co-cultured with DCs. To further determine the inhibitory characteristic of α-LacCer, we performed a functional assay using NK1.2 hybridomas and measured the IC50 as 2.917 μg/ml against α-GalCer (**Figure 2F**).

To determine the inhibitory effect of α-LacCer *in vivo*, BALB/c mice were injected intraperitoneally with 1 μg α-GalCer in the presence or absence of 1 μg α-LacCer. We found that α-LacCer co-treatment reduced α-GalCer-induced lung iNKT

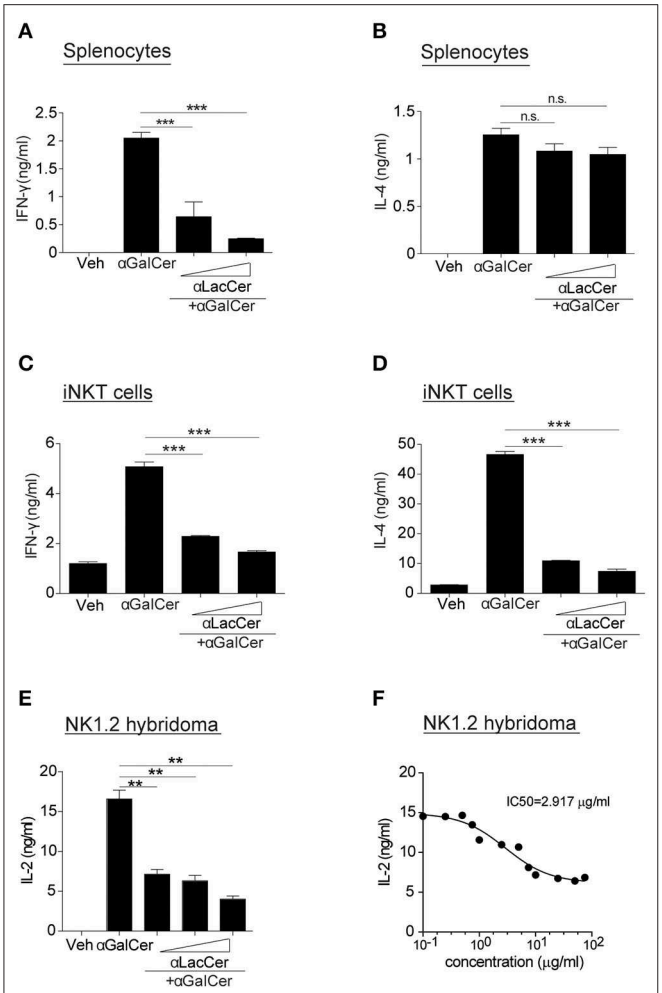

FIGURE 2 | α-LacCer suppresses α-GalCer-induced cytokine production *in vitro*. **(A,B)** Splenocytes from BALB/c mice were stimulated with 100 ng/ml α-GalCer in the presence or absence of α-LacCer (5 or 20 μg/ml) for 48 h. The levels of IFN-γ **(A)** and IL-4 **(B)** in the supernatant were measured ($n = 3$). **(C,D)** Sorted mouse iNKT cells were co-cultured with irradiated BMDCs and stimulated with α-GalCer (100 ng/ml) in the presence or absence of α-LacCer (5 or 20 μg/ml) for 48 h. The levels of IFN-γ **(C)** and IL-4 **(D)** in the supernatant were measured ($n = 3$). **(E)** NK1.2 cells in co-culture with A20-CD1d cells were stimulated with 100 ng/ml α-GalCer in the presence or absence of α-LacCer (100, 1,000, or 10,000 ng/ml) for 48 h. The level of IL-2 in supernatants was measured ($n = 3$). **(F)** NK1.2 cells in co-culture with A20-CD1d cells were stimulated with 100 ng/ml α-GalCer in the presence of incremental levels of α-LacCer (0.1–100 μg/ml) for 48 h. The level of IL-2 in supernatants was measured ($n = 4$), and GraphPad Prism was utilized for calculating the IC50. Data are representative of three independent experiments and presented as means ± s.e.m. [n.s., not significant; $^{**}P < 0.01$ and $^{***}P < 0.001$; Student's *t*-test **(A–F)**].

cell activation (**Figure 3A**) and proliferation (**Figure 3B**), as determined by the expressions of CD69 and Ki67, respectively. Furthermore, mice receiving α-GalCer and α-LacCer showed lower levels of lung IFN-γ and IL-4 comparing to α-GalCer-treated mice (**Figure 3C**). Taken together, these data indicate that α-LacCer suppress α-GalCer-induced iNKT activation, proliferation and cytokine production *in vitro* and *in vivo*.

α-LacCer Inhibits α-GalCer-Induced Lung iNKT Cell Activation and Airway Hyperreactivity (AHR)

Previous studies have shown that activation of lung iNKT cells by α-GalCer mediated the development of AHR and airway inflammation (Meyer et al., 2006; Wingender et al., 2011). Thus, we wondered whether α-LacCer could suppress α-GalCer-induced AHR. We treated mice intranasally with α-GalCer in the presence or absence of α-LacCer for 24 h. We found α-LacCer co-treatment attenuated α-GalCer-induced AHR (**Figure 4A**) and neutrophil infiltration in the bronchoalveolar lavage fluid (BALF) (**Figure 4B**). Accordingly, α-GalCer-induced IL-4 and IL-13 production were significantly inhibited by α-LacCer (**Figure 4C**). Similar suppression was observed in the GSL-1-induced AHR model (**Figure 4D**), further highlighting the therapeutic potential of α-LacCer for the treatment of asthma.

α-LacCer Protects Against ConA-Induced Liver Injury

iNKT cells have been shown to participate in ConA-induced liver damage (Mattner, 2013). Hence, we examined whether α-LacCer could protect against iNKT cell-mediated liver damage. In accordance to a previous study (Takeda et al., 2000), ConA induced liver damage in WT, but not iNKT cell-deficient $CD1d^{-/-}$ mice (**Figures 5A,B**). Likewise, serum levels of alanine aminotransferase (ALT) and aspartate aminotransferase (AST) were markedly lower in ConA-treated $CD1d^{-/-}$ mice compared to their WT counterpart (**Figure 5C**), implying that ConA-induced hepatitis was iNKT cell-dependent.

We next examined whether the pre-treatment with α-LacCer could protect against ConA-induced liver damage. α-LacCer was injected intraperitoneally 24 h before ConA injection, and the extent of liver damage was measured. We found that α-LacCer pre-treatment significantly reduced the percentage of liver damage area (**Figures 5D,E**). Similarly, ConA-induced AST, ALT (**Figure 5F**), and IFN-γ (**Figure 5G**) production in sera were suppressed by α-LacCer. These data demonstrated the protective effect of α-LacCer against ConA-induced liver injury.

α-LacCer Suppresses α-GalCer-Induced Activation and Cytokine Production by Human iNKT Cells

To examine the possible effects of α-LacCer in human, human iNKT cells were isolated and co-cultured with irradiated DCs with α-GalCer or α-LacCer in the presence or absence of anti-human CD1b or anti-human CD1d antibody. Human iNKT cells showed little to no induction of IFN-γ and IL-4 when treated with α-LacCer comparing to α-GalCer (**Figure 6A**). Additionally, the induction was CD1d-dependent as blocking CD1d, but not CD1b, impaired cytokine production induced by α-GalCer. α-LacCer also failed to induce iNKT cell proliferation ($Ki67^+$ cells) and activation ($CD69^+$ cells) in terms of percentage (**Figure 6B**) and frequency (**Figure 6C**). Furthermore, α-LacCer co-treatment

significantly suppressed α-GalCer-induced IFN-γ secretion from human PBMC (**Figure 6D**) and human iNKT cells (**Figure 6E**). Overall, these data indicated that α-LacCer effectively inhibited both human and mouse iNKT cell activation and cytokine production.

α-LacCer Suppresses α-GalCer-Stimulated Cytokine Production by iNKT Cells by Competing for CD1d Binding

Since α-LacCer could be docked into both mouse CD1-iNKT TCR and human CD1d-iNKT TCR complexes (Data not shown), we hypothesized that the suppressive effect exhibited by α-LacCer toward α-GalCer might be due to the competitive binding to CD1d. We examined this hypothesis by performing the cell-free plate-bound CD1d assay. We pre-loaded mouse CD1d and human CD1d-coated plates with α-GalCer or α-LacCer, followed by a second loading with α-LacCer or α-GalCer, respectively. Pre-loading with α-LacCer reduced α-GalCer-induced IFN-γ (**Figure 7A**) and IL-4 (**Figure 7B**) production in mouse iNKT cells. Similar results were obtained with human iNKT cells (**Figures 7C,D**). In short, our results suggested that α-LacCer suppressed α-GalCer-stimulated cytokine production by mouse and human iNKT cells by competing for CD1d binding.

DISUCSSION

In this study, we demonstrated that α-LacCer is a weak activator of mouse and human iNKT cells comparing to α-GalCer. Yet, when co-administered with α-GalCer *in vitro*, α-LacCer suppressed α-GalCer-induced mouse and human iNKT cell activation and cytokine production. Through a NK1.2 hybridoma-based functional assay, we measured the IC50 of α-LacCer as 2.917 μg/ml against α-GalCer. When co-administered with α-GalCer or GSL-1 *in vivo*, α-LacCer suppressed AHR development by both glycolipids, as well as α-GalCer-induced neutrophilic inflammation by inhibiting lung iNKT cell activation and cytokine production. Furthermore, α-LacCer protected against ConA-induced liver injury in a CD1d-dependent manner. Lastly, pre-loaded α-LacCer inhibited α-GalCer-stimulated IL-4 and IFN-γ production by iNKT cells in the plate-bound CD1d binding assay, suggesting the inhibitory effect of α-LacCer is due to its competition for CD1d binding. Results from this study highlighted the potential therapeutic utility of α-LacCer for the treatment of iNKT cell-associated diseases.

iNKT cells are associated with various allergic and non-allergic diseases. For instance, iNKT cells contribute to the induction of pathology in mucosal tissues of the airways and the gastrointestinal tract and drive allergic inflammatory reactions through the production of Th2 cytokines, as well as the recruitment and degranulation of mast cells and eosinophils (Nau et al., 2014). iNKT cells also contribute to lupus development by augmenting Th1-biased immune responses and autoantibody secretion (Zeng et al., 2003). Additionally, collagen-induced arthritis (CIA) is associated with iNKT cells because CIA can be ameliorated by blocking the interaction between CD1d and iNKT cells using anti-CD1d neutralizing antibody (Chiba et al., 2005). Furthermore, α-GalCer treatment in mice often leads to detrimental side

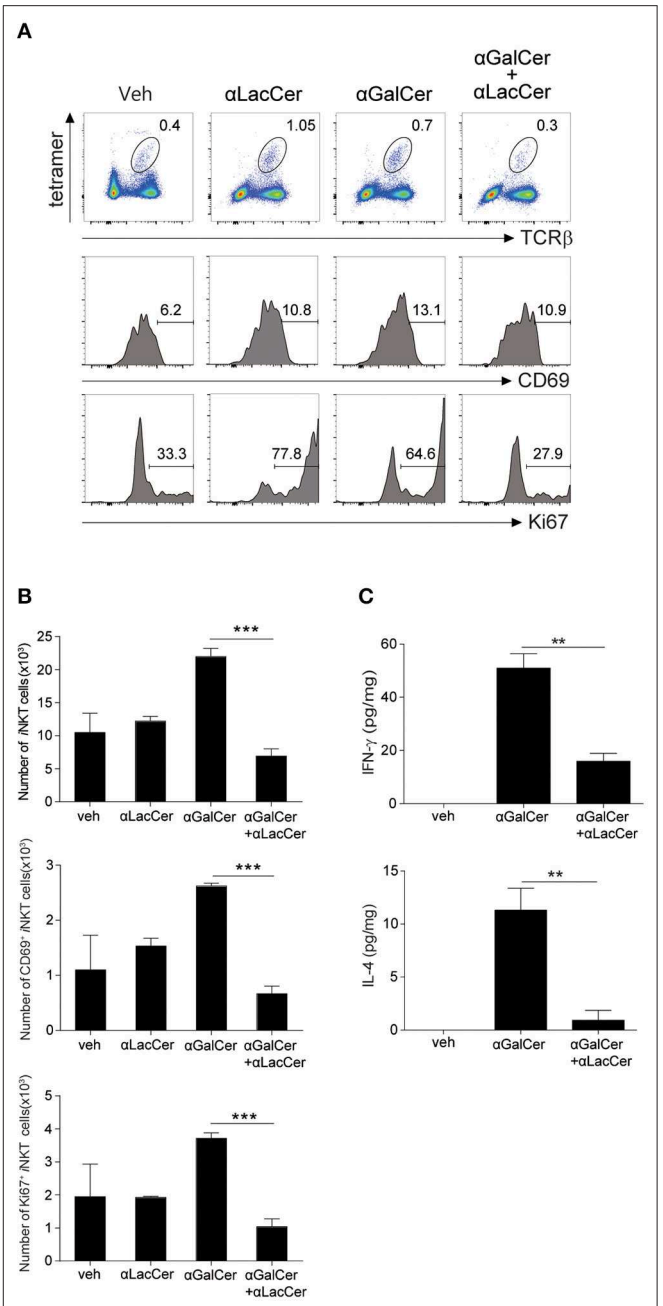

FIGURE 3 | α-GalCer-induced iNKT cell activation and proliferation are suppressed by α-LacCer *in vivo*. BALB/c mice were injected intraperitoneally with 1 μg of α-GalCer and α-LacCer, and the lungs were harvested 3 days post-injection. **(A)** Flow cytometry analysis of CD69 and Ki67 expressions in iNKT cells ($CD45^+TCR\beta^+CD1d$ tetramer$^+$ cells). **(B)** Absolute numbers of total, $CD69^+$, and $Ki67^+$ iNKT cells calculated from the flow cytometry data ($n = 3$). **(C)** IFN-γ and IL-4 levels in the lung lysates were measured by ELISA ($n = 3$). Data are representative of three independent experiments and presented as means ± s.e.m. [$^{**}P < 0.01$ and $^{***}P < 0.001$, Student's *t*-test **(B,C)**].

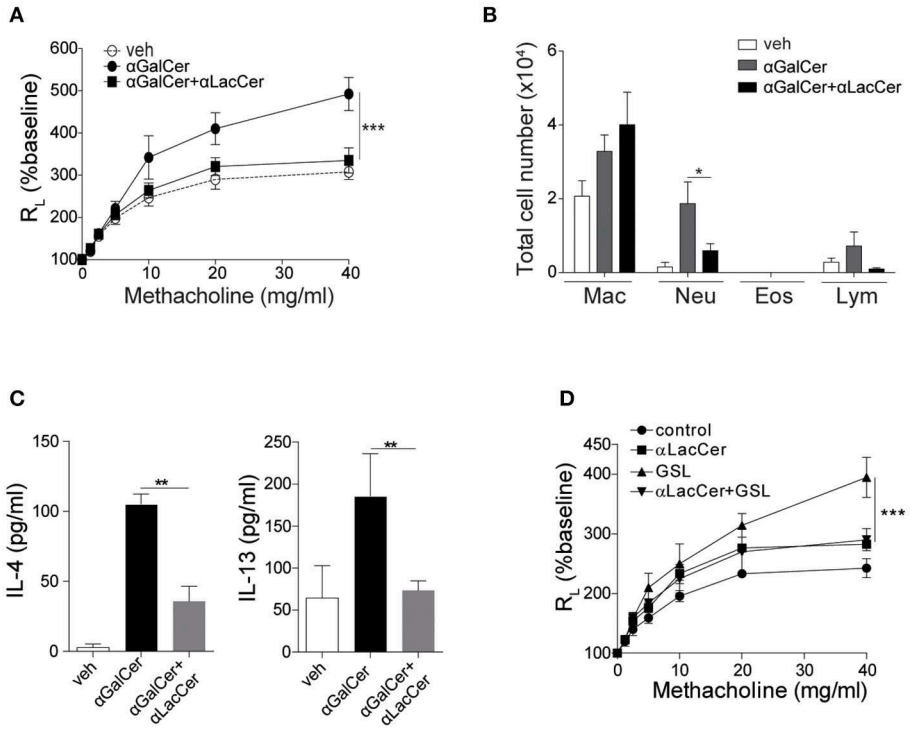

FIGURE 4 | α-LacCer suppresses α-GalCer and GSL-1-induced airway hyperreactivity. BALB/c mice were treated intranasally with 1 μg α-GalCer **(A–C)** or 10 μg GSL-1 **(D)** in the presence or absence of 1 μg α-LacCer for 24 h. **(A,D)** Changes in lung resistance (R_L) in response to increasing doses of methacholine [n = 6–8/group in **(A)**; n = 3–5/group in **(D)**]. **(B)** The numbers of macrophage (Mac), neutrophil (Neu), eosinophil (Eos), and lymphocyte (Lym) in the BALF (n = 7–8). **(C)** The levels of IL-4 and IL-13 in the lungs assessed using ELISA (n = 4). Data are representative of three independent experiments and presented as means ± s.e.m. [$^*P < 0.05$, $^{**}P < 0.01$, and $^{***}P < 0.001$; Two-way ANOVA **(A,D)** and Student's t-test **(B,C)**].

effects, resulting in disease exacerbation rather than protection (Wu and Van Kaer, 2009). Hence, the pathogenic roles of activated iNKT cells in various diseases justify the need to develop new and improved therapeutic approaches targeting these cells.

Several lipids have been shown to suppress iNKT cell activation, but none have been developed pharmacologically. For instance, An et al. revealed that GSL-Bf717, a bacterial glycol sphingolipids extracted from *Bacteroides fragilis*, did not activate iNKT but could inhibit iNKT hybridoma activation when treated together with α-GalCer (An et al., 2014). In another study, 1,2-dipalmitoyl-sn-glycero-3-phosphoethanolamine-N[methoxy(polyethyleneglycol)-350 (DPPE-PEG_{350}) was developed and reported to be effective in inhibiting iNKT cell activation and attenuating the development of allergen-induced AHR (Lombardi et al., 2010) and atherosclerosis (Li et al., 2016). Furthermore, a non-lipid based antagonist, *Griffonia simplicifolia*-derived isolectin B4 (IB4), has been shown to inhibit the sphingolipid isoglobotrihexosylceramide (iGb3)-induced iNKT cell stimulation by binding to the terminal Gal α1,3 Gal of iGb3, thus preventing its recognition by mouse Vα14 and human Vα24 iNKT cells (Keusch et al., 2000; Zhou et al., 2004). Hence, our findings add to the growing list of iNKT cell antagonists that can be exploited for therapeutic purposes. Mechanistically, the inhibitory function of α-LacCer on α-GalCer activity seems to involve the competitive binding of CD1d. However, this does not mean α-LacCer prevents the activation of iNKT through the inhibition of CD1d function. Rather, α-LacCer could still induce iNKT activation through CD1d while it is occupying the binding site, but at a much weaker level comparing to α-GalCer. This speculation is supported by the *in vitro* data showing that α-LacCer could activate iNKT in a CD1d-dependent manner, but with a much lower intensity in comparison to α-GalCer. However, the exact mechanism may require further investigation to reveal.

A similar glycolipid with lactose head, also called α-LacCer, was previously synthesized and found to activate both human and mouse iNKT cells as effectively as α-GalCer in terms of inducing IL-4, but not IFN-γ production (Zhang et al., 2008). This Th2-biased glycolipid exhibited both antitumor and anti-autoimmune disease effects, with greater potency than α-GalCer in ameliorating the latter disease. Contrary to this, the α-LacCer synthesized for our study is a weak iNKT cell activator when compared with the prototypical α-GalCer, as evidenced by the lower IFN-γ and IL-4 production, as well as the lack of iNKT cell expansion and activation when administered *in vivo*. The difference in potency is likely due to the different

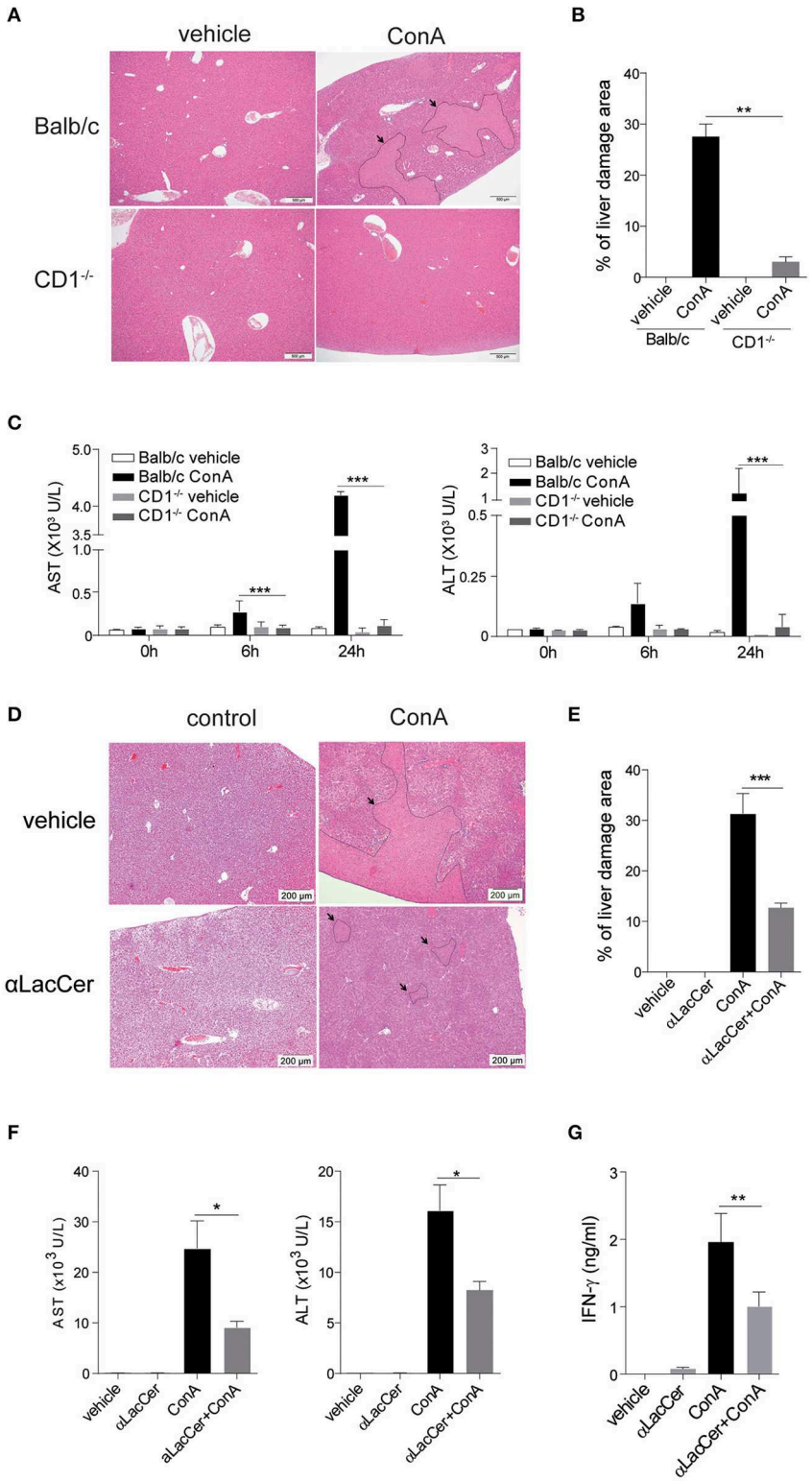

FIGURE 5 | α-LacCer protects against ConA-induced liver injury. **(A–C)** ConA was injected intravenously (25 mg/kg) into BALB/c ($n = 3$) or CD1d$^{-/-}$ mice ($n = 3$). Sera were collected at 0, 6, and 24 h post-injection, and mice were sacrificed at 24 h post-injection. **(A)** H&E stained liver sections (Scale bar = 500 μm). **(B)** Percentage of liver damage area. **(C)** Serum levels of ALT and AST. **(D–G)** BALB/c mice were first pre-treated intraperitoneally with α-LacCer (5 μg/ml) for 24 h and followed by ConA (25 mg/kg; i.v.) administration. Sera and livers were harvested 24 h post-ConA treatment. **(D)** H&E stained liver sections (Scale bar = 200 μm). **(E)** Percentage of liver damage area ($n = 3$). **(F)** Serum levels of AST and ALT ($n = 4$). **(G)** The serum IFN-γ level measured by ELISA ($n = 4$). Data are representative of three independent experiments and are presented as means ± s.e.m. [$^*P < 0.05$, $^{**}P < 0.01$, and $^{***}P < 0.001$; Student's t-test **(B,C,E–G)**].

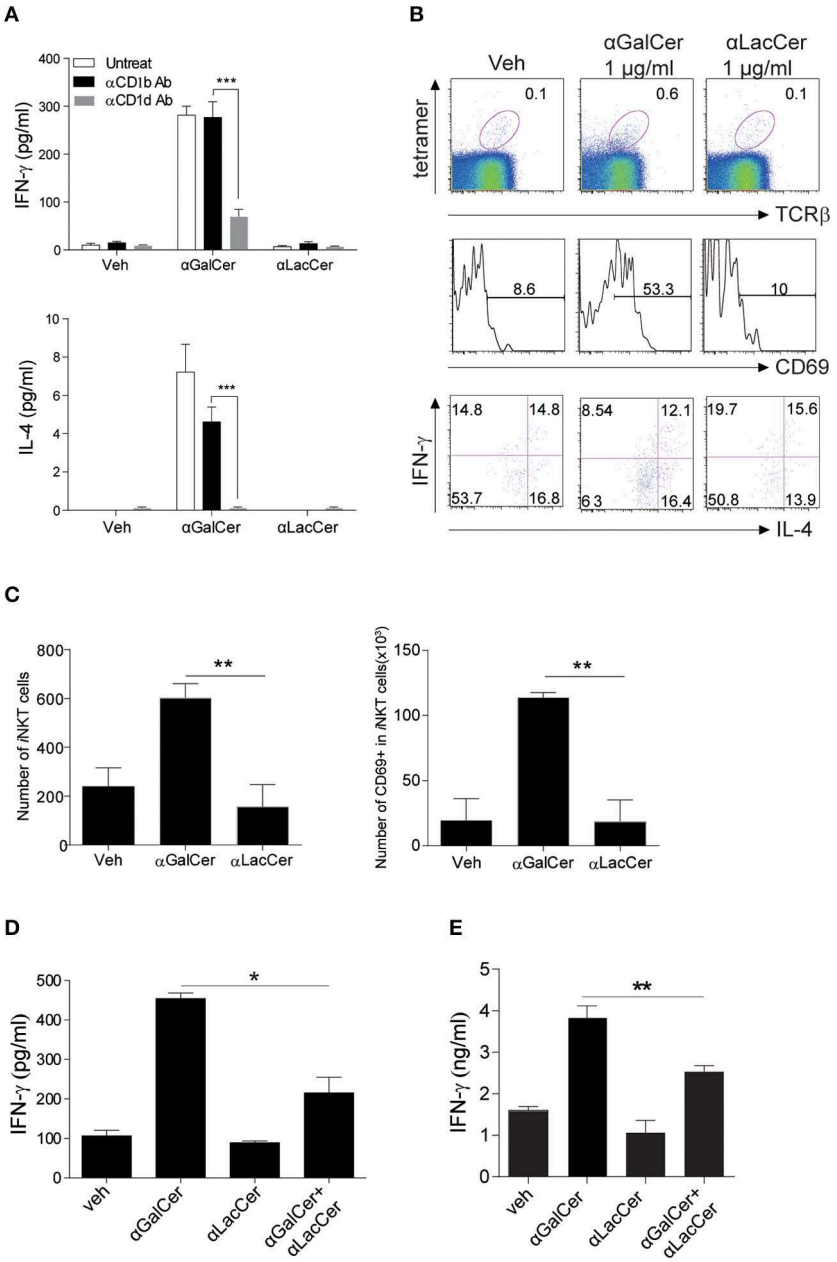

FIGURE 6 | α-LacCer suppresses α-GalCer-induced cytokine production by human iNKT cells *in vitro*. **(A)** Sorted human iNKT cells were stimulated with α-GalCer and α-LacCer (1 μg/ml) in the absence or presence of anti-CD1b or anti-CD1d antibody for 72 h. The levels of IFN-γ and IL-4 in the supernatant were analyzed (n = 3–6). **(B,C)** Human PBMCs were cultured with 1 μg/ml α-GalCer and α-LacCer for 7 days. **(B)** FACS analysis of CD69, IFN-γ, and IL-4 expressions in human iNKT cells ($CD45^+$tetra-$CD1d^+TCR\beta^+$). **(C)** Absolute numbers of total and $CD69^+$ iNKT cells. **(D)** Human PBMCs were stimulated with α-GalCer (100 ng/ml) in the presence or absence of α-LacCer (1 μg/ml) for 3 days. The level of IFN-γ was analyzed (n = 3). **(E)** Human iNKT cells were cultured with irradiated DCs pre-treated with 100 ng/ml α-GalCer in the absence or presence of 1 μg/ml α-LacCer for 3 days. The levels of IFN-γ and IL-4 were analyzed (n = 3–5). Data are representative of three independent experiments and presented as means ± s.e.m. [*n.s.*, not significant; $^*P < 0.05$, $^{**}P < 0.01$, and $^{***}P < 0.001$; Student's t-test **(A,C–E)**].

acyl chain length. The reported α-LacCer retains the 26-carbon long acyl chain found in the prototypical α-GalCer, whereas the α-LacCer synthesized in our study is 8 carbons shorter (C18). Truncation of the acyl chain has previously been shown to reduce the binding stability of glycolipids to CD1d without affecting TCR affinity (McCarthy et al., 2007). While this may explain the weaker activating property of our α-LacCer, it does not justify the observation that α-LacCer can effectively suppress α-GalCer-induced iNKT cell activation and the downstream effects through competitive

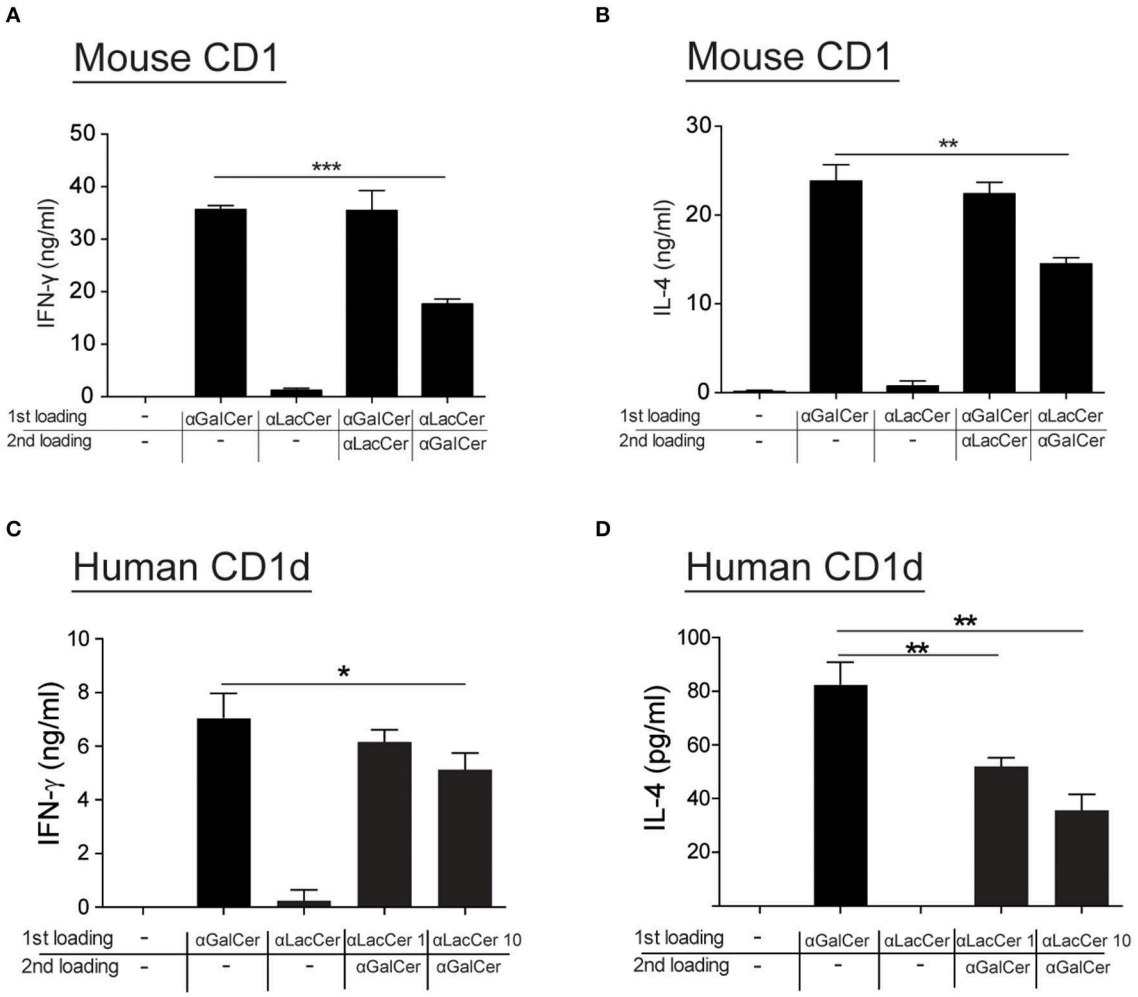

FIGURE 7 | α-LacCer suppresses α-GalCer-stimulated cytokine production by competing for CD1d binding. **(A,B)** Sorted mouse iNKT cells were cultured in the CD1-coated plate pre-loaded with 100 ng/ml α-GalCer or 1 μg/ml α-LacCer with or without the second loading of α-GalCer or α-LacCer for 48 h. The levels of IFN-γ **(A)** and IL-4 **(B)** in the culture supernatant were assessed ($n = 3$). **(C,D)** Sorted human iNKT cells were cultured in the CD1d-coated plate pre-loaded with α-LacCer (1 or 10 μg/ml) with the second loading of α-GalCer (100 ng/ml) for 48 h. The levels of IFN-γ **(C)** and IL-4 **(D)** in the supernatant were assessed ($n = 3$–6). Data are representative of three independent experiments and are presented as means ± s.e.m. [$^{*}P < 0.05$, $^{**}P < 0.01$, and $^{***}P < 0.001$; Student's *t*-test **(A–D)**].

CD1d binding. Hence, the difference in the activation potency between the reported α-LacCer and ours may be caused by other factors, and additional studies will be required to unravel the mechanisms involved.

We observed that α-LacCer effectively suppressed ConA-induced liver injury. Although it has been suggested that ConA-induced liver injury is CD1d-independent (Zeissig et al., 2017), a recent study reported that CD1d-mediated activation of iNKT cells is required for further activation of these cells in response to ConA (Wei et al., 2016). In their study, the authors demonstrated the importance of gut bacteria-derived glycolipids in driving hepatic iNKT cell activation. When comparing to specific pathogen-free mice, germ-free mice had lower levels of gut bacteria-derived glycolipids and were resistant to ConA-induced liver injury. Based on this finding, we postulate that α-LacCer may reduce ConA-induced liver damage by preventing the initial iNKT cell activation.

In summary, the data indicate that even though α-LacCer failed to potently activate iNKT cells, it did effectively suppress the iNKT cell-activating properties of α-GalCer both *in vitro* and *in vivo*. Moreover, α-LacCer attenuated α-GalCer, and GSL-1-induced AHR and ConA-triggered liver injury. As determined by the plate-bound CD1d binding assay, the pre-loading of α-LacCer prior to α-GalCer treatment attenuated the stimulatory properties of α-GalCer, suggesting that α-LacCer competed with α-GalCer for CD1d binding. In conclusion, this study characterized the biological function of α-LacCer highlighting the use of this glycolipid for the clinical treatment of iNKT cell-associated diseases.

DATA AVAILABILITY STATEMENT

The datasets generated for this study are available on request to the corresponding author.

ETHICS STATEMENT

The animal study was reviewed and approved by Institutional Animal Care and Use Committee of Academia Sinica (AS IACUC), which is affiliated to Academia Sinica.

AUTHOR CONTRIBUTIONS

AL planned and performed experiments and wrote the manuscript. P-YC performed the AHR experiments and assisted with experiments. CT assisted with experiments and helped writing the manuscript. Y-CH and H-NK performed the *in vitro* experiments. H-WH and JG-H synthesized and supplied glycolipids. Y-JC conceived and initiated the project, planned experiments, and wrote the manuscript.

FUNDING

This work was supported in part by the Ministry of Science and Technology (105-2628-B-001-009-MY3 to Y-JC) and by the Academia Sinica Career Development Award (104-CDA-L05 to Y-JC) in Taiwan. JG-H acknowledges support from the United States National Institutes of Health (R01GM090262).

ACKNOWLEDGMENTS

We thank the NIH NIAID Tetramer Facility for providing GSL-1 and CD1d tetramers, and we also thank the staff of IBMS Flow Cytometry Core Facility for the services and facilities provided.

SUPPLEMENTARY MATERIAL

The Supplementary Material for this article can be found online at: https://www.frontiersin.org/articles/10.3389/fchem.2019.00811/full#supplementary-material

REFERENCES

Akbari, O., Stock, P., Meyer, E., Kronenberg, M., Sidobre, S., Nakayama, T., et al. (2003). Essential role of NKT cells producing IL-4 and IL-13 in the development of allergen-induced airway hyperreactivity. *Nat. Med.* 9, 582–588. doi: 10.1038/nm851

An, D., Oh, S. F., Olszak, T., Neves, J. F., Avci, F. Y., Erturk-Hasdemir, D., et al. (2014). Sphingolipids from a symbiotic microbe regulate homeostasis of host intestinal natural killer T cells. *Cell* 156, 123–133. doi: 10.1016/j.cell.2013.11.042

Aspeslagh, S., Nemcovic, M., Pauwels, N., Venken, K., Wang, J., Van Calenbergh, S., et al. (2013). Enhanced TCR footprint by a novel glycolipid increases NKT-dependent tumor protection. *J. Immunol.* 191, 2916–2925. doi: 10.4049/jimmunol.1203134

Brigl, M., Bry, L., Kent, S. C., Gumperz, J. E., and Brenner, M. B. (2003). Mechanism of CD1d-restricted natural killer T cell activation during microbial infection. *Nat. Immunol.* 4, 1230–1237. doi: 10.1038/ni1002

Cameron, G., Pellicci, D. G., Uldrich, A. P., Besra, G. S., Illarionov, P., Williams, S. J., et al. (2015). Antigen specificity of type I NKT cells is governed by tcr beta-chain diversity. *J. Immunol.* 195, 4604–4614. doi: 10.4049/jimmunol.1501222

Carnaud, C., Lee, D., Donnars, O., Park, S. H., Beavis, A., Koezuka, Y., et al. (1999). Cutting edge: cross-talk between cells of the innate immune system: NKT cells rapidly activate NK cells. *J. Immunol.* 163, 4647–4650.

Carreno, L. J., Saavedra-Avila, N. A., and Porcelli, S. A. (2016). Synthetic glycolipid activators of natural killer T cells as immunotherapeutic agents. *Clin. Transl. Immunol.* 5:e69. doi: 10.1038/cti.2016.14

Chiba, A., Kaieda, S., Oki, S., Yamamura, T., and Miyake, S. (2005). The involvement of V(alpha)14 natural killer T cells in the pathogenesis of arthritis in murine models. *Arthritis Rheum.* 52, 1941–1948. doi: 10.1002/art.21056

Hsieh, H. W., Schombs, M. W., and Gervay-Hague, J. (2014). Integrating ReSET with glycosyl iodide glycosylation in step-economy syntheses of tumor-associated carbohydrate antigens and immunogenic glycolipids. *J. Org. Chem.* 79, 1736–1748. doi: 10.1021/jo402736g

Kaneko, Y., Harada, M., Kawano, T., Yamashita, M., Shibata, Y., Gejyo, F., et al. (2000). Augmentation of valpha14 NKT cell-mediated cytotoxicity by interleukin 4 in an autocrine mechanism resulting in the development of concanavalin a-induced hepatitis. *J. Exp. Med.* 191, 105–114. doi: 10.1084/jem.191.1.105

Kawano, T., Cui, J., Koezuka, Y., Toura, I., Kaneko, Y., Motoki, K., et al. (1997). CD1d-restricted and TCR-mediated activation of valpha14 NKT cells by glycosylceramides. *Science* 278, 1626–1629. doi: 10.1126/science.278.5343.1626

Kawano, T., Nakayama, T., Kamada, N., Kaneko, Y., Harada, M., Ogura, N., et al. (1999). Antitumor cytotoxicity mediated by ligand-activated human V alpha24 NKT cells. *Cancer Res.* 59, 5102–5105.

Keusch, J. J., Manzella, S. M., Nyame, K. A., Cummings, R. D., and Baenziger, J. U. (2000). Expression cloning of a new member of the ABO blood group glycosyltransferases, iGb3 synthase, that directs the synthesis of isoglobo-glycosphingolipids. *J. Biol. Chem.* 275, 25308–25314. doi: 10.1074/jbc.M002629200

Kim, H. Y., Eyheramonho, M. B., Pichavant, M., Gonzalez Cambaceres, C., Matangkasombut, P., Cervio, G., et al. (2011). A polymorphism in TIM1 is associated with susceptibility to severe hepatitis a virus infection in humans. *J. Clin. Invest.* 121, 1111–1118. doi: 10.1172/JCI44182

Kinjo, Y., Wu, D., Kim, G., Xing, G. W., Poles, M. A., Ho, D. D., et al. (2005). Recognition of bacterial glycosphingolipids by natural killer T cells. *Nature* 434, 520–525. doi: 10.1038/nature03407

Kitamura, H., Ohta, A., Sekimoto, M., Sato, M., Iwakabe, K., Nakui, M., et al. (2000). alpha-galactosylceramide induces early B-cell activation through IL-4 production by NKT cells. *Cell. Immunol.* 199, 37–42. doi: 10.1006/cimm.1999.1602

Kjer-Nielsen, L., Borg, N. A., Pellicci, D. G., Beddoe, T., Kostenko, L., Clements, C. S., et al. (2006). A structural basis for selection and cross-species reactivity of the semi-invariant NKT cell receptor in CD1d/glycolipid recognition. *J. Exp. Med.* 203, 661–673. doi: 10.1084/jem.20051777

Laurent, X., Bertin, B., Renault, N., Farce, A., Speca, S., Milhomme, O., et al. (2014). Switching invariant natural killer T (iNKT) cell response from anticancerous to anti-inflammatory effect: molecular bases. *J. Med. Chem.* 57, 5489–5508. doi: 10.1021/jm4010863

Li, Y., Kanellakis, P., Hosseini, H., Cao, A., Deswaerte, V., Tipping, P., et al. (2016). A CD1d-dependent lipid antagonist to NKT cells ameliorates atherosclerosis in ApoE$^{-/-}$ mice by reducing lesion necrosis and inflammation. *Cardiovasc. Res.* 109, 305–317. doi: 10.1093/cvr/cvv259

Lisbonne, M., Diem, S., De Castro Keller, A., Lefort, J., Araujo, L. M., Hachem, P., et al. (2003). Cutting edge: invariant V alpha 14 NKT cells are required for allergen-induced airway inflammation and hyperreactivity in an experimental asthma model. *J. Immunol.* 171, 1637–1641. doi: 10.4049/jimmunol.171.4.1637

Lombardi, V., Stock, P., Singh, A. K., Kerzerho, J., Yang, W., Sullivan, B. A., et al. (2010). A CD1d-dependent antagonist inhibits the activation of invariant NKT cells and prevents development of allergen-induced airway hyperreactivity. *J. Immunol.* 184, 2107–2115. doi: 10.4049/jimmunol.0901208

Long, X., Deng, S., Mattner, J., Zang, Z., Zhou, D., Mcnary, N., et al. (2007). Synthesis and evaluation of stimulatory properties of sphingomonadaceae glycolipids. *Nat. Chem. Biol.* 3, 559–564. doi: 10.1038/nchembio.2007.19

Mattner, J. (2013). Natural killer T (NKT) cells in autoimmune hepatitis. *Curr. Opin. Immunol.* 25, 697–703. doi: 10.1016/j.coi.2013.09.008

McCarthy, C., Shepherd, D., Fleire, S., Stronge, V. S., Koch, M., Illarionov, P. A., et al. (2007). The length of lipids bound to human CD1d molecules modulates the affinity of NKT cell TCR and the threshold of NKT cell activation. *J. Exp. Med.* 204, 1131–1144. doi: 10.1084/jem.20062342

Meyer, E. H., Goya, S., Akbari, O., Berry, G. J., Savage, P. B., Kronenberg, M., et al. (2006). Glycolipid activation of invariant T cell receptor+ NK T cells is sufficient to induce airway hyperreactivity independent of conventional CD4+ T cells. *Proc. Natl. Acad. Sci. U.S.A.* 103, 2782–2787. doi: 10.1073/pnas.0510282103

Nau, D., Altmayer, N., and Mattner, J. (2014). Mechanisms of innate lymphoid cell and natural killer T cell activation during mucosal inflammation. *J. Immunol. Res.* 2014:546596. doi: 10.1155/2014/546596

Perola, O., Nousiainen, T., Suomalainen, S., Aukee, S., Karkkainen, U. M., Kauppinen, J., et al. (2002). Recurrent *Sphingomonas paucimobilis* - bacteraemia associated with a multi-bacterial water-borne epidemic among neutropenic patients. *J. Hosp. Infect.* 50, 196–201. doi: 10.1053/jhin.2001.1163

Singh, A. K., Wilson, M. T., Hong, S., Olivares-Villagomez, D., Du, C., Stanic, A. K., et al. (2001). Natural killer T cell activation protects mice against experimental autoimmune encephalomyelitis. *J. Exp. Med.* 194, 1801–1811. doi: 10.1084/jem.194.12.1801

Takeda, K., Hayakawa, Y., Van Kaer, L., Matsuda, H., Yagita, H., and Okumura, K. (2000). Critical contribution of liver natural killer T cells to a murine model of hepatitis. *Proc. Natl. Acad. Sci. U.S.A.* 97, 5498–5503. doi: 10.1073/pnas.040566697

Wei, Y., Zengs B., Chen, J., Cui, G., Lu, C., Wu, W., et al. (2016). Enterogenous bacterial glycolipids are required for the generation of natural killer T cells mediated liver injury. *Sci. Rep.* 6:36365. doi: 10.1038/srep36365

Wingender, G., Rogers, P., Batzer, G., Lee, M. S., Bai, D., Pei, B., et al. (2011). Invariant NKT cells are required for airway inflammation induced by environmental antigens. *J. Exp. Med.* 208, 1151–1162. doi: 10.1084/jem.20102229

Wu, L., and Van Kaer, L. (2009). Natural killer T cells and autoimmune disease. *Curr. Mol. Med.* 9, 4–14. doi: 10.2174/156652409787314534

Wu, L., and Van Kaer, L. (2011). Natural killer T cells in health and disease. *Front. Biosci.* 3, 236–251. doi: 10.2741/s148

Zeissig, S., Peuker, K., Iyer, S., Gensollen, T., Dougan, S. K., Olszak, T., et al. (2017). CD1d-Restricted pathways in hepatocytes control local natural killer T cell homeostasis and hepatic inflammation. *Proc. Natl. Acad. Sci. U.S.A.* 114, 10449–10454. doi: 10.1073/pnas.1701428114

Zeng, D., Liu, Y., Sidobre, S., Kronenberg, M., and Strober, S. (2003). Activation of natural killer T cells in NZB/W mice induces Th1-type immune responses exacerbating lupus. *J. Clin. Invest.* 112, 1211–1222. doi: 10.1172/JCI200317165

Zhang, W., Zheng, X., Xia, C., Perali, R. S., Yao, Q., Liu, Y., et al. (2008). Alpha-lactosylceramide as a novel "sugar-capped" CD1d ligand for natural killer T cells: biased cytokine profile and therapeutic activities. *Chembiochem* 9, 1423–1430. doi: 10.1002/cbic.200700625

Zhou, D., Mattner, J., Cantu, C. III., Schrantz, N., Yin, N., Gao, Y., Sagiv, Y., et al. (2004). Lysosomal glycosphingolipid recognition by NKT cells. *Science* 306, 1786–1789. doi: 10.1126/science.1103440

Conflict of Interest: The authors declare that the research was conducted in the absence of any commercial or financial relationships that could be construed as a potential conflict of interest.

frontiers in Chemistry

REVIEW
published: 03 December 2019
doi: 10.3389/fchem.2019.00823

The Structural Biology of Galectin-Ligand Recognition: Current Advances in Modeling Tools, Protein Engineering, and Inhibitor Design

Carlos P. Modenutti[1,2]*, *Juan I. Blanco Capurro*[1,2], *Santiago Di Lella*[1,2] and *Marcelo A. Martí*[1,2]*

[1] Departamento de Química Biológica, Facultad de Ciencias Exactas y Naturales, Buenos Aires, Argentina, [2] Instituto de Química Biológica de la Facultad de Ciencias Exactas y Naturales (IQUIBICEN), CONICET, Buenos Aires, Argentina

Galectins (formerly known as "S-type lectins") are a subfamily of soluble proteins that typically bind β-galactoside carbohydrates with high specificity. They are present in many forms of life, from nematodes and fungi to animals, where they perform a wide range of functions. Particularly in humans, different types of galectins have been described differing not only in their tissue expression but also in their cellular location, oligomerization, fold architecture and carbohydrate-binding affinity. This distinct yet sometimes overlapping distributions and physicochemical attributes make them responsible for a wide variety of both intra- and extracellular functions, including tremendous importance in immunity and disease. In this review, we aim to provide a general description of galectins most important structural features, with a special focus on the molecular determinants of their carbohydrate-recognition ability. For that purpose, we structurally compare the human galectins, in light of recent mutagenesis studies and novel X-ray structures. We also offer a detailed description on how to use the solvent structure surrounding the protein as a tool to get better predictions of galectin-carbohydrate complexes, with a potential application to the rational design of glycomimetic inhibitory compounds. Finally, using Gal-1 and Gal-3 as paramount examples, we review a series of recent advances in the development of engineered galectins and galectin inhibitors, aiming to dissect the structure-activity relationship through the description of their interaction at the molecular level.

Keywords: galectin, structure, carbohydrate, water sites, docking, drug-design, glycomimetic

OPEN ACCESS

Edited by:
Karina Valeria Mariño, Institute of Biology and Experimental Medicine (IBYME), Argentina

Reviewed by:
Paripok Phitsuwan, King Mongkut's University of Technology Thonburi, Thailand
Mario Antonio Bianchet, Johns Hopkins University, United States

***Correspondence:**
Carlos P. Modenutti
cmodenutti@qb.fcen.uba.ar
Marcelo A. Martí
marti.marcelo@gmail.com

Specialty section:
This article was submitted to Chemical Biology, a section of the journal Frontiers in Chemistry

Received: *28 July 2019*
Accepted: *12 November 2019*
Published: *03 December 2019*

Citation:
Modenutti CP, Capurro JIB, Di Lella S and Martí MA (2019) The Structural Biology of Galectin-Ligand Recognition: Current Advances in Modeling Tools, Protein Engineering, and Inhibitor Design. Front. Chem. 7:823. doi: 10.3389/fchem.2019.00823

GALECTINS IN CELLULAR BIOLOGY

Deciphering the complex structure of the sweet pattern elegantly disposed over different cell surfaces requires a wide variety of biomolecules specifically designed to interact with each particular moiety. Understanding the structure, dynamics, and recognition mechanism of the proteins responsible for this role is therefore of fundamental relevance to gain a deeper understanding of the underlying biological processes involved and develop potential therapeutic interventions. Galectins are one of the main groups of carbohydrate recognition proteins, and in humans, they are involved in a variety of physiological processes, many of which are directly linked with immunity and disease.

Galectins arose lately as novel actors in the modulation of physio-pathological processes. They have been implicated in many biological activities, ranging from functional early developmental processes, vascularization programs, cell migration, and regulation of immune system cells to either pro- or anti-inflammatory resolutions (Liu and Rabinovich, 2010; Di Lella et al., 2011; Thiemann and Baum, 2016). Galectins are deeply involved in pathogen recognition and killing, and in facilitating entry of microbial pathogens and parasites into the host (Vasta, 2009; Yang et al., 2011; Baum et al., 2014; Lujan et al., 2018). During infection, they are the subtle intermediators that decipher glycan-containing information about the host immune cells and microbial structures, and therefore modulate a diversity of signaling events that lead to cellular proliferation, survival, chemotaxis, trafficking, cytokine secretion, and cell-cell communication.

Extracellularly, most galectins act as soluble cell surface pattern recognition receptors, by these means regulating cell-cell communication (Arthur et al., 2015b). Their lectin activity, specifically directed toward β-galactoside moieties, is either coupled with a dimerization equilibrium, in tandem multi carbohydrate binding domain structure, or other oligomerization strategies, that prompt the formation of very complex supramolecular structures, often described as lattices (Sacchettini et al., 2001). In summary, the mechanism through which galectin extracellular functions are accomplished relies both on their carbohydrate-binding specificity, as well as on their lattice formation capabilities which are tightly related to galectin structure.

GALECTIN STRUCTURE

As described originally by Hirabayashi and Kasai (1993), galectins can be classified according to their domain organization in three groups: (i) the prototype galectins, which display a single Carbohydrate Recognition Domain (CRD) per polypeptide and usually form dimers, represented in humans by Gal-1,−2,−7,−10,−13, and−14; (ii) tandem repeat-type galectins, displaying two CRDs in tandem, represented by Gal-4,−8,−9, and−12; and finally the (iii) chimera-type galectins, where the CRD is fused to another non-lectin domain, represented by Gal-3 (Liu and Rabinovich, 2010; Di Lella et al., 2011; Thiemann and Baum, 2016). On the other hand, phylogenetic analysis based on sequence and intron/exon positions revealed two monophyletic groups referred to as F3 and F4 CRD types (Houzelstein et al., 2004). Interestingly, all tandem repeat-type galectins are composed of one CRD of each type.

Galectin's CRD (**Figure 1**) can be described as an about ∼130–140 residue domain which folds as a two antiparallel β-sheet sandwich that adopts a closing hand shape. The backhand is formed by strands F1 to FX (which form the F-sheet), while the palm consists of strands S1 to SY (the S-sheet). In all galectins, the carbohydrate-binding site (CBS) is located in a groove in the S-sheet side of the sandwich, and the β-galactoside recognition core motif is mediated by sheets S4, S5, and S6.

Comparative sequence and structural analysis, shows some interesting trends of galectin structural divergence. The first thing to notice is that despite having a low (∼30% average) sequence identity, the CRD fold structure is highly conserved: the maximum backbone Root Mean Square Deviation (RMSD) between all human galectins is below 2.2 Å, with the main differences observed in specific loop regions (**Figure 2A**). The structure also seems to follow sequence evolution, with all galectins from the same CRD type (F3/F4) clustering together in the RMSD tree (**Figure 2B**), and close sequence pairs (i.e., Gal-1/Gal-2 or Gal-10/Gal-13) displaying very similar structures. A particular interesting observation concerns tandem type galectins, since they always combine two domains which are both sequence and structural divergent. Finally, it is worth mentioning that the C-terminal domain of Gal-12 seems to be the most divergent galectin domain, sharing <20% sequence identity to any other galectin, and whose structure is currently unknown.

LINKING OLIGOMERIC STRUCTURE TO FUNCTION

Going back to the oligomeric structure, it is important to note that prototype galectins form dimers of two CRDs back to back and that both states seem to exist in a dynamical equilibrium, which has been shown, at least in Gal-1, to affect ligand binding kinetics and affinity (Di Lella et al., 2010; Nesmelova et al., 2010; Romero et al., 2016). A clear example of the oligomeric state affecting immune function is that only dimeric Gal-1, but not its permanent monomeric mutant form, is able to induce phosphatidylserine exposure and enhance phagocytic recognition of leukocytes (Dias-Baruffi et al., 2003).

Tandem repeat-type galectins, as their name evidence, display two CRDs covalently connected in tandem by a hinge region, thus no dynamical equilibrium is possible. This constitutive bivalency of tandem repeat-type galectins has been proposed as an explanation of why and how they induce cell signaling at lower concentrations than those of proto-type galectins. Supporting this idea, many independent studies have shown dissimilar potencies of different galectins upon triggering particular cellular responses. For example, when looking at T lymphocytes and neutrophils signaling, tandem repeat-type Gal-4,−8, and−9 are more potent than the chimera-type Gal-3, the latter being more potent than the proto-type Gal-1 (Sturm et al., 2004; Levy et al., 2006; Stowell et al., 2007). Supporting key role of (supra) domain structure, the orientation, rotational flexibility, and spacing of the CRDs in tandem repeat-type galectins has been shown to modulate its lattice forming capabilities (Rabinovich et al., 2007). The above described structural mechanisms of lattice formation, impacts directly in galectin-based protein engineering strategies for therapeutic purposes, as exemplified by a covalently linked form of the Gal-1 dimer (i.e., an engineered tandem repeat type Gal-1), which was found to be a potent pro-apoptotic agent on mouse thymocytes as well as mature T lymphocytes at lower concentrations compared to the wild-type (Bättig et al., 2004).

Concerning Gal-3, its unique type of possible oligomeric states deserves particular attention. Gal-3 is monovalent in the absence

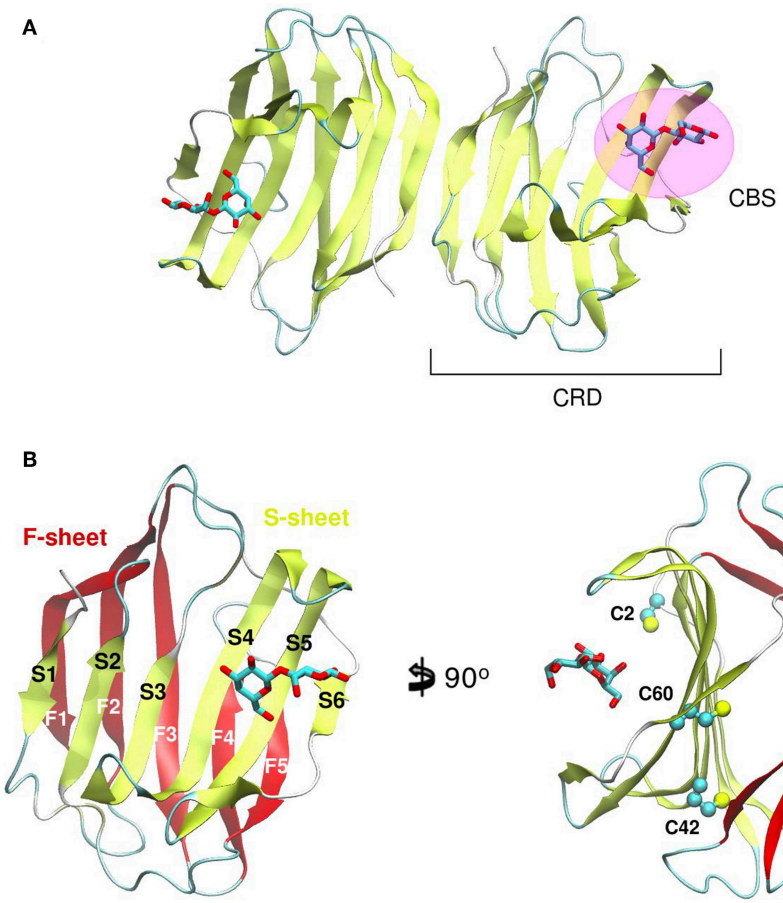

FIGURE 1 | Structure of a Galectin. **(A)** Gal-1 dimer. **(B)** Detail of the Gal-1 monomer differentiating the "S-sheet" (strands S1–S6) in yellow, and the "F-sheet" (strands F1–F5) in red. All cysteine side chains drawn as Balls and sticks.

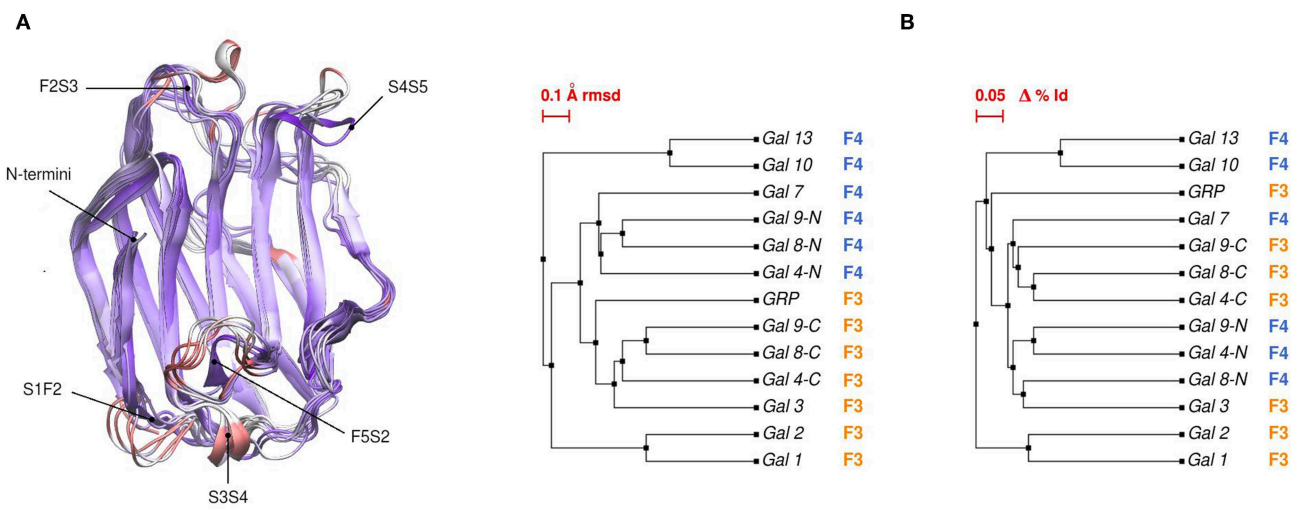

FIGURE 2 | (A) Structural alignment of all available human Galectin CRDs X-ray structures. Blue-colored regions correspond to the lowest RMSD values and red to the highest values. Gal-1 structure used as reference. Each loop is named after the two β-strands it connects. **(B)** Backbone RMSD-based tree (left) and amino acid sequence identity tree (right) of the X-ray structures.

of ligands, but can oligomerize through its N-terminal non-lectin domain upon ligand recognition by its lectin C-terminal galectin CRD (Ahmad et al., 2004). This oligomerization, and further lattice formation process, leads to cross-linking of glycoprotein receptors on the cell surface, which is an essential event for the majority of Gal-3 extracellular functions, such as cell adhesion and T cell activation (Yang et al., 2008).

While the macromolecular structure of organized clustered assemblies could be evidenced by electron microscopy of homogeneous and heterogeneous lectin-carbohydrate cross-linked complexes in other lectins (Dam et al., 2017), only blobs in EMs of precipitates of Gal-3 with bivalent pentasaccharides has been observed (Ahmad et al., 2004). The functional activity of a pro- or anti-inflammatory galectin could be explained in terms of the quaternary structure -the organization of these supramolecular assemblies. While Gal-1, displaying anti-inflammatory features, remains a dimer in cross-linked complexes with a bivalent oligosaccharide, Gal-3, a pro-inflammatory lectin, is predominantly a monomer in solution, converting into a pentamer in the presence of a precipitating multivalent carbohydrate. Additionally, and due to its dimeric equilibrium, Gal-1 can form one-dimensional and homogeneous lattices, while Gal-3 forms heterogeneous cross-linked complexes with multivalent carbohydrates (Ahmad et al., 2004).

GALECTIN CARBOHYDRATE RECOGNITION

Galectins' CBS is formed by the residues within the groove comprising the S-sheet. From a general point of view, binding of carbohydrates involves at least two major interactions: hydrophilic, through an extensive complementary hydrogen-bond network, and hydrophobic, through CH-π interactions between the sugar and aromatic amino acid sidechains in the CRD. An in-depth binding affinity analysis of a large oligosaccharide library covering a diverse set of mammals, fungi, nematode and Porifera galectins has been carried by Hirabayashi et al. (2002).

In galectins, the minimum binding determinant, usually a Lactose or N-acetyl-lactosamine disaccharide, binds to the far side of the CBS (strands S4–S6), although there are several reported complex structures with larger saccharides. Using one of the largest available as reference -the Gal-9N hexasaccharide complex (PDB id: 2zhm)- in order to facilitate the analysis the whole CBS can be divided into six different "monosaccharide binding subsites," which we will refer to as sites Y, Z, A, B, C, and D. Comparative analysis of the protein residues related to each subsite in several human galectins (**Figure 3A**) show that while there are highly conserved topological positions, others seem to allow the presence of many types of amino acids. Most conserved residues give shape to subsites C and D (**Figure 3B**). Particularly, "subsite C" deserves a detailed structural description, since it is the one that comes into most intimate contact with the β-galactoside moiety, hence could be the most implicated in galectins' characteristic specificity. It essentially consists of a pocket-shaped region formed by three conserved positions along the S4 strand, His at 4-S4, Asn at 6-S4, and Arg at 8-S4, plus a conserved Trp at position 2-S6 (**Figure 3C**). The three polar residues of S4 are implicated in accommodating the axial C4-OH -the distinctive feature of galactoside epimers- through multiple hydrogen-bonding interactions, while the Trp interacts with the opposite face of the sugar through its CH-π cloud.

Computational calculation of each individual site-monosaccharide interaction energy by the Generalized Born (GB) method also showed some interesting trends (Guardia et al., 2011). As it can be observed in **Figure 3D**, sites that contribute most to the binding affinity are subsites C and D. Particularly, subsite C showed a high contribution of Van Der Waals interactions to the total energy, that can be explained by the pocket-like shape of the site. On the other hand, subsite D showed mainly electrostatic contributions, due to the presence of a conserved negatively-charged Asp at position 5-S6, and a less well-conserved positively-charged residue at position 7-S6. Most of these characteristics are in agreement with a broader analysis made by our group for a larger and more diverse set of lectins, which show that even if some lectins are able to accommodate large oligosaccharides, most lectins typically recognize a core of one or two monosaccharide units, and usually no more than 2–3 OH groups per monosaccharide are in contact with the protein, with a total average of 4-OH groups being responsible for ligand recognition (Modenutti et al., 2015).

Despite being commonly considered as galectins for exhibiting the characteristic jelly roll-like CRD, from a ligand-binding perspective there are special cases to underscore that arguably deserve to be included in this classification. One is the C-terminal domain of the human hematopoietic stem cell precursor, commonly called GRP for "galectin-related protein," which has no apparent ability to bind carbohydrates (Zhou et al., 2008). **Figure 3C** shows that these could be due to the fact it lacks 4 out of the 6 most conserved residues, the previously described His, Asn, Arg, and Trp of subsite C. A second special case is Gal-13 (also known as Placenta Protein 13), which has proven to be unable to bind lactose by both crystallographic and biochemical analysis. However, the Gal-13 R53H-H57R double mutant (PDB id: 6a62) was proven to recover the lactose-binding capabilities (Su et al., 2018a), thus suggesting that it possibly changed its binding capacity due to a few recent evolutionary steps. The structural explanation behind this clever work of re-engineering lays in the fact that in Gal-13 position 53 corresponds to the key His and position 57 to the Arg of subsite C, which as mentioned above are necessary for hydrogen bonding the axial C4-OH. Finally, the most controversial case is possibly that of Gal-10, which has shown little affinity toward β-galactosides, yet its structure has been co-crystallized with mannose (PDB id: 1qkq) (Swaminathan et al., 1999). A close inspection of the structure immediately reveals that the mannose ring is distorted from its classical low-energy chair conformation and that it is not completely buried into the CBS, thus making it difficult to think of mannose as its endogenous ligand.

The difference in Gal-10 behavior seems to concern domain organization, as recently demonstrated by Su et al., who showed that Gal-10 dimerizes in a different way to other prototype lectins, that is, through the S-sheet face of the CRD; in this

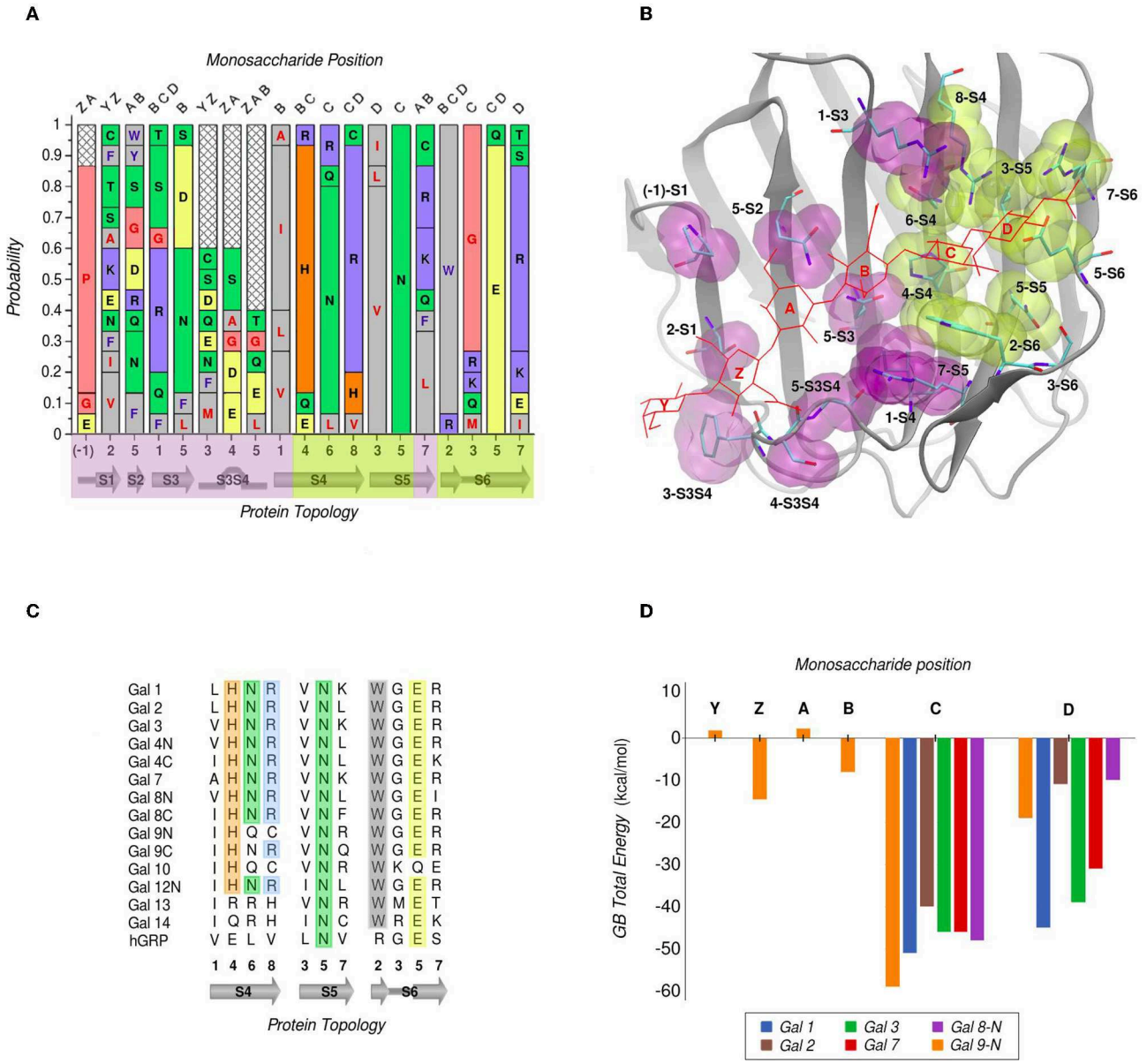

FIGURE 3 | Amino Acid composition of human galectins' CBS based on a topological analysis (Gal-12C excluded). **(A)** Probability graph for each topological position. Each residue is colored by its physicochemical properties. The protein topology naming corresponds to the piece of secondary structure under study, preceded by a number which indicates the relative position of each particular residue in that piece of secondary structure (e.g., "5-S2" corresponds to the position no. "5" of the "S2" β-strand). **(B)** Tridimensional representation of the Gal-9N, with the main residues of the CBS surface, highlighted as yellow (most conserved) or purple (least conserved). Hexasaccharide molecule is depicted with red lines and its monosaccharide units named with letters Z-Y-A-B-C-D. **(C)** Residue comparison along S4-S6 β-strands. **(D)** Individual contribution per monosaccharide to the total Binding Energy, calculated with the General Born method (Guardia et al., 2011). "Reprinted (adapted) with permission from Guardia et al. (2011). Copyright (2011) American Chemical Society".

novel dimerization mode, the F2S3 loop residue Glu 33 from one monomer partially occludes the CBS of the other and vice versa, hence preventing the binding of lactose (Su et al., 2018b). However, when this Glu is mutated to Ala, dimerization equilibria is altered and now the monomeric Gal-10 E33A can bind lactose. This idea is strongly supported by the recently solved crystal structure of the Gal-10 E33A mutant in complex with lactose (PDB id: 6a1t), and by hemagglutination inhibition experiments. Also, the CBS involvement in Gal-10 dimerization is further backed up by the mutation of the conserved C subsite Trp to Ala; Gal-10 W72A mutant is indeed a monomer, hence confirming the participation of Trp 72 in dimerization. Gal-10 W72A agglutination capabilities are enhanced with respect to wild-type, as well as its ability of binding to lactose-modified

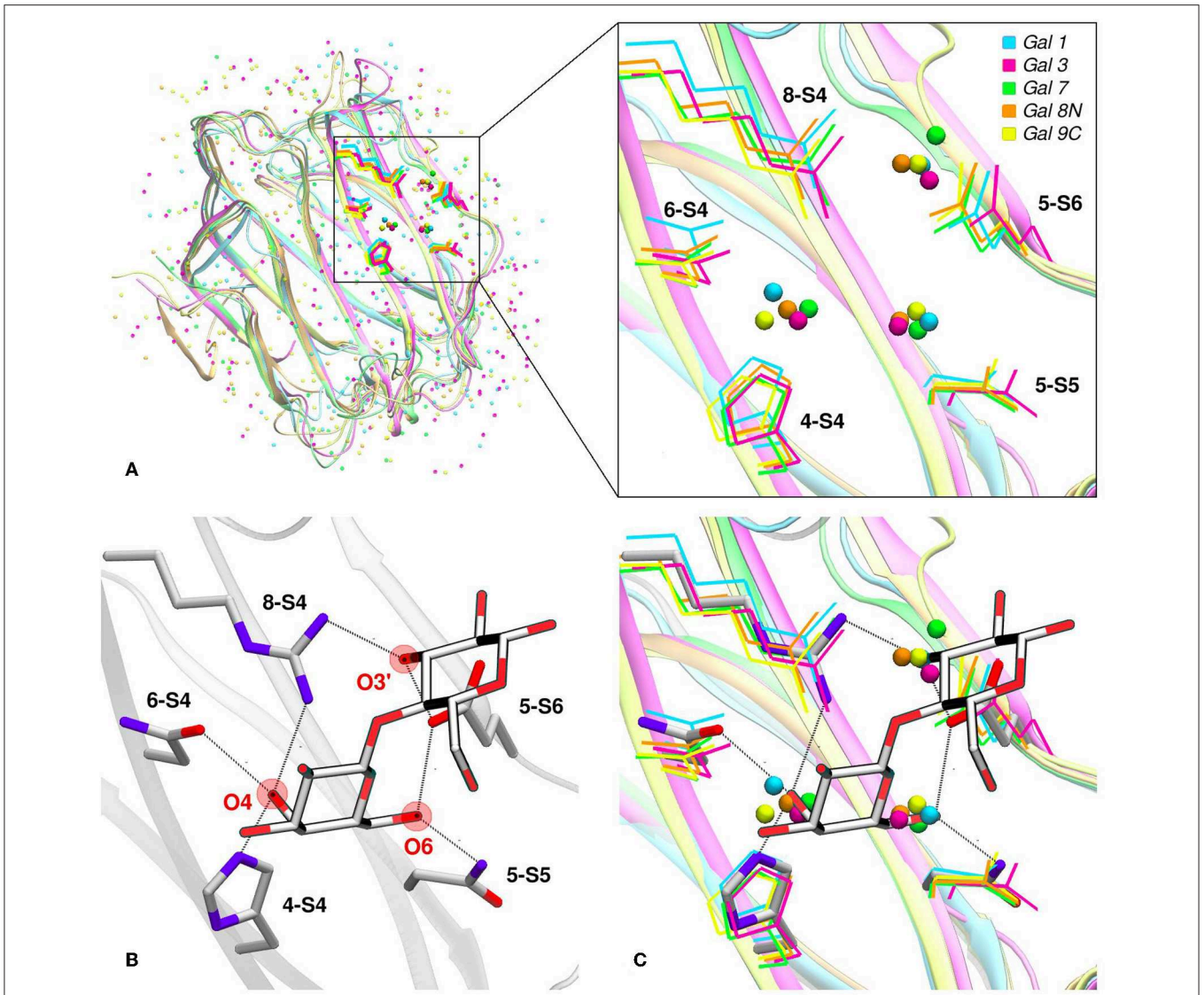

FIGURE 4 | Solvent structure of several human galectins. **(A)** Apo X-rays superimposition showing highly ordered crystallographic water molecules in the CBS. Color code is cyan for Gal-1 (1w6n-B), magenta for Gal-3 (3zsm-A), green for Gal-7 (4gal-A), orange for Gal-8N (3apb-B), and yellow for Gal-9C (3nv1-A). **(B)** Detail of Gal-1 (1w6o-A) in complex with lactose, showing the main polar residues and the Hydrogen bond network (dotted lines) established with the ligand. **(C)** Superimposition of A and B, showing that a clear displacement of water molecules is needed for binding to proceed.

sepharose-6B beads in solid-phase assays (Su et al., 2019). This raises the question as to whether the conserved C subsite Trp regulates lactose binding negatively, and more shallow binding sites such as that of Gal-10 W72A could rather increase affinity.

THE ROLE OF WATER IN GALECTIN CARBOHYDRATE RECOGNITION

Water molecules play an important role in protein structure and function. During the ligand-binding process, the water molecules from the corresponding binding site must be displaced to make room from the incoming ligand, which is also partially solvated. Several works have shown that this solvent reorganization process has an important contribution to the binding free energy (Lazaridis, 1998; Abel et al., 2008). Most importantly, the hydrophilic nature of both the carbohydrate ligands and the galectins CBS makes this contribution a key element in the recognition process and the resulting affinity. From a structural point of view, and as a result of the specific interactions between the CBS surface and the water solvent, water molecules tend to occupy specific positions and orientations (i.e., they are highly ordered), resulting in a well-defined solvent structure. This ordered solvent structure can be revealed for example by the presence of crystallographic waters (**Figure 4A**), or as will be described below, using Molecular Dynamics simulations, yielding the so-called "Water Sites" (WS). Previous analysis from our group for a large dataset of

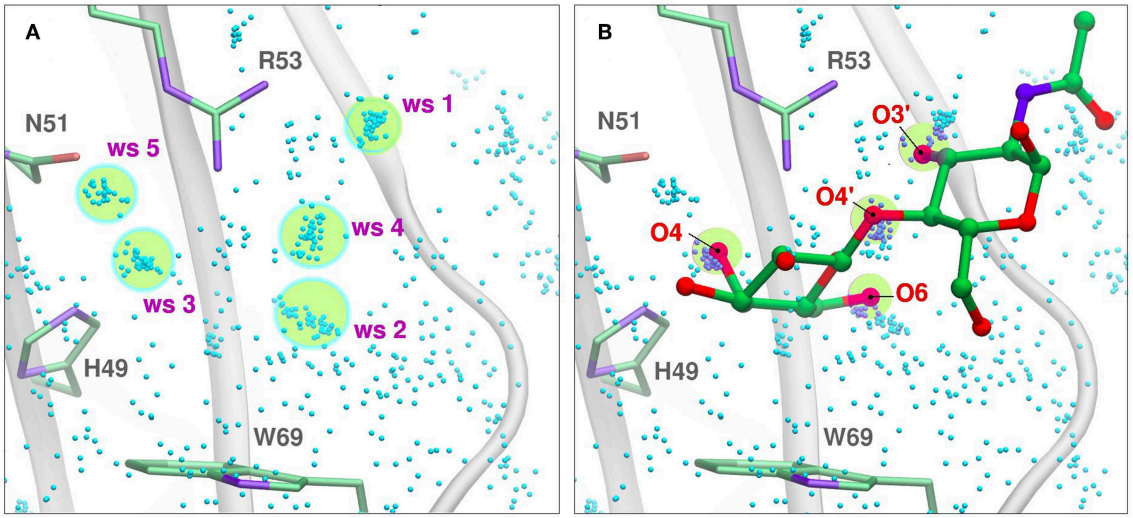

FIGURE 5 | Solvent structure determination by Molecular Dynamics of Gal-7 CBS (PDB id: 1bkz). Water molecules from many snapshots along the simulation trajectory are superimposed and shown as small cyan dots (Hydrogens atoms omitted for clarity). **(A)** Water Sites 1–5 are depicted as transparent yellow circles. **(B)** N-acetyl-lactosamine coordinates of "PDB id: 5gal" superimposed into the previous image, highlighting all the oxygen atoms that displace a Water Site.

lectin-carbohydrate complexes showed that up to 80% of all observed ligand -OH groups that interact with their receptors are, when the ligand is absent, occupied by a WS. On the other hand, of all WS found in the CBS of lectins, about 40% tend to be replaced by ligand-OH groups (Modenutti et al., 2015). **Figure 4A** shows how these WS are precisely located and perfectly describe the binding mode of β-galactosides in galectins.

Looking at the sugar ligand, it is evident as the name "carbohydrate" suggests, that they can be structurally/chemically described as "hydrated carbons," and upon binding their -OH groups perform the same interactions with the protein as those performed by the WS (**Figures 4B,C**, **5B**). In other words, the WS structure mimics the ligand -OH framework that interacts with the protein and therefore can be an excellent predictor for recognition and affinity.

MOLECULAR SIMULATION METHODS AS STRUCTURAL BIOLOGY TOOLS FOR STUDYING GALECTINS AND CARBOHYDRATES

Molecular simulation methods, mainly classical force field-based Molecular Dynamics simulations and Molecular Docking, have been extensively used to study carbohydrates, lectins, and their complexes. In particular, explicit water simulations allow a detailed description of the solvent structure in the Lectin CBS in terms of WS (Gauto et al., 2009). A WS corresponds to a definite region in the space adjacent to the protein surface, where the probability of finding a water molecule is significantly higher than that observed in the bulk solvent. It has been proven that there is a correlation between the WS and the crystallographic waters (Modenutti et al., 2015) and can be structurally and thermodynamically characterized in the context of the Inhomogeneous Fluid Solvation Theory (Lazaridis, 1998). Several methods are available for WS determination, like WaterMap (Abel et al., 2008), WATsite (Hu and Lill, 2014), GIST (Nguyen et al., 2012), and WATclust (López et al., 2015), to cite a few.

In WATclust, for example, WS is detected through clustering of explicit water molecules, through a graphic interface implemented in the commonly spread Visual Molecular Dynamics software (Humphrey et al., 1996). Briefly, to detect WS, the program should be fed with a collection of trajectory snapshots (∼500–1,000, which usually cover 5–20 ns) derived from the corresponding simulation of the desired protein embedded in a large explicit water box. The snapshots are superimposed using a local RMSD-based structural alignment, in which the residues selected for the alignment should reflect the region of interest, usually the CBS. Subsequently, the number of snapshots harboring a water oxygen atom in a previously defined space region (with an arbitrary spherical volume of 1 $Å^3$) are determined, and those regions with a high population (>10–50% of the total number of snapshots) are selected as candidate WS (**Figure 5A**).

Once identified, for each candidate WS two important parameters are computed, namely: (i) The "Water Finding Probability" (WFP), defined as the probability of finding a water molecule in the 1 $Å^3$ volume and normalized with respect to the probability of the bulk water; (ii) The "R90", which corresponds to the radius in which 90% of the water molecules can be found. This parameter gives a notion of the WS dispersion, and thus its translational entropy; candidate water clusters whose WFP is below 2–5 are usually discarded, and the remaining are considered the true WS. As will be described below, the WS predictive capacity leads us to develop a WS-biased docking methodology which significantly improves the quality of structure predictions both in terms of accuracy and specificity.

WATER SITES AS PREDICTORS OF GALECTIN-CARBOHYDRATE BINDING

Molecular Docking methods, such as the widely used Autodock (Forli et al., 2016), aim to determine the structure of a protein-ligand complex and the corresponding affinity (i.e., the Binding free energy'), starting from the structure of the protein receptor and the ligand separately. Therefore, they are commonly utilized to determine the precise complex structure of a known binding protein-ligand pair (usually referred as "pose prediction"), or to predict the structure and affinity of a series of potential ligands for a given receptor (referred to as "virtual screening") (Arcon et al., 2019a). Docking methods usually consist of a conformational search algorithm coupled to an energy scoring function that estimates the Binding Free Energy (Morris et al., 1998). Scoring functions are usually developed and calibrated for rigid hydrophobic drug-like compounds stored in deep hydrophobic pockets of their respective receptors, hence, they typically perform poorly when trying to dock polar ligands such as carbohydrates that bind to lectins' shallow and solvent-exposed CBSs.

Based on our previous finding that WS tend to mimic the carbohydrate -OH groups in the resulting lectin-sugar complexes, we hypothesized this information could be used to improve carbohydrate docking performance. The idea, which we called the "Solvent-Site Bias Docking Method" (SSBDM) was implemented in Autodock 4 (Arcon et al., 2019b), and it basically adds a correction term to the Autodock energy scoring function to bias the ligand oxygen atoms toward replacing the WS coordinates, as described by Equation (1):

$$\Delta G_0^M = \Delta G_0 - RT \sum_{i=1}^{N} \ln\left(WFP_i\right) e^{\frac{-\sqrt{((x - x_{WS,i})^2 + (y - y_{WS,i})^2 + (z - z_{WS,i})^2)}}{R_{90}}} \quad (1)$$

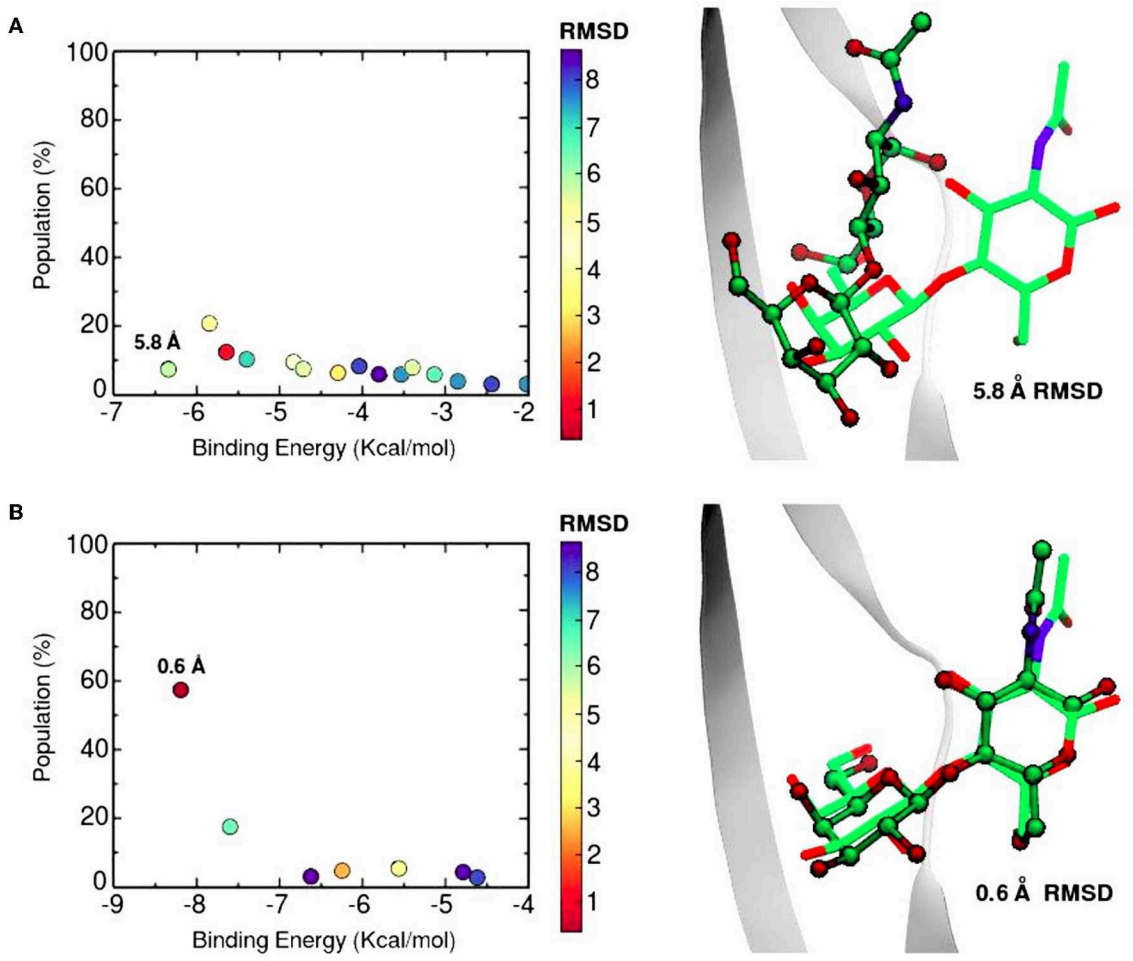

FIGURE 6 | Docking calculations of N-acetyl-lactosamine disaccharide to Gal-1 structure (PDB id: 1y1u). Results are presented as "Population vs. Binding Energy," and a picture of the Best energy-ranked result for each docking method. **(A)** Conventional Autodock Docking Method. **(B)** Solvent-site Bias Docking Method (SSBDM). The values next to the dots represent the ligand heavy atom RMSD between the predicted ligand pose and the reference X-ray pose. The red dot indicates the location of the most accurate result.

Here, ΔG_0 corresponds to the original Autodock 4 scoring function Binding Energy, WFP_i is the water-finding probability of the "ith" WS. X_{WS}, Y_{WS}, and Z_{WS} are the corresponding WS cartesian coordinates, and R_{90} is the WS dispersion factor.

This way, in the SSBDM each WS provides a favorable interaction energy between the center of the WS position and any oxygen atom of the ligand, with a magnitude that is proportional to the "Ln(WFP)" and an amplitude related to the WS dispersion "R90." In other words, those poses of the carbohydrate that maximize superposition of the -OH groups to where the WS with highest WFP were located are favored in terms of Binding Energy.

The SSBDM has proven to be an efficient structure predictor for many protein-carbohydrate complexes, including some galectins (Gauto et al., 2013). An example of the method increase in performance is shown in **Figure 6**. Docking calculations typically return a set of probable ligand poses, ranked by their Binding Energy and sometimes reporting the pose "population" (understood as the percentage of times that the corresponding pose was found). **Figure 6** shows a classic "Population vs. Binding Energy" plot for 100 Docking runs of N-acetyl-lactosamine to Gal-1, where each dot corresponds to a different ligand pose. Highlighted in red is the "correct pose" (i.e., that with a 0.6 Å heavy-atom RMSD with respect to the N-acetyl-lactosamine in the reference complex, PDB id: 1y1u). **Figure 6A** shows that for conventional docking the correct pose is indistinguishable from other poses with similar values of energy and/or population. **Figure 6B**, on the other hand, illustrates how the SSBDM increases the predictive power of Docking, since it enriches the correct pose both in terms of energy and population, making it now easily distinguishable from false positives.

Currently, as of 2019, the SSBDM has been officially integrated into the AutoDock suite as an easy-to-use script, by the name of "AutoDock Bias" (Arcon et al., 2019a).

Nevertheless, the pose prediction of larger saccharides (i.e., beyond the trisaccharide level) is still a challenging task and requires additional patches. Common docking calculations often decrease their success rate when dealing with large ligands that have several active torsions, especially when these torsions result in a large conformational space, as in the case of short oligosaccharides. To address this problem, Nivedha et al. successfully implemented an *ad hoc* potential function for Autodock Vina scoring function, which energetically penalizes those conformations that fall too far from the glycosidic dihedral angles minima, significantly optimizing the performance for large carbohydrates. This method is called "Vina-Carb"(Nivedha et al., 2014, 2016), and as shown in **Table 1**, it was proven successful for the prediction of many galectin-oligosaccharide complexes. Noteworthy examples are the case of the sialyllactose trisaccharide docking to both Gal-8N and Gal-9C receptor structures. Even more strikingly, it was able to give an accurate prediction of the N-acetyl-lactosemine hexasaccharide pose in Gal-9N (RMSD 1.90 Å). Yet strangely, Vina Carb performed poorly (RMSD $>$ 3) for the two disaccharide complexes listed. This could be indicating that for small saccharides the Carb energy functions are still not enough for a guaranteed success, and might support the idea that a combination of techniques - torsional penalties and the incorporation of the solvent structure- is probably the best strategy.

Molecular Docking methods enable the investigator to access an atomistic-detailed comprehension of the protein-carbohydrate interaction and thus provide a state of the art tool for the rational design of glycomimetic binders. Furthermore, it would be interesting to know the aftermath of applying such methods to predictively discern binders from non-binders in glycan-array experiments. Currently, an important line of work in this direction is being developed in our lab.

TABLE 1 | Docking results of carbohydrates of different sizes onto their respective Galectin receptors, using Autodock Vina Carb.

Galectin	PDB id-chain	Ligand	Oligomer	RMSD
Gal-2	1HLC-B	Lactose	Disaccharide	6.1
Bovine Gal-1	1SLT-B	N-acetyl-lactosamine	Disaccharide	7.0
Gal-8N	3AP7-A	Sialyllactose	Trisaccharide	1.0
Gal-9C	3NV4-A	Sialyllactose	Trisaccharide	0.8
Gal-9N	2EAL-A	Forssman antigen	Trisaccharide	0.4
Fungal CGL2	1ULF-A	Blood group A antigen	Tetrasaccharide	8.0
Gal-9N	2ZHM-A	N-acetyl-lactosamine	Hexasaccharide	1.9
Adenovirus fiber C-term domain	2WT2-B	N-acetyl-lactosamine	Hexasaccharide	2.5

GALECTINS AS THERAPEUTIC AGENTS AND DRUG TARGETS

The identification of critical regions in galectin's structure that determine their biophysical properties and interactions with the microenvironment can be exploited in the design of novel proteins with particular features. Furthermore, understanding their unique structural features is the key to overcoming the difficulties in designing specific glycomimetic ligands for therapeutic purposes. Two of the most studied galectins to date in this respect are Gal-1 and Gal-3, being in the bullseye of the scientific community as well as the pharmaceutical industry, they both serve as examples of the paramount importance of galectins and their ligands in immunology related Translational Medicine (St-Pierre et al., 2012; Téllez-Sanz et al., 2013).

GALECTIN-1 AND PROTEIN-ENGINEERING

The high levels of expression of Gal-1 in the thymus, lymph nodes, as well as in immune cells such as T cells and activated macrophages, suggested from the very beginning a key role in immune response regulation. Early evidence for the potential of Gal-1 therapeutic applications came from several experiments with rodent models (Levi et al., 1983; Offner et al., 1990; Santucci et al., 2003), as well as from evidence of low expression

levels of Gal-1 and increased anti-Gal-1 antibodies in human patients with diverse forms of arthritis (Harjacek et al., 2001; Xibillé-Friedmann et al., 2013). In order to utilize Gal-1 as a therapeutic agent, first difficulties to overcome were those related to its varying functionality and efficiency due to its different physicochemical states, namely the oxidized vs. reduced forms, and monomer-dimer equilibrium (Blanchard et al., 2016).

A distinctive characteristic of some galectins is the requirement of a reducing environment for carbohydrate-binding activity. The rationale behind this property is based on the presence of a variable number of cysteine residues. Gal-1 for example, contains 6 cysteines in its 135 residue monomer (**Figure 1B**), and many studies have established a critical interplay between Gal-1 ligand binding activity and cysteine redox state (Stowell et al., 2009; Guardia et al., 2014; Arthur et al., 2015a). This characteristic should not go unnoticed given the sensitivity of Gal-1 to oxidative inactivation and its functional role in inflammatory microenvironments, where there is a high propensity toward oxidation. Sensitivity of Gal-1 to oxidation was cleverly addressed by Nishi et. al., with the generation of a cysteine-less Gal-1 mutant. This "perpetually reduced" mutant showed enhanced stability over the wild-type, while retaining its hemagglutination and inhibition of cell-growth capabilities intact (Nishi et al., 2008). On the other hand, an "oxidized" form of Gal-1 with a disulfide bond between Cys16-Cys88 has been patented for nerve regeneration treatments (Horie et al., 2005). This oxidized variant is to be further covalently bound to soluble polymers such as polyethylene glycol, to enhance both stability and solubility. A detailed analysis of the involvement of every cysteine residue revealed a different correlation on their importance for disulfide bond formation and further lectin activity inactivation (Guardia et al., 2014).

Regarding the dimerization state, wild type Gal-1 and several dimer-interface mutants with notably higher dimerization constants were patented for inflammatory modulation applications, in which the dimer were to be used to kill

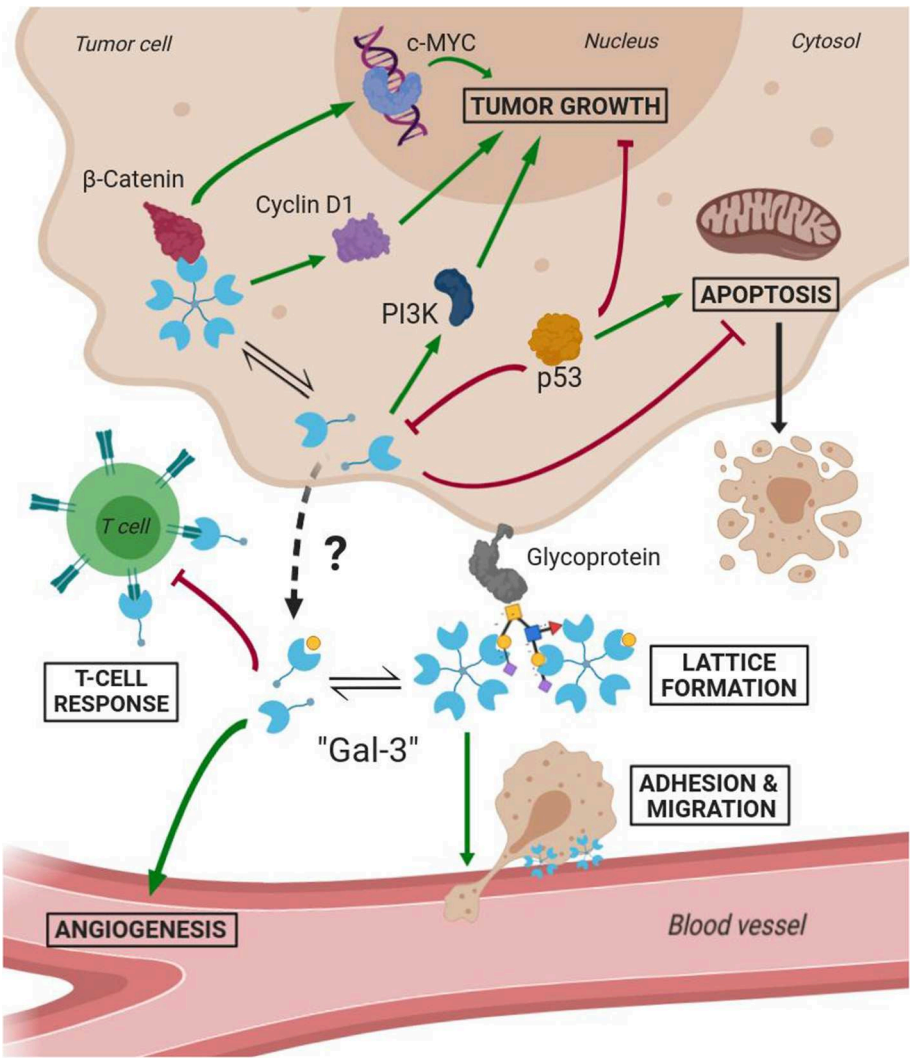

FIGURE 7 | Scheme of Gal-3 most important cellular functions in tumoral environments (Green arrows mean activation and bordeaux lines mean inhibition).

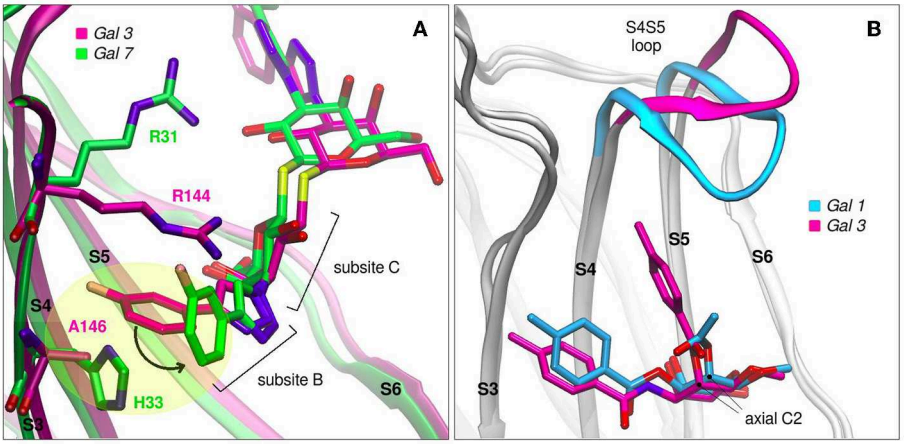

FIGURE 8 | Galectins in complex with carbohydrate-derived monovalent inhibitors. **(A)** Thiodigalactoside "TD139" superimposed complexes of Gal-3 (magenta, PDB id: 5h9p) and Gal-7 (green, PDB id: 5h9q) **(B)** Taloside inhibitors superimposed complexes. Gal-1 and methyl 2-O-acetyl-3-O-toluoyl-beta-D-talopyranoside (cyan, PDB id: 3T2T), Gal-3 and methyl 3-deoxy-2-O-toluoyl-3-N-toluoyl-beta-D-talopyranoside (magenta, PDB id: 3T1M).

activated neutrophils (anti-inflammatory effect), while the monomeric stable mutants were to be used to block the neutrophils apoptosis (pro-inflammatory effect) (Cummings and Cho, 1999). These dimer-interface mutants include single mutations (such as C2S or V5D), as well as a multisite mutant called "N-Gal-1" (bearing C2S, L4Q, V5D, and A6S mutations) (Cho and Cummings, 1996). In the opposite direction, in an effort to increase the relatively low *in vivo* potency of monomeric forms, a rational design of a series of covalently-linked Gal-1 dimers have been engineered. Following the pioneer "two-glycine covalent linker" (Bättig et al., 2004), various linkers of different lengths and flexibilities were explored, such as the 14 residue long random coil linker of Gal-9 (Bi et al., 2008), the 34 residue long helix linker from bacterial ribosomal L9 protein (Earl et al., 2011), and a 33 residue long flexible linker of Gal-8 (Vértesy et al., 2015). Each of these linker variants led to both increased hemagglutination and increased T-cell apoptosis promotion. The rationale behind the improved potency could presumably be the formation of more stable supramolecular structures (Baum, 2011).

Last but not least, Dimitroff et al. engineered a chimera protein of murine Gal-1 and the Fc region of human Immunoglobulin G1, which showed similar levels of activity as the native Gal-1 but stronger stability. This peculiar protein product showed pro-inflammatory toward activated leukocytes of rheumatoid arthritis patients and bears a patent for the treatment of immune disorders (Dimitroff et al., 2013). In summary, it is clear that a deep understanding of structural and physicochemical characteristics of Gal-1 in the context of its biological function, has been a key issue for the development of therapeutic approaches.

GALECTIN 3 AND DRUG-DESIGN

Several studies have demonstrated Gal-3 involvement in tumorigenesis, malignant form transformation, and metastasis (Radosavljevic et al., 2012). Gal-3 helps tumor cells them to escape immune surveillance by blocking both the afferent arm (T cell proliferation) and efferent arm (T cell attack) of the immune system response. A summary of both Gal-3 intratumoral and extracellular functions is schematized in **Figure 7**. As a result, inhibition of Gal-3 is strongly considered as a way of helping to restore the immune system's ability to fight cancer.

Most popular inhibitors of Gal-3 fall into one of three categories: Firstly, the peptide-derived inhibitors, perhaps headed by the sixteen amino acid long peptide "G3-C12," obtained from phage display (Zou et al., 2005); Secondly, The carbohydrate-derived multivalent inhibitors, represented mostly by the pectin derivatives, examples of which are the citrus-pectin derived "GBC-590" and "GCS-100" (both by Safescience, Inc.), or the galactomannan "GM-CT-01" (Davanat™) and galactoarabino-rhamnogalacturonan "GR-MD-02" (both by Galectin Therapeutics, former Pro-Pharmaceuticals, Inc.). Inhibitors from these two categories are already undergoing phase II clinical trials, and have been extensively described by Blanchard et al. (2014).

The third category and perhaps the most relevant to describe in detail under the structural scope of this review is comprised by the carbohydrate-derived monovalent inhibitors. They originally consisted of either galactose, lactose or N-acetyllactosamine scaffolds, in which their free -OH groups were to be modified with diverse chemical substituents. This fragment-based approach of drug design soon established the so-called "thio-digalactoside" (TDG) scaffold" and its derivatives as some of the most prominent small-molecule inhibitors of Gal-3 (Cumpstey et al., 2005), given the extra resistance to both chemical and enzymatic hydrolysis conferred by a sulfur bond. Among these compounds, we can cite the C2-symmetric "TD139" (by Galecto Biotech) or its asymmetrical derivative "TAZTDG" by Hsieh et al. (2016).

Modifications of TDG scaffold as a strategy to increase the binding affinity and, at the same time, improve specificity

is supported under the premise that the different galectins present variations in their protein sequences at subsites Z, Y, A, and B. Taking as an example the case of TD139, this antagonist has been co-crystallized with Gal-1 (PDB id: 4y24), Gal-3 (PDB id: 5h9p) and Gal-7 (PDB id: 5h9q). Although the ligand exhibits similar binding modes for Gal-1 and Gal-3, a remarkably different conformation is observed in the Gal-7 complex (**Figure 8A**), involving a disfavourable rotation of one of its 4-fluorophenyl substituents, prompted by the presence of a His residue at position 3 of the S3 strand (near the subsite B), in contrast to the less bulky Val occupying this same position in Gal-1 or the Ala in Gal-3. This difference in the structure offers a simple albeit elegant explanation to the several orders of magnitude in their ITC-determined dissociation constants (Gal-7 K_d = 38 μM, Gal-3 K_d = 0.068 μM) (Chan et al., 2018).

Another promising carbohydrate scaffold that is able to bind in the galectins subsite C is the taloside. Talose is the C2 epimer of galactose, featuring an axial C2-OH group (as opposed to the equatorial of galactose) (Collins et al., 2012). This enables the incorporation of axial substituents at this position which, depending on their shape, can interact with the surface of strands S4 and S5, as well as with the S4–S5 loop. This particular loop (as previously shown in **Figure 2A**) has both variable amino acid composition and length across the several lectins, and has been proven to have a wide flexibility as evidenced by Molecular Dynamics simulations (Guardia et al., 2011). Each particular loop structural difference and dynamical behavior could be rationally exploited in favor of improving ligand specificity. Examples that support this idea are shown in **Figure 8B**, where it can be clearly shown that Gal-3 is able to accommodate larger C2 substituents than Gal-1, due to its shorter S4–S5 loop.

As a final remark, we would like to emphasize that, while peptide and multivalent carbohydrate-derived inhibitors show very promising results in experiments and clinical trials, their weak spot lies in the fact that their structural mechanisms of binding are unknown. On the contrary, this is the small-molecule monovalent inhibitors strongest feature, since their development involves a rational understanding of both the ligand and the target physicochemical characteristics. An in depth description of carbohydrate-derived monovalent inhibitors for Gal-3 has been thoroughly reviewed by St-Pierre et al. (2012) and Téllez-Sanz et al. (2013).

CONCLUSIONS

When looking at galectins overall fold, it is clear that the conserved scaffold of the CRD allows for a subtle shaping of each CBS, which are expected to result in different affinities for different carbohydrate ligands, yielding a possibly unique selectivity which combined with particular domain architecture and environmental modulation (i.e., redox state, level of expression) produces a potential variety of biological responses. A comparative analysis on CBS amino acid composition across several human galectins reveals conserved positions that strongly correlate with having important roles in binding, especially regarding the binding pocket of the β-galactoside moiety. This pocket is formed by conserved residues His, Asn, Arg and Trp, which apparently cannot be freely mutated without producing serious consequences to ligand affinity.

Water molecules play an important role in lectin-carbohydrate recognition. The identification of Water Sites allows for an accurate description of the solvent structure surrounding the CBS, information which in turn can be craftily taken advantage of by incorporating it to Docking schemes, enhancing their predictive power. Carbohydrate dihedral angle energy penalties might also be of great aid when dealing with complex oligosaccharides. Molecular Docking for prediction of protein-ligand complexes is becoming an essential tool in structural biology.

All the above mentioned roles played by galectins in cell communication, proliferation, and migration, plus their active participation in immunological processes, make clear that galectins are directly involved in many diseases, such as cancer development and progression, HIV and microbial infections, autoimmune disorders, allergies, cardiovascular diseases, and the list continues. In this context, Gal-1 and Gal-3 have particularly withdrawn the attention of the scientific and pharmaceutical community, given their ubiquity and their direct relation to disease. They have been subject not only of protein engineering studies with therapeutic purposes, but also as extensive drug-design protocols.

AUTHOR CONTRIBUTIONS

CM, JC, SD, and MM wrote the review.

FUNDING

This work was supported by grants from CONICET (112201 501003 03CO) and the UBA (20020150100023BA), to MM, and a return fellowship from the Alexander von Humboldt Foundation in Germany to SD. CM is University of Buenos Aires postdoctoral fellow, JB is doctoral of Argentinean National Research Council, SD and MM are career members of the Argentinean National Research Council.

REFERENCES

Abel, R., Young, T., Farid, R., Berne, B. J., and Friesner, R. A. (2008). Role of the active-site solvent in the thermodynamics of factor Xa ligand binding. *J. Am. Chem. Soc.* 130, 2817–2831. doi: 10.1021/ja0 771033

Ahmad, N., Gabius, H.-J., André, S., Kaltner, H., Sabesan, S., Roy, R., et al. (2004). Galectin-3 precipitates as a pentamer with synthetic multivalent carbohydrates and forms heterogeneous cross-linked complexes. *J. Biol. Chem.* 279, 10841–10847. doi: 10.1074/jbc.M312834200

Arcon, J. P., Defelipe, L. A., Lopez, E. D., Burastero, O., Modenutti, C. P., Barril, X., et al. (2019a). Cosolvent-based protein pharmacophore for

ligand enrichment in virtual screening. *J. Chem. Inf. Model.* 59, 3572–3583. doi: 10.1021/acs.jcim.9b00371

Arcon, J. P., Modenutti, C. P., Avendano, D., Lopez, E. D., Defelipe, L. A., Ambrosio, F. A., et al. (2019b). AutoDock bias: improving binding mode prediction and virtual screening using known protein-ligand interactions. *Bioinformatics* 35, 3836–3838. doi: 10.1093/bioinformatics/btz152

Arthur, C. M., Baruffi, M. D., Cummings, R. D., and Stowell, S. R. (2015a). Evolving mechanistic insights into galectin functions. *Methods Mol. Biol.* 1207, 1–35. doi: 10.1007/978-1-4939-1396-1_1

Arthur, C. M., Rodrigues, L. C., Baruffi, M. D., Sullivan, H. C., Heimburg-Molinaro, J., Smith, D. F., et al. (2015b). Examining galectin binding specificity using glycan microarrays. *Methods Mol. Biol.* 1207, 115–131. doi: 10.1007/978-1-4939-1396-1_8

Bättig, P., Saudan, P., Gunde, T., and Bachmann, M. F. (2004). Enhanced apoptotic activity of a structurally optimized form of galectin-1. *Mol. Immunol.* 41, 9–18. doi: 10.1016/j.molimm.2004.02.004

Baum, L. G. (2011). Burn control, an adipocyte-specific function for galectin-12. *Proc. Natl. Acad. Sci. U.S.A.* 108, 18575–18576. doi: 10.1073/pnas.1115738108

Baum, L. G., Garner, O. B., Schaefer, K., and Lee,B. (2014). Microbe–host interactions are positively and negatively regulated by galectin–glycan interactions. *Front. Immunol.* 5:284. doi: 10.3389/fimmu.2014.00284

Bi, S., Earl, L. A., Jacobs, L., and Baum, L. G. (2008). Structural features of galectin-9 and galectin-1 that determine distinct t cell death pathways. *J. Biol. Chem.* 283, 12248–12258. doi: 10.1074/jbc.M800523200

Blanchard, H., Bum-Erdene, K., Bohari, M. H., and Yu, X. (2016). Galectin-1 inhibitors and their potential therapeutic applications: a patent review. *Expert Opin. Ther. Pat.* 26, 537–554. doi: 10.1517/13543776.2016.1163338

Blanchard, H., Yu, X., Collins, P. M., and Bum-Erdene, K. (2014). Galectin-3 inhibitors: a patent review (2008-present). *Expert Opin. Ther. Pat.* 24, 1053–1065. doi: 10.1517/13543776.2014.947961

Chan, Y.-C., Lin, H.-Y., Tu, Z., Kuo, Y.-H., Danny Hsu, S.-T., and Lin, C.-H. (2018). Dissecting the structure-activity relationship of galectin-ligand interactions. *Int. J. Mol. Sci.* 19:392. doi: 10.3390/ijms19020392

Cho, M., and Cummings, R. D. (1996). Characterization of monomeric forms of galectin-1 generated by site-directed mutagenesis. *Biochemistry* 35, 13081–13088. doi: 10.1021/bi961181d

Collins, P. M., Oberg, C. T., Leffler, H., Nilsson, U. J., and Blanchard, H. (2012). Taloside inhibitors of galectin-1 and galectin-3. *Chem. Biol. Drug Des.* 79, 339–346. doi: 10.1111/j.1747-0285.2011.01283.x

Cummings, R. D., and Cho, M.-J. (1999). *Methods of Screening for Compounds Which Mimic Galectin-1. USPTO 5948628.* US Patent. Available online at: https://patentimages.storage.googleapis.com/be/7d/0b/e1a0156c3486ae/US5948628.pdf

Cumpstey, I., Sundin, A., Leffler, H., and Nilsson, U. J. (2005). C2-symmetrical thiodigalactoside bis-benzamido derivatives as high-affinity inhibitors of galectin-3: efficient lectin inhibition through double arginine-arene interactions. *Angew. Chem.* 44, 5110–5112. doi: 10.1002/anie.200500627

Dam, T. K., Fan, N., Talaga, M. L., and Brewer, C. F. (2017). "8.08 - stoichiometry regulates macromolecular recognition and supramolecular assembly: examples from lectin-glycoconjugate interaction," in *Comprehensive Supramolecular Chemistry II*, ed J. L. Atwood (Oxford: Elsevier), 161–77.

Di Lella, S., Martí, M. A., Croci, D. O., Guardia, C. M. A., Díaz-Ricci, J. C., Rabinovich, G. A., et al. (2010). Linking the structure and thermal stability of β-galactoside-binding protein galectin-1 to ligand binding and dimerization equilibria. *Biochemistry.* 49, 7652–7658. doi: 10.1021/bi100356g

Di Lella, S., Sundblad, V., Cerliani, J. P., Guardia, C. M., Estrin, D. A., Vasta, G. R., et al. (2011). When galectins recognize glycans: from biochemistry to physiology and back again. *Biochemistry* 50, 7842–7857. doi: 10.1021/bi201121m

Dias-Baruffi, M., Zhu, H., Cho, M., Karmakar, S., McEver, R. P., and Cummings, R. D. (2003). Dimeric galectin-1 induces surface exposure of phosphatidylserine and phagocytic recognition of leukocytes without inducing apoptosis. *J. Biol. Chem.* 278, 41282–41293. doi: 10.1074/jbc.M306624200

Dimitroff, C. J., Laurent, F. C., and Barthel, S. R. (2013). *Galectin-Immunoglobulin Chimeric Molecules. USPTO 8598323.* US Patent. Available online at: https://patentimages.storage.googleapis.com/59/0b/ec/d534bba62ea4ca/US8598323.pdf

Earl, L. A., Bi, S., and Baum, L. G. (2011). Galectin multimerization and lattice formation are regulated by linker region structure. *Glycobiology* 21, 6–12. doi: 10.1093/glycob/cwq144

Forli, S., Huey, R., Pique, M. E., Sanner, M. F., Goodsell, D. S., and Olson, A. J. (2016). Computational protein-ligand docking and virtual drug screening with the AutoDock suite. *Nat. Protoc.* 11, 905–919. doi: 10.1038/nprot.2016.051

Gauto, D. F., Di Lella, S., Guardia, C. M. A., Estrin, D. A., and Martí, M. A. (2009). Carbohydrate-binding proteins: dissecting ligand structures through solvent environment occupancy. *J. Phys. Chem. B* 113, 8717–8724. doi: 10.1021/jp901196n

Gauto, D. F., Petruk, A. A., Modenutti, C. P., Blanco, J. I., Di Lella, S., and Mart,í, M. A. (2013). Solvent structure improves docking prediction in lectin-carbohydrate complexes. *Glycobiology* 23, 241–258. doi: 10.1093/glycob/cws147

Guardia, C. M., Caramelo, J. J., Trujillo, M., Méndez-Huergo, S. P., Radi, R., Estrin, D. A., et al. (2014). Structural basis of redox-dependent modulation of galectin-1 dynamics and function. *Glycobiology* 24, 428–441. doi: 10.1093/glycob/cwu008

Guardia, C. M. A., Gauto, D. F., Di Lella, S., Rabinovich, G. A., Martí, M. A., and Estrin, D. A. (2011). An integrated computational analysis of the structure, dynamics, and ligand binding interactions of the human galectin network. *J. Chem. Inf. Model.* 51, 1918–1930. doi: 10.1021/ci200180h

Harjacek, M., Diaz-Cano, S., De Miguel, M., Wolfe, H., Maldonado, C. A., and Rabinovich, G. A. (2001). Expression of galectins-1 and−3 correlates with defective mononuclear cell apoptosis in patients with juvenile idiopathic arthritis. *J. Rheumatol.* 28, 1914–1922.

Hirabayashi, J., Hashidate, T., Arata, Y., Nishi, N., Nakamura, T., Hirashima, M., et al. (2002). Oligosaccharide specificity of galectins: a search by frontal affinity chromatography. *Biochim. Biophys. Acta* 1572, 232–254. doi: 10.1016/S0304-4165(02)00311-2

Hirabayashi, J., and Kasai, K. (1993). The family of metazoan metal-independent beta-galactoside-binding lectins: structure, function and molecular evolution. *Glycobiology* 3, 297–304. doi: 10.1093/glycob/3.4.297

Horie, H., Inagaki, Y., Sohma, Y., and Kadoya, T. (2005). *Neuronal Growth Factor Galectin-1. USPTO 6890531.* US Patent. Available online at: https://patentimages.storage.googleapis.com/0c/98/54/7fe9239b69e10b/US6890531.pdf

Houzelstein, D., Gonçalves, I. R., Fadden, A. J., Sidhu, S. S., Cooper, D. N. W., Drickamer, K., et al. (2004). Phylogenetic analysis of the vertebrate galectin family. *Mol. Biol. Evol.* 21, 1177–1187. doi: 10.1093/molbev/msh082

Hsieh, T.-J., Lin, H.-Y., Tu, Z., Lin, T.-C., Wu, S.-C., Tseng, Y.-Y., et al. (2016). Dual hio-digalactoside-binding modes of human galectins as the structural basis for the design of potent and selective inhibitors. *Sci. Rep.* 6:29457. doi: 10.1038/srep29457

Hu, B., and Lill, M. A. (2014). WATsite: hydration site prediction program with PyMOL interface. *J. Comput. Chem.* 35, 1255–1260. doi: 10.1002/jcc.23616

Humphrey, W., Dalke, A., and Schulten, K. (1996). VMD: visual molecular dynamics. *J. Mol. Graphics* 14, 33–38. doi: 10.1016/0263-7855(96)00018-5

Lazaridis, T. (1998). Inhomogeneous fluid approach to solvation thermodynamics. 1. theory. *J. Phys. Chem. B* 102, 3531–41. doi: 10.1021/jp9723574

Levi, G., Tarrab-Hazdai, R., and Teichberg, V. I. (1983). Prevention and therapy with electrolectin of experimental autoimmune myasthenia gravis in rabbits. *Eur. J. Immunol.* 13, 500–507. doi: 10.1002/eji.1830130613

Levy, Y., Auslender, S., Eisenstein, M., Vidavski, R. R., Ronen, D., Bershadsky, A. D., et al. (2006). It depends on the hinge: a structure-functional analysis of galectin-8, a tandem-repeat type lectin. *Glycobiology* 16, 463–476. doi: 10.1093/glycob/cwj097

Liu, F.-T., and Rabinovich, G. A. (2010). Galectins: regulators of acute and chronic inflammation. *Ann. N. Y. Acad. Sci.* 1183, 158–182. doi: 10.1111/j.1749-6632.2009.05131.x

López, E. D., Arcon, J. P., Gauto, D. F., Petruk, A. A., Modenutti, C. P., Dumas, V. G., et al. (2015). WATCLUST: a tool for improving the design of drugs based on protein-water interactions. *Bioinformatics* 31, 3697–3699. doi: 10.1093/bioinformatics/btv411

Lujan, A. L., Croci, D. O., and Tudela, J. A. G. (2018). Glycosylation-dependent galectin–receptor interactions promote chlamydia trachomatis infection. *Proc. Natl. Acad. Sci. U.S.A.* 115, E6000–E6009. doi: 10.1073/pnas.1802188115

Modenutti, C., Gauto, D., Radusky, L., Blanco, J., Turjanski, A., Hajos, S., et al. (2015). Using crystallographic water properties for the analysis

and prediction of lectin-carbohydrate complex structures. *Glycobiology* 25, 181–196. doi: 10.1093/glycob/cwu102

Morris, G. M., Goodsell, D. S., Halliday, R. S., Huey, R., Hart, W. E., Belew, R. K., et al. (1998). Automated docking using a lamarckian genetic algorithm and an empirical binding free energy function. *J. Comput. Chem.* 19, 1639–1662. doi: 10.1002/(SICI)1096-987X(19981115)19:14<1639::AID-JCC10>3.0.CO;2-B

Nesmelova, I. V., Ermakova, E., Daragan, V. A., Pang, M., Menéndez, M., Lagartera, L., et al. (2010). Lactose binding to galectin-1 modulates structural dynamics, increases conformational entropy, and occurs with apparent negative cooperativity. *J. Mol. Biol.* 397, 1209–1230. doi: 10.1016/j.jmb.2010.02.033.

Nguyen, C. N., Young, T. K., and Gilson, M. K. (2012). Grid inhomogeneous solvation theory: hydration structure and thermodynamics of the miniature receptor cucurbit[7]uril. *J. Chem. Phys.* 137:044101. doi: 10.1063/1.4733951

Nishi, N., Abe, A., Iwaki, J., Yoshida, H., Itoh, A., Shoji, H., et al. (2008). Functional and structural bases of a cysteine-less mutant as a long-lasting substitute for galectin-1. *Glycobiology* 18, 1065–1073. doi: 10.1093/glycob/cwn089

Nivedha, A. K., Makeneni, S., Foley, B. L., Tessier, M. B., and Woods, R. J. (2014). Importance of ligand conformational energies in carbohydrate docking: sorting the wheat from the chaff. *J. Comput. Chem.* 35, 526–539. doi: 10.1002/jcc.23517

Nivedha, A. K., Thieker, D. F., Makeneni, S., Hu, H., and Woods, R. J. (2016). Vina-carb: improving glycosidic angles during carbohydrate docking. *J. Chem. Theory Comput.* 12, 892–901. doi: 10.1021/acs.jctc.5b00834

Offner, H., Celnik, B., Bringman, T. S., Casentini-Borocz, D., Nedwin, G. E., and Vandenbark, A. A. (1990). Recombinant human β-galactoside binding lectin suppresses clinical and histological signs of experimental autoimmune encephalomyelitis. *J. Neuroimmunol.* 28, 177–184. doi: 10.1016/0165-5728(90)90032-I

Rabinovich, G. A., Toscano, M. A., Jackson, S. S., and Vasta,G. R. (2007). Functions of cell surface galectin-glycoprotein lattices. *Curr. Opin. Struct. Biol.* 17, 513–520. doi: 10.1016/j.sbi.2007.09.002

Radosavljevic, G., Volarevic, V., Jovanovic, I., Milovanovic, M., Pejnovic, N., Arsenijevic, N., et al. (2012). The roles of galectin-3 in autoimmunity and tumor progression. *Immunol. Res.* 52, 100–110. doi: 10.1007/s12026-012-8286-6

Romero, J. M., Trujillo, M., Estrin, D. A., Rabinovich, G. A., and Di Lella S. (2016). Impact of human galectin-1 binding to saccharide ligands on dimer dissociation kinetics and structure. *Glycobiology*. 26, 1317–1327. doi: 10.1093/glycob/cww052

Sacchettini, J. C., Baum, L., G., and Brewer, C. F. (2001). Multivalent protein–carbohydrate interactions. a new paradigm for supermolecular assembly and signal transduction. *Biochemistry* 40, 3009–3015. doi: 10.1021/bi002544j

Santucci, L., Fiorucci, S., Rubinstein, N., Mencarelli, A., Palazzetti, B., Federici, B., et al. (2003). Galectin-1 suppresses experimental colitis in mice. *Gastroenterology* 124, 1381–1394. doi: 10.1016/S0016-5085(03)00267-1

Stowell, S. R., Cho, M., Feasley, C. L., Arthur, C. M., Song, X., Colucci, J. K., et al. (2009). Ligand reduces galectin-1 sensitivity to oxidative inactivation by enhancing dimer formation. *J. Biol. Chem.* 284, 4989–4999. doi: 10.1074/jbc.M808925200

Stowell, S. R., Karmakar, S., Stowell, C. J., Dias-Baruffi, M., McEver, R. P., and Cummings, R. D. (2007). Human galectin-1,−2, and−4 induce surface exposure of phosphatidylserine in activated human neutrophils but not in activated T cells. *Blood* 109, 219–227. doi: 10.1182/blood-2006-03-007153

St-Pierre, C., Ouellet, M., Giguère, D., Ohtake, R., Roy, R., Sato, S., et al. (2012). Galectin-1-specific inhibitors as a new class of compounds to treat HIV-1 infection. *Antimicrob. Agents Chemother.* 56, 154–162. doi: 10.1128/AAC.05595-11

Sturm, A., Lensch, M., Andr,é, S., Kaltner, H., Wiedenmann, B., Rosewicz, S., et al. (2004). Human galectin-2: novel inducer of t cell apoptosis with distinct profile of caspase activation. *J. Immunol.* 173, 3825–3837. doi: 10.4049/jimmunol.173.6.3825

Su, J., Cui, L., Si, Y., Song, C., Li, Y., Yang, T., et al. (2018a). Resetting the ligand binding site of placental protein 13/galectin-13 recovers its ability to bind lactose. *Biosci. Rep.* 38:BSR20181787. doi: 10.1042/BSR20181787

Su, J., Gao, J., Si, Y., Cui, L., Song, C., Wang, Y., et al. (2018b). Galectin-10: a new structural type of prototype galectin dimer and effects on saccharide ligand binding. *Glycobiology* 28, 159–168. doi: 10.1093/glycob/cwx107

Su, J., Song, C., Si, Y., Cui, L., Yang, T., Li, Y., et al. (2019). Identification of key amino acid residues determining ligand binding specificity, homodimerization and cellular distribution of human galectin-10. *Glycobiology* 29, 85–93. doi: 10.1093/glycob/cwy087

Swaminathan, G. J., Leonidas, D. D., Savage, M. P., Ackerman, S. J., and Acharya, K. R. (1999). Selective recognition of mannose by the human eosinophil charcot-leyden crystal protein (galectin-10): a crystallographic study at 1.8 a resolution. *Biochemistry* 38, 13837–13843. doi: 10.1021/bi990756e

Téllez-Sanz, R., García-Fuentes, L., and Vargas-Berenguel, A. (2013). Human galectin-3 selective and high affinity inhibitors. present state and future perspectives. *Curr. Med. Chem.* 20, 2979–2990. doi: 10.2174/09298673113209990163

Thiemann, S., and Baum, L. G. (2016). Galectins and immune responses—just how do they do those things they do? *Annu. Rev. Immunol.* 34, 243–264. doi: 10.1146/annurev-immunol-041015-055402

Vasta, G. R. (2009). Roles of galectins in infection. *Nat. Rev. Microbiol.* 7, 424–438. doi: 10.1038/nrmicro2146

Vértesy, S., Michalak, M., Miller, M. C., Schnölzer, M., André, S., Kopitz, J., et al. (2015). Structural significance of galectin design: impairment of homodimer stability by linker insertion and partial reversion by ligand presence. *Protein Eng. Des. Sel.* 28, 199–210. doi: 10.1093/protein/gzv014

Xibillé-Friedmann, D., Bustos Rivera-Bahena, C., Rojas-Serrano, J., Burgos-Vargas, R., and Montiel-Hernández, J. L. (2013). A decrease in galectin-1 (gal-1) levels correlates with an increase in anti-gal-1 antibodies at the synovial level in patients with rheumatoid arthritis. *Scand. J. Rheumatol.* 42, 102–107. doi: 10.3109/03009742.2012.725769

Yang, M.-L., Chen, Y.-H., Wang, S.-W., Huang, Y.-J., Leu, C.-H., Yeh, N.-C., et al. (2011). Galectin-1 binds to influenza virus and ameliorates influenza virus pathogenesis. *J. Virol.* 85, 10010–10020. doi: 10.1128/JVI.00301-11

Yang, R.-Y., Rabinovich, G. A., and Liu, F.-T. (2008). Galectins: structure, function and therapeutic potential. *Expert Rev. Mol. Med.* 10:e17. doi: 10.1017/S1462399408000719

Zhou, D., Ge, H., Sun, J., Gao, Y., Teng, M., and Niu, L. (2008). Crystal structure of the C-terminal conserved domain of human GRP, a galectin-related protein, reveals a function mode different from those of galectins. *Proteins* 71, 1582–1588. doi: 10.1002/prot.22003

Zou, J., Glinsky, V. V., Landon, L. A., Matthews, L., and Deutscher, S. L. (2005). Peptides specific to the galectin-3 carbohydrate recognition domain inhibit metastasis-associated cancer cell adhesion. *Carcinogenesis* 26, 309–318. doi: 10.1093/carcin/bgh329

Conflict of Interest: The authors declare that the research was conducted in the absence of any commercial or financial relationships that could be construed as a potential conflict of interest.

frontiers in Chemistry

REVIEW
published: 13 December 2019
doi: 10.3389/fchem.2019.00833

Glycan Microarrays as Chemical Tools for Identifying Glycan Recognition by Immune Proteins

*Chao Gao, Mohui Wei, Tanya R. McKitrick, Alyssa M. McQuillan, Jamie Heimburg-Molinaro and Richard D. Cummings**

Department of Surgery, National Center for Functional Glycomics, Beth Israel Deaconess Medical Center, Harvard Medical School, Boston, MA, United States

Glycans and glycan binding proteins (GBPs or lectins) are essential components in almost every aspect of immunology. Investigations of the interactions between glycans and GBPs have greatly advanced our understanding of the molecular basis of these fundamental immunological processes. In order to better study the glycan-GBP interactions, microscope glass slide-based glycan microarrays were conceived and proved to be an incredibly useful and successful tool. A variety of methods have been developed to better present the glycans so that they mimic natural presentations. Breakthroughs in chemical biology approaches have also made available glycans with sophisticated structures that were considered practically impossible just a few decade ago. Glycan microarrays provide a wealth of valuable information in immunological studies. They allow for discovery of detailed glycan binding preferences or novel binding epitopes of known endogenous immune receptors, which can potentially lead to the discovery of natural ligands that carry the glycans. Glycan microarrays also serve as a platform to discover new GBPs that are vital to the process of infection and invasion by microorganisms. This review summarizes the construction strategies and the immunological applications of glycan microarrays, particularly focused on those with the most comprehensive sets of glycan structures. We also review new methods and technologies that have evolved. We believe that glycan microarrays will continue to benefit the growing research community with various interests in the field of immunology.

Keywords: glycans, microarrays, glycoimmunology, glycan-binding proteins, immunology, immune receptors, immune proteins

OPEN ACCESS

Edited by:
Christoph Rademacher, Max Planck Institute of Colloids and Interfaces, Germany

Reviewed by:
Felix Broecker, Icahn School of Medicine at Mount Sinai, United States
Hiroaki Tateno, National Institute of Advanced Industrial Science and Technology (AIST), Japan

****Correspondence:***
Richard D. Cummings
rcummin1@bidmc.harvard.edu

Specialty section:
This article was submitted to Chemical Biology, a section of the journal Frontiers in Chemistry

Received: *20 September 2019*
Accepted: *15 November 2019*
Published: *13 December 2019*

Citation:
Gao C, Wei M, McKitrick TR, McQuillan AM, Heimburg-Molinaro J and Cummings RD (2019) Glycan Microarrays as Chemical Tools for Identifying Glycan Recognition by Immune Proteins. Front. Chem. 7:833. doi: 10.3389/fchem.2019.00833

INTRODUCTION

Immunology as a field is continuously evolving and expanding. With thousands of publications every year, it fundamentally impacts many aspects of biomedical sciences and has led to fascinating breakthroughs in a large number of biomedical areas, including primary immunodeficiencies, immunometabolism, neuroimmunology, mucosal immunology, cancer immunotherapy, and vaccine development. It is becoming increasingly clear that major components of our immune system include glycoproteins and recognition of glycans by glycan-binding proteins (GBPs) or lectins (Rabinovich et al., 2012; Colomb et al., 2019; Läubli and Varki, 2019; Pascoal et al., 2019; Taylor and Drickamer, 2019). These components are involved in all aspects of cellular recognition and signaling, both biological and pathological. Glycans are essential modulators in both innate and

adaptive immune systems. They are binding ligands for innate immune receptors, such as selectins, galectins, and Siglecs, many of which are targets for cancer immunotherapy (RodrÍguez et al., 2018). Glycans are also indirectly involved in the protein-protein interactions by contributing to protein conformations and oligomerization. Immune checkpoint molecules PD-1 (Okada et al., 2017) and PD-L1 (Li et al., 2018; Lee et al., 2019) are both heavily glycosylated, and the glycans are required for their normal interactions and subsequent suppression of T cell activities. In addition, human glycans are receptors of surface proteins of pathogens, such as bacteria, fungi and viruses that are involved in virtually all types of infectious disease processes (Li et al., 2017; Byrd-Leotis et al., 2019b).

Identifying the interactions between glycans and GBPs is, therefore, key to understanding the molecular mechanisms of these immunological events. There is a need for facile methods to study such interactions in a miniaturized and high throughput manner. A major breakthrough in this effort was the development of printed glycan microarrays (Fukui et al., 2002; Wang et al., 2002; Blixt et al., 2004; Geissner et al., 2019), which enable simultaneous binding analyses of GBPs to hundreds of glycan structures. The public availability of the glycan microarrays built by the Consortium for Functional Glycomics (www.functionalglycomics.org, CFG) facilitated the analyses of many GBPs in various aspects of immunology. With the technology developments at the National Center for Functional Glycomics (NCFG), these key immunological players have been re-examined with a larger variety of glycan sequences. This review introduces glycan microarray technologies from a historical point of view, summarizes the recent developments in the chemical and chemoenzymatic methods and new glycan microarrays with the focus on the CFG and NCFG approaches. We highlight the biological applications of glycan microarrays in immunology studies, and discuss current challenges and future perspectives of this technology.

HISTORICAL ASPECTS OF BINDING ASSAYS TO PROBE GLYCAN-GBP INTERACTIONS

Early efforts in the investigation of glycan-GBP interactions involved indirect methods such as hemagglutination inhibition and inhibition of precipitation assays. In these assays, free monosaccharides or oligosaccharides were tested as inhibitors against the binding between glycan-bearing substances, such as red blood cells or glycoprotein-containing extracts, and GBPs such as plant lectins and antisera. These methods led to the discovery of major blood group A, B, O (H) epitopes by Morgan and Watkins, and Kabat and colleagues between the 1950's and 1970's (Watkins, 2001). They have been adapted to different fields of biological research and are still widely used nowadays. For instance, hemagglutination inhibition assay is routinely used to determine the titer of antibodies against influenza viruses in human serum.

Solid phase direct binding assays were developed thereafter, in which GBPs were directly radio-labeled and the binding assays were performed on thin-layer chromatography (TLC). Breakthrough discoveries in this stage include the identification of GM1 as the ligand for cholera toxin (Magnani et al., 1980), the pancreatic cancer-associated biomarker CA19-9 (Magnani et al., 1982) and stage-specific embryonic antigens (Gooi et al., 1981; Kannagi et al., 1982, 1983). This method was superseded by EL'-based binding assays in which secondary proteins were enzyme-conjugated or fluorescently labeled. Glycans or glycopeptides labeled with biotin can be immobilized to wells of a microtiter plate pre-coated with streptavidin and directly assayed (Blixt et al., 2003; Alvarez and Blixt, 2006). This assay format enabled the comparison of the binding activities of dozens of glycans at the same time and is the prototype of glycan microarrays. The results revealed many features on the binding specificities of P- and L-selectin with PSGL-1 glycopeptide (Leppänen et al., 2002, 2003), and of galectin-1 (Leppänen et al., 2005).

One drawback of prior methods is that they required relatively large quantities of GBPs and often milligram levels of glycans. Due to their structural heterogeneity and complexity, the glycans cannot be easily acquired either by isolation and purification from natural sources, or by synthetic routes using chemical synthesis or chemoenzymatic synthesis. Moreover, the diversity of the glycan structures with sufficient amounts available for study is not comparable to the diversity of glycans in nature. It is estimated that the human glycome contains ∼3,000 glycan species or more on glycoproteins and glycolipids, and ∼4,000 theoretical pentasaccharide sequences on GAGs (Cummings, 2009) but only a small proportion of these sequences are currently available for bioactivity studies. Both of these factors highlight the demand for a microarray platform with structurally diverse glycans and minimal sample consumption, thus marks the era of glycan microarray.

Since their invention, glycan microarrays have become an essential tool in glycobiology, with increasing number and diversity of glycans and extremely small amounts of glycan consumption (Li and Feizi, 2018; Cummings, 2019). In particular, the glycan microarrays provided by NCFG and CFG not only revealed the fine binding specificities of known GBPs, they also helped in identification of novel GBPs and their novel biological activities through collaborative projects with investigators all over the world, which, altogether led to hundreds of published papers. The arrays have also served as a screening tool to provide investigators with leads to follow in subsequent assays that delve deeper into binding interactions between glycans and their immune protein of interest.

CHEMISTRY ASPECTS OF GLYCAN MICROARRAYS

The key step to creating glycan microarrays is to establish proper methods to immobilize the glycans onto the solid phase, via either non-covalent or covalent approaches. There have been extensive reviews discussing the available chemical methods for glycan immobilization (Fukui et al., 2002; Rillahan and Paulson, 2011; Park et al., 2013; Palma et al., 2014; Song et al., 2014, 2015).

The strategy taken by the CFG and NCFG to generate glycan microarrays is covalent attachment, which requires glycans to be covalently derivatized with a specific bi-functional chemical group that can subsequently be used to covalently react with a functionalized solid surface. Although glycans produced by *de novo* chemical or chemo-enzymatic synthesis are usually provided with a reactive handle to allow subsequent immobilization, free reducing glycans, such as milk oligosaccharides or natural glycans released enzymatically, need proper derivatization to enable quantification and attachment. The ability to label glycans from natural sources is of particular importance, as it allows the field to overcome the limitations of synthetic routes and vastly expand the repertoire of glycans that could be incorporated into the microarray platform. Due to the wide availability of N-hydroxysuccinimide (NHS) ester- or epoxy-derivatized glass slides, much effort has been devoted to the development of amine-containing bi-functional linkers, which can be coupled to the reducing end of the glycan and contains a reactive amine group to covalently attach to solid supports.

Development of Fluorescent Bi-Functional Linker

Initially, the commercially available 2,6-diaminopyridine (DAP) (Xia et al., 2005) was used to generate glycan-DAP conjugates (GDAPs) that are fluorescent and contain a primary aryl amine for immobilization (**Figure 1**). A wide variety of glycans were successfully converted to GDAPs which were reactive to NHS-activated surface, maleimide-activated protein, carboxylated microspheres and NHS-biotin, demonstrating the general utility of DAP for glycan labeling and glycan microarray construction. However, these DAP derivatives showed higher immobilization efficiency on epoxy slides compared to NHS-activated glass (Song et al., 2008). The low reactivity of the aromatic amine of DAP and the weak fluorescence restricted the utility of GDAPs.

Song et al. therefore developed another bifunctional fluorescent linker, 2-amino-N-(2-amino-ethyl)-benzamide (AEAB, **Figure 1**) (Song et al., 2009). AEAB selectively reacts with free reducing glycans through its aryl amine to form glycan-AEAB conjugates (GAEABs). The remaining primary alkyl amine is suitable for efficient immobilization on epoxy or NHS slides, and therefore makes it a great linker for glycan microarray construction. Moreover, due to its high fluorescence sensitivity and conjugation yield, AEAB is ideal for development of natural glycan microarrays or shotgun glycomics, whereby all types of glycans could be isolated from natural sources and be fluorescently-tagged, purified by multi-dimensional chromatography, quantified and eventually printed on glass slides to create natural glycan microarrays. With this approach, we developed a variety of sequence-defined and shotgun glycan microarrays, including a human milk glycan array, a microbial glycan microarray (MGM), sequence-defined and shotgun Schistosome glycan arrays, a pig lung N-glycan array and more recently, a sequence-defined NCFG array, a lectin QA/QC array and a human lung shotgun N-glycan array (Byrd-Leotis et al., 2019b).

It should be noted that another approach using 2-aminobenzamide (2-AB) and 2-aminobenzoic acid (2-AA) has also been developed, whereby glycans reductively labeled with 2-AB can be isolated by chromatography and then directly covalently coupled to epoxy-activated glass slides via secondary amine chemistry to generate 2-AB or 2-AA-glycan microarrays (de Boer et al., 2007; van Diepen et al., 2015). These approaches may be considered equivalent to the use of AEAB and DAP.

A major drawback of using DAP, AEAB, 2-AA, and 2-AB is that their conjugation reaction relies on reductive amination which, although highly efficient, opens the sugar ring at the reducing end monosaccharide (**Figure 1**). This destroys the reducing end integrity of the glycan (Prasanphanich et al., 2015) and potentially results in non-natural presentation of glycans on the array. This would affect the binding affinities of smaller glycans, and particularly those with modifications in the core region, such as core Fuc on N-glycans (Prasanphanich et al., 2015). We, therefore, have been developing new strategies to overcome this weakness while retain the merits mentioned above.

New Strategies to Display Sequence-Defined and Natural Glycans

F-MAPA

N-alkyl oxime can react with hemiacetal of reducing glycans and form intact closed-ring reducing end, thereby preserving the integrity of glycans. We have developed a reversible fluorescent linker F-MAPA, which contains an N-alkyl oxime active motif and an Fmoc protected alkyl amine (Wei et al., 2019). F-MAPA can efficiently derivatize reducing glycans via N-alkyl oxime mediated ligation and preserve the structure integrity (**Figure 2**). Fmoc serves as a transient fluorophore for monitoring and quantification, as well as a hydrophobic tag for glycan enrichment, separation and purification via C-18 solid phase extraction (SPE). Fmoc also can be easily removed to generate an active alkyl amine, enabling further manipulation and application of glycans for multiple purposes (e.g., glycan microarray, neoglycoprotein synthesis, etc.).

F-MAPA is more versatile than ordinary bi-functional linkers. It can be facilely cleaved under mild conditions, such as treatment by *N*-chlorosuccinimide (NCS) to regenerate free reducing glycans, which particularly facilitates glycomics and functional glycomics. This "catch and release" approach provided by F-MAPA enables selective enrichment of free reducing glycans from complex biological samples, which can be followed by mass spectrometry (MS)-based structural analysis upon release of the linker, and parallel microarray binding analysis upon release of Fmoc. Moreover, the successful recycling of the reaction system and synthesis of neoglycoprotein indicate that F-MAPA has great potential for industrial application in the synthesis of neoglycoprotein therapeutics and vaccines. The facile and scalable synthesis, high conjugation efficiency and operational simplicity of the derivatization reaction make the linker highly accessible to general research laboratories, thereby enabling general accessibility of glycan microarrays to the research community.

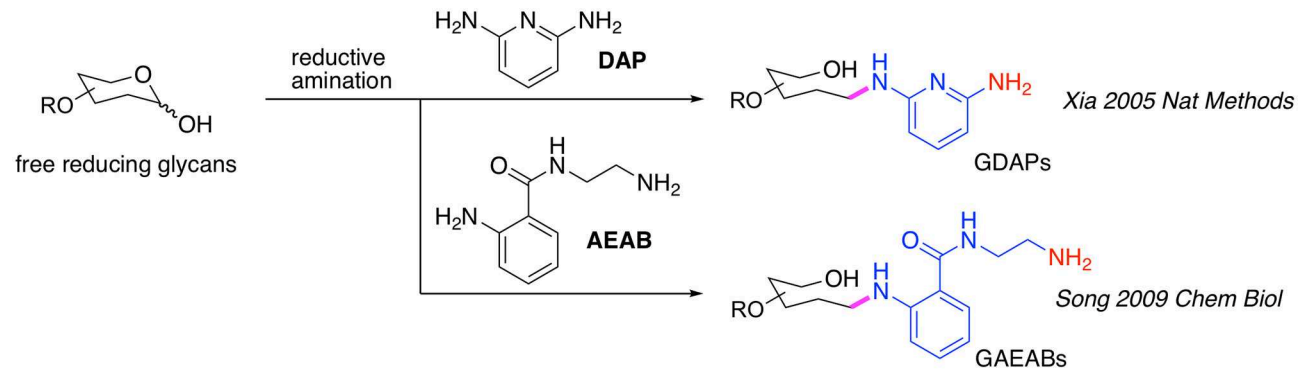

FIGURE 1 | Bifunctional fluorescent glycan linkers developed in the Cummings Lab.

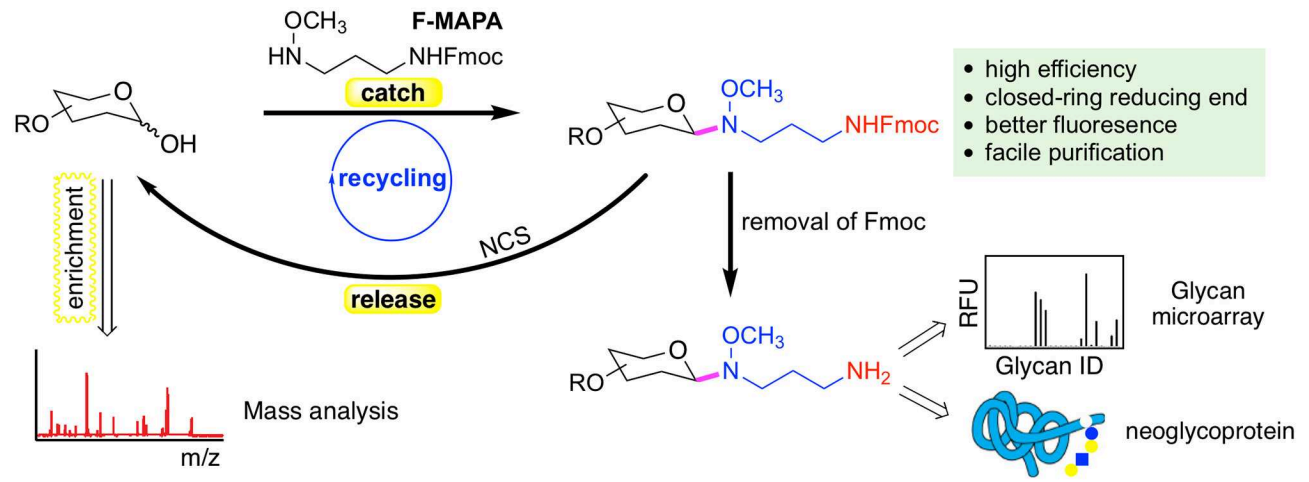

FIGURE 2 | A reversible fluorescent linker F-MAPA recently developed in the Cummings Lab. The linker enables highly efficient conjugation of glycans with their reducing end preserved. The Fmoc group in the F-MAPA linker renders strong fluorescence and hydrophobicity, both of which facilitates the purification. The Fmoc (fluorenylmethyloxycarbonyl) can be easily removed to support further manipulation and applications such as glycan microarrays and neoglycoprotein synthesis. The F-MAPA can also be cleaved upon treatment of *N*-chlorosuccinimide (NCS) to regenerate free reducing glycans. This figure is reprinted (adapted) with permission from Wei et al. (2019) Copyright 2019 American Chemical Society.

Fmoc-Labeled Asparagine

Because of the key consideration to preserve as much as possible the natural linkage of a glycan to its aglycone, e.g., amino acid, another approach we recently developed was the chemoenzymatic synthesis using a naturally occurring amino acid as the linker (Gao et al., 2019). Due to the structural complexity and heterogeneity, *de novo* chemical synthesis or isolation from natural sources had been intimidating for N-glycan production. Although chemoenzymatic synthesis has provided an alternative route, many of the methods rely on sophisticated chemical synthesis to produce the core structures to start with. These suffered from low yield and efficiency due to the usage of non-mammalian glycosyltransferases and poor substrates in which the aglycone potentially interferes with the reactivity. Moreover, evidence has shown that the linkers also play a role in microarray binding experiments (Padler-Karavani et al., 2012; Tessier et al., 2013; Grant et al., 2014).

As the natural N-glycan carrier, asparagine (Asn) guarantees the beta-configuration of the N-glycans, thus at least partially retains the natural presentation of N-glycans within context of N-glycopeptides. Asn-linked biantennary N-glycan core is abundant in chicken egg yolk. Fmoc can be selectively installed on the primary amine of the asparagine residue. Similar to F-MAPA, it renders strong fluorescence, adequate hydrophobicity and can be easily removed. The Asn-linked N-glycans have also been shown to be great substrates for enzymatic reactions. They are often quantitatively converted to products with the presence of mammalian glycosyltransferases.

Using this approach, we successfully synthesized a library of 32 multiantennary Asn-linked N-glycans and prepared the Asn-linked N-glycan array (designated N-glycan array). All of them are naturally occurring complex N-glycan structures found in human and other mammals. We will discuss the application of this glycan microarray in detail in the next section.

Future Directions in Linker Development

The Asn-linked chemoenzymatic approach holds great promise in expansion to more asymmetric complex N-glycan structures. In combination with specifically designed sugar donors, it is now possible to generate asymmetric multiantennary N-glycans without specially synthesized core structures in the initial steps, and thus can significantly reduce the difficulty in total chemical synthesis of N-glycans (Liu et al., 2019). We envisage that there will soon be N-glycan arrays with extremely complex structures available for function assays.

Versatile as it is, the F-MAPA does not contain a fluorophore on the backbone but rather, relies on the Fmoc protecting group attached to the primary amine. Thus, an extra step to remove Fmoc is needed prior to any further treatments. This also applies to the natural amino acid linker Asn. Therefore, it would be ideal to develop new linkers with fluorophores that do not require these additional steps.

One obstacle in studying glycan-GBP interaction is the potentially low affinity of some GBPs for certain types of glycans. In the natural state, the glycan-GBP interaction often occurs in a multivalent fashion, accomplished by clustered presentation of ligands and/or carbohydrate recognition domains. Many labs have, thus, developed natural protein or synthetic polymers to generate glycan microarrays (Maierhofer et al., 2007; Jayaraman, 2009; Huang et al., 2015; Mende et al., 2019). It would be beneficial to have easily accessible and facile technologies to generate linker-bearing scaffolds to achieve higher binding avidity in the future.

APPLICATION OF GLYCAN MICROARRAYS IN IMMUNOLOGY

With the above-mentioned chemical methods in position, we have generated glycan microarrays that encompass various types of glycan structures to facilitate the biological studies both from our group at the NCFG and through the use of the CFG glycan microarray by investigators world-wide. We summarize below a few with highlights on their applications in addressing key aspects of immunological studies.

Natural Ligands for Endogenous Immune Receptors

The innate immune system recognizes pathogens and self-antigens by endogenous receptors expressed on the surface of or secreted by immune cells. A large variety of these receptors have been identified, including Siglecs, galectins and C-type lectins. Typically, they recognize the pathogen-associated and damage-associated molecular patterns (PAMPs and DAMPs, respectively), as well as self-associated molecular patterns (SAMPs) and many of these interactions involve binding to carbohydrates. Due to their myriad of functions in anti-microbial defense and immune homeostasis, understanding of the fine binding specificities of these receptors is critical in our understanding of how the innate immune system responds selectively in the context of infections, autoimmunity and cancer.

Siglecs

Siglecs are a family of sialic acid-binding lectins that are mostly located on the surface of hematopoietic cells. They are involved in cell signaling and adhesion, and are particularly important in immune cell regulation (Bornhofft et al., 2018). There are 14 different Siglecs in the human genome. The detailed binding specificity of these Siglecs was mainly investigated in 2000's (Blixt et al., 2003; Campanero-Rhodes et al., 2006; Crocker et al., 2007) and early 2010's (Macauley et al., 2014) when only a limited number and diversity of glycans were available. Particularly, their binding preferences to sialic acid linkage in the context of N-glycans were not fully characterized due to a lack of paired multiantennary complex-type N-glycans. Therefore, we sought to take a systematic chemoenzymatic approach for N-glycan synthesis and address the specificities by microarray analyses.

We synthesized an array of Asn-linked isomeric multiantennary N-glycans with varying terminal non-reducing sialic acid, galactose, and N-acetylglucosamine residues, as well as core fucose (**Figure 3**). Using this microarray, and together with the sequence-defined glycan array from CFG, we investigated 11 human Siglecs, Siglec-1 to Siglec-11, and a rat-derived Siglec-4, all in human Fc chimera form, with particular focus on their binding to multiantennary N-glycans. As the affinity of Siglec-ligand interaction is generally thought to be low, we also performed the binding assays with Siglecs precomplexed with the secondary antibodies to increase the binding avidity.

Of the twelve Siglecs tested, only four showed binding to the N-glycan array (**Figure 3A**). Siglec-1 and-9 preferentially recognized glycans containing the determinant NeuAcα2-3Galβ1-4GlcNAc-, irrespective of the presence of core fucosylation (**Figure 3D**). The binding was independent of the branching patterns, but there was a clear trend that glycans with more α2,3-linked NeuAc elicited stronger signals. The binding of the two Siglecs without precomplex was comparable to or higher than with precomplex, suggesting that the affinities of Siglec-1 and-9 are high (**Figure 3A**). In contrast to Siglec-1 and-9, we observed that Siglec-2 and-10 both preferentially bound N-glycans terminating in α2,6-linked sialic acid, although some weak binding of Siglec-10 was detected to N-glycans with α2,3-linked sialic acid (**Figures 3C,D**). Preincubation with the secondary antibody significantly increased the binding intensity of Siglec-10, suggesting multivalency may be important to this protein (**Figure 3A**). This was also reflected by the observation that glycans containing higher numbers of branches (and thus more binding epitopes) elicited higher binding signals. Interestingly, no binding was detected with the other Siglecs on the N-glycan array, indicating their lack of recognition of N-glycans in these formats.

Collectively, our data indicates that sialylated, multiantennary N-glycans are potential endogenous receptors for Siglecs-1,-2,-9, and -10. These results shed lights on the biological functions of these Siglecs considering the potential high density of these natural N-glycan ligands on the cell surface.

In order to compare our results to those previously published, we tested the Siglecs on the CFG glycan microarray, one of the most comprehensive glycan microarray screening platforms. This array provides a great tool for researchers to determine if

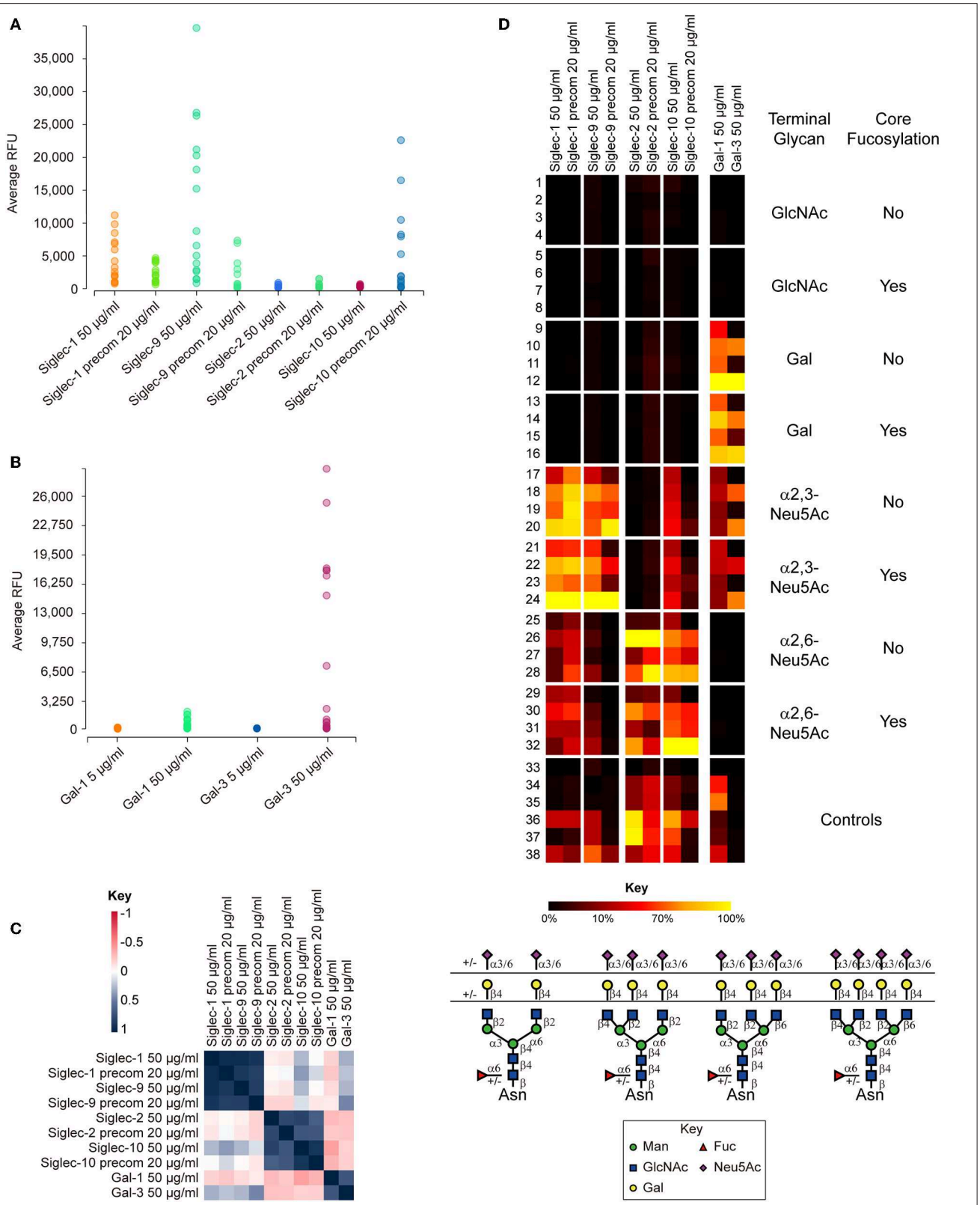

FIGURE 3 | Summary of the binding results of human Siglecs-1, -2, -9, -10, galectin-1 (Gal-1), and galectin-3 (Gal-3) on N-glycan microarray. **(A)** Binding RFUs of Siglecs tested at 50 μg/ml without precomplex with the secondary antibody, or at 20 μg/ml with precomplex to sixteen sialylated N-glycans on the microarray. **(B)**

(Continued)

FIGURE 3 | Binding RFUs of galectins tested at 5 or 50 μg/ml to all complex N-glycans on the array. Each colored bubble represents the binding signal elicited by one N-glycan. **(C)** Correlation of the overall binding results between samples on the N-glycan microarray. The Siglec-1 and 9, Siglec-2 and 10, Galectin-1 and -3 are segregated into three different groups, suggesting similar binding patterns found within each group. The key represents the correlation coefficiency between two samples. **(D)** Relative binding intensities of the Siglecs and galectins. The RFUs of the top binder of each protein was set 100% (colored in yellow). Color reflects the relative binding intensity relative to the strongest signal within the results of each protein. The N-glycans were grouped according to the structural features listed on right: GlcNAc, Gal, α2,3-Neu5Ac, and α2,6-Neu5Ac, without or with core Fuc. Within each subgroup, the glycans were listed according to the branching patterns in the order of biantennary, 224-triantennary, 226-triantennary and tetraantennary as shown at the bottom. The data was processed and presented by the GLAD toolkit (https://www.glycotoolkit.com/Tools/GLAD/) developed in house (Mehta and Cummings, 2019). precom, precomplex; RFU, relative fluorescent units; GLAD, GLycan Array Dashboard.

their protein of interest has glycan binding capabilities. The most current version of the CFG slides contains 585 unique, diverse mammalian-type glycans that are either synthetically made or chemoenzymatically modified. The glycans have amino linkers, of which there are twenty distinct structures, which are covalently attached to NHS-activated glass microscope slides. This array consists of a number of different classes of glycans that are common epitopes observed in biological interactions, among which there are 114 N-linked glycans with 28 sialylated species (summarized in **Table 1**).

Moderate to strong binding was observed with human Siglec-3,-6,-8,-9,-10, and -11, as well as the rat Siglec-4. The others human Siglecs including-1,-2,-4,-5, and -7 showed weak or no binding. Siglecs-8 and-9 showed binding toward α2,3-sialylic acid-containing sulfated glycans (**Figure 4**). Siglec-8 binding was extremely strong and exclusive to Neu5Acα2-3(6S)Galβ1-4GlcNAc-. This was in accordance with the data obtained with lipid-linked glycan arrays showing that the α2,3-linked sialic acid, and the 6-sulfation on the Gal, but not on the GlcNAc, is critical (Campanero-Rhodes et al., 2006), although the exact same sequence had not been available on that array. Consistent with the previous data (Campanero-Rhodes et al., 2006; Macauley et al., 2014), the top binder of Siglec-9 was 6-sulfo-sLeX (Neu5Acα2-3Galβ1-4(Fucα1-3)(6S)GlcNAc-). This protein also exhibited strong binding to α2,3-sialic acid-containing glycans that lack either sulfate or fucose, suggesting that sulfation and fucosylation may not be essential. Similar to our data on the N-glycan array, Siglec-10 showed binding to both α2,3- and α2,6-sialylated glycans, in particular, the N-glycolyl form, Neu5Gc. However, Siglec-10 binding to N-glycans on the CFG glycan microarray, albeit weak, showed preference to the α2,6-sialylated probes (**Figure 4**).

Despite the weak binding intensities, Siglec-2 showed binding to the α2,6-sialic acid-containing glycans, with or without sulfation (Neu5Acα2-6Galβ1-4(6S)GlcNAc- and Neu5Gcα2-6Galβ1-4GlcNAc-, **Figure 4**), which suggests the possibility that Siglec-2 can indeed bind similar structures presented on N-glycans.

We also observed novel specificities that have not been reported previously. Siglec-3 bound strongly to Neu5Acα2-3(6S)Galβ1-4GlcNAc- (**Figure 4**), which is different from the previously reported Neu5Acα2-6Galβ1-4GlcNAc-. It has been known that the human and mouse Siglec-4 bind the α2,3-sialylated core 1 (Neu5Acα2-3Galβ1-3GalNAc-). Our data suggest that both the human and rat Siglec-4 in fact bound Neu5Acα2-3Galβ1-3(6S)GalNAc- and Neu5Acα2-6(Neu5Acα2-3Galβ1-3)GalNAc- stronger (**Figure 4**), suggesting the requirement of the negatively charged group on the core GalNAc. In addition, Siglec-4 from both human and rat bound the α2,8-sialic acid terminating glycan, which has not been observed previously.

Notably, none of the N-glycans on the CFG glycan microarray were among the highest binders. This may be due to multiple factors. First, most of the multi-sialylated highly branched N-glycans (i.e., tri- and tetraantennary) on the CFG array contain a bisecting GlcNAc (**Table 1**), a key structural feature that may alter glycan conformation and prevent glycan recognition. Second, the synthetic 2-amino-methyl N,O-hydroxyethyl linker which was used to immobilize all of these tri- and tetraantennary fully sialylated N-glycans may cause suboptimal presentation of the binding determinants, in comparison to the Asn-linked N-glycans on new N-glycan array.

Galectins

Galectins are another key family of GBPs implicated in virtually all aspects of the immune system (Brinchmann et al., 2018; Elola et al., 2018; Robinson et al., 2019). Galectins are expressed in many cell types including those of squamous epithelia, gastrointestinal tract, adipocytes, immune cells, and even erythrocytes (Thiemann and Baum, 2016). They share a common carbohydrate recognition domain (CRD) composed of two extended antiparallel β-sheets that fold into a β-sandwich structure forming the binding pocket. While certain amino acids within the CRDs are highly conserved (termed common carbohydrate-binding cassette) supporting the interaction with galactose, the variations outside of the binding cassette determine the fine specificities of different galectins. Knowledge of the fine binding preference of galectins can help identify the glycoproteins bearing these structures which in turn, facilitate the design of reagents that could specifically promote or prevent galectin binding activity.

We and others previously profiled in detail the binding specificities of many galectins to various Gal-containing glycans ranging from small monosaccharides to poly-LacNAc-containing glycoconjugates, with or without modifications of sialic acid, sulfation and blood group antigens (Hirabayashi et al., 2002; Leppänen et al., 2005; Stowell et al., 2008, 2010; Song et al., 2009; Horlacher et al., 2010). As evidence showed that some galectins can accommodate sialic acid (Leppänen et al., 2005; Stowell et al., 2008) and the N-glycan preferences of these galectins were not clear, we analyzed galectin-1 and -3 as examples on the newly generated N-glycan array.

TABLE 1 | All of the sialylated N-glycans on the CFG array; α2,3- and α2,6-linked sialic acids are colored in blue and red, respectively.

ID	Glycan sequence
341	Neu5Acα2-6Galβ1-4GlcNAcβ1-2Manα1-6Manβ1-4GlcNAcβ1-4GlcNAcβ-Sp12
342	Neu5Acα2-6Galβ1-4GlcNAcβ1-2Manα1-3Manβ1-4GlcNAcβ1-4GlcNAcβ-Sp12
339	Neu5Acα2-6Galβ1-4GlcNAcβ1-2Manα1-6(Manα1-3)Manβ1-4GlcNAcβ1-4GlcNAcβ-Sp12
340	Manα1-6(Neu5Acα2-6Galβ1-4GlcNAcβ1-2Manα1-3)Manβ1-4GlcNAcβ1-4GlcNAcβ-Sp12
304	Neu5Acα2-6Galβ1-4GlcNAcβ1-2Manα1-6(GlcNAcβ1-2Manα1-3)Manβ1-4GlcNAcβ1-4GlcNAcβ-Sp12
297	Neu5Acα2-6Galβ1-4GlcNAcβ1-2Manα1-6(Galβ1-4GlcNAcβ1-2Manα1-3)Manβ1-4GlcNAcβ1-4GlcNAcβ-Sp12
315	Galβ1-4GlcNAcβ1-2Manα1-6(Neu5Acα2-6Galβ1-4GlcNAcβ1-2Manα1-3)Manβ1-4GlcNAcβ1-4GlcNAcβ-Sp12
55	Neu5Acα2-6Galβ1-4GlcNAcβ1-2Manα1-6(Neu5Acα2-6Galβ1-4GlcNAcβ1-2Manα1-3)Manβ1-4GlcNAcβ1-4GlcNAcβ-Sp12
56	Neu5Acα2-6Galβ1-4GlcNAcβ1-2Manα1-6(Neu5Acα2-6Galβ1-4GlcNAcβ1-2Manα1-3)Manβ1-4GlcNAcβ1-4GlcNAcβ-Sp21
57	Neu5Acα2-6Galβ1-4GlcNAcβ1-2Manα1-6(Neu5Acα2-6Galβ1-4GlcNAcβ1-2Manα1-3)Manβ1-4GlcNAcβ1-4GlcNAcβ-Sp24
314	Neu5Acα2-6Galβ1-4GlcNAcβ1-2Manα1-6(Neu5Acα2-3Galβ1-4GlcNAcβ1-2Manα1-3)Manβ1-4GlcNAcβ1-4GlcNAcβ-Sp12
320	Neu5Acα2-3Galβ1-4GlcNAcβ1-2Manα1-6(Neu5Acα2-3Galβ1-4GlcNAcβ1-2Manα1-3)Manβ1-4GlcNAcβ1-4GlcNAcβ-Sp12
321	Neu5Acα2-3Galβ1-4GlcNAcβ1-2Manα1-6(Neu5Acα2-6Galβ1-4GlcNAcβ1-2Manα1-3)Manβ1-4GlcNAcβ1-4GlcNAcβ-Sp12
474	Neu5Acα2-6Galβ1-4GlcNAcβ1-2Manα1-6(Neu5Acα2-6Galβ1-4GlcNAcβ1-2Manα1-3)Manβ1-4GlcNAcβ1-4(Fucα1-6)GlcNAcβ-Sp24
475	Neu5Acα2-3Galβ1-4GlcNAcβ1-2Manα1-6(Neu5Acα2-3Galβ1-4GlcNAcβ1-2Manα1-3)Manβ1-4GlcNAcβ1-4(Fucα1-6)GlcNAcβ-Sp24
452	Neu5Acα2-3Galβ1-4GlcNAcβ1-2Manα1-6(GlcNAcβ1-4)(Neu5Acα2-3Galβ1-4GlcNAcβ1-2Manα1-3)Manβ1-4GlcNAcβ1-4GlcNAcβ-Sp21
456	Neu5Acα2-6Galβ1-4GlcNAcβ1-2Manα1-6(GlcNAcβ1-4)(Neu5Acα2-6Galβ1-4GlcNAcβ1-2Manα1-3)Manβ1-4GlcNAcβ1-4GlcNAcβ-Sp21
478	Neu5Acα2-3Galb1-3GlcNAcβ1-2Manα1-6(GlcNAcβ1-4)(Neu5Acα2-3Galb1-3GlcNAcβ1-2Manα1-3)Manβ1-4GlcNAcβ1-4GlcNAcβ-Sp21
578	Neu5Acα2-3Galβ1-4GlcNAcb1-3Galβ1-4GlcNAcβ1-2Manα1-6(Neu5Acα2-3Galβ1-4GlcNAcb1-3Galβ1-4GlcNAcβ1-2Manα1-3)Manβ1-4GlcNAcβ1-4GlcNAcβ-Sp12
583	Neu5Acα2-6Galβ1-4GlcNAcb1-3Galβ1-4GlcNAcβ1-2Manα1-6(Neu5Acα2-6Galβ1-4GlcNAcb1-3Galβ1-4GlcNAcβ1-2Manα1-3)Manβ1-4GlcNAcβ1-4GlcNAcβ-Sp12
581	Neu5Acα2-6Galβ1-4GlcNAcb1-3Galβ1-4GlcNAcb1-3Galβ1-4GlcNAcβ1-2Manα1-6(Neu5Acα2-6Galβ1-4GlcNAcb1-3Galβ1-4GlcNAcb1-3Galβ1-4GlcNAcβ1-2Manα1-3)Manβ1-4GlcNAcβ1-4GlcNAcβ-Sp12
582	Neu5Acα2-3Galβ1-4GlcNAcb1-3Galβ1-4GlcNAcb1-3Galβ1-4GlcNAcβ1-2Manα1-6(Neu5Acα2-3Galβ1-4GlcNAcb1-3Galβ1-4GlcNAcb1-3Galβ1-4GlcNAcβ1-2Manα1-3)Manβ1-4GlcNAcβ1-4GlcNAcβ-Sp12
453	Neu5Acα2-3Galβ1-4GlcNAcβ1-4Manα1-6(GlcNAcβ1-4)(Neu5Acα2-3Galβ1-4GlcNAcβ1-4(Neu5Acα2-3Galβ1-4GlcNAcβ1-2)Manα1-3)Manβ1-4GlcNAcβ1-4GlcNAcβ-Sp21
457	Neu5Acα2-6Galβ1-4GlcNAcβ1-4Manα1-6(GlcNAcβ1-4)(Neu5Acα2-6Galβ1-4GlcNAcβ1-4(Neu5Acα2-6Galβ1-4GlcNAcβ1-2)Manα1-3)Manβ1-4GlcNAcβ1-4GlcNAcβ-Sp21
454	Neu5Acα2-3Galβ1-4GlcNAcβ1-6(Neu5Acα2-3Galβ1-4GlcNAcβ1-2)Manα1-6(GlcNAcβ1-4)(Neu5Acα2-3Galβ1-4GlcNAcβ1-2Manα1-3)Manβ1-4GlcNAcβ1-4GlcNAcβ-Sp21
458	Neu5Acα2-6Galβ1-4GlcNAcβ1-6(Neu5Acα2-6Galβ1-4GlcNAcβ1-2)Manα1-6(GlcNAcβ1-4)(Neu5Acα2-6Galβ1-4GlcNAcβ1-2Manα1-3)Manβ1-4GlcNAcβ1-4GlcNAcβ-Sp21
455	Neu5Acα2-3Galβ1-4GlcNAcβ1-6(Neu5Acα2-3Galβ1-4GlcNAcβ1-2)Manα1-6(GlcNAcβ1-4)(Neu5Acα2-3Galβ1-4GlcNAcβ1-4(Neu5Acα2-3Galβ1-4GlcNAcβ1-2)Manα1-3)Manβ1-4GlcNAcβ1-4GlcNAcβ-Sp21
459	Neu5Acα2-6Galβ1-4GlcNAcβ1-6(Neu5Acα2-6Galβ1-4GlcNAcβ1-2)Manα1-6(GlcNAcβ1-4)(Neu5Acα2-6Galβ1-4GlcNAcβ1-4(Neu5Acα2-6Galβ1-4GlcNAcβ1-2)Manα1-3)Manβ1-4GlcNAcβ1-4GlcNAcβ-Sp21

Linkers: Sp12 = Asparagine; Sp21 = -N(CH$_3$)-O-(CH$_2$)$_2$-NH$_2$; Sp24 = KVANKT.

Both of the galectins showed binding at 50 μg/mL (but not 5 μg/mL) to all of the LacNAc (Galβ1-4GlcNAc)-containing glycans, with or without core fucose (**Figures 3B,D**). Not surprisingly, the tetra-antennary N-glycans with four LacNAc sequences were most strongly bound. This observation, together with the absence of binding at lower protein concentration (**Figure 3B**), is reflective of the multivalent interactions of the two galectins with their glycan ligands. Our result clearly showed the tolerance of the two galectins to α2,3- but not to α2,6-linked sialic acid (**Figure 3D**), which has been reported in previous microarray studies using small glycan epitopes (Stowell et al., 2008) and cell-based assays (Patnaik et al., 2006; Stowell et al., 2008).

Moreover, our result identified the branching preference of galectin-1 and -3: the 2,2,4-form triantennary structures were always more strongly bound than the 2,2,6-isomeric triantennary counterparts; in galectin-3, the binding to 2,2,6-form triantennary structures was completely diminished (**Figure 3D**). This is a novel discovery in itself as MGAT5, the glycosyltransferase that initiates the β1,6-linked GlcNAc branch, was previously found to support the galectin-3 binding (Demetriou et al., 2001) on T-cells. Our results indicated that the expression of the 2,2,6-form triantennary N-glycan does not necessarily lead to the generation of the galectin-3 ligand. It is worth testing if the poly-LacNAc extension on either the 6- or the 4-linked arms affects galectin-3 binding.

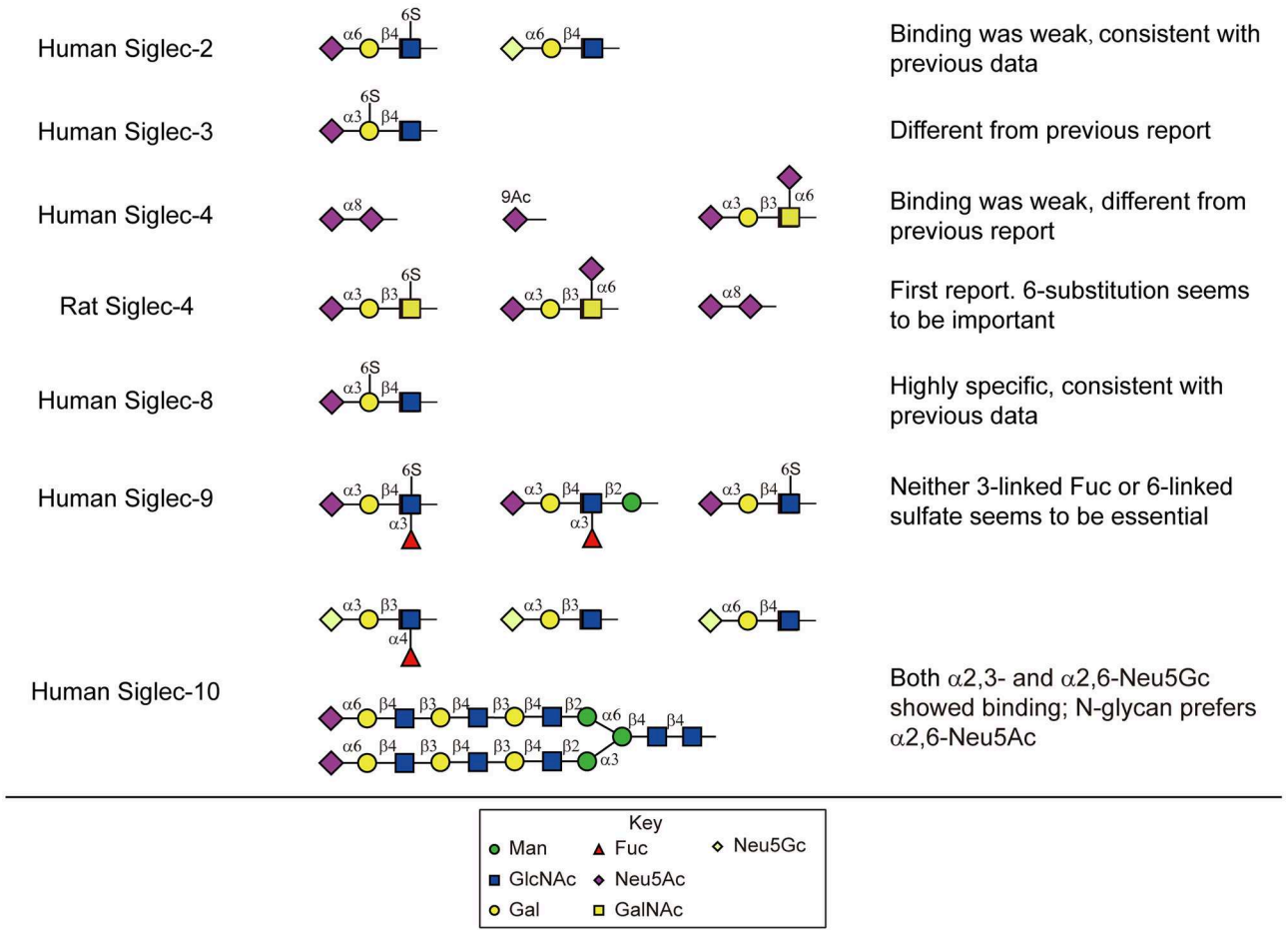

FIGURE 4 | Major sialylated binding motifs bound by human and rat Siglecs on the CFG array. These results were compared to the previous report summarized by the Macauley et al. (2014) and the comments were listed in the table.

It has been known that the human milk glycans (HMGs) are not significantly digested in the infant GI tract (Gnoth et al., 2000; Chaturvedi et al., 2001), besides lactose, which is typically digested prior to entering the small intestine. Thus, due to spatial correlation, HMGs can encounter and interact with galectins that are highly expressed locally. To explore these potential interactions, we took advantage of two glycan microarrays generated in house. One is a human milk shotgun glycan microarray containing 247 natural glycans purified from human milk, termed the HM-SGM array (Yu et al., 2014); the other is an array with defined, simple HMG structures, termed the HMG microarray. These arrays provide a unique collection of type 1 backbone (Galβ1-3GlcNAc)-containing glycans, which were underrepresented on other non-HMG glycan microarrays. All of the tested recombinant galectins, galectin-1,-3,-4,-7,-8, and -9, except for galectin-2, showed unique binding profiles on the HM-SGM array (**Table 2**). The majority of the binding signals were toward neutral glycan fractions or sialylated glycans with a non-sialylated branch (**Table 2**). These results were also corroborated by the HMG microarray and by isothermal titration microcalorimetry and hapten inhibition assays (Noll et al., 2016). This study extended these earlier observations and also identified more complex HMGs as additional targets of specific galectins.

Collectively, these data highlighted the distinct binding specificities of galectins against the human milk metaglycome (Cummings and Pierce, 2014). This may at least partially account for the fact that each galectin has more or less unique physiological activities.

In summary, glycan microarray-based technology is not only useful for comparing binding patterns of different GBPs to deduce their specificities, it also supports the identification and characterization of novel carbohydrate ligands of the endogenous immune receptors. This information sheds light on the identification of the corresponding glycoprotein counterreceptors, and the functional intervention of these interactions.

TABLE 2 | Major binding motifs bound by human galectins on the HMG array. Modified from Table II of Noll et al. (2016).

Protein	HMG binding motif(s)
Galectin-1	Galβ1-4GlcNAcβ1-6(Galβ1-3/4GlcNAcβ1-3)Galβ1-4Glc Galβ1-4GlcNAcβ1-6(Galβ1-3/4GlcNAcβ1-3)Galβ1-4GlcNAcβ1-
Galectin-3	Galβ1-4GlcNAcb1-3Galβ1-4GlcNAcb1-3Galβ1-4Glc
Galectin-4	Fucα1-2Galβ1-4GlcNAcb1-3Galβ1-4Glc Fucα1-2Galβ1-4GlcNAcb1-3Galβ1-4GlcNAcβ1-3
Galectin-7	Galβ1-3GlcNAcβ1-3Galβ1-4GlcNAcβ1-6(Galβ1-3GlcNAcβ1-3)Galβ1-4Glc
Galectin-8	Galβ1-4GlcNAcβ1-3Galβ1-4GlcNAcβ1-3Galβ1-4Glc
Galectin-9	Undefined neutral, nonfucosylated motif

Motifs are proposed structures based on manual inspection of HMG-260 microarray data and the known HMG structure(s) within the bound samples.

Discovery of Natural Glycan Ligands Involved in Infection and Microorganism Invasion

One major goal in the area of Functional Glycomics has been to identify naturally occurring host ligands for various microorganisms, which could help to understand their pathogenicity and infectivity. The CFG glycan array and other array platforms, such as the lipid-linked glycan array, have been used to study the glycan interactions with microorganisms such as bacteria and influenza viruses, as well as components of microorganisms that are important in various pathways of attachment and virulence, such as toxins, adhesins, and agglutinins (Childs et al., 2009; Liu et al., 2010; Petrova et al., 2016; Littler et al., 2017; Sun et al., 2018a; Yang et al., 2018). The glycan arrays, with both defined glycan structures as well as natural, undefined structures, have allowed for a deeper view of what glycan structures and classes play a role in the binding of relevant components or whole organisms.

As described above for galectins, the human milk glycan array has also been a critical tool for understanding microbial interactions, especially rotaviruses and influenza virus (Yu et al., 2012, 2014; Ashline et al., 2014; Hu et al., 2015; Sun et al., 2018a,b). We separated the soluble milk glycans into 247 different targets for printing on the array, which was one of the first instances of capturing all of the compounds of a "soluble glycome" for binding interaction purposes. Rotavirus VP domains were tested for their ability to bind, since rotaviruses are a main cause of gastrointestinal illness in infants and children. Interestingly, different VP proteins tested all bound to unique glycan structure subsets, many of which are believed to be non-metabolizable in the GI tract, leading to the hypothesis that these soluble glycans act as decoy receptors and prevent the rotavirus from attaching to the GI tract. These studies, in which the glycan arrays were a key tool, have been important to understanding the transmission and tropism of these viruses and the role that glycans play in the infection process.

Another example of the glycan array platform as a biochemical tool for ligand discovery has been the work with pig and human lung tissue for the main goal of searching for glycan ligands of influenza viruses. Sequence-defined glycan arrays have been utilized to assign the receptor-binding specificities of pandemic influenza viruses (H1N1) (Childs et al., 2009; Liu et al., 2010). Our initial studies focused on generating a "shotgun" or natural glycan microarray of the glycan materials isolated directly from pig lung tissue (Byrd-Leotis et al., 2014). This was the proof-of-concept that the tissue could be processed in such a way that the glycans could be isolated and printed for functional assays. Several 2,3- and 2,6-sialylated biantennary N-glycans were identified to be positively bound by influenza strains, which was an exciting development for studying endogenous glycan ligands. This led to the broad screening of various strains of influenza viruses, including these H3N2 strains that have progressively undergone "antigenic drift" in their head domains (Byrd-Leotis et al., 2019a) Surprisingly, the H3N2 drift strains almost completely lost their capacity in binding of canonical sialylated N-glycans on the sequence-defined N-glycan array (Byrd-Leotis et al., 2019a). Moreover, the discoveries with the pig lung glycan array opened the door to later studies with actual human lung tissue to search for endogenous receptors for influenza viruses (Byrd-Leotis et al., 2019b). Interestingly, it was discovered that many of the influenza viruses tested not only bound to sialylated structures, but also to phosphorylated glycans present in human lung tissue (Byrd-Leotis et al., 2019b). This novel finding will lead to brand new lines of study into viral pathogenesis and treatment options.

A complementary avenue to the "natural arrays" from human and other mammalian host tissues, is the generation of natural arrays from the microorganisms themselves. This strategy is important for being able to profile the innate and adaptive immune response toward the glycan-containing components of the organism. Our studies with *Schistosoma mansoni* and the human response to this parasitic infection led us to generate a natural shotgun N-glycan microarray from the schistosome egg glycoproteins (Mickum et al., 2016). The schistosome eggs, which were isolated from infected mice, were treated with PNGase F and A to isolate as many N-glycans as possible, separated and printed to create the arrays. These arrays, in conjunction with a defined schistosome-related glycan array (Luyai et al., 2014) were then interrogated with antibodies and sera from infected mammals. Both defined and shotgun arrays helped to define the FLDNF epitope (Fucα1-3GalNAcβ1-4(Fucα1-3)GlcNAc-), which was the target of a monoclonal antibody F2D2 derived from an infected mouse. Further, the arrays showed that the profile of the F2D2 antibody overlapped in distinct areas with infected rhesus monkeys and humans, leading to the presumption that the FLDNF glycan is a major antigenic target during schistosomiasis infections. The defined and shotgun array studies were complementary and informative, and helped to guide additional assays to characterize the immune response toward *S. mansoni* infection.

Characterization of Natural Human Anti-glycome

The characterization of the human anti-glycome has benefited from both broad and specific glycan microarrays. The CFG

microarray has been extensively utilized in studying the binding of GBPs including pathogenic toxins, intact viruses such as influenza and bacteria like *Escherichia coli*, various immune molecules including lectins and anti-carbohydrate antibodies (Blixt et al., 2004; Stowell et al., 2008; Hickey et al., 2010; Gulati et al., 2013; Jobling, 2016; Jones et al., 2016; Collins et al., 2017). As each array is conducted and data is collected, the results are published onto the CFG website, which is open to the public. This database is an invaluable resource for the glycobiology community, as it can inform researchers on which data has already been collected and point researchers in the right direction for additional experiments. Another useful resource produced by the CFG to screen mammalian GBPs is the Microbial Glycan Microarray (MGM). The most recent version of the array consists of 313 glycan targets from the polysaccharide material derived from different bacterial strains such as *E. coli, Proteus mirabilis, Pseudomonas aeruginosa, Providencia alcalifaciens, Providencia rustigianii, Providencia stuartii, Shigella boydii*, and *Shigella dysenteriae* (Bunker et al., 2017). These bacterial strains were largely provided by Dr. Yuri Knirel's group at the ND Zelinsky Institute of Organic Chemistry in Moscow, Russia. The bacterial polysaccharides presented on this array are coupled to NHS-activated glass microscope slides. Another microbe-focused glycan array has recently been developed by Seeberger group (Geissner et al., 2019). Complementary to the natural glycan approach, this new glycan array was generated by combining a variety of synthetic strategies. Together with the large collection of accumulated glycans from previous studies, the Max Planck Society (MPS) glycan library now contains more than 300 unique structures, making it one of the largest collections of microbial glycans. All of these microarray platforms have provided a unique resource to decipher the roles that certain proteins and antibodies (Bunker et al., 2017) may be playing in innate and adaptive immune detection of microbial carbohydrates.

Considering that the compounds for both of the CFG and MGM microarrays are limited in their quantity and accessibility, other defined arrays have been made using several classes of synthetic glycans such as α-glucans, β-glucans, xyloglucans, chitins, lacto-, globo-, and sialyl-series, gangliosides, blood groups A/B/O, Forssman and P antigen, Lewis antigen, Galα1-3R/Galili antigens, HNK1/GlcA, isoglobo, asialo-ganglio series, N-glycans and O-glycans. Many of these glycans have been shown to have biological relevance, and can be used for larger scale screenings. The NCFG has developed many of these arrays that are accessible to the public and is anticipated to serve as a key screening tool that is complementary to the CFG glycan array.

Each of these glycan microarrays has been used to characterize the specificity of human anti-glycan antibodies. Pooled IgG from healthy donors and IVIG (von Gunten et al., 2009; Schneider et al., 2015) have been profiled on a variety of different microarray platforms and have revealed a large diversity of anti-glycan antibody repertoires, including antibodies specific for cellulose and monosaccharides (Schwarz et al., 2003). Individual serum has been tested from healthy individuals (Muthana and Gildersleeve, 2016) as well as in HIV positive individuals (Scheepers et al., 2017) from the array platforms generated by Gildersleeve's group (see discussion in section Other Approaches in Glycan Microarray Generation). We have also surveyed the anti-carbohydrate antibody repertoire (ACAR) of 105 healthy donors, ranging from 20 to 60+ years old on the NCFGv1 array (Luetscher et al. in review). We discovered that the antibody profiles found within these individuals are relatively unique, with each individual displaying their own anti-carbohydrate signature. Additionally, we found that there are several glycan antigens that are highly immunogenic, with most individuals containing antibodies, which recognize the Forssman antigen, chitins and β-glucans. While it is difficult to compare certain aspects of the results of our study with Muthana and Gildersleeve (2016), as the glycan presentation and array platforms are not directly comparable, there were several common patterns of recognition by antibodies in both populations assayed. The NCFGv1 array has also been used to screen a cohort of Ugandan individuals with chronic exposure to *Mycobacterium tuberculosis* (Mtb), however these individuals never progress to active disease or result in a positive Mtb test. These resistant individuals were profiled for their anti-glycan antibody response, and compared to individuals with active and latent Mtb infections. The results of the NCFGv1 antibody profile from these distinct cohorts were indistinguishable, meaning that the resisters did not possess an anti-glycan antibody response that differed from active and latent patients. However, the data in its entirety has suggested that individuals resistant to Mtb infection have a unique and distinctive adaptive immune profile against Mtb specifically, although their deficiency in antibody response to carbohydrate antigens was eliminated by our results from the NCFGv1 array (Lu et al., 2019).

Understanding the repertoires of anti-glycan antibodies detected by glycan microarray analysis is important, and can be used to identify immunogens for glycoconjugate vaccines. This has been demonstrated by the development of glycan-based vaccines toward *Clostridium difficile* (Martin et al., 2013a,b), in which fragments of surface glycan PS-I were chemically synthesized and examined by microarray analyses with patient samples to identify the minimal antigenic epitopes. These candidates were coupled to carriers and yielded potent antigenic response in a mouse model.

Plant Lectins and Antibodies as Essential Tools for Probing Sequence-Specific Glycans

Plant lectins and anti-glycan antibodies are essential tools in biological studies. The binding profiles of common plant lectins, which are naturally occurring GBPs, are very well-studied and they are vital for researchers identifying and characterizing specific glycan epitopes. Therefore, lectins are often used as sequence-specific controls in microarray assays.

Targeted glycan arrays have allowed for discovery of new information on the binding profiles of these already well-characterized lectins. For example, plant lectins have been utilized in detecting N-glycans based on what is currently known about their binding profiles. However, information on the exact relationship between the lectins and N-glycan variants is limited due to a lack of a variety of these structures on

arrays. Using the new 32 N-Glycan Array created by Gao et al. (2019), each individual lectin was seen to have preferences for different N-glycan structures. Wheat germ agglutinin (WGA) and *Lens culinaris* agglutinin (LCA) bound the biantennary and 2,2,6- triantennary forms but not to the 2,2,4-counterparts or tetra-antennary N-glycans, which suggests that these lectins prefer branching; among the N-glycan backbone-binding lectins, only LCA, *Pisum sativum* agglutinin (PSA), and Concanavalin A (ConA) can accommodate both the α2,3- and α2,6-linked sialic acid. Other lectins, such as WGA, *Phaseolus vulgaris* erythroagglutinin (E-PHA), *Phaseolus vulgaris* leukoagglutinin (L-PHA), and *Datura stramonium* agglutinin (DSA) can only accommodate the α2,3-sialic acid (Gao et al., 2019). This level of detailed information was not previously known. Demonstrating these kinds of observable differences between binding to branched, core, and other modified glycans validates the necessity of expanding the repertoire of glycans available. With access to a number of slightly modified and varied structures, we can uncover new binding capabilities of lectins and expand upon the knowledge available about the lectin binding motifs.

As noted above, anti-glycan antibodies can be characterized on the array platforms, and many have been studied over the years on the CFG glycan array (Agrawal-Gamse et al., 2011; Zipser et al., 2012; Noble et al., 2013; Falkowska et al., 2014; Chua et al., 2015; Mickum et al., 2016; Tati et al., 2017; Nkurunungi et al., 2019), such as characterization of a new Lewis x antibody (Mandalasi et al., 2013) and multiple iterations of an anti-Tn antigen antibody (Chaturvedi et al., 2008; Tati et al., 2017). While antibody specificities are not the main focus of this review, it is clear from past work that the glycan microarrays have been and will continue to be very useful tools for their characterization, especially as the glycans and the types of linkers diversify.

Glycan Array as a Platform for Developing Lamprey-Derived Smart Anti-glycan Reagents (SAGRs)

While glycan microarrays have been an essential tool for determining the specificity of a particular GBP, recently we have developed an alternative use of the technology to isolate and enrich for anti-glycan monoclonal antibodies. We have recently reported that the sea lamprey, *Petromyzon marinus*, generates a broad repertoire of anti-glycan antibodies in response to immunization with a variety of cell lines and biological tissues (McKitrick et al., in review). In contrast to the gnathostomes which produce antibodies made of immunoglobulin domains, the agnathans or jawless vertebrates, utilize a class of proteins constructed with leucine rich repeat motifs called Variable Lymphocyte Receptors (VLRs) as antigen receptors (Pancer et al., 2004; Alder et al., 2005, 2008; Boehm et al., 2018). These single-chain antibodies are produced and secreted by the VLRB lymphocyte lineage, and several groups have discovered and characterized monoclonal VLRB proteins that are specific for distinct carbohydrate structures (Han et al., 2008; Hong et al., 2013; Luo et al., 2013; Collins et al., 2017).

In order to utilize the VLRB proteins as traditional reagents in a laboratory setting, one must identify and enrich for VLRBs of a defined specificity and subsequently express them in a soluble form. To accomplish this, we as well as others have expressed the repertoire of VLRB proteins in a yeast surface display (YSD) platform (Xu et al., 2011; Velásquez et al., 2017; McKitrick et al., in review). We have then developed the methodology to incubate the VLRB expressing YSD library onto the glycan microarrays, where the VLRB antibodies will bind to the arrays in an antigen specific manner. The bound yeast colonies can then be transferred to solid media via replica plating, where monoclonals can be sequenced and screened individually for specificity (McKitrick et al., in review; McKitrick et al., accepted). Clones of interest are then expressed as a VLRB-Fc chimeric soluble protein, which we are calling Smart Anti-Glycan Reagents (SAGRs), and can be used for most routine research applications such as ELISA, western blotting etc. Thus, by combining YSD and glycan microarray technology, we have developed a high throughput methodology for the isolation and enrichment of glycan-specific reagents, which will greatly enhance the field of glycobiology.

OTHER APPROACHES IN GLYCAN MICROARRAY GENERATION

Diversity of Glycan Microarray Platforms

In addition to the widely used amine-based coupling method, other covalent attachment approaches have also been explored. One of the arrays that encompasses a large number of glycans is from the Gildersleeve group at NIH, in which glycans were covalently linked to a carrier protein bovine serum albumin (BSA) in the form of neoglycoproteins (Manimala et al., 2006). These glycoconjugates can be directly printed onto epoxy slides. The key feature of this array platform is multivalent presentation, which is similar to how natural glycans are found on glycoproteins. With a total of 60 amines, BSA has 54 that are expected to be solvent exposed (Oyelaran et al., 2009) and are fairly evenly distributed on the protein surface. The density of glycans on BSA can be controlled to some extent so that it becomes a multivalent scaffold to present glycans in a clustered or multivalent format to achieve high binding avidity. Thus, a neoglycoprotein-based glycan microarray has been developed and used in multiple studies, including the characterization of lectins (Luo et al., 2013) and monoclonal antibodies (Gildersleeve and Wright, 2016; Trabbic et al., 2019). In a recent screening of anti-glycan antibodies in the sera of pancreatic cancer patients, a glycan microarray containing 407 glyco-epitopes was generated and probed with sera from patients immunized with a whole cell vaccine. Antibody response was detected against many glycans including tumor-associated glycans, blood group antigen and α-Gal epitope (Xia et al., 2016). The anti-α-Gal antibodies, in particular, were inversely correlated with the overall survival rate and thus could be used as a potential biomarker to evaluate the immune responses to the vaccine.

In addition to the covalent methods, non-covalent attachment methods have also been developed and become the foundation of another comprehensive glycan microarray platform. Feizi and colleagues attached glycans to phospholipid carriers via reductive amination or oxime ligation (Tang et al., 1985;

Chai et al., 2003; Liu et al., 2007; Li and Feizi, 2018). The products, neoglycolipids (NGLs) have hydrophobic lipid tails which facilitate immobilization on hydrophobic surfaces such as nitrocellulose through non-covalent hydrophobic interaction. This binding was so strong that the NGLs cannot be washed away by aqueous solution in microarray assays. Moreover, NGLs can be conveniently incorporated into liposomes supporting a clustered presentation. These NGL-carrying liposomes also enable microarray printing in aqueous solutions rather than in volatile solvents.

Since the generation of the first NGL-based glycan microarray (Fukui et al., 2002), the number and diversity of glycans in the libraries have been steadily growing (Palma et al., 2006; Gao et al., 2014; Li et al., 2017). Now there are more than 800 probes in their sequence-defined glycan microarray, making it one of the world largest resources (Li and Feizi, 2018). One of the recent applications of the NGL-based glycan microarray is the "Beam Search" which is an activity-chasing approach. In this effort, a minor O-glycan component from mucin-type glycoproteins was pinpointed and characterized as the binding ligand for rotaviruses (Li et al., 2017).

New Concepts and Approaches in Glycan Microarray

Luminex/Multiplex Assays

As mentioned above, the glass slide-based glycan microarrays enable screening of GBPs against hundreds of structurally diverse glycans with minimal sample consumption. However, the traditional form of glycan microarrays on microscope glass slides is inconvenient in simultaneous analyses of multiple GBPs. Under different settings, one can probably investigate dozens (typically < 32) of samples in parallel. As a screening method, the glass slide-printed microarrays do not allow for analyses of large numbers (hundreds) of samples in a high-throughput manner. Recently, She et al. developed a multiplex glycan bead array platform based on the Luminex technology (Purohit et al., 2018). Each Luminex bead contains a unique fluorescent label among 500 labels that can be distinguished by the instrument. The binding assays can be easily performed in microwell plates, meaning the platform has the potential to simultaneous analyze 384 samples against up to 500 glycans in a single assay. The assembled bead array contained over 100 covalently attached glycans and was used in the studies of plant lectins, anti-glycan antibodies and human sera. Given the high-throughput and the prevalence of the Luminex instrument, this method could be adopted in clinical settings and benefit larger research and clinical community.

DNA-Coded Arrays

Several DNA-based glycan arrays have been generated (Chevolot et al., 2014; Yan et al., 2019). For example, Song et al. developed a DNA-coded glycan microarray platform by attaching glycans with DNA sequences and adopting next-generation sequencing (NGS) as the decoding method (Yan et al., 2019). Each glycan was tagged with a unique, defined oligonucleotide sequence. A library of DNA-coded glycans were mixed in a single vial, incubated with a biologically relevant GBP, then "pull down" bound glycans by microsphere beads immobilized with secondary antibody. For cells or intact microorganisms, bound glycans were "pulled down" by direct centrifugation. The DNA codes on bound glycans were sequenced by NGS, and the copy numbers of DNA codes represent relative binding intensities of the corresponding glycan structures. This microarray platform allows high throughput assays and the solution-phase binding assay is directly applicable to identifying glycan binding to intact cells (Yan et al., 2019).

Cell-Based Arrays

A cell-based platform has been reported in characterization of the structure of glycan ligands (Nonaka et al., 2014). A similar but more powerful and comprehensive approach was taken by Clausen and Yang's groups at the Copenhagen Center for Glycomics, where they developed a methodology to display the glycans on the surface of HEK293 or CHO cells. The overall approach has been to develop a panel of cell lines, genetically engineer to express a substantial portion of the human glycome (Narimatsu et al., 2019) and glycosaminoglycan or GAGome (Chen et al., 2018). Using a rather elegant combination of CRISPR/Cas9 knock-in and knock-outs of human glycosyltransferases (Narimatsu et al., 2018), the authors were able to drive the expression of unique glycan structures onto the cell surface glycoproteins. These panels of cell lines were then used to investigate the binding specificity of Siglecs, influenza viruses and Streptococcus adhesion proteins by flow cytometry. There are several advantages to using this approach, of particular note is the glycans on the cell surface are presented in the context of a fully folded protein, which is closest to their most native confirmation. In addition, upon identification of the binding profile of a given GBP, the full sequence of glycosyltransferases that are required to build the structure interacting with the GBP is also known, which provides a level of information that may not be given by the printed glycan microarrays. The authors have also developed the technology to secrete the glycans into the culture media, using the amino derivative XylNap,2-(6-((3-aminopropyl)oxy)-naphthyl)β-d-xylopyranoside ($XylNapNH_2$) (Chen et al., 2018). Ultimately, the glycans are amine functionalized, and can be used for direct immobilization onto a microarray surface.

CONCLUSIONS

As a robust high-throughput and high-content screening platform, glycan microarray represents a unique tool to define protein-glycan interactions in immunological studies. Glycan microarrays require minute amount of glycans that can be assayed with low background and high specificity. They enable functional screening and comparison in binding specificity of GBPs including antibodies, proteins, and viruses. Glycan microarrays provide information on both positively and negatively bound glycan structures which is particularly informative when placed in the relevant biological context.

Under current parameters, glycan microarray analyses cannot provide solutions to all scientific demands. For instance,

this platform is not suitable for quantitative studies such as determining the binding constants. Several technical details are also yet to be addressed, and array robustness is related to the number and diversity of the printed compounds. The printing efficiency is generally low due to the efficiency in the underlying chemical reaction. The density and the presentation have also been shown to have a variable impact on the glycan interactions, and there may be cases where in-solution assays are more appropriate. Nonetheless, we and other groups have made many biologically important observations and advancements through glycan microarray interaction studies.

The glycan microarrays represent a *hypothesis-generating discovery tool* that can be effectively used to screen many types of immune proteins against hundreds of glycans simultaneously and provide leads to further experiments into these interactions. Sequence-defined and Shotgun microarrays are well complemented from distinct aspects of biological research: shotgun glycan arrays capture natural glycans that cannot be synthesized for defined arrays, sequence-defined glycan arrays corroborate the discovery made by shotgun glycan arrays. Therefore, they serve as a first-line screening that can guide further experimentation. An enormous amount of information can be gained from the array binding experiments themselves, especially if multiple types of arrays are utilized in a comparative fashion. They can also be coupled with creative steps such as enzyme treatments of the glycans, hapten inhibition, titration curves, and mutant proteins to obtain next-level binding characteristics. With increased sensitivity and throughput and the development of new formats including beads-based, cell-based and DNA-coded, glycan microarrays are now playing more and more important roles in discovering new GBPs and defining their essential functions in the host and microbiome interactome and in the immune system.

AUTHOR CONTRIBUTIONS

CG, MW, TM, AM, JH-M, and RC contributed to the writing and editing of the final review.

FUNDING

The authors acknowledge NIH grant P41GM103694 for support.

ACKNOWLEDGMENTS

The authors would like to thank Dr. Akul Mehta for help with the GLAD software program.

REFERENCES

Agrawal-Gamse, C., Luallen, R. J., Liu, B., Fu, H., Lee, F. H., Geng, Y., et al. (2011). Yeast-elicited cross-reactive antibodies to HIV Env glycans efficiently neutralize virions expressing exclusively high-mannose N-linked glycans. *J. Virol.* 85, 470–480. doi: 10.1128/JVI.01349-10

Alder, M. N., Herrin, B. R., Sadlonova, A., Stockard, C. R., Grizzle, W. E., Gartland, L. A., et al. (2008). Antibody responses of variable lymphocyte receptors in the lamprey. *Nat. Immunol.* 9:319. doi: 10.1038/ni1562

Alder, M. N., Rogozin, I. B., Iyer, L. M., Glazko, G. V., Cooper, M. D., and Pancer, Z. (2005). Diversity and function of adaptive immune receptors in a jawless vertebrate. *Science* 310, 1970–1973. doi: 10.1126/science.1119420

Alvarez, R. A., and Blixt, O. (2006). Identification of ligand specificities for glycan-binding proteins using glycan arrays. *Meth. Enzymol.* 415, 292–310. doi: 10.1016/S0076-6879(06)15018-1

Ashline, D. J., Yu, Y., Lasanajak, Y., Song, X., Hu, L., Ramani, S., et al. (2014). Structural characterization by MSn of human milk glycans recognized by human rotaviruses. *Mol. Cell. Proteom.* 13, 2961–2974. doi: 10.1074/mcp.M114.039925

Blixt, O., Collins, B. E., van den Nieuwenhof, I. M., Crocker, P. R., and Paulson, J. C. (2003). Sialoside specificity of the siglec family assessed using novel multivalent probes: identification of potent inhibitors of myelin-associated glycoprotein. *J. Biol. Chem.* 278, 31007–31019. doi: 10.1074/jbc.M304331200

Blixt, O., Head, S., Mondala, T., Scanlan, C., Huflejt, M. E., Alvarez, R., et al. (2004). Printed covalent glycan array for ligand profiling of diverse glycan binding proteins. *Proc. Natl. Acad. Sci. U.S.A.* 101, 17033–17038. doi: 10.1073/pnas.0407902101

Boehm, T., Hirano, M., Holland, S. J., Das, S., Schorpp, M., and Cooper, M. D. (2018). Evolution of alternative adaptive immune systems in vertebrates. *Annu. Rev. Immunol.* 36, 19–42. doi: 10.1146/annurev-immunol-042617-053028

Bornhofft, K. F., Goldammer, T., Rebl, A., and Galuska, S. P. (2018). Siglecs: a journey through the evolution of sialic acid-binding immunoglobulin-type lectins. *Dev. Comp. Immunol.* 86, 219–231. doi: 10.1016/j.dci.2018.05.008

Brinchmann, M. F., Patel, D. M., and Iversen, M. H. (2018). The role of galectins as modulators of metabolism and inflammation. *Mediators Inflamm.* 2018:9186940. doi: 10.1155/2018/9186940

Bunker, J. J., Erickson, S. A., Flynn, T. M., Henry, C., Koval, J. C., Meisel, M., et al. (2017). Natural polyreactive IgA antibodies coat the intestinal microbiota. *Science* 358:eaan6619. doi: 10.1126/science.aan6619

Byrd-Leotis, L., Jia, N., Dutta, S., Trost, J. F., Gao, C., Cummings, S. F., et al. (2019b). Influenza binds phosphorylated glycans from human lung. *Sci. Adv.* 5:eaav2554. doi: 10.1126/sciadv.aav2554

Byrd-Leotis, L., Liu, R., Bradley, K. C., Lasanajak, Y., Cummings, S. F., Song, X., et al. (2014). Shotgun glycomics of pig lung identifies natural endogenous receptors for influenza viruses. *Proc. Natl. Acad. Sci. U.S.A.* 111, E2241–2250. doi: 10.1073/pnas.1323162111

Byrd-Leotis, L. Gao, C., Jia, N., Mehta, A., Trost, J., Cummings, S. F., Heimburg-Molinaro, J., et al. (2019a). Antigenic pressure on H3N2 influenza drift strains imposes constraints on binding to sialylated receptors, but not phosphorylated glycans. *J. Virol.* 4, 1178–1119. doi: 10.1128/JVI.01178-19

Campanero-Rhodes, M. A., Childs, R. A., Kiso, M., Komba, S., Le Narvor, C., Warren, J., et al. (2006). Carbohydrate microarrays reveal sulphation as a modulator of siglec binding. *Biochem. Biophys. Res. Commun.* 344, 1141–1146. doi: 10.1016/j.bbrc.2006.03.223

Chai, W., Stoll, M. S., Galustian, C., Lawson, A. M., and Feizi, T. (2003). "Neoglycolipid technology: deciphering information content of glycome," in *Methods in Enzymology*. Vol. 362, eds C. Lee Yuan, and T. Lee Reiko (Cambridge, MA: Academic Press), 160–195.

Chaturvedi, P., Warren, C. D., Buescher, C. R., Pickering, L. K., and Newburg, D. S. (2001). Survival of human milk oligosaccharides in the intestine of infants. *Adv. Exp. Med. Biol.* 501, 315–323. doi: 10.1007/978-1-4615-1371-1_39

Chaturvedi, R., Heimburg, J., Yan, J., Koury, S., Sajjad, M., Abdel-Nabi, H. H., et al. (2008). Tumor immunolocalization using (124)I-Iodine labeled JAA-F11 antibody to Thomsen-Friedenreich alpha-linked antigen. *Appl. Radiat. Isot.* 66, 278–287. doi: 10.1016/j.apradiso.2007.07.029

Chen, Y. H., Narimatsu, Y., Clausen, T. M., Gomes, C., Karlsson, R., Steentoft, C., et al. (2018). The GAGOme: a cell-based library of displayed glycosaminoglycans. *Nat. Methods* 15, 881–888. doi: 10.1038/s41592-018-0086-z

Chevolot, Y., Laurenceau, E., Phaner-Goutorbe, M., Monnier, V., Souteyrand, E., Meyer, A., et al. (2014). DNA directed immobilization glycocluster array: applications and perspectives. *Curr. Opin. Chem. Biol.* 18, 46–54. doi: 10.1016/j.cbpa.2013.12.009

Childs, R. A., Palma, A. S., Wharton, S., Matrosovich, T., Liu, Y., Chai, W., et al. (2009). Receptor-binding specificity of pandemic influenza A (H1N1) 2009 virus determined by carbohydrate microarray. *Nat. Biotechnol.* 27, 797–799. doi: 10.1038/nbt0909-797

Chua, J. X., Vankemmelbeke, M., McIntosh, R. S., Clarke, P. A., Moss, R., Parsons, T., et al. (2015). Monoclonal antibodies targeting LecLex-related glycans with Potent antitumor activity. *Clin. Cancer Res.* 21, 2963–2974. doi: 10.1158/1078-0432.CCR-14-3030

Collins, B. C., Gunn, R. J., McKitrick, T. R., Cummings, R. D., Cooper, M. D., Herrin, B. R., et al. (2017). Structural insights into VLR fine specificity for blood group carbohydrates. *Structure* 25, 1667–1678.e1664. doi: 10.1016/j.str.2017.09.003

Colomb, F., Giron, L. B., Trbojevic-Akmacic, I., Lauc, G., and Abdel-Mohsen, M. (2019). Breaking the glyco-code of HIV persistence and immunopathogenesis. *Curr. HIV/AIDS Rep.* 16, 151–168. doi: 10.1007/s11904-019-00433-w

Crocker, P. R., Paulson, J. C., and Varki, A. (2007). Siglecs and their roles in the immune system. *Nat. Rev. Immunol.* 7, 255–266. doi: 10.1038/nri2056

Cummings, R. D. (2009). The repertoire of glycan determinants in the human glycome. *Mol. Biosyst.* 5, 1087–1104. doi: 10.1039/b907931a

Cummings, R. D. (2019). Stuck on sugars – how carbohydrates regulate cell adhesion, recognition, and signaling. *Glycoconj. J.* 36, 241–257. doi: 10.1007/s10719-019-09876-0

Cummings, R. D., and Pierce, J. M. (2014). The challenge and promise of glycomics. *Chem. Biol.* 21, 1–15. doi: 10.1016/j.chembiol.2013.12.010

de Boer, A. R., Hokke, C. H., Deelder, A. M., and Wuhrer, M. (2007). General microarray technique for immobilization and screening of natural glycans. *Anal. Chem.* 79, 8107–8113. doi: 10.1021/ac071187g

Demetriou, M., Granovsky, M., Quaggin, S., and Dennis, J. W. (2001). Negative regulation of T-cell activation and autoimmunity by Mgat5N-glycosylation. *Nature* 409, 733–739. doi: 10.1038/35055582

Elola, M. T., Ferragut, F., Méndez-Huergo, S. P., Croci, D. O., Bracalente, C., and Rabinovich, G. A. (2018). Galectins: multitask signaling molecules linking fibroblast, endothelial and immune cell programs in the tumor microenvironment. *Cell. Immunol.* 333, 34–45. doi: 10.1016/j.cellimm.2018.03.008

Falkowska, E., Le, K. M., Ramos, A., Doores, K. J., Lee, J. H., Blattner, C., et al. (2014). Broadly neutralizing HIV antibodies define a glycan-dependent epitope on the prefusion conformation of gp41 on cleaved envelope trimers. *Immunity* 40, 657–668. doi: 10.1016/j.immuni.2014.04.009

Fukui, S., Feizi, T., Galustian, C., Lawson, A. M., and Chai, W. (2002). Oligosaccharide microarrays for high-throughput detection and specificity assignments of carbohydrate-protein interactions. *Nat. Biotech.* 20, 1011–1017. doi: 10.1038/nbt735

Gao, C., Hanes, M. S., Byrd-Leotis, L. A., Wei, M., Jia, N., Kardish, R. J., et al. (2019). Unique binding specificities of proteins toward isomeric asparagine-linked glycans. *Cell Chem. Biol.* 26, 535–547.e534. doi: 10.1016/j.chembiol.2019.01.002

Gao, C., Liu, Y., Zhang, H., Zhang, Y., Fukuda, M. N., Palma, A. S., et al. (2014). Carbohydrate sequence of the prostate cancer-associated antigen F77 assigned by a mucin O-glycome designer array. *J. Biol. Chem.* 289, 16462–16477. doi: 10.1074/jbc.M114.558932

Geissner, A., Reinhardt, A., Rademacher, C., Johannssen, T., Monteiro, J., Lepenies, B., et al. (2019). Microbe-focused glycan array screening platform. *Proc. Nat. Acad. Sci. U.S.A.* 116, 1958–1967. doi: 10.1073/pnas.1800853116

Gildersleeve, J. C., and Wright, W. S. (2016). Diverse molecular recognition properties of blood group A binding monoclonal antibodies. *Glycobiology* 26, 443–448. doi: 10.1093/glycob/cwv171

Gnoth, M. J., Kunz, C., Kinne-Saffran, E., and Rudloff, S. (2000). Human milk oligosaccharides are minimally digested *in vitro*. *J. Nutr.* 130, 3014–3020. doi: 10.1093/jn/130.12.3014

Gooi, H. C., Feizi, T., Kapadia, A., Knowles, B. B., Solter, D., and Evans, M. J. (1981). Stage-specific embryonic antigen involves αl→ 3 fucosylated type 2 blood group chains. *Nature* 292, 156–158. doi: 10.1038/292156a0

Grant, O. C., Smith, H. M., Firsova, D., Fadda, E., and Woods, R. (2014). J. Presentation, presentation, presentation! Molecular-level insight into linker effects on glycan array screening data. *Glycobiology* 24, 17–25. doi: 10.1093/glycob/cwt083

Gulati, S., Smith, D. F., Cummings, R. D., Couch, R. B., Griesemer, S. B., St. George, K., et al. (2013). Human H3N2 influenza viruses isolated from 1968 To 2012 show varying preference for receptor substructures with no apparent consequences for disease or spread. *PLoS ONE* 8:e66325. doi: 10.1371/journal.pone.0066325

Han, B. W., Herrin, B. R., Cooper, M. D., and Wilson, I. A. (2008). Antigen recognition by variable lymphocyte receptors. *Science* 321, 1834–1837. doi: 10.1126/science.1162484

Hickey, T. B., Ziltener, H. J., Speert, D. P., and Stokes, R. W. (2010). Mycobacterium tuberculosis employs Cpn60.2 as an adhesin that binds CD43 on the macrophage surface. *Cell. Microbiol.* 12, 1634–1647. doi: 10.1111/j.1462-5822.2010.01496.x

Hirabayashi, J., Hashidate, T., Arata, Y., Nishi, N., Nakamura, T., Hirashima, M., et al. (2002). Oligosaccharide specificity of galectins: a search by frontal affinity chromatography. *Biochim. Biophy. Acta* 1572, 232–254. doi: 10.1016/S0304-4165(02)00311-2

Hong, X., Ma, M. Z., Gildersleeve, J. C., Chowdhury, S., Barchi, J. J., Mariuzza, R. A., et al. (2013). Sugar-binding proteins from fish: selection of high affinity "lambodies" that recognize biomedically relevant glycans. *ACS Chem. Biol.* 8, 152–160. doi: 10.1021/cb300399s

Horlacher, T., Oberli, M. A., Werz, D. B., Kröck, L., Bufali, S., Mishra, R., et al. (2010). Determination of carbohydrate-binding preferences of human galectins with carbohydrate microarrays. *Chembiochem.* 11, 1563–1573. doi: 10.1002/cbic.201000020

Hu, L., Ramani, S., Czako, R., Sankaran, B., Yu, Y., Smith, D. F., et al. (2015). Structural basis of glycan specificity in neonate-specific bovine-human reassortant rotavirus. *Nat. Commun.* 6:8346. doi: 10.1038/ncomms9346

Huang, M. L., Cohen, M., Fisher, C. J., Schooley, R. T., Gagneux, P., and Godula, K. (2015). Determination of receptor specificities for whole influenza viruses using multivalent glycan arrays. *Chem. Commun.* 51, 5326–5329. doi: 10.1039/C4CC08613A

Jayaraman, N. (2009). Multivalent ligand presentation as a central concept to study intricate carbohydrate-protein interactions. *Chem. Soc. Rev.* 38, 3463–3483. doi: 10.1039/b815961k

Jobling, M. G. (2016). The chromosomal nature of LT-II enterotoxins solved: a lambdoid prophage encodes both LT-II and one of two novel pertussis-toxin-like toxin family members in type II enterotoxigenic *Escherichia coli*. *Pathog. Dis.* 74:ftw001. doi: 10.1093/femspd/ftw001

Jones, M. B., Oswald, D. M., Joshi, S., Whiteheart, S. W., Orlando, R., and Cobb, B. A. (2016). B-cell–independent sialylation of IgG. *Proc. Natl. Acad. Sci. U.S.A.* 113, 7207–7212. doi: 10.1073/pnas.1523968113

Kannagi, R., Cochran, N. A., Ishigami, F., Hakomori, S., Andrews, P. W., Knowles, B. B., et al. (1983). Stage-specific embryonic antigens (SSEA-3 and−4) are epitopes of a unique globo-series ganglioside isolated from human teratocarcinoma cells. *EMBO J.* 2, 2355–2361. doi: 10.1002/j.1460-2075.1983.tb01746.x

Kannagi, R., Nudelman, E., Levery, S. B., and Hakomori, S. (1982). A series of human erythrocyte glycosphingolipids reacting to the monoclonal antibody directed to a developmentally regulated antigen SSEA-1. *J. Bio. Chem.* 257, 14865–14874.

Läubli, H., and Varki, A. (2019). Sialic acid–binding immunoglobulin-like lectins (Siglecs) detect self-associated molecular patterns to regulate immune responses. *Cell. Mol. Life Sci.* doi: 10.1007/s00018-019-03288-x. [Epub ahead of print].

Lee, H. H., Wang, Y. N., Xia, W., Chen, C. H., Rau, K. M., Ye, L., et al. (2019). Removal of N-linked glycosylation enhances PD-L1 detection and predicts anti-PD-1/PD-L1 therapeutic efficacy. *Cancer Cell* 36, 168–178.e4. doi: 10.1016/j.ccell.2019.06.008

Leppänen, A., Penttila, L., Renkonen, O., McEver, R. P., and Cummings, R. D. (2002). Glycosulfopeptides with O-glycans containing sialylated and polyfucosylated polylactosamine bind with low affinity to P-selectin. *J. Bio. Chem.* 277, 39749–39759. doi: 10.1074/jbc.M206281200

Leppänen, A., Stowell, S., Blixt, O., and Cummings, R. D. (2005). Dimeric galectin-1 binds with high affinity to α2,3-sialylated and non-sialylated terminal N-acetyllactosamine units on surface-bound extended glycans. *J. Bio. Chem.* 280, 5549–5562. doi: 10.1074/jbc.M412019200

Leppänen, A., Yago, T., Otto, V. I., McEver, R. P., and Cummings, R. D. (2003). Model glycosulfopeptides from P-selectin glycoprotein ligand-1 require tyrosine sulfation and a core 2-branched O-glycan to bind to L-selectin. *J. Bio. Chem.* 278, 26391–26400. doi: 10.1074/jbc.M303551200

Li, C. W., Lim, S. O., Chung, E. M., Kim, Y. S., Park, A. H., Yao, J., et al. (2018). Eradication of triple-negative breast cancer cells by targeting glycosylated PD-L1. *Cancer Cell* 33, 187–201.e10. doi: 10.1016/j.ccell.2018.01.009

Li, Z., and Feizi, T. (2018). The neoglycolipid (NGL) technology-based microarrays and future prospects. *FEBS Lett.* 592, 3976–3991. doi: 10.1002/1873-3468.13217

Li, Z., Gao, C., Zhang, Y., Palma, A. S., Childs, R. A., Silva, L. M., et al. (2017). *O-Glycome beam search arrays for carbohydrate ligand discovery*. *Mol. Cell Proteomics.* 17, 121–133. doi: 10.1074/mcp.RA117.000285

Littler, D. R., Ang, S. Y., Moriel, D. G., Kocan, M., Kleifeld, O., Johnson, M. D., et al. (2017). Structure and function analyses of a pertussis-like toxin from pathogenic *Escherichia coli* reveal a distinct mechanism of inhibition of trimeric proteins. *J. Biol. Chem.* 292, 15143–15158. doi: 10.1074/jbc.M117.796094

Liu, L., Prudden, A. R., Capicciotti, C. J., Bosman, G. P., Yang, J. Y., Chapla, D. G., et al. (2019). Streamlining the chemoenzymatic synthesis of complex N-glycans by a stop and go strategy. *Nat. Chem.* 11, 161–169. doi: 10.1038/s41557-018-0188-3

Liu, Y., Childs, R. A., Matrosovich, T., Wharton, S., Palma, A. S., Chai, W., et al. (2010). Altered receptor specificity and cell tropism of d222g hemagglutinin mutants isolated from fatal cases of pandemic A(H1N1) 2009 influenza virus. *J. Virol.* 84, 12069–12074. doi: 10.1128/JVI.01639-10

Liu, Y., Feizi, T., Campanero-Rhodes, M. A., Childs, R. A., Zhang, Y., Mulloy, B., et al. (2007). Neoglycolipid probes prepared via oxime ligation for microarray analysis of oligosaccharide-protein interactions. *Chem. Biol.* 14, 847–859. doi: 10.1016/j.chembiol.2007.06.009

Lu, L. L., Smith, M. T., Yu, K. K. Q., Luedemann, C., Suscovich, T. J., Grace, P. S., et al. (2019). IFN-γ-independent immune markers of Mycobacterium tuberculosis exposure. *Nat. Med.* 25, 977–987. doi: 10.1038/s41591-019-0441-3

Luo, M., Velikovsky, C. A., Yang, X., Siddiqui, M. A., Hong, X., Barchi, J. J., et al. (2013). Recognition of the Thomsen-Friedenreich pancarcinoma carbohydrate antigen by a lamprey variable lymphocyte receptor. *J. Biol. Chem.* 288, 23597–23606. doi: 10.1074/jbc.M113.480467

Luyai, A. E., Heimburg-Molinaro, J., Prasanphanich, N. S., Mickum, M. L., Lasanajak, Y., Song, X., et al. (2014). Differential expression of anti-glycan antibodies in schistosome-infected humans, rhesus monkeys and mice. *Glycobiology* 24, 602–618. doi: 10.1093/glycob/cwu029

Macauley, M. S., Crocker, P. R., and Paulson, J. C. (2014). Siglec-mediated regulation of immune cell function in disease. *Nat. Rev. Immunol.* 14, 653–666. doi: 10.1038/nri3737

Magnani, J. L., Nilsson, B., Brockhaus, M., Zopf, D., Steplewski, Z., Koprowski, H., et al. (1982). A monoclonal antibody-defined antigen associated with gastrointestinal cancer is a ganglioside containing sialylated lacto-N-fucopentaose II. *J. Biol. Chem.* 257, 14365–14369.

Magnani, J. L., Smith, D. F., and Ginsburg, V. (1980). Detection of gangliosides that bind cholera toxin: direct binding of 125I-labeled toxin to thin-layer chromatograms. *Anal. Biochem.* 109, 399–402. doi: 10.1016/0003-2697(80)90667-3

Maierhofer, C., Rohmer, K., and Wittmann, V. (2007). Probing multivalent carbohydrate-lectin interactions by an enzyme-linked lectin assay employing covalently immobilized carbohydrates. *Bioorg. Med. Chem.* 15, 7661–7676. doi: 10.1016/j.bmc.2007.08.063

Mandalasi, M., Dorabawila, N., Smith, D. F., Heimburg-Molinaro, J., Cummings, R. D., and Nyame, A. K. (2013). Development and characterization of a specific IgG monoclonal antibody toward the Lewis x antigen using splenocytes of *Schistosoma mansoni*-infected mice. *Glycobiology* 23, 877–892. doi: 10.1093/glycob/cwt025

Manimala, J. C., Roach, T. A., Li, Z., and Gildersleeve, J. C. (2006). High-throughput carbohydrate microarray analysis of 24 lectins. *Angew. Chem. Int. Ed.* 45, 3607–3610. doi: 10.1002/anie.200600591

Martin, C. E., Broecker, F., Eller, S., Oberli, M. A., Anish, C., Pereira, C. L., et al. (2013a). Glycan arrays containing synthetic *Clostridium difficile* lipoteichoic acid oligomers as tools toward a carbohydrate vaccine. *Chem. Commun.* 49, 7159–7161. doi: 10.1039/c3cc43545h

Martin, C. E., Broecker, F., Oberli, M. A., Komor, J., Mattner, J., Anish, C., et al. (2013b). Immunological evaluation of a synthetic *Clostridium difficile* oligosaccharide conjugate vaccine candidate and identification of a minimal epitope. *J. Am. Chem. Soc.* 135, 9713–9722. doi: 10.1021/ja401410y

McKitrick, T. R., Hanes, M. S., Rosenberg, C. S., Heimburg-Molinaro, J., Cooper, M. D., Herrin, B. R., et al. (accepted). Identification of glycan-specific variable lymphocyte receptors using yeast surface display and glycan microarrays. *Methods Mol. Biol.*

Mehta, A. Y., and Cummings, R. D. (2019). GLAD: GLycan array dashboard, a visual analytics tool for glycan microarrays. *Bioinformatics* 35, 3536–3537. doi: 10.1093/bioinformatics/btz075

Mende, M., Bordoni, V., Tsouka, A., Loeffler, F. F., Delbianco, M., and Seeberger, P. H. (2019). Multivalent glycan arrays. *Faraday Discuss.* 219, 9–32. doi: 10.1039/C9FD00080A

Mickum, M. L., Prasanphanich, N. S., Song, X., Dorabawila, N., Mandalasi, M., Lasanajak, Y., et al. (2016). Identification of antigenic glycans from *Schistosoma mansoni* using a shotgun egg glycan microarray. *Infect. Immun.* 84, 1371–1386. doi: 10.1128/IAI.01349-15

Muthana, S. M., and Gildersleeve, J. C. (2016). Factors affecting anti-glycan IgG and IgM repertoires in human serum. *Sci. Rep.* 6:19509. doi: 10.1038/srep19509

Narimatsu, Y., Joshi, H. J., Nason, R., Van Coillie, J., Karlsson, R., Sun, L., et al. (2019). An atlas of human glycosylation pathways enables display of the human glycome by gene engineered cells. *Mol. Cell* 75, 394–407.e395. doi: 10.1016/j.molcel.2019.05.017

Narimatsu, Y., Joshi, H. J., Yang, Z., Gomes, C., Chen, Y. H., Lorenzetti, F. C., et al. (2018). A validated gRNA library for CRISPR/Cas9 targeting of the human glycosyltransferase genome. *Glycobiology* 28, 295–305. doi: 10.1093/glycob/cwx101

Nkurunungi, G., van Diepen, A., Nassuuna, J., Sanya, R. E., Nampijja, M., Nambuya, I., et al. (2019). Microarray assessment of N-glycan-specific IgE and IgG profiles associated with *Schistosoma mansoni* infection in rural and urban Uganda. *Sci. Rep.* 9:3522. doi: 10.1038/s41598-019-40009-7

Noble, P., Spendlove, I., Harding, S., Parsons, T., and Durrant, L. G. (2013). Therapeutic targeting of lewisy and lewisb with a novel monoclonal antibody 692/29. *PLoS ONE* 8:e54892. doi: 10.1371/journal.pone.0054892

Noll, A. J., Gourdine, J. P., Yu, Y., Lasanajak, Y., Smith, D. F., and Cummings, R. D. (2016). Galectins are human milk glycan receptors. *Glycobiology* 26, 655–669. doi: 10.1093/glycob/cww002

Nonaka, M., Fukuda, M. N., Gao, C., Li, Z., Zhang, H., Greene, M. I., et al. (2014). Determination of carbohydrate structure recognized by prostate-specific F77 monoclonal antibody through expression analysis of glycosyltransferase genes. *J. Biol. Chem.* 289, 16478–16486. doi: 10.1074/jbc.M114.559047

Okada, M., Chikuma, S., Kondo, T., Hibino, S., Machiyama, H., Yokosuka, T., et al. (2017). Blockage of core fucosylation reduces cell-surface expression of PD-1 and promotes anti-tumor immune responses of T cells. *Cell Rep.* 20, 1017–1028. doi: 10.1016/j.celrep.2017.07.027

Oyelaran, O., Li, Q., Farnsworth, D., and Gildersleeve, J. C. (2009). Microarrays with varying carbohydrate density reveal distinct subpopulations of serum antibodies. *J. Proteome Res.* 8, 3529–3538. doi: 10.1021/pr9002245

Padler-Karavani, V., Song, X., Yu, H., Hurtado-Ziola, N., Huang, S., Muthana, S., et al. (2012). Cross-comparison of protein recognition of sialic acid diversity on two novel sialoglycan microarrays. *J. Biol. Chem.* 287, 22593–22608. doi: 10.1074/jbc.M112.359323

Palma, A. S., Feizi, T., Childs, R. A., Chai, W., and Liu, Y. (2014). The neoglycolipid (NGL)-based oligosaccharide microarray system poised to decipher the meta-glycome. *Curr. Opin. Chem. Biol.* 18, 87–94. doi: 10.1016/j.cbpa.2014.01.007

Palma, A. S., Feizi, T., Zhang, Y., Stoll, M. S., Lawson, A. M., Díaz-Rodríguez, E., et al. (2006). Ligands for the β-glucan receptor, dectin-1, assigned using "designer" microarrays of oligosaccharide probes (neoglycolipids) generated from glucan polysaccharides. *J. Biol. Chem.* 281, 5771–5779. doi: 10.1074/jbc.M511461200

Pancer, Z., Amemiya, C. T., Ehrhardt, G. R., Ceitlin, J., Gartland, G. L., and Cooper, M. D. (2004). Somatic diversification of variable lymphocyte receptors in the agnathan sea lamprey. *Nature* 430, 174–180. doi: 10.1038/nature02740

Park, S., Gildersleeve, J. C., Blixt, O., and Shin, I. (2013). Carbohydrate microarrays. *Chem. Soc. Rev.* 42, 4310–4326. doi: 10.1039/C2CS35401B

Pascoal, C., Francisco, R., Ferro, T., Dos Reis Ferreira, V., Jaeken, J., and Videira, P. A. (2019). CDG and immune response: from bedside to bench and back. *J. Inherit. Metab. Dis*. doi: 10.1002/jimd.12126. [Epub ahead of print].

Patnaik, S. K., Potvin, B., Carlsson, S., Sturm, D., Leffler, H., and Stanley, P. (2006). Complex N-glycans are the major ligands for galectin-1,−3, and−8 on Chinese hamster ovary cells. *Glycobiology* 16, 305–317. doi: 10.1093/glycob/cwj063

Petrova, M. I., Lievens, E., Verhoeven, T. L., Macklaim, J. M., Gloor, G., Schols, D., et al. (2016). The lectin-like protein 1 in Lactobacillus rhamnosus GR-1 mediates tissue-specific adherence to vaginal epithelium and inhibits urogenital pathogens. *Sci. Rep.* 6:37437. doi: 10.1038/srep37437

Prasanphanich, N. S., Song, X., Heimburg-Molinaro, J., Luyai, A. E., Lasanajak, Y., Cutler, C. E., et al. (2015). Intact reducing glycan promotes the specific immune response to lacto-N-neotetraose-BSA neoglycoconjugates. *Bioconjug. Chem.* 26, 559–571. doi: 10.1021/acs.bioconjchem.5b00036

Purohit, S., Li, T., Guan, W., Song, X., Song, J., Tian, Y., et al. (2018). Multiplex glycan bead array for high throughput and high content analyses of glycan binding proteins. *Nat. Commun.* 9:258. doi: 10.1038/s41467-017-02747-y

Rabinovich, G. A., van Kooyk, Y., and Cobb, B. A. (2012). Glycobiology of immune responses. *Ann. N. Y. Acad. Sci.* 1253, 1–15. doi: 10.1111/j.1749-6632.2012.06492.x

Rillahan, C. D., and Paulson, J. C. (2011). Glycan microarrays for decoding the glycome. *Annu. Rev. Biochem.* 80, 797–823. doi: 10.1146/annurev-biochem-061809-152236

Robinson, B. S., Arthur, C. M., Evavold, B., Roback, E., Kamili, N. A., Stowell, C. S., et al. (2019). The sweet-side of leukocytes: galectins as master regulators of neutrophil function. *Front. Immunol.* 10:1762. doi: 10.3389/fimmu.2019.01762

RodrÍguez, E., Schetters, S. T. T., and van Kooyk, Y. (2018). The tumour glyco-code as a novel immune checkpoint for immunotherapy. *Nat. Rev. Immunol.* 18:204. doi: 10.1038/nri.2018.3

Scheepers, C., Chowdhury, S., Wright, W. S., Campbell, C. T., Garrett, N. J., Abdool Karim, Q., et al. (2017). Serum glycan-binding IgG antibodies in HIV-1 infection and during the development of broadly neutralizing responses. *AIDS* 31, 2199–2209. doi: 10.1097/QAD.0000000000001643

Schneider, C., Smith, D. F., Cummings, R. D., Boligan, K. F., Hamilton, R. G., Bochner, B. S., et al. (2015). The human IgG anti-carbohydrate repertoire exhibits a universal architecture and contains specificity for microbial attachment sites. *Sci. Transl. Med.* 7, 269ra261–269ra261. doi: 10.1126/scitranslmed.3010524

Schwarz, M., Spector, L., Gargir, A., Shtevi, A., Gortler, M., Altstock, R. T., et al. (2003). A new kind of carbohydrate array, its use for profiling antiglycan antibodies, and the discovery of a novel human cellulose-binding antibody. *Glycobiology* 13, 749–754. doi: 10.1093/glycob/cwg091

Song, X., Heimburg-Molinaro, J., Cummings, R. D., and Smith, D. F. (2014). Chemistry of natural glycan microarrays. *Curr. Opin. Chem. Biol.* 18, 70–77. doi: 10.1016/j.cbpa.2014.01.001

Song, X., Heimburg-Molinaro, J., Smith, D. F., and Cummings, R. D. (2015). Glycan microarrays of fluorescently-tagged natural glycans. *Glycoconj. J.* 32, 465–473. doi: 10.1007/s10719-015-9584-8

Song, X., Xia, B., Lasanajak, Y., Smith, D. F., and Cummings, R. D. (2008). Quantifiable fluorescent glycan microarrays. *Glycoconj. J.* 25, 15–25. doi: 10.1007/s10719-007-9066-8

Song, X., Xia, B., Stowell, S. R., Lasanajak, Y., Smith, D. F., and Cummings, R. D. (2009). Novel fluorescent glycan microarray strategy reveals ligands for galectins. *Chem. Biol.* 16, 36–47. doi: 10.1016/j.chembiol.2008.11.004

Stowell, S. R., Arthur, C. M., Dias-Baruffi, M., Rodrigues, L. C., Gourdine, J. P., Heimburg-Molinaro, J., et al. (2010). Innate immune lectins kill bacteria expressing blood group antigen. *Nat. Med.* 16, 295–301. doi: 10.1038/nm.2103

Stowell, S. R., Arthur, C. M., Mehta, P., Slanina, K. A., Blixt, O., Leffler, H., et al. (2008). Galectin-1,−2, and−3 exhibit differential recognition of sialylated glycans and blood group antigens. *J. Biol. Chem.* 283, 10109–10123. doi: 10.1074/jbc.M709545200

Sun, X., Li, D., Qi, J., Chai, W., Wang, L., Wang, L., et al. (2018a). Glycan binding specificity and mechanism of human and porcine P[6]/P[19] rotavirus VP8*s. *J. Virol.* 92, e00538–e00518. doi: 10.1128/JVI.00538-18

Sun, X., Wang, L., Qi, J., Li, D., Wang, M., Cong, X., et al. (2018b). Human group C rotavirus VP8*s recognize type A histo-blood group antigens as ligands. *J. Virol.* 92, e00442–e00418. doi: 10.1128/JVI.00442-18

Tang, P. W., Gool, H. C., Hardy, M., Lee, Y. C., and Feizi, T. (1985). Novel approach to the study of the antigenicities and receptor functions of carbohydrate chains of glycoproteins. *Biochem. Biophys. Res. Commun.* 132, 474–480. doi: 10.1016/0006-291X(85)91158-1

Tati, S., Fisk, J. C., Abdullah, J., Karacosta, L., Chrisikos, T., Philbin, P., et al. (2017). Humanization of JAA-F11, a highly specific anti-thomsen-friedenreich pancarcinoma antibody and *in vitro* efficacy analysis. *Neoplasia* 19, 716–733. doi: 10.1016/j.neo.2017.07.001

Taylor, M. E., and Drickamer, K. (2019). Mammalian sugar-binding receptors: known functions and unexplored roles. *FEBS J.* 286, 1800–1814. doi: 10.1111/febs.14759

Tessier, M. B., Grant, O. C., Heimburg-Molinaro, J., Smith, D., Jadey, S., Gulick, A. M., et al. (2013). Computational screening of the human TF-glycome provides a structural definition for the specificity of anti-tumor antibody JAA-F11. *PLoS ONE* 8:e54874. doi: 10.1371/journal.pone.0054874

Thiemann, S., and Baum, L. G. (2016). Galectins and immune responses—just how do they do those things they do? *Annu. Rev. Immunol.* 34, 243–264. doi: 10.1146/annurev-immunol-041015-055402

Trabbic, K. R., Whalen, K., Abarca-Heideman, K., Xia, L., Temme, J. S., Edmondson, E. F., et al. (2019). A Tumor-selective monoclonal antibody from immunization with a tumor-associated mucin glycopeptide. *Sci. Rep.* 9:5662. doi: 10.1038/s41598-019-42076-2

van Diepen, A., van der Plas, A. J., Kozak, R. P., Royle, L., Dunne, D. W., and Hokke, C. H. (2015). Development of a *Schistosoma mansoni* shotgun O-glycan microarray and application to the discovery of new antigenic schistosome glycan motifs. *Int. J. Parasitol.* 45, 465–475. doi: 10.1016/j.ijpara.2015.02.008

Velásquez, A. C., Nomura, K., Cooper, M. D., Herrin, B. R., and He, S. Y. (2017). Leucine-rich-repeat-containing variable lymphocyte receptors as modules to target plant-expressed proteins. *Plant Methods* 13:29. doi: 10.1186/s13007-017-0180-8

von Gunten, S., Smith, D. F., Cummings, R. D., Riedel, S., Miescher, S., Schaub, A., et al. (2009). Intravenous immunoglobulin contains a broad repertoire of anticarbohydrate antibodies that is not restricted to the IgG2 subclass. *J. Allergy Clin. Immunol.* 123, 1268–1276.e1215. doi: 10.1016/j.jaci.2009.03.013

Wang, D., Liu, S., Trummer, B. J., Deng, C., and Wang, A. (2002). Carbohydrate microarrays for the recognition of cross-reactive molecular markers of microbes and host cells. *Nat. Biotechnol.* 20, 275–281. doi: 10.1038/nbt0302-275

Watkins, W. M. (2001). The ABO blood group system: historical background. *Transfus. Med.* 11, 243–265. doi: 10.1046/j.1365-3148.2001.00321.x

Wei, M., McKitrick, T. R., Mehta, A. Y., Gao, C., Jia, N., McQuillan, A. M., et al. (2019). Novel reversible fluorescent glycan linker for functional glycomics. *Bioconj. Chem.* 30, 2897–2908. doi: 10.1021/acs.bioconjchem.9b00613

Xia, B., Kawar, Z. S., Ju, T., Alvarez, R. A., Sachdev, G. P., and Cummings, R. D. (2005). Versatile fluorescent derivatization of glycans for glycomic analysis. *Nat. Meth.* 2, 845–850. doi: 10.1038/nmeth808

Xia, L., Schrump, D. S., and Gildersleeve, J. C. (2016). Whole-cell cancer vaccines induce large antibody responses to carbohydrates and glycoproteins. *Cell Chem. Biol.* 23, 1515–1525. doi: 10.1016/j.chembiol.2016.10.012

Xu, G., Tasumi, S., and Pancer, Z. (2011). Yeast surface display of lamprey variable lymphocyte receptors. *Methods Mol. Biol.* 748, 21–33. doi: 10.1007/978-1-61779-139-0_2

Yan, M., Zhu, Y., Liu, X., Lasanajak, Y., Xiong, J., Lu, J., et al. (2019). Next-generation glycan microarray enabled by DNA-coded glycan library and next-generation sequencing technology. *Anal. Chem.* 91, 9221–9228. doi: 10.1021/acs.analchem.9b01988

Yang, H., Carney, P. J., Chang, J. C., Guo, Z., and Stevens, J. (2018). Structural and molecular characterization of the hemagglutinin from the fifth epidemic wave A (H7N9) influenza viruses. *J. Virol.* 92, e00375–e00318. doi: 10.1128/JVI.00375-18

Yu, Y., Lasanajak, Y., Song, X., Hu, L., Ramani, S., Mickum, M. L., et al. (2014). Human milk contains novel glycans that are potential decoy

receptors for neonatal rotaviruses. *Mol. Cell. Proteom.* 13, 2944–2960. doi: 10.1074/mcp.M114.039875

Yu, Y., Mishra, S., Song, X., Lasanajak, Y., Bradley, K. C., Tappert, M. M., et al. (2012). Functional glycomic analysis of human milk glycans reveals the presence of virus receptors and embryonic stem cell biomarkers. *J. Biol. Chem.* 287, 44784–44799. doi: 10.1074/jbc.M112.425819

Zipser, B., Bello-DeOcampo, D., Diestel, S., Tai, M.-H., and Schmitz, B. (2012). Mannitou monoclonal antibody uniquely recognizes paucimannose, a marker for human cancer, stemness, and inflammation. *J. Carbohydr. Chem.* 31, 504–518. doi: 10.1080/07328303.2012.661112

Conflict of Interest: The authors declare that the research was conducted in the absence of any commercial or financial relationships that could be construed as a potential conflict of interest.

frontiers in Chemistry

BRIEF RESEARCH REPORT
published: 10 January 2020
doi: 10.3389/fchem.2019.00898

A Synthetic Tetramer of Galectin-1 and Galectin-3 Amplifies Pro-apoptotic Signaling by Integrating the Activity of Both Galectins

Shaheen A. Farhadi[†], *Margaret M. Fettis*[†‡], *Renjie Liu and Gregory A. Hudalla*[*]

J. Crayton Pruitt Family Department of Biomedical Engineering, University of Florida, Gainesville, FL, United States

OPEN ACCESS

Edited by:
Karina Valeria Mariño, Institute of Biology and Experimental Medicine (IBYME), Argentina

Reviewed by:
Mare Cudic, Florida Atlantic University, United States
Bernd Lepenies, University of Veterinary Medicine Hannover, Germany

***Correspondence:**
Gregory A. Hudalla
ghudalla@bme.ufl.edu

[†]*These authors have contributed equally to this work*

[‡]***Present address:***
Margaret M. Fettis, George W. Woodruff School of Mechanical Engineering, Georgia Institute of Technology, Atlanta, GA, United States

Specialty section:
This article was submitted to Chemical Biology, a section of the journal Frontiers in Chemistry

Received: *27 August 2019*
Accepted: *12 December 2019*
Published: *10 January 2020*

Citation:
Farhadi SA, Fettis MM, Liu R and Hudalla GA (2020) A Synthetic Tetramer of Galectin-1 and Galectin-3 Amplifies Pro-apoptotic Signaling by Integrating the Activity of Both Galectins. Front. Chem. 7:898. doi: 10.3389/fchem.2019.00898

Galectin-1 (G1) and galectin-3 (G3) are carbohydrate-binding proteins that can signal apoptosis in T cells. We recently reported that a synthetic tetramer with two G1 and two G3 domains ("G1/G3 Zipper") induces Jurkat T cell death more potently than G1. The pro-apoptotic signaling pathway of G1/G3 Zipper was not elucidated, but we hypothesized based on prior work that the G1 domains acted as the signaling units, while the G3 domains served as anchors that increase glycan-binding affinity. To test this, here we studied the involvement of different cell membrane glycoproteins and intracellular mediators in pro-apoptotic signaling via G1/G3 Zipper, G1, and G3. G1/G3 Zipper induced Jurkat T cell death more potently than G1 and G3 alone or in combination. G1/G3 Zipper, G1, and G3 increased caspase-8 activity, yet only G1 and G3 depended on it to induce cell death. G3 increased caspase-3 activity more than G1/G3 Zipper and G1, while all three galectin variants required it to induce cell death. JNK activation had similar roles downstream of G1/G3 Zipper, G1, and G3, whereas ERK had differing roles. CD45 was essential for G1 activity, and was involved in signaling via G1/G3 Zipper and G3. CD7 inhibited G1/G3 Zipper activity at low galectin concentrations but not at high galectin concentrations. In contrast, CD7 was necessary for G1 and G3 signaling at low galectin concentration but antagonistic at high galectin concentrations. Collectively, these observations suggest that G1/G3 Zipper amplifies pro-apoptotic signaling through the integrated activity of both the G1 and G3 domains.

Keywords: galectin-1, galectin-3, glycobiology, protein engineering, protein-carbohydrate binding

INTRODUCTION

Galectins are a family of soluble carbohydrate-binding proteins that regulate cell phenotype and function in development and disease (Cummings et al., 2015). For example, galectins are integral to fetal-maternal tolerance, mediators of cell-cell and cell-matrix adhesion, prevent the onset and progression of various autoimmune diseases, activate pro-inflammatory responses during osteoarthritis, can enhance or inhibit pathogen entry into host cells, and confer immune privilege to various tissues as well as tumors (Rabinovich et al., 1999; Hughes, 2001; Santucci et al., 2003; St-Pierre et al., 2011; Than et al., 2012; Li et al., 2013; Baum et al., 2014; Hu et al., 2017). Galectin-1

(G1) and galectin-3 (G3) are expressed by many immune cells and receive considerable attention in the context of immunity (Rabinovich and Toscano, 2009; Thiemann and Baum, 2016). They can act on various cell types, including monocytes, macrophages, neutrophils, dendritic cells, and T cells to regulate cell adhesion, migration, proliferation, cytokine secretion, or death (Elola et al., 2005; Vasta et al., 2012; Chung et al., 2013). Among immune cells, the activity of G1 and G3 on T cells has been studied most extensively. Notably, G1 and G3 demonstrate similar biological activities toward T cells in some contexts, yet divergent activity in others. For example, both G1 and G3 can induce T cell apoptosis (Stillman et al., 2006), whereas only G3 has been shown to induce T cell secretion of interleukin-2 (Hsu et al., 1996). Further, G1 can stimulate antigen-specific T cell responses, whereas G3 failed to stimulate these responses (Tribulatti et al., 2012). Moreover, G3 induced activated human T cell death, whereas G1 did not, instead promoting immunosuppressive interleukin-10 production and suppressing interferon-γ secretion (Stowell et al., 2008b). Thus, understanding the pathways by which G1 and G3 evoke changes in immune cell behavior, as well as any interplay between them, presents opportunities to regulate innate and adaptive immune responses.

Both G1 and G3 activate apoptosis of T cells by crosslinking glycoproteins displayed on the plasma membrane, yet evidence suggests that they may signal through distinct intracellular pathways. For example, early reports suggested that G1 induces apoptosis in a caspase- and cytochrome c-independent manner through nuclear translocation of endonuclease G (Hahn et al., 2004). More recently, it has been shown that G1 can induce Jurkat T cell death due to activation of c-Jun N-terminal kinase (JNK) which, in turn, activates c-Jun and AP-1 (Brandt et al., 2010). G1 has also been reported to sensitize resting human T cells to Fas-mediated cell death (Matarrese et al., 2005), as well as induce Fas-dependent apoptosis of Jurkat T cells via activation of caspase-8 and caspase-3 (Brandt et al., 2008). The pathways through which extracellular G3 induces apoptosis are less understood at present. Early reports demonstrated that extracellular G3 signals apoptosis via cytochrome c-release and caspase-3 activation independent of caspase-8 activation (Fukumori et al., 2003), with more recent data suggesting that G3 activates caspase-9 upstream of caspase-3 through phosphorylation of extracellular signal-regulated kinase (ERK) (Xue et al., 2017).

Differences in the pro-apoptotic signaling pathways activated by extracellular G1 and G3 may arise because they recognize different cell surface glycoproteins by way of their selectivity for different oligosaccharide ligands (Stowell et al., 2008a). Among glycoprotein receptors implicated in T cell death (e.g., CD7, CD29, CD43, CD45, and CD71) (Brown et al., 1996; Lesage et al., 1997; Lesnikov et al., 2001; Arencibia et al., 2002), apoptosis induced by G1 has been suggested to depend on CD7 but not CD45 (Pace et al., 1999, 2000; Walzel et al., 1999; Stillman et al., 2006), whereas other studies have identified a role for CD45 in G1 pro-apoptotic signaling (Nguyen et al., 2001). In contrast, apoptosis via extracellular G3 has been suggested to depend on CD45 but not CD43, whereas conflicting roles of CD7 and CD29 have been reported (Fukumori et al., 2003; Stillman et al., 2006). Further, CD71 was observed to cluster on dying cells treated with G3, whereas G1 cannot bind CD71 (Stillman et al., 2006).

Combination therapies that engage different receptors or pathways can be used to regulate T cell responses by amplifying apoptosis and/or modulating activation (Strauss et al., 2002; Reddy et al., 2012). Intriguingly, the combination of native G1 and G3 was neither additive nor synergistic for activating T cell apoptosis despite engaging different receptors and distinct pathways (Stillman et al., 2006). Consistent with this, we previously reported that a fusion protein consisting of G1 linked to the N-terminus of G3 (i.e., "G1/G3") failed to induce Jurkat T cell apoptosis; however, a synthetic tetramer developed by engineering G1/G3 to self-assemble (i.e., "G1/G3 Zipper") induced apoptosis at a significantly lower concentration than G1 alone (Fettis et al., 2019). We hypothesized that the G1 domains acted as the signaling units, while the G3 domains served as anchors that increase the apparent glycan-binding affinity (**Figure 1**, left). This was based on two previous observations. First, G1 fixed in a homodimeric configuration has increased pro-apoptotic signaling activity when compared to native G1, regardless of whether the dimeric structure is established by a peptide linker, α-helical coiled-coil, Fc fusion, or synthetic polymer (van der Leij et al., 2007; Cedeno-Laurent et al., 2010; Earl et al., 2011; Farhadi and Hudalla, 2016; Fettis and Hudalla, 2018). Second, a synthetic homotrimer of G3 lacked signaling activity when compared to native G3 (Farhadi et al., 2018), likely because its carbohydrate-recognition domain valency was insufficient to activate intracellular signaling pathways to a measurable extent.

Here, we sought to determine whether the G1 domains of G1/G3 Zipper act as signaling units while G3 domains serve as anchors (**Figure 1**, left), or if both galectin domains of G1/G3 Zipper act as signaling units (**Figure 1**, right). To this end, we studied the involvement of different cell membrane receptors and intracellular mediators in pro-apoptotic signaling via G1/G3 Zipper, G1, and G3. In particular, we evaluated the role of caspase activity (e.g., caspase-8 and caspase-3), as well as ERK and JNK activation. Additionally, we used CD7- and CD45-deficient T cell lines to assess G1/G3 Zipper-, G1-, and G3-induced transmembrane signal transduction.

MATERIALS AND METHODS

Protein Expression and Purification

All proteins in this study were expressed from recombinant DNA in Origami™ B(DE3) Competent *E. coli* (70837-4, Novagen) and purified according to established protocols (Fettis et al., 2019). Protein sequences of G1, which has been mutated to lack surface cysteines, G3, and G1/G3 Zipper have been published elsewhere (Restuccia et al., 2018; Fettis et al., 2019). After purification, molecular weight and purity of each protein were determined via denaturing gel electrophoresis and Coomassie staining. Molar concentration of each purified protein was determined using the Pierce™ 660 nm Protein Assay Reagent (22660, ThermoFisher). Finally, endotoxin content was reduced to <1 EU/mL via Triton X-114 cloud-point precipitation and then confirmed using the

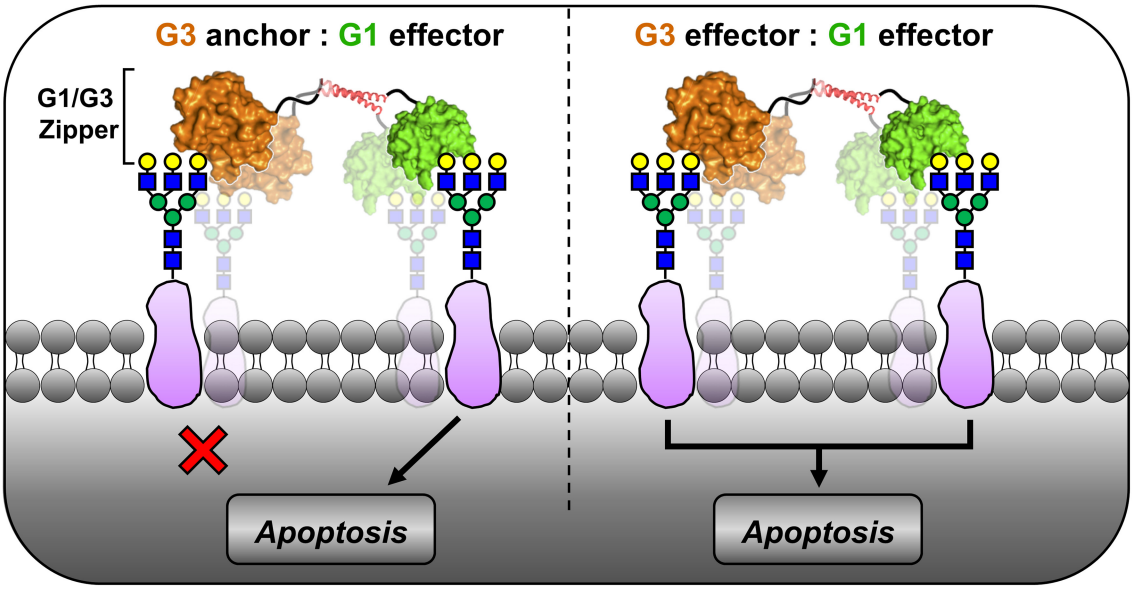

FIGURE 1 | Proposed models of G1/G3 Zipper pro-apoptotic signaling activity. In one model, G3 binding to membrane glycoproteins anchors G1 at the cell surface, where G1 acts as the only signaling domain **(Left)**. In an alternative model, both G1 and G3 act as signaling domains to amplify apoptosis **(Right)**.

Pierce™ Chromogenic Endotoxin Quantitation kit (A39552, ThermoFisher), according to manufacturer instructions.

Cell Death Assays

Protocols for flow cytometric analysis of apoptosis were adapted from previously reported methods (Pace et al., 2003). Jurkat E6-1 (ATCC® TIB-152™), HuT 78 (ATCC® TIB-161™), and J45.01 (ATCC® CRL-1990™) T cells were expanded in complete media (RPMI 1640 supplemented with 10% heat-inactivated fetal bovine serum, 1% penicillin–streptomycin, 200 mM L-glutamine, 1% HEPES buffer) at 37°C, 5% CO_2. For all apoptosis experiments, 100 μL of cells were aliquoted at 200,000 cells into round-bottom 12 × 75 mm culture test tubes (14-956-3D, ThermoFisher) and incubated with 100 μL of sterile 1x PBS (Hyclone™ SH30256) alone (i.e., untreated), G1, G3, G1 + G3, or G1/G3 Zipper in sterile 1x PBS (final galectin concentration depending on assay) in the presence or absence of 100 μM caspase-8 inhibitor Z-IETD-FMK (FMK007, R&D Systems), caspase-3/7 inhibitor I (218826, MilliporeSigma), ERK inhibitor U0126 (662005, MilliporeSigma), or JNK inhibitor II SP600125 (420119, MilliporeSigma) for 4 or 24 h at 37°C, 5% CO_2. Note, inhibitors were dissolved in American Chemical Society grade dimethyl sulfoxide (DMSO) and an equivalent amount of DMSO (1 μL or 0.5% final concentration) was added to all groups not receiving inhibitors as vehicle control. Further, cells received inhibitor alone as control to calculate a final percentage of cell death after data were collected. Positive single stain controls for flow cytometric analysis were produced by treating cells with 1 μM (S)-(+)-Camptothecin (C9911, MilliporeSigma) for 4 or 24 h at 37°C, 5% CO_2. After incubation, half the volume of cells treated with (S)-(+)-Camptothecin was heated to 56°C for 5 min and then cooled on ice for 5 min before being recombined with the other half of (S)-(+)-Camptothecin-treated cells. All cells were treated with 1 mL of ice-cold 100 mM lactose in sterile 1x PBS, then pelleted via centrifugation (500 × *g* for 5 min at 4°C) and resuspended in 1 mL of ice-cold sterile 1x PBS. Cells were then stained with 1 μL (1:1,000 dye:PBS volume ratio) of LIVE/DEAD® Near-IR dye (excitation λ = 633 nm and emission λ = 750 nm) on ice for 30 min while protected from light, according to protocols from a LIVE/DEAD® Fixable Near-IR Dead Cell Stain Kit (L34975, ThermoFisher). After staining, cells were washed with 1 mL of ice-cold 1x PBS via centrifugation and the supernatant was carefully discarded. Cells were then resuspended in 100 μL of 1x Annexin V Binding Buffer (556454, BD Biosciences) with 5 μL BV421 Annexin V (563973, BD Biosciences) to stain for phosphatidylserine exposure, and then mixed gently followed by 15 min incubation at room temperature in the dark, according to manufacturer protocols. Finally, 200 μL of 1x Annexin V Binding Buffer was further added to the cells before flow cytometric data was acquired on a BD FACSCelesta™ flow cytometer equipped with BD FACSDiva™ software, a violet laser (405 nm) for BV421 detection (excitation λ = 407 nm and emission λ = 421 nm), and a red laser (640 nm) for LIVE/DEAD® detection (excitation λ = 650 nm and emission λ = 785 nm). Data were analyzed and graphed as scatter plots using BD FlowJo™ software (version 10.0.7). Percentage of cell death was then calculated as follows: [(% annexin V^- and LIVE/DEAD®$^-$ cells in untreated group)—(% annexin V^- and LIVE/DEAD®$^-$ cells in treated group)]/(% annexin V^- and LIVE/DEAD®$^-$ cells in untreated group). Values less than zero were reported as zero. Percentages of cell death that were positive after treatment with inhibitor alone (**Supplementary Figure 2**) were, respectively, subtracted from protein plus inhibitor treated

groups to yield a final percentage of galectin-induced cell death in experimental groups.

Caspase Activity

Jurkat T cells were expanded in complete media as described above. Jurkat T cells were aliquoted (500,000 cells/well) into sterile, clear, tissue culture treated 6-well microplates. Cells were then incubated with 5 μM G1, 5 μM G3, or 0.5 μM G1/G3 Zipper for 24 h at 37 °C, 5% CO_2. Cells were washed with sterile 1x PBS prior to measuring caspase activity with the following commercially available assay kits: FLICE/Caspase-8 Colorimetric Assay Kit (K113100, ThermoFisher) and EnzCheck® Caspase-3 Assay Kit #1 (E13183, ThermoFisher). Note, the substrate Z-DEVD-AMC in the EnzCheck® Caspase-3 Assay Kit #1 can also be activated by caspase-7. Herein, we refer to any measured activity as "caspase-3 activity" in accordance with the manufacturer's naming convention. For caspase-8 activity measurements, groups of cells were pooled together at 1.5 * 10^6 cells per replicate.

Statistical Analysis

All experimental and control groups had $N = 3$, and the data were reported as mean ± standard deviation. Data were analyzed for statistically significant differences using one-way ANOVA with Tukey's *post hoc* ($p < 0.05$) in GraphPad Prism 8.0 (GraphPad Software, San Diego, CA, USA).

RESULTS

G1/G3 Zipper Induces Jurkat T Cell Death More Potently Than G1 and G3 Alone or in Combination

Jurkat T cell apoptosis induced by G1 and G3 is associated with early exposure of phosphatidylserine on the outer leaflet of the plasma membrane, followed by late membrane permeability (Pace et al., 1999, 2003; Stowell et al., 2008b). Here, we used a combination of annexin V staining of phosphatidylserine and a membrane-impermeable DNA-binding dye (LIVE/DEAD®, Invitrogen) to quantify Jurkat T cell death induced by G1/G3 Zipper, G1, or G3 as a function of galectin concentration and time. Note, cells were treated with as low as 0.5 μM G1/G3 Zipper in all experiments based on a prior report showing that high concentration of this protein led to loss of cell integrity (Fettis et al., 2019), whereas cells were treated with as high as 5 μM G1 or G3 based on the reported effective dose of these proteins (Restuccia et al., 2015, 2018; Farhadi et al., 2018; Fettis and Hudalla, 2018; Fettis et al., 2019). For each concentration of galectin (0.5, 1, 2.5, and 5 μM) tested, G1/G3 Zipper induced significantly more cell death by 24 h than an equimolar combination of G1 and G3 (**Figure 2A**). At 4 h, 0.5 μM G1/G3 Zipper induced significantly more cell death than either 5 μM G1 or 5 μM G3 alone (**Figure 2B**). By 24 h, 5 μM G1 and 5 μM G3 induced a comparable extent of Jurkat T cell death as 0.5 μM G1/G3 Zipper (**Figure 2B**).

G1/G3 Zipper, G1, and G3 Differentially Activate Caspase-8 and Caspase-3

We characterized caspase-8 activity induced by G1/G3 Zipper, G1, or G3 by quantifying Jurkat T cell cleavage of the caspase-8 substrate, IETD-*p*-nitroanilide. At 24 h, cells treated with 5 μM G3 and 0.5 μM G1/G3 Zipper demonstrated comparable caspase-8 activity, whereas cells treated with 5 μM G1 demonstrated significantly weaker caspase-8 activity (**Figure 3A**).

We characterized caspase-3 activity induced by G1/G3 Zipper, G1, or G3 by quantifying Jurkat T cell cleavage of the substrate, Z-DEVD-AMC. At 4 h, cells treated with 0.5 μM G1/G3 Zipper, 5 μM G1, or 5 μM G3 demonstrated no measurable caspase-3 activity relative to untreated cells (**Supplementary Figure 1**). At 24 h, cells treated with 5 μM G3 demonstrated high caspase-3 activity. In contrast, cells treated with 0.5 μM G1/G3 Zipper demonstrated moderate caspase-3 activity, while cells treated with 5 μM G1 had low caspase-3 activity (**Figure 3B**).

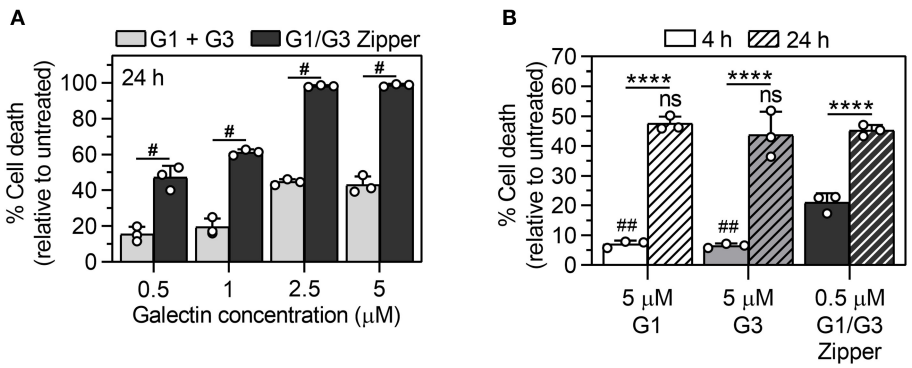

FIGURE 2 | Quantification of Jurkat T cell death via G1/G3 Zipper, G1, G3, or G1 + G3. **(A)** Percentage of dead Jurkat T cells treated with 0.5–5 μM of G1 + G3 (equimolar ratio) or G1/G3 Zipper for 24 h relative to untreated cells. **(B)** Percentage of dead Jurkat T cells treated with 5 μM G1, 5 μM G3, or 0.5 μM G1/G3 Zipper for 4 or 24 h relative to untreated cells. For **(A)**, # indicates significant differences between G1 + G3 and G1/G3 Zipper at each concentration tested and denotes $p < 0.0001$. For **(B)**, *indicates significant differences between time; # indicates significant differences relative to G1/G3 Zipper at $t = 4$ h; "ns" indicates no significant difference relative to G1/G3 Zipper at $t = 24$ h; two symbols denote $p < 0.01$ and four symbols denote $p < 0.0001$. All data shown are $N = 3$, mean ± standard deviation, and tested for statistically significant differences using one-way ANOVA with Tukey's *post-hoc*.

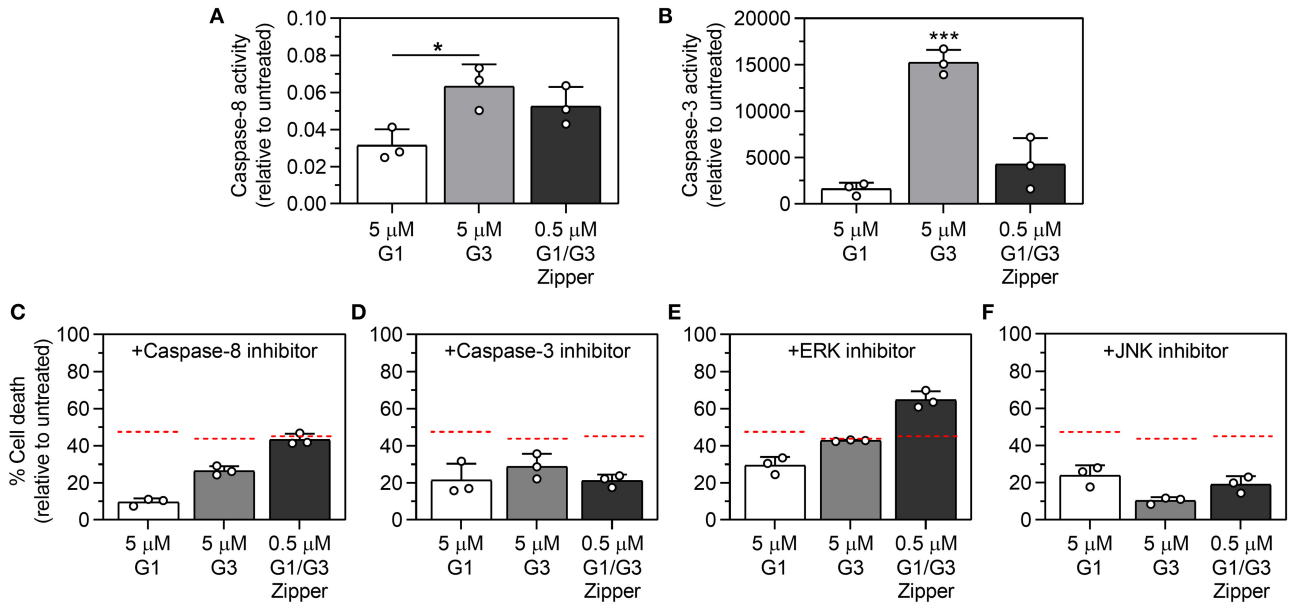

FIGURE 3 | Characterization of the role of caspase-8, caspase-3, ERK, and JNK activation in Jurkat T cell apoptosis induced by G1/G3 Zipper, G1, or G3. **(A)** Quantification of caspase-8 activity and **(B)** quantification of caspase-3 activity in Jurkat T cells treated with 5 μM G1, 5 μM G3, or 0.5 μM G1/G3 Zipper for 24 h relative to untreated cells. Percentage of dead Jurkat T cells (relative to untreated cells) following treatment with 5 μM G1, 5 μM G3, or 0.5 μM G1/G3 Zipper for 24 h in the presence of **(C)** caspase-8 inhibitor (Z-IETD-FMK), **(D)** caspase-3 inhibitor I, **(E)** ERK inhibitor (U0126), or **(F)** JNK inhibitor II (SP600125). For comparison, the red dashed lines in **(C–F)** indicate the percentage of dead Jurkat T cells following treatment with 5 μM G1, 5 μM G3, or 0.5 μM G1/G3 Zipper for 24 h, respectively, from **Figure 2B**. For **(A,B)**, * indicates significant differences between groups; one symbol denotes $p < 0.05$, three symbols denote $p < 0.001$; statistically significant differences were determined using one-way ANOVA with Tukey's *post-hoc*. All data shown are $N = 3$, mean ± standard deviation.

The Intracellular Mediators Involved in G1/G3 Zipper Pro-apoptotic Signaling Differ Relative to G1 and G3

We first evaluated the involvement of caspase-8 in Jurkat T cell death induced by G1/G3 Zipper, G1, or G3 using the caspase-8 inhibitor, Z-IETD-FMK. Inhibiting caspase-8 significantly reduced the activity of 5 μM G1 over 4 and 24 h (**Figure 3C**, **Supplementary Figure 3**). Inhibiting caspase-8 diminished the activity of 5 μM G3 over 24 h (**Figure 3C**), albeit to a lesser extent than G1, yet had only a weak effect on G3 over 4 h (**Supplementary Figure 3**). In contrast, inhibiting caspase-8 had no significant effect on 0.5 μM G1/G3 Zipper activity over 4 or 24 h (**Figure 3C**, **Supplementary Figure 3**).

Next, we evaluated the involvement of caspase-3 in Jurkat T cell death induced by G1/G3 Zipper, G1, or G3 using a commercially available caspase-3 inhibitor. Inhibiting caspase-3 significantly decreased the extent of cell death induced by 5 μM G1, 5 μM G3, or 0.5 μM G1/G3 Zipper over 24 h (**Figure 3D**). Notably, the caspase-3 inhibitor decreased the activity of G1/G3 Zipper, G1, and G3 to a similar extent. In contrast, inhibiting caspase-3 decreased the activity of G1/G3 Zipper over 4 h, yet had no effect on G1 or G3 (**Supplementary Figure 3**).

We characterized the role of ERK in Jurkat T cell death induced by G1/G3 Zipper, G1, or G3 using the ERK inhibitor, U0126. Inhibiting ERK increased the extent of cell death induced by G1/G3 Zipper, G1, or G3 over 4 h (**Supplementary Figure 3**). Over 24 h, inhibiting ERK also increased the pro-apoptotic activity of 0.5 μM G1/G3 Zipper (**Figure 3E**). In contrast, inhibiting ERK decreased the activity of 5 μM G1 over 24 h, but had no significant effect on the activity of 5 μM G3 (**Figure 3E**).

We characterized the role of JNK activation in Jurkat T cell death induced by G1/G3 Zipper, G1, or G3 using the ATP-competitive JNK inhibitor, SP600125 ("JNK inhibitor"). Inhibiting JNK activation significantly increased the extent of cell death induced by G3 and weakly increased the extent of cell death induced by G1/G3 Zipper over 4 h, whereas it had no effect on G1 activity over 4 h (**Supplementary Figure 3**). In contrast, inhibiting JNK activation decreased the extent of cell death induced by 5 μM G1, 5 μM G3, or 0.5 μM G1/G3 Zipper over 24 h (**Figure 3F**). Notably, inhibiting JNK decreased the pro-apoptotic activity of G3 over 24 h more than the activity of G1/G3 Zipper and G1, which were inhibited to a similar extent.

Collectively, these data suggest that the intracellular mediators that signal apoptosis downstream of G1/G3 Zipper, G1, and G3 differ relative to each other, as well as with time. In particular, caspase-8 was required to signal apoptosis via G1 over 4 h, while ERK activation was inhibitory. Caspase-3 and JNK activation played no role in G1 signaling at this time point. In contrast, over 24 h, caspase-8, caspase-3, ERK, and JNK all contributed to Jurkat T cell death via G1. Over 24 h, both JNK activation and ERK were inhibitory downstream of G3, whereas caspase-8 and caspase-3 were not involved. In contrast, caspase-8, caspase-3, and JNK contributed to pro-apoptotic signaling via G3 over 24 h, whereas ERK was not involved. Caspase-8 was never involved in

pro-apoptotic signaling downstream of G1/G3 Zipper, whereas caspase-3 was involved at both early and late time points. Further, inhibiting ERK always amplified pro-apoptotic signaling downstream of G1/G3 Zipper, whereas JNK activation inhibited apoptosis induced by G1/G3 Zipper early but amplified it late.

G1/G3 Zipper-Induced Cell Death Is Mediated by CD45 and Hindered by CD7

We treated Jurkat ($CD7^+$, $CD45^+$), HuT 78 ($CD7^-$, $CD45^+$), and J45.01 ($CD7^+$, $CD45^-$) T cells with a range of G1/G3 Zipper, G1, or G3 concentrations to characterize the role of the cell surface glycoprotein receptors CD7 and CD45 in galectin-induced cell death. At 5 μM, G1 induced significantly less death of HuT 78 and J45.01 T cells than Jurkat T cells (**Figure 4A**). The extent of HuT 78 T cell death increased with G1 concentration (**Figure 4A**, gray bars), reaching a maximum that was slightly higher, although not significantly greater, than the extent of Jurkat T cell death induced by G1. In contrast, G1 only weakly induced J45.01 cell death at the concentrations tested (**Figure 4A**, black bars).

At 5 μM, G3 induced significantly less death of HuT 78 and J45.01 T cells than Jurkat T cells (**Figure 4B**), similar to G1. The extent of HuT 78 T cell death increased with G3 concentration (**Figure 4B**, gray bars), reaching a maximum that was slightly higher, although not significantly greater, than the extent of Jurkat T cell death induced by G3, similar to G1. In contrast to G1, the extent of J45.01 T cell death also increased with G3 concentration (**Figure 4B**, black bars), reaching a maximum that was comparable to the extent of Jurkat T cell death induced by G3.

At low concentrations, G1/G3 Zipper induced significantly more death of HuT 78 T cells than Jurkat T cells (**Figure 4C**, gray bars), similar to G1 and G3 at high concentration. At 0.5 μM, G1/G3 Zipper induced significantly less J45.01 T cell death than Jurkat T cell death, whereas the extent of J45.01 T cell and Jurkat T cell death at all other G1/G3 Zipper concentrations were similar.

Collectively, these data suggest that G1/G3 Zipper, G1, and G3 require CD45 to signal apoptosis. These data also suggest that CD7 antagonizes G1/G3 Zipper signaling at low galectin concentration, and may also inhibit G1 and G3 signaling at high galectin concentrations, whereas it is necessary for G1 and G3 signaling at low galectin concentrations.

DISCUSSION

Here we report a comparison of the pro-apoptotic signaling pathways activated by a synthetic G1/G3 tetramer referred to as G1/G3 Zipper, G1, and G3. Collectively, the data demonstrate that each protein differentially employs CD45, CD7, caspase-8, caspase-3, ERK, and JNK to induce apoptosis. In particular, G1/G3 Zipper, G1, and G3 all depend on caspase-3 to induce apoptosis. However, G3 induces significantly greater caspase-3 activity than G1/G3 Zipper or G1. Further, caspase-3 inhibition has a similar effect on G1/G3 Zipper and G1 activity, which is greater than the effect on G3 activity. Taken together, these observations suggest that G1/G3 Zipper behaves more like G1 than G3, in agreement with our initial hypothesis.

With regard to caspase-8, however, G1/G3 Zipper differs from both G1 and G3. For example, while G1/G3 Zipper, G1, and G3 all activate caspase-8, G1/G3 Zipper does not depend on it to induce apoptosis. In contrast, G1 depends on caspase-8 at both early and late time points, whereas G3 depends on it only at a later time point.

The role of JNK activation in G1/G3 Zipper signaling is more similar to its role in G3 signaling than G1 signaling. In particular, inhibition of JNK activation weakly increased the activity of G1/G3 Zipper at an early time point, but weakly decreased it at a late time point. In contrast, JNK inhibition strongly potentiated G3 activity at an early time point and significantly decreased it at a late time point, whereas JNK inhibition only decreased G1 activity at a late time point. This latter observation was consistent with a previous report which demonstrated that G1 induces Jurkat T cell death via activation of JNK and, in turn, c-Jun and

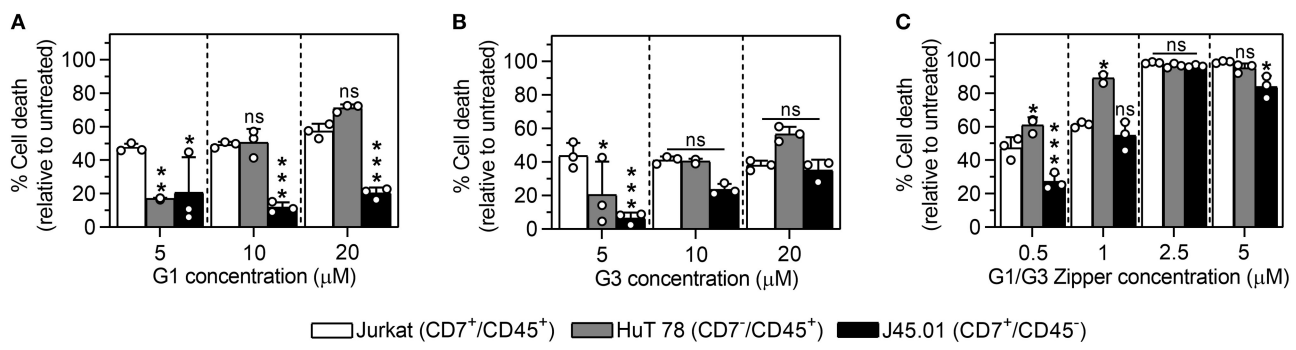

FIGURE 4 | Comparison of Jurkat, HuT 78, and J45.01 T cell death via G1/G3 Zipper, G1, or G3. Percentage of dead cells following treatment of Jurkat, HuT 78, or J45.01 T cells with **(A)** 5–20 μM G1, **(B)** 5–20 μM G3, or **(C)** 0.5–5 μM G1/G3 Zipper for 24 h relative to untreated cells. For **(A–C)**, * indicates significant differences relative to Jurkat T cells; "ns" indicates no significant difference between cells. In all panels, one symbol denotes $p < 0.05$, two symbols denote $p < 0.01$, and three symbols denote $p < 0.001$. All data shown are $N = 3$, mean ± standard deviation, and tested for statistically significant differences using one-way ANOVA with Tukey's *post-hoc*.

AP-1 (Brandt et al., 2010). These observations suggest that G1/G3 Zipper does not induce apoptosis exclusively through G1-related pathways, which contrasts with our hypothesis. Instead, these data suggest that the G3 domains of G1/G3 Zipper are active as extracellular signals, but that their activity is diminished when compared to the native protein, which may be due to differences in carbohydrate-recognition domain valency.

Unexpectedly, ERK activation has contrasting roles in G1/G3 Zipper, G1, and G3 signaling. In particular, inhibiting ERK increased G1 activity early but diminished it at a later time point, increased G3 activity early but had no effect later, and increased G1/G3 Zipper activity at both early and late time points. These observations suggest that pro-apoptotic signaling via G1/G3 Zipper is not simply an additive combination of the signaling pathways activated by G1 and G3, but instead may involve an alternative pathway that integrates aspects of the pathways activated by both galectins.

Differences in the pro-apoptotic signaling pathways activated by G1/G3 Zipper, G1, and G3 may stem from differences in the role of the membrane glycoproteins CD7 and CD45 as signal transducers. For example, high CD45 expression was required for G1 activity under all conditions tested, whereas the activity of G1/G3 Zipper and G3 toward CD45 low cells increased with their concentration. Toward CD7 low cells, the activity of both G1 and G3 increased with their concentration, but was weakened relative to their activity toward CD7 high cells at low galectin concentration. In contrast, low CD7 expression enhanced G1/G3 Zipper activity at low concentrations, whereas it had no effect at high G1/G3 Zipper concentrations. Collectively, these data suggest that CD7 is not directly involved as a signal transducer of G1/G3 Zipper, but instead may act as an antagonist, whereas it is involved in both G1 and G3 signaling, as suggested in prior reports (Pace et al., 1999, 2000; Fukumori et al., 2003; Stillman et al., 2006). Note that any differences in the role of CD7 in galectin signaling observed here and reported elsewhere may be due to differences in protein concentration, culture time, or cell type which often vary across studies. Further, these data suggest that G1/G3 Zipper signals at least in part through CD45, which could be mediated by either the G1 or G3 domain, as both have been implicated in G1 and G3 signaling previously (Nguyen et al., 2001; Stillman et al., 2006). However, the observation that G1/G3 Zipper induces considerable death of CD45 low cells at all concentrations tested suggests that other membrane glycoproteins likely also act as signal transducers or binding partners. Future research efforts will work to identify membrane glycoproteins that are recognized by G1/G3 Zipper, as well as those that act as transducers of pro-apoptotic signals.

Both caspase-8 and JNK activation can induce changes in metabolic activity that lead to pro-apoptotic signaling (Li et al., 1998; Dhanasekaran and Reddy, 2017). We previously reported that G1/G3 Zipper decreased NADH content of Jurkat T cells to a greater extent than both native G1 and a polymer-stabilized G1 homodimer, as measured by conversion of resazurin to resorufin with the CellTiter-Blue® cell viability assay (Promega) (Fettis et al., 2019). Here we observed that both caspase-8 and JNK activation are involved in pro-apoptotic signaling via G1. In contrast, pro-apoptotic signaling via G1/G3 Zipper depends on JNK activation but not caspase-8 activity. The observation that G1/G3 Zipper induced higher caspase-8 activity than G1 suggests that the increased metabolic dysfunction induced by G1/G3 Zipper relative to G1 reported previously is due to caspase-8. But why is caspase-8 a bystander in pro-apoptotic signaling downstream of G1/G3 Zipper but not G1? The answer may lie in the observed disparity in the role of ERK downstream of G1/G3 Zipper and G1. JNK and/or caspase-8 acting on mitochondria can lead to activation of caspase-9 that amplifies cell death by increasing caspase-3 activity (Li et al., 1998; Dhanasekaran and Reddy, 2008). Consistent with this, we observed higher caspase-3 activity in cells treated with G1/G3 Zipper relative to cells treated with G1. Further, phosphorylation via ERK inhibits caspase-9 (Allan et al., 2003), and here inhibiting ERK activity increased the extent of cell death induced by G1/G3 Zipper. Collectively, these observations suggest a role for caspase-9 downstream of mitochondrial dysfunction as a contributor to G1/G3 Zipper pro-apoptotic signaling. Future work will take a closer look at the interplay between JNK activation, mitochondrial function, ERK activity, and caspase−8,−9, and−3 in pro-apoptotic signaling induced by G1/G3 Zipper.

CONCLUSIONS

G1/G3 Zipper, a synthetic engineered tetramer with two G1 and two G3 domains, induces apoptosis to a greater extent than G1 and G3 alone or in combination. The results reported here suggest that G1/G3 Zipper signals apoptosis through a pathway that depends on caspase-3 and JNK, like G1 and G3, but is independent of caspase-8 activity and is amplified by ERK inhibition, which contrasts with G1 and G3. G1/G3 Zipper signaling is mediated in part by CD45, similar to G1 and G3, but inhibited by CD7, which contrasts with G1 and G3. Collectively, these observations call into question our prior mechanistic hypothesis which suggested that G1 acts as the signal while G3 acts as an anchor. Instead, G1/G3 Zipper amplifies pro-apoptotic signaling by integrating the activities of both G1 and G3. Although we have not yet elucidated the particular intracellular signals through which G1/G3 Zipper induces apoptosis in exhaustive detail, we have begun to understand the roles of common pro-apoptotic signaling molecules in this pathway. Further, we have identified key differences between an engineered galectin variant and the native proteins from which it was created. Finally, we demonstrated that co-integrating galectins into a single construct can enhance their signaling activity. Increasing understanding of the interplay between G1 and G3 assembled into non-native architectures may provide new opportunities to therapeutically regulate innate and adaptive immunity.

DATA AVAILABILITY STATEMENT

The raw data supporting the conclusions of this article will be made available by the authors, without undue reservation, to any qualified researcher.

AUTHOR CONTRIBUTIONS

GH designed experiments, analyzed data, and wrote the paper. SF designed and conducted flow cytometry experiments, analyzed data, and contributed to writing and editing of the paper. MF designed and conducted caspase activity experiments, analyzed data, and edited the paper. RL assisted with collection and analysis of flow cytometry data and edited the paper.

FUNDING

Research reported in this publication was supported by National Institutes of Health grants: R03 EB019684, R01 DE027301, R21 EB024762. Research reported in this publication was also supported by the National Center for Advancing Translational Sciences of the National Institutes of Health under University of Florida Clinical and Translational Science Awards TL1TR001428 and UL1TR001427. The content is solely the responsibility of the authors and does not necessarily represent the official views of the National Institutes of Health.

ACKNOWLEDGMENTS

The authors would like to acknowledge Dr. Benjamin G. Keselowsky for kindly providing Jurkat T cells.

SUPPLEMENTARY MATERIAL

The Supplementary Material for this article can be found online at: https://www.frontiersin.org/articles/10.3389/fchem.2019.00898/full#supplementary-material

REFERENCES

Allan, L. A., Morrice, N., Brady, S., Magee, G., Pathak, S., and Clarke, P. R. (2003). Inhibition of caspase-9 through phosphorylation at Thr 125 by ERK MAPK. *Nat Cell Biol* 5, 647–654. doi: 10.1038/ncb1005

Arencibia, I., Frankel, G., and Sundqvist, K. G. (2002). Induction of cell death in T lymphocytes by invasin via beta1-integrin. *Eur J Immunol* 32, 1129–1138. doi: 10.1002/1521-4141(200204)32:4<1129::AID-IMMU1129>3.0.CO;2-G

Baum, L. G., Garner, O. B., Schaefer, K., and Lee, B. (2014). Microbe-host interactions are positively and negatively regulated by galectin-glycan interactions. *Front Immunol* 5:284. doi: 10.3389/fimmu.2014.00284

Brandt, B., Abou-Eladab, E. F., Tiedge, M., and Walzel, H. (2010). Role of the JNK/c-Jun/AP-1 signaling pathway in galectin-1-induced T-cell death. *Cell Death Dis.* 1:e23. doi: 10.1038/cddis.2010.1

Brandt, B., Buchse, T., Abou-Eladab, E. F., Tiedge, M., Krause, E., Jeschke, U., et al. (2008). Galectin-1 induced activation of the apoptotic death-receptor pathway in human Jurkat T lymphocytes. *Histochem. Cell Biol.* 129, 599–609. doi: 10.1007/s00418-008-0395-x

Brown, T. J., Shuford, W. W., Wang, W. C., Nadler, S. G., Bailey, T. S., Marquardt, H., et al. (1996). Characterization of a CD43/leukosialin-mediated pathway for inducing apoptosis in human T-lymphoblastoid cells. *J. Biol. Chem.* 271, 27686–27695. doi: 10.1074/jbc.271.44.27686

Cedeno-Laurent, F., Barthel, S. R., Opperman, M. J., Lee, D. M., Clark, R. A., and Dimitroff, C. J. (2010). Development of a nascent galectin-1 chimeric molecule for studying the role of leukocyte galectin-1 ligands and immune disease modulation. *J. Immunol.* 185, 4659–4672. doi: 10.4049/jimmunol.1000715

Chung, A. W., Sieling, P. A., Schenk, M., Teles, R. M., Krutzik, S. R., Hsu, D. K., et al. (2013). Galectin-3 regulates the innate immune response of human monocytes. *J. Infect. Dis.* 207, 947–956. doi: 10.1093/infdis/jis920

Cummings, R. D., Liu, F. T., and Vasta, G. R. (2015). "Galectins," in *Essentials of Glycobiology*, eds A. Varki and D. Richard (Cold Spring Harbor, NY: Cold Spring Harbor Laboratory Press), 469–480.

Dhanasekaran, D. N., and Reddy, E. P. (2008). JNK signaling in apoptosis. *Oncogene* 27, 6245–6251. doi: 10.1038/onc.2008.301

Dhanasekaran, D. N., and Reddy, E. P. (2017). JNK-signaling: a multiplexing hub in programmed cell death. *Genes Cancer* 8, 682–694. doi: 10.18632/genesandcancer.155

Earl, L. A., Bi, S., and Baum, L. G. (2011). Galectin multimerization and lattice formation are regulated by linker region structure. *Glycobiology* 21, 6–12. doi: 10.1093/glycob/cwq144

Elola, M. T., Chiesa, M. E., Alberti, A. F., Mordoh, J., and Fink, N. E. (2005). Galectin-1 receptors in different cell types. *J. Biomed. Sci.* 12, 13–29. doi: 10.1007/s11373-004-8169-5

Farhadi, S. A., Bracho-Sanchez, E., Fettis, M. M., Seroski, D. T., Freeman, S. L., Restuccia, A., et al. (2018). Locally anchoring enzymes to tissues via extracellular glycan recognition. *Nat. Commun.* 9:4943. doi: 10.1038/s41467-018-07129-6

Farhadi, S. A., and Hudalla, G. A. (2016). Engineering galectin-glycan interactions for immunotherapy and immunomodulation. *Exp. Biol. Med.* 241, 1074–1083. doi: 10.1177/1535370216650055

Fettis, M. M., Farhadi, S. A., and Hudalla, G. A. (2019). A chimeric, multivalent assembly of galectin-1 and galectin-3 with enhanced extracellular activity. *Biomater. Sci.* 7, 1852–1862. doi: 10.1039/C8BM01631C

Fettis, M. M., and Hudalla, G. A. (2018). Engineering reactive oxygen species-resistant galectin-1 dimers with enhanced lectin activity. *Bioconjug. Chem.* 29, 2489–2496. doi: 10.1021/acs.bioconjchem.8b00425

Fukumori, T., Takenaka, Y., Yoshii, T., Kim, H. R., Hogan, V., Inohara, H., et al. (2003). CD29 and CD7 mediate galectin-3-induced type II T-cell apoptosis. *Cancer Res.* 63, 8302–8311.

Hahn, H. P., Pang, M., He, J., Hernandez, J. D., Yang, R. Y., Li, L. Y., et al. (2004). Galectin-1 induces nuclear translocation of endonuclease G in caspase- and cytochrome c-independent T cell death. *Cell Death Differ.* 11, 1277–1286. doi: 10.1038/sj.cdd.4401485

Hsu, D. K., Hammes, S. R., Kuwabara, I., Greene, W. C., and Liu, F. T. (1996). Human T lymphotropic virus-I infection of human T lymphocytes induces expression of the beta-galactoside-binding lectin, galectin-3. *Am. J. Pathol.* 148, 1661–1670.

Hu, Y., Yelehe-Okouma, M., Ea, H. K., Jouzeau, J. Y., and Reboul, P. (2017). Galectin-3: a key player in arthritis. *Joint Bone Spine* 84, 15–20. doi: 10.1016/j.jbspin.2016.02.029

Hughes, R. C. (2001). Galectins as modulators of cell adhesion. *Biochimie* 83, 667–676. doi: 10.1016/S0300-9084(01)01289-5

Lesage, S., Steff, A. M., Philippoussis, F., Page, M., Trop, S., Mateo, V., et al. (1997). CD4+ CD8+ thymocytes are preferentially induced to die following CD45 cross-linking, through a novel apoptotic pathway. *J. Immunol.* 159, 4762–4771.

Lesnikov, V., Lesnikova, M., and Deeg, H. J. (2001). Pro-apoptotic and anti-apoptotic effects of transferrin and transferrin-derived glycans on hematopoietic cells and lymphocytes. *Exp. Hematol.* 29, 477–489. doi: 10.1016/S0301-472X(00)00687-1

Li, H., Zhu, H., Xu, C. J., and Yuan, J. (1998). Cleavage of BID by caspase 8 mediates the mitochondrial damage in the Fas pathway of apoptosis. *Cell* 94, 491–501. doi: 10.1016/S0092-8674(00)81590-1

Li, S., Yu, Y., Koehn, C. D., Zhang, Z., and Su, K. (2013). Galectins in the pathogenesis of rheumatoid arthritis. *J. Clin. Cell Immunol.* 4:1000164. doi: 10.4172/2155-9899.1000164

Matarrese, P., Tinari, A., Mormone, E., Bianco, G. A., Toscano, M. A., Ascione, B., et al. (2005). Galectin-1 sensitizes resting human T lymphocytes to Fas (CD95)-mediated cell death via mitochondrial hyperpolarization, budding, and fission. *J. Biol. Chem.* 280, 6969–6985. doi: 10.1074/jbc.M409752200

Nguyen, J. T., Evans, D. P., Galvan, M., Pace, K. E., Leitenberg, D., Bui, T. N., et al. (2001). CD45 modulates galectin-1-induced T cell death:

regulation by expression of core 2 O-glycans. *J. Immunol.* 167, 5697–5707. doi: 10.4049/jimmunol.167.10.5697

Pace, K. E., Hahn, H. P., and Baum, L. G. (2003). Preparation of recombinant human galectin-1 and use in T-cell death assays. *Methods Enzymol.* 363, 499–518. doi: 10.1016/S0076-6879(03)01075-9

Pace, K. E., Hahn, H. P., Pang, M., Nguyen, J. T., and Baum, L. G. (2000). CD7 delivers a pro-apoptotic signal during galectin-1-induced T cell death. *J. Immunol.* 165, 2331–2334. doi: 10.4049/jimmunol.165.5.2331

Pace, K. E., Lee, C., Stewart, P. L., and Baum, L. G. (1999). Restricted receptor segregation into membrane microdomains occurs on human T cells during apoptosis induced by galectin-1. *J. Immunol.* 163, 3801–3811.

Rabinovich, G. A., Daly, G., Dreja, H., Tailor, H., Riera, C. M., Hirabayashi, J., et al. (1999). Recombinant galectin-1 and its genetic delivery suppress collagen-induced arthritis via T cell apoptosis. *J. Exp. Med.* 190, 385–398. doi: 10.1084/jem.190.3.385

Rabinovich, G. A., and Toscano, M. A. (2009). Turning 'sweet' on immunity: galectin-glycan interactions in immune tolerance and inflammation. *Nat. Rev. Immunol.* 9, 338–352. doi: 10.1038/nri2536

Reddy, P. B., Schreiber, T. H., Rajasagi, N. K., Suryawanshi, A., Mulik, S., Veiga-Parga, T., et al. (2012). TNFRSF25 agonistic antibody and galectin-9 combination therapy controls herpes simplex virus-induced immunoinflammatory lesions. *J. Virol.* 86, 10606–10620. doi: 10.1128/JVI.01391-12

Restuccia, A., Fettis, M. M., Farhadi, S. A., Molinaro, M. D., Kane, B., and Hudalla, G. A. (2018). Evaluation of self-assembled glycopeptide nanofibers modified with N,N '-diacetyllactosamine for selective galectin-3 recognition and inhibition. *ACS Biomater. Sci. Eng.* 4, 3451–3459. doi: 10.1021/acsbiomaterials.8b00611

Restuccia, A., Tian, Y. F., Collier, J. H., and Hudalla, G. A. (2015). Self-assembled glycopeptide nanofibers as modulators of galectin-1 bioactivity. *Cell Mol. Bioeng.* 8, 471–487. doi: 10.1007/s12195-015-0399-2

Santucci, L., Fiorucci, S., Rubinstein, N., Mencarelli, A., Palazzetti, B., Federici, B., et al. (2003). Galectin-1 suppresses experimental colitis in mice. *Gastroenterology* 124, 1381–1394. doi: 10.1016/S0016-5085(03)00267-1

Stillman, B. N., Hsu, D. K., Pang, M., Brewer, C. F., Johnson, P., Liu, F. T., et al. (2006). Galectin-3 and galectin-1 bind distinct cell surface glycoprotein receptors to induce T cell death. *J. Immunol.* 176, 778–789. doi: 10.4049/jimmunol.176.2.778

Stowell, S. R., Arthur, C. M., Mehta, P., Slanina, K. A., Blixt, O., Leffler, H., et al. (2008a). Galectin-1,−2, and−3 exhibit differential recognition of sialylated glycans and blood group antigens. *J. Biol. Chem.* 283, 10109–10123. doi: 10.1074/jbc.M709545200

Stowell, S. R., Qian, Y., Karmakar, S., Koyama, N. S., Dias-Baruffi, M., Leffler, H., et al. (2008b). Differential roles of galectin-1 and galectin-3 in regulating leukocyte viability and cytokine secretion. *J. Immunol.* 180, 3091–3102. doi: 10.4049/jimmunol.180.5.3091

St-Pierre, C., Manya, H., Ouellet, M., Clark, G. F., Endo, T., Tremblay, M. J., et al. (2011). Host-soluble galectin-1 promotes HIV-1 replication through a direct interaction with glycans of viral gp120 and host CD4. *J. Virol.* 85, 11742–11751. doi: 10.1128/JVI.05351-11

Strauss, G., Osen, W., and Debatin, K. M. (2002). Induction of apoptosis and modulation of activation and effector function in T cells by immunosuppressive drugs. *Clin. Exp. Immunol.* 128, 255–266. doi: 10.1046/j.1365-2249.2002.01777.x

Than, N. G., Romero, R., Kim, C. J., McGowen, M. R., Papp, Z., and Wildman, D. E. (2012). Galectins: guardians of eutherian pregnancy at the maternal-fetal interface. *Trends Endocrinol. Metab.* 23, 23–31. doi: 10.1016/j.tem.2011.09.003

Thiemann, S., and Baum, L. G. (2016). Galectins and immune responses-just how do they do those things they do? *Annu. Rev. Immunol.* 34, 243–264. doi: 10.1146/annurev-immunol-041015-055402

Tribulatti, M. V., Figini, M. G., Carabelli, J., Cattaneo, V., and Campetella, O. (2012). Redundant and antagonistic functions of galectin-1, −3, and −8 in the elicitation of T cell responses. *J. Immunol.* 188, 2991–2999. doi: 10.4049/jimmunol.1102182

van der Leij, J., van den Berg, A., Harms, G., Eschbach, H., Vos, H., Zwiers, P., et al. (2007). Strongly enhanced IL-10 production using stable galectin-1 homodimers. *Mol. Immunol.* 44, 506–513. doi: 10.1016/j.molimm.2006.02.011

Vasta, G. R., Ahmed, H., Nita-Lazar, M., Banerjee, A., Pasek, M., Shridhar, S., et al. (2012). Galectins as self/non-self recognition receptors in innate and adaptive immunity: an unresolved paradox. *Front. Immunol.* 3:199. doi: 10.3389/fimmu.2012.00199

Walzel, H., Schulz, U., Neels, P., and Brock, J. (1999). Galectin-1, a natural ligand for the receptor-type protein tyrosine phosphatase CD45. *Immunol. Lett.* 67, 193–202. doi: 10.1016/S0165-2478(99)00012-7

Xue, H., Liu, L., Zhao, Z., Zhang, Z., Guan, Y., Cheng, H., et al. (2017). The N-terminal tail coordinates with carbohydrate recognition domain to mediate galectin-3 induced apoptosis in T cells. *Oncotarget* 8, 49824–49838. doi: 10.18632/oncotarget.17760

Conflict of Interest: The authors declare that the research was conducted in the absence of any commercial or financial relationships that could be construed as a potential conflict of interest.

frontiers in Chemistry

MINI REVIEW
published: 05 February 2020
doi: 10.3389/fchem.2020.00055

Biological and Technical Challenges in Unraveling the Role of N-Glycans in Immune Receptor Regulation

*Paola de Haas[1], Wiljan J. A. J. Hendriks[1], Dirk J. Lefeber[2,3] and Alessandra Cambi[1]**

[1] Department of Cell Biology, Radboud Institute for Molecular Life Sciences, Radboud University Medical Center, Nijmegen, Netherlands, [2] Department of Laboratory Medicine, Translational Metabolic Laboratory, Radboud Institute for Molecular Life Sciences, Radboud University Medical Center, Nijmegen, Netherlands, [3] Department of Neurology, Donders Institute for Brain, Cognition and Behaviour, Radboud University Medical Center, Nijmegen, Netherlands

N-glycosylation of membrane receptors is important for a wide variety of cellular processes. In the immune system, loss or alteration of receptor glycosylation can affect pathogen recognition, cell-cell interaction, and activation as well as migration. This is not only due to aberrant folding of the receptor, but also to altered lateral mobility or aggregation capacity. Despite increasing evidence of their biological relevance, glycosylation-dependent mechanisms of receptor regulation are hard to dissect at the molecular level. This is due to the intrinsic complexity of the glycosylation process and high diversity of glycan structures combined with the technical limitations of the current experimental tools. It is still challenging to precisely determine the localization and site-occupancy of glycosylation sites, glycan micro- and macro-heterogeneity at the individual receptor level as well as the biological function and specific interactome of receptor glycoforms. In addition, the tools available to manipulate N-glycans of a specific receptor are limited. Significant progress has however been made thanks to innovative approaches such as glycoproteomics, metabolic engineering, or chemoenzymatic labeling. By discussing examples of immune receptors involved in pathogen recognition, migration, antigen presentation, and cell signaling, this Mini Review will focus on the biological importance of N-glycosylation for receptor functions and highlight the technical challenges for examination and manipulation of receptor N-glycans.

Keywords: membrane receptor, glycocalyx, N-glycans, immune receptor, glycoprotein, galectin, cell membrane, protein glycoforms

OPEN ACCESS

Edited by:
Karina Valeria Mariño, Institute of Biology and Experimental Medicine (IBYME), Argentina

Reviewed by:
Yoshiki Yamaguchi, Tohoku Medical and Pharmaceutical University, Japan
Morten Thaysen-Andersen, Macquarie University, Australia

***Correspondence:**
Alessandra Cambi
alessandra.cambi@radboudumc.nl

Specialty section:
This article was submitted to Chemical Biology, a section of the journal Frontiers in Chemistry

Received: *29 August 2019*
Accepted: *17 January 2020*
Published: *05 February 2020*

Citation:
de Haas P, Hendriks WJAJ, Lefeber DJ and Cambi A (2020) Biological and Technical Challenges in Unraveling the Role of N-Glycans in Immune Receptor Regulation. Front. Chem. 8:55. doi: 10.3389/fchem.2020.00055

INTRODUCTION

Protein glycosylation, the enzymatic addition of glycans to amino acid side chains, is the most common post-translational modification. It is exerted by an intricate set of enzymes that prunes and grafts the carbohydrate moieties on proteins traveling the endoplasmic reticulum (ER)—Golgi apparatus secretory route toward the cell surface (Ohtsubo and Marth, 2006).

Glycans are composed of different monosaccharides, that can be covalently bound via alpha or beta linkages, rendering a wide range of glycan structures. Competition and dynamics of glycosylation enzymes lead to varying glycan structures not only on different proteins but also within the same protein, a phenomenon called glycan microheterogeneity. Also, one protein can have multiple glycosylation sites that may be partially occupied, reflecting variations in

enzymes, substrate, and protein acceptor fluxes (Zacchi and Schulz, 2016), resulting in glycan macroheterogeneity. Glycan heterogeneity occurs among different tissues (Medzihradszky et al., 2015), biomarks developmental and activation stages (Clark and Baum, 2012), and correlates to aging and disease processes (Kristic et al., 2014; Reily et al., 2019).

Two major types of protein glycosylation are discerned: N-glycosylation, the addition of glycan chains on the amide nitrogen of asparagine residues in the ER, and O-glycosylation, the addition of glycan chains to the oxygen atom of serine/threonine residues in the Golgi. For many membrane proteins, removal of N-glycosylation sites leads to intracellular retention, degradation, and reduced membrane expression (Barbosa et al., 1987; Fischer et al., 2017). Moreover, after arrival on the cell surface, the stability and functionality of glycoproteins remain dependent on their glycosylation pattern (Dennis et al., 2009a,b; Skropeta, 2009). This partly relates to the existence of membrane-associated β-galactoside-binding lectins, known as galectins, which bind and crosslink different glycoproteins (Nabi et al., 2015). Since galectins have multiple binding sites and form multimers, they enable the formation of galectin lattices: an intricate network of glycoproteins and glycan-binding proteins, which shapes and regulates cell surface subdomains of clustered macromolecules and ultimately influences cell functions (Lajoie et al., 2009).

Aberrant protein glycosylation impacts viability and functionality of cells and organisms. This is underlined by the Congenital Disorders of Glycosylation, where defects in the synthesis or processing of glycans affect glycoprotein activities and cause a large variety of systemic symptoms (Peanne et al., 2018). Furthermore, Mkhikian et al. demonstrated that in multiple sclerosis environmental factors and genetic variants of immune receptors and glycosylation enzymes collectively dysregulate the N-glycosylation pathway (Mkhikian et al., 2011). Finally, malignant transformation is notoriously associated with altered glycosylation (Marsico et al., 2018). Despite its clear biomedical relevance, addressing the involvement of glycosylation in protein activity is challenging due to the complexity of the glycosylation process and the relatively limited experimental tools available.

Recent reviews highlight the importance of protein-glycan interactions in immunity (Marth and Grewal, 2008; Van Kooyk and Rabinovich, 2008; Zhou et al., 2018). In this review, we highlight key examples of how N-glycosylation of membrane immune receptors influences receptor properties, such as lateral interactions with neighboring molecules, clustering and diffusion behavior, all modulating receptor function (**Figure 1**). We also discuss tools and approaches for detection and manipulation of membrane receptor glycosylation, emphasizing current challenges and opportunities (**Table 1**).

MEMBRANE IMMUNE RECEPTOR GLYCOSYLATION: BEYOND PROTEIN FOLDING

Pathogen Recognition

Many membrane receptors involved in pathogen-recognition are glycosylated and their glycans can influence their function. For example, Dendritic Cell Immunoreceptor (DCIR) has one N-glycosylation site inside its carbohydrate-recognition domain. Removing or truncating this glycan increases the affinity for DCIR-binding ligands, but the underlying mechanism is still undefined (Bloem et al., 2013). For other pathogen recognition receptors, more information on N-glycosylation impact is available and will be discussed.

DC-SIGN is a homo-tetramer expressed by human macrophages and dendritic cells (Geijtenbeek et al., 2000) and organizes in nanoclusters at the cell membrane, which are specifically important for binding of virus-size particles (Cambi et al., 2004). Mutagenesis of its single N-glycosylation site (N80A) does not alter the expression levels and overall binding capacity nor nanocluster formation. However, unlike the wild-type receptor, the DC-SIGN-N80A mutant exhibits clathrin-independent internalization of virus particles and reduced adhesion strengthening when binding *Candida albicans* (Torreno-Pina et al., 2014; Te Riet et al., 2017). This could be explained by DC-SIGN-N80A inability to laterally interact with actin-anchored transmembrane glycoproteins like CD44. Wildtype DC-SIGN diffusion pattern—but not that of DC-SIGN-N80A—indeed overlaps with that of CD44, being restricted to membrane areas of high clathrin density (Torreno-Pina et al., 2014). This interaction is possibly regulated by galectins since proteomic studies show colocalization of DC-SIGN, CD44, and Galectin-9 at the phagosome (Buschow et al., 2012), and lactose addition, which competes with binding of extracellular galectins to N-glycan chains, prevents adhesion strengthening during DC-SIGN-pathogen binding (Te Riet et al., 2017).

The pathogen-recognition receptor Dectin-1, which binds fungal β-glucan, is also shown to be dependent on galectin interactions. A N-glycan-dependent close association of Dectin-1 with Galectin-3 is demonstrated on murine macrophage membranes, which is required for the proinflammatory response to pathogenic fungi (Esteban et al., 2011; Leclaire et al., 2018). Removal of Dectin-1 N-glycans lowers surface expression levels, negatively influencing ligand-binding and the collaboration with Toll-like Receptor 2 (TLR2; Kato et al., 2006).

Interactions of TLR2 and TLR4 with Galectin-3 are also documented. Macrophages differently sense pathogenic and non-pathogenic fungi thanks to a TLR2-Galectin-3 association induced by ligands specifically present on the pathogen's surface (Jouault et al., 2006). Galectin-3-dependent TLR4 activation contributes to sustained microglia activation, prolonging the inflammatory response in neuroinflammatory diseases (Esteban et al., 2011; Burguillos et al., 2015). TLR4 has 9 N-linked glycosylation sites and is part of the lipopolysaccharide (LPS) receptor complex together with the glycoproteins CD14 and MD-2. The N-linked glycans of both MD-2 and TLR4 are essential in maintaining the functional integrity of the LPS receptor (Da Silva Correia and Ulevitch, 2002).

Antigen Presentation

Not only antigen recognition and uptake but also antigen presentation is influenced by N-glycosylation. All major histocompatibility (MHC) glycoprotein family members contain evolutionary highly conserved putative sites for N-glycosylation, suggesting functional relevance (Ryan and Cobb, 2012). Indeed,

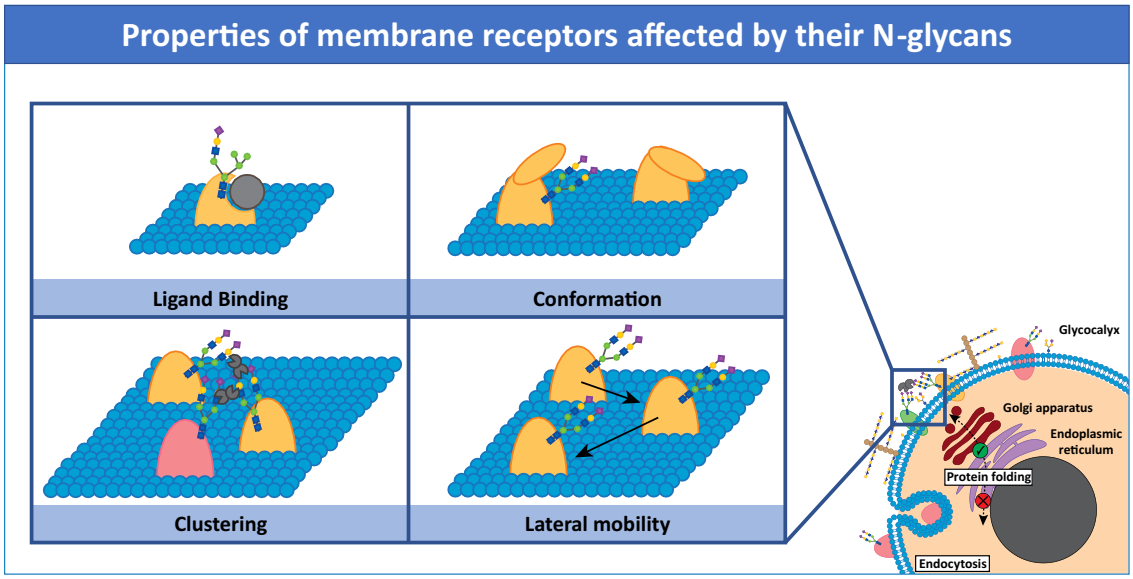

FIGURE 1 | Properties of membrane receptors influenced by N-glycans. The presence or absence of N-glycans on receptor molecules can modulate receptor function by affecting not only folding but also ligand binding, conformation, clustering, and lateral mobility. Glycan-crosslinking proteins, such as galectins, can influence these properties.

removal of N-glycans from MHCIa molecules by mutagenesis of glycosylation sites significantly increases protein misfolding thus decreasing surface expression levels (Barbosa et al., 1987). Additionally, the MHC-I glycan chains are critical for its association with calreticulin, which is required to form a stable MHCI-antigenic peptide loading complex that is necessary to elicit a T cell response (Van Der Burg et al., 1996; Wearsch et al., 2011; Zhang et al., 2011).

Removal of the complex N-glycans on MHCII molecules, using inhibitors catanospermine and kifunensine or by knockout of the glycosyltransferase gene *MGAT2*, reduces binding and presentation of glycoantigens, but not of peptide antigens, and reduces T cell activation (Ryan et al., 2011). Authors speculate that the MHCII peptide-binding groove requires N-glycans on its protein backbone to be sufficiently large for capturing glycoantigens, suggesting direct MHCII N-glycan involvement in glycoantigen binding (Ryan et al., 2011). MHCII N-glycosylation seems to be very different depending on the type of antigen-presenting cell, which could fine-tune the information exchange with T cells (Ryan and Cobb, 2012).

Immune Signaling

Signaling immune receptors on B and T lymphocytes are also glycosylation-dependent. The receptor of the proinflammatory cytokine IFNγ (IFNγR) is composed of two IFNγR1 and two IFNγR2 subunits. In several children suffering from hypersensitivity to non-tuberculous mycobacterial infections, a homozygous T168N mutation is present in the IFNγR2 extracellular domain, creating an additional N-glycosylation site (Vogt et al., 2005; Moncada-Velez et al., 2013). This additional N-glycan negatively affects folding leading to slightly decreased IFNγR expression levels (Moncada-Velez et al., 2013). In contrast to wild-type IFNγR2, which is localized in lipid nanodomains, T168N mutants that do reach the cell surface are confined by the cortical actin meshwork (Blouin et al., 2016). Upon IFNγ binding, the wild-type receptor undergoes a conformational change resulting in JAK activation. However, the actin meshwork prevents IFNγR2-T168N to change conformation thus blocking IFNγ signaling. In line, galectin depletion rescues the T168N phenotype and galectin addition to wild-type IFNγR2 impaired IFNγ signaling (Blouin et al., 2016). These studies show that not only glycan loss or truncation can lead to receptor malfunction but that also additional receptor glycosylation sites may lead to disease.

Glycan-galectin interactions are important for many more receptors, including the T cell receptor (TCR). T cells from mice deficient in the glycosyltransferase GnT-V show a lack of complex branching N-glycans, which reduces Galectin-3 binding and enhances TCR clustering, resulting in autoimmunity (Demetriou et al., 2001; Chen et al., 2007). On B cells, BCR signaling is influenced by Galectin-9 dependent N-glycan mediated lateral interactions between the BCR and CD22, an ITIM bearing member of the sialic acid-binding immunoglobulin-like lectin (Siglec) family (Wasim et al., 2019). CD22 is heavily glycosylated and forms homo-oligomers by binding glycans of neighboring CD22 molecules in cis on the B cell membrane (Han et al., 2005). CD22 function as inhibitor of BCR signaling is hampered by removing five of its 12 glycosylation sites (Wasim et al., 2019). These glycans on CD22 may be bound by Galectin-9 and crosslinked with the BCR, thus explaining the inhibitory function of CD22 and Galectin-9 on BCR signaling (Cao et al., 2018; Wasim et al., 2019).

TABLE 1 | Overview of the techniques to study membrane receptor glycosylation: applications and limitations.

Tools for studying membrane receptor glycosylation				
Method	**Working principle**	**Applications**	**Limitations**	**References**
Quantitative and qualitive measurement of receptor glycosylation				
SDS-PAGE and glycan-cleaving enzymes	Separating glycoforms by differences in molecular weight, using cell lysates treated with or without glycan-cleaving enzymes.	Quick and easy way to observe different glycoforms and roughly assess localization: membrane vs. cytosol.	No detailed information on glycan structure. Glycoforms with small or no differences in molecular weight cannot be separated.	Freeze and Kranz, 2010
Lectin blot	Separating glycoforms by differences in molecular weight and staining with glycan binding lectins.	Analyze different glycoforms in cell lysates and provides insights regarding glycan composition.	Low binding affinity and specificity of lectins. No detailed information on glycan structure.	Cao et al., 2013
Chemoenzymatic labeling	Building a monosaccharide analog into the glycan chain to introduce a chemical modification compatible with click chemistry reactions.	Specific glycan structures can be labeled on live cells or cell lysates.	No detailed information on glycan structure or site occupancy. Labeling is not specific for the protein of interest.	Lopez Aguilar et al., 2017
Lectin and antibody labeling	Visualizing specific glycan structures by lectin or antibody staining.	Labeling specific glycan structures for microscopy or flow cytometry.	Low binding affinity and specificity of lectins. Labeling is not specific for the protein of interest.	Tommasone et al., 2019
In situ proximity ligation assay	Antibodies conjugated to oligonucleotides can only ligate and be visualized when the antibody targets are in close proximity.	Provides information on the location of glycoforms within the cell and on the cell membrane.	No detailed information on glycan structure. Distance between the detected entities can be up to 40 nm, sometimes complicating data interpretation.	Soderberg et al., 2006
Glycomics	Analyzing glycan structure with mass spectrometry-based techniques.	Provides detailed structural information on glycans released from their protein backbone.	No information on the location of the glycosylation site within the protein.	Lauc and Wuhrer, 2017
Glycoproteomics	Analyzing glycopeptides with mass spectrometry-based techniques.	Provides information on the location of the glycosylation site and the glycan structure as well as micro- and macro-heterogeneity.	Glycan fine structures cannot be dissected when using large scale glycopeptide analysis. Complicated data analysis creating many false positive identifications.	Lauc and Wuhrer, 2017; Yang et al., 2017; Narimatsu H. et al., 2018
FRET-based labeling of glycoproteins	Energy transfer from a donor fluorophore to an acceptor fluorophore can only occur when the antibody targets are in close proximity.	Provides information on the cellular location of glycoforms.	No detailed information on glycan structure and site-occupancy.	Lin et al., 2014
Strategies for manipulation of membrane receptor glycosylation				
Metabolic inhibitors	Different strategies, examples are sugar analogs, oligosaccharyltransferase inhibitors or inhibitors of glycosyltransferases.	Inhibition of the glycosylation pathway resulting in loss, truncation or modification of glycans.	Unwanted side-effects. Effect not specific for protein of interest.	Wojtowicz et al., 2012
Knockdown or knockout of glycosyltransferases	RNA interference or CRISPR-Cas9 genome editing.	Inhibition of the glycosylation pathway resulting in loss, truncation or modification of glycans.	Need for easy-to-transfect cell-line. Effect not specific for protein of interest.	Stolfa et al., 2016; Narimatsu Y. et al., 2018
Site-directed mutagenesis	Changing the glycosylation consensus sequence by changing the amino acid sequence of the protein and therefore removing the glycosylation site.	Removing one or multiple glycan chains from a specific protein.	Need for easy-to-transfect cell-line. Amino-acid substitution can affect other protein properties besides glycan presence. Modification of glycans is not possible.	Barbosa et al., 1987; Bordo and Argos, 1991; Weber et al., 2004

Adhesion and Migration

Dynamic leukocyte-leukocyte and leukocyte-matrix interactions shape immunity and depend on many different adhesion receptors, including cadherins, selectins, and integrins. Integrins form a big family of heavily glycosylated transmembrane α/β heterodimeric proteins (Marsico et al., 2018). Although most integrin glycosylation studies focus on cancer cells or fibroblasts, integrin-mediated adhesion and migration is also key to elicit effective immune responses. Adhesion of the fibronectin-binding integrin α5β1 during myeloid differentiation into macrophages,

e.g., is regulated via phorbol myristate acetate (PMA)-induced reduction of sialyltransferase ST6GAL1 activity, which causes β1-integrin hyposialylation and increased fibronectin binding (Semel et al., 2002). In fact, complex integrin glycosylation is required for heterodimerization, clustering, activation as well as lateral interactions with other membrane proteins (Zheng et al., 1994; Guo et al., 2002; Isaji et al., 2006, 2009; Hou et al., 2016). Leukocyte-specific β2-integrins are also highly glycosylated (Miller and Springer, 1987), and interactions between αLβ2 and galectins on human monocytes and dendritic cells are revealed by proteomics (Eich et al., 2016). However, information on glycan-mediated functional consequences is lacking. The β2-integrin ligands ICAM-1 and JAM-A on the endothelium carry N-glycans that are only marginally important for protein transport to the membrane but strongly influence protein conformation, dimerization, and binding to αLβ2 (Jimenez et al., 2005; Scott et al., 2015). Recently, two distinct N-glycoforms of ICAM-1 have been detected on activated endothelial cells: a complex, highly abundant N-glycoform and a less abundant oligomannose glycoform. These differ in their signaling capacity and dynamic interactions with the cortical actin cytoskeleton, possibly modulating distinct aspects of the inflammatory response (Scott et al., 2013).

Considering the importance of integrins and their ligands in many aspects of immune cell function, their glycan micro- and macroheterogeneity could be additional regulatory mechanisms of immune cell functions for which further investigation is warranted.

QUANTITATIVE AND QUALITATIVE MEASUREMENT OF RECEPTOR GLYCOSYLATION: CHASING A MOVING TARGET

To determine functional differences of receptor glycoforms, one needs methodologies (**Table 1**) that determine localization and site-occupancy of glycosylation sites, structure of glycan chains, glycan micro- and macroheterogeneity and glycoform-specific localization and interactome at the cell membrane. Ideally, these methodologies should also be able to capture the dynamic changes in these parameters.

First insights into the glycosylation status of immune receptors can be obtained by size-separating proteins using SDS-PAGE and immuno-detection of the protein of interest, before and after treatment with glycan-cleaving enzymes (Freeze and Kranz, 2010). Glycan removal reduces the molecular weight and results in a mobility shift of the protein. To obtain information about glycan composition, the so-called lectin blotting can be used on the intact glycoproteins (Sato, 2014). Recombinant lectins can also be used to label glycans present on the membrane of intact cells for detection by flow cytometry or microscopy (Bull et al., 2015), but their multimeric nature and relatively weak binding strength (Debray et al., 1981) may complicate data interpretation. Antibodies against glycan antigens are limited due to glycan low immunogenicity and high structural similarity (Tommasone et al., 2019). Another way to label membrane-exposed glycan structures on intact cells or in cell lysates is chemoenzymatic labeling, which exploits engineered recombinant glycosyltranferases that add monosaccharide analogs, suitable for click chemistry reactions, to specific structures in glycan chains (Lopez Aguilar et al., 2017). Although these techniques enable labeling of specific glycan structures, several limitations should be considered. It is plausible that glycocalyx thickness influences binding of lectins or access of glycosyltranferases and this can complicate data interpretation when variations in the glycocalyx composition are expected, such as between cell types, different metabolic states or in disease. Furthermore, staining and labeling methods provide ensemble measurements, thus lacking information about glycan microheterogeneity, and do not focus on a particular receptor of interest.

A solution may come from the combined use of a receptor-specific antibody and a glycan-specific probe, both adapted to serve in the so-called *in situ* proximity ligation assay (PLA) (Soderberg et al., 2006). The resulting co-detection of protein and glycosylation on the cell surface (Conze et al., 2010) has been successfully employed to demonstrate increased Sialyl Lewis X glycosylation of the RON receptor tyrosine kinase in cells overexpressing α2,3-sialyltransferase (Mereiter et al., 2016) and to reveal aberrant glycan modification of E-cadherin in human gastric carcinoma cells (Carvalho et al., 2016). However, since the distance between the two detected entities can be up to 40 nm, signals represent close proximity but may not reflect intramolecular co-occurrence (Alsemarz et al., 2018).

A technique that shows great potential for studying spatiotemporal organization of receptor glycoforms is the cis-membrane Förster resonance energy transfer (FRET)-based method for protein-specific imaging of cell surface glycans (Lin et al., 2014). This method introduces a FRET acceptor onto a specific monosaccharide of protein glycans, by metabolic labeling, and additionally a FRET donor onto the receptor of interest. FRET signals therefore solely originate from the labeled monosaccharide-containing protein of interest. Currently sialic acids and GalNAc residues can be labeled on membrane receptors in this way (Lin et al., 2014; Yuan et al., 2018) but future expansion of the monosaccharide toolbox will hopefully allow metabolic labeling of any sugar moiety on the glycoprotein of interest.

The techniques discussed above are of great value to detect glycoforms on the membrane, but do not provide detailed structural information about the glycan chains. To obtain this information, mass spectrometry can be used in a glycomics or glycoproteomics approach (Lauc and Wuhrer, 2017; Yang et al., 2017; Narimatsu H. et al., 2018). Although glycomics provides detailed structural information about the glycan chain without protein information and is therefore not suitable to study glycan position on receptors. For this, glycoproteomics is the preferred approach. Tryptic digestion of immunopurified glycoprotein receptors is required to generate glycosylated peptides for analysis by liquid chromatography-mass spectrometry (LC-MS). MS-based glycopeptide analysis is challenging since ionization efficiencies are much lower as compared to non-glycosylated peptides. In addition, the existence of multiple glycoforms of the same peptide reduces the abundance of the individual glycopeptide isoforms. Therefore,

glycopeptides are commonly first enriched, e.g., via solid-phase extraction on polar cartridges. Recent advances further improve analytical sensitivity for glycopeptides (Narimatsu H. et al., 2018). Fragmentation of glycopeptides by tandem mass spectrometry (MS/MS) yields information on the glycan and peptide sequence to provide site-specific information on glycan heterogeneity (Stavenhagen et al., 2017).

A combination of labeling techniques to detect specific glycoforms and structural analysis of glycan composition and site-occupancy would greatly benefit our understanding of membrane receptor glycosylation.

STRATEGIES FOR MANIPULATION OF MEMBRANE RECEPTOR GLYCOSYLATION

To study the function of glycan chains on membrane receptors, tools are needed to manipulate glycan site-occupancy and composition in a well-controlled manner. Thus far, the tools are rather generic. Metabolic glycosylation inhibitors, e.g., can block transport of proteins from the Golgi to the ER or interfere with the synthesis of nucleotide sugars, which are the building block of the lipid-linked oligosaccharide. Naturally, occurring glycan chain elongation inhibitors (e.g., plant alkaloids) block glycosylation enzymes and glycoside primers that mimic the natural glycosyltranferase substrates can divert glycan chain synthesis from the endogenous substrate (Wojtowicz et al., 2012; Esko et al., 2017).

The most widely used glycosylation inhibitor is the antibiotic tunicamycin, that inhibits GlcNAc phosphotransferase responsible for the initial steps in N-glycosylation, causing protein misfolding (Foufelle and Fromenty, 2016). Other inhibitors interfere with the enzyme oligosaccharyltransferase that is responsible for the transfer of the lipid-linked oligosaccharide to the protein (Lopez-Sambrooks et al., 2016; Rinis et al., 2018). Also, the development of specific glycosyltransferase inhibitors is pursued (Tedaldi and Wagner, 2014). Inhibitors, however, can have additional effects on general cellular functions, inducing ER stress and general toxicity, limiting their application.

Another way to manipulate protein glycosylation is through genetic means. The role of α1,3-fucosyltransferases and α(2,3)sialyltransferases on leukocyte rolling, e.g., was studied using shRNA-mediated knock-down (Buffone et al., 2013; Mondal et al., 2015). CRISPR/Cas9-mediated gene editing allowed the simultaneous determination of N-glycan, O-glycan and glycosphingolipid contributions to leukocyte rolling and adhesion (Stolfa et al., 2016). Recently, a gRNA library for CRISPR/Cas9 knockout of 186 glycosyltransferases has been validated in HEK293T cells (Narimatsu Y. et al., 2018), and its application to immune cell biology is an exciting opportunity.

The most specific way to manipulate the glycan content of a given receptor remains site-directed mutagenesis. The substitute amino acid should be carefully chosen, since it may affect protein structure independently from the loss/gain of the glycosylation site (Bordo and Argos, 1991). Moreover, expression of the mutant in presence of the endogenous protein should be avoided. This can be achieved by exploiting CRISPR/Cas9-triggered homology-directed repair in cells to introduce the glycosite mutation in the immune-receptor gene. Unfortunately, this technique allows only the loss or gain of complete glycans and not their editing. Further development of tools for targeted modification of receptor glycosylation and for dedicated assessment of glycan structure and site-occupancy is required.

OUTLOOK

Pioneering studies combining super-resolution microscopy with bioorthogonal chemistry have recently provided the first nanoscale images of membrane glycans and measurements of glycocalyx height differences (Letschert et al., 2014; Mockl et al., 2019). Since each methodology for glycan quantification and editing has limitations, smart combinations of techniques may be the way forward to reveal novel aspects of membrane glycan biology.

AUTHOR CONTRIBUTIONS

AC and PH designed and wrote the review with input from WH and DL for conceiving, writing, and editing the manuscript.

FUNDING

PH was supported by an intramural Ph.D. fellowship from the Radboud University Medical Center.

ACKNOWLEDGMENTS

We apologize to all those authors whose work could not be cited due to space limitations.

REFERENCES

Alsemarz, A., Lasko, P., and Fagotto, F. (2018). Limited significance of the *in situ* proximity ligation assay. *bioRxiv [Preprint]* 411355. doi: 10.1101/411355

Barbosa, J. A., Santos-Aguado, J., Mentzer, S. J., Strominger, J. L., Burakoff, S. J., and Biro, P. A. (1987). Site-directed mutagenesis of class I HLA genes. role of glycosylation in surface expression and functional recognition. *J. Exp. Med.* 166, 1329–1350. doi: 10.1084/jem.166.5.1329

Bloem, K., Vuist, I. M., Van Der Plas, A. J., Knippels, L. M., Garssen, J., Garcia-Vallejo, J. J., et al. (2013). Ligand binding and signaling of dendritic cell immunoreceptor (DCIR) is modulated by the glycosylation of the carbohydrate recognition domain. *PLoS ONE* 8:e66266. doi: 10.1371/journal.pone.0066266

Blouin, C. M., Hamon, Y., Gonnord, P., Boularan, C., Kagan, J., Viaris De Lesegno, C., et al. (2016). Glycosylation-dependent IFN-gammaR partitioning in lipid and actin nanodomains is critical for JAK activation. *Cell* 166, 920–934. doi: 10.1016/j.cell.2016.07.003

Bordo, D., and Argos, P. (1991). Suggestions for safe residue substitutions in site-directed mutagenesis. *J. Mol. Biol.* 217, 721–729. doi: 10.1016/0022-2836(91)90528-E

Buffone, A. Jr., Mondal, N., Gupta, R., McHugh, K. P., Lau, J. T., and Neelamegham, S. (2013). Silencing α1,3-fucosyltransferases in human

leukocytes reveals a role for FUT9 enzyme during E-selectin-mediated cell adhesion. *J. Biol. Chem.* 288, 1620–1633. doi: 10.1074/jbc.M112.400929

Bull, C., Boltje, T. J., Van Dinther, E. A., Peters, T., De Graaf, A. M., Leusen, J. H., et al. (2015). Targeted delivery of a sialic acid-blocking glycomimetic to cancer cells inhibits metastatic spread. *ACS Nano* 9, 733–745. doi: 10.1021/nn5061964

Burguillos, M. A., Svensson, M., Schulte, T., Boza-Serrano, A., Garcia-Quintanilla, A., Kavanagh, E., et al. (2015). Microglia-secreted galectin-3 acts as a toll-like receptor 4 ligand and contributes to microglial activation. *Cell Rep.* 10, 1626–1638. doi: 10.1016/j.celrep.2015.02.012

Buschow, S. I., Lasonder, E., Szklarczyk, R., Oud, M. M., De Vries, I. J., and Figdor, C. G. (2012). Unraveling the human dendritic cell phagosome proteome by organellar enrichment ranking. *J. Proteomics* 75, 1547–1562. doi: 10.1016/j.jprot.2011.11.024

Cambi, A., De Lange, F., Van Maarseveen, N. M., Nijhuis, M., Joosten, B., Van Dijk, E. M., et al. (2004). Microdomains of the C-type lectin DC-SIGN are portals for virus entry into dendritic cells. *J. Cell Biol.* 164, 145–155. doi: 10.1083/jcb.200306112

Cao, A., Alluqmani, N., Buhari, F. H. M., Wasim, L., Smith, L. K., Quaile, A. T., et al. (2018). Galectin-9 binds IgM-BCR to regulate B cell signaling. *Nat. Commun.* 9:3288. doi: 10.1038/s41467-018-05771-8

Cao, J., Guo, S., Arai, K., Lo, E. H., and Ning, M. (2013). Studying extracellular signaling utilizing a glycoproteomic approach: lectin blot surveys, a first and important step. *Methods Mol. Biol.* 1013, 227–233. doi: 10.1007/978-1-62703-426-5_15

Carvalho, S., Catarino, T. A., Dias, A. M., Kato, M., Almeida, A., Hessling, B., et al. (2016). Preventing E-cadherin aberrant N-glycosylation at Asn-554 improves its critical function in gastric cancer. *Oncogene* 35, 1619–1631. doi: 10.1038/onc.2015.225

Chen, I. J., Chen, H. L., and Demetriou, M. (2007). Lateral compartmentalization of T cell receptor versus CD45 by galectin-N-glycan binding and microfilaments coordinate basal and activation signaling. *J. Biol. Chem.* 282, 35361–35372. doi: 10.1074/jbc.M706923200

Clark, M. C., and Baum, L. G. (2012). T cells modulate glycans on CD43 and CD45 during development and activation, signal regulation, and survival. *Ann. N.Y. Acad. Sci.* 1253, 58–67. doi: 10.1111/j.1749-6632.2011.06304.x

Conze, T., Carvalho, A. S., Landegren, U., Almeida, R., Reis, C. A., David, L., et al. (2010). MUC2 mucin is a major carrier of the cancer-associated sialyl-Tn antigen in intestinal metaplasia and gastric carcinomas. *Glycobiology* 20, 199–206. doi: 10.1093/glycob/cwp161

Da Silva Correia, J., and Ulevitch, R. J. (2002). MD-2 and TLR4 N-linked glycosylations are important for a functional lipopolysaccharide receptor. *J. Biol. Chem.* 277, 1845–1854. doi: 10.1074/jbc.M109910200

Debray, H., Decout, D., Strecker, G., Spik, G., and Montreuil, J. (1981). Specificity of twelve lectins towards oligosaccharides and glycopeptides related to N-glycosylproteins. *Eur. J. Biochem.* 117, 41–55. doi: 10.1111/j.1432-1033.1981.tb06300.x

Demetriou, M., Granovsky, M., Quaggin, S., and Dennis, J. W. (2001). Negative regulation of T-cell activation and autoimmunity by Mgat5 N-glycosylation. *Nature* 409, 733–739. doi: 10.1038/35055582

Dennis, J. W., Lau, K. S., Demetriou, M., and Nabi, I. R. (2009a). Adaptive regulation at the cell surface by N-glycosylation. *Traffic* 10, 1569–1578. doi: 10.1111/j.1600-0854.2009.00981.x

Dennis, J. W., Nabi, I. R., and Demetriou, M. (2009b). Metabolism, cell surface organization, and disease. *Cell* 139, 1229–1241. doi: 10.1016/j.cell.2009.12.008

Eich, C., Lasonder, E., Cruz, L. J., Reinieren-Beeren, I., Cambi, A., Figdor, C. G., et al. (2016). Proteome based construction of the lymphocyte function-associated antigen 1 (LFA-1) interactome in human dendritic cells. *PLoS ONE* 11:e0149637. doi: 10.1371/journal.pone.0149637

Esko, J. D., Bertozzi, C., and Schnaar, R. L. (2017). "Chemical tools for inhibiting glycosylation," in *Essentials of Glycobiology,* eds A. Varki, R. D. Cummings, J. D. Esko, H. H. Freeze, P. Stanley, C. R. Bertozzi, G. W. Hart, and M. E. Etzler (New York, NY: Cold Spring Harbor Laboratory Press).

Esteban, A., Popp, M. W., Vyas, V. K., Strijbis, K., Ploegh, H. L., and Fink, G. R. (2011). Fungal recognition is mediated by the association of dectin-1 and galectin-3 in macrophages. *Proc. Natl. Acad. Sci. U.S.A.* 108, 14270–14275. doi: 10.1073/pnas.1111415108

Fischer, M., Muller, J. P., Spies-Weisshart, B., Grafe, C., Kurzai, O., Hunniger, K., et al. (2017). Isoform localization of dectin-1 regulates the signaling quality of anti-fungal immunity. *Eur. J. Immunol.* 47, 848–859. doi: 10.1002/eji.201646849

Foufelle, F., and Fromenty, B. (2016). Role of endoplasmic reticulum stress in drug-induced toxicity. *Pharmacol. Res. Perspect.* 4:e00211. doi: 10.1002/prp2.211

Freeze, H. H., and Kranz, C. (2010). Endoglycosidase and glycoamidase release of N-linked glycans. *Curr. Protoc. Mol. Biol.* 8:13A. doi: 10.1002/0471142727.mb1713as89

Geijtenbeek, T. B., Torensma, R., Van Vliet, S. J., Van Duijnhoven, G. C., Adema, G. J., Van Kooyk, Y., et al. (2000). Identification of DC-SIGN, a novel dendritic cell-specific ICAM-3 receptor that supports primary immune responses. *Cell* 100, 575–585. doi: 10.1016/S0092-8674(00)80693-5

Guo, H. B., Lee, I., Kamar, M., Akiyama, S. K., and Pierce, M. (2002). Aberrant N-glycosylation of beta1 integrin causes reduced alpha5beta1 integrin clustering and stimulates cell migration. *Cancer Res.* 62, 6837–6845.

Han, S., Collins, B. E., Bengtson, P., and Paulson, J. C. (2005). Homomultimeric complexes of CD22 in B cells revealed by protein-glycan cross-linking. *Nat. Chem. Biol.* 1, 93–97. doi: 10.1038/nchembio713

Hou, S., Hang, Q., Isaji, T., Lu, J., Fukuda, T., and Gu, J. (2016). Importance of membrane-proximal N-glycosylation on integrin β1 in its activation and complex formation. *FASEB J.* 30, 4120–4131. doi: 10.1096/fj.201600665R

Isaji, T., Sato, Y., Fukuda, T., and Gu, J. (2009). N-glycosylation of the I-like domain of β1 integrin is essential for β1 integrin expression and biological function: identification of the minimal N-glycosylation requirement for α5β1. *J. Biol. Chem.* 284, 12207–12216. doi: 10.1074/jbc.M807920200

Isaji, T., Sato, Y., Zhao, Y., Miyoshi, E., Wada, Y., Taniguchi, N., et al. (2006). N-glycosylation of the beta-propeller domain of the integrin alpha5 subunit is essential for alpha5beta1 heterodimerization, expression on the cell surface, and its biological function. *J. Biol. Chem.* 281, 33258–33267. doi: 10.1074/jbc.M607771200

Jimenez, D., Roda-Navarro, P., Springer, T. A., and Casasnovas, J. M. (2005). Contribution of N-linked glycans to the conformation and function of intercellular adhesion molecules (ICAMs). *J. Biol. Chem.* 280, 5854–5861. doi: 10.1074/jbc.M412104200

Jouault, T., El Abed-El Behi, M., Martinez-Esparza, M., Breuilh, L., Trinel, P. A., Chamaillard, M., et al. (2006). Specific recognition of *Candida albicans* by macrophages requires galectin-3 to discriminate Saccharomyces cerevisiae and needs association with TLR2 for signaling. *J. Immunol.* 177, 4679–4687. doi: 10.4049/jimmunol.177.7.4679

Kato, Y., Adachi, Y., and Ohno, N. (2006). Contribution of N-linked oligosaccharides to the expression and functions of beta-glucan receptor, dectin-1. *Biol. Pharm. Bull.* 29, 1580–1586. doi: 10.1248/bpb.29.1580

Kristic, J., Vuckovic, F., Menni, C., Klaric, L., Keser, T., Beceheli, I., et al. (2014). Glycans are a novel biomarker of chronological and biological ages. *J. Gerontol. A Biol. Sci. Med. Sci.* 69, 779–789. doi: 10.1093/gerona/glt190

Lajoie, P., Goetz, J. G., Dennis, J. W., and Nabi, I. R. (2009). Lattices, rafts, and scaffolds: domain regulation of receptor signaling at the plasma membrane. *J. Cell Biol.* 185, 381–385. doi: 10.1083/jcb.200811059

Lauc, G., and Wuhrer, M. (2017). *High-Throughput Glycomics and Glycoproteomics: Methods and Protocols*. New York, NY: Humana Press. doi: 10.1007/978-1-4939-6493-2

Leclaire, C., Lecointe, K., Gunning, P. A., Tribolo, S., Kavanaugh, D. W., Wittmann, A., et al. (2018). Molecular basis for intestinal mucin recognition by galectin-3 and C-type lectins. *FASEB J.* 32, 3301–3320. doi: 10.1096/fj.201700619R

Letschert, S., Gohler, A., Franke, C., Bertleff-Zieschang, N., Memmel, E., Doose, S., et al. (2014). Super-resolution imaging of plasma membrane glycans. *Angew. Chem. Int. Ed. Engl.* 53, 10921–10924. doi: 10.1002/anie.201406045

Lin, W., Du, Y., Zhu, Y., and Chen, X. (2014). A cis-membrane FRET-based method for protein-specific imaging of cell-surface glycans. *J. Am. Chem. Soc.* 136, 679–687. doi: 10.1021/ja410086d

Lopez Aguilar, A., Briard, J. G., Yang, L., Ovryn, B., Macauley, M. S., and Wu, P. (2017). Tools for studying glycans: recent advances in chemoenzymatic glycan labeling. *ACS Chem. Biol.* 12, 611–621. doi: 10.1021/acschembio.6b01089

Lopez-Sambrooks, C., Shrimal, S., Khodier, C., Flaherty, D. P., Rinis, N., Charest, J. C., et al. (2016). Oligosaccharyltransferase inhibition induces senescence in RTK-driven tumor cells. *Nat. Chem. Biol.* 12, 1023–1030. doi: 10.1038/nchembio.2194

Marsico, G., Russo, L., Quondamatteo, F., and Pandit, A. (2018). Glycosylation and integrin regulation in cancer. *Trends Cancer* 4, 537–552. doi: 10.1016/j.trecan.2018.05.009

Marth, J. D., and Grewal, P. K. (2008). Mammalian glycosylation in immunity. *Nat. Rev. Immunol.* 8, 874–887. doi: 10.1038/nri2417

Medzihradszky, K. F., Kaasik, K., and Chalkley, R. J. (2015). Tissue-specific glycosylation at the glycopeptide level. *Mol. Cell Proteomics* 14, 2103–2110. doi: 10.1074/mcp.M115.050393

Mereiter, S., Magalhaes, A., Adamczyk, B., Jin, C., Almeida, A., Drici, L., et al. (2016). Glycomic analysis of gastric carcinoma cells discloses glycans as modulators of RON receptor tyrosine kinase activation in cancer. *Biochim. Biophys. Acta* 1860, 1795–1808. doi: 10.1016/j.bbagen.2015.12.016

Miller, L. J., and Springer, T. A. (1987). Biosynthesis and glycosylation of p150,95 and related leukocyte adhesion proteins. *J. Immunol.* 139, 842–847.

Mkhikian, H., Grigorian, A., Li, C. F., Chen, H. L., Newton, B., Zhou, R. W., et al. (2011). Genetics and the environment converge to dysregulate N-glycosylation in multiple sclerosis. *Nat. Commun.* 2:334. doi: 10.1038/ncomms1333

Mockl, L., Pedram, K., Roy, A. R., Krishnan, V., Gustavsson, A. K., Dorigo, O., et al. (2019). Quantitative super-resolution microscopy of the mammalian glycocalyx. *Dev. Cell* 50, 57–72.e56. doi: 10.1016/j.devcel.2019.04.035

Moncada-Velez, M., Martinez-Barricarte, R., Bogunovic, D., Kong, X. F., Blancas-Galicia, L., Tirpan, C., et al. (2013). Partial IFN-γR2 deficiency is due to protein misfolding and can be rescued by inhibitors of glycosylation. *Blood* 122, 2390–2401. doi: 10.1182/blood-2013-01-480814

Mondal, N., Buffone, A. Jr., Stolfa, G., Antonopoulos, A., Lau, J. T., Haslam, S. M., et al. (2015). ST3Gal-4 is the primary sialyltransferase regulating the synthesis of E-, P-, and L-selectin ligands on human myeloid leukocytes. *Blood* 125, 687–696. doi: 10.1182/blood-2014-07-588590

Nabi, I. R., Shankar, J., and Dennis, J. W. (2015). The galectin lattice at a glance. *J. Cell Sci.* 128, 2213–2219. doi: 10.1242/jcs.151159

Narimatsu, H., Kaji, H., Vakhrushev, S. Y., Clausen, H., Zhang, H., Noro, E., et al. (2018). Current technologies for complex glycoproteomics and their applications to biology/disease-driven glycoproteomics. *J. Proteome Res.* 17, 4097–4112. doi: 10.1021/acs.jproteome.8b00515

Narimatsu, Y., Joshi, H. J., Yang, Z., Gomes, C., Chen, Y. H., Lorenzetti, F. C., et al. (2018). A validated gRNA library for CRISPR/Cas9 targeting of the human glycosyltransferase genome. *Glycobiology* 28, 295–305. doi: 10.1093/glycob/cwx101

Ohtsubo, K., and Marth, J. D. (2006). Glycosylation in cellular mechanisms of health and disease. *Cell* 126, 855–867. doi: 10.1016/j.cell.2006.08.019

Peanne, R., De Lonlay, P., Foulquier, F., Kornak, U., Lefeber, D. J., Morava, E., et al. (2018). Congenital disorders of glycosylation (CDG): quo vadis? *Eur. J. Med. Genet.* 61, 643–663. doi: 10.1016/j.ejmg.2017.10.012

Reily, C., Stewart, T. J., Renfrow, M. B., and Novak, J. (2019). Glycosylation in health and disease. *Nat. Rev. Nephrol.* 15, 346–366. doi: 10.1038/s41581-019-0129-4

Rinis, N., Golden, J. E., Marceau, C. D., Carette, J. E., Van Zandt, M. C., Gilmore, R., et al. (2018). Editing N-glycan site occupancy with small-molecule oligosaccharyltransferase inhibitors. *Cell Chem. Biol.* 25, 1231–1241 e1234. doi: 10.1016/j.chembiol.2018.07.005

Ryan, S. O., Bonomo, J. A., Zhao, F., and Cobb, B. A. (2011). MHCII glycosylation modulates *Bacteroides fragilis* carbohydrate antigen presentation. *J. Exp. Med.* 208, 1041–1053. doi: 10.1084/jem.20100508

Ryan, S. O., and Cobb, B. A. (2012). Roles for major histocompatibility complex glycosylation in immune function. *Semin. Immunopathol.* 34, 425–441. doi: 10.1007/s00281-012-0309-9

Sato, T. (2014). Lectin-probed western blot analysis. *Methods Mol. Biol.* 1200, 93–100. doi: 10.1007/978-1-4939-1292-6_8

Scott, D. W., Dunn, T. S., Ballestas, M. E., Litovsky, S. H., and Patel, R. P. (2013). Identification of a high-mannose ICAM-1 glycoform: effects of ICAM-1 hypoglycosylation on monocyte adhesion and outside in signaling. *Am. J. Physiol. Cell Physiol.* 305, C228–C237. doi: 10.1152/ajpcell.00116.2013

Scott, D. W., Tolbert, C. E., Graham, D. M., Wittchen, E., Bear, J. E., and Burridge, K. (2015). N-glycosylation controls the function of junctional adhesion molecule-A. *Mol. Biol. Cell* 26, 3205–3214. doi: 10.1091/mbc.e14-12-1604

Semel, A. C., Seales, E. C., Singhal, A., Eklund, E. A., Colley, K. J., and Bellis, S. L. (2002). Hyposialylation of integrins stimulates the activity of myeloid fibronectin receptors. *J. Biol. Chem.* 277, 32830–32836. doi: 10.1074/jbc.M202493200

Skropeta, D. (2009). The effect of individual N-glycans on enzyme activity. *Bioorg. Med. Chem.* 17, 2645–2653. doi: 10.1016/j.bmc.2009.02.037

Soderberg, O., Gullberg, M., Jarvius, M., Ridderstrale, K., Leuchowius, K. J., Jarvius, J., et al. (2006). Direct observation of individual endogenous protein complexes *in situ* by proximity ligation. *Nat. Methods* 3, 995–1000. doi: 10.1038/nmeth947

Stavenhagen, K., Hinneburg, H., Kolarich, D., and Wuhrer, M. (2017). Site-specific N- and O-glycopeptide analysis using an integrated C18-PGC-LC-ESI-QTOF-MS/MS approach. *Methods Mol. Biol.* 1503, 109–119. doi: 10.1007/978-1-4939-6493-2_9

Stolfa, G., Mondal, N., Zhu, Y., Yu, X., Buffone, A. Jr., and Neelamegham, S. (2016). Using CRISPR-Cas9 to quantify the contributions of O-glycans, N-glycans and glycosphingolipids to human leukocyte-endothelium adhesion. *Sci. Rep.* 6:30392. doi: 10.1038/srep30392

Te Riet, J., Joosten, B., Reinieren-Beeren, I., Figdor, C. G., and Cambi, A. (2017). N-glycan mediated adhesion strengthening during pathogen-receptor binding revealed by cell-cell force spectroscopy. *Sci. Rep.* 7:6713. doi: 10.1038/s41598-017-07220-w

Tedaldi, L., and Wagner, G. K. (2014). Beyond substrate analogues: new inhibitor chemotypes for glycosyltransferases. *Med. Chem. Comm.* 5, 1106–1125. doi: 10.1039/C4MD00086B

Tommasone, S., Allabush, F., Tagger, Y. K., Norman, J., Kopf, M., Tucker, J. H. R., et al. (2019). The challenges of glycan recognition with natural and artificial receptors. *Chem. Soc. Rev.* 48, 5488–5505. doi: 10.1039/C8CS00768C

Torreno-Pina, J. A., Castro, B. M., Manzo, C., Buschow, S. I., Cambi, A., and Garcia-Parajo, M. F. (2014). Enhanced receptor-clathrin interactions induced by N-glycan-mediated membrane micropatterning. *Proc. Natl. Acad. Sci. U.S.A.* 111, 11037–11042. doi: 10.1073/pnas.1402041111

Van Der Burg, S. H., Visseren, M. J., Brandt, R. M., Kast, W. M., and Melief, C. J. (1996). Immunogenicity of peptides bound to MHC class I molecules depends on the MHC-peptide complex stability. *J. Immunol.* 156, 3308–3314.

Van Kooyk, Y., and Rabinovich, G. A. (2008). Protein-glycan interactions in the control of innate and adaptive immune responses. *Nat. Immunol.* 9, 593–601. doi: 10.1038/ni.f.203

Vogt, G., Chapgier, A., Yang, K., Chuzhanova, N., Feinberg, J., Fieschi, C., et al. (2005). Gains of glycosylation comprise an unexpectedly large group of pathogenic mutations. *Nat. Genet.* 37, 692–700. doi: 10.1038/ng1581

Wasim, L., Buhari, F. H. M., Yoganathan, M., Sicard, T., Ereno-Orbea, J., Julien, J. P., et al. (2019). N-linked glycosylation regulates CD22 organization and function. *Front. Immunol.* 10:699. doi: 10.3389/fimmu.2019.00699

Wearsch, P. A., Peaper, D. R., and Cresswell, P. (2011). Essential glycan-dependent interactions optimize MHC class I peptide loading. *Proc. Natl. Acad. Sci. U.S.A.* 108, 4950–4955. doi: 10.1073/pnas.1102524108

Weber, A. N., Morse, M. A., and Gay, N. J. (2004). Four N-linked glycosylation sites in human toll-like receptor 2 cooperate to direct efficient biosynthesis and secretion. *J. Biol. Chem.* 279, 34589–34594. doi: 10.1074/jbc.M403830200

Wojtowicz, K., Szaflarski, W., Januchowski, R., Zawierucha, P., Nowicki, M., and Zabel, M. (2012). Inhibitors of N-glycosylation as a potential tool for analysis of the mechanism of action and cellular localisation of glycoprotein P. *Acta Biochim. Pol.* 59, 445–450. doi: 10.18388/abp.2012_2076

Yang, Y., Franc, V., and Heck, A. J. R. (2017). Glycoproteomics: a balance between high-throughput and in-depth analysis. *Trends Biotechnol.* 35, 598–609. doi: 10.1016/j.tibtech.2017.04.010

Yuan, B., Chen, Y., Sun, Y., Guo, Q., Huang, J., Liu, J., et al. (2018). Enhanced imaging of specific cell-surface glycosylation based on multi-FRET. *Anal. Chem.* 90, 6131–6137. doi: 10.1021/acs.analchem.8b00424

Zacchi, L. F., and Schulz, B. L. (2016). N-glycoprotein macroheterogeneity: biological implications and proteomic characterization. *Glycoconj. J.* 33, 359–376. doi: 10.1007/s10719-015-9641-3

Zhang, W., Wearsch, P. A., Zhu, Y., Leonhardt, R. M., and Cresswell, P. (2011). A role for UDP-glucose glycoprotein glucosyltransferase in expression and quality control of MHC class I molecules. *Proc. Natl. Acad. Sci. U.S.A.* 108, 4956–4961. doi: 10.1073/pnas.1102527108

Zheng, M., Fang, H., and Hakomori, S. (1994). Functional role of N-glycosylation in alpha 5 beta 1 integrin receptor. De-N-glycosylation induces dissociation or altered association of alpha 5 and beta 1 subunits and concomitant loss of fibronectin binding activity. *J. Biol. Chem.* 269, 12325–12331.

Zhou, J. Y., Oswald, D. M., Oliva, K. D., Kreisman, L. S. C., and Cobb, B. A. (2018). The glycoscience of immunity. *Trends Immunol.* 39, 523–535. doi: 10.1016/j.it.2018.04.004

Conflict of Interest: The authors declare that the research was conducted in the absence of any commercial or financial relationships that could be construed as a potential conflict of interest.

frontiers in Chemistry

REVIEW
published: 25 February 2020
doi: 10.3389/fchem.2020.00098

Biochemical Characterization of Oyster and Clam Galectins: Selective Recognition of Carbohydrate Ligands on Host Hemocytes and *Perkinsus* Parasites

Gerardo R. Vasta[1]*, *Chiguang Feng*[1], *Satoshi Tasumi*[1†], *Kelsey Abernathy*[1], *Mario A. Bianchet*[2], *Iain B. H. Wilson*[3], *Katharina Paschinger*[3], *Lai-Xi Wang*[4], *Muddasar Iqbal*[1], *Anita Ghosh*[2], *Mohammed N. Amin*[4], *Brina Smith*[1,5], *Sean Brown*[1,6] and *Aren Vista*[1,6]

[1] Department of Microbiology and Immunology, University of Maryland School of Medicine, Institute of Marine and Environmental Technology, Baltimore, MD, United States, [2] Departments of Neurology, and Biophysics and Biophysical Chemistry, The Johns Hopkins University School of Medicine, Baltimore, MD, United States, [3] Department für Chemie, Universität für Bodenkultur, Vienna, Austria, [4] Department of Chemistry and Biochemistry, University of Maryland, College Park, MD, United States, [5] Coppin State University, Baltimore, MD, United States, [6] University of Maryland Baltimore County, Baltimore, MD, United States

OPEN ACCESS

Edited by:
Matthew S. Macauley,
University of Alberta, Canada

Reviewed by:
Vered Padler-Karavani,
Tel Aviv University, Israel
Sean Stowell,
Emory University, United States
Jessica Kramer,
The University of Utah, United States

***Correspondence:**
Gerardo R. Vasta
gvasta@som.umaryland.edu

†Present address:
Satoshi Tasumi,
Fisheries Laboratory, Graduate School of Agricultural and Life Sciences, The University of Tokyo, Shizuoka, Japan

Specialty section:
This article was submitted to Chemical Biology, a section of the journal Frontiers in Chemistry

Received: 01 October 2019
Accepted: 31 January 2020
Published: 25 February 2020

Citation:
Vasta GR, Feng C, Tasumi S, Abernathy K, Bianchet MA, Wilson IBH, Paschinger K, Wang L-X, Iqbal M, Ghosh A, Amin MN, Smith B, Brown S and Vista A (2020) Biochemical Characterization of Oyster and Clam Galectins: Selective Recognition of Carbohydrate Ligands on Host Hemocytes and Perkinsus Parasites. Front. Chem. 8:98. doi: 10.3389/fchem.2020.00098

Both vertebrates and invertebrates display active innate immune mechanisms for defense against microbial infection, including diversified repertoires of soluble and cell-associated lectins that can effect recognition and binding to potential pathogens, and trigger downstream effector pathways that clear them from the host internal milieu. Galectins are widely distributed and highly conserved lectins that have key regulatory effects on both innate and adaptive immune responses. In addition, galectins can bind to exogenous ("non-self") carbohydrates on the surface of bacteria, enveloped viruses, parasites, and fungi, and function as recognition receptors and effector factors in innate immunity. Like most invertebrates, eastern oysters (*Crassostrea virginica*) and softshell clams (*Mya arenaria*) can effectively respond to most immune challenges through soluble and hemocyte-associated lectins. The protozoan parasite *Perkinsus marinus*, however, can infect eastern oysters and cause "Dermo" disease, which is highly detrimental to both natural and farmed oyster populations. The sympatric *Perkinsus chesapeaki*, initially isolated from infected *M. arenaria* clams, can also be present in oysters, and there is little evidence of pathogenicity in either clams or oysters. In this review, we discuss selected observations from our studies on the mechanisms of *Perkinsus* recognition that are mediated by galectin-carbohydrate interactions. We identified in the oyster two galectins that we designated CvGal1 and CvGal2, which strongly recognize *P. marinus* trophozoites. In the clam we also identified galectin sequences, and focused on one (that we named MaGal1) that also recognizes *Perkinsus* species. Here we describe the biochemical characterization of CvGal1, CvGal2, and MaGal1 with focus on the detailed study of the carbohydrate specificity, and the glycosylated moieties on the surfaces of the oyster hemocytes and the two *Perkinsus* species (*P. marinus* and *P. chesapeaki*). Our

goal is to gain further understanding of the biochemical basis for the interactions that lead to recognition and opsonization of the *Perkinsus* trophozoites by the bivalve hemocytes. These basic studies on the biology of host-parasite interactions may contribute to the development of novel intervention strategies for parasitic diseases of biomedical interest.

Keywords: galectin, biochemical characterization, carbohydrate recognition, bivalve hemocyte, perkinsus parasites

INTRODUCTION

In both invertebrates and vertebrates, the immediate recognition of surface moieties on the surface of potential pathogens and parasites or their soluble extracellular products is a critical step for a successful innate immune response (Janeway and Medzhitov, 2002). Among these, bacterial lipopolysaccharides and exopolysaccharides, viral envelope glycoproteins, and surface carbohydrate structures from eukaryotic parasites encode complex information that is "decoded" by the host's soluble or membrane-associated carbohydrate-binding proteins (lectins) (Laine, 1997). Upon recognition and binding to exogenous carbohydrate moieties, lectins can activate signaling pathways and initiate downstream events that include agglutination, immobilization, and opsonization, and activation of effector pathways, such as prophenoloxidase and complement, that can promote killing and clearance of the potential pathogen or parasite (Vasta and Ahmed, 2008). Therefore, lectins are key recognition and effector factors of innate immune responses (Vasta et al., 2007). Most lectins are oligomeric associations of peptide subunits that can be covalently or non-covalently bound, and are characterized by the presence of one or more carbohydrate recognition domains (CRDs) (Vasta et al., 2007; Vasta and Ahmed, 2008)[1]. Initially based on canonical amino acid sequence motifs in their CRD, and most recently on their structural fold, lectins are currently classified in distinct major families, such as galectins (formerly S-type lectins), C-, P-, X-, and I-types, and others (Vasta et al., 2007; Vasta and Ahmed, 2008)[1]. In addition to a unique sequence motif in their CRD and their structural fold, galectins are characterized by their binding preference for β-galactosides, wide taxonomic distribution (Leffler et al., 2004; Vasta and Ahmed, 2008), and functional diversification (Leffler et al., 2004; Vasta, 2009; Rabinovich and Croci, 2012; Vasta et al., 2012). By binding to endogenous ("self") glycans, galectins mediate developmental processes (Leffler et al., 2004; Vasta and Ahmed, 2008), and regulate immune responses (Rabinovich and Croci, 2012). Galectins also bind exogenous ("non-self") glycans on the surface of viruses, bacteria, and parasites, and participate in innate immunity (Vasta, 2009; Vasta et al., 2012).

Like most invertebrates, eastern oysters (*Crassostrea virginica*) and softshell clams (*Mya arenaria*) lack the typical adaptive immune responses of vertebrates mediated by immunoglobulins, B and T cells, and rely upon innate immune responses for defense against infection (Janeway and Medzhitov, 2002). This comprises both cellular and humoral defense responses initiated by multiple cell-associated and soluble receptors, including galectins that can recognize the infectious challenge and lead to effector functions, such as opsonization and phagocytosis by hemolymph cells (hemocytes). Thus, invertebrates, including oysters and softshell clams can effectively respond to most immune challenges through soluble and hemocyte-associated recognition and effector factors (Vasta et al., 1982, 1984, 2004a; Kennedy et al., 1996; Dame et al., 2002). The eukaryotic parasite *Perkinsus marinus*, however, successfully infects the oyster and causes "Dermo" disease along the east and Gulf coasts of the USA, resulting in mass mortalities with serious consequences for both natural and farmed shellfisheries, and the water quality of coastal environments (Andrews, 1996; Kennedy et al., 1996; Perkins, 1996; Harvell et al., 1999; Dame et al., 2002; Caceres-Martinez et al., 2012). Transmission of the parasite from infected oysters is thought to occur through the release of *P. marinus* trophozoites, which are filtered by the healthy oysters together with the phytoplankton (**Figure 1A**). Trophozoites released into the water column can mature into hypnospores that release numerous flagellated zoospores, but their potential infective capacity is not fully understood (**Figure 1B**). Once in contact with the mucosal surfaces, trophozoites are phagocytosed by hemocytes (**Figure 1C**), survive intracellular killing, and proliferate, causing systemic infection and death of the oyster (Chu, 1996; Bushek et al., 2002; Ford et al., 2002). The sympatric *Perkinsus chesapeaki*, initially isolated from infected *M. arenaria* clams, can also be present in oysters, but there is little evidence of pathogenicity for either bivalve species. The detailed mechanisms of parasite recognition and entry, and the determinants of host preference and pathogenicity of *Perkinsus* species remain to be fully understood (Reece et al., 2008).

In this review, we discuss selected observations from our studies aimed at gaining further insight into the molecular basis of recognition and opsonization of *Perkinsus* trophozoites by the bivalve hemocytes. During our initial studies on the oyster and the clam, we examined the possibility that recognition of *Perkinsus* parasites by their phagocytic hemocytes could be mediated by protein-carbohydrate interactions. Our results revealed complex lectin repertoires in both bivalve species, among which we identified novel galectins. We then used

Abbreviations: CvGal1, *Crassostrea virginica* galectin 1; CvGal2, *Crassostrea virginica* galectin 2; MaGal1, *Mya arenaria* galectin 1; BaGal1, *Bufo arenarum* galectin-1; hGal-1, human galectin-1; CGL2, *Coprinus cinereus* galectin-2; CRD, carbohydrate recognition domain; GalNAc, N-acetyl-D-galactosamine; GlcNAc, N-acetyl-D-glucosamine; LacNAc, N-acetyllactosamine; TDG, thiodigalactose; BSM, bovine submaxillary mucin; OSM, ovine submaxillary mucin; PSM, porcine stomach mucin; SPR, surface plasmon resonance; PRR, pattern recognition receptors.

[1]A genomics resource for animal lectins. Available online at: http://www.imperial.ac.uk/research/animallectins/

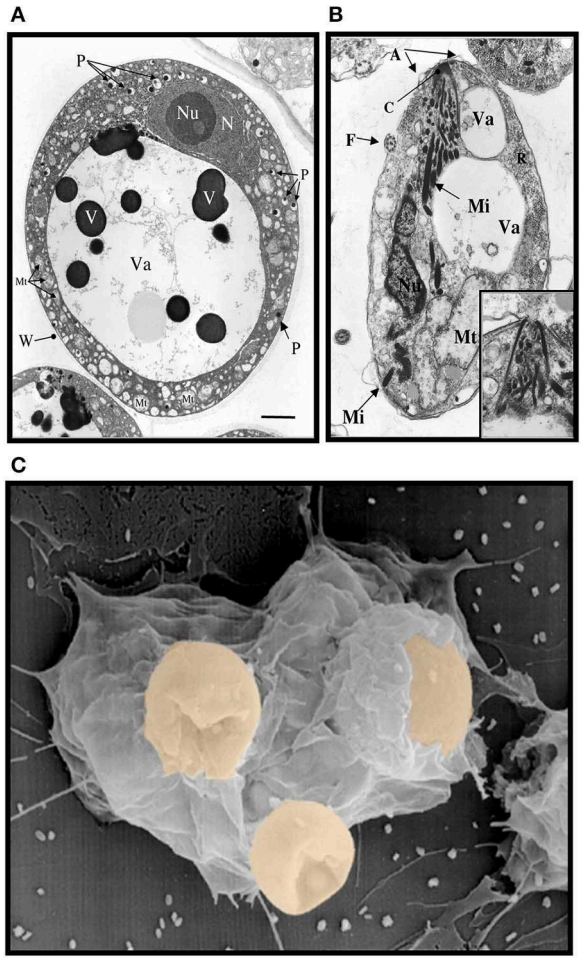

FIGURE 1 | Electron micrographs of *Perkinsus* sp. **(A)** Mature trophozoites of *Perkinsus* sp. isolated from the Baltic clam, *Macoma balthica*. Scale bar = 2 μm. A, cortical alveoli expansion; Mt, mitochondria; N, nucleus; Nu, nucleolus; P, vacuoplast precursors; Va, vacuole; W, wall; Mi, rectilinear micronemes; F, flagellum; C; conoid. Scale bar = 1 μm. **(B)** Longitudinal section of mature zoospores of *Perkinsus* sp. isolated from *Macoma balthica*. Insert shows detail of anterior end of another zoospore. **(C)** Phagocytosis of *Perkinsus marinus* by eastern oyster (*Crassostrea virginica*) hemocytes in a scanning electron micrograph [Adapted from Harvell et al. (1999) with permission from the American Association for the Advancement of Science].

biochemical, molecular, glycomic, and structural approaches to address the carbohydrate specificity of the oyster and clam galectins, and the identification of glycosylated moieties on the surfaces of the hemocytes and the *Perkinsus* parasites that may be responsible for the host-parasite interactions.

IDENTIFICATION AND RECOMBINANT EXPRESSION OF OYSTER AND CLAM GALECTINS: INTERACTIONS WITH SYMPATRIC *PERKINSUS* SPECIES

Mining public genomic and EST databases from the oyster *C. virginica* revealed the presence of multiple galactosyl-binding lectins. Their sequences indicated that these belong either to the C-type lectin or galectin families. Based on their domain organization, galectins from vertebrate species are currently classified as "proto", "chimera," and "tandem-repeat" types, each endowed with unique molecular structure, biochemical properties, and taxonomic distribution (Hirabayashi and Kasai, 1993). Proto type galectins contain one CRD per subunit, and are usually homodimers of non-covalently-linked subunits. Chimera type galectins comprise a C-terminal CRD and an proline-rich N-terminal domain that participates in subunit oligomerization. In the tandem-repeat galectins, two CRDs are joined by a linker peptide. Surprisingly, the oyster sequence identified as a galectin, revealed the presence of four tandemly arrayed CRDs, which represents a novel feature for a member of the galectin family, and poses interesting questions about its structural and functional aspects. The oyster galectin, which we designated as CvGal1 (*C. virginica* galectin 1), contained most residues responsible for recognition of galactosyl moieties in the four CRDs and therefore, was considered as a potential receptor for *P. marinus* trophozoites (Tasumi and Vasta, 2007; Feng et al., 2013). To test this possibility, we examined the presence of galectin transcripts in oyster hemocytes and selected tissues (gills, gut, muscle, and mantle) by RT-PCR (Tasumi and Vasta, 2007). The results clearly indicated that both CvGal1 is expressed in all tissues tested and based on the similar intensity of the amplicons, it seemed likely that the signals observed in the tissues tested originated from the hemocytes that infiltrate these tissues. Further, it is noteworthy that hemocytes, gills, gut, and mantle, which are cells and tissues that are in direct contact with the external environment, have all been proposed as portals for *P. marinus* infection (Chu, 1996; Bushek et al., 2002; Ford et al., 2002; Reece et al., 2008).

To gain further understanding of the oyster's galectin repertoire and the recognition and effector function(s) of its members, we screened the oyster cDNA library to search for proteins that may display the galectin canonical sequence motif. This search identified a second novel galectin which we named CvGal2 (*C. virginica* galectin 2), that was also expressed mostly in the oyster hemocytes, and displayed four tandemly arrayed similar but yet distinct CRDs (Feng et al., 2015). It is noteworthy that the preliminary sequence alignment of CvGal1 CRDs with those of bovine, zebrafish and *C. elegans* galectins showed that two amino acid residues (His^{52} and Asp^{54}, based on the mammalian numbering), that interact with the nitrogen of the *N*-acetyl group of the sugar, are missing in all four CvGal1 CRDs (**Figure 2A**). The oyster galectin CvGal2 also displays short forms of loop 4 in its four CRDs (Feng et al., 2015). The missing tetrapeptide includes His^{52} and Asp^{54} (based on the mammalian numbering; Liao et al., 1994; **Figure 2B**), which interact with the *N*-acetyllactosamine ligand. Although all four CRDs of the oyster galectins CvGal1 and CvGal2 have very similar primary structure, as in the case of the *C. elegans* galectin LEC-6 (formerly, N16; Tasumi and Vasta, 2007; Feng et al., 2015), the shorter loop 4 and the lack of His^{52} and Asp^{54} confers a different carbohydrate specificity (Liao et al., 1994; Ahmed et al., 2002; Tasumi and Vasta, 2007; Feng et al., 2013, 2015).

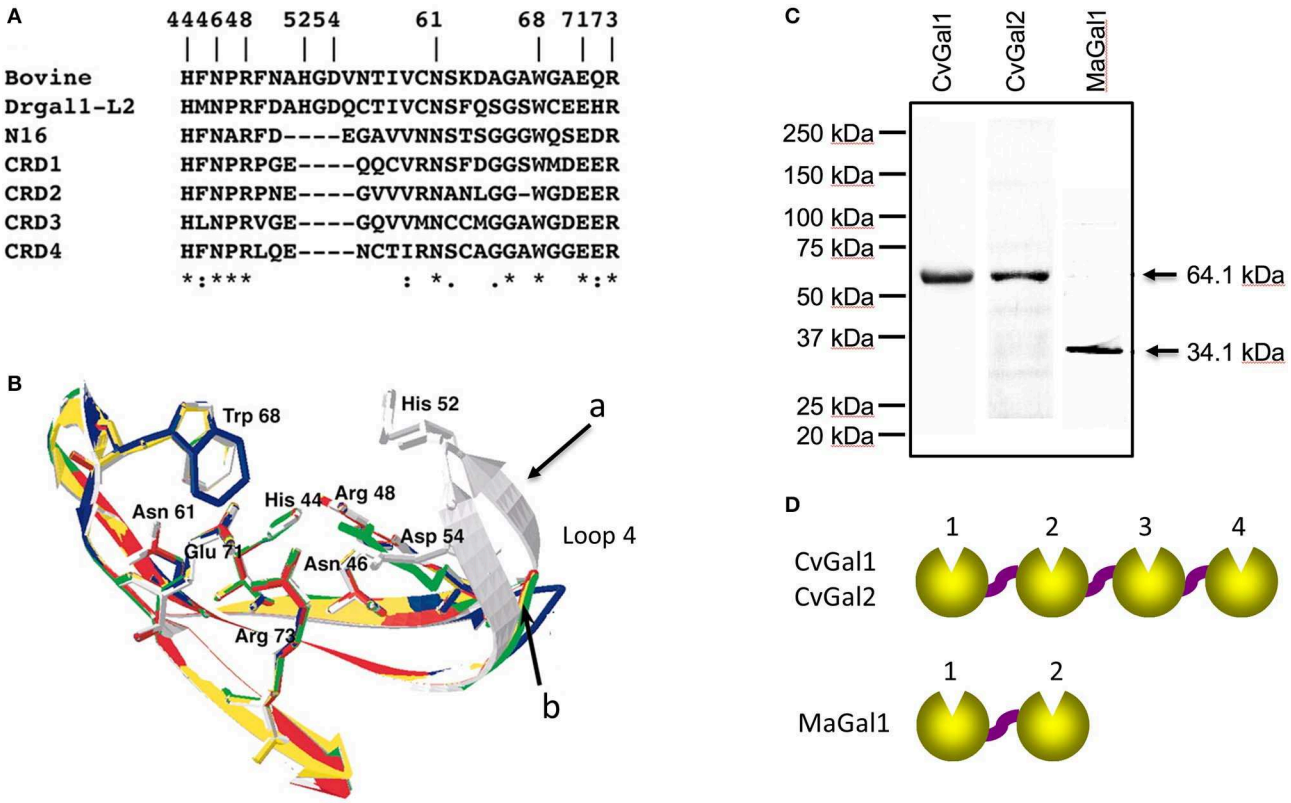

FIGURE 2 | Galectins in bivalves. **(A)** Alignment of bovine galectin−1, zebrafish Drgal1−L2, *C. elegans* LEC−6 (formerly N16), and CRD1 to −4 of CvGal1. **(B)** Homology modeling of CvGal1 CRDs. Bovine galectin−1, CRD−1,−2,−3, and−4 are shown in white, blue, yellow, red, and green, respectively. Numbering of amino acid residues is based on bovine galectin−1. Loop 4 of the CvGal1 CRDs (arrow b) is shorter than the loop 4 of BaGal1 (arrow a). **(C)** Coomassie stain of recombinant CvGal1, CvGal2, and MaGal1 containing either four or two CRDs. Arrows indicate the expected molecular weight of the proteins. **(D)** Schematic illustration of four CRDs of CvGal1 and CvGal2 and two CRDs of MaGal1 [Adapted from Tasumi and Vasta (2007) with permission from the American Association of Immunologists].

Subsequently, we carried out an RNAseq-based transcriptomic analysis of tissues from the softshell clam *M. arenaria* (a bivalve species sympatric with the eastern oyster *C. virginica* in Chesapeake Bay), and identified a galectin-encoding sequence with two tandemly arrayed CRDs, which we designated MaGal1. The two CRDs of MaGal1 also display a short loop 4, and like the oyster galectins CvGal1 and CvGal2, the MaGal1 transcript is mostly expressed in hemocytes (Tasumi and Vasta, 2007; Feng et al., 2013, 2015; Vasta et al., 2015).

The identification of galectins in oyster and clam hemocytes, the phagocytic cells that are the primary defense mechanism in these filter-feeding bivalves, supported our hypothesis that they may function as *Perkinsus* receptors, and we proceeded to develop tools to enable structural and functional studies on these proteins, with focus on their potential role(s) in parasite recognition and host entry. For this, we started by elucidating the full cDNA and gene sequences, and expressed the recombinant proteins (Tasumi and Vasta, 2007; Feng et al., 2013, 2015). The electrophoretic mobilities of the recombinant proteins rCvGal1, rCvGal2, and rMaGal1 are shown in **Figure 2C**. The relative electrophoretic mobility of rCvGal1 and rCvGal2, and rMaGal1 confirmed the molecular mass and CRD organization expected from the transcripts' sequences, illustrated in **Figure 2D**. The recognition properties of rCvGal1, rCvGal2, and rMaGal1 for the two sympatric *Perkinsus* species of interest, *P. marinus* and *P. chesapeaki,* are shown in **Figure 3**. Most interesting was the observation that while CvGal1 and CvGal2 strongly recognize *P. marinus*, the recognition of *P. chesapeaki* is very weak (**Figures 3A,B**). In contrast, MaGal1 strongly recognizes *P. chesapeaki* (**Figure 3C**), suggesting that host preference of the parasite for either bivalve host may be related to galectin-mediated recognition and entry into the hemocyte.

Based on these results we characterized the oyster and clam galectins in their molecular, structural, and carbohydrate-binding properties, and proceeded to identify and characterize their carbohydrate ligands on the surface of their hemocytes and the *Perkinsus* trophozoites. Accomplishment of these goals would contribute further understanding of the potential roles of bivalve galectins as soluble and hemocyte-associated receptors for *Perkinsus* parasites. These studies will be discussed in the following sections, and mostly illustrated with results obtained on CvGal1 (Tasumi and Vasta, 2007; Feng et al., 2013; Kurz et al., 2013).

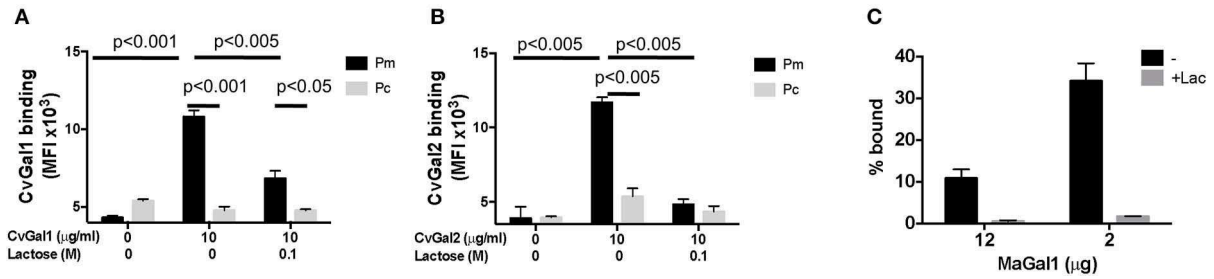

FIGURE 3 | Selective binding of CvGals and MaGal to Perkinsus parasites. **(A,B)** *Perkinsus marinus* (Pm) or *P. chesapeaki* (Pc) were incubated with recombinant CvGal1 **(A)** and CvGal2 **(B)** with or without 0.1 M lactose. The galectin binding was detected with galectin-specific antibodies followed by Fitc-conjugated anti-rabbit secondary antibody incubated, and analyzed in C6 cytometer. **(C)** *P. chesapeaki* was incubated with purified MaGal1 (12 or 2 μg) with (+Lac) or without (–) 0.1 M lactose and the bound galectin was pelleted along with the parasites by centrifugation. The bound galectin was eluted and run in SDS-PAGE along with the unbound galectin remaining in supernatant, and subjected to Coomassie staining. The intensities of both fractions from each samples were quantified (NIH Image J) and % bound was calculated as bound/(bound + unbound) [Adapted from Feng et al. (2015) with permission from the American Chemical Society].

BIOCHEMICAL CHARACTERIZATION OF OYSTER AND CLAM GALECTINS

The initial characterization of the carbohydrate specificity of CvGal1 using a panel of mono-, oligo-, and polysaccharides, and glycoproteins revealed that CvGal1 has a preference for GalNAc relative to Gal or LacNAc, which are typically recognized by most galectins (Tasumi and Vasta, 2007). Furthermore, the glycoproteins porcine stomach mucin (PSM), asialofetuin, thyroglobulin, lactoferrin, and laminin behaved as strong inhibitors, whereby PSM is a complex mixture of glycans, rich in blood group ABH moieties. To elucidate the fine specificity of CvGal1, the binding of recombinant CvGal1 to a glycan microarray was analyzed at the Core H, Consortium for Functional Glycomics, Emory University, Atlanta. The study confirmed the preliminary results by revealing that CvGal1 preferentially binds to carbohydrates containing non-reducing terminal GalNAc (Tasumi and Vasta, 2007). The strongest binders in the glycan microarray were complex bi-antennary oligosaccharides carrying blood group A type 2 moieties, followed by the type 1 structures and, with less affinity, similar type-2 B oligosaccharides (**Figure 4A**; Feng et al., 2013).

In contrast with rCvGal1, the glycan array binding profile of rCvGal2 showed that it recognizes with high affinity carbohydrates displaying either blood group A or B type 2 moieties (Feng et al., 2015). Thus, like CvGal1, CvGal2 also prefers type-2 backbone structures Galβ1-4GlcNAc in LacNAc and Gal, and a Fuc linked in α1-2 to the subterminal Gal. Unlike most galectins described to date, which recognize oligosaccharides exhibiting galactosyl units at the non-reducing end, such as *N*-acetyllactosamine moieties (Leffler et al., 2004; Vasta and Ahmed, 2008), our studies revealed that the oyster galectins CvGal1 and CvGal2 preferentially bind to ABH blood groups (Tasumi and Vasta, 2007; Feng et al., 2013, 2015). Unlike CvGal1 and CvGal2, however, a glycan microarray analysis of MaGal1, confirmed the preliminary solid phase assays that suggested preference for galactosyl moieties, and showed that MaGal1 preferentially recognizes Galα1-3Galβ1-4GlcNAcβ1-2Manα1-6(Galα1-3Galβ1-4GlcNAcβ1-2Manα1-3)Manβ1-4GlcNAcβ1-4GlcNAcβ-R and other bi-antennary structures with non-reducing terminal Galα1-3Galβ1-4GlcNAc, followed by those with terminal Galα/β1-4Galβ1-4GlcNAc (Vasta et al., 2015).

To elucidate the structural basis for the binding specificity of CvGal1 and CvGal2 we modeled their structure using the toad *Bufo arenarum* galectin-1 (BaGal1) as template (Bianchet et al., 2000) and analyzed the interactions of the CRDs with the preferred carbohydrate ligands for both oyster galectins identified in the solid phase assays and glycan array analysis (**Figures 4B–D**). The structures of the four CRDs of CvGal1 overlap very closely with each other (**Figure 4B**) and with BaGal1 (**Figure 4C**). Only minor differences among the four CRDs, mostly located in loops 3, 4, and 5, were predicted by the CvGal1 model (**Figure 4B**). Alignment of the CvGal1 CRDs with BaGal1 showed that amino acid residues that are involved participate in the recognition of the Galβ(1-4)GlcNAc by BaGal1 are mostly conserved in all four CvGal1 CRDs (Feng et al., 2013). In BaGal1 these residues establish interactions with the galactoside moieties as follows (**Figures 4C,D**): [1] (Arg^{49}, His^{45}, Asn^{47})—4-OH of Gal, [2](Arg^{49}, Glu^{72})—[3-OH in core 1, or 4-OH in core 2 galactosides] of GlcNAc, [3](Asn^{62}, Glu^{72})-—5-OH of Gal, and [4] Trp^{69}–ring of Gal. The modeling alignment also revealed differences in the secondary structure elements of CvGal1's CRDs with respect to the BaGal1 template, such as the short loop 4 (the sequence between strands 4 and 5) (**Figure 4C**), as discussed above (**Figures 2A,B**). In BaGal1 and other vertebrate prototype galectins only loop 4 participates in the recognition of the galactose moiety, whereby a histidine residue (His^{53}) makes an apolar contact with the C2 and O2 atoms of the Gal moiety of the core 2 galactoside. This histidine residue is absent in the short loop 4 of all CvGal1 CRDs (Feng et al., 2013).

To rationalize the recognition of ABH blood group oligosaccharides by CvGal1, the type 2 blood group A oligosaccharide (A2) was docked into the first CvGal1 CRD as guided by the *N*-acetyllactosamine bound to BaGal1 (Feng et al.,

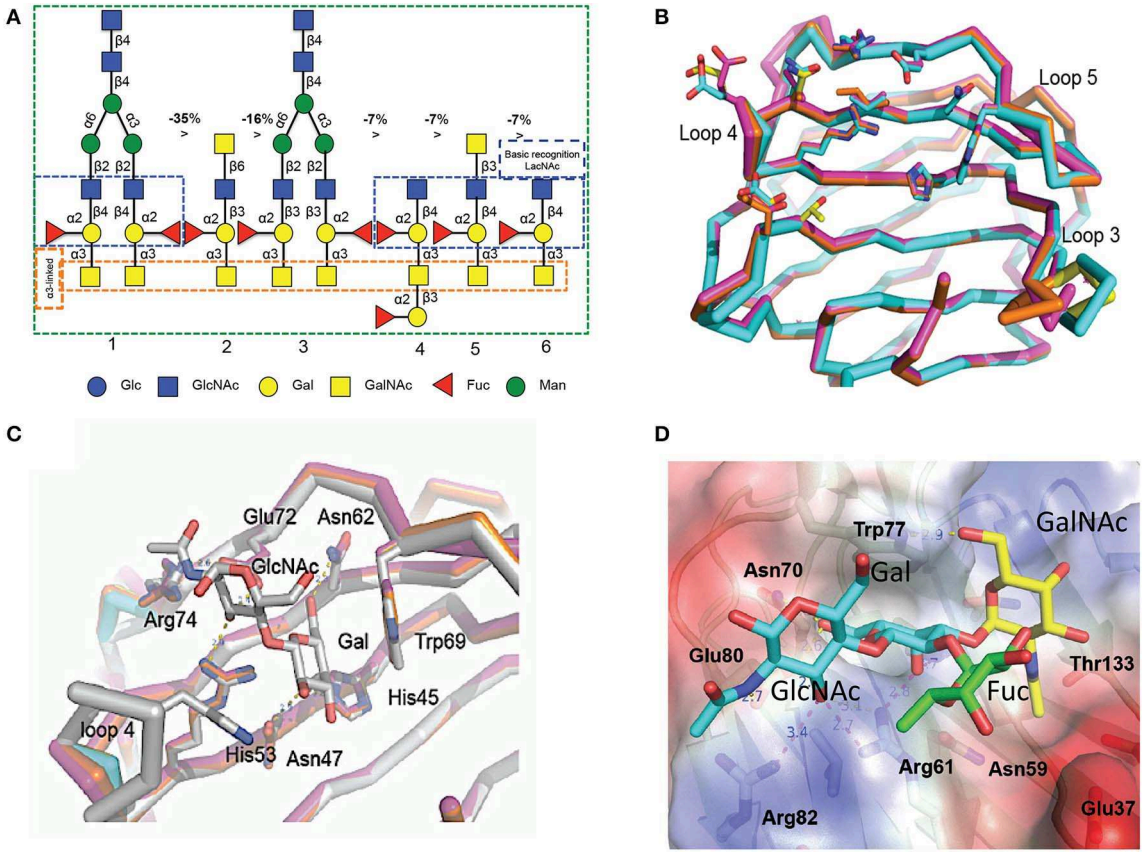

FIGURE 4 | Binding ligand analysis through glycan array and homology modeling. **(A)** Six best glycans ranked by their affinity for CvGal1 in glycan array analysis. The negative percentages are the evaluation of the % change in the fluorescent signal $(F_j - F_i)/F_i \times 100\%$). **(B)** Model of the four CRDs of CvGal1: Chain A in orange, chain B in cyan, chain C in magenta and chain D in yellow. **(C)** Overlay between the modeled CvGal1 CRDs and BaGal1: Loop 4 of the CvGal1 CRDs (chain colors as in A above) is shorter than the loop 4 of BaGal1 (in gray), allowing bulkier structure next to the N-acetylglucosamine residue. **(D)** A2 blood oligosaccharide docked at the binding pocket of the CvGal1 model of the first CRD, using the observed common *N*-acetyllactosamine disaccharide bound to the template. CvGal1-binding site is shown as semi-transparent solvent-accessible surface colored by its vacuum electrostatic potential (positive in *blue* to negative in *red*). The schematic model of the protein is visible across the surface showing the interacting residues in a *stick* representation. H-bonds recognizing hydroxyl groups of the A2 oligosaccharide are displayed as *dashed lines* with their distances (in Å) between heavy atoms indicated [Adapted from Feng et al. (2013) with permission from the American Society for Biochemistry and Molecular Biology].

2013) (**Figure 4D**). The space generated by the shortening of loop 4 enabled fitting the 2'-fucosyl moiety common to both the A and B blood group tetrasaccharides, with its 6-methyl group placed on top of the arginine that coordinates the axial 4- and equatorial 3-OH groups of the first and second moieties of the core galactoside, respectively (**Figure 4D**). Thus, the glutamate at the tip of loop 4 holds this conserved arginine in position. Distances from Glu^{37}, in the 1st CRD, Asn^{199} in the 2nd CRD; and Glu^{449} and Glu^{474}, in the 4th CRD to the fucose 4-OH group could support water-mediated bridges, although no direct interaction of polar group from the protein with any fucose hydroxyls could be established (Feng et al., 2013). Similarly, the CvGal2 structural model enabled a visual interpretation of the glycan array results, in particular the preferential binding to ABH blood group bi-antennary structures, and the recognition of sulfated moieties and Forssman antigens (Feng et al., 2015). In contrast with CvGal1, the glycan array analysis revealed that CvGal2 recognizes oligosaccharides displaying both blood group A and B moieties. Like in CvGal1 (Feng et al., 2013) and CGL2 (Walser et al., 2004), the longer loop 3 and shorter loop 4 in CvGal2 as compared to the typical proto type galectins (Bianchet et al., 2000; Feng et al., 2013) supports the structural basis for a preference for blood group oligosaccharides. In blood group A, the methyl-group of the *N*-acetyl moiety in the non-reducing GalNAc is coordinated by residues from a pocket formed on the N-terminus, similar to that observed in the CGL2-A2 antigen complex (Walser et al., 2004). As for CvGal1, the shorter loop 4 enables accommodating simultaneously the 2'-fucosyl group and the α(1-3)Gal[NAc] of A and B moieties. This feature results in an apparent higher affinity relative to that of the vertebrate prototype galectins that possess the typical long loop 4 (Liao et al., 1994; Vasta et al., 2015). It is noteworthy that in all four CvGal2 CRDs (A-D, or 1-4) sequence variations at key positions are suggestive of differences in their

fine specificity for glycans displaying ABH moieties (Feng et al., 2015).

The experimental validation of the CvGal1 and CvGal2 models, was carried out by first comparatively assessing by ELISA the binding of the recombinant galectins to neoglycoproteins displaying either a monosaccharide (GalNAc), a blood group A trisaccharide [GalNAcα3(Fucα2)Gal], or a type 2 tetrasaccharide [GalNAcα3(Fucα2)Galβ3GlcNAc] conjugated to BSA (Feng et al., 2013). The results showed that CvGal1 strongly bound to the blood group A tetrasaccharide, while the trisaccharide-BSA and GalNAc-BSA were not recognized (**Figure 5A**). A similar study using an anti-A monoclonal antibody showed that it equally recognized both the blood group A tri- and tetrasaccharides, but displayed negligible binding to GalNAc-BSA. A quantitative analysis of binding affinity by SPR revealed that rCvGal1 binds to the neoglycoprotein with conjugated blood group A type 2 tetrasaccharide with a K_D value of 1.5 μM (**Figure 5B**), while no binding was observed to blood group A trisaccharide-BSA (**Figure 5C**), or neoglycoproteins displaying GalNAc, Gal or GlcNAc (results not shown) (Feng et al., 2013). A similar analysis showed that in contrast with CvGal1, CvGal2 recognized both the blood group A tetra- and the trisaccharide-BSA (**Figure 5D**; Feng et al., 2015). SPR analysis confirmed that CvGal2 recognized both blood group A tetra- and trisaccharide-BSA, but displayed higher affinity for the tetrasaccharide than the trisaccharide (4.8 and 60 nM, respectively) (**Figures 5E,F**). Further SPR assessment of CvGal2 binding affinity with various blood group ABH oligosaccharides showed that it binds to type 1, 2, and 3/4 of blood group A tetrasaccharides (K_D = 2.5–21 μM) (Feng et al., 2015). In conclusion, although CvGal1 and CvGal2 are structurally similar, their fine specificities for ABH blood group oligosaccharides are both quali- and quantitatively different. Ongoing studies in our lab are aimed at expressing the recombinant individual CRDs from both CvGal1 and CvGal2 to enable the identification of potential differences in binding specificity among them.

IDENTIFICATION OF GALECTIN LIGANDS ON THE HEMOCYTE AND PARASITE SURFACE

As discussed above, analysis of CvGal1 expression suggested that it takes place in the hemocytes (Tasumi and Vasta, 2007; Feng et al., 2013). We experimentally assessed the subcellular localization of the CvGal1 protein, by raising an antiserum

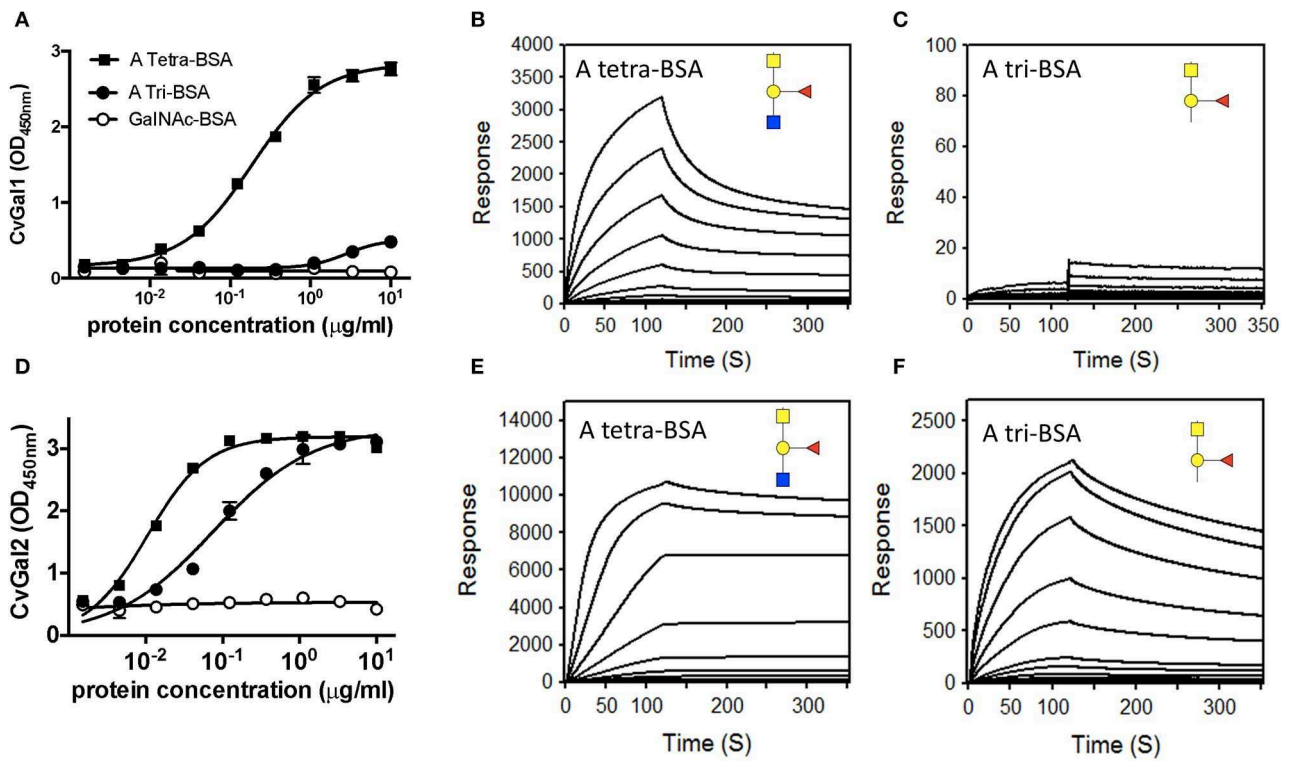

FIGURE 5 | Binding of recombinant CvGal1 and CvGal2 to blood group A antigen. **(A,D)** blood group A tetrasaccharide-BSA (A Tetra-BSA), blood group A trisaccharide-BSA (A Tri-BSA), or *N*-acetylgalactosamine-BSA (GalNAc-BSA) were added at the concentrations indicated (serial dilution starting from 10 μg/ml, 100 μl/well) into 96-well plates and the binding of 0.2 μg/ml of rCvGal1 **(A)** or rCvGal2 **(D)** was assessed by ELISA. Data show optical density at 450 nm (OD_{450nm}) in triplicates with standard error (SEM). **(B,C,E,F)** Blood group A tetrasaccharide-BSA (A Tetra-BSA) or blood group A trisaccharide-BSA (A Tri-BSA) were immobilized up to 1,000 response units on CM5 chips, and the binding of rCvGal1 **(B,C)** or rCvGal2 **(E,F)** was assessed by SPR with either lectin being injected as analyte. The SPR sensorgrams were recorded with 2-fold serial dilutions of the analyte starting from 100 μg/ml. Negligible responses were observed on sensorgrams for the GalNAc-BSA (data not shown) [Adapted from Feng et al. (2013) with permission from the American Society for Biochemistry and Molecular Biology].

against rCvGal1, and validating the specificity of the purified anti-rCvGal1 immunoglobulins by Western blot against a crude hemocyte extract, using rCvGal1 as control (Tasumi and Vasta, 2007). In agreement with the detection of the CvGal1 transcripts in hemocytes, the Western blot results revealed that the mature protein was also localized in the cytoplasm of the circulating hemocytes, suggesting that the gene is transcribed, translated, and the protein accumulates in the hemocyte. Because upon attachment and spreading on a foreign surface, the oyster hemocytes become motile and avidly phagocytic, we examined by blotting the presence of CvGal1 in plasma and hemocytes [circulating (unattached), and attached/spread]. Both the circulating and attached hemocytes showed a strong CvGal1 band, whereas the attached hemocytes secreted soluble CvGal1 into the extracellular space (**Figure 6A**). Next, we used immunofluorescence to assess the subcellular distribution of CvGal1 in unattached and attached hemocytes (**Figure 6B**). In the unattached hemocytes, CvGal1 was localized to the cytoplasm of approximately one third of the permeabilized hemocytes (+ Triton-X), but no signal was observed in the untreated cells (– Triton-X). In contrast, in both permeabilized and untreated attached hemocytes, intense diffuse staining was observed approximately in the same proportion as in the unattached permeabilized cells (Tasumi and Vasta, 2007). Based on their subcellular morphology under phase contrast microscopy, these cells were identified as granulocytes (Kennedy et al., 1996; Terahara et al., 2006). Unlike the CvGal1 localization in circulating hemocytes, the high concentration of CvGal1 detected on the plasma membrane of the untreated attached hemocytes, particularly on the surface of filopodia (**Figure 6B**), suggest that upon attachment and spreading, the cytoplasmic CvGal1 is secreted to the extracellular space and binds to the hemocyte

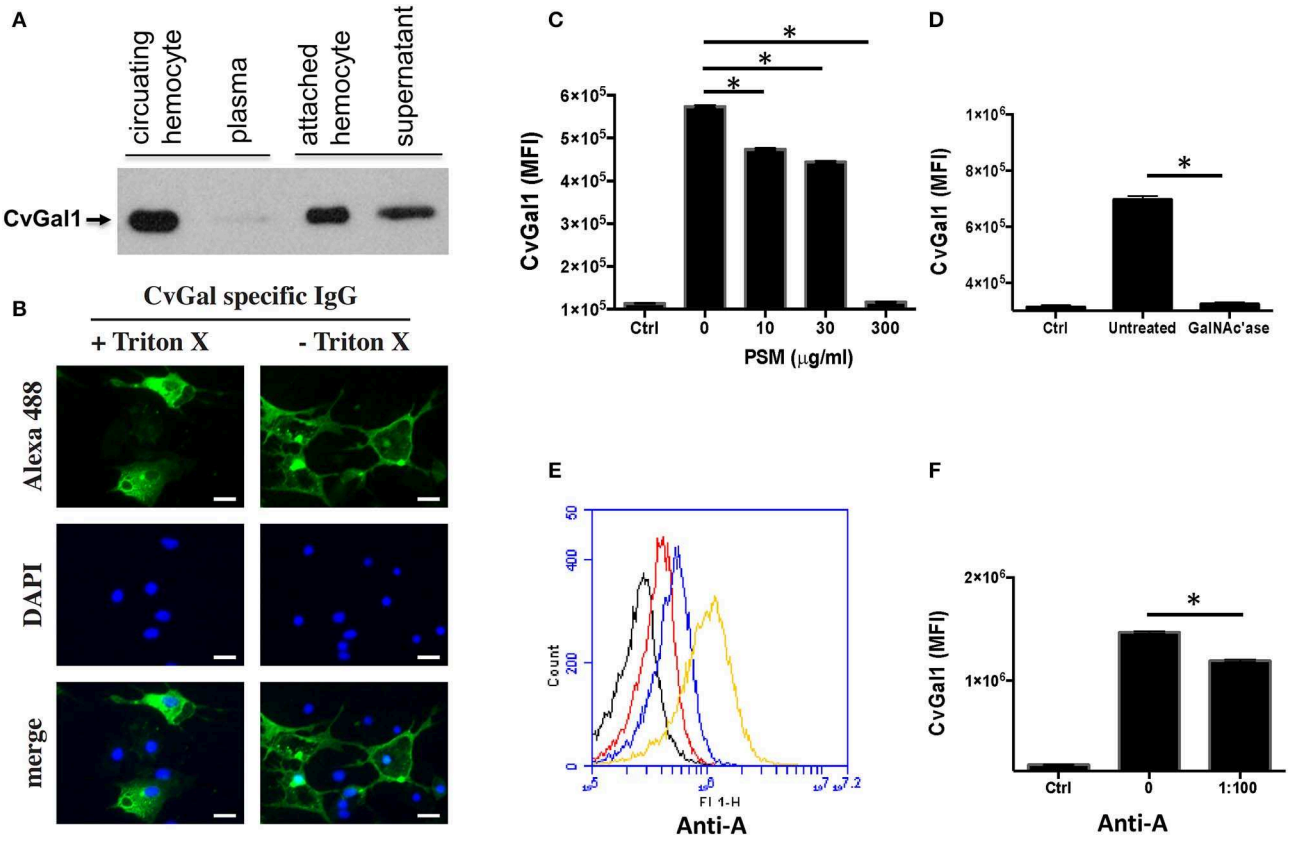

FIGURE 6 | Binding of CvGal1 and CvGal2 to oyster hemocytes. **(A)** Upon hemocyte attachment and spreading, CvGal1 is translocated to the periphery and secreted. Western blotting of unattached hemocytes, plasma, attached-spread hemocytes, and supernatant. **(B)** Immunofluorescence staining with anti-CvGal1 and DAPI staining of attached-spread hemocytes with (+) or without (–) Triton X treatment, showing the presence of CvGal1 in the cytoplasm, and on the external surface of the hemocyte plasma membrane, respectively. Scale bar, 10 μm. **(C)** Binding of rCvGal1 (100 μg/ml) to hemocytes in the presence of PSM (0–300 μg/ml), whereby the control (*Ctrl*) is sample without exogenous rCvGal1 and inhibitor. **(D)** Binding of rCvGal1 to unattached hemocytes with α-*N*-acetylgalactosaminidase treatment (*GalNAc'ase*) or no treatment (*Untreated*) were measured by flow cytometry, whereby a sample without rCvGal1 was the control (*Ctrl*). Data show mean fluorescence intensity (*MFI*) ± S.E. of each sample. **(E)** Fixed hemocytes were stained with dilutions of anti-blood group A antibody (*red,* 1:2000; *blue,* 1:500; *yellow,* 1:100) or buffer only (*black*) in flow cytometry analysis. **(F)** Fixed cells were preincubated with anti-blood group A antibody (1:100), and the binding of rCvGal1 (100 μg/ml) was measured by flow cytofluorometry; the control (*Ctrl*) was recorded in the absence of rCvGal1. *Indicates significant difference ($p < 0.05$) between samples from One-Way ANOVA analysis [Adapted from Tasumi and Vasta (2007) and Feng et al. (2013) with permission from the American Association of Immunologists and the American Society for Biochemistry and Molecular Biology].

surface glycans. Galectins are secreted by an unconventional mechanism not yet fully elucidated, as they lack the signal peptide typical of secreted proteins (Hughes, 1999). Therefore, galectins are not exported via the typical secretory pathway but through a mechanism that resembles vesicle exocytosis (Hughes, 1999). CvGal1, which also lacks a signal peptide, may be no exception to this observation, and may be secreted by the non-classical mechanism common to other galectins (Tasumi and Vasta, 2007). We also examined the possibility that the CvGal1 released by the attached granulocytes binds to the external surface of circulating hemocytes by binding to surface moieties. For this, we tested by immunofluorescence the potential binding of rCvGal1 to unattached hemocytes (Tasumi and Vasta, 2007). Intense staining was observed in virtually 100% of the cells examined, indicating that CvGal1 can strongly bind to both attached and unattached hemocytes subpopulations, including hyalinocytes. These observations suggest that the CvGal1 secreted by the attached granulocytes binds to carbohydrate moieties on the cell surface and upon saturation, the secreted galectin remains in plasma as a soluble protein (Tasumi and Vasta, 2007). Similar observations were made with CvGal2 (Feng et al., 2015).

Based on our studies on the specificity of CvGal1 and CvGal2 for ABH blood group moieties described above, we addressed the question about the identity of the carbohydrate moieties on the hemocyte surface that are recognized by the oyster galectins (Feng et al., 2013, 2015). For this, we used flow cytometry, to assess the binding of CvGal1 to fixed, non-permeabilized hemocytes and its inhibition by increasing concentrations of PSM, a mixture of glycoproteins rich in ABH moieties, using BSA as control (Feng et al., 2013). Strong binding of CvGal1 to the hemocyte surface was observed, and this interaction could be specifically prevented by pre-incubation of CvGal1 with PSM (300 μg/ml) (**Figure 6C**). Pre-treatment of the hemocytes with α-*N*-acetylgalactosaminidase also significantly prevented CvGal1 binding (**Figure 6D**), confirming that non-reducing terminal αGalNAc on the hemocyte surface is required for

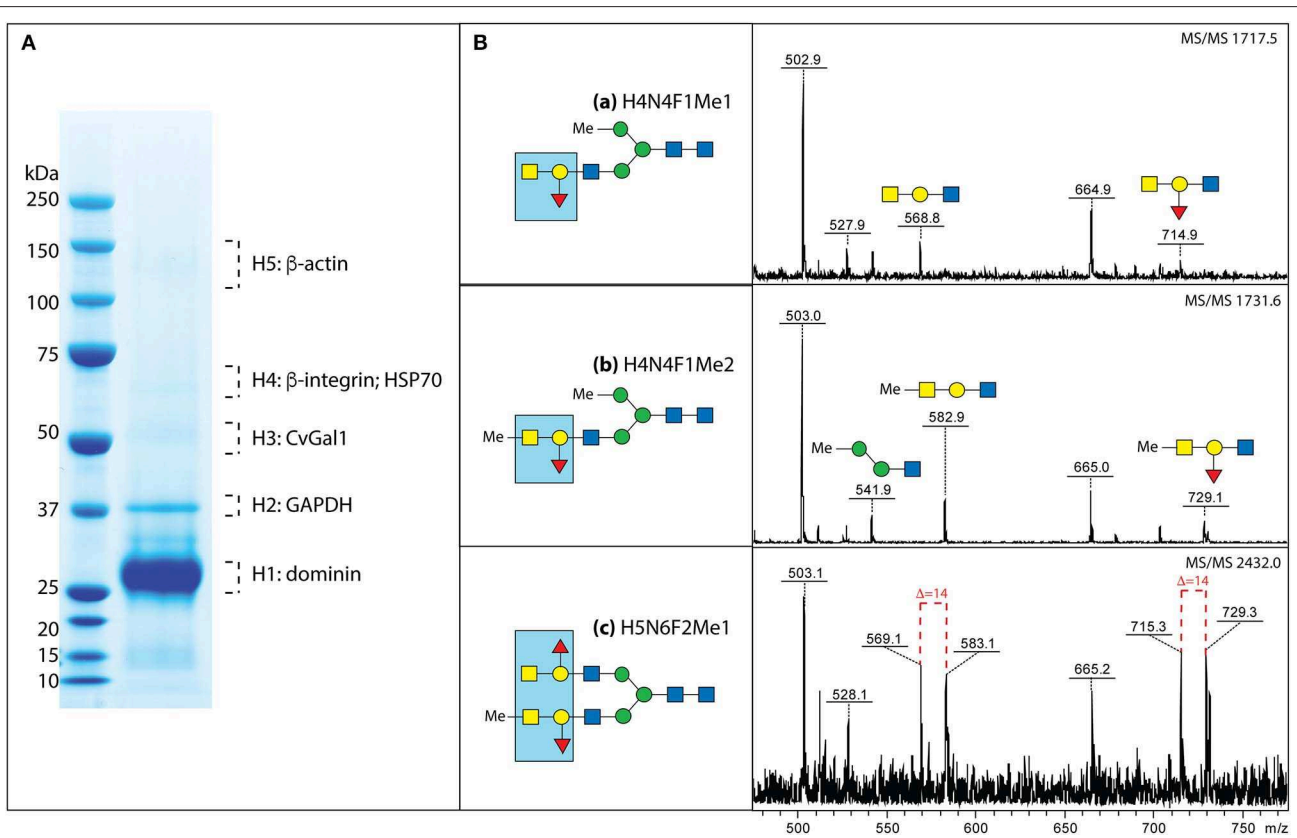

FIGURE 7 | Binding ligands of CvGals on oyster hemocyte surface. **(A)** Isolation and identification of CvGal1 ligands from oyster hemocytes. Oyster hemocyte extracts were eluted from a rCvGal1-column (rCvGal1 cross-linked to Affi-Gel 15, BioRad) using 50 mM lactose, prior to analysis by SDS-PAGE. The Coomassie blue-stained protein bands (H1–H5) were excised from the gel and subjected to proteomic analysis as described (Feng et al., 2013). Peptide sequences were identified using Mascot software to search the NCBInr 167 database, processed in Scaffold and the proteins identified based on the identification of at least two peptides at 95% or greater confidence. **(B)** MS/MS analysis of oyster glycans carrying the histo-blood group A modification. *a–c, N*-glycans from selected NP-HPLC fractions (6.0, 5.7, and 7.7 g.u., respectively) were subject to MS/MS of their protonated forms in positive mode with the focus on the fragments in the range *m/z* 500–800, which are indicative of modification by the blood group A and methyl groups; for the glycan carrying both non-methylated and methylated forms of the blood group A, the differences of 14 Da between the sets of fragments are shown with *dashed lines*. The blue boxes emphasize the identified blood group A tetrasaccharide structure (for further details, see Feng et al., 2013 and Kurz et al., 2013).

CvGal1 binding. Monoclonal anti-A antibodies strongly bound to the hemocyte surface (**Figure 6E**) revealing that exposed blood group A moieties are present, and that the αGalNAc detected may possibly be the terminal moiety on the hemocyte ligands recognized by CvGal1 (Tasumi and Vasta, 2007). In contrast, the anti-B antibodies failed to bind to the intact hemocytes. Furthermore, we observed partial inhibition of rCvGal1 binding to the intact hemocytes by anti-A monoclonal antibodies, and *vice versa*, that pre-treatment with anti-A antibodies could partially inhibit binding of CvGal1(**Figure 6F**), whereas the anti-B antibodies had no effect (Feng et al., 2013). Taken together, these observations suggested that blood group A moieties on the hemocyte surface are, at least in part, the ligands for CvGal1.

Next, we used affinity chromatography of the oyster hemocyte extracts on a rCvGal1-Affi-Gel 15 column to isolate the CvGal1 ligands, and selected bands from SDS-PAGE were subjected to proteomic analysis for the identification of these glycans (Feng et al., 2013). The mass spectrometry analysis identified multiple peptides that matched β-integrin, dominin, GAPDH, and HSP70 in the bands of the expected electrophoretic mobilities (**Figure 7A**; Feng et al., 2013). Dominin is a major plasma protein that houses a Cu/Zn superoxide-like domain, and is highly similar to cavortin, an iron binding-protein from the Pacific oyster (*C. gigas*) (Itoh et al., 2011). Iron is critical for *P. marinus* intracellular survival in oyster hemocytes (Schott and Vasta, 2003; Schott et al., 2003a; Fernández-Robledo et al., 2008; Alavi et al., 2009), and the iron transporters (Nramp; Robledo et al., 2004; Lin et al., 2011) in both the parasite and the oyster host are involved in their competition for available iron (Cellier et al., 2007). Another interesting ligand for CvGal1 identified on the hemocyte surface is β-integrin (Zhuo et al., 2008; Feng et al., 2013), and this was of particular interest as this transmembrane signaling glycoprotein is a key receptor in cell activation processes (Mayadas and Cullere, 2005; Lim and Hotchin, 2012). We have observed that the addition of PSM to attached and spread hemocytes, promotes activation and phagocytosis of *P. marinus*. It is possible that this results from clustering of hemocyte β-integrin-bound CvGal1 by the multivalent PSM, which acts as a three-component glycoprotein-CvGal1-β-integrin lattice that leads to cell activation.

A rigorous *N*-glycomic study on selected glycoproteins isolated on a CvGal1 column and identified by proteomic analysis, together with plasma and hemocyte glycoproteins, demonstrated the presence of blood group A oligosaccharide moieties on some hemocyte N-glycans (Kurz et al., 2013; **Figure 7B**). Frequent methylation and sulfation of the identified hemocyte glycans was observed, with the latter likely to confer a significant negative charge to the hemocyte glycocalyx (Kurz et al., 2013). These observations are consistent with the results of our CvGal1-ligand interaction model which revealed that methyl groups can be present at the 4-OH and 6-OH of the GalNAcα(1-3), without any negative effect on CvGal1 recognition by the protein (Feng et al., 2013). The results of the glycomic analysis are supported by identification of an α1,2-fucosyltransferase gene in the oyster genome, which is predicted to encode an enzyme that can transfer L-Fuc to Gal (Zhang et al., 2012).

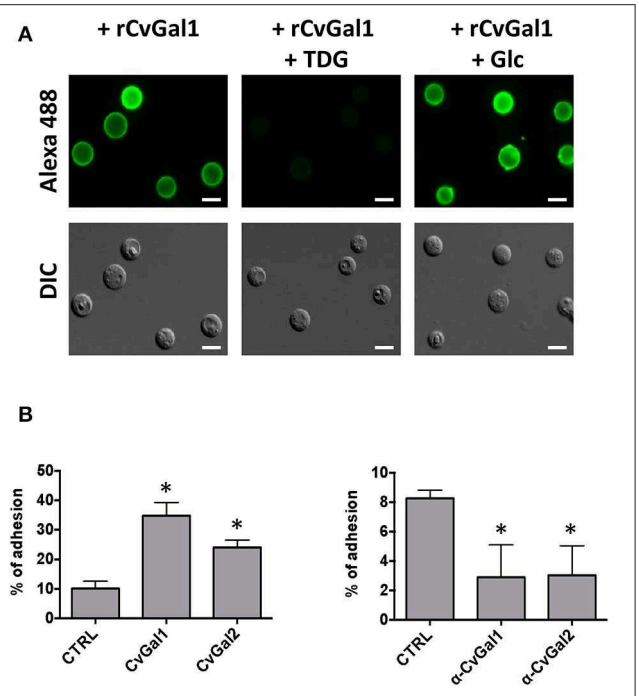

FIGURE 8 | CvGals mediate *P. marinus* trophozoites adhesion onto oyster hemocytes. **(A)** Carbohydrate -specific binding of rCvGal1 to *P. marinus* trophozoites in the presence and absence of thiodigalactose (inhibits rCvGal1 binding) or glucose (does not inhibit rCvGal1 binding) was analyzed by immunofluorescence staining. Scale bar, 10 μm. **(B)** Adhesion of *P. marinus* trophozoites to hemocytes was enhanced by addition of recombinant CvGal1 or CvGal2 (left) or inhibited by addition of anti-CvGal1 or anti-CvGal2 antibody (right). *Indicates significant difference ($p < 0.05$) from control sample [Adapted from Tasumi and Vasta (2007), and Feng et al. (2013) with permission from the American Association of Immunologists and the American Society for Biochemistry and Molecular Biology].

We then carried out experiments to identify the nature of the glycan moieties recognized by CvGal1 and CvGal2 on the surface of the *Perkinsus* trophozoites. CvGal1 binds strongly and in a carbohydrate-specific manner to *P. marinus* trophozoites (**Figure 8A**; Tasumi and Vasta, 2007). The binding can be fully prevented by thiodigalactose (TDG), an effective galectin inhibitor, but not by glucose. Furthermore, pre-incubation of *P. marinus* trophozoites with either CvGal1 or CvGal2 enhances their adhesion to the hemocyte surface, whereas pre-treating the hemocytes with anti-CvGal1 or -CvGal2 antibodies significantly decreases adhesion, suggesting that both galectins can function either as opsonins or cell surface receptors for the parasite (**Figure 8B**; Feng et al., 2013). Based on the identification of blood group A oligosaccharides as the hemocyte surface ligands for the oyster galectins, we investigated the possibility that the CvGal1 ligands on the parasite surface were also ABH blood group moieties. Thus, we first assessed the binding of CvGal1 and its inhibition by PSM by flow cytometry. CvGal1 bound strongly to the trophozoites, and pre-incubation with PSM reduces the binding in a dose-dependent manner, similar to our observations with hemocytes (**Figure 9A**; Feng et al., 2013). Strikingly, however, we observed no binding of the anti-A or

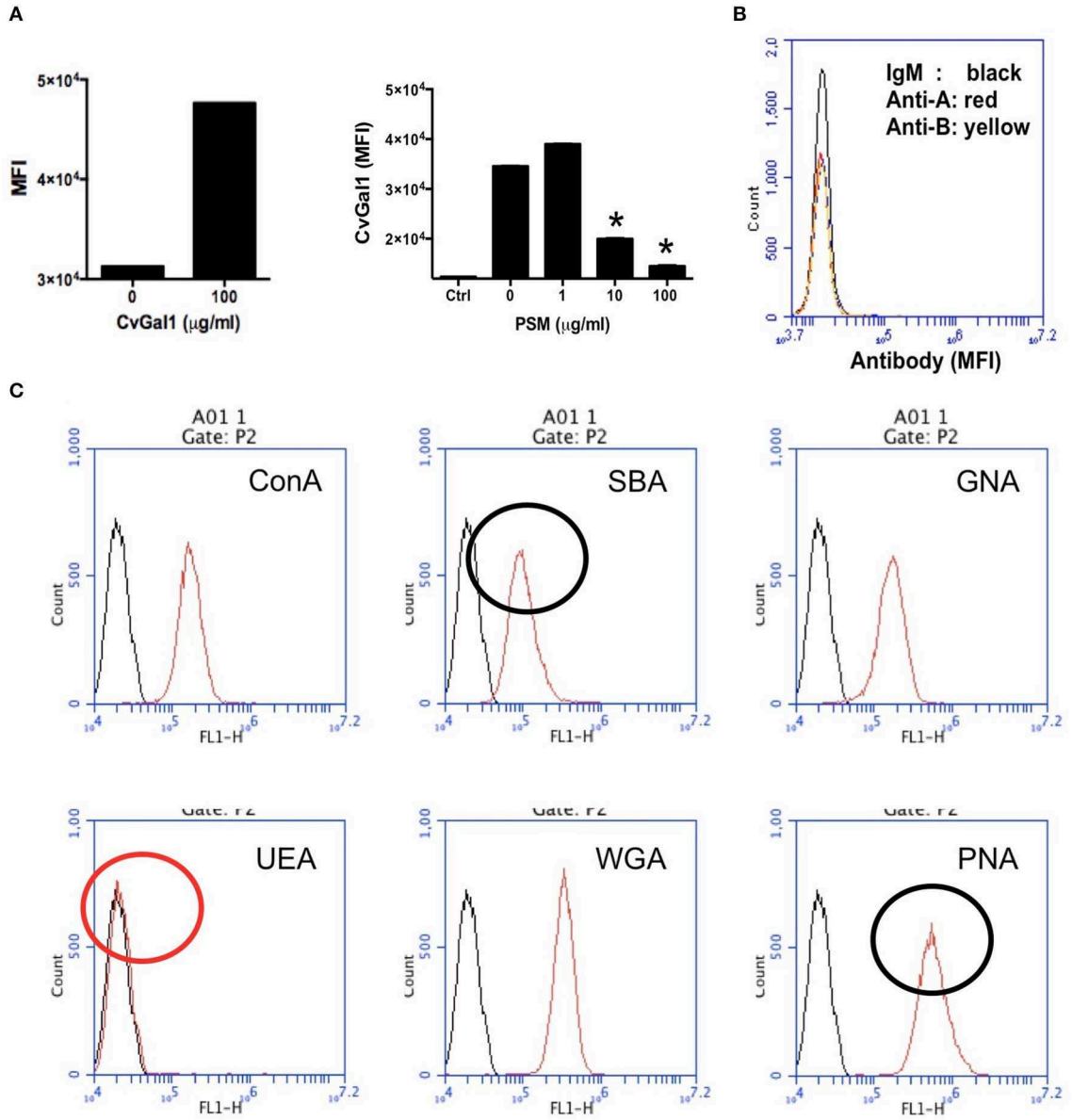

FIGURE 9 | Binding of rCvGal1 to *P. marinus* trophozoites. **(A)** Binding of rCvGal1 (100 μg/ml) to *P. marinus* trophozoites was measured by flow cytometry analysis. Data show mean fluorescence intensity (*MFI*) ± S.E. of each sample. The binding of rCvGal1 (100 μg/ml) to *P. marinus* trophozoites in the presence of PSM (0–100 μg/ml) is shown on the right hand panel of A. *Indicates significant difference ($p < 0.05$) from sample without PSM inhibition (*0*). Sample without exogenous rCvGal1 and inhibitor was shown (*Ctrl*). **(B)** anti-A or anti-B binding to *P. marinus* revealed the absence of exposed A and B blood group moieties. **(C)** *P. marinus* trophozoites were stained with fluorochrome-labeled lectins (*red lines*) or buffer alone (*black lines*) in flow cytometry analysis. Black circles indicate significant staining of SBA (soybean agglutinin) and PNA (peanut agglutinin) over background, and red circle indicates no significant staining of UEA (*Ulex europaeus* agglutinin) [Adapted from Feng et al. (2013) and Kurz et al. (2013) with permission from the American Society for Biochemistry and Molecular Biology].

anti-B monoclonal antibodies to the *P. marinus* trophozoites (**Figure 9B**). This revealed that no blood group A or B moieties are exposed on the parasite surface, and suggested that the GalNAc or related sugars recognized by CvGal1 are linked to different glycan structures (Feng et al., 2013).

To tentatively identify these carbohydrate moieties on the surface of *P. marinus* trophozoites we used labeled plant lectins to carry out a glycotyping analysis of the parasite surface (**Figure 9C**; Feng et al., 2013). We observed strong signals with ConA (concanavalin A; binding αMan, GlcNAc, and αGlc), SBA (α,βGalNAc and α,βGal), GNA (*Galanthus nivalis* agglutinin; α1-3 and α1-6 high mannose oligosaccharides), WGA (Wheat germ agglutinin; Neu5Ac or β4-linked terminal HexNAc), and PNA (Galβ1-3GalNAcα). UEA (*Ulex europaeus* agglutinin), showed no binding, indicating the absence of exposed Fucα1-2Gal moieties. This was supported by the absence of fucosyltransferase genes in

the *P. marinus* genome (Caler et al., in preparation). In contrast, the binding of SBA and PNA to *P. marinus* trophozoites revealed the presence of exposed GalNAc and Gal moieties on the parasite surface. The absence of Fucα1-2Gal and lack of anti-A and anti-B antibody staining suggest that the strong binding of CvGal1 and CvGal2 to the parasite surface is based on the recognition of exposed GalNAc and Gal as components of carbohydrate moieties that may be topologically similar to A or B blood group oligosaccharides, but chemically different (Feng et al., 2013). Ongoing glycomic studies are aimed at the identification and structural characterization of the glycans that function as CvGal1, CvGal2 and MaGal1 ligands on *Perkinsus* trophozoites.

SUMMARY AND CONCLUSIONS

Among the various lectin families, galectins are evolutionarily conserved and taxonomically widely distributed lectins endowed with key regulatory and effector functions in multiple biological processes (Leffler et al., 2004; Vasta et al., 2007, 2012; Vasta and Ahmed, 2008; Vasta, 2009; Rabinovich and Croci, 2012)[1]. Within the marine environment, galectins seem to be ubiquitous among both invertebrates (reviewed in Vasta et al., 2004a, 2015; Vasta and Ahmed, 2008; Vasta, 2009; Wang and Wang, 2013) and vertebrates (reviewed in Vasta et al., 2004b, 2011; Shirai et al., 2006; Cummings et al., 2017). By the use of biochemical, molecular, glycomic, and structural approaches we identified and characterized the specificity of the oyster galectins CvGal1, CvGal2 and the clam galectin MaGal1, and have gained novel insights into the nature of their carbohydrate ligands on the surfaces of the oyster hemocyte and *Perkinsus* parasites (Tasumi and Vasta, 2007; Feng et al., 2013, 2015; Vasta et al., 2015). This work is ongoing in our lab and those of our collaborators, and we aim to achieve a detailed and comprehensive view of the protein-carbohydrate interactions and mechanisms that determine host preference, recognition, and entry of *Perkinsus* parasites into their bivalve hosts. We expect that the bivalve-*Perkinsus* system will constitute a useful model to address the role(s) of galectins in host defense against parasites, as well as their unique glycan adaptations for host colonization.

The binding profiles of the oyster galectins CvGal1 and CvGal2 in the glycan microarray revealed that they preferentially recognize ABH blood group oligosaccharides, whereas the clam galectin MaGal1 binds to oligosaccharides with terminal Gal. The modeling of the galectins's CRDs and docking of selected ABH oligosaccharides into their binding pockets, enabled a detailed visualization of the interactions that take place between the protein and the carbohydrate ligand. Most galectins typically recognize oligosaccharides exhibiting non-reducing terminal galactosyl moieties, particularly *N*-acetyllactosamine units (Di Lella et al., 2011). Selected galectins, however, may recognize non-reducing terminal GalNAc on surface carbohydrate moieties of parasites or microbial pathogens, such as the human galectin-3 that binds to glycans displaying GalNAcβ1–4GlcNAc from the parasite helminth *Schistosoma mansoni* (van den Berg et al., 2004). Other galectins described in taxa from fungi to mammals display specificity for ABH blood groups (Stowell et al., 2008a,b, 2010). For example, CGL2, a galectin from the mushroom *Coprinus cinereus*, can bind blood group A oligosaccharides (Cooper et al., 1997; Walser et al., 2004), while the mammalian galectins 2, 3, 4, and 8 can recognize both A and B oligosaccharides (Stowell et al., 2008a,b). The glycomic study carried out on selected hemocyte surface glycans recognized by CvGal1 rigorously demonstrated the presence of blood group A oligosaccharides (Kurz et al., 2013), thereby confirming results from biochemical approaches (Tasumi and Vasta, 2007; Feng et al., 2013).

As mentioned above, the oyster galectins CvGal1 and CvGal2 that have been secreted by the hemocytes upon recognition of a foreign surface or particle, can bind to the hemocyte surface, with some CvGal1 and CvGal2 remaining as soluble protein in extracellular space (Tasumi and Vasta, 2007). The strong recognition of *P. marinus* trophozoites, their enhanced adhesion to hemocytes by pre-incubation with CvGal1 and CvGal2, and the specific inhibition of adhesion and phagocytosis by anti-CvGal1 and anti-CvGal2 antibodies strongly suggest that host galectins can recognize and mediate uptake of phytoplankton, bacteria, and *Perkinsus* parasites either as cell surface receptors or as opsonins by cross-linking glycans on the parasite to those on the hemocyte (Tasumi and Vasta, 2007; Vasta, 2009; **Figure 10**). The internalized *Perkinsus* parasites use their powerful anti-oxidative machinery to inhibit the hemocyte's typical oxidative burst (Wright et al., 2002; Ahmed et al., 2003; Schott and Vasta, 2003; Schott et al., 2003a,b, 2019; Asojo et al., 2006), they survive and proliferate, and eventually lyse the infected hemocytes (Alavi et al., 2009). The parasite progeny released by the desintegrating hemocytes are phagocytosed by other attached hemocytes, or circulating cells that are activated by the binding of secreted CvGal1 or CvGal2 to their surface and recognition of the released parasites (Tasumi and Vasta, 2007; Feng et al., 2013, 2015; Vasta et al., 2015).

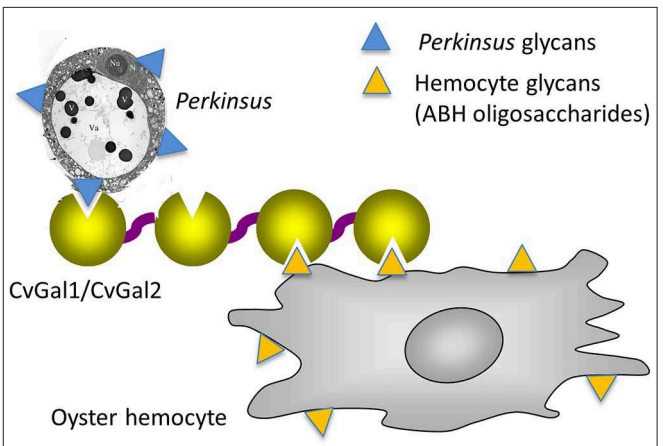

FIGURE 10 | Schematic model of CvGals-mediated *Perkinsus* sp. infection. Yellow triangles represent the binding ligands on hemocytes (mainly ABH oligosaccharides on dominin) and blue triangles represent the chemically different binding ligands on *Perkinsus* sp. parasites.

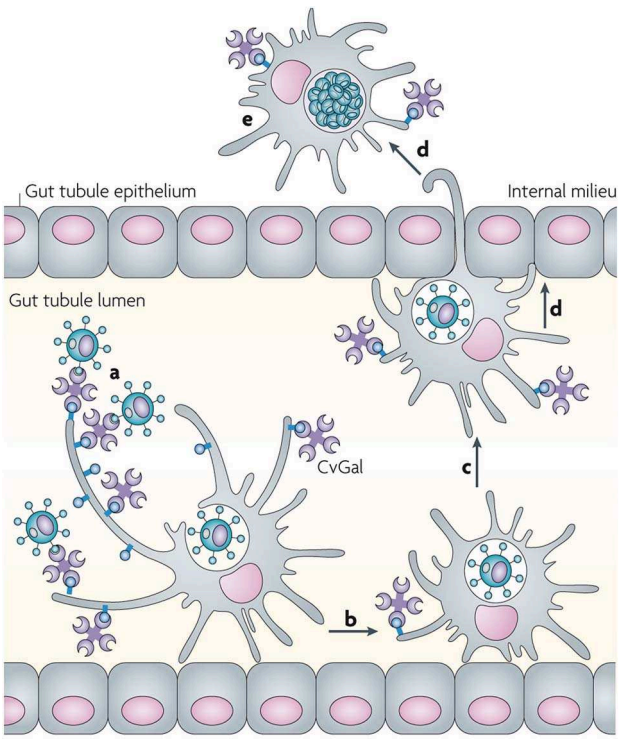

FIGURE 11 | Recognition of *Perkinsus marinus* trophozoites by the oyster (*Crassostrea virginica*) galectin CvGals facilitates infection: CvGals displays four canonical galectin carbohydrate-recognition domains (CRDs), a domain organization that is unlike any of the known galectin types. CvGal is translocated to the periphery and secreted by attached hemocytes, and binds to the cell surface. *P. marinus* trophozoites (a) ingested by filter-feeding are recognized by CvGal on the surface of hemocytes that coat the gut tubules, phagocytosed (b) and transported through the gut epithelium (c,d) into the internal milieu. The parasite inhibits intracellular killing by the host hemocytes and proliferates (e), thereby causing systemic infection and eventually death of the host [Adapted from Vasta (2009) with permission from the Springer Nature].

Although CvGal1 or CvGal2 strongly recognize ABH blood group oligosaccharides on the surface of hemocyte surface, the carbohydrate moieties recognized on the *Perkinsus* surface may be topologically similar, albeit chemically different, as no A or B oligosaccharides could be detected by the specific monoclonal antibodies (Tasumi and Vasta, 2007; Feng et al., 2013, 2015; Kurz et al., 2013). Further, as the presence of exposed GalNAc and Gal moieties on the parasite surface was revealed by glycotyping analysis with labeled plant lectins, the lack of binding of the lectin UEA to the trophozoite surface, suggested that Fuc(α1–2)Gal moieties are absent (**Figure 9**). Additionally, the absence of fucosyltransferase genes in the *Perkinsus* genome support the lack of *bona fide* A or B oligosaccharides on the trophozoite surface. Based on this experimental evidence it is tempting to speculate that the *Perkinsus* parasite has co-evolved with the oyster host and adapted its glycocalyx to acquire effective mimicry of the "self" ligands recognized by CvGal1 on the hemocyte surface, and gained galectin-mediated entry into the oyster phagocytic hemocytes, survive the oxidative attack, and proliferate (Vasta, 2009; **Figures 10**, **11**). ABH blood group oligosaccharides have been identified in most vertebrate species (Marionneau et al., 2001), as well as in some invertebrates and bacteria (Tasumi and Vasta, 2007; Stowell et al., 2010; Feng et al., 2013, 2015; Kurz et al., 2013). Their taxonomic distribution, however, has not been investigated in a comprehensive manner, and their biological role(s) and evolutionary aspects are subject of current discussion (Marionneau et al., 2001; Gagneux et al., 2017; Stanley and Cummings, 2017).

In recent years, evidence has accumulated to support a role of galectins as carbohydrate-specific receptors that recognize surface carbohydrate moieties of viruses, bacteria and parasites, although in very few examples the identity of the recognized moieties has been rigorously identified (Vasta, 2009). Based on these observations, galectins are often considered to function as PRRs. However, the Janeway and Medzhitov model (Janeway and Medzhitov, 2002) for self/non-self recognition, proposes that PRRs recognize pathogen- or microbe-associated molecular patterns (PAMPs or MAMPs), such as LPS or peptidoglycan, that are highly conserved and widely distributed among viruses, microbes, and parasites, but are absent from the host. Therefore, galectins do not fit a *sensu stricto* definition of PRRs as they can recognize endogenous ("self") and exogenous ("non-self") carbohydrate moieties with the same binding site. This apparent paradox reveals significant gaps in our understanding of galectin-carbohydrate binding equilibrium dynamics, the subcellular compartmentalization and secretion of galectins and their carbohydrate ligands, as well as structural and biophysical aspects of their recognition of multivalent glycans (Dam and Brewer, 2008; Vasta, 2009; Vasta et al., 2012). Although substantial progress has been achieved in the past few years, these aspects warrant further investigation.

AUTHOR CONTRIBUTIONS

GV wrote the article draft and all co-authors listed have made a substantial, direct and intellectual contribution to the work, and approved it for publication.

FUNDING

Studies reviewed in this article were supported by grants IOB-0618409, IOS-0822257, and IOS-1063729 from the National Science Foundation, grant NA05NMF4571243 from the National Oceanic and Atmospheric Administration, and grant R01 GM070589 from the National Institutes of Health to GV, grant P21946 from the Austrian Fonds zur Förderung der Wissenschaftlichen Forschung Grant to KP, and grant R01 GM080374 from the National Institutes of Health to L-XW.

ACKNOWLEDGMENTS

We are grateful to Prof. Richard D. Cummings, Dr. David Smith, and Dr. Jamie Molinaro from the Core H, Consortium for Functional Glycomics, Emory University, Atlanta, GA, and National Center for Functional Glycomics, Harvard University, Boston, MA for the glycan array analysis of galectins discussed in this review.

REFERENCES

Ahmed, H., Bianchet, M. A., Amzel, L. M., Hirabayashi, J., Kasai, K., Giga-Hama, Y., et al. (2002). Novel carbohydrate specificity of the 16-kDa galectin from Caenorhabditis elegans: binding to blood group precursor oligosaccharides (type 1, type 2, Tαβ, and Tβ) and gangliosides. *Glycobiology* 12, 451–461. doi: 10.1093/glycob/cwf052

Ahmed, H., Schott, E. J., Gauthier, J. D., and Vasta, G. R. (2003). Superoxide dismutases from the oyster parasite *Perkinsus marinus*: purification, biochemical characterization, and development of a plate microassay for activity, *Anal. Biochem.* 318, 132–141. doi: 10.1016/S0003-2697(03)00192-1

Alavi, M. R., Fernandez-Robledo, J. A., and Vasta, G. R. (2009). Development of an *in vitro* assay to examine intracellular survival of *Perkinsus marinus* trophozoites upon phagocytosis by oyster (*Crassostrea virginica* and *Crassostrea ariakensis*) hemocytes. *J. Parasitol.* 95, 900–907. doi: 10.1645/GE-1864.1

Andrews, J. D. (1996). History of *Perkinsus marinus*, a pathogen of oysters in Chesapeake Bay 1950-1984. *J. Shellfish Res.* 15, 13–16.

Asojo, O. A., Schott, E. J., Vasta, G. R., Silva, A. M. (2006). Structures of PmSOD1 and PmSOD2, two superoxide dismutases from the protozoan parasite *Perkinsus marinus*. *Acta Crystallogr. Sect. F. Struct. Biol. Cryst. Commun.* 62, 1072–1075. doi: 10.1107/S17443091060 40425

Bianchet, M. A., Ahmed, H., Vasta, G. R., and Amzel, L. M. (2000). Soluble beta-galactosyl-binding lectin (galectin) from toad ovary: crystallographic studies of two protein-sugar complexes. *Proteins* 40, 378–388. doi: 10.1002/1097-0134(20000815)40:3<378::AID-PROT40>3.0.CO;2-7

Bushek, D., Ford, S. E., and Chintala, M. M. (2002). Comparison of *in vitro*-cultured and wild-type *Perkinsus marinus*. III. Fecal elimination and its role in transmission. *Dis. Aquat. Organ.* 51, 217–225. doi: 10.3354/dao051217

Caceres-Martinez, J., Ortega, M. G., Vasquez-Yeomans, R., Garcia Tde, J., Stokes, N. A., and Carnegie, R. B. (2012). Natural and cultured populations of the mangrove oyster Saccostrea palmula from Sinaloa, Mexico, infected by *Perkinsus marinus*. *J. Invertebr. Pathol.* 110, 321–325. doi: 10.1016/j.jip.2012.03.019

Cellier, M. F., Courville, P., and Campion, C. (2007). Nramp1 phagocyte intracellular metal withdrawal defense. *Microbes Infect.* 9, 1662–1670. doi: 10.1016/j.micinf.2007.09.006

Chu, F.-L. E. (1996). Laboratory investigations of susceptibility, infectivity, and transmission of *Perkinsus marinus* in oysters. *J. Shellfish Res.* 15, 57–66.

Cooper, D. N., Boulianne, R. P., Charlton, S., Farrell, E. M., Sucher, A., and Lu, B. C. (1997). Fungal galectins, sequence and specificity of two isolectins from Coprinus cinereus. *J. Biol. Chem.* 272, 1514–1521. doi: 10.1074/jbc.272.3.1514

Cummings, R. D., Liu, F.-T., and Vasta, G. R. (2017). "Chapter 36 galectins," in *Essentials of Glycobiology, 3rd Edn*. eds A. Varki, R. D. Cummings, J. D. Esko, P. Stanley, G. W. Hart, M. Aebi, et al. (New York, NY: Cold Spring Harbor Laboratory Press), 469–480.

Dam, T. K., and Brewer, C. F. (2008). Effects of clustered epitopes in multivalent ligand-receptor interactions. *Biochemistry* 47, 8470–8476. doi: 10.1021/bi801208b

Dame, R., Bushek, D., Allen, D., Lewitus, A., Edwards, D., Koepfler, E., et al. (2002). Ecosystem response to bivalve density reduction: management implications. *Aquat. Ecol.* 36, 51–65. doi: 10.1023/A:1013354807515

Di Lella, S., Sundblad, V., Cerliani, J. P., Guardia, C. M., Estrin, D. A., Vasta, G. R., et al. (2011). When galectins recognize glycans: from biochemistry to physiology and back again. *Biochemistry* 50, 7842–7857. doi: 10.1021/bi201121m

Feng, C., Ghosh, A., Amin, M. N., Bachvaroff, T. R., Tasumi, S., Pasek, M., et al. (2015). The Galectin CvGal2 from the eastern oyster (*Crassostrea virginica*) displays unique specificity for ABH blood group oligosaccharides and differentially recognizes sympatric Perkinsus species. *Biochemistry* 54, 4711–4730. doi: 10.1021/acs.biochem.5b00362

Feng, C., Ghosh, A., Amin, M. N., Giomarelli, B., Shridhar, S., Banerjee, A., et al. (2013). The galectin CvGal1 from the eastern oyster (*Crassostrea virginica*) binds to blood group A oligosaccharides on the hemocyte surface. *J. Biol. Chem.* 288, 24394–24409. doi: 10.1074/jbc.M113.476531

Fernández-Robledo, J. A., Schott, E. J., and Vasta, G. R. (2008). *Perkinsus marinus* superoxide dismutase 2 (PmSOD2) localizes to single-membrane subcellular compartments. *Biochem. Biophys. Res. Commun.* 375, 215–219. doi: 10.1016/j.bbrc.2008.07.162

Ford, S. E., Chintala, M. M., and Bushek, D. (2002). Comparison of *in vitro*-cultured and wild-type *Perkinsus marinus*. I. Pathogen virulence. *Dis. Aquat. Organ.* 51, 187–201. doi: 10.3354/dao051187

Gagneux, P., Aebi, M., and Varki, A. (2017). "Chapter 20. evolution of glycan diversity," in *Essentials of Glycobiology, 3rd Edn*, eds A. Varki, R. D. Cummings, J. D. Esko, P. Stanley, G. W. Hart, M. Aebi, et al. (New York, NY: Cold Spring Harbor Laboratory Press), 253–264.

Harvell, C. D., Kim, K., Burkholder, J. M., Colwell, R. R., Epstein, P. R., Grimes, D. J., et al. (1999). Emerging marine diseases–climate links and anthropogenic factors. *Science* 285, 1505–1510. doi: 10.1126/science.285.5433.1505

Hirabayashi, J., and Kasai, K. (1993). The family of metazoan metal-independent beta-galactoside binding lectins: structure, function and molecular evolution. *Glycobiology* 3, 297–304. doi: 10.1093/glycob/3.4.297

Hughes, R. C. (1999). Secretion of the galectin family of mammalian carbohydrate binding proteins. *Biochim. Biophys. Acta* 1473, 172–185. doi: 10.1016/S0304-4165(99)00177-4

Itoh, N., Xue, Q. G., Schey, K. L., Li, Y., Cooper, R. K., and La Peyre, J. F. (2011). Characterization of the major plasma protein of the eastern oyster, *Crassostrea virginica*, and a proposed role in host defense. *Comp. Biochem. Physiol.-B: Biochem. Mol. Biol.* 158, 9–22 doi: 10.1016/j.cbpb.2010.06.006

Janeway, C. A. Jr., and Medzhitov, R. (2002). Innate immune recognition. *Annu. Rev. Immunol.* 20:197–216. doi: 10.1146/annurev.immunol.20.083001.084359

Kennedy, V. S., Newell, R. I. E., and Eble, A. F. (1996). *The Eastern Oyster: Crassostrea virginica, 2nd Edn.* College Park, MD: University of Maryland Sea Grant Publications. 734.

Kurz, S., Jin, C., Hykollari, A., Gregorich, D., Giomarelli, B., Vasta, G. R., et al. (2013). Hemocytes and plasma of the eastern oyster (*Crassostrea virginica*) display a diverse repertoire of sulfated and blood group A-modified N-glycans. *J. Biol. Chem.* 288, 24410–24428. doi: 10.1074/jbc.M113.478933

Laine, R. A. (1997). "The information-storing potential of the sugar code," in *Glycosciences: Status and Perspectives*, eds H. -J. Gabius and S. Gabius (Weinheim: Chapman & Hill). 5–14.

Leffler, H., Carlsson, S., Hedlund, M., Qian, Y., and Poirier, F. (2004). Introduction to galectins. *Glycoconj J.* 19, 433–440. doi: 10.1023/B:GLYC.0000014072.34840.04

Liao, D. I., Kapadia, G., Ahmed, H., Vasta, G. R., and Herzberg, O. (1994). Structure of S-lectin, a developmentally regulated vertebrate beta-galactoside-binding protein. *Proc. Natl. Acad. Sci. U.S.A.* 91, 1428–1432. doi: 10.1073/pnas.91.4.1428

Lim, J., and Hotchin, N. A. (2012). Signalling mechanisms of the leukocyte integrin alphaMbeta2: current and future perspectives. *Biol. Cell* 104, 631–640 doi: 10.1111/boc.201200013

Lin, Z., Fernández-Robledo, J. A., Cellier, M. F., and Vasta, G. R. (2011). The natural resistance-associated macrophage protein from the protozoan parasite *Perkinsus marinus* mediates iron uptake. *Biochemistry* 50, 6340–6355. doi: 10.1021/bi200343h

Marionneau, S., Cailleau-Thomas, A., Rocher, J., Le Moullac-Vaidye, B., Ruvoën, N., Clément, M., et al. (2001). histo-blood group antigens, a model for the meaning of oligosaccharide diversity in the face of a changing world. *J. Biochimie.* 83, 565–573. doi: 10.1016/S0300-9084(01)01321-9

Mayadas, T. N., and Cullere, X. (2005). Neutrophil β2 integrins: moderators of life or death decisions. *Trends Immunol.* 26, 388–395. doi: 10.1016/j.it.2005.05.002

Perkins, F. O. (1996). The structure of *Perkinsus marinus* (Mackin, Owen and Collier, 1950) Levine, 1978 with comments on taxonomy and phylogeny of *Perkinsus* spp. *J Shellfish Res.* 15, 67–87.

Rabinovich, G. A., and Croci, D. O. (2012). Regulatory circuits mediated by lectin-glycan interactions in autoimmunity and cancer. *Immunity* 36, 322–335. doi: 10.1016/j.immuni.2012.03.004

Reece, K. S., Dungan, C. F., and Burreson, E. M. (2008). Molecular epizootiology of *Perkinsus marinus* and *P. chesapeaki* infections among wild oysters and clams in Chesapeake Bay, USA. *Dis. Aquat. Organ.* 82, 237–248. doi: 10.3354/dao01997

Robledo, J. A., Courville, P., Cellier, M. F., and Vasta, G. R. (2004). Gene organization and expression of the divalent cation transporter Nramp in the protistan parasite *Perkinsus marinus*. *J. Parasitol.* 90, 1004–1014. doi: 10.1645/GE-240R

Schott, E. J., Di Lella, S., Bachvaroff, T. R., Amzel, L. M., and Vasta, G. R. (2019). Lacking catalase, a protistan parasite draws on its photosynthetic ancestry to complete an antioxidant repertoire with ascorbate peroxidase. *BMC Evol. Biol.* 19:146. doi: 10.1186/s12862-019-1465-5

Schott, E. J., Pecher, W. T., Okafor, F., and Vasta, G. R. (2003b). The protistan parasite *Perkinsus marinus* is resistant to selected reactive oxygen species. *Exp. Parasitol.* 105, 232–240. doi: 10.1016/j.exppara.2003.12.012

Schott, E. J., Robledo, J. A. F., Wright, A. C., Silva, A. M., and Vasta, G. R. (2003a). Gene organization and homology modeling of two iron superoxide dismutases of the early branching protist *Perkinsus marinus*. *Gene* 309, 1–9. doi: 10.1016/S0378-1119(03)00469-4

Schott, E. J., and Vasta, G. R. (2003). The PmSOD1 gene of the protistan parasite *Perkinsus marinus* complements the sod2D mutant of *Saccharomyces cerevisiae*, and directs an iron superoxide dismutase to mitochondria. *Mol. Biochem. Parasitol.* 126, 81–92. doi: 10.1016/S0166-6851(02)00271-2

Shirai, T., Shionyu-Mitsuyama, C., Ogawa, T., and Muramoto, K. (2006). Structure based studies of the adaptive diversification process of congerins. *Mol. Divers* 10, 567–573. doi: 10.1007/s11030-006-9030-8

Stanley, P., and Cummings, R. D. (2017). "Chapter 14. Structures common to different glycans," in *Essentials of Glycobiology, 3rd Edn*, eds A. Varki, R. D. Cummings, J. D. Esko, P. Stanley, G. W. Hart, M. Aebi, et al. (New York, NY: Cold Spring Harbor Laboratory Press), 161–178.

Stowell, S. R., Arthur, C. M., Dias-Baruffi, M., Rodrigues, L. C., Gourdine, J. P., Heimburg-Molinaro, J., et al. (2010). Innate immune lectins kill bacteria expressing blood group antigen. *Nat. Med.* 16, 295–301. doi: 10.1038/nm.2103

Stowell, S. R., Arthur, C. M., Mehta, P., Slanina, K. A., Blixt, O., Leffler, H., et al. (2008a). Galectin-1,−2, and−3 exhibit differential recognition of sialylated glycans and blood group antigens. *J. Biol. Chem.* 283, 10109–10123. doi: 10.1074/jbc.M709545200

Stowell, S. R., Arthur, C. M., Slanina, K. A., Horton, J. R., Smith, D. F., and Cummings, R. D. (2008b). Dimeric Galectin-8 induces phosphatidylserine exposure in leukocytes through polylactosamine recognition by the C-terminal domain. *J. Biol. Chem.* 283, 20547–20559. doi: 10.1074/jbc.M802495200

Tasumi, S., and Vasta, G. R. (2007). A galectin of unique domain organization from hemocytes of the Eastern oyster (*Crassostrea virginica*) is a receptor for the protistan parasite *Perkinsus marinus*. *J. Immunol.* 179, 3086–3098. doi: 10.4049/jimmunol.179.5.3086

Terahara, K., Takahashi, K. G., Nakamura, A., Osada, M., Yoda, M., Hiroi, T., et al. (2006). Differences in integrin-dependent phagocytosis among three hemocyte subpopulations of the Pacific oyster "*Crassostrea gigas*." *Dev. Comp. Immunol.* 30, 667–683. doi: 10.1016/j.dci.2005.09.009

van den Berg, T. K., Honing, H., Franke, N., van Remoortere, A., Schiphorst, W. E., Liu, F. T., et al. (2004). LacdiNAc-glycans constitute a parasite pattern for galectin-3-mediated immune recognition. *J. Immunol.* 173, 1902–1907. doi: 10.4049/jimmunol.173.3.1902

Vasta, G. R. (2009). Roles of galectins in infection. *Nat. Rev. Microbiol.* 7, 424–438. doi: 10.1038/nrmicro2146

Vasta, G. R., and Ahmed, H. (2008). "Animals lectins: a functional view," in *Animals Lectins: A Functional View*, eds G. R. Vasta and H. Ahmed (Boca Raton, FL: CRC Press), 538.

Vasta, G. R., Ahmed, H., Du, S., and Henrikson, D. (2004b). Galectins in teleost fish: Zebrafish (*Danio rerio*) as a model species to address their biological roles in development and innate immunity. *Glycoconj J.* 21, 503–521. doi: 10.1007/s10719-004-5541-7

Vasta, G. R., Ahmed, H., Nita-Lazar, M., Banerjee, A., Pasek, M., Shridhar, S., et al. (2012). Galectins as self/non-self recognition receptors in innate and adaptive immunity: an unresolved paradox. *Front. Immunol.* 3:199. doi: 10.3389/fimmu.2012.00199

Vasta, G. R., Ahmed, H., and Odom, E. W. (2004a). Structural and functional diversity of lectin repertoires in invertebrates, protochordates and ectothermic vertebrates. *Curr. Opin. Struct. Biol.* 14, 617–630. doi: 10.1016/j.sbi.2004.09.008

Vasta, G. R., Ahmed, H., Tasumi, S., Odom, E. W., and Saito, K. (2007). Biological roles of lectins in innate immunity: molecular and structural basis for diversity in self/non-self recognition. *Adv. Exp. Med. Biol.* 598, 389–406. doi: 10.1007/978-0-387-71767-8_27

Vasta, G. R., Cheng, T. C., and Marchalonis, J. J. (1984). A lectin on the hemocyte membrane of the oyster (*Crassostrea virginica*). *Cell. Immunol.* 88, 475–488. doi: 10.1016/0008-8749(84)90179-5

Vasta, G. R., Feng, C., Bianchet, M. A., Bachvaroff, T. R., and Tasumi, S. (2015). Structural, functional, and evolutionary aspects of galectins in aquatic mollusks: From a sweet tooth to the Trojan horse. *Fish Shellfish Immunol.* 46, 94–106. doi: 10.1016/j.fsi.2015.05.012

Vasta, G. R., Nita-Lazar, M., Giomarelli, B., Ahmed, H., Du, S., Cammarata, M., et al. (2011). Structural and functional diversity of the lectin repertoire in teleost fish: relevance to innate and adaptive immunity. *Dev. Comp. Immunol.* 35, 1388–1399. doi: 10.1016/j.dci.2011.08.011

Vasta, G. R., Sullivan, J. T., Cheng, T. C., Marchalonis, J. J., and Warr, G. W. (1982). A cell membrane-associated lectin of the oyster hemocyte. *J. Invertebr. Pathol.* 40, 367–377. doi: 10.1016/0022-2011(82)90175-6

Walser, P. J., Haebel, P. W., Kunzler, M., Sargent, D., Kues, U., Aebi, M., et al. (2004). Structure and functional analysis of the fungal galectin CGL2. *Structure* 12, 689–702. doi: 10.1016/j.str.2004.03.002

Wang, X. W., and Wang, J. X. (2013). Pattern recognition receptors acting in innate immune system of shrimp against pathogen infections. *Fish Shellfish Immunol.* 34, 981–989. doi: 10.1016/j.fsi.2012.08.008

Wright, A. C., Ahmed, H., Gauthier, J. D., Silva, A. M., and Vasta, G. R. (2002). cDNA cloning and characterization of two iron superoxide dismutases from the oyster parasite *Perkinsus marinus*. *Mol. Biochem. Parasitol.* 123, 73–77. doi: 10.1016/S0166-6851(02)00090-7

Zhang, G., Fang, X., Guo, X., Li, L., Luo, R., Xu, F., et al. (2012). The oyster genome reveals stress adaptation and complexity of shell formation. *Nature* 490, 49–54. doi: 10.1038/nature11413

Zhuo, Y., Chammas, R., and Bellis, S. L. (2008). Sialylation of beta1 integrins blocks cell adhesion to galectin-3 and protects cells against galectin-3-induced apoptosis. *J. Biol. Chem.* 283, 22177–22185. doi: 10.1074/jbc.M800015200

Conflict of Interest: The authors declare that the research was conducted in the absence of any commercial or financial relationships that could be construed as a potential conflict of interest.

frontiers in Chemistry

ORIGINAL RESEARCH
published: 28 February 2020
doi: 10.3389/fchem.2020.00138

A Matrix-Assisted Laser Desorption/Ionization—Mass Spectrometry Assay for the Relative Quantitation of Antennary Fucosylated *N*-Glycans in Human Plasma

*Osmond D. Rebello[1,2], Simone Nicolardi[1], Guinevere S. M. Lageveen-Kammeijer[1], Jan Nouta[1], Richard A. Gardner[2], Wilma E. Mesker[3], Rob A. E. M. Tollenaar[3], Daniel I. R. Spencer[2], Manfred Wuhrer[1] and David Falck[1]**

[1] Center for Proteomics and Metabolomics, Leiden University Medical Center, Leiden, Netherlands, [2] Ludger Ltd, Culham Science Centre, Abingdon, United Kingdom, [3] Department of Surgery, Leiden University Medical Center, Leiden, Netherlands

Changes in the abundance of antennary fucosylated glycans in human total plasma *N*-glycome (TPNG) have been associated with several diseases ranging from diabetes to various forms of cancer. However, it is challenging to address this important part of the human glycome. Most commonly, time-consuming chromatographic separations are performed to differentially quantify core and antenna fucosylation. Obtaining sufficient resolution for larger, more complex glycans can be challenging. We introduce a matrix-assisted laser desorption/ionization—mass spectrometry (MALDI-MS) assay for the relative quantitation of antennary fucosylation in TPNG. *N*-linked glycans are released from plasma by PNGase F and further treated with a core fucosidase before performing a linkage-informative sialic acid derivatization. The core fucosylated glycans are thus depleted while the remaining antennary fucosylated glycans are quantitated. Simultaneous quantitation of α2,3-linked sialic acids and antennary fucosylation allows an estimation of the sialyl-Lewis x motif. The approach is feasible using either ultrahigh-resolution Fourier-transform ion cyclotron resonance mass spectrometry or time-of-flight mass spectrometry. The assay was used to investigate changes of antennary fucosylation as clinically relevant marker in 14 colorectal cancer patients. In accordance with a previous report, we found elevated levels of antennary fucosylation pre-surgery which decreased after tumor resection. The assay has the potential for revealing antennary fucosylation signatures in various conditions including diabetes and different types of cancer.

Keywords: antennary fucose, glycomics, sialyl-Lewis x, MALDI-MS, FT-ICR-MS, CE-MS, colorectal cancer, exoglycosidase

OPEN ACCESS

Edited by:
Karina Valeria Mariño, Institute of Biology and Experimental Medicine (IBYME), Argentina

Reviewed by:
Jeongkwon Kim, Chungnam National University, South Korea
Xin Liu, Huazhong University of Science and Technology, China
Ganglong Yang, Jiangnan University, China

***Correspondence:**
David Falck
d.falck@lumc.nl

Specialty section:
This article was submitted to Chemical Biology, a section of the journal Frontiers in Chemistry

Received: *14 October 2019*
Accepted: *14 February 2020*
Published: *28 February 2020*

Citation:
Rebello OD, Nicolardi S, Lageveen-Kammeijer GSM, Nouta J, Gardner RA, Mesker WE, Tollenaar RAEM, Spencer DIR, Wuhrer M and Falck D (2020) A Matrix-Assisted Laser Desorption/Ionization—Mass Spectrometry Assay for the Relative Quantitation of Antennary Fucosylated N-Glycans in Human Plasma. Front. Chem. 8:138. doi: 10.3389/fchem.2020.00138

INTRODUCTION

Changes in the relative abundance of either core or antennary fucosylation have been associated with certain diseases or disease states (Blomme et al., 2009; Testa et al., 2015). Here, we focus on antennary fucosylation in human total plasma *N*-glycome (TPNG) as a clinically relevant disease marker. For instance, the abundance of antennary fucosylation in TPNG has been correlated with (1) certain cancers such as hepatocellular carcinoma (Benicky et al., 2014; Zhu et al., 2014), ovarian cancer (Saldova et al., 2007) and colorectal cancer (Holst et al., 2016; de Vroome et al., 2018; Doherty et al., 2018); (2) hepatocyte nuclear factor 1 homeobox A—maturity-onset diabetes of the young (HNF1A—MODY) (Thanabalasingham et al., 2013; Juszczak et al., 2019); (3) inflammatory conditions (Brinkman-van der Linden et al., 1998; Higai et al., 2005) and (4) with attention-deficit hyperactivity disorder in children (Pivac et al., 2011). These correlations have created a need for the development of assays for quantitation of antennary fucosylation in TPNG. Quantitation of changes in core fucosylated glycans will remain relevant as well, but can better covered by existing approaches.

The quantitation of antennary fucosylation in TPNG was also used for more specialized clinical purposes such as for prognosis or for differentiating between closely related diseases. For example, a lowered incidence of antennary fucosylation on triantennary glycans was shown to discriminate HNF1A-MODY patients from Type 1 and Type 2 diabetes (Thanabalasingham et al., 2013). Current genetic tests for diagnosing HNF1A-MODY are sometimes inconclusive, and there is a demand for additional diagnostic markers (Schober et al., 2009; Thanabalasingham and Owen, 2011; Hattersley and Patel, 2017). Plasma *N*-glycome antennary fucosylation has been reported to be regulated by HNF1A making it a proxy of HNF1A expression levels and functions (Lauc et al., 2010). Hence, quantitation of antennary fucosylation in TPNG has been found to be an HNF1A-MODY disease biomarker with potential for complementing genetic tests in disease diagnosis (Lauc et al., 2010; Thanabalasingham et al., 2013). For colorectal cancer, both better diagnosis and prediction of long-term survival are urgent clinical needs. Currently, long-term survival predictions are mostly based on tumor node metastasis classification which has low success rates (Cserni, 2003; de Vroome et al., 2018). This negatively affects the decision making on therapy given to the patients. Antennary fucosylation was shown to be associated with the recovery of colorectal cancer patients after tumor resection (de Vroome et al., 2018), and thus may have the potential for long-term survival prediction.

TPNG is a rich and convenient source of valuable associations with diseases and disease states. It reflects the loss of systemic or cellular homeostasis which may affect the regulation of glycosylation pathways (Nairn et al., 2008; Blomme et al., 2009; Lauc et al., 2010). Enabling a bird's-eye view, TPNG analysis is highly complementary to the target analysis of specific proteins. Quantitation of low abundant antennary fucosylated glycans in human TPNG is complicated by the structural diversity of its component glycans. This diversity is a combination of monosaccharide composition variants and linkage isomers (Royle et al., 2008; Stumpo and Reinhold, 2010).

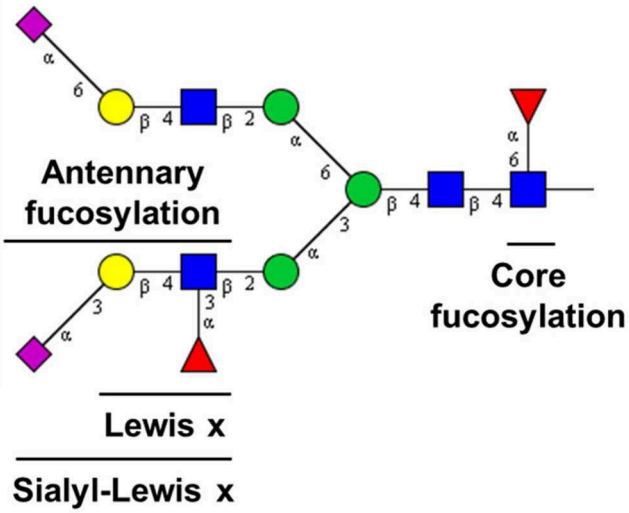

FIGURE 1 | Fucose epitopes on *N*-glycans in human plasma. [Blue square: *N*-acetylglucosamine, green circle: mannose, yellow circle: galactose, red triangle: fucose, pink diamond: *N*-acetylneuraminic acid (+45° α2,6-linked; −45° α2,3-linked). For compositions see **Figure 6**].

Composed of diantennary, triantennary and tetraantennary *N*-glycans, TPNG also features bisecting *N*-acetylglucosamine and glycans with *N*-acetyllactosamine repeats, and complexity is added by different levels of galactosylation, sialylation and fucosylation (Stumpo and Reinhold, 2010; Vreeker et al., 2018; Lageveen-Kammeijer et al., 2019). Fucosylation can be classified as either core or antennary (**Figure 1**). Core fucosylation is linked by an α(1-6) glycosidic bond to the reducing end *N*-acetylglucosamine. Antennary fucosylation in TPNG mainly features fucose residues that are linked by an α(1-3) glycosidic bond (Lewis x epitope) to antennary *N*-acetylglucosamine residues (Staudacher et al., 1999).

Methods for sample preparation and analysis of human TPNG have been developed on a number of analytical platforms. This includes liquid chromatography (LC)—fluorescence detection (FLD) (Royle et al., 2008; Knezevic et al., 2011; Pivac et al., 2011; Doherty et al., 2018), MALDI-MS (Reiding et al., 2014; Bladergroen et al., 2015; Vreeker et al., 2018), and capillary gel electrophoresis—laser-induced fluorescence (Ruhaak et al., 2010; Vanderschaeghe et al., 2010). Each method has its advantages and disadvantages when it comes to measuring antennary fucosylation. Capillary gel electrophoresis—laser-induced fluorescence (Vanderschaeghe et al., 2010) and LC-FLD (Pivac et al., 2011; Doherty et al., 2018) are able to resolve some antennary fucosylated glycans in TPNG along their chromatographic dimension. However, LC-FLD often requires extensive measurement time. Nonetheless, due to its high precision and robustness, one of the most attractive techniques for routine applications is LC-FLD. MALDI-MS is gaining popularity in biomarker analysis since it features short measurement time and high molecular resolution. This, combined with linkage-informative sialic acid

derivatization, is the ideal basis for an high throughput TPNG glycomic assay in a research setting (Reiding et al., 2014; Bladergroen et al., 2015; Vreeker et al., 2018). However, due to identical mass, the differentiation between core fucosylation and antennary fucosylation in monofucosylated glycans of the same composition is not achieved by MALDI-MS. Therefore, additional experiments are needed such as tandem mass spectrometry (Chen and Flynn, 2007; Wuhrer et al., 2011; Lattova et al., 2019) or exoglycosidase treatment (Royle et al., 2008). Unfortunately, relative quantitation of fucose isomers by tandem MS is hindered by the vastly different efficiencies of the fragmentation pathways (Banazadeh et al., 2019; Lattova et al., 2019). Additionally, potential fucose rearrangement influences the ratios of diagnostic fragment ion(s), further interfering with the assessment of mixtures by tandem MS (Harvey et al., 2002; Chen and Flynn, 2007; Wuhrer et al., 2011). Alternatively, endoglycosidases can be used for glycomic assays (Benicky et al., 2014; Vanderschaeghe et al., 2018). For example, a combination of Endo F2 and Endo F3 has been used to quantify antennary fucosylation on diantennary and triantennary glycans on hemopexin and complement factor H in patients suffering from liver diseases (Benicky et al., 2014). However, until now, this approach has not been demonstrated on TPNG. Due to the narrow specificity of these endoglycosidases in contrast to the vast structural diversity of TPNG, such an approach may not be suitable for TPNG.

We developed an assay for the relative quantitation of antennary fucosylation in human TPNG by combining MALDI-MS and exoglycosidase approaches. It can be viewed as complementing the existing approach for TPNG measurement by MALDI-MS. The assay was applied to 14 colorectal cancer patient samples. Consistent antennary fucosylation changes pre vs. post tumor resection were detected which revealed the assays potential for addressing biomedical research questions.

MATERIALS AND METHODS

Reagents and Samples

Disodium hydrogen phosphate dihydrate, potassium dihydrogen phosphate, sodium chloride, 85% phosphoric acid, 30–33% (*v/v%*) ammonium hydroxide, nonidet P-40 substitute (NP-40), 1-hydroxybenzotriazole 97% (HOBt), ammonium acetate and super-DHB (9:1 mixture of 2,5-dihydroxybenzoic acid and 2-hydroxy-5-methoxybenzoic acid) were purchased from Sigma Aldrich Chemie GmbH (Steinheim, Germany). 1-Ethyl-3-[3-(dimethylamino)-propyl]carbodiimide hydrochloride (EDC) was purchased from Fluorochem (Hadfield, UK). Analytical grade ethanol, analytical grade glacial acetic acid, sodium dodecyl sulfate (SDS), trifluoroacetic acid, and potassium hydroxide were purchased from Merck KGaA (Darmstadt, Germany). HPLC-grade acetonitrile was purchased from Biosolve (Valkenswaard, The Netherlands). Girard's Reagent P (GiRP) was purchased from TCI Development Co. Ltd. (Tokyo, Japan). 5× phosphate buffered saline solution (PBS; 175 mM; pH 7.3) was prepared by dissolving 285 g of disodium hydrogen phosphate dihydrate, 23.8 g of potassium dihydrogen phosphate and 425 g of sodium chloride in 10 L deionized water. The 5× acidic PBS was prepared by adding 68 μL of 85% phosphoric acid (14.7 M) to 9.93 mL of the 5× PBS. Recombinant Peptide *N*-glycosidase F (PNGase F) was obtained from Roche Diagnostics (Mannheim, Germany). The recombinant core fucosidase, commercially known as α1-2,4,6 Fucosidase O, was purchased from New England BioLabs (MA, USA). However, activity on the α1,4-linkage is reported as very low. Under the employed conditions, the enzyme did not noticeably act on antennary fucoses present in TPNG (see section *Result and Discussion*). Peptide Calibration Standard II was purchased from Bruker Daltonic (Bremen, Germany).

Human plasma standard (Visucon-F frozen normal control plasma, pooled from a minimum of 20 human donors, citrated and buffered in 0.02 M 4-(2-hydroxyethyl)-1-piperazineethanesulfonic acid) was purchased from Affinity Biologicals (Ancaster, Ontario, Canada).

The pre-operative vs. 45 days post-operative pairs of 14 colorectal cancer patient samples were collected as part of a biobank as was previously described (de Vroome et al., 2018). These serum samples were collected between October 2002 and March 2013 by the Leiden University Medical Center Surgical Oncology Biobank. This study was approved by the Medical Ethics Committee of the Leiden University Medical Center and was performed in accordance with the Code of Conduct of the Federation of Medical Scientific Societies in the Netherlands (http://www.federa.org/).

N-Glycan Release

PNGase F release of human TPNG was performed similarly as previously described (Vreeker et al., 2018). Briefly, 4 μL of plasma was added to 8 μL of 2% SDS in a polypropylene 96 well V-bottom plate (V-96 microwell, NUNC, Roskilde, Denmark). The plate was sealed (adhesive plate seals, Thermo Scientific, UK) and mildly shaken on a plate shaker for 5 min, before incubating at 60°C for 10 min. Additionally, 8 μL of the PNGase F releasing mixture (4 μL of 4% NP-40 solution, 4 μL of 5× acidic PBS and 0.4 μL of PNGase F) was then added to the plasma samples. The plate was sealed and mildly shaken on a plate shaker for 5 min before incubating overnight (15–18 h) at 37°C.

Depletion of Core Fucosylation

The overnight incubated plasma release mixture (5 μL) was diluted with 45 μL of 1× acidic PBS solution in a 96 well V-bottom plate (V-96 microwell, Grenier Bio-one, Germany). The plate was mildly shaken on a plate shaker for 5 min, before transferring 1–2 μL of core fucosidase mixture (0.65 μL deionized water, 0.75 μL of 4% NP-40 solution, 0.4 μL of 5× acidic PBS and 0.2 μL/0.4 Units of core fucosidase) in a 96 well V-bottom plate. After sealing of the plate, the samples were incubated overnight (15–18 h) at 37°C in an enclosed, humidified chamber to prevent evaporation.

Linkage Specific Sialic Acid Derivatization

Sialic acid derivatization was performed as previously described (Lageveen-Kammeijer et al., 2019), but with minor alterations. With this approach, the carboxylic acid groups of α(2,6)-linked sialic acids are ethyl esterified while the α(2,3)-linked sialic acids are amidated. Briefly, 60 μL of ethyl esterification reagent

(solution of 0.25 M EDC and 0.25 M HOBt in ethanol) was added to the core defucosylated samples. The plate was sealed and incubated at 37°C for 30 min. Twelve microliters of 30–33% (*v/v%*) NH_4OH solution were added to the wells and the sealed plate incubated for another 30 min at 37°C. Seventy-two microliters of acetonitrile was added to the wells, after which cotton hydrophilic interaction liquid chromatography (HILIC)—solid-phase extraction (SPE) microtip purification was performed immediately.

Cotton Hydrophilic Interaction Liquid Chromatography—Solid-Phase Extraction Microtip Purification

This purification step was performed as previously described (Selman et al., 2011) with minor modifications. The cotton HILIC-SPE microtips were prepared by inserting a cotton strand of length 3–4 mm into a 20 μL capacity microtip (Mettier-Toledo, Switzerland) and pushing it into place with a stream of pressurized air/nitrogen. Conditioning was performed by pipetting 5 times 20 μL of water, followed by an equilibration step of pipetting 3 times 20 μL of 85% acetonitrile. The derivatized samples were loaded onto the HILIC-SPE by pipetting 20 μL of it 20 times. Washing was performed with 3 times 20 μL of 85% acetonitrile containing 1% trifluoroacetic acid and 3 times 20 μL of 85% acetonitrile, consecutively. The glycans were eluted from the HILIC-SPE by repeatedly, 10 times, pipetting 4 μL of deionized water in a 96 well V-bottom plate (V-96 microwell, Grenier Bio-one, Germany). All steps were performed with a 12 channel multi-channel pipette.

Purified glycan samples (1 μL) were spotted on an MTP anchor chip 600/384 TF MALDI target plate (Bruker Daltonics, Bremen, Germany), followed by the addition of 1 μL of the MALDI matrix solution (50% acetonitrile solution of 2.5 mg/mL super-DHB and 0.1 mM sodium hydroxide). The solutions were mixed on the plate with a pipette. The spotted samples were allowed to air dry before performing MALDI- time-of-flight -MS (MALDI-TOF-MS) or MALDI- Fourier-transform ion cyclotron resonance -MS (MALDI-FT-ICR-MS) measurements.

MALDI-TOF-MS Analysis

The analysis was performed on an UltrafleXtreme Mass spectrometer in reflectron positive ion mode (Bruker Daltonics, Bremen, Germany) which was operated by FlexControl version 3.4 (Build 135). A Bruker Smartbeam-II laser was used for ionization at an irradiation frequency of 1 kHz using the "small" predefined laser shot pattern. Each sample spot was irradiated by 20,000 shots with 200 shots at each laser raster. Irradiation was performed randomly over the complete sample spot. Spectra were recorded within an *m/z* range of 900–5,000. Samples were measured in an automated manner using the AutoXecute function of FlexControl. Before each measurement, the instrument was calibrated with a peptide standard mix (Peptide Calibration Standard II, Bruker Daltonics).

MALDI-FT-ICR-MS Analysis

The analysis was performed in positive ion mode on a Bruker 15T solariX XR FT-ICR mass spectrometer equipped with a CombiSource and a ParaCell (Bruker Daltonics). The system was operated by ftmsControl version 2.2.0 (Build 150). A Bruker Smartbeam- II laser was used for ionization at an irradiation frequency of 500 Hz using the "medium" predefined laser shot pattern. Each sample spot was irradiated with a raster of 200 laser shots. Ten such scans were performed randomly over the complete sample spot. Spectra were acquired within an *m/z*-range 1,011–5,000 with 1 million data points (transient time 2.3069 s). Samples were measured in an automated manner using the AutoXecute function of ftmsControl.

Processing of MALDI-MS Data

The MALDI-TOF-MS spectra were internally calibrated using FlexAnalysis version 3.4 (Build 76; Bruker Daltonic). The glycan calibrants used were $[H3N4 + Na]^+$ of *m/z* 1,339.476, $[H5N4 + Na]^+$ of *m/z* 1,663.581, $[H5N4E1 + Na]^+$ of *m/z* 1,982.708, $[H5N4E2 + Na]^+$ of *m/z* 2,301.835, $[H5N5E2 + Na]^+$ of *m/z* 2,504.914, $[H6N5E2Am1 + Na]^+$ of *m/z* 2,957.078 and $[H7N6E2Am2 + Na]^+$ of *m/z* 3,612.322. The.xy files generated by Flexanalysis were further processed with Massy Tools (Jansen et al., 2015). A second round of internal spectral calibration was performed with at least four calibrants in the low *m/z* range and at least three calibrants in the medium *m/z* range, having to pass signal to noise ratio (S/N) at least above 15. The *m/z* window for calibration, peak detection, and spectral data integration was taken at ± 0.45 Th. The background detection windows were set to 20 Th.

The MALDI-FT-ICR-MS spectra were acquired in serial mode. Thus, a single combined file was generated. This file was split into individual compound spectra and transformed into.xy files using DataAnalysis version 5 (Bruker Daltonics). Calibration of these spectra was performed in Massy Tools, for which at least four calibrants in the low *m/z* range and at least three calibrants in the medium *m/z* range, have to pass S/N at least above 50. The *m/z* window for calibration was taken at ± 0.10 Th. Peak detection and spectral data integration was performed using an extraction window depending on the defined glycans in the analyte list. This was done so as to exclude interferences in the spectra. The background detection windows were set at the value of 20 Th.

The calibrant list and analyte list for MALDI-TOF-MS spectra and MALDI-FT-ICR-MS spectra are shown in **Supplementary Tables S1, S2**, respectively. The table of all identified and quantitated glycans by MALDI-FT-ICR-MS and MALDI-TOF-MS, respectively, are shown in **Supplementary Table S3**. At least 85% of the theoretical isotopic distribution of each glycan analyte was integrated. The Massy tools output was used further for analyte curation, which was based on multiple criteria. These were S/N ≥ 9, isotopic pattern quality ≤ 0.25 and mass accuracy between ± 20 ppm (MALDI-TOF-MS) or ± 10 ppm (MALDI-FT-ICR-MS). Spectra for which the number of glycan analytes passing these criteria were <50% of the total number of defined glycans in the analyte list, were not considered for further processing as these spectra were deemed of low quality. The absolute area of the curated glycans was corrected to 100% of their respective isotopic distribution, before using them in total area normalization.

Derived traits, focusing on features rather than individual glycans, were calculated from the relative areas of the glycan compositions using an in-house prepared R script (**Supplementary Table S4**). Statistical significance of the differences between pre-operative vs. post-operative colorectal cancer patient samples was assessed by a Wilcoxon matched-pairs signed-rank test with $\alpha = 0.05$. Multiple-testing correction was performed using a false discovery rate of 1% calculated with the Benjamini and Hochberg method. These statistical tests were performed in GraphPad Prism version 8.0.1. The box and whisker plots used for representing the features were made by an in-house prepared R script.

Method Optimization and Assay Performance

All optimization experiments of the assay were measured on the MALDI-TOF-MS (**Supplementary Material** "*Assay optimization*"). Data processing for these mentioned optimization experiments was done using the mass list of the negative control (fucosidase untreated TPNG) (**Supplementary Table S2**). Quantitation of residual core fucosylated glycans allowed the assessment of the completeness of the core defucosylation. Importantly, all identified antennary fucosylated glycans were also included in the mass list of the negative control (fucosidase untreated TPNG).

The intermediate precision of the antennary fucose assay for combined sample preparation and measurements on the MALDI-TOF-MS or MALDI-FT-ICR-MS were performed in three independent experiments on three different days within a period of 5 days. For each of these experiments, the assay was performed with nine replicates of glycan releases from a human plasma pool (Visucon-F, Affinity Biologicals). Data processing was performed as mentioned in the subsection "*Processing of MALDI-TOF-MS/MALDI-FT-ICR-MS data*".

Capillary Electrophoresis—Electrospray Ionization—Mass Spectrometry

Identification of core fucosylated glycans, antennary fucosylated glycans, and composition containing both isomers was done by comparing the MALDI-FT-ICR-MS spectra from the assay (core fucosidase treated) to the negative control (fucosidase untreated). The identified antennary fucosylated glycans and mixed fucosylated isomeric glycans were structurally confirmed by targeted collision induced dissociation (CID) fragmentation on a capillary electrophoresis—electrospray ionization–tandem MS (CE-ESI-MS/MS) platform. The samples were performed in 12 replicates of which nine were used for MALDI-FT-ICR-MS measurements while the remaining three were used for CE-ESI-MS/MS measurements ($n = 3$).

For the CE-ESI-MS/MS measurement, the replicates from the assay and the negative controls were, respectively, pooled together and dried down in a vacuumed centrifuge (Salm en Kipp, Breukelen, Netherlands) at 50°C. They were used for permanent cationic labeling with GiRP as previously described (Lageveen-Kammeijer et al., 2019) but with certain alterations. Briefly, 10 μL of GiRP labeling solution (7.5 mg GiRP dissolved in a solution of 720 μL ethanol and 80 μL glacial acetic acid) was added to the dried samples. The plate was sealed and mildly shaken on a plate shaker for 5 min before incubating at 60°C for 1 h. After incubation, the samples were dried down in a vacuumed centrifuge at 50°C and then re-suspended in 5 μL of deionized water. In total, 3.6 μL of the GiRP labeled glycans were mixed with 2.4 μL of 250 mM ammonium acetate solution as leading electrolytes (250 mM ammonium acetate solution adjusted to pH 4 with glacial acetic acid) before being transferred into a vial (nanoVial, Sciex, Framingham, USA).

All CE-ESI-MS/MS analyses were performed on a static coated neutral capillary cartridge (Neutral OptiMS cartridge, Sciex), fitted into a CESI 8000 system (Sciex). The CE system was coupled with an Impact HD UHR-QTOF-MS system (Bruker Daltonics). When the capillary was not in use, a continuous flow of water at 10 psi was applied to the separation line. Prior to usage, the separation line and reverse line were filled with the background electrolyte containing 10% acetic acid (sonicated in a water bath for 10 min). Prior to sample injection, the separation line was flushed with 0.1 M HCl at a pressure of 100 psi for 5 min. This was followed by flushing the reverse line with background electrolyte at 75 psi for 3 min. The separation line was filled with background electrolyte by applying a pressure of 100 psi for 10 min. The sample was injected into the separation line of the capillary from the nanovials via a hydrodynamic injection of 12.5 psi for 24 s (about 5% of the capillary volume). The tip of the separation line was washed by momentary dipping it into a vial of background electrolyte, followed by injecting a background electrolyte plug with a pressure of 2.5 psi for 15 s. A 20 kV voltage of normal polarity (cathode toward the end of the capillary) was applied on the capillary for 30 min. During this step, a continuous flow of 2 psi was applied only on the reverse line. After 30 min, a flow of background electrolyte is applied to both the separation line and reverse line by applying a pressure of 2 psi on both lines for 40 min. Finally, the voltage on the capillary was ramped down over 5 min to 1 kV before termination of the run. The capillary was maintained at 30°C throughout the analysis.

For the MS analysis, a dopant enriched nitrogen gas (acetonitrile as dopant) at 0.2 bar was used for nebulization at the ESI captive sprayer. The drying gas of nitrogen at 150°C was introduced at the source at 1.2 L/min and the internal capillary of the MS was maintained at 1,200 V. A targeted CID fragmentation was performed on 20 glycan analytes of interested. This list was divided into two inclusion lists on the software otof control version 3.4 (Build 14; Bruker Daltonics) which was used for operating the MS and MS/MS analysis. Hence each sample was measured twice in-order to fragment all the glycan analytes of interest. The MS/MS fragmentation spectra were collected at a rate of 1 Hz within an *m/z*-range of 150–2,000 and at an absolute intensity threshold at 2,274 on the *m/z* values of interest. The targeted precursor ions were isolated with a width of 8–15 Th depending on the *m/z* values. The collision energies of the CID cell was set in an *m/z* dependent manner, ranging from 35 eV for singly charged precursor ions of *m/z* 500 to 70 eV for singly charged precursor ions at *m/z* 2,000. Data analysis was done using DataAnalysis version 5 (Bruker Daltonics).

Hydrophilic Interaction Liquid Chromatography Analysis

PNGase F released *N*-glycans from 12 replicates of human plasma samples (Visucon-F) were used for procainamide labeling and analysis on a HILIC-FLD-MS^n platform as previously described (Kozak et al., 2015). Following PNGase F treatment, 8 μL of each sample was dried down and the released *N*-glycans converted to aldoses with 0.1% formic acid, filtered through a protein binding plate (LC-PBM-96, Ludger, Oxford, UK), washed twice with 100 μL of water and dried. *N*-glycans were labeled by reductive amination in 10 μL of water and 10 μL procainamide labeling solution (LT-KPROC-24 containing $NaCNBH_3$, Ludger) and incubated at 65°C for 1 h. A HILIC-type clean-up plate (LC-PROC-96, Ludger) was used to remove unreacted procainamide dye. Procainamide labeled *N*-glycans were eluted in 300 μL of water. The samples were dried and resuspended in water (50 μL) for further analysis.

Procainamide-labeled samples were analyzed by HILIC-FLD-MS^n. 12.5 μL of each sample was injected into an ACQUITY BEH Glycan column (1.7 μm, 2.1 × 150 mm) at 40°C on a Dionex Ultimate 3000 UHPLC instrument with a fluorescence detector (ex = 310 nm and em = 370 nm attached to an Amazon Speed ETD (Bruker Daltonics). The running conditions used were as follows: solvent A was 50 mM ammonium formate (pH 4.4) (LS-NBUFFX40, Ludger), and solvent B was acetonitrile.

Gradient conditions were as follows: 0–53.5 min, 76–51% B, 0.4 mL/min; 53.5–55.5 min, 51–0% B, 0.4–0.2 mL/min; 55.5–57.5 min, 0% B at a flow rate of 0.2 mL/min; 57.5–59.5 min, 0–76% B, 0.2 mL/min; 59.5–65.5 min, 76% B, 0.2 mL/min; 65.5–66.5 min, 76% B, 0.2–0.4 mL/min; 66.5–70.0 min, 76% B, 0.4 mL/min. The Amazon Speed settings used were as follows: source temperature, 250°C; gas flow, 10 L/min; capillary voltage, 4,500 V; ICC target, 200,000; Max. accu. time (Maximum Accumulation Time), 50.00 ms; rolling average, 2; number of precursor ions selected, 3; release after 0.2 min; positive ion mode; scan mode, enhanced resolution; mass range scanned, 400–1,500; target mass, 900.

RESULTS AND DISCUSSIONS

The workflow for the antennary fucose assay is shown in **Figure 2**. Released *N*-glycans from human plasma were treated with an α1,6-linkage-selective fucosidase (core fucosidase) to deplete core fucosylation. Antennary fucosylation remained and was relatively quantified by MALDI-FT-ICR-MS or MALDI-TOF-MS. Information on sialic linkage is obtained in parallel, potentially improving the estimation of sialyl-Lewis x abundance. An overview of all analytical methods used during the development of the assay is shown in **Supplementary Figure S1**.

Human TPNG was 28.3% ± 0.5% fucosylated. Most of this is core fucosylation (**Supplementary Table S5**). Hence, it was important to optimize the assay with a focus on a robust and complete depletion of core fucosylation of TPNG. This aids a robust relative quantitation of the remaining antennary fucosylated glycans by MALDI-MS. The efficient use of costly reagents, specifically the core fucosidase, was also addressed. During the optimization steps, completeness of core defucosylation was judged by the inability to quantify by MALDI-MS (signal to noise ratio (S/N) < 9) some of the most abundant core fucosylated glycans namely $[H3N4F1 + Na]^+$ of *m/z* 1,485.53 and $[H4N4F1 + Na]^+$ of *m/z* 1,647.59 (**Supplementary Figure S4**). Details pertaining to assay optimization are described in the **Supplementary Material** section "*Assay optimization*." For these optimized assay conditions, a complete core defucosylation of TPNG could already be achieved with 0.2 units of core fucosidase (**Figure 3**). However, to facilitate robustness of the core defucosylation a 2-fold greater amount (0.4 units) was chosen for further experiments. Equally important is the preservation of antennary fucosylation. A fucosidase specific, or at least highly selective, for the α1,6-linkage over other linkages significant in TPNG (mainly α1,3-linkage) is therefore essential. The MS/MS spectra provided in the **Supplementary Material** demonstrate that core fucoses are removed while antennary fucoses remain (see also following sub-section) with the chosen enzyme. The integrity of the antennary fucosylation under increased enzyme concentrations (**Figure 3**) and incubation times (data not shown) further supports the α1,6-linkage selectivity. An absence of the oxonium ion of *m/z* 658.26 [galactose—*N*-acetylglucosamine(fucose)$_2$+H]$^+$ excluded a significant presence of Lewis y or Lewis b structures.

Identification of Antennary Fucosylated Glycans in Total Plasma *N*-Glycome

Core fucosylated glycans and antennary fucosylated glycans in TPNG were identified by comparing the TPNG profile with and without core fucosidase treatment (**Figure 4**). A more detailed view can be found in **Supplementary Figures S2, S3**

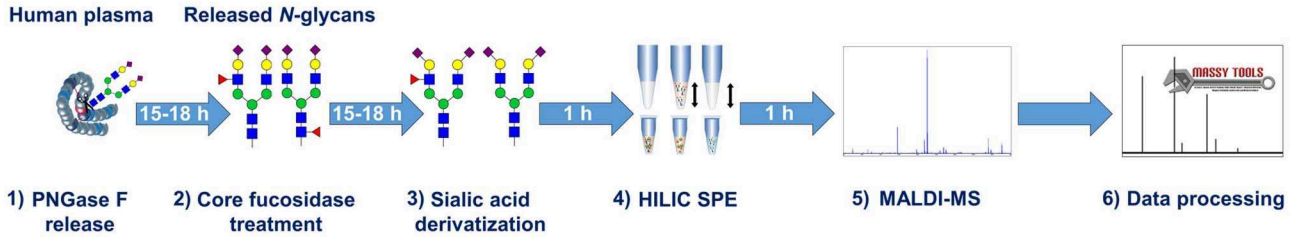

FIGURE 2 | Workflow of the antennary fucose assay for human plasma.

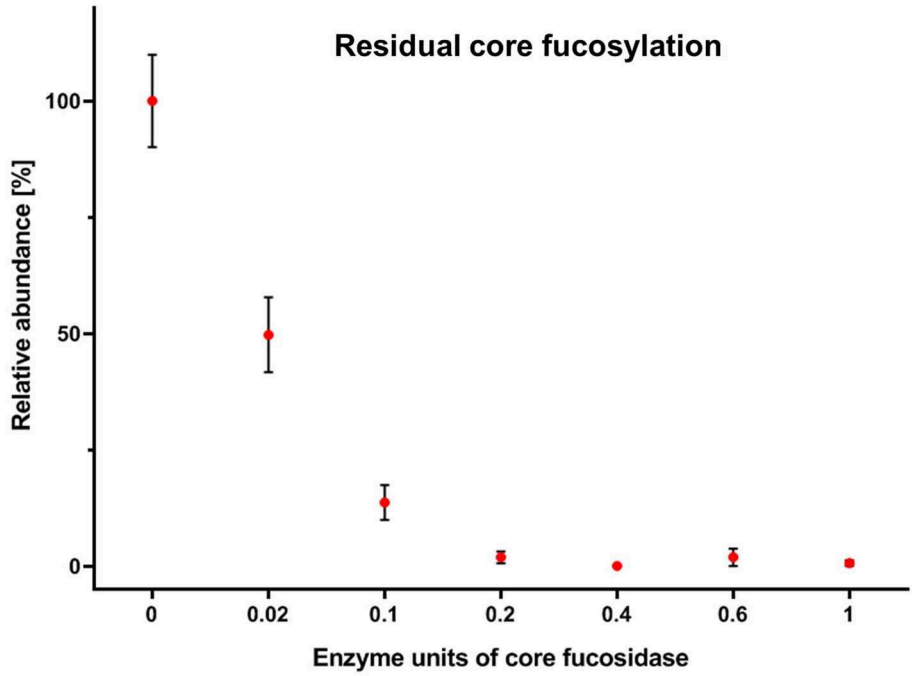

FIGURE 3 | Residual core fucosylation on TPNG after incubation with varying amounts of core fucosidase. The amounts of core fucosylation on complex *N*-glycans were calculated and were normalized to their lowest and highest mean values. Error bars show the standard deviation of the mean of three replicates.

for MALDI-FT-ICR-MS and MALDI-TOF-MS spectra, respectively. Interestingly, some monofucosylated glycan compositions in TPNG showed a mixture of both core and antennary fucosylated isomers (**Supplementary Figure S4**). CID spectra, obtained on a CE-ESI-MS/MS platform, provided an orthogonal layer of evidence (**Figure 5**). CID spectra for all identified antennary fucosylated glycans are shown in **Supplementary Figures S5–S24**. Antennary fucosylation was identified by the formation of the diagnostic B-ion of *m/z* 512.198 assigned as [galactose-*N*-acetylglucosamine(fucose)+H]$^+$ (Wuhrer et al., 2011). Core fucosylation was identified by the formation of the Y-ion of *m/z* 501.219 assigned as [*N*-acetylglucosamine(fucose)-GiRP]$^+$. Core fucosylation also generates, to a lesser extent, the B-ion of *m/z* 512.198 assigned as [mannose-*N*-acetylglucosamine(fucose)+H]$^+$ caused by fucose rearrangement (Harvey et al., 2002; Chen and Flynn, 2007; Wuhrer et al., 2011; Lettow et al., 2019). This complicates the assessment of mixtures, especially relative quantitation by MS/MS. Although, fucose rearrangement also limits the sensitivity of antennary fucose identification in the presence of core fucose isomers, significant contributions of antennary fucose are still readily identified (**Figure 5**).

Notably, no core fucosylation remained after core fucosidase treatment. This was assessed by the absence of the core fucosylated glycans H3N4F1and H4N4F1 (S/N < 9) (**Supplementary Figure S25**). As expected the corresponding afucosylated glycoforms increased in abundance (**Figure 4**). The remaining fucosylated glycans are suggested to be solely antennary fucosylated.

As similar relative abundances were maintained after core fucosidase treatment, the species, H6N5F2Am2E1, H6N5F1Am1E2, H7N6F1Am1E1, H7N6F1Am2E1, H7N6F1Am1E2, H7N6F1Am3E1, H7N6F2Am3E1, H7N6F1Am2E2, H7N6F2Am2E2, and H7N6F1Am1E3, are assigned as antennary fucosylated in human TPNG. This was confirmed by MS/MS (**Supplementary Figures S14–S23**). Interestingly, we were able to prove that the difucosylated glycans, H6N5F2Am2E1, H7N6F2Am3E1, and H7N6F2Am2E2, contained only antennary fucosylation and no core fucosylation. Previously, these glycans have often been assigned as containing one core and one antennary fucose (Vreeker et al., 2018). In fact, we were unable to identify any multifucosylated glycan compositions in TPNG having both core and antennary fucose residues on the same glycan. However, at low abundances (<0.5%), two such mixed, multifucosylated glycans, H6N5F2Am2E1 and H6N5F2Am1E2, have been convincingly demonstrated (Lageveen-Kammeijer et al., 2019). On haptoglobin, multifucosylated glycans having both core and antennary residues were shown to have clinical relevance in subtyping hepatocellular carcinoma patients (Zhu et al., 2014). Thus, it may be very important to differentiate between glycans with multiple antennary fucoses and glycans containing both a core and an antennary fucose. The former may be directly assessed with our assay, the latter indirectly, either via an increase of the resulting monofucosylated species or by comparison to the negative control (fucosidase untreated).

A range of monofucosylated compositions were found to be a mixture of core fucosylated and antennary fucosylated

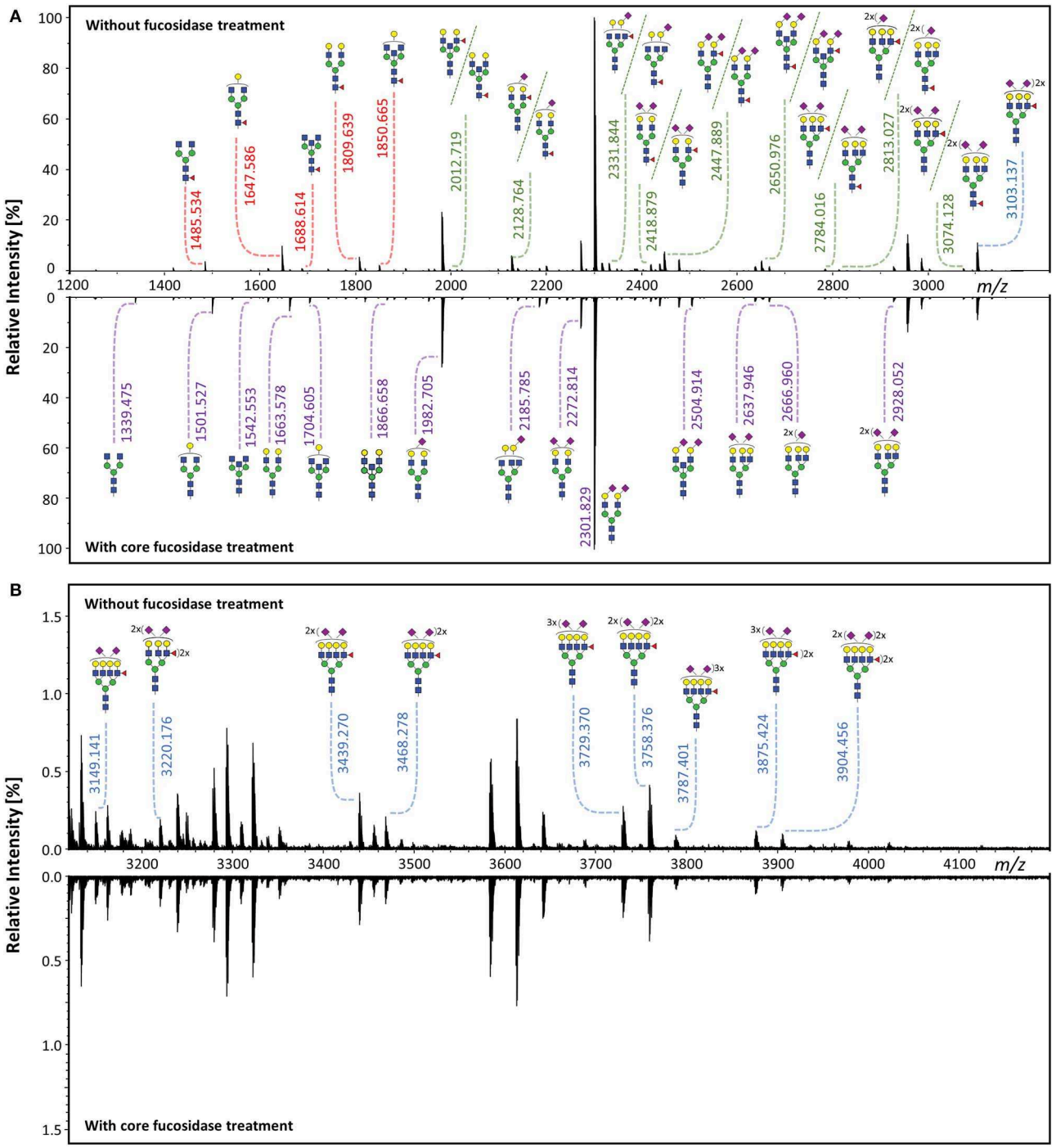

FIGURE 4 | Identification of core fucosylated glycans and antennary fucosylated glycans by exoglycosidase and MALDI-FT-ICR-MS. The TPNG profile without core fucosidase treatment was compared to the profile after treatment, within **(A)** the *m/z* range of 1,200–3,200 and **(B)** the *m/z* range of 3,120–4,200. Core fucosylated glycans [red *m/z* values] are converted to their corresponding afucosylated glycans [purple *m/z* values], upon core fucosidase treatment. Only the antennary fucosylated glycans [blue *m/z* values] and the antennary fucose isomers of the mixed fucose isomeric (core or antennary fucosylation) glycans [green *m/z* values] remain after core fucosidase treatment. All *m/z* values of annotated glycans belong to $[M + Na]^+$ ions. The description of the glycan cartoons are shown in **Figure 1**.

isomers, including for the following glycan compositions: H5N5F1, H5N4F1E1, H5N5F1E1, H5N4F1Am1E1, H5N4F1E2, H5N5F1E2, H6N5F1Am1E1, H6N5F1E2, and H6N5F1Am2E1. Their relative abundances were significantly lowered, but signals did not disappear after core fucosidase treatment (**Supplementary Figure S4** and **Supplementary Table S4**).

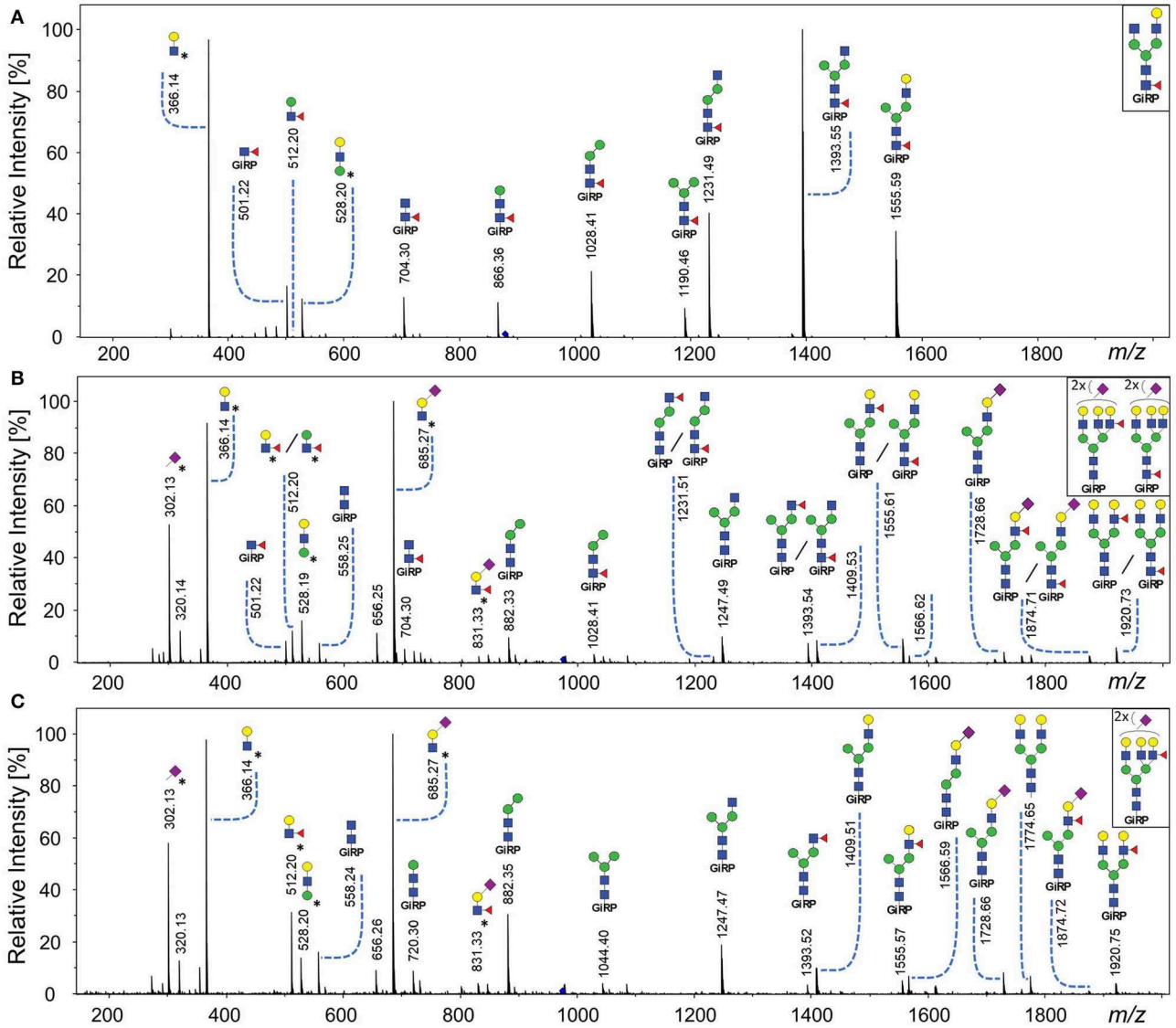

FIGURE 5 | CE-ESI-MS/MS spectra of sialic acid derivatized and GiRP labeled TPNG for the confirmation of antennary, mixed isomeric (core or antennary fucosylation) and core fucosylated glycans. **(A)** The $[M+H]^{2+}$ ion of H4N4F1 (*m/z* 879.838) is fragmented for fucosidase untreated TPNG. Its fragment ions are indicative of core fucosylation. **(B)** The $[M+2H]^{3+}$ ion of H6N5F1E2 (*m/z* 975.709) [second isotope] is fragmented for fucosidase untreated TPNG. Its fragment ions are indicative of both core fucosylated and antennary fucosylated isomers. **(C)** The ion $[M+2H]^{3+}$ of H6N5F1E2 (*m/z* 975.709) [second isotope] is again fragmented, but for core fucosidase treated TPNG. Its fragmentation pattern is indicative of only antennary fucosylation. The descriptions of the glycan cartoons are shown in **Figure 1**. GiRP represents Girard's reagent P label; * represents an oxonium ion.

These findings were further supported by their MS/MS spectra (**Supplementary Figures S5–S13**). As a representative example, the MS/MS fragmentation of the monofucosylated composition H6N5F1E2 is shown without and with core defucosylation in **Figures 5B,C**, respectively. Fragmentation of this glycan from untreated human TPNG resulted in the formation of similar abundances of both a Y-ion of *m/z* 501.219 and a B-ion of *m/z* 512.198. This is typical of a mixture of core and antennary fucosylation (**Figure 5B**). Expectedly, the fragmentation of this glycan after core defucosylation, results in the formation of only the B-ion of *m/z* 512.198 which is indicative of only antennary fucosylation (**Figure 5C**). Thus, H6N5F1E2 in human TPNG is comprised of a mixture of core fucose isomers and antennary fucose isomers. Such monofucosylated glycan compositions which include mixtures of core fucose and antennary fucose isomers contribute to a total abundance of 12.1% ± 1.0% in human TPNG. Our assay determined 3.1% ± 0.3% of them to be antennary fucosylated (**Supplementary Table S5**).

A B-ion of *m/z* 831.325 was observed in several CID spectra which was tentatively assigned as [*N*-acetylneuraminic acid(amidated)-*N*-acetylglucosamine(fucose)+H]$^{+}$. This is an unconventional motif, because antenna fucosylation is generally

observed on α2-3 sialylated antennae. The ion may be caused by fucose rearrangement between the antennae (Wuhrer et al., 2011). For the composition H6N5F1E2 (**Figure 5C**), the higher abundance of the B-ion of *m/z* 512.198 compared to *m/z* 831.325, indeed indicates a Lewis x structure to be more likely. Additionally, for the compositions with only α2-6 sialylated antennae, H5N4F1E2 and H5N5F1E2, we did not observe a B-ion of *m/z* 831.325 but rather the Y-ion of *m/z* 501.219 (**Supplementary Figures S9B, S10B**). Thus, these compositions are partly explained by incomplete core defucosylation. Their antennary fucosylated portion, suggested by the significant abundance of the Y-ion of *m/z* 512.198, could be due to side-products of the esterification of α(2-3) linked sialic acids (Toyoda et al., 2008; Pongracz et al., 2019; Suzuki et al., 2019).

After core fucosidase treatment, H6N5F2Am2E1 and H7N6F1Am1E2 showed a lower abundance (**Supplementary Table S6**). However, from the MS/MS spectra without fucosidase treatment, core fucosylation could not be confirmed on these glycans due to the lack of the Y-ion of *m/z* 501.219 (**Supplementary Figures S16A, S18A**). H6N5F2Am2E1 and H7N6F2Am2E1 both contribute to <0.25% to TPNG, and the ratio of their abundances for *core fucosidase treated / untreated* is 0.83 and 0.88, respectively (**Supplementary Table S5**). Thus, if their core fucosylated isomers are present in TPNG, they might be too low abundant (≤0.03%) to be identified in MS/MS spectra of our CE-ESI-MS/MS platform. Furthermore, a complete depletion of core fucosylation for H5N5F1, H5N4F1E1, H5N5F1E1, H5N4F1E2, and H5N5F1E2 was not achieved as the Y-ion of *m/z* 501.219 was still observed in their MS/MS spectra, although the B-ion of *m/z* 512.198 is equally, if not more abundant (**Supplementary Figures S5–S7, S9, S10**). However, most of the core fucosylation was removed (**Supplementary Figure S4**). Due to the relatively low abundance of the affected glycans, this small overestimation is not likely to have a significant impact on the measurements. A pessimistic estimate is an 0.1% bias in relative quantitation of total antennary fucosylation (<3% for affected glycans, such as H5N4F1E1).

Assay Performance

Intermediate precision was assessed by three independent experiments on different days each with nine replicates of glycan releases from a human plasma pool measured by MALDI-FT-ICR-MS. Seventy glycans were quantified (**Supplementary Table S7**, **Supplementary Figure S26**), which included 19 antennary fucosylated glycans (**Figure 6**). These antennary fucosylated glycans make up 11.8% ± 0.9% of total abundance in human TPNG, with the three most abundant antennary fucosylated glycans, H6N5F1Am1E2, H5N4F1Am1E1, and H6N5F1Am2E1, contributing 6.80% ± 0.63%, 0.84% ± 0.03% and 0.66% ± 0.06%, respectively (**Figure 6B**). The abundance of H6N5F1Am1E2 is consistent with previous quantitation using MALDI-FT-ICR-MS (Vreeker et al., 2018). The median of intermediate precisions for the 19 quantitated antennary fucosylated glycans is 12.4% (9.1–18.5% interquartile range; **Supplementary Figure S27**), which is in-line with the ca. 10% previously described for MALDI-FT-ICR-MS analysis of all TPNG glycans (Vreeker et al., 2018). Notably, neither the focus on low abundant antennary fucosylated glycans (<1%, except H6N5F1Am1E2) nor the additional processing steps resulted in a marked loss of precision.

Previous research quantified 21 antennary fucosylated glycans in human TPNG using a MALDI-FT-ICR-MS platform (Vreeker et al., 2018). These antennary fucosylated glycans are consistent with our findings. However, we were also able to identify a mixture of both core fucose isomers and antennary fucose isomers for nine of these monofucosylated glycan compositions (**Supplementary Figure S4**). For example, we have identified H6N5F1E2 and H5N4F1Am1E1 as being a mixture of core fucose isomers and antennary fucose isomers. Previously, these glycans were assumed to be antennary fucosylated (H6N5F1E2) and core fucosylated (H5N4F1Am1E1), respectively. The specific measurement of antennary fucosylated glycans using our assay may increase the accuracy of the relative quantitation of antennary fucose.

To demonstrate the accuracy of the quantitation of antennary fucosylated glycans, procainamide labeled human TPNG was analyzed on a HILIC-FLD-MS^n platform (Kozak et al., 2015). This analytical platform was chosen for its accuracy and precision of measurements. Antennary fucosylated glycan peaks were identified from their CID spectra while relative quantitation was performed from the FLD chromatograms. By using the FLD chromatogram instead of the MS spectra for quantification, we overcome the ionization bias resulting from charge differences conferred by underivatized sialic acids (which applies to most antennary fucosylated glycans), as compared to the neutral glycans (Wheeler et al., 2009). As the HILIC-FLD-MS^n platform did not identify antennary fucosylated tetraantennary glycans, we based the comparison to our MALDI-MS method on antennary fucosylation of triantennary glycans only. This includes nearly 70% of the total abundance of antennary fucosylated glycans in TPNG (**Supplementary Table S7**). With 32.4 ± 1.1% result from our MALDI-MS method were highly comparable results to the 34.7 ± 1.3% quantified with the HILIC-FLD-MS^n reference method. Thus, our assay is capable of accurately quantifying antennary fucosylation in TPNG.

MALDI-FT-ICR-MS is not widely available. Therefore, we also demonstrated that the assay can be measured with a somewhat more widespread MALDI-TOF-MS instrument (**Supplementary Figure S28**). In total, 58 glycans could be relatively quantitated of which 15 were antennary fucosylated glycans with a total abundance of 7.3% ± 0.7% using MALDI-TOF-MS (**Supplementary Table S8**). In contrast, 19 antennary fucosylation glycans out of 70 glycans in total were quantified with a total abundance of 11.8% ± 0.9% using MALDI-FT-ICR-MS (**Supplementary Table S7**). Thus, fewer antennary fucosylated glycans were quantified with MALDI-TOF-MS due to the expectedly lower sensitivity of the instrument. Furthermore, the differences in quantified antennary fucosylation between the instruments can be accounted for by the different efficiencies of ionization and ion transfer to the detector over the *m/z* range; the MALDI-FT-ICR-MS having been more efficiently tuned for good sensitivity in the high mass range. Consistent with the overall trend, the three

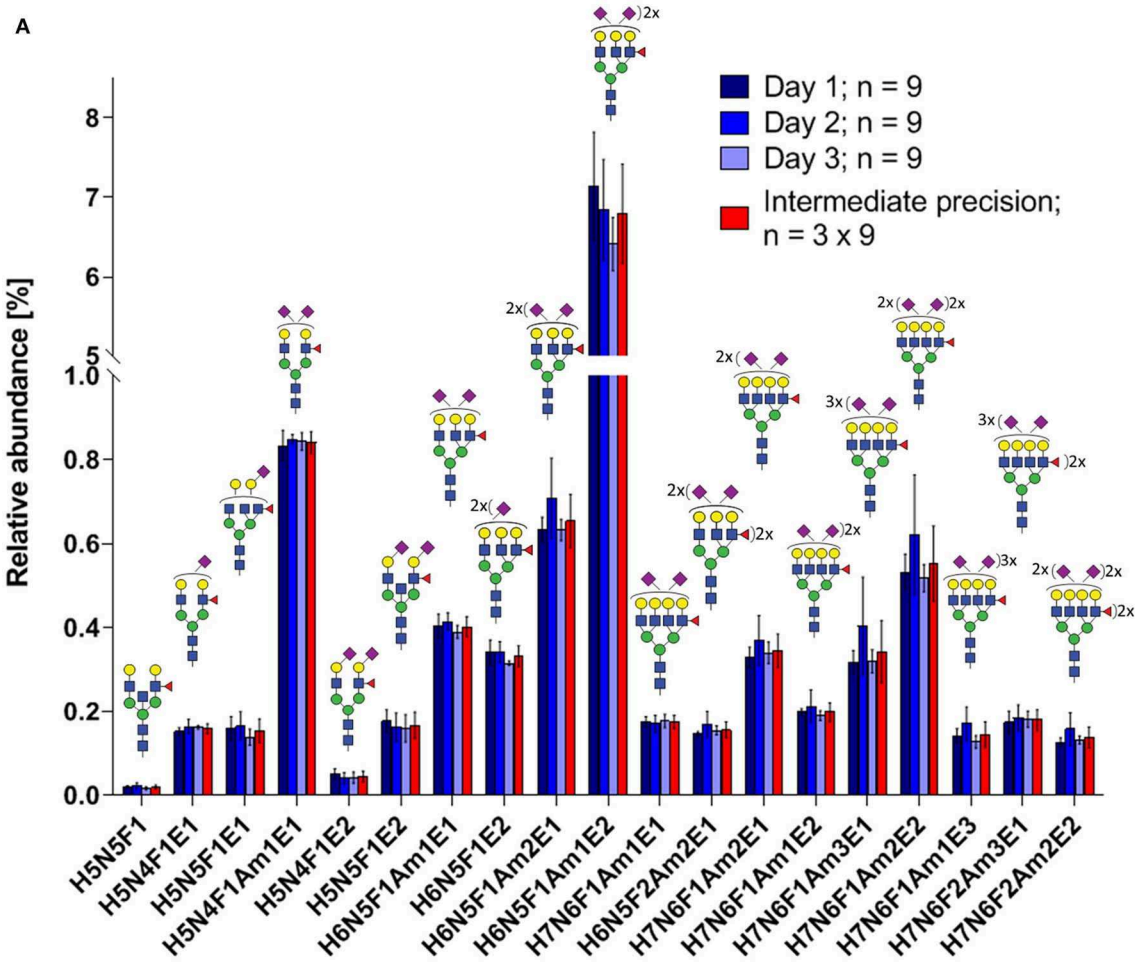

B

Relative standard deviations of the three most abundant AFGs in TPNG			
	H6N5F1Am1E2	H5N4F1Am1E1	H6N5F1Am2E1
Day 1; n = 9	9.5%	4.4%	4.7%
Day 2; n = 9	9.3%	1.3%	13.5%
Day 3; n = 9	5.2%	2.5%	4.0%
Intermediate precision; n = 3 x 9	9.2%	3.1%	9.6%

FIGURE 6 | Intermediate precision of sample preparation for assay and MALDI-FT-ICR-MS measurements of antennary fucosylated glycans in human TPNG. **(A)** The mean relative abundances of the 19 quantified antennary fucosylated glycans are shown with the error bars representing standard deviation ($n = 9$). **(B)** The relative standard deviations of the three most abundant antennary fucosylated glycans are shown. The description of the glycan cartoons are as described in **Figure 1**. [H = hexose, N = *N*-acetylhexosamine, F = deoxyhexose (fucose), Am = amidated *N*-acetylneuraminic acid (α2,3-linked), E = ethyl esterified *N*-acetylneuraminic acid (α2,6-linked)].

most abundant antennary fucosylated glycans also show lower (or equal) values in the MALDI-TOF-MS, H6N5F1Am1E2, H5N4F1Am1E1, and H6N5F1Am2E1, contributing to 3.9% ± 0.4%, 0.81% ± 0.07% and 0.41% ± 0.05% of the total abundance, respectively (**Supplementary Figure S28B**). The abundance of H6N5F1Am1E2 is consistent with previous MALDI-TOF-MS analysis of TPNG (Reiding et al., 2014; Bladergroen et al., 2015). The median of intermediate precisions for the 15 quantitated antennary fucosylated glycans is 12.5% (10.6–13.6% interquartile range; **Supplementary Figure S29**), which is virtually identical to our MALDI-FT-ICR-MS measurements of the 19 antennary fucosylated glycans. The intermediate precision of all *N*-glycans quantitated by MALDI-TOF-MS is shown in **Supplementary Figure S30**. Thus, the assay measured on either instrument can be used for detailed quantitation of antennary fucosylation in human TPNG.

Quantitation of Antennary Fucosylation in Colorectal Cancer Patient Samples

To demonstrate the applicability of the developed antennary fucose assay and especially its ability to reveal clinically relevant markers of antennary fucosylation, total serum *N*-glycome (TSNG) samples were analyzed from colorectal cancer patients pre and post tumor resection. This is of specific interest, as colorectal cancer has been associated with an increase in antennary fucosylation and a decrease in core fucosylation, next to an increase in *N*-glycan antennarity and sialylation (de Vroome et al., 2018; Doherty et al., 2018). Previously, TSNG has been analyzed by MALDI-TOF-MS on sample pairs (pre-operative vs. post-operative) of 61 colorectal cancer patients from the same cohort (de Vroome et al., 2018). The derived traits that were a proxy for antennary fucosylation on *N*-glycans are especially relevant to our study. Multifucosylation on triantennary glycans and α2,3-sialylation per antenna in fucosylated triantennary glycans were significantly

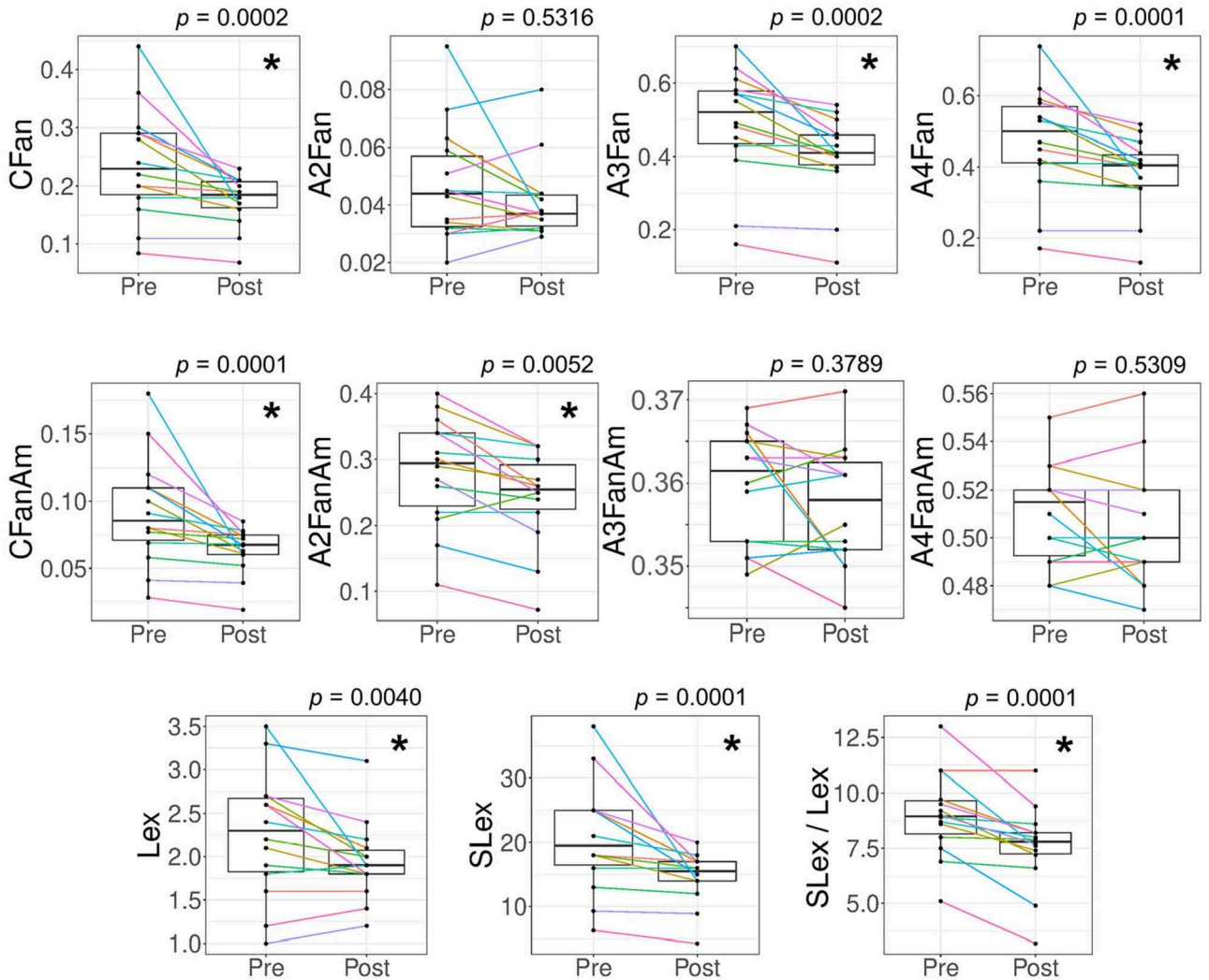

FIGURE 7 | Alteration in features related to antennary fucosylated glycans for colorectal cancer patient samples. Derived traits for glycans were calculated to evaluate antennary fucosylation changes between the 14 pairs of pre-operative (Pre) vs. post-operative (Post) colorectal cancer patient samples. The patient samples were measured with the antennary fucose assay (MALDI-FT-ICR-MS readout). Significant changes were observed for antennary fucosylation in complex *N*-glycans (**CFan**), antennary fucosylation in triantennary glycans (**A3Fan**), antennary fucosylation in tetraantennary glycans (**A4Fan**), α2,3-sialylation per antenna of total antennary fucosylated glycans (**CFanAm**), α2,3-sialylation per antenna of diantennary antennary fucosylated glycans (**A2FanAm**), sialyl-Lewis x abundance (relative area%) in TPNG (**SLex**), Lewis x abundance in TPNG (**Lex**) and the ratio of sialyl-Lewis x to Lewis x abundances in TPNG (**SLex / Lex**). No significant changes were observed for antennary fucosylation in diantennary glycans (**A2Fan**), α2,3-sialylation per antenna of triantennary antennary fucosylated glycans (**A3FanAm**) and α2,3-sialylation per antenna of tetraantennary antennary fucosylated glycans (**A4FanAm**). The *p*-values shown are from a Wilcoxon matched-pairs signed-rank test with confidence level taken as 95%. Multiple-testing correction was performed using a false discovery rate of 1% calculated with the Benjamini and Hochberg method. The *p*-values < 0.0073 are considered significant and are represented with an asterisk (*).

lowered in the post-operative patient samples as compared to pre-operative samples (de Vroome et al., 2018). The latter derived trait was used as a proxy for sialyl-Lewis x epitopes in TSNG. These changes were thought to be associated with the recovery of the patients since values were closer to healthy controls in the post-operative than in the pre-operative samples.

The feasibility to analyze clinically relevant markers of antennary fucosylation with our assay was demonstrated on sample pairs (pre-operative vs. post-operative) of 14 colorectal cancer patients. Glycosylation changes in colorectal cancer patient samples are shown in **Figure 7** and **Supplementary Figure S31**. Details on features and their calculations are shown in **Supplementary Table S4**. In line with previous findings, we were able to show that post-operative patient samples had a significantly lower total antennary fucosylation on total complex *N*-glycans (CFan) as compared to pre-operative samples (**Figure 7**). Unlike previously, no significant differences were observed in α2,3-sialylation per antenna of antennary fucosylated triantennary glycans (A3FanAm), but rather a significantly lowered α2,3-sialylation per antenna of antennary fucosylation diantennary glycans (A2FanAm) in post-operative patient samples as compared to pre-operative samples (**Figure 7**). Since we used only a quarter of the samples, compared to the previous study, missing statistical power provides a simple explanation for missing the sialylation effect on fucosylated triantennary glycans. However, when we focused on the quantitation of sialyl-Lewis x epitopes, it was possible to reproduce the finding. We are able to calculate highly specific derived traits based on antennary fucosylated glycans structures, allowing us to study more specific glycan features. For example, assuming α2,6-sialylated antennae are not fucosylated, there is no preference for fucosylation of α2,3-sialylated or asialylated antennae and multiple fucoses are on different arms, the relative abundances of sialyl-Lewis x can be calculated. This is indeed lowered in the post-operative samples (**Figure 7**). The discovery of a novel association with A2FanAm is also easily explained by the increased specificity of our assay. The trait is largely composed of compositions representing a mixture of core and antennary fucose isomers before core defucosylation. Hence, in a regular TPNG/TSNG MALDI-MS analysis unrelated variations in core fucosylation would interfere with the detection of changes in antennary fucosylation of diantennary glycans.

The changes in CFan are mainly contributed by the triantennary glycans (A3Fan) and tetraantennary glycans (A4Fan) rather than the diantennary glycans (A2Fan) and bisecting diantennary glycans (A2BFan) (A2BFan shown in **Supplementary Figure S31**). We did not observe a change in A2Fan and A2BFan. Without core defucosylation, these traits would largely measure core fucosylation (**Supplementary Figure S4**). Furthermore, we also observed a significantly lowered multiantennary fucosylation (CFm_an) in post-operative patient samples as compared to pre-operative samples (**Supplementary Figure S31**). Finally, we also approximated the abundance of glycans having Lex or sialyl-Lewis x epitopes in TPNG. sialyl-Lewis x / Lewis x ratio was significantly lowered in post-operative patient samples as compared to pre-operative samples. This change was mainly contributed by a decreased abundance of sialyl-Lewis x in post-operative samples, although the Lewis x abundance was also lowered. This may be associated with a decreased inflammatory state of the recovering patient (Brinkman-van der Linden et al., 1998; Higai et al., 2005).

All studied features, except for Lewis x ($p = 0.0513$), were replicated for the MALDI-TOF-MS measurements of the samples (**Supplementary Figure S32**). Thus, MALDI-TOF-MS measurements are sufficient to detect many of the clinical changes.

CONCLUSION

We developed an assay for the relative quantitation of antennary fucosylation and approximation of Lewis x and sialyl-Lewis x abundances in TPNG, based on high-throughput MALDI-MS analysis. This assay is compatible with high sensitivity and ultrahigh-resolution MALDI-FT-ICR-MS or with MALDI-TOF-MS. In total, 19 antennary fucosylated glycans were relatively quantified with precision and accuracy expectable of a MALDI-MS approach. Furthermore, the assay was applied to measuring biomedically relevant changes in antennary fucosylation in colorectal cancer patients pre vs. post tumor resection. Next to previous findings that could be repeated, despite the reduced sample size, the increased specificity enabled the discovery of novel associations. Additionally, we were able to investigate more specialized features based on antennary fucosylation which would not be possible with regular TPNG analysis. The next steps would include further automatization of the assay and perform a high throughput analysis on a large set of patient samples.

DATA AVAILABILITY STATEMENT

The datasets generated for this study are available on request to the corresponding author.

ETHICS STATEMENT

The studies involving human participants were reviewed and approved by the pre-operative vs. 45 days post-operative pairs of 14 CRC patient samples were collected as part of a biobank as was previously described (de Vroome et al., 2018). These serum samples were collected between October 2002 and March 2013 by the Leiden University Medical Center (LUMC) Surgical Oncology Biobank. This study was approved by the Medical Ethics Committee of the LUMC and was performed in accordance with the Code of Conduct of the Federation of Medical Scientific Societies in the Netherlands (http://www.federa.org/). The patients/participants provided their written informed consent to participate in this study.

AUTHOR CONTRIBUTIONS

OR performed all experiments (except HILIC-FLD-MS measurements) and analyzed all data with the help of DF. OR was supervised by SN for the MALDI-FT-ICR-MS experiments and by JN and GL-K for the CE-ESI-MS/MS experiments, respectively. DF supervised the sample preparation and MALDI-TOF-MS experiments. RG performed the HILIC-FLD-MS experiments supervised by DS. WM and RT managed the colorectal cancer samples. OR and DF designed the experiments, aided by SN, GL-K, and MW. OR, SN, GL-K, and DF drafted the manuscript. All authors contributed to finalizing the manuscript.

FUNDING

This research was supported by the European Union (GlySign, Grant No. 722095) and the NWO (Vernieuwingsimpuls Veni Project No. 722.016.008).

SUPPLEMENTARY MATERIAL

The Supplementary Material for this article can be found online at: https://www.frontiersin.org/articles/10.3389/fchem.2020.00138/full#supplementary-material

REFERENCES

Banazadeh, A., Nieman, R., Goli, M., Peng, W., Hussein, A., Bursal, E., et al. (2019). Characterization of glycan isomers using magnetic carbon nanoparticles as a MALDI co-matrix. *RSC Adv.* 9, 20137–20148. doi: 10.1039/C9RA02337B

Benicky, J., Sanda, M., Pompach, P., Wu, J., and Goldman, R. (2014). Quantification of fucosylated hemopexin and complement factor H in plasma of patients with liver disease. *Anal. Chem.* 86, 10716–10723. doi: 10.1021/ac502727s

Bladergroen, M. R., Reiding, K. R., Hipgrave Ederveen, A. L., Vreeker, G. C., Clerc, F., Holst, S., et al. (2015). Automation of high-throughput mass spectrometry-based plasma N-glycome analysis with linkage-specific sialic acid esterification. *J. Proteome Res.* 14, 4080–4086. doi: 10.1021/acs.jproteome.5b00538

Blomme, B., Van Steenkiste, C., Callewaert, N., and Van Vlierberghe, H. (2009). Alteration of protein glycosylation in liver diseases. *J. Hepatol.* 50, 592–603. doi: 10.1016/j.jhep.2008.12.010

Brinkman-van der Linden, E. C., de Haan, P. F., Havenaar, E. C., and van Dijk, W. (1998). Inflammation-induced expression of sialyl LewisX is not restricted to alpha1-acid glycoprotein but also occurs to a lesser extent on alpha1-antichymotrypsin and haptoglobin. *Glycoconj. J.* 15, 177–182. doi: 10.1023/A:1006972307166

Chen, X., and Flynn, G. C. (2007). Analysis of N-glycans from recombinant immunoglobulin G by on-line reversed-phase high-performance liquid chromatography/mass spectrometry. *Anal. Biochem.* 370, 147–161. doi: 10.1016/j.ab.2007.08.012

Cserni, G. (2003). Nodal staging of colorectal carcinomas and sentinel nodes. *J. Clin. Pathol.* 56, 327–335. doi: 10.1136/jcp.56.5.327

de Vroome, S. W., Holst, S., Girondo, M. R., van der Burgt, Y. E. M., Mesker, W. E., Tollenaar, R., et al. (2018). Serum N-glycome alterations in colorectal cancer associate with survival. *Oncotarget* 9, 30610–30623. doi: 10.18632/oncotarget.25753

Doherty, M., Theodoratou, E., Walsh, I., Adamczyk, B., Stockmann, H., Agakov, F., et al. (2018). Plasma N-glycans in colorectal cancer risk. *Sci. Rep.* 8:8655. doi: 10.1038/s41598-018-26805-7

Harvey, D. J., Mattu, T. S., Wormald, M. R., Royle, L., Dwek, R. A., and Rudd, P. M. (2002). "Internal residue loss": rearrangements occurring during the fragmentation of carbohydrates derivatized at the reducing terminus. *Anal. Chem.* 74, 734–740. doi: 10.1021/ac0109321

Hattersley, A. T., and Patel, K. A. (2017). Precision diabetes: learning from monogenic diabetes. *Diabetologia* 60, 769–777. doi: 10.1007/s00125-017-4226-2

Higai, K., Aoki, Y., Azuma, Y., and Matsumoto, K. (2005). Glycosylation of site-specific glycans of alpha1-acid glycoprotein and alterations in acute and chronic inflammation. *Biochim. Biophys. Acta* 1725, 128–135. doi: 10.1016/j.bbagen.2005.03.012

Holst, S., Deuss, A. J., van Pelt, G. W., van Vliet, S. J., Garcia-Vallejo, J. J., Koeleman, C. A., et al. (2016). N-glycosylation profiling of colorectal cancer cell lines reveals association of fucosylation with differentiation and caudal type homebox 1 (CDX1)/Villin mRNA expression. *Mol. Cell Proteomics* 15, 124–140. doi: 10.1074/mcp.M115.051235

Jansen, B. C., Reiding, K. R., Bondt, A., Hipgrave Ederveen, A. L., Palmblad, M., Falck, D., et al. (2015). MassyTools: a high-throughput targeted data processing tool for relative quantitation and quality control developed for glycomic and glycoproteomic MALDI-MS. *J. Proteome Res.* 14, 5088–5098. doi: 10.1021/acs.jproteome.5b00658

Juszczak, A., Pavic, T., Vuckovic, F., Bennett, A. J., Shah, N., Pape Medvidovic, E., et al. (2019). Plasma fucosylated glycans and C-reactive protein as biomarkers of HNF1A-MODY in young adult-onset nonautoimmune diabetes. *Diabetes Care* 42, 17–26. doi: 10.2337/dc18-0422

Knezevic, A., Bones, J., Kracun, S. K., Gornik, O., Rudd, P. M., and Lauc, G. (2011). High throughput plasma N-glycome profiling using multiplexed labelling and UPLC with fluorescence detection. *Analyst.* 136, 4670–4673. doi: 10.1039/c1an15684e

Kozak, R. P., Tortosa, C. B., Fernandes, D. L., and Spencer, D. I. (2015). Comparison of procainamide and 2-aminobenzamide labeling for profiling and identification of glycans by liquid chromatography with fluorescence detection coupled to electrospray ionization-mass spectrometry. *Anal. Biochem.* 486, 38–40. doi: 10.1016/j.ab.2015.06.006

Lageveen-Kammeijer, G. S. M., de Haan, N., Mohaupt, P., Wagt, S., Filius, M., Nouta, J., et al. (2019). Highly sensitive CE-ESI-MS analysis of N-glycans from complex biological samples. *Nat. Commun.* 10:2137. doi: 10.1038/s41467-019-09910-7

Lattova, E., Skrickova, J., and Zdrahal, Z. (2019). Applicability of phenylhydrazine labeling for structural studies of fucosylated N-glycans. *Anal. Chem.* 91, 7985–7990. doi: 10.1021/acs.analchem.9b01321

Lauc, G., Essafi, A., Huffman, J. E., Hayward, C., Knezevic, A., Kattla, J. J., et al. (2010). Genomics meets glycomics-the first GWAS study of human N-Glycome identifies HNF1alpha as a master regulator of plasma protein fucosylation. *PLoS Genet* 6:e1001256. doi: 10.1371/journal.pgen.1001256

Lettow, M., Mucha, E., Manz, C., Thomas, D. A., Marianski, M., Meijer, G., et al. (2019). The role of the mobile proton in fucose migration. *Anal. Bioanal. Chem.* 411, 4637–4645. doi: 10.1007/s00216-019-01657-w

Nairn, A. V., York, W. S., Harris, K., Hall, E. M., Pierce, J. M., and Moremen, K. W. (2008). Regulation of glycan structures in animal tissues: transcript profiling of glycan-related genes. *J Biol. Chem.* 283, 17298–17313. doi: 10.1074/jbc.M801964200

Pivac, N., Knezevic, A., Gornik, O., Pucic, M., Igl, W., Peeters, H., et al. (2011). Human plasma glycome in attention-deficit hyperactivity disorder and autism spectrum disorders. *Mol. Cell. Proteomics* 10:M110.004200. doi: 10.1074/mcp.M110.004200

Pongracz, T., Wuhrer, M., and de Haan, N. (2019). Expanding the reaction space of linkage-specific sialic acid derivatization. *Molecules* 24:3617. doi: 10.3390/molecules24193617

Reiding, K. R., Blank, D., Kuijper, D. M., Deelder, A. M., and Wuhrer, M. (2014). High-throughput profiling of protein N-glycosylation by MALDI-TOF-MS employing linkage-specific sialic acid esterification. *Anal. Chem.* 86, 5784–5793. doi: 10.1021/ac500335t

Royle, L., Campbell, M. P., Radcliffe, C. M., White, D. M., Harvey, D. J., Abrahams, J. L., et al. (2008). HPLC-based analysis of serum N-glycans on a 96-well plate platform with dedicated database software. *Anal. Biochem.* 376, 1–12. doi: 10.1016/j.ab.2007.12.012

Ruhaak, L. R., Hennig, R., Huhn, C., Borowiak, M., Dolhain, R. J., Deelder, A. M., et al. (2010). Optimized workflow for preparation of APTS-labeled N-glycans allowing high-throughput analysis of human plasma glycomes using 48-channel multiplexed CGE-LIF. *J. Proteome Res.* 9, 6655–6664. doi: 10.1021/pr100802f

Saldova, R., Royle, L., Radcliffe, C. M., Abd Hamid, U. M., Evans, R., Arnold, J. N., et al. (2007). Ovarian cancer is associated with changes in glycosylation in both acute-phase proteins and IgG. *Glycobiology* 17, 1344–1356. doi: 10.1093/glycob/cwm100

Schober, E., Rami, B., Grabert, M., Thon, A., Kapellen, T., Reinehr, T., et al. (2009). Phenotypical aspects of maturity-onset diabetes of the young (MODY diabetes) in comparison with Type 2 diabetes mellitus (T2DM) in children and adolescents: experience from a large multicentre database. *Diabet. Med.* 26, 466–473. doi: 10.1111/j.1464-5491.2009.02720.x

Selman, M. H., Hemayatkar, M., Deelder, A. M., and Wuhrer, M. (2011). Cotton HILIC SPE microtips for microscale purification and enrichment of glycans and glycopeptides. *Anal. Chem.* 83, 2492–2499. doi: 10.1021/ac1027116

Staudacher, E., Altmann, F., Wilson, I. B., and Marz, L. (1999). Fucose in N-glycans: from plant to man. *Biochim. Biophys. Acta* 1473, 216–236. doi: 10.1016/S0304-4165(99)00181-6

Stumpo, K. A., and Reinhold, V. N. (2010). The N-glycome of human plasma. *J. Proteome Res.* 9, 4823–4830. doi: 10.1021/pr100528k

Suzuki, N., Abe, T., and Natsuka, S. (2019). Quantitative LC-MS and MS/MS analysis of sialylated glycans modified by linkage-specific alkylamidation. *Anal. Biochem.* 567, 117–127. doi: 10.1016/j.ab.2018.11.014

Testa, R., Vanhooren, V., Bonfigli, A. R., Boemi, M., Olivieri, F., Ceriello, A., et al. (2015). N-glycomic changes in serum proteins in type 2 diabetes mellitus correlate with complications and with metabolic syndrome parameters. *PLoS ONE* 10:e0119983. doi: 10.1371/journal.pone.0119983

Thanabalasingham, G., Huffman, J. E., Kattla, J. J., Novokmet, M., Rudan, I., Gloyn, A. L., et al. (2013). Mutations in HNF1A result in marked alterations of plasma glycan profile. *Diabetes* 62, 1329–1337. doi: 10.2337/db12-0880

Thanabalasingham, G., and Owen, K. R. (2011). Diagnosis and management of maturity onset diabetes of the young (MODY). *BMJ* 343:d6044. doi: 10.1136/bmj.d6044

Toyoda, M., Ito, H., Matsuno, Y. K., Narimatsu, H., and Kameyama, A. (2008). Quantitative derivatization of sialic acids for the detection of sialoglycans by MALDI MS. *Anal. Chem.* 80, 5211–5218. doi: 10.1021/ac800457a

Vanderschaeghe, D., Meuris, L., Raes, T., Grootaert, H., Van Hecke, A., Verhelst, X., et al. (2018). Endoglycosidase S enables a highly simplified clinical chemistry procedure for direct assessment of serum IgG undergalactosylation in chronic inflammatory disease. *Mol. Cell Proteomics* 17, 2508–2517. doi: 10.1074/mcp.TIR118.000740

Vanderschaeghe, D., Szekrenyes, A., Wenz, C., Gassmann, M., Naik, N., Bynum, M., et al. (2010). High-throughput profiling of the serum N-glycome on capillary electrophoresis microfluidics systems: toward clinical implementation of GlycoHepatoTest. *Anal. Chem.* 82, 7408–7415. doi: 10.1021/ac101560a

Vreeker, G. C. M., Nicolardi, S., Bladergroen, M. R., van der Plas, C. J., Mesker, W. E., Tollenaar, R., et al. (2018). Automated plasma glycomics with linkage-specific sialic acid esterification and ultrahigh resolution MS. *Anal. Chem.* 90, 11955–11961. doi: 10.1021/acs.analchem.8b02391

Wheeler, S. F., Domann, P., and Harvey, D. J. (2009). Derivatization of sialic acids for stabilization in matrix-assisted laser desorption/ionization mass spectrometry and concomitant differentiation of alpha(2 –> 3)- and alpha(2 –> 6)-isomers. *Rapid Commun. Mass Spectrom.* 23, 303–312. doi: 10.1002/rcm.3867

Wuhrer, M., Deelder, A. M., and van der Burgt, Y. E. (2011). Mass spectrometric glycan rearrangements. *Mass Spectrom. Rev.* 30, 664–680. doi: 10.1002/mas.20337

Zhu, J., Lin, Z., Wu, J., Yin, H., Dai, J., Feng, Z., et al. (2014). Analysis of serum haptoglobin fucosylation in hepatocellular carcinoma and liver cirrhosis of different etiologies. *J. Proteome Res.* 13, 2986–2997. doi: 10.1021/pr500128t

Conflict of Interest: OR, RG, and DS were employed by Ludger Ltd.

The remaining authors declare that the research was conducted in the absence of any commercial or financial relationships that could be construed as a potential conflict of interest.

Advantages of publishing in Frontiers

OPEN ACCESS
Articles are free to read for greatest visibility and readership

FAST PUBLICATION
Around 90 days from submission to decision

HIGH QUALITY PEER-REVIEW
Rigorous, collaborative, and constructive peer-review

TRANSPARENT PEER-REVIEW
Editors and reviewers acknowledged by name on published articles

Frontiers
Avenue du Tribunal-Fédéral 34
1005 Lausanne | Switzerland

Visit us: www.frontiersin.org
Contact us: info@frontiersin.org | +41 21 510 17 00

REPRODUCIBILITY OF RESEARCH
Support open data and methods to enhance research reproducibility

DIGITAL PUBLISHING
Articles designed for optimal readership across devices

FOLLOW US
@frontiersin

IMPACT METRICS
Advanced article metrics track visibility across digital media

EXTENSIVE PROMOTION
Marketing and promotion of impactful research

LOOP RESEARCH NETWORK
Our network increases your article's readership